Volume 2

Exploring Assur

Assur 2024

Continuing the excavations in the New Town and other research across the site

edited by

Karen Radner and Andrea Squitieri

PeWe-Verlag

Exploring Assur
Volume 2

Exploring Assur

edited by

Karen Radner and F. Janoscha Kreppner

Assur 2024
Continuing the excavations in the New Town and other research across the site

edited by

Karen Radner and Andrea Squitieri

PeWe-Verlag
2025

Gedruckt mit Unterstützung der Deutschen Forschungsgemeinschaft (Gottfried Wilhelm Leibniz-Preis 2022)

Bibliografische Information der Deutschen Nationalbibliothek
Die Deutsche Nationalbibliothek verzeichnet diese Publikation in der Deutschen Nationalbibliografie; detaillierte bibliografische Daten sind im Internet über http://dnb.dnb.de abrufbar.

Layout und Prepress: PeWe-Verlag, Gladbeck
Umschlaggestaltung: PeWe-Verlag, Gladbeck
Umschlagabbildung: Dronenfoto der Schnitte NT1 und "New Town 4" in der Neustadt von Assur im Februar 2024 (Jens Rohde für das Assur Excavation Project)
Druck und Bindung: Rudolph Druck, Schweinfurt

Gedruckt auf alterungsbeständigem Papier

Printed in Germany

ISBN: 978-3-935012-70-6

Table of contents

Preface

Karen Radner

To the memory of Mario Fales, in love and admiration

The 2024 field season at Assur was the second of a series of planned excavations in the New Town funded by my 2022 Gottfried Wilhelm Leibniz Award from the German Research Foundation (DFG). I am very grateful to Ali Obeid Shalgham, the new chairman of the State Board of Antiquities and Heritage, for his unwavering support, as well as to all the many other SBAH members who enable our work. Most prominently, these are Salim Abdullah Ali, director of SBAH Salaheddin, Amr Mohammad Jasim, the head of its Sherqat branch, and his colleagues Sakhar Mohammad Ajaj and Omar Leith Allawi. Among the local staff, special mention must again go to Ahmed Khidr Ahmed, known as "Arabi", who not only served as the mission's driver and mechanic but also gave all of us much joy with his musical gifts, and Mahjub Mohammad Jar, one of the last remaining "Sherqatis" who so generously shares his expertise and is instrumental in training a new generation of excavation workmen from Sherqat and Sdera that also includes some of his sons.

Most members of the field team my intrepid co-director F. Janoscha Kreppner and I assembled for the 2024 season have worked together since the early days of the Peshdar Plain Project, which has been exploring the Dinka Settlement Complex in the Autonomous Kurdish Region of Iraq since 2015. Beyond the Munich and Münster staff (Veronica Hinterhuber, Jana Richter, Jens Rohde, Andrea Squitieri, and Marco Wolf), the core team again included Assur veterans Mark Altaweel and Jörg Fassbinder as well as Christoph Forster. I am much indebted to Mark for coming out to Assur despite the poor compatibility with his academic year at University College London and to Jörg and Christoph for making time for us when we needed them most despite their terrifyingly busy schedules. Huge thanks are due to our head of logistics Kamal Rasheed Raheem who has made it his mission to make both the excavation house and our working and living conditions as comfortable as possible; he continues to perform miracles, and while work in Assur might just about be feasible without him I simply would not want to imagine it. In 2024, Kamal was supported at Assur by Aziz Sharif and his wife Kwestan Raheem Abdullah as our cooks and housekeepers who did everything to keep the excavation household free of illness and full of bodily comforts. The entire team owes a tremendous debt of gratitude to Kamal, Aziz, Kwestan and our conservator, Akam Omar Ahmed Al-Qaradaghi, for their friendship and their support in matters small and great.

On a very personal note, I am very grateful to the entire team for tolerating the sometimes considerable discomfort of having a three-month-old puppy in the excavation house: Ningal, whom we found injured from coyote bites on the first day of excavations in the old SBAH trench and who then happily resided with me in Munich. The latter would not have been possible without the help of my old friend Nineb Lamassu, who generously gave her a home in April and May in Qaraqosh among the Assyrian Christians before she was permitted to enter Germany. Her young life was cruelly cut short by a train accident in Kirchseeon on 24 April 2025, on the same day this manuscript was completed. She was the most wonderful of dogs and worthy of her name in every aspect.

My heartfelt thanks must now turn to my co-editor Andrea Squitieri for kindly yet mercilessly shepherding all contributors towards completing their chapters in the shortest of times. The stellar publication track of the Peshdar Plain Project and now of the fieldwork in the New Town of Assur would be entirely impossible without Andrea's drive and talent; may our close collaboration continue as successfully as it has been in this past decade once Andrea takes up his newly created, much deserved professorship in Ancient Near Eastern Archaeology at the University of Padova in May 2025. With me for a good junk of time incapacitated by illness, Andrea and Denise Bolton, who again expertly dealt with language corrections and copy-editing, took on many of the tasks that I usually handle for our fieldwork publications, and I am very grateful to my dear friends for this and all their other acts of kindness over the past months. This gratitude also extends to Veronica Hinterhuber and Jana Richter.

Our publisher, Peter Werner, deserves my thanks for overseeing the production of this second volume of the se-

ries *Exploring Assur* (ExA). The first volume, entitled *Assur 2023: Excavations and Other Research in the New Town*, is available in print at www.pewe-verlag.de and as an open-access download at https://epub.ub.uni-muenchen.de/115818. As of 3 April 2025, there were 837 downloads and 1493 hits, and I hope that the present volume will find its audience as quickly as the first one.

Finally, my thanks are due to the institutions that provided the funding for our work in 2024: in addition to the already mentioned German Research Foundation, which is the principal sponsor of the project, we received funding from the Gerda Henkel Foundation and LMU Munich, through the endowment of the Alexander von Humboldt Chair for the Ancient History of the Near and Middle East which I hold since 2015.

I dedicate this second volume of the series "Exploring Assur" to the memory of Mario Fales, who has been a generous mentor and good friend to me ever since we first met in the study room of the Vorderasiatisches Museum in Berlin in the autumn of 1993. Mario was a giant in Assyrian studies. One of our last conversations before his death on 15 April 2024 was about the new fieldwork in Assur, which he naturally promised to visit as soon as possible. He was enthusiastic and full of reminiscences about his own experiences when excavating nearby at Tell Karrana and Tell Jikan in 1984 with Gernot Wilhelm and Carlo Zaccagnini. We had often collaborated over the past thirty years, and I am very happy that we were in frequent exchange until his untimely death, especially while he worked on his masterful chapter "The Assyrian Empire: Perspectives on Culture and Society" for the fourth volume of the Oxford History of the Ancient Near East (*The Age of Assyria*, OUP 2023), which I edited with Nadine Moeller and Dan Potts. Mario liked to joke that we were academic siblings, due to the role of the unforgotten Karlheinz Deller in our doctoral training: "I am Deller's oldest Assyrian child, and you are his youngest." Indeed, Mario was the best elder brother one could have in Assyrian studies, and I owe him so much, from invitations to international conferences when I just started in academia to our joint publication of the tablets from Ma'allanate (Tell Shiukh Fawqani) to sharing moments with our families in Hatfield, London, Munich and Verona. Thank you, Mario.

A. Continuing fieldwork at Assur: An introduction to the work programme of 2024

Karen Radner

After the promising results of the first year of fieldwork of the Assur Excavation Project in 2023,[1] the team returned to Sherqat and the restored excavation house in early February 2024 and stayed until early April 2024. The weather, while cold, was less inclement than it had been in the previous spring. The temperatures and the rain proved less challenging, although we still lost several days to storms and their aftermaths. The fact that the conditions were generally better than in the spring of 2023 is perhaps best demonstrated by the fact that we could take boat trips on the Tigris, most importantly upstream to Kar-Tukulti-Ninurta (Tulul al-ʿAqar), where our party was cordially welcomed by the archaeologists of SBAH Sdera on 23 February 2024 (**Fig. A1**).

The excavation programme of the second spring campaign continued with work in the same trench (**§C2**) and a new second trench nearby (**§C4**). Three old hands from our days in the Peshdar Plain were able to join us: John MacGinnis (Cambridge University) added many valuable perspectives from the excavations he is currently undertaking at Nineveh (Mosul) and Kalhu (Nimrud). He and our former LMU Munich colleagues Eileen Eckmeier (now Professor for Geoarchaeology and Environmental Risks at Kiel University since 2021) and Alessio Palmisano (Professor of Research Methods for Archaeology at Turin University since 2023) were, as ever, invaluable out in the field but to all of us, their good cheer and optimism were just as important as their expertise.

Serendipity brought us a new team member in the shape of Helen Gries (Vorderasiatisches Museum Berlin), who had first meant only briefly to visit en route to Nineveh; as circumstances changed, she instead joined us for good, putting to excellent use her decades-long familiarity with all things Assur in analysing the small finds of 2023 and 2024. It is a great pleasure to extend the close collaboration with the Vorderasiatisches Museum in Berlin to the fieldwork at Assur and include a member of the current leadership team of the Deutsche Orientgesellschaft in our roster. We were joined by Rafał Fetner (University of Warsaw) and Marta Lorenzon (University of Helsinki), who brought us much-needed expertise in their respective fields of human anthropology and mudbrick technology. Poppy Tushingham further strengthened the Munich contingent as a jack-of-all-trades who had wisely decided that a true Assyrian specialist must know Assyria itself. She assisted in the excavation and quickly became an integral part of the pottery team.

Fig. A1: Part of the team, including John MacGinnis (centre back) and Alessio Palmisano (third from left) as well as our puppy Ningal, at Kar-Tukulti-Ninurta (Tulul al-ʿAqar) with SBAH Sdera archaeologists Mazhar Abdel Karim Hijab and Awad Mohammed Abdel Rahman (first and third on the right). 23 February 2024. Photo by Omar Laith Allawi.

1 For the publication of the 2023 fieldwork, see Radner/Squitieri 2024a.

Joint heads of mission (Fig. A2):
- Karen Radner (LMU Munich): 10 February–3 April 2024, also epigraphist;
- F. Janoscha Kreppner (University of Münster): 6 February–3 April 2024.

SBAH archaeologists (Fig. A3):
- Salim Abdullah Ali (SBAH Salaheddin), as principal representative;
- Amr Mohammad Jasim (SBAH Sherqat), as representative; also pottery team;
- Sakhar Mohammad Ajaj (SBAH Sherqat), as representative; also field team;
- Omar Laith Allawi (SBAH Sherqat), pottery processing.

Local logistics unit (Fig. A2):
- Kamal Rasheed Raheem (Sulaymaniyah Directorate of Antiquities and Heritage; retired), as head of logistics;
- Ahmed Khidr Ahmed, known as "Arabi" (SBAH Sherqat), as driver (**Fig. A9**);
- Aziz Sharif (Sulaymaniyah Directorate of Antiquities), as cook and housekeeper;
- Kwestan Raheem Abdullah, as cook and housekeeper;
- Hussein Abdallah (SBAH Sherqat), as house guard;
- Ali Hussein (SBAH Sherqat), as house guard.

House team (Fig. A2):
- Jana Richter (LMU Munich), joint head of house: 10 February–3 April 2024;
- Andrea Squitieri (LMU Munich), joint head of house: 6 February–3 April 2024, also sediment coring;
- Christoph Forster (Fa. Datalino, Berlin), digital documentation and database: 23 February–9 March 2024;
- Helen Gries (Vorderasiatisches Museum, Berlin), small finds: 19 March–3 April 2024;
- Poppy Tushingham (LMU Munich), pottery processing: 10 February–3 April 2024, also field team.

Field team (Fig. A4):
- Jens Rohde (LMU Munich), field director: 6 February–3 April 2024;
- Veronica Hinterhuber (LMU Munich), trench supervisor: 10 February–3 April 2024;
- John MacGinnis (Cambridge University), trench supervisor: 10 February–22 March 2024 (**Figs. A1 and A5**);
- Alessio Palmisano (University of Turin), trench supervisor: 10 February–9 March 2024 (**Figs. A1 and A5**);
- Marco Wolf (LMU Munich), trench supervisor: 6 February–3 April 2024, also magnetometer and ERT prospecting;
- Mahjub Mohammad Jar, as foreman ("Sherqati") (**Fig. A6**);

Fig. A2: Most members of the logistics, house and field teams with specialists Akam Omar Ahmed Al-Qaradaghi (standing, first on left), Eileen Eckmeier (seated, first on right) and Marta Lorenzon (seated, third from left) in the garden of the excavation house. Photo by Omar Laith Allawi.

Fig. A3: Just before our departure to Baghdad airport on 3 April 2024 with our local SBAH colleagues: Salim Abdullah Ali, Omar Laith Allawi, Sakhar Mohammad Ajaj (seated, second to fourth from left), Amr Mohammad Jasim (seated, second from right), and Ahmed Khidr Ahmed, known as "Arabi" (standing on the far left). Drone photo by Jens Rohde.

- Abu Hais Sa'la, as site guard;
- Issa Ibrahim Atiyah, as site guard;
- 27 workers from Sherqat and Sdera.

Specialists:

- Mark Altaweel (University College London), geoarchaeology and sediment coring: 10 February–17 February 2024 (**Fig. A5**);
- Eileen Eckmeier (University of Kiel), sedimentology and erosion studies: 19 March–3 April 2024 (**Fig. A2**);
- Jörg Fassbinder (LMU Munich), magnetometer and ERT prospecting: 23 February–9 March 2024;
- Rafał Fetner (University of Warsaw), physical anthropology: 23 February–9 March 2024;
- Marta Lorenzon (University of Helsinki), mudbrick analysis: 19 March–3 April 2024 (**Fig. A2**);
- Akam Omar Ahmed Al-Qaradaghi (Sulaymaniyah Directorate of Antiquities and Heritage), find restoration: 6 February–3 April 2024, with some interruptions (**Fig. A2**).

As in the Peshdar Plain and at Gird-i Rostam, where Aziz Sharif had been our driver since 2015, he masterfully resolved various mechanical and engineering issues that had plagued us previously, including problems with heating, bathrooms and the flotation tank. All of these previous areas of concern massively benefitted from the installation in August 2023 of solar panels and a photovoltaic system that provide the power needed to run the house reliably. We are very grateful for the funding received from the Bavarian State Ministry for Science and Art and the Austrian Embassy in Baghdad.

The Austrian ambassador, His Excellency Dr Andrea Nasi, honoured us with a visit on 6 March 2024 to formally inaugurate the photovoltaic system (**Fig. A6**). On that occasion, we also welcomed many local dignitaries (**Fig. A7**) and transformed the excavation house's hall, which is normally used for pottery processing and the restoration of large objects, into a concert venue. The guests were treated to a musical performance by Ismail Khalaf Abdelkarim, the director of the Al-Khusm Elementary

Fig. A4: Most of the field team in trench NT1 on 23 March 2024, with foreman Mahjub Mohammad Jar standing second from left (holding a trowel). Drone photo by Jens Rohde.

Fig. A5: Walking on Sennacherib's stone-paved procession road on 16 February 2024, with Mark Altaweel (centre front), John MacGinnis (second from right) and Alessio Palmisano (third from left). Drone photo by Jens Rohde.

Fig. A6: Karen Radner shows some of the solar panels installed on the excavation house's southern roof to the Austrian ambassador Dr Andrea Nasi and Nineb Lamassu, director of the Sustainable Peace Foundation in Mosul. 6 March 2024. Photo by Omar Laith Allawi.

School in Sherqat, on the oud and the violin (**Fig. A8**) and by our own Ahmed Khidr Ahmed ("Arabi") on the rababa (rebab), a traditional string instrument that he had built himself (**Fig. A9**).

Later on that same day, we also received an official visit from the new chairman of the State Board of Antiquities and Heritage, Ali Obeid Shalgham (**Fig. A10**), for whose ongoing support we are very grateful.

During the spring campaign, Kamal Rasheed Raheem and I discussed with the SBAH Sherqat team the possibility of restoring the ruined building next to the Andrae excavation house that had been used for pottery storage before it was destroyed when the ISIS cell that had used the excavation house as its base was driven out by aerial attacks by Iraqi state forces in late 2016. The building had originally served as the lodgings of the excavation's original bookkeeper Shaul Salman, a well-known member of the Jewish community of Hillah and a longtime associate of Robert Koldewey and his Babylon excavation team. The structure, therefore, is as old as the excavation house and is a historical monument in its own right. Funding for its restoration was generously awarded in May 2024 by the Gerda Henkel Foundation (AZ 22/BE/24: "Renovation of the House of Shaul Salman in Assur"), and the ensuing building work took place from August to October 2024, overseen by Kamal Rasheed Raheem.

Fig. A7: The Austrian ambassador Dr Andrea Nasi (centre) and local dignitaries visiting the ziggurat of the Aššur temple with Kamal Rasheed Raheem, Janoscha Kreppner (third and fourth from left), Karen Radner and Sakhar Mohammad Ajaj (sixth and fifth from right). 6 March 2024. Photo by Omar Laith Allawi.

Fig. A8: The Austrian ambassador Dr Andrea Nasi and Ismail Khalaf Abdelkarim, director of the Al-Khusm Elementary School in Sherqat, with his oud in the hall of the excavation house after the concert on 6 March 2024. Photo by Karen Radner.

Fig. A9: Ahmed Khidr Ahmed ("Arabi") in concert, performing on a rababa (rebab) constructed from an oil canister. 6 March 2024. Photo by Karen Radner.

Fig. A10: The chairman of the State Board of Antiquities and Heritage, Ali Obeid Shalgham (centre), with Kamal Rasheed Raheem, Salim Abdullah Ali, Karen Radner and Janoscha Kreppner (from right to left) during his visit on 6 March 2024. Photo by Omar Laith Allawi.

The restoration effort was completed by the time a second, short autumn campaign took place from 24 October to 11 November 2024. It served a dual purpose: firstly, to conclude the initial processing of the pottery unearthed in spring 2024 and secondly, to more closely investigate a promising sondage dug within the 2002 SBAH trench (**§C3**). The team consisted of Jana Richter, Jens Rohde, Andrea Squitieri and Poppy Tushingham, our local logistics unit headed by Kamal Rasheed Raheem (see above) and 10 workers from Sherqat and Sdera led by Mahjub Mohammad Jar as their foreman, with Ahmed Al-Wru acting as site guard. The team also started furnishing the restored Shaul Salman building so that it could again be used as a storage facility, especially for pottery that had already been processed and analysed.

When Janoscha Kreppner and I first met with the SBAH Sherqat authorities in February 2022, a dog called Fleah caught our attention as he accompanied us through the ruins of Assur. Highly unusually for the region, Fleah had a name because he was friendly with the archaeologists and the antiquities police, who tolerated him as they considered him a guardian of the archaeological site. While we lived in the excavation house in 2023 and 2024, Fleah moved there too and diligently kept watch over the river entrance of the building, keeping at bay coyotes, sheep flocks and the occasional bovine invaders swimming over from the river island where cattle are brought for grazing. Clever and self-assured, Fleah was the grizzled patriarch of the pack of wild dogs that resides in Assur and introduced some of its more adventurous members to us; most wisely stay out of sight of humans. Sadly, Fleah died in autumn 2024 before the team's return. I will always remember him as the watcher on the walls of Assur (**Fig. A11**).

Fig. A11: Fleah, patriarch of the wild dogs of Assur, on the rampart walls of the city he guarded all his life. 22 March 2024. Photo by Karen Radner.

As already in the first field season of 2023, Ali Obeid Shalgham and his SBAH team in Baghdad again enabled us to export various kinds of samples for scientific analysis, for which we are very grateful. The samples were brought back to Munich in May 2024 by Jana Richter and Poppy Tushingham after Kamal Rasheed Raheem had prepared the extensive paperwork necessary on behalf of the Assur Excavation Project. The return of the leftovers of these samples was formally accepted by SBAH in Baghdad on 27 March 2025.

In addition to the already-mentioned researchers who had worked on-site in Assur and later continued their analyses in their home labs, several other researchers and research teams have taken on the processing and analysing of specific finds and samples collected during our fieldwork:

- Human DNA analysis: Johannes Krause, Philipp Stockhammer and the team of the Max-Planck-Institut für evolutionäre Anthropologie, Leipzig;
- Material studies: Silvia Amicone and the Competence Center Archaeometry - Baden Wuerttemberg (University of Tübingen) and Melis Uzdurum (University of Helsinki): **§D2** and **§G**;
- Numismatics: Kay Ehling (Staatliche Münzsammlung München): **§E2**;
- Paleobotanical analysis: Claudia Sarkady and the Archäobotanisches Labor Eggstädt: **§I2**;
- Phytolith analysis: Doğa Karakaya (University of Helsinki): **§I3**;
- Pottery studies: Alessandra Cellerino and Enrico Foietta (both University of Turin) and Mustafa Ahmad (Goethe University Frankfurt): **§D1**;
- Radiocarbon dating: Curt-Engelhorn-Zentrum Archäometrie, Reiss-Engelhorm-Museen, Mannheim: **§C1.2**;
- Sedimentology: Andreas Stele (Bayerisches Landesamt für Denkmalpflege);
- Wood analysis from charcoals: Katleen Deckers (University of Tübingen): **§I1**;
- XRF analysis: Michaela Schauer (University of Vienna): **§D2**.

As in the previous year, we are again very fortunate that some of our research partners have already been able to produce reports for this second publication of the Assur Excavation Project, in addition to the reports on the erosion damage to the archaeological site (**§B1**), on the continuing coring (**§B2**) and geophysical prospecting programmes (**§B3**), on the excavation (**§C**), as well as on the small finds (**§E1**), the cuneiform texts (**§F**) and the human remains (**§H**), all of which result from work conducted by the authors on the site.

B. Environment, coring and remote sensing in and around Assur, 2024

This section consists of three chapters addressing aspects of Assur's modern and ancient environment. Chapter **§B1** examines the impact of water and wind erosion on the archaeological site. Chapter **§B2** provides a detailed visual description of the sediment cores extracted from various locations on-site. Chapter **§B3** is dedicated to the geophysical survey, detailing the results of Electrical Resistivity Tomography (ERT) conducted in the New Town.

B1. Documentation of damage due to erosion at the site of Assur

Eileen Eckmeier

Assur is situated in a region with a distinct climate that renders it highly susceptible to land and soil degradation. Early accounts, such as those by Walter Andrae,[2] highlight the area's characteristic weather phenomena, including dust storms, torrential rains, and flooding from the Tigris River. Andrae described the landscape as hostile, underscoring the inherent fragility of Iraq's soils and ecosystems. This vulnerability has only intensified recently due to the escalating impacts of climate change.

Erosion is also a significant issue for archaeological and historical monuments, including Assur, a UNESCO World Heritage Site, which was listed in 2003 as a World Heritage Site in Danger. While the primary concern has been the risks associated with ongoing conflicts in the region, the challenges of erosion, weathering, and the decay of mudbrick structures have also been recognised as critical issues. In response, a joint mission by the World Heritage Centre (WHC) and ICOMOS carried out a reactive monitoring visit to document the current state of Assur and assess the extent of these threats.[3]

The damages and threats, documented in March 2024 by the author, encompass mainly processes that are related to the specific geographical characteristics of the region, to the anthropogenic activities on the site and to the material from which the buildings in Assur had been constructed. The WHC/ICOMOS documentation reports that large quantities of materials were eroded from the constructions and redeposited on their base and that the artificial topography of the site as a result of excavations is aggravating erosion and increasing surface runoff due to the lack of sufficient drainage.[4]

Erosion is primarily influenced by five key factors: climate (precipitation, temperature, wind), vegetation cover, soil characteristics (particle-size distribution, humidity, composition), topography, and human activities.

The weather station in Mosul (36° 19' N; 43° 09' E) recorded an average of 359 mm of precipitation per year (average in the period 1941-1970) and a mean annual temperature of 19.8° C.[5] However, the annual variations are relevant: while the precipitation in winter (December to March) reaches values of 60-70 mm/month, with strong precipitation events, the amount of rain can be zero in summer, leading to bare surfaces and dry soils. Wind direction is mostly S-SE, as documented for the years 2023-2024.[6]

Therefore, the area's climatic conditions are characterised by high precipitation in spring, which triggers water erosion. Arid and hot summers, combined with prevailing winds, add to the effects of wind erosion. In March 2024, the site's current damage was documented by the present author following a period of heavy rainfall. Visual inspection revealed that most surfaces remained largely bare of vegetation and unprotected, even after the winter rains. Exceptions were observed in depressions, such as former excavation pits or erosion gullies, where moisture lingered, allowing vegetation to persist for extended periods.

A notable feature of the site is the absence of significant soil formation. The surface sediment appears to consist predominantly of decayed mudbrick material, likely mixed with windblown dust, and lacks any humic topsoil that would support plant growth. The ancient structures, including the ziggurat and city walls, were primarily con-

2 Andrae 1938; 1977.

3 See https://whc.unesco.org/en/list/1130/documents.

4 See https://whc.unesco.org/en/list/1130/documents.

5 Data source: Deutscher Wetterdienst: www.dwd.de/DE/leistungen/klimadatenwelt/asien/fj/irak/irak_node.html.

6 Data source: Meteoblue: www.meteoblue.com/en/weather/historyclimate/weatherarchive/mosul_iraq_99072.

structed from unbaked mudbricks. These mudbricks were made from a loamy mixture of silt, clay, and sand, with a high proportion of silt-sized particles. Silt, in particular, is highly susceptible to erosion by both water and wind, contributing to the site's vulnerability.

Moreover, the site's surface level slopes towards the river. The rainwater flows downhill, resulting in gully erosion and deterioration near the cliff's edge. Gully and tunnel erosion were also documented in the area at other locations.

Fig. B1.1: Pathways and traces of trampling erosion due to the passage of sheep and goats. Photo by Eileen Eckmeier.

Fig. B1.2: Pathways and traces of trampling erosion due to the passage of sheep and goats. Photo by Eileen Eckmeier.

Fig. B1.3: Pathways and traces of trampling erosion due to the passage of sheep and goats. Photo by Eileen Eckmeier.

Human-made alteration of the surfaces and their contours enhanced damage to the site. The excavations by Andrae left behind deep and long trenches, which cross the whole area from west to east, dipping from the city walls to the river, as well as mounds of spoil. Previously excavated areas have not been refilled,[7] creating a strongly incised and disturbed surface. Currently, visitors use the area for recreational purposes, especially the ziggurat, and create cavities and grooves on the surface when they climb the constructions. Finally, the vegetation growing in the depressions and the wide space attracts herds of sheep and goats from the site's surrounding areas. They cross the city walls and leave clear pathways and traces of trampling erosion on the slopes (**Figs. B1.1-3**).

Overall, erosion due to water and wind leads to:

1. severe damage to the mudbrick constructions;
2. loss of material on the surface of the site;
3. reformation of surface contours due to the accumulation of eroded material;
4. loss of material at the embankments of the Tigris.

1. The deterioration of the mudbrick structures is particularly severe at the ziggurat. Its surface shows significant damage caused by rainfall and the activity of visitors climbing the monument. Cavities have developed both on the exterior and within the structure. Most notably, a large tunnel at the base, excavated in modern times,[8] shows evidence of water flow down into the ziggurat's structure. Mudbricks frequently detach from damaged sections of the walls or erode under rainfall, resulting in

Fig. B1.4: The remains of the ziggurat with deep incisions due to the rain flow. Photo by Eileen Eckmeier.

7 The sole exception are the trenches dug by the Assur Excavation Project since 2023, which are all backfilled at the end of each excavation season and re-excavated as needed at the beginning of the next season.

8 Andrae 1977, 129.

Fig. B1.5: The tunnel excavated in modern times within the ziggurat core. Photo by Eileen Eckmeier.

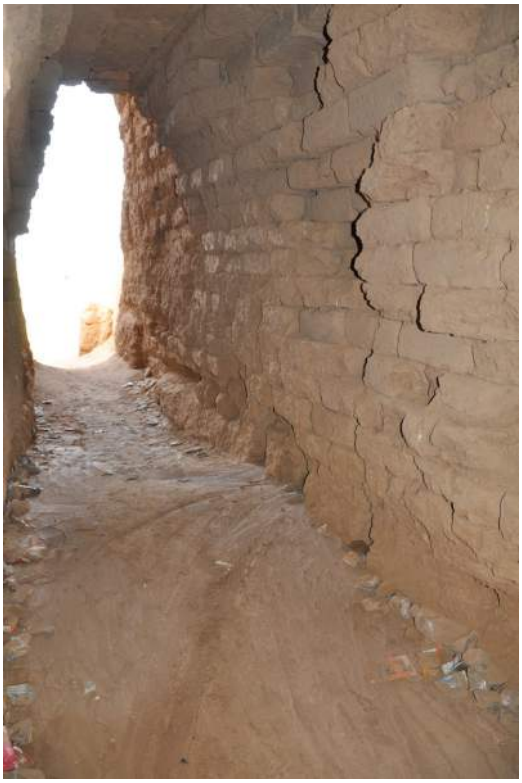

Fig. B1.6: The tunnel excavated in modern times within the ziggurat core. Photo by Eileen Eckmeier.

Fig. B1.7: Erosion at the base of the ziggurat. Photo by Eileen Eckmeier.

Fig. B1.8: Damage caused by slope erosion in the area below the ziggurat. Photo by Eileen Eckmeier.

Fig. B1.9: Damage caused by rapid runoff during heavy rainfall. Photo by Eileen Eckmeier.

deep incisions (**Figs. B1.4-7**). Furthermore, the slope erosion leading to the lower fluvial bank poses an additional threat to the ziggurat's stability, potentially undermining its structural integrity (**Fig. B1.8**).

2. The excavation trenches created by Andrae, which cut downhill across the site, along with the surface characteristics, contribute to rapid runoff during heavy rainfall. This runoff accelerates water erosion, carving gullies and tunnels into and through the archaeological site. This process not only transports material from the site into the river but also displaces archaeological artefacts within the site (**Figs. B1.9-14**). A striking example of this is the severe tunnel erosion, which has formed a prominent channel extending downhill (**Figs. B1.15-17**).

3. The eroded material accumulates at the edges of the constructions. The former city walls, for example, were completely reshaped by either material loss (**Figs. B1.18-20**) or accumulation in the surrounding areas. A test core at the outer area of the wall (Core C28, **Fig. B1.21**) revealed eroded sediment up to a depth of 4.70 m, where a layer of gravel marked the end of the sedimentation. The sediment was a homogeneous silt-rich material throughout the coring, without specific features or artefacts.

4. The erosion damage at the fluvial embankment is critical. A visual inspection of the cliffs shows that the river had cut mudbrick structures, and parts of these structures were found at the river bank (**Fig. B1.22**). Another issue is that gravel is mined at the site's southern edge, leading to larger disruptions near the city wall (**Figs. B1.23**).

In conclusion, the archaeological site of Assur faces severe threats from erosion, primarily driven by its distinct climate, human activities, and the fragile mudbrick construction of its ancient structures. Water and wind erosion are exacerbated by the site's sloping terrain, lack of vegetation, and the legacy of excavation trenches, leading to significant material loss, damage to key monuments such as the ziggurat, and destabilisation of the river embankment. These challenges highlight the urgent need for targeted conservation efforts to mitigate the ongoing degradation of this UNESCO World Heritage Site.

Fig. B1.10: Damage caused by rapid runoff during heavy rainfall. Photo by Eileen Eckmeier.

Fig. B1.11: Damage caused by rapid runoff during heavy rainfall. Photo by Eileen Eckmeier.

Fig. B1.12: Damage caused by rapid runoff during heavy rain. Photo by Eileen Eckmeier.

Fig. B1.13: Damage caused by rapid runoff during heavy rainfall. Photo by Eileen Eckmeier.

Fig. B1.14: Sediment being transported into one of Andrae's old east-west excavation trenches.. Photo by Eileen Eckmeier.

Fig. B1.15: Severe tunnel erosion. Photo by Eileen Eckmeier.

Fig. B1.16: Severe tunnel erosion. Photo by Eileen Eckmeier.

Fig. B1.17: Severe tunnel and gully erosion. Photo by Eileen Eckmeier.

Fig. B1.18: Erosion along the city walls. Photo by Eileen Eckmeier.

Fig. B1.19: Erosion along the city walls. Photo by Eileen Eckmeier.

Fig. B1.20: Erosion along the city walls. Photo by Eileen Eckmeier.

Fig. B1.21: A test core taken at the outer area of the wall (Core C28). Photo by Eileen Eckmeier.

Fig. B1.22: Mudbrick structures cut by the river. Photo by Eileen Eckmeier.

Fig. B1.23: Mudbrick structures cut by the river. Photo by Eileen Eckmeier.

B2. The 2024 geoarchaeological coring at Assur

Mark Altaweel

B2.1 Work plan and objectives

During the 2024 campaign, geoarchaeological coring efforts expanded substantially, with 20 new cores completed (**Fig. B2.1**), building on the previous season's work.[9] 11 cores were obtained in the New Town area (C9-C12, C14-C18, C27, C28), and six in the Inner City (C21-C24, C25, C26). Additionally, three cores for clay analysis (C13, C19, C20) were taken by the Tigris river, north of Assur, with results used in Chapter **§D2** on the petrographic analysis of pottery.

The geophysical data collected in 2023 informed the coring activity in the New Town.[10] This data enabled us to pinpoint key areas where evidence of building activity located just below the site surface was either inconclusive or scant. The primary objective of coring in these areas was to access deeper strata, potentially dating back to the Iron Age, and to compare the findings with the results of the ERT survey (**§C3**).

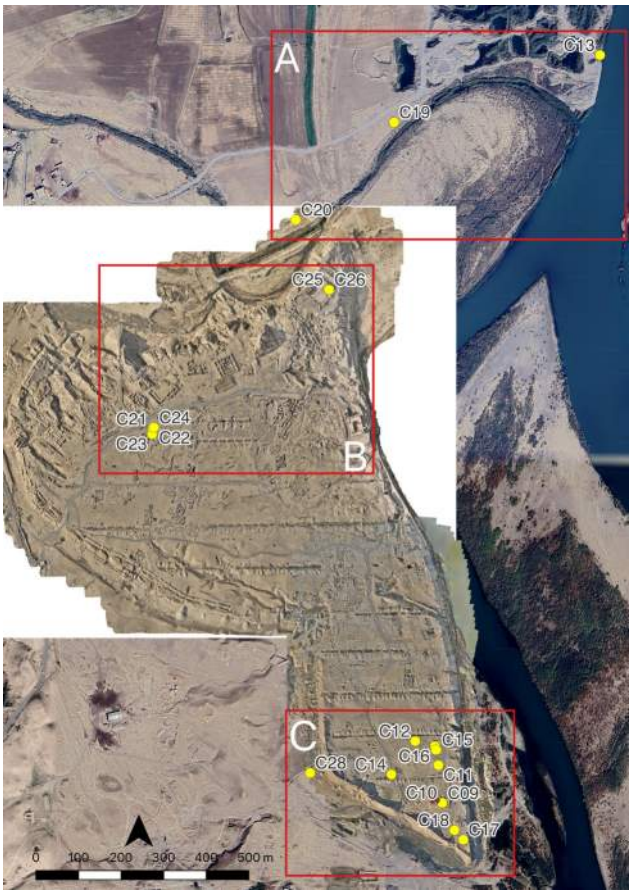

Fig. B2.1: Location of the 2024 cores: to the north of Assur (A), in the Inner City (B) and the New Town (C). Prepared by Andrea Squitieri.

Within the Inner City, the coring activity investigated the construction history of Assur's two major temples: the Ishtar temple and the Aššur temple (Ešarra). The origins of the Ishtar temple, initially documented by Andrae[11] and later revisited by Bär[12] and Schmitt,[13] remain only partially understood. Current evidence suggests that the earliest phase (Temple H) may date to the Early Dynastic period (c. 2500 BC) and was likely established on virgin soil. Statues discovered at the site have prompted scholarly debate, with some attributing Assur's cultural influences to Sumerian origins while others propose a uniquely local origin for the Ishtar cult at Assur.[14] Notably, the earliest occupational levels in Assur are accessible in the Ishtar temple area, where these layers remain close to the modern surface, allowing further exploration of the Ishtar temple's foundational phases.

The oldest layers of Assur are likely situated beneath the Aššur temple. However, extensive ancient and more recent construction, including the old Ottoman military barracks, complicates access to these strata. While Andrae's early excavations did not fully reach the city's earliest layers, evidence indicates that Assur's origins may lie in and around this northeastern section, dating back to the early third millennium BC.[15] Coring beneath the currently excavated temple levels could potentially reveal these foundational layers, offering insights into both the earliest phases of the temple complex and the initial settlement of Assur.

B2.2 The cores from the New Town and their descriptions

Cores C9-C12, C14-C18, and C27-C28 were taken from the New Town (**Fig. B2.2**). **Figs. B2.3—B2.4** present summaries in the form of sediment drawings for some of these cores, with a detailed description provided below. The absolute elevation (metres above sea level) of the highest point of the cores is indicated next to each core name.

Core C9 (top point: 160.41 m asl)
This core reached less than 1 m in depth due to hitting a rock or some other obstruction. It is located within a large,

9 Altaweel 2024.
10 Fassbinder *et al.* 2024a.
11 Andrae 1922; 1935.
12 Bär 2003a.
13 Schmidt 2012.
14 Bär 2003b.
15 Gries 2017; Miglus 1996; Haller/Andrae 1955.

Fig. B2.2: Location of the 2024 cores in the New Town. Prepared by Andrea Squitieri.

likely Neo-Assyrian building excavated by SBAH in 2002. The surface material, down to 43 cm, included silty-clay debris with small pebbles. Evidence of a wall or architecture collapse is found between 43-54 cm with larger gypsum stone pieces. This could also be evidence of a paved courtyard, but the stones were rough, suggesting wall material. Below, between 54-90 cm, was clean silty-clay sediment with little evidence of architectural debris. This could be the bottom level of the architectural layer. As mentioned, a large stone or some other obstruction was reached around 90 cm, preventing the corer from penetrating further.

Core 10 (top point: 160.40 m asl)
Given the obstruction in C9, it was decided to open a new core very near to C9. This proved more successful as the core reached 3 m. At 0-20 cm, fill debris, which was mixed silty-clay and stone content, was evident. At 25-55 cm, silty-clay sediment mixed with small calcium nodules and pottery was evident. Between 55-94 cm, an ashy layer was found with some pottery fragments, pebbles, and calcite nodules. No apparent architectural remains were visible. The pebbles increase in frequency between 94-97 cm, which could signify a floor or a debris layer. Observations at 97-104 cm indicated a clean silty-clay layer with calcium nodules and no ash. Ash was evident, and evidence of mudbrick remains was seen at 104-116 cm below the surface. Between 116-158 cm, pottery fragments, silty-clay remains, and calcite nodules were found. At 158-191 cm, reddish sediment, consisting of harder, more clayey mudbrick remains (likely mudbrick), was evident, along with some calcite nodules. The reddish remains became lighter around 191-200 cm with less evidence of ceramics or anthropogenic remains. At 200-230 cm, pottery again was evident with a bit of ash, calcite nodules, and small pebbles. At 230-300 cm, the sediment was light brown and became very clean, with no evidence of anthropogenic remains. This suggests building activity may not have reached below 230 cm in this area.

Core 11 (top point: 160.13 m asl)
This core was placed inside a large building identified during the 2023 magnetic survey and dubbed "Secondary Parthian Palace," about 75 m to the north of the NT1 trench.[16] The core reached 250 cm before stopping. The surface materials (0-37 cm) consisted of very loose sediment, light grey, that was likely windblown. At 37-95 cm, light brown sediment was more compact with silty-clay sediment mixed with ash, pottery, pebbles, and calcium nodules. More pottery was found at 95-145 cm, but sediment became loose, windblown and brown. Pebbles and calcium nodules were mixed in with some ash. Between 145-174 cm, harder sediment with mudbrick debris was mixed with ash, charcoal, and calcium modules. At 174-200 cm, a lot of ash was found with baked bricks, pottery, and silty-clay material. A possible floor was evident at 200-215 cm, where loose sediments were found, along with many pebbles and baked brick fragments lying flat. A very ashy layer was found below this at 215-220 cm. At 220-250 cm, more ash was found, but here mixed with pottery, mudbrick, and calcium nodules. Some pottery sherds appear burnt, and charcoal samples were taken at 235 cm, with sediments mostly silty-clayey.

Core 12 (top point: 162.27 m asl)
This core was drilled in a small building, also identified in the magnetic survey, about 60 m northwest of the "Secondary Parthian Palace." The depth of occupation appears to be deep here, reaching at least 3 m. The top level (0-60 cm) consisted of loose material, likely windblown, with grey sediment and some calcium nodules. From 60-100 cm, pottery and ash were encountered with a large pebble/rock at 65 cm. At 100-200 cm, the sediments were

16 Fassbinder *et al.* 2024a, 74.

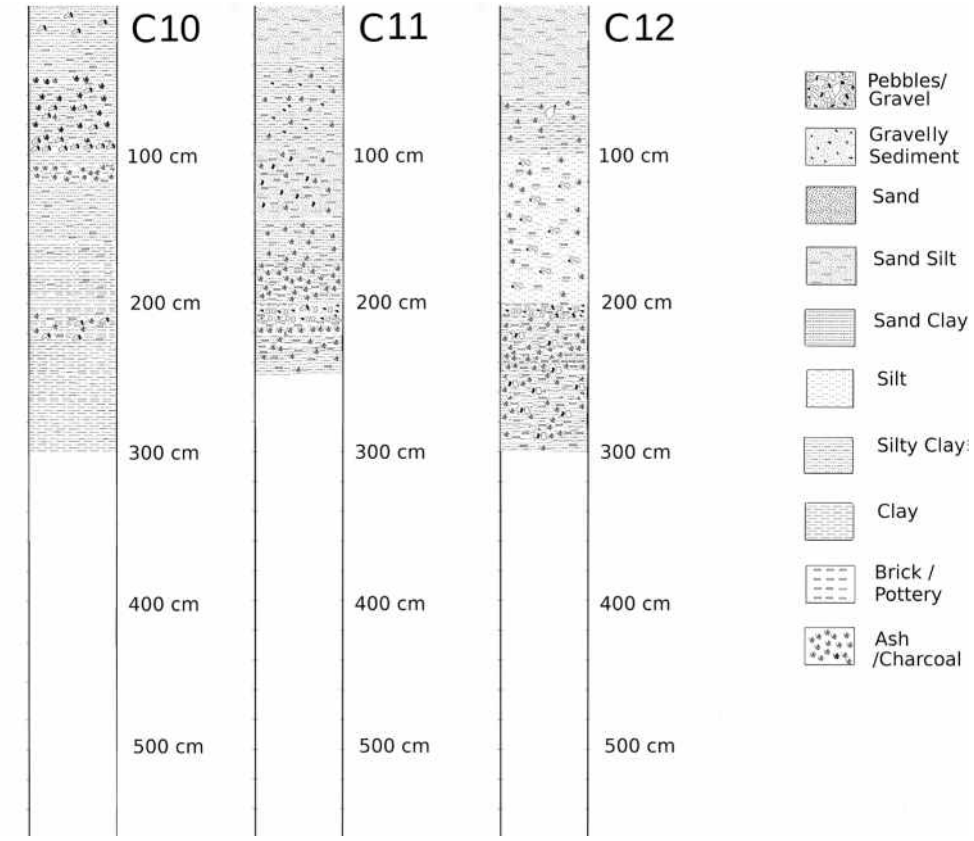

Fig. B2.3: The profiles of cores C10, C11 and C12 drilled in the New Town. Prepared by Mark Altaweel.

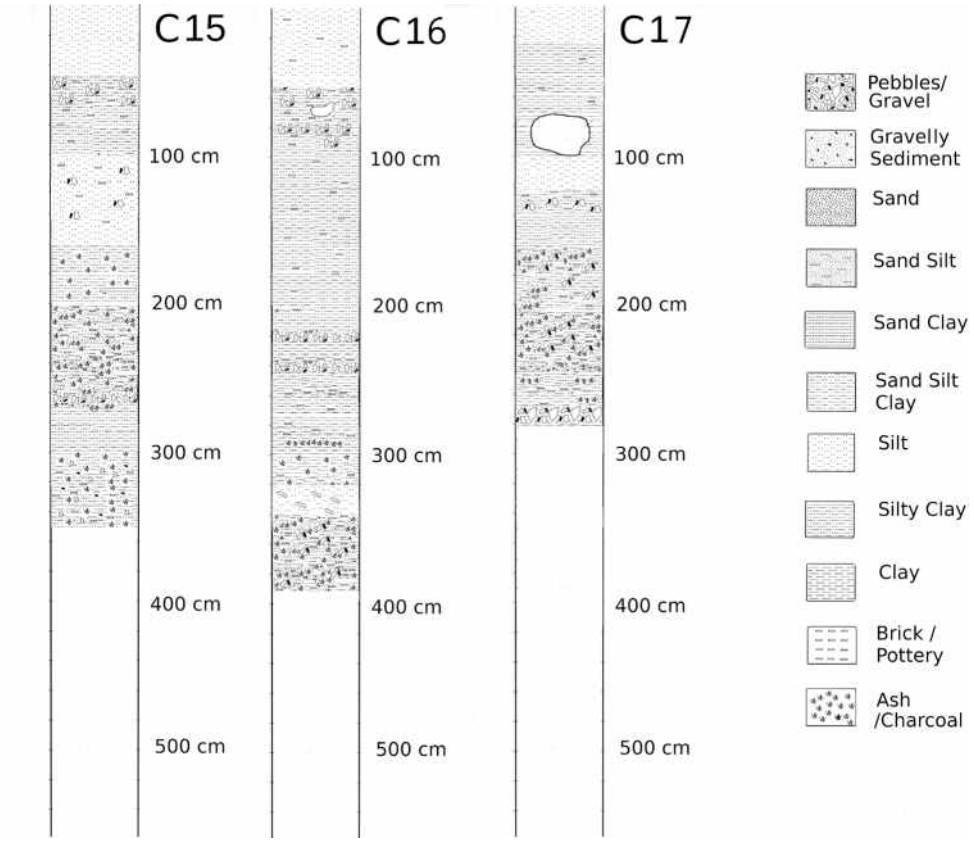

Fig. B2.4: The profiles of cores C15, C16 and C17 drilled in the New Town. Prepared by Mark Altaweel.

consistent, showing silty material, a lot of pottery, pebbles, and many small scattered charcoal pieces and ash. Calcium nodules were found scattered. At around 200 cm, baked bricks, pottery, and many pebbles were concentrated, suggesting a possible floor. The layer could be evidence of destruction to habitation at this level. Between 210-300 cm, the layer consisted of mudbrick fill, a lot of ash, pebbles, pottery, calcite nodules, and silty-clayey content throughout, but it was generally harder and contained more clay material than the above layers. The sediment colour was greyish to brown. Baked brick fragments were found to be around 240 cm, with ash concentrated around 240 cm and a darker grey colour. At around 270 cm, the layer was more brown but clayey. Pottery fragments were evident. The layer could be consistent with occupation debris with some evidence of burning or even a conflagration.

Core 14 (top point: 155.88 m asl)
This core was placed closer to the city wall, where the magnetic survey showed no clear architecture. The core reached about 2 m but we became stuck in gravel sediment when trying to go further, requiring the core to be abandoned at this level. Near the surface, at 0-40 cm, windblown loose sediment was light brown, and some pottery was found. At 40-100 cm, more compact sediment with some calcium nodules was found, particularly around 70 cm, with some pebbles but generally very clean and with no evidence of pottery. Some pebbles were evident at around 100 cm. At 100-135 cm, loose sediment was once again encountered that was relatively clean. At 135-137 cm, many pebbles were seen. Some bricks and ash also became evident just below this level, but it was difficult to tell the depth because the remains came out of the core sampler upon retrieval.

Core 15 (top point: 160.91 m asl)
This core was drilled in an area just north of the "Secondary Parthian Palace," where the magnetic survey showed no clear architecture. It reached 3.5 m below the surface. The top layers, 0-50 cm, were of very loose silty material, light brown, and relatively devoid of ceramic remains and other evidence of occupation. This could be windblown sediment embedded in the layer. At around 50-100 cm, evidence of pebbles (53 cm) was found, and more compact sedimen below this. Some pottery was present, but the sediment lacked other anthropogenic remains. At 100-160 cm, loose silty sediment with some pebbles, pottery, and calcium nodules were found. Like the previous layers, it was relatively clean of anthropogenic occupation remains, and no ash was evident. At 160-200 cm, the sediment became darker and contained ash. It was compact, with calcium nodules and some pottery fragments. A large piece of pottery was found at 190 cm, which could derive from a more complete vessel. At 200-250 cm, mudbrick material with baked brick remains were found. Pottery, calcium nodules, ash, compact silty-clay sediment, and dark, grey sediment were seen. An Iron Age/Neo-Assyrian diagnostic rim fragment was found at 230 cm, which provides a rough date for the layer. Charcoal samples were also taken at 230 cm. At 250-260 cm, the sediment became slightly looser, with many pebbles around 260-270 cm. Some charcoal pieces were evident around 273 cm. The 260-270 cm layer could be a floor. At 273-300 cm, light brown sediment with calcium nodules that was relatively clean and devoid of occupation material was seen. At 300-350 cm, pebbly and ashy sediment was encountered. This was mixed with silty-clay sediment, including mudbrick fragments, calcium nodules, pebbles, and ash. This suggests that occupation levels likely continued deeper, but the coring had to be stopped as we probably hit a large stone.

Core 16 (top point: 161.79 m asl)
This core, immediately northwest of C15, reached nearly 4 m in depth. At 0-56 cm, loose, silty, light brown material with some pottery was evident. The sediment became more compact at 56-100 cm, with pebbles, pottery, calcium nodules, and mudbrick mixed in the debris. A larger rock was seen at 65 cm. There was a pebble concentration at around 80 cm mixed with mudbrick. Between 100-200 cm, a light-coloured material was found, including calcium nodules, pottery, and compact silty-clay sediment. However, no ash or charcoal was evident. At 200-240 cm, silty-clay sediment with calcium nodules was seen. At 220 cm, a street level or floor may be apparent by a concentration of stones. Another possible floor was evident at 240 cm with a concentration of pottery and stone at this level. Below 240-257 cm, compact silty-clay and calcium nodules were found. Some pottery was seen at 257 cm. At 260-294 cm, mudbrick debris and very compact sediment were evident, with a large charcoal piece at 294 cm which was sampled. At 294-320 cm, compact sediment with ash, calcium nodules, and some pottery was evident. Starting at 320 cm, the sediment became very loose, with a few stones and mostly powdery silty material. Between 340-390 cm, mudbrick remains, baked bricks, stones, and burnt material were all mixed with ash and darker-coloured sediment.

Core 17 (top point: 160.31 m asl)
The core was placed inside the far southern tip of Assur, to determine if any building evidence was present in this area; the core reached 270 cm below the surface. At 0-23 cm, loose, windblown light brown sediment was found.

At 34-75 cm, sediment was more compact but relatively clean from building or occupation evidence. A gypsum rock between 75-100 cm was encountered, possibly wall debris. Between 100-120 cm, there was a space with no remains recovered. The debris may have fallen out of the core because it was loose. Generally, loose sediment was likely at this depth. This may also distort some of the remains below this gap in the core. Remains between 130-140 cm showed gypsum stones with some pottery above the stones (at around 120-130 cm). Mudbrick was also evident below 160 cm with pottery, some ash, and larger pieces of charcoal. Overall, the debris had some mudbrick mixed with stones and loose material. White stones, likely gypsum stones, were mixed in. Around 250 cm, a mix of ash, pottery, and stones suggested accumulated occupation material mixed with silty-clayey and compact remains. At 270 cm, there was stone material that the corer had hit, potentially wall debris from the city wall or a nearby building. Pottery was also evident and collected.

Fig. B2.5: The location of the cores C21, C22, C23 and C24 in the Ishtar temple. Left: orthophoto created by Jan Heiler (courtesy of Peter Miglus, Heidelberg University); right: plan after Andrae 1922, pl. 4 (the oldest temple levels are shown in red). Prepared by Andrea Squitieri.

Core 18 (top point: 159.03 m asl)
Given the resistance that the corer encountered in C17, a new core was drilled to its northeast. This, however, also came upon resistance in the form of what is likely to be wall debris, given its proximity to the city wall. The top 0-50 cm material was loose, composed of brown silty material that was relatively clean and had no evidence of pottery. Deposits were likely formed mainly through rain or wind action. Between 50-100 cm, some pottery, calcite nodules, ash, and mudbrick debris were encountered, but the quantities were small and scattered. Nevertheless, in the final 5 cm, there were some larger pebbles with ash and charcoal, suggesting some type of floor. Two charcoal samples were taken at 85 and 100 cm, with a diagnostic pottery sherd collected at 75 cm. At 100 cm, a large stone was likely encountered as the corer could not penetrate further. The coring was blocked here by what may be a large piece of wall debris.

Core 27 (top point: 160.92 m asl)
This was taken next to C15, using a clear tube. This tube was exported in May 2024 and is currently being analysed in lab conditions.

Core 28 (top point: 157.16 m asl)
This core was taken outside of the city wall of the New Town. Loose samples were collected at specific intervals, exported in May 2024 and will be analysed at a later stage (see also **§B1**).

B2.3 The cores from the Inner City and their descriptions

The Inner City coring consisted of four cores (C21-C24) from inside the Ishtar temple and two cores (C25-C26) in the Aššur temple (**Figs. B2.5-6**). Cores C21-C24 were extracted from the area where the oldest levels of the Ishtar temple once stood (Phases H and G). C25 and C26 were positioned close to the probable location of the main cella of the Aššur temple. **Figs. B2.7-8** provide the sediment drawings that detail some of the descriptions given below. The absolute elevation (in m asl) of the highest point of the cores is indicated next to each core name.

Core 21 (top point: 176.14 m asl)
The top 0-20 cm layer consisted of clay fill; small pieces of white calcite stones and ash were seen at around 15-20 cm. Between 20-30 cm, some small charcoal pieces were encountered, along with some pottery at around 40 cm, although these remains were limited. Sediments were clayey and relatively clean; around 60-70 cm, some

Fig. B2.6: The cores C25 and C26 in the Aššur temple. Left: orthophoto created by Jan Heiler (courtesy of Peter Miglus, Heidelberg University); right: plan after Andrae 1938. Prepared by Andrea Squitieri.

ash and charcoal became evident. Below 70 cm, however, clear sandy and yellowish remains were encountered, with no pottery or other contents seen. A charcoal sample was taken at 70 cm immediately above the sandy layer.[17] Between 100-190 cm, a sandy yellow layer was evident with limited small charcoal pieces. Around 190 cm, the sand layer stopped, and the sediment became clayey, with mixed calcite granules evident. No cultural material was seen. The clay layer continued to around 235 cm. Below this point, the remains consisted of rocks, potentially the natural bedrock, with the corer stopping around 250 cm as the layer became full of stone content. This could be evidence of the natural bedrock that Assur sits on.

Core 22 (top point: 176.40 m asl)
To confirm what was seen in C21, C22 was opened about 4 m away from the former. At 0-26 cm, the top material consisted of clayey sediment with some pottery, indicating mixed fill. Below 26 cm, the clay sediment became harder and clayey with some calcium flakes, pottery, and a mix of silts. At around 50 cm, calcium flakes and charcoal were encountered, but the layer was still mostly clay. At 73-80 cm, a gravel level mixed with big stones was evident, with some intermixed pottery. This could be a floor, perhaps the floor for Temple H. Below 80 cm, once again, there was a yellow silty layer mixed with some sand similar to the previous core. At 100-190 cm, this consisted of yellow sand material. Around 165 cm, some pebbles were mixed with sand and calcium nodules. No cultural material, however, was evident. At around 190-200 cm, rocks were once again encountered, potentially at the level of the natural bedrock.

Core 23 (top point: 176.62 m asl)
To further confirm cores C21 and C22, another core was placed in the Ishtar temple, about 15 m south of C22. Here, results showed 0-15 cm of topsoil fill consisting of clayey material, with some silt mixed in at 15 cm and pottery and pebbles mixed with loose sediment and larger stones, including possible mudbrick remains. This continued to about 50 cm. Below 50 cm, the sediment was more of a silty-clay compact material with a few ceramic sherds found, with some pebbles and likely some mudbrick material through much of the matrix. Neither ash nor charcoal were encountered. At around 95 cm, many pebbles were seen, forming a layer down to 100 cm. This could have been a floor. At 100-135 cm, silty-clay material with possible mudbrick debris was seen, but no pottery or pebbles were encountered. Ash and charcoal were mixed in the material at around 135-150 cm with pottery. This appears to have been a floor of compacted ash and charcoal material. Below 150 cm, the yellow sand layer was again seen, although it was mixed with some gypsum stones to about 180 cm. At around 180 cm, pebbly gypsum material was mixed with sand and no cultural material. Below this, stones and likely the bedrock were again encountered.

Core 24 (top point: 176.32 m asl)
Core C24 was a clear tube sample taken next to C22. The tube was exported in May 2024, and the sand and other sediment content are currently being analysed in lab conditions.

Core 25 (top point: 172.07 m asl)
This was the first of the Aššur temple's cores taken close to the likely location of the main temple cella. At 0-20 cm, topsoil material consisting of loose material with plant roots was encountered. Below 20 cm, compact clay-silt sediment with many pebbles was seen. Some calcium nodules, pottery, and possibly baked bricks were evident

17 This and the other charcoal samples from coring in the Ishtar temple were exported in May 2025.

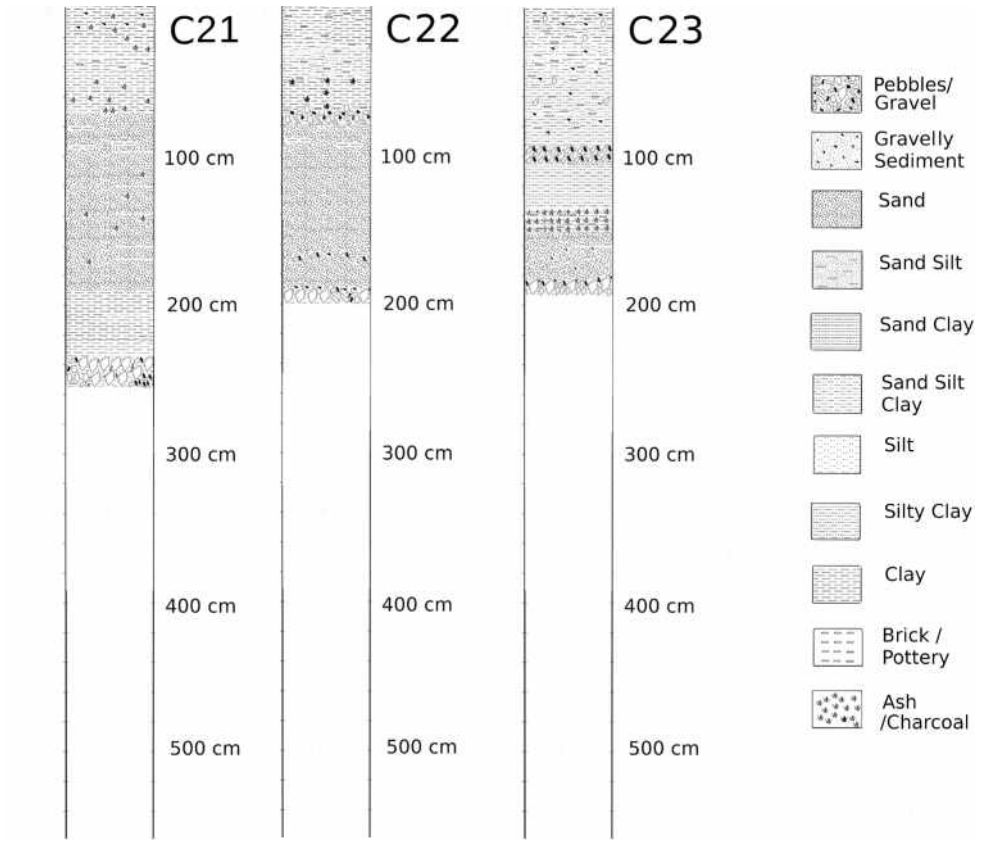

Fig. B2.7: The profiles of cores C21, C22, and C23, drilled in the Ishtar Temple. Prepared by Mark Altaweel.

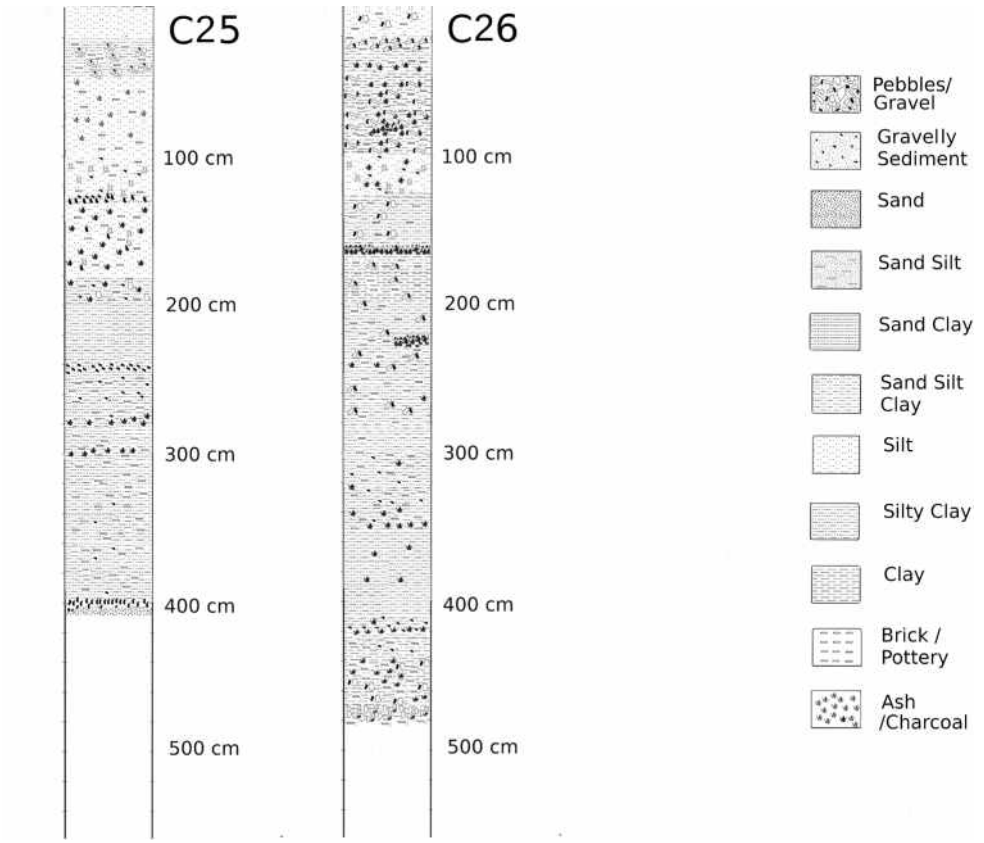

Fig. B2.8: The profiles of cores C25 and C26, drilled in the Aššur Temple. Prepared by Mark Altaweel.

to 50 cm. Below 50 cm, a fill with silty material was evident, which was mixed with pottery, some ash and charcoal, and possible mudbrick debris; this continued to 100 cm. At 100-130 cm, the sediments were again loose with fill mixed with pottery, calcium nodules, mostly silts, pebbles, and some stones. At 130 cm, a concentration of pebbles was found, but this was probably not a floor. Below 130 cm, the sediments were again composed of silty fill mixed with pottery and pebbles, with some ash. At around 180 cm, more compact material with some remains of mudbrick mixed with ash, pebbles, and some pottery was encountered, which continued to 200 cm. Silty-clay loose fill was evident at 240-245 cm, where a small pebble layer was encountered, although this was probably not a floor. Below this, again, a silty-clay fill with some pebbles, calcium nodules, baked bricks, mudbrick fragments, and pottery was found. Charcoal samples were taken at 280 cm. The silty-clay fill, mixed with brick, mudbrick material, and calcium nodules, continued to 400 cm. Some ash was seen around 300 cm with some loose silty-clay sediment. At about 400 cm, some pebbles may indicate a floor level. The corer had difficulties going through this level, only reaching 410 cm before stopping. However, some reddish sandy material was seen at this level, and samples were taken. Nevertheless, it seems that the depth of the temple debris in this area was likely deeper.

Core 26 (top point: 171.90 m asl)
An additional Aššur temple core was taken next to C25 to verify the remains from the latter. At 0-20 cm, the topsoil was mixed with rocks and bricks. Between 20-30 cm, a pebble layer mixed with pottery and clay was seen, charcoal at around 40 cm, and a rim sherd was also evident. This sherd may date to the Hellenistic or Parthian periods. Below 40 cm was a clayey layer that was mixed with gypsum. From 50 cm, there was a lot of charcoal mixed with baked bricks, stones, pebbles, and pottery, with this level continuing to 100 cm. A large piece of charcoal was seen at 80 cm.

From 100 cm, the material was more silty, crumbly, and loose, and it was mixed with small stones and some charcoal pieces to 125 cm. At 125-160 cm, sediments became more clayey, and some pebbles, gypsum flakes, and possible mudbrick fragments were seen. Below 160 cm, an ashy layer and mudbrick broken material were seen, and these remains lasted until 165 cm. Below 165 cm, mudbrick-clayey material mixed with pottery and stones continued until 200 cm. At approximately 200 cm, the fill became more of a silty-clay mixed with possible mudbrick debris, some pottery, and small pebbles. This continued to 300 cm, with some ash and charcoal at 230 cm. From 300 cm, sediments were crumbly and loose with small stones, charcoal, and baked brick debris, but no floor evidence. This continued to 400 cm, although some ash was below 350 cm. No pottery was seen below 350 cm, and the clay fill does not have much evidence of occupation content. However, at 420 cm, the material again became crumbly and loose and mixed with charcoal and calcite nodules. From 430 cm, the sediment was lighter in appearance and more clayey, with potential mudbrick debris evident. There was some pottery, calcite stone, other stones, and charcoal around 440-465 cm. More pebbles were encountered at the bottom of the core at around 470 cm, which could be a possible floor or collapse. More evidence of pottery and pebbles continued to 480 cm, suggesting that the debris or floor material continued even deeper.

B2.4 Discussion

The coring work from 2024 has helped to further elucidate the results of the 2023 geophysical prospection. Cores in the New Town revealed architectural debris in spaces that appeared empty in the geophysical results. This suggests that these spaces were courtyards, rooms, gardens, or empty areas just outside of prominent buildings that were now filled with collapse. Some cores did provide clear evidence of floors and/or architectural remains. Occupation is seen to be deep in places, particularly where cores C15 and C16 were taken. Other cores, including C11 and C12, also show evidence of relatively deep occupation (more than 3 m) and that building activity was likely to occur there. Some cores, including C10-12, C15-16 and C18, show potential floors of buildings, although it is also possible that these could be streets or courtyard floors. The debris and depth of human occupation potentially showed that in some places, occupation occurred in multiple periods and reached deep levels, even if the magnetic survey results did not show evident architecture near the surface (see also the ERT results in **§B3**).

In the Ishtar temple, not only was the foundation of the oldest temple (level H) found, but sand deposits underneath this earliest level were recovered. The sand was likely placed underneath the floor to purify the ground on which the temple was to be built, a tradition mainly known in southern Mesopotamia.[18] We intend to analyse the sand further to demonstrate the likely origin of this material. However, judging by its colour and grain aspect, the sand does not appear similar to the sand we observed around Assur.

18 Leacroft/Leacroft 1974.

The Aššur temple proved to be more challenging, as the two cores there did not reach deep enough to document the original temple construction level. The fact that the temple levels go very deeply down is clear, as it is doubtful that we could reach Early or Middle Bronze Age levels even after over 4 m of coring. However, the red sand encountered in our cores is an another interesting feature that we hope to verify in other cores.

B3. The 2024 Earth Resistivity Tomography (ERT) prospecting in the New Town of Assur

Jörg Fassbinder, Andrea Squitieri & Marco Wolf

Geophysical prospection in Assur during the campaigns in 1989, 2023, and 2024 focused on large-scale magnetometer surveys of the entire city area.[19] In 2024, we employed ERT measurements to ascertain the depth of archaeological layers, sediments, and building foundations in selected areas. We had conducted the first successful tests using the ERT method in the New Town of Assur during the 2023 campaign.[20] Unfortunately, due to transport issues from Germany and subsequent customs inspections, along with confusion and delays at border customs, some cables were damaged, and the devices were available in Assur for only two days of measurements. Thankfully, the device was repaired and could be fully utilised in the 2024 campaign.

The study of apparent resistance and earth resistance tomography (ERT) is among the oldest and most widely employed geophysical exploration methods for archaeological purposes.[21] For instance, the first resistance measurements for archaeology in Iraq were conducted as early as 1973 in Hatra and Seleucia on the Tigris by Ratti and Lanza,[22] albeit with limited success, attributed to the unfavourable soil conditions in late summer. Consequently, our measurements were scheduled for spring, when sufficient soil moisture was anticipated after the winter rains.

For soil resistance measurements, which are fundamentally based on Ohm's Law, a variety of electrode configurations can be employed to introduce electrical current into the soil.[23] The resolution and penetration depth of the resistance measurement, particularly when investigating archaeological features near the surface, depend on the distance between electrodes, the chosen electrode configurations, as well as the soil moisture and temperature.[24]

The most commonly used configurations for ERT profiles in archaeological sites are dipole-dipole, Schlumberger, and Wenner. The process involves injecting electrical current into the subsurface and utilising resistivity metres to detect anomalies with either high or low resistance compared to the background resistance of the ground. Anomalies primarily arise from local variations in soil water content. These anomalies may indicate the presence of stone structures and cavities or clay, sand, or organic material concentrations in trenches and pits. Significant improvements in instrumentation, computing, and data inversion technology over the last twenty years have made it possible to perform extensive 2D and 3D profiles and process and interpret the data in a reasonable time.[25]

B3.1 ERT data acquisition and processing

The ERT instrument employed for this project is a 4-point light 10 W model from Erich Lippmann (Lippmann Geophysical Messgeräte, Germany), featuring what is known as "active" electrodes, which allow for an electrode distance ranging from 25 cm to 5 m.[26] The two-dimensional (2D) switched array is often called "Electrical Resistivity Tomography" or ERT. This method facilitates simultaneous measurements of resistivity variations in both horizontal and vertical dimensions, resulting in what is known as a resistivity pseudo-section. Consequently, the instrument is adapted explicitly for archaeological prospecting; with an appropriate number of electrodes and displays, it can accurately record the deeper sediment layers in detail. The three electrode configurations utilised for our research are dipole-dipole, Schlumberger, and Wenner arrays. While the dipole-dipole array is sensitive to lateral variations, the Wenner and Schlumberger arrays are more responsive to vertical variations.[27] The main inversion method employed is the smoothness-constrained inversion method with a convergence limit of 5%, whilst the forward model calculations are based on the finite element method.[28]

We collected the ERT field data using GeoTest software and converted and exported it to the Res2Dinv data format. Here, we view, check, and eliminate erroneous data

19 Becker 1991; Fassbinder/Wolf 2024; Fassbinder *et al.* 2024b.
20 Fassbinder/Wolf 2024.
21 Schlumberger 1912; Atkinson 1946; Clark,1980; Kunetz 1966; Hulin *et al.* 2018.
22 Ratti 1971; Lanza/Mancini/Ratti 1972; Fassbinder *et al.* 2024b.
23 Everett 2013; Schmidt 2013.
24 Clark 1968; 1980; 1996; Herring/Pidlisecky/Cey 2021.
25 Loke/Acworth/Dahlin 2003.
26 Parsi 2022, Parsi *et al.* 2019; 2020; 2023.
27 Griffiths/Barker 1993.
28 Constable/Parker/Constable 1987; Loke *et al.* 2003.

Parameters	
Damping factors	1.500
Minimum Damping Factor	0.0200
Use a higher damping factor for the first layer	3
Vertical to Horizontal Flatness Filter Ratio (Weight)	1.00
Robust model Constrain cut off factor	0.05
Robust model Constrain cut off factor	0.005
Forward modelling method setting	Finite-element method
Use model refinement	Use model cells with widths of half the unit electrode spacing
Use incomplete Gauss-Newton	0.005
Number of Iterations	5
Contour Interval	Logarithmic Contour Interval

Table B3.1: Parameters used for 2D electrical resistivity inverse for the measured data. Prepared by Jörg Fassbinder.

points, sorting the measurements before performing the 2D inversion. Significantly, few data points were removed from specific profiles in our case study. We then executed the 2D model inversion using the RES2DINVx64 computer programme developed by Geotomosoft; it processes the resistivity data and calculates the inverse model of the field data, which we ultimately use for our archaeological interpretation.[29]

The processing parameters applied to the data are listed in **Table B3.1**. The same inversion parameters were applied to all data sets, allowing the software to generate three inverse resistivity depth images for each profile. The results are based on inverse resistivity model studies of dipole-dipole arrays spaced at 1.0 m.

The locations of the ERT profiles were chosen based on the 2023 magnetometer measurements[30] and the results obtained from coring (**§B2**). In total, we conducted 15 profile measurements, each 40 m long (**Fig. B3.1**). We selected a west-to-east orientation for all profiles and a south-to-north orientation for the perpendicular profiles. Additionally, we adopted a probe distance of 1 m for all our profiles, which allows us to discern sufficient details of buildings, such as individual walls, while utilising 40 electrodes and a profile length of 39 m, providing ample information from deeper archaeological sediments. This configuration enables us to gather data from up to 8 m penetration depths. Consequently, we can reach at least the undisturbed layers beneath the ancient city and differentiate between the various settlement layers. Below, we present the results of all 15 profiles, which reflect the subsurface conditions of the different areas within the New Town of Assur that we explored.

29 Loke 2012.

30 Fassbinder *et al.* 2024a.

B3.2 Results

To aid the interpretation of the ERT results, **Fig. B3.2** shows the location of the ERT profiles, the cores taken during the 2024 campaign (**§B2**), and the interpretation of the magnetogram produced after the 2023 magnetic prospection.[31] In the magnetogram, the built structures are indicated in yellow, and the green areas lack constructions (at least at the most superficial levels), while the pink bands indicate possible roads based on Andrae's insights.[32] The information from the magnetogram corresponds to all levels measured with the ERT method. However, since the latter can distinguish the depths, we can gain insights into the different levels, which cannot be achieved through magnetometer measurements.

Figs. B3.3 to B3.17 present the ERT measurements arranged by profile in the diploe-dipole, Schlumberger, and Wenner configurations. For each profile, we show the measured apparent and calculated inverse model without topographical correction, the inverse results, and the topographical details. The anomalies, which arise from varying resistance values in the subsurface, facilitate the identification of the remains of walls and rooms filled with rubble. The different sediment layers can be distinguished in deeper regions based on their varying electrical conductivities.

The profiles were measured from west to east and from south to north, meaning that in the west-east profiles, the left side corresponds to the west, while in the south-north profiles, the left side corresponds to the south (for the direction of the profiles, see **Fig. B3.2**).

31 Fassbinder *et al.* 2024a, figs. C2.6, C2.7, and C2.8.

32 Fassbinder *et al.* 2024a, figs. C2.6, C2.7, and C2.8; Andrae/Lenzen 1933, pl. 2.

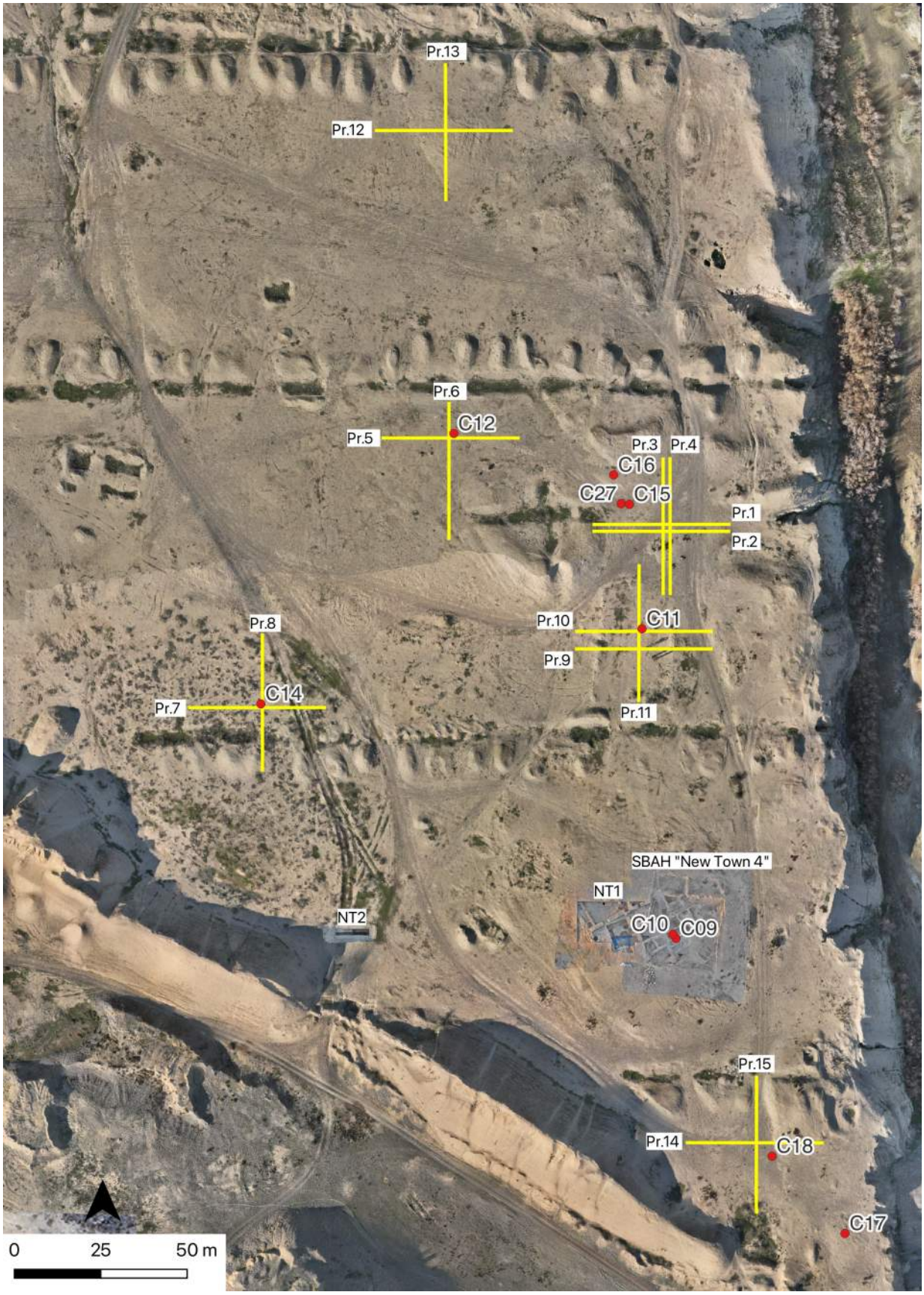

Fig. B3.1: Location of the ERT profiles (yellow lines) and sediment cores (red dots) taken in 2024 in the New Town of Assur. Prepared by Andrea Squitieri.

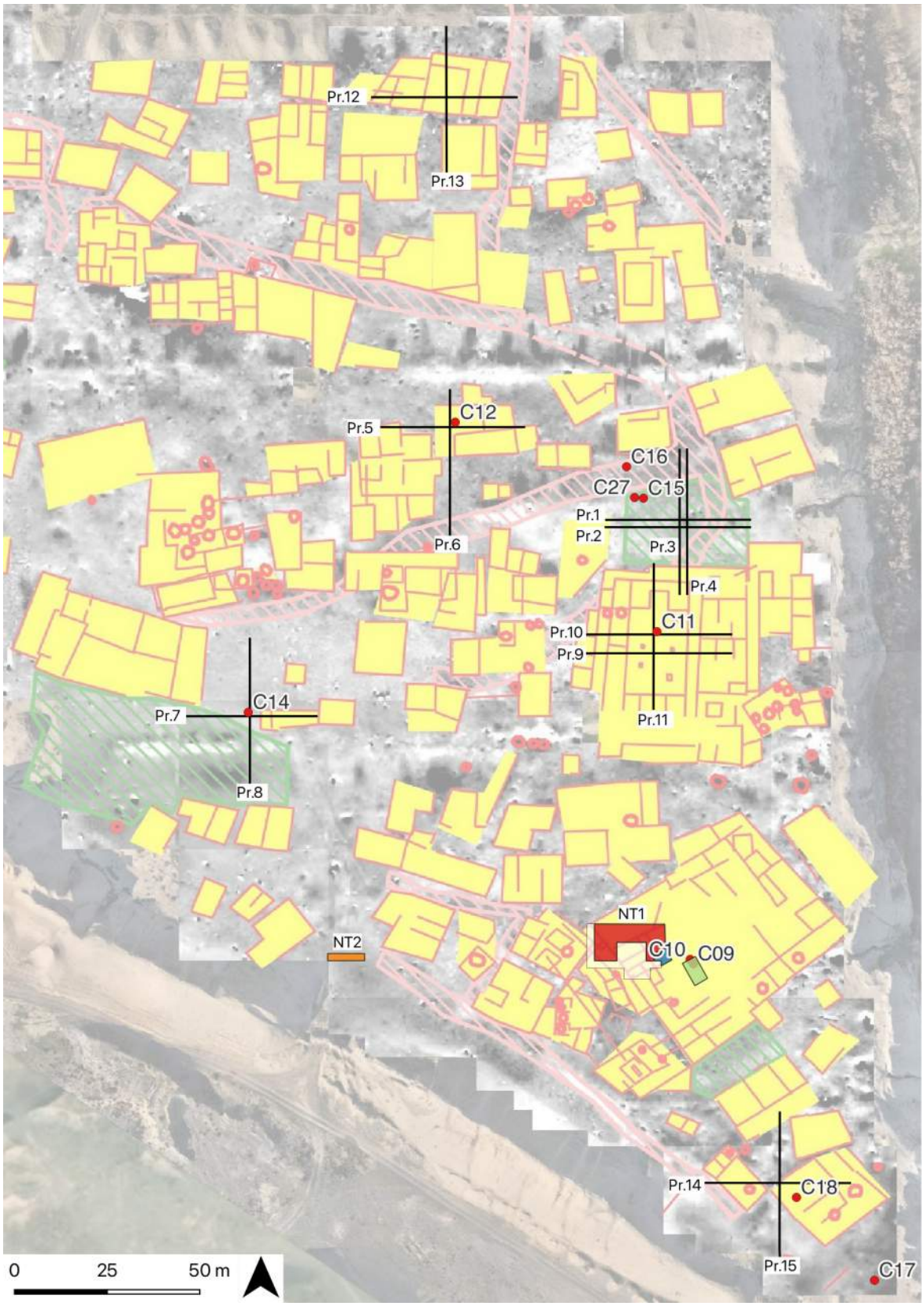

Fig. B3.2: The ERT profiles (black lines) and cores (red dots) taken in 2024 in the New Town of Assur as well as the excavation trenches NT1 and NT2 overlaid onto the 2023 magnetogram interpretation by Jean-Jacques Herr (published in Fassbinder *et al.* 2024a), with built structures indicated in yellow, open areas in green, and roads in pink. Prepared by Andrea Squitieri.

Overall, the resistivity zones shown in the ERT results can be interpreted as follows:

- Low-resistivity zones (blue/light blue colour):
  Low-resistivity zones often indicate materials with higher moisture content. They could represent shallow groundwater, a buried water channel, or a past excavation filled with wetter sediment. If located near known archaeological features, they might indicate a moat, trench, or ditch that retains moisture differently from the surrounding soil. Clay has a low resistivity due to its ability to retain water; hence, a regular-shaped light blue feature could suggest a filled-in pit, ancient construction material (such as mudbrick), or a natural clay lens. At an archaeological site, low-resistivity anomalies might correspond to buried clay/mudbrick structures, backfilled excavation pits, or decayed organic material (such as former wooden structures or graves).
- High-resistivity zones (red/purple colour):
  High resistivity is often linked to stone or compacted features, such as ancient walls, foundations, buried stone roads, rubble-filled structures or compacted soil layers. The red bands near the surface suggest shallow stone structures or ruins close to the surface. On the other hand, a wide red/yellow patch extending along the profile length towards the bottom is usually interpreted as the natural bedrock or gravel layer.
- Gradual resistivity zones (green/yellow colour):
  These moderate resistivity areas indicate typical compacted soils with moderate moisture content. They may indicate the background resistivity of the site's typical soil composition if they appear consistent and widespread. Meanwhile, if the green/yellow area is not uniform and has a trench-like shape, it could suggest artificial fills, ancient pathways, refilled ditches, or variably compacted layers from human activity.

B3.2.1 Profiles 1 to 4

Profiles 1, 2, 3, and 4 (**Figs. B3.3 to B3.6**) were measured near the locations of cores C15, C16, and C27 (**§B2**).

Profiles 1 and 2, running parallel from west to east, cross a seemingly open area in the magnetogram and reach a possible road towards the east. In the ERT measurements of these two profiles, we notice the following:

- A red/yellow patch is visible towards the east, close to the surface. This may indicate the ancient road, made of pebbles.
- Two light/dark blue wide and quite regular patches are located to the west and the east; the latter is below the red/yellow patch mentioned above. These two light/dark blue patches indicate clay-rich, water-saturated soil, which reaches a depth of about 4 m. Such an anomaly can be interpreted as collapsed mudbrick structures, which, because of their depth, may point to the existence of a deep archaeological layer. In this respect, it is worth noting that cores C15 and C16 encountered evidence of human occupation down to 3.5 m (**§B2**).

Profiles 3 and 4 run parallel to each other and perpendicular to the previous profiles, from south to north. In both, we notice the following:

- Two red/yellow patches are located to the south and the north of the profiles. In contrast, in the middle, these patches are not visible close to the surface. The red/yellow patches to the south may be related to the built structures visible in **Fig. B3.2**, while those to the north may indicate the road also visible in the same figure. The absence of red/yellow patches in the middle of the profiles (also close to the surface) may confirm that an open area is present in the area crossed by both profiles.
- Light/dark blue patches are visible to the south and to the north, below the red/yellow patches, and reach a depth of more than 4 m. As in Profiles 1 and 2, these patches may indicate the presence of deep archaeological features composed of clay-rich soil and mudbrick material.

B3.2.2 Profiles 5 and 6

Profiles 5 and 6 meet at 90 degrees, with the spot where core C12 (**§B2**) was taken at the intersection point between the two profiles. They cross an area where the magnetogram shows the presence of built structures. In Profile 5, we notice the following:

- Localised red/yellow patches are visible towards the west and near the surface. They may correspond to the wall foundations of the structures visible in the magnetogram or stone/pebble floors. On the westernmost side of the profile, these anomalies seem to reach a depth of more than 3 m. This depth is consistent with core C12, which has evidenced occupation material (including pebbles) down to about 3 m. Towards the middle and the eastern side of the profile, these red/yellow surface patches are lost; this indicates that the built structures visible in the magnetogram and crossed by this profile have shallower foundations or a different nature from those to the west.
- A broad and localised light blue anomaly is visible in the middle of the profile. This may indicate clay-rich soil from mudbrick debris, possibly belonging to a structure about 4 m below the surface. It may also be

an older archaeological phase than that visible in the magnetogram.

In Profile 6, we notice the following:

- Small red/yellow patches near the surface, located at regular distances from one another, may also indicate the wall foundations of the structures visible in the magnetogram. The superficial patches towards the south may correspond to a road, but this is unclear.
- Towards the middle of the profile, a regular and wide green patch at about 4 m depth may be connected to the light blue anomaly visible in Profile 5 and indicate deep archaeological features.

B3.2.3 Profiles 7 and 8

Profiles 7 and 8 meet at 90 degrees, with core C14 taken at the intersection point. They are located where the magnetic survey showed little evidence of built structures. Core C14 became stuck into the ground at about 2 m depth as it encountered a hard stone layer (**§B2**).

The ERT measurements from both profiles show the following:

- A broad red/purple anomaly begins at approximately 1.8 to 2 m depth. This anomaly may be interpreted as the natural gravel layer. Since this area of New Town is significantly lower than the western region, where the previous profiles were measured, the natural ground may be higher here than in the west. Furthermore, the inability to core deeper than 2 m is likely due to a high natural ground level (see core C14 in **§B2**). One can compare the large red/purple anomaly visible in Profiles 7 and 8 with the substantial gravel accumulation excavated in trench NT2, which reached a depth of about 6 m. Here, the 2023 ERT measurement revealed the same broad red/purple anomaly as in Profiles 7 and 8, visible on both sides of the shaft dug through the natural ground (see **Fig. C4.2**).
- A localised and seemingly regular green patch in Profile 7, towards the west, at about 4.8 m depth. Green and regular zones usually indicate a refilled ditch, construction pits, ancient roads or artificial fills. In our case, the area crossed by Profile 7 lacked more superficial structures in the magnetogram; however, an archaeological feature may be at a higher depth.
- Two significant dark blue anomalies in Profile 8, towards the south and quite close to the surface, may indicate water-saturated erosion channels filled with clay or sand rather than mudbrick structures, as the magnetogram did not indicate the presence of built structures.

B3.2.4 Profiles 9, 10, and 11

These profiles cross an area where the magnetogram showed the presence of a large building, dubbed the "Secondary Parthian Palace," characterised by a central court surrounded by rooms.[33] While Profiles 9 and 10 run parallel in the direction of west-east, Profile 11 runs south-north, meeting the previous profiles at 90 degrees. Core C11 was taken at the intersection point between Profiles 10 and 11.

In these profiles, we notice the following:

- Two localised red/yellow patches, close to the surface, are located respectively in the western and eastern portions of Profiles 9 and 10. These two patches are separated by an area characterised by a broad light blue patch. This pattern may be consistent with the "Secondary Parthian Palace" layout as interpreted after the magnetogram. The vast blue patch in the middle may correspond to the courtyard, while the two red/yellow patches should correspond to the wall foundations of the rooms at opposite sides of the courtyard itself. The two red/yellow patches are separated by a distance of about 15-20 m, roughly corresponding to the courtyard's width.
- Superficial and localised red/yellow patches in Profile 11 continue along the profile's length. They may indicate the presence of foundations or collapses of structures in the middle of the courtyard, which were not intercepted by Profile 10.
- Below the red/yellow patches mentioned above, light/dark blue localised and regular patches are visible in both profiles, reaching a depth of about 3.5 m. These patches may indicate the presence of mudbrick features belonging to an older occupation phase below the "Secondary Parthian Palace."

B3.2.5 Profiles 12 and 13

Profiles 12 and 13 cross an area where the magnetogram showed built structures. In both profiles, we notice the following:

- A series of localised red/yellow patches near the surface that recur along the profiles' length. These patches can be interpreted as the wall foundations of the structures identified in the magnetogram.
- Large, localised, and regular light/dark blue zones between 2 and 5 m depth below the red/yellow patches mentioned above. These zones may be interpreted as

33 Fassbinder *et al.* 2024a, 74.

mudbrick structures or other archaeological features retaining moisture (e.g., pits, burials, room fills) located below the structures visible in the magnetogram.

B3.2.6 Profiles 14 and 15

Profiles 14 and 15 were measured very close to the city wall in an area where the magnetogram indicated built structures. Core C18 was taken near the intersection point where the two profiles meet at a right angle. However, this core only reached a depth of 1 m due to encountered resistance (**§B2.2**).

In Profile 14, we observe the following:

- A series of red/yellow patches very close to the surface may indicate the wall foundations of the structures visible in the magnetogram.
- Light blue regular patches are below the previous red/yellow patches, reaching a depth of about 5 m. These patches may indicate archaeological features (mudbrick structures, burials, pits) located below the features visible in the magnetogram.

In Profile 15, we notice the following:

- Localised red/yellow patches close to the surface, located to the south, may correspond to structures not visible in the magnetogram.
- A wide, dark blue, irregular patch extending for most of the profile may indicate a water-saturated zone that may represent pits, voids or lower density features. Alternatively, this wide blue anomaly may be connected to the mudbrick collapse from the nearby city wall.

B3.3 Conclusions and future plans

The ERT profiles reveal key archaeological and geological features across the surveyed areas in the Assur New Town. Here is a summary of the findings:

- Profiles 1-4 indicate clay-rich soil linked to collapsed mudbrick structures and potential deep archaeological layers. Open areas and built structures are also identified.
- Profiles 5-6 show wall foundations of structures detected in the magnetogram, with deeper anomalies suggesting older archaeological phases.
- Profiles 7-8 reveal a high bedrock level at about 2 m depth at some locations, while potential deep-seated archaeological features, such as refilled ditches, channels, or construction pits, may be present in others.
- Profiles 9-11 cross the "Secondary Parthian Palace" and show resistivity patterns matching a courtyard and surrounding rooms. Deeper layers suggest earlier occupation phases.
- Profiles 12-13 confirm the wall foundations of structures seen in the magnetogram and deeper mudbrick features.
- Profiles 14-15, located near the city wall, identify surface structures and deep anomalies, suggesting prominent and collapsed built features or natural clay-rich accumulations.

Overall, the results highlight a complex stratigraphy with multiple occupation phases, buried structures, and areas of human activity, supporting and enhancing interpretations from the magnetic prospection and coring. For the 2025 field campaign, we plan to collect additional cores at targeted locations along the ERT profiles, ensuring we go deep enough to investigate the anomalies discussed in this chapter and confirm their nature.[34]

34 In the meantime, this coring work was undertaken by Eileen Eckmeier and Andrea Squitieri in March 2025.

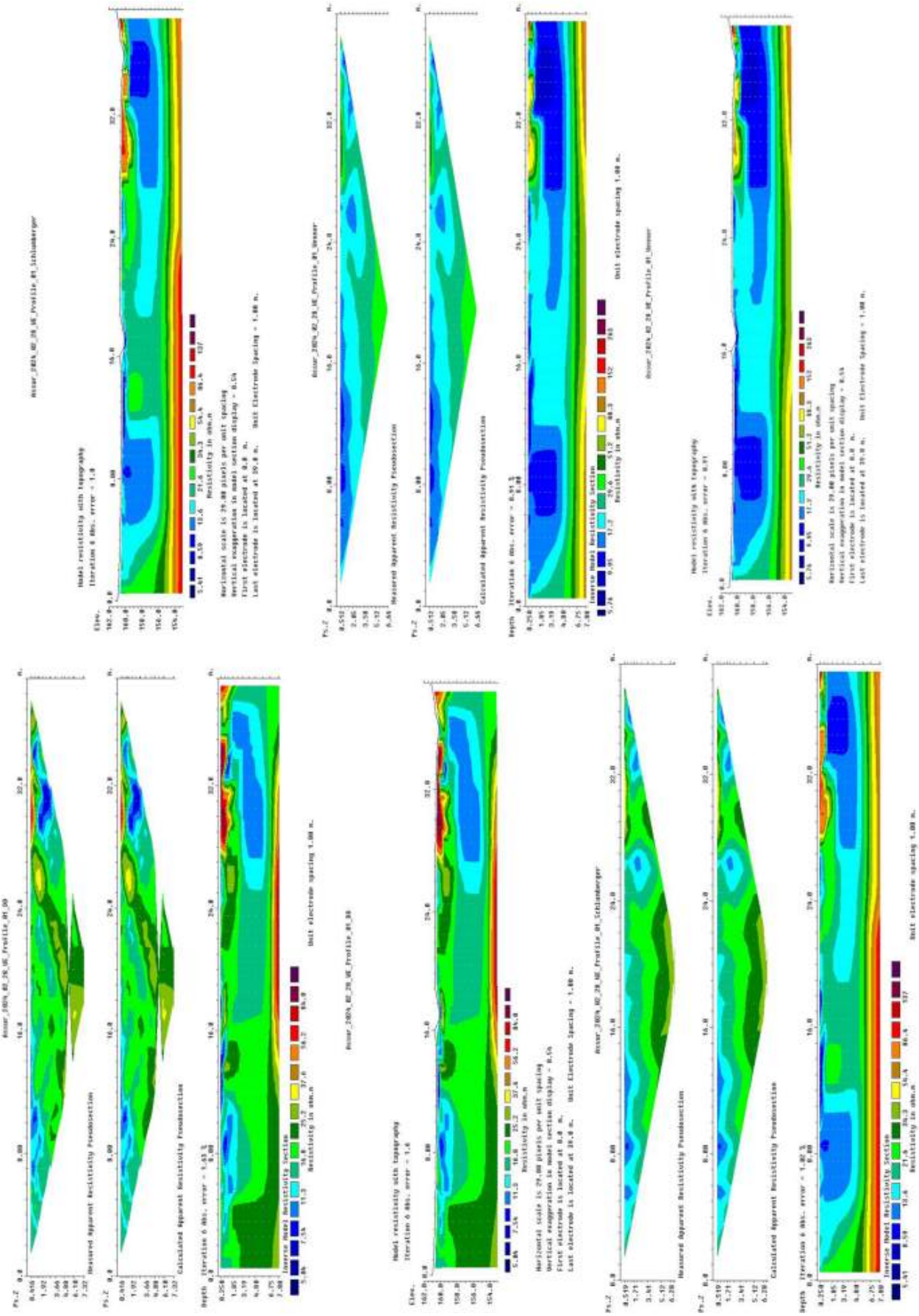

Fig. B3.3: ERT Profile 1. Measured and calculated apparent resistivity ERT profile in dipole-dipole, Schlumberger and Wenner configuration with the corresponding topographical correction. Probe separation 1 m. Profile length 0–39 m. West-to-east orientation.

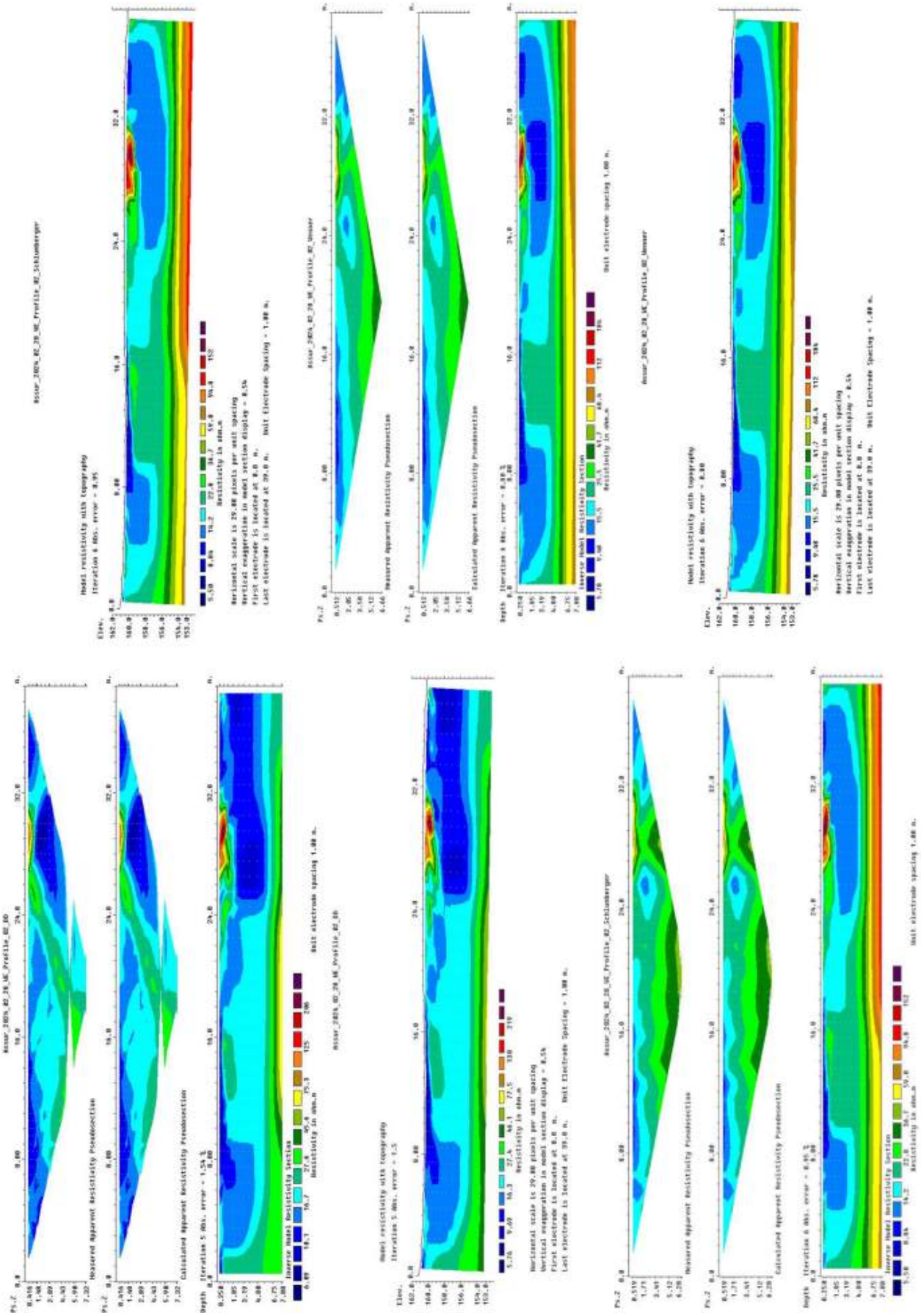

Fig. B3.4: ERT Profile 2. Measured and calculated apparent resistivity ERT profile in dipole-dipole, Schlumberger and Wenner configuration with the corresponding topographical correction. Probe separation 1 m. Profile length 0–39 m. West-to-east orientation.

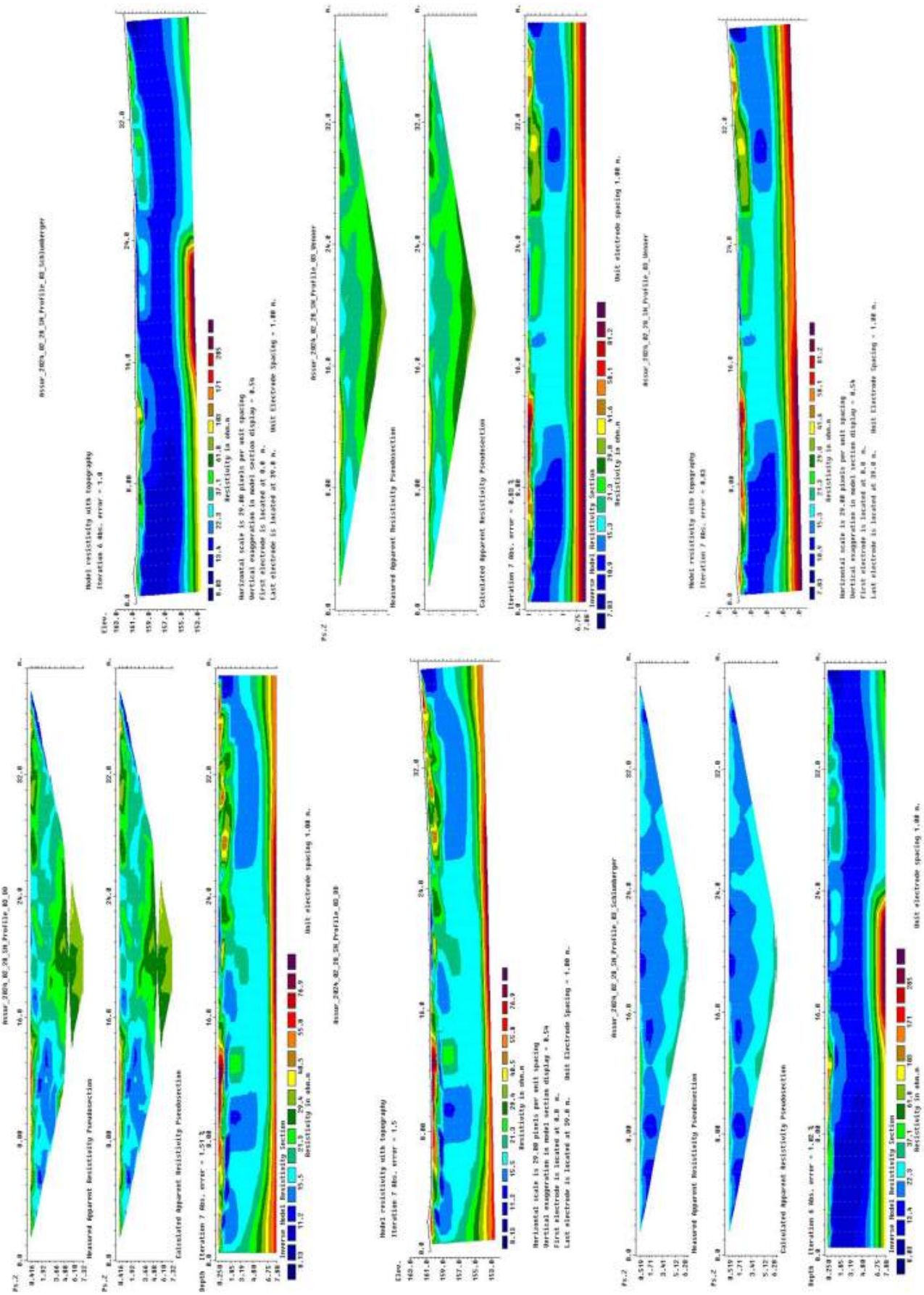

Fig. B3.5: ERT Profile 3. Measured and calculated apparent resistivity ERT profile in dipole-dipole, Schlumberger and Wenner configuration with the corresponding topographical correction. Probe separation 1 m. Profile length 0–39 m. North-to-south orientation.

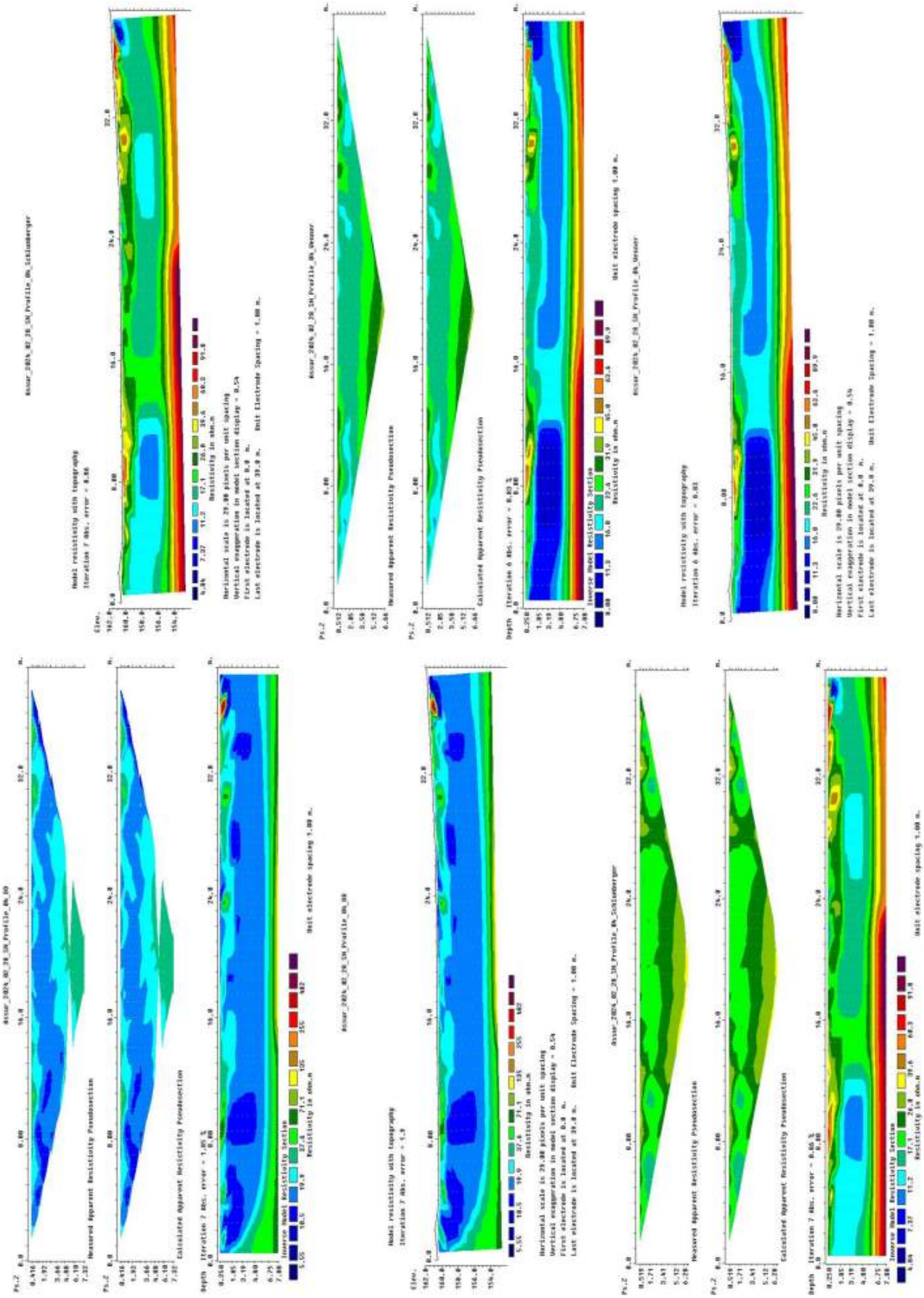

Fig. B3.6: ERT Profile 4. Measured and calculated apparent resistivity ERT profile in dipole-dipole, Schlumberger and Wenner configuration with the corresponding topographical correction. Probe separation 1 m. Profile length 0–39 m. North-to-south orientation.

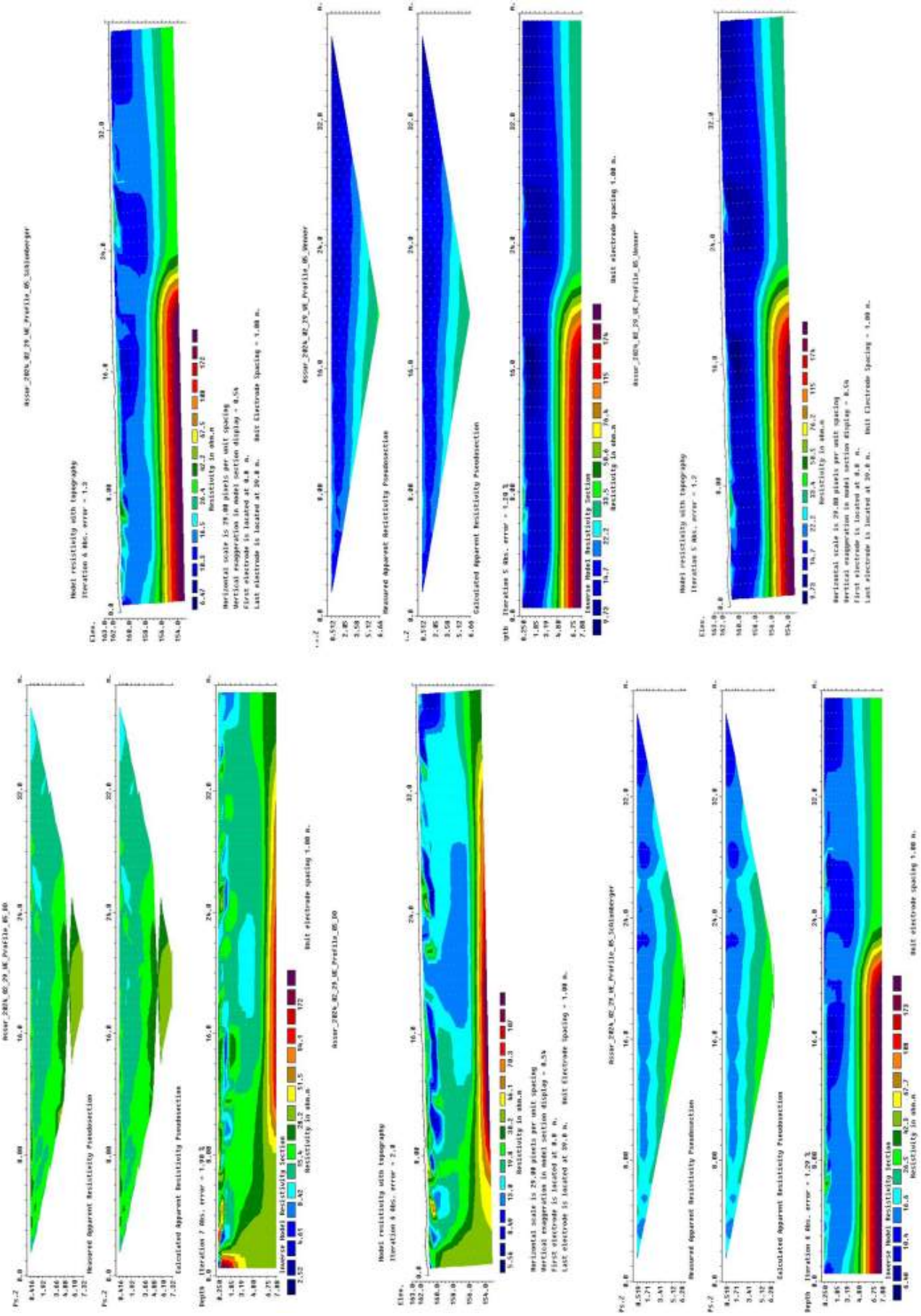

Fig. B3.7: ERT Profile 5. Measured and calculated apparent resistivity ERT profile in dipole-dipole, Schlumberger and Wenner configuration with the corresponding topographical correction. Probe separation 1 m. Profile length 0–39 m. West-to-east orientation.

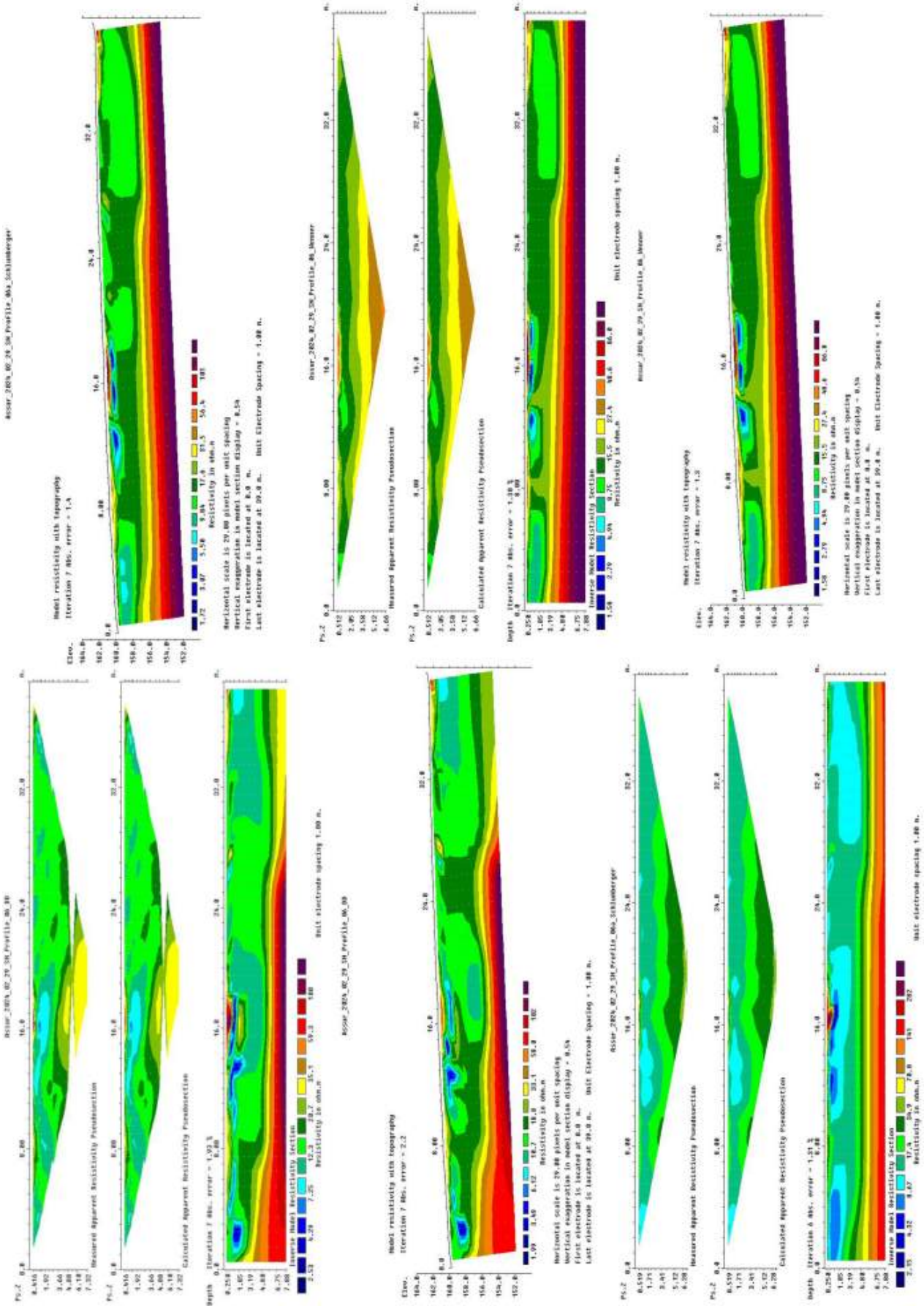

Fig. B3.8: ERT Profile 6. Measured and calculated apparent resistivity ERT profile in dipole-dipole, Schlumberger and Wenner configuration with the corresponding topographical correction. Probe separation 1 m. Profile length 0–39 m. North-to-south orientation.

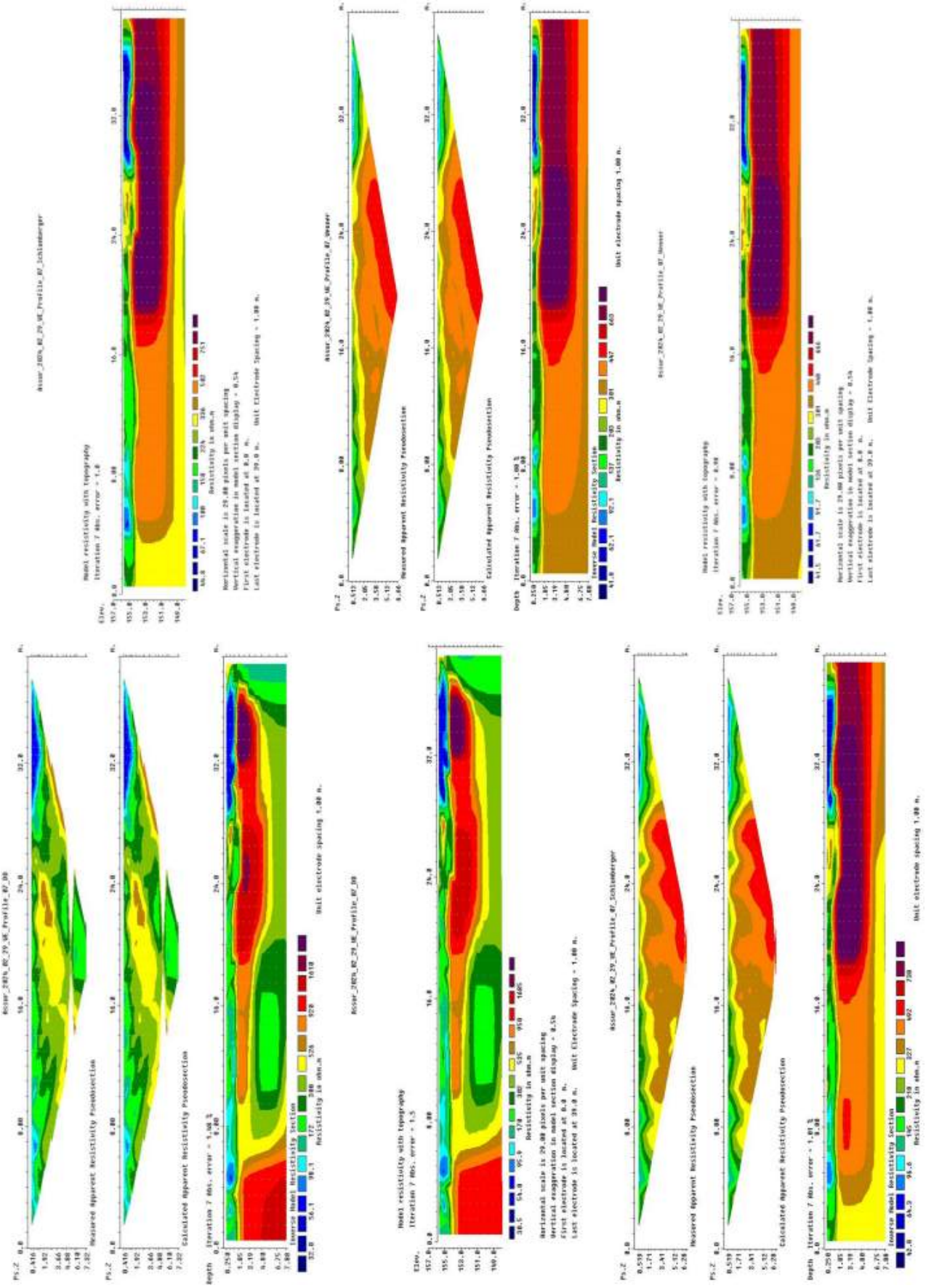

Fig. B3.9: ERT Profile 7. Measured and calculated apparent resistivity ERT profile in dipole-dipole, Schlumberger and Wenner configuration with the corresponding topographical correction. Probe separation 1 m. Profile length 0–39 m. West-to-east orientation.

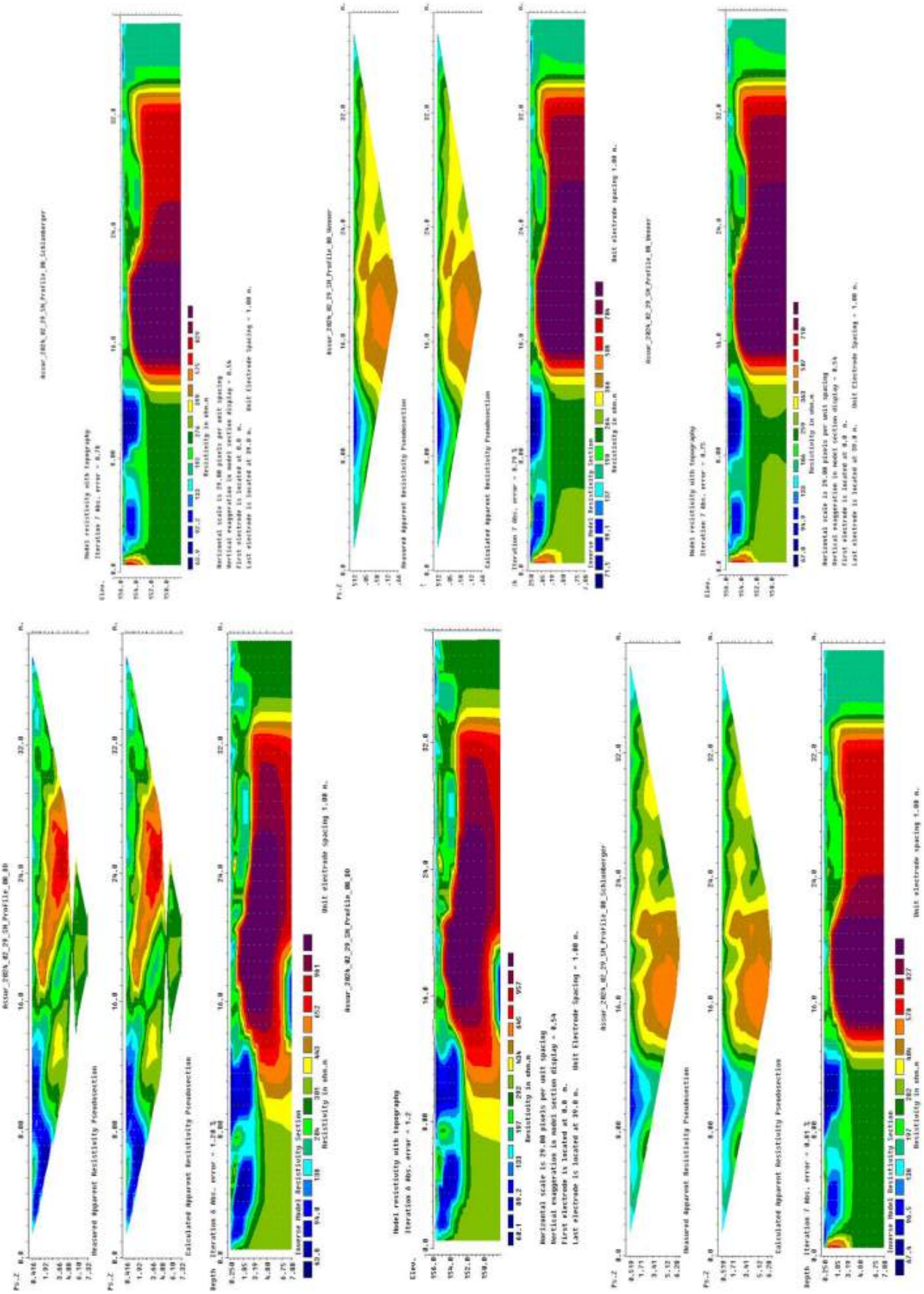

Fig. B3.10: ERT Profile 8. Measured and calculated apparent resistivity ERT profile in dipole-dipole, Schlumberger and Wenner configuration with the corresponding topographical correction. Probe separation 1 m. Profile length 0–39 m. North-to-south orientation.

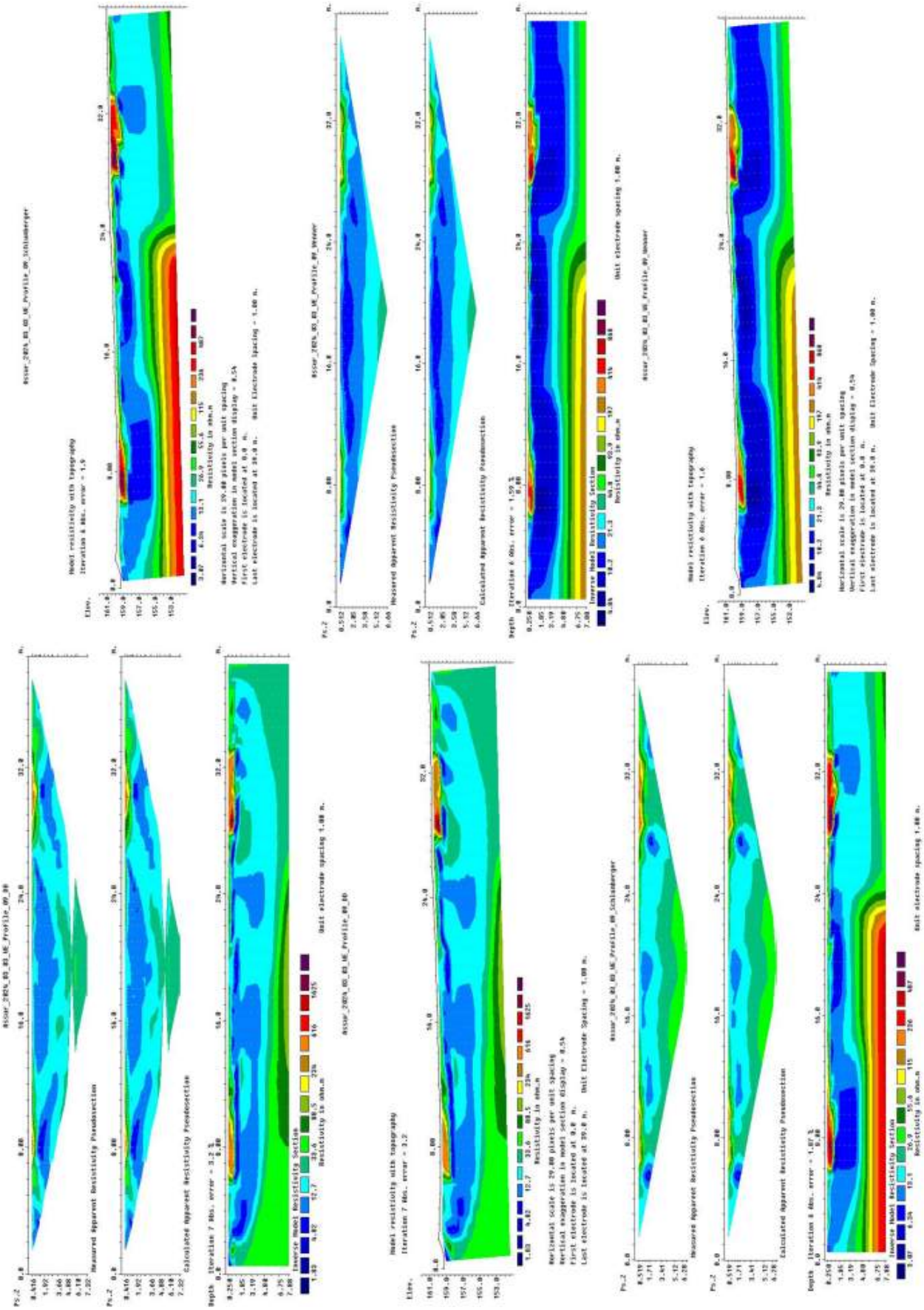

Fig. B3.11: ERT Profile 9. Measured and calculated apparent resistivity ERT profile in dipole-dipole, Schlumberger and Wenner configuration with the corresponding topographical correction. Probe separation 1 m. Profile length 0–39 m. West-to-east orientation.

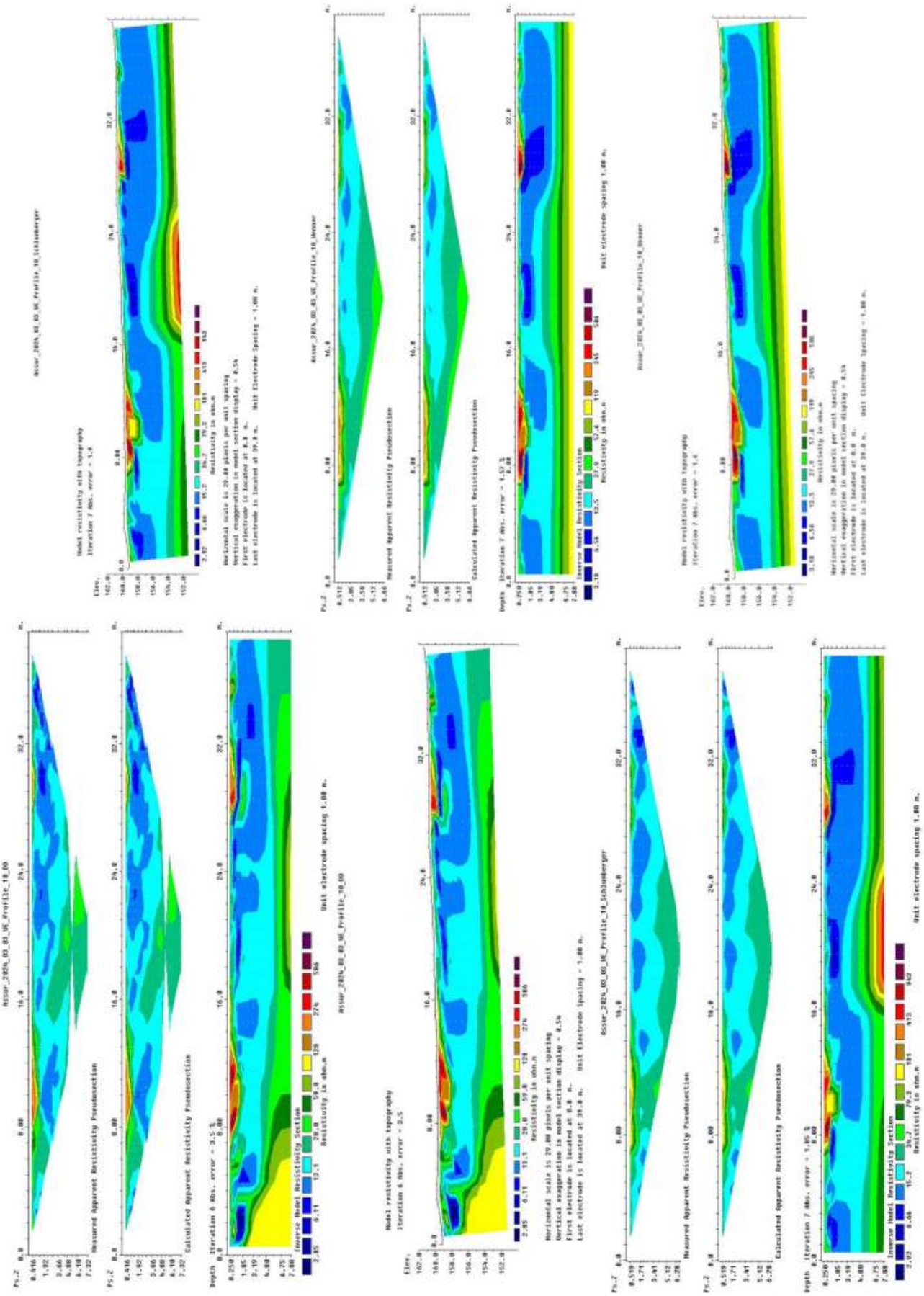

Fig. B3.12: ERT Profile 10. Measured and calculated apparent resistivity ERT profile in dipole-dipole, Schlumberger and Wenner configuration with the corresponding topographical correction. Probe separation 1 m. Profile length 0–39 m. West-to-east orientation.

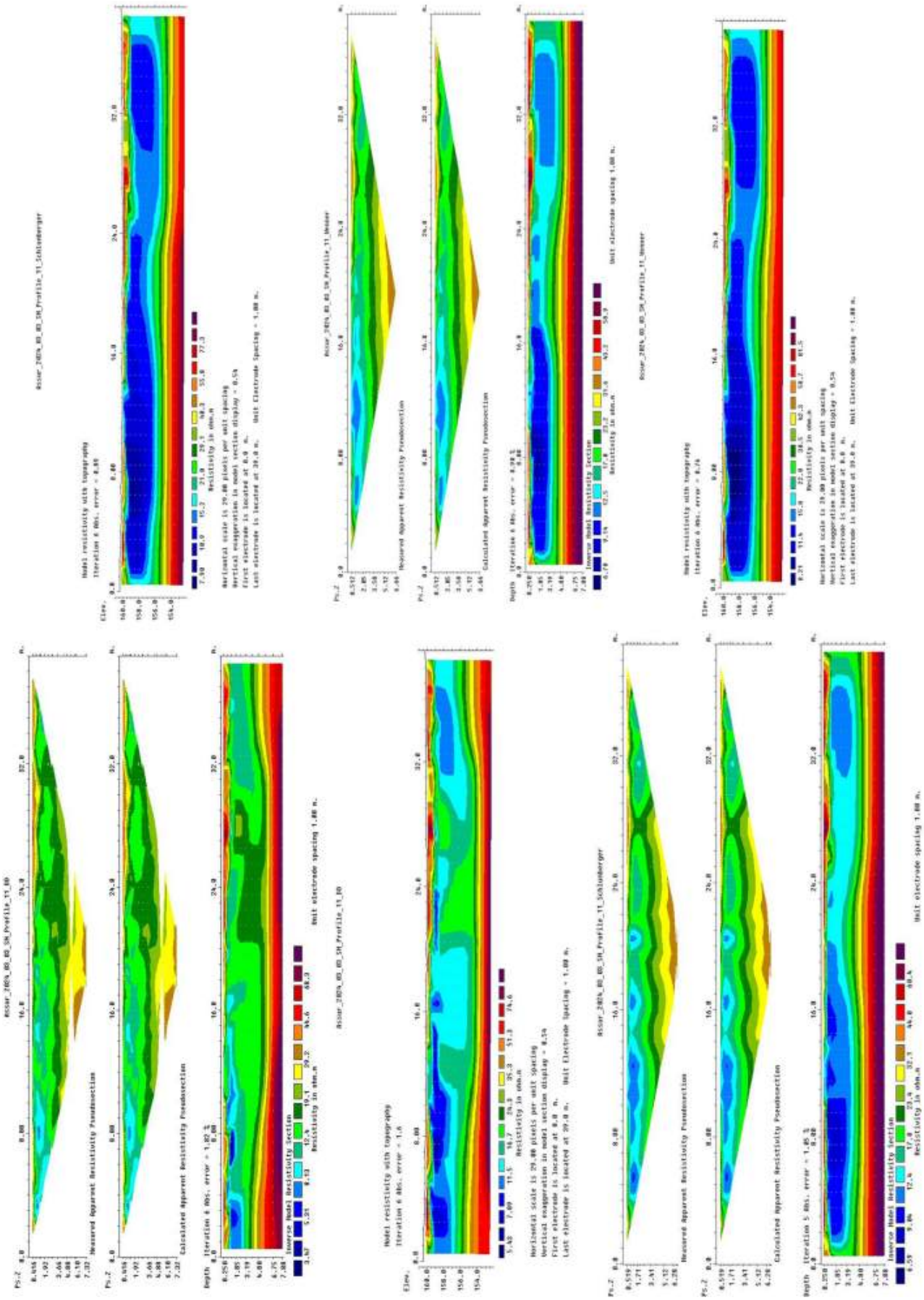

Fig. B3.13: ERT Profile 11. Measured and calculated apparent resistivity ERT profile in dipole-dipole, Schlumberger and Wenner configuration with the corresponding topographical correction. Probe separation 1 m. Profile length 0–39 m. North-to-south orientation.

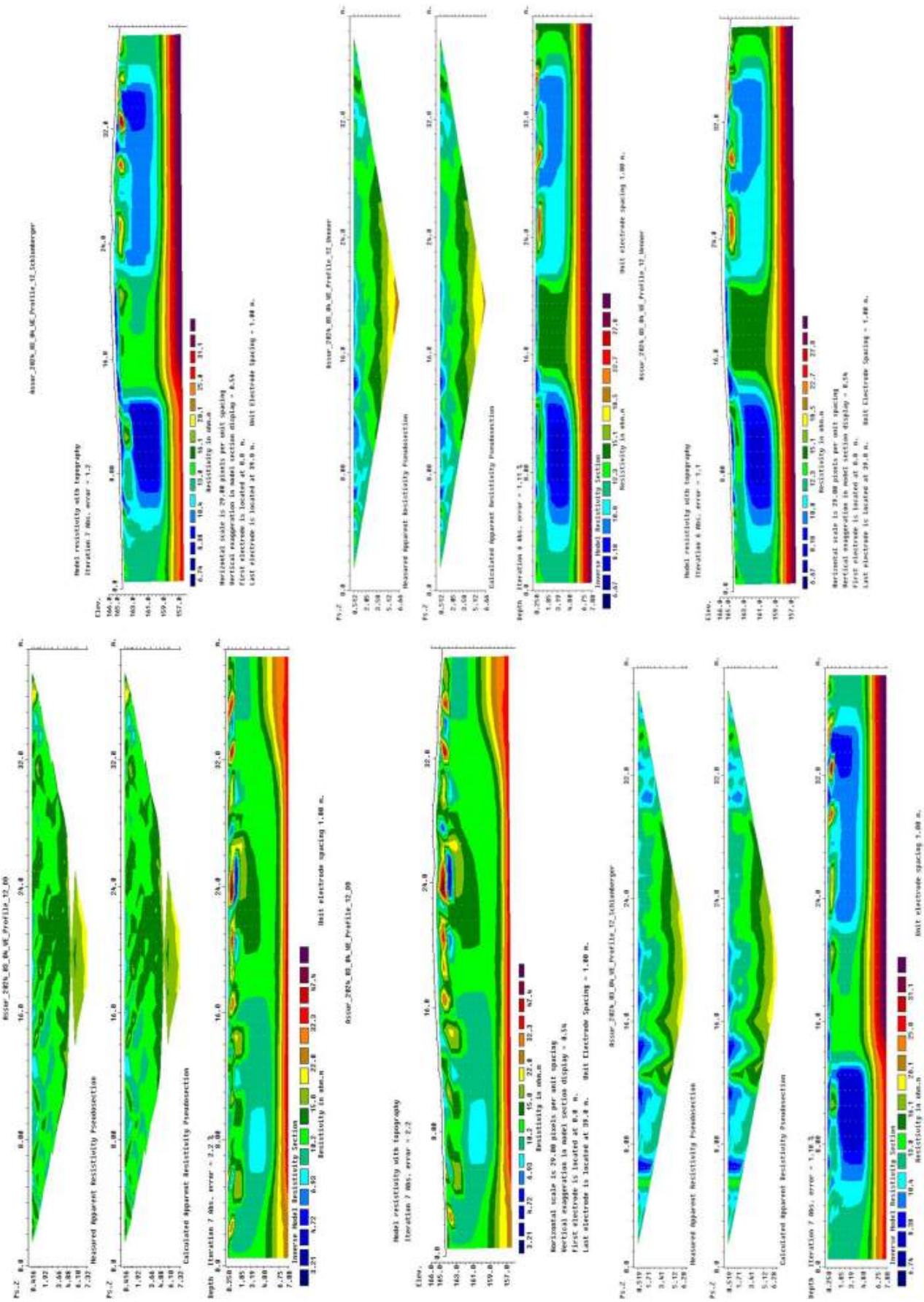

Fig. B3.14: ERT Profile 12. Measured and calculated apparent resistivity ERT profile in dipole-dipole, Schlumberger and Wenner configuration with the corresponding topographical correction. Probe separation 1 m. Profile length 0–39 m. West-to-east orientation.

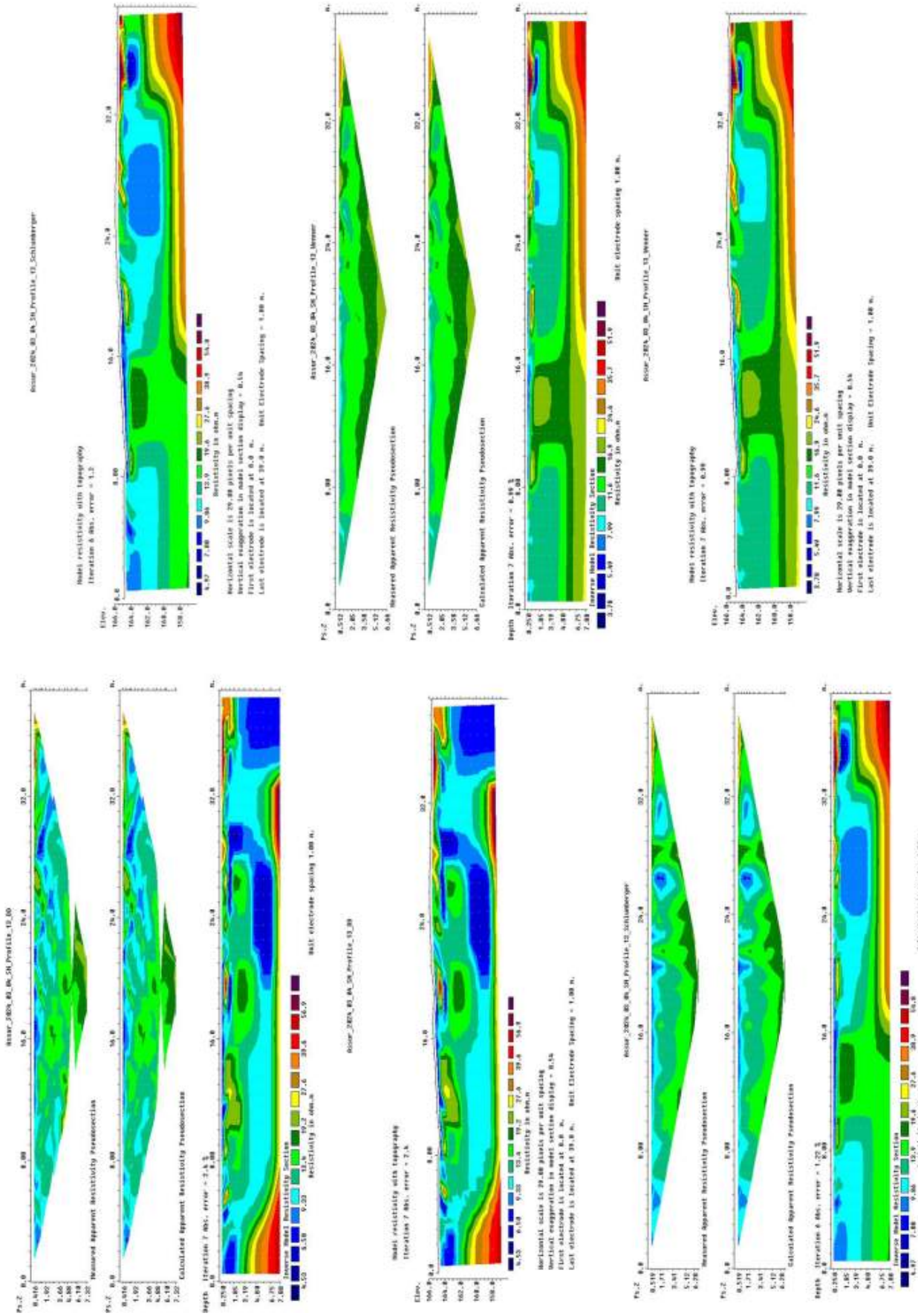

Fig. B3.15: ERT Profile 13. Measured and calculated apparent resistivity ERT profile in dipole-dipole, Schlumberger and Wenner configuration with the corresponding topographical correction. Probe separation 1 m. Profile length 0–39 m. North-to-south orientation.

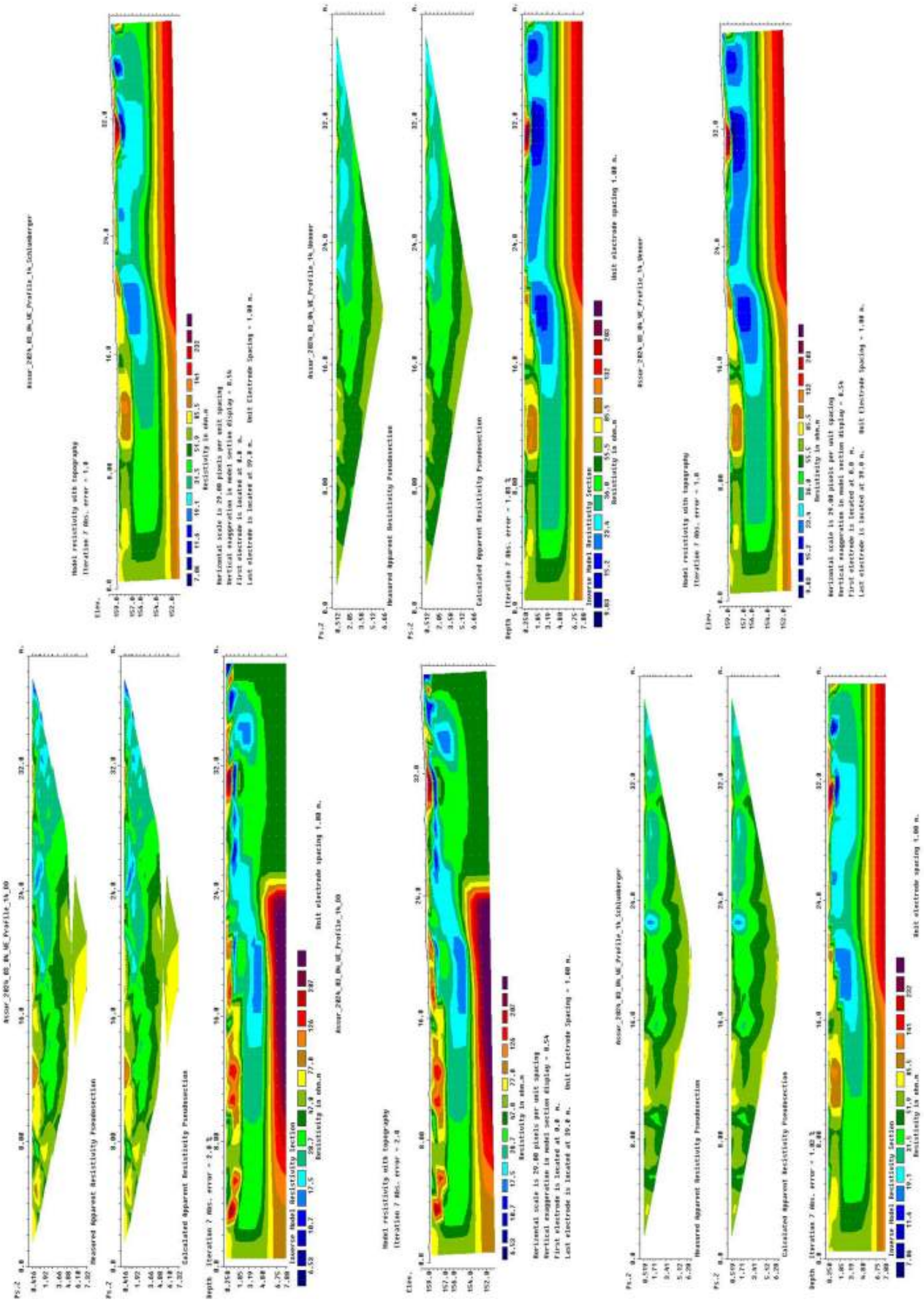

Fig. B3.16: ERT Profile 14. Measured and calculated apparent resistivity ERT profile in dipole-dipole, Schlumberger and Wenner configuration with the corresponding topographical correction. Probe separation 1 m. Profile length 0–39 m. West-to-east orientation.

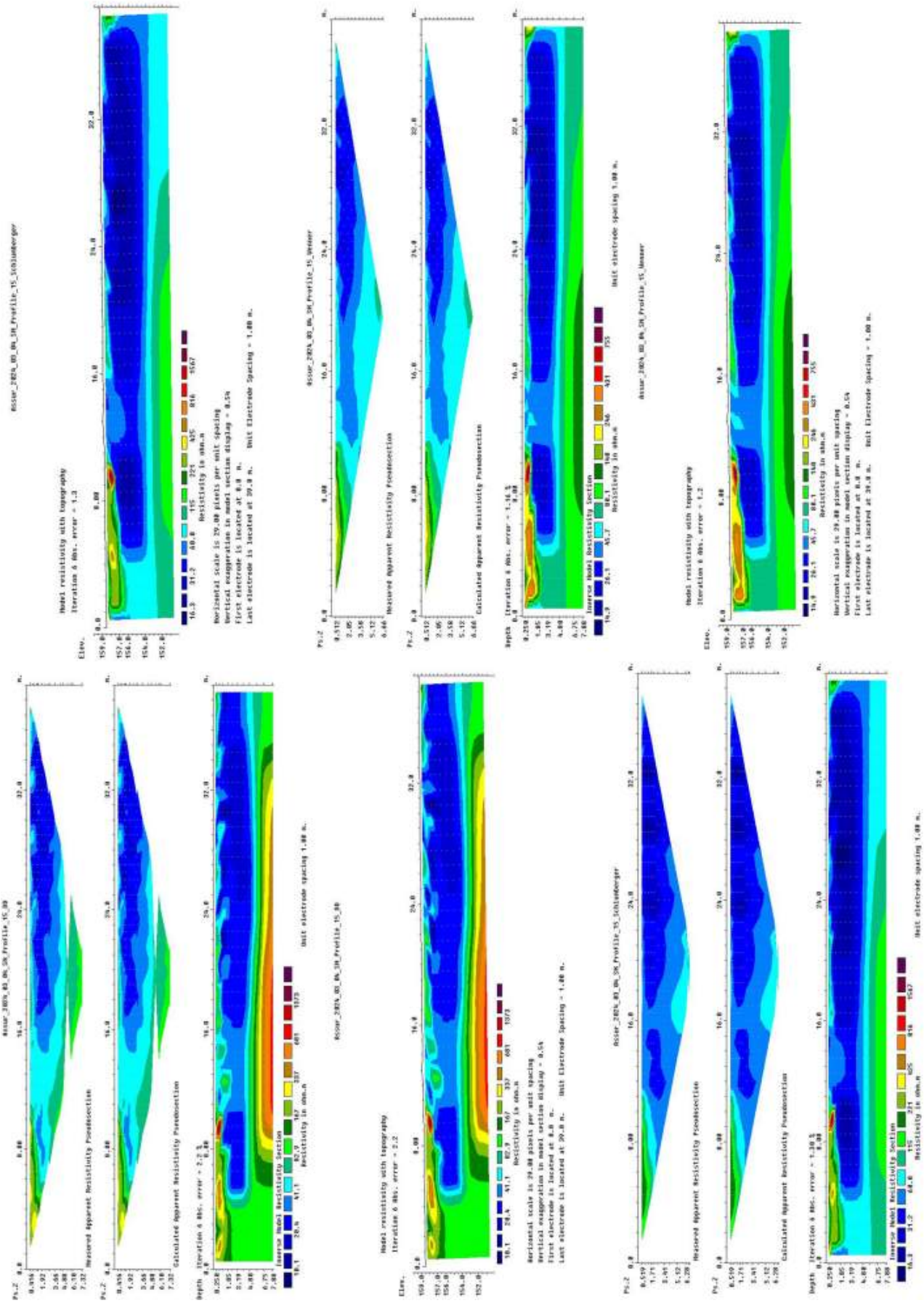

Fig. B3.17: ERT Profile 15. Measured and calculated apparent resistivity ERT profile in dipole-dipole, Schlumberger and Wenner configuration with the corresponding topographical correction. Probe separation 1 m. Profile length 0–39 m. North-to-south orientation.

C. Excavating in the New Town of Assur in 2024

C1. The 2024 work plan and its implementation

Karen Radner & Andrea Squitieri

The 2024 work plan was designed to address questions and test hypotheses that arose from the results of the 2023 campaign. At the end of the 2023 campaign, three main goals were achieved:

- The excavation of a 120 m² trench, named NT1 (white colour in **Fig. C1.1**), located to the west of the trench excavated by SBAH in 2002, called at the time "New Town 4." NT1 revealed a stratigraphic sequence and architectural features ranging from the Late Bronze Age/Middle Assyrian period to the Parthian period. In particular, the excavations uncovered the remains of a Parthian chamber tomb (Grave 1), which had damaged a building named Building A, dated to the Hellenistic period.[35] Below Building A, an older building called Building B, dated to the Iron Age,[36] was also explored. In 2024, we continued the excavation of both Building A and Building B.

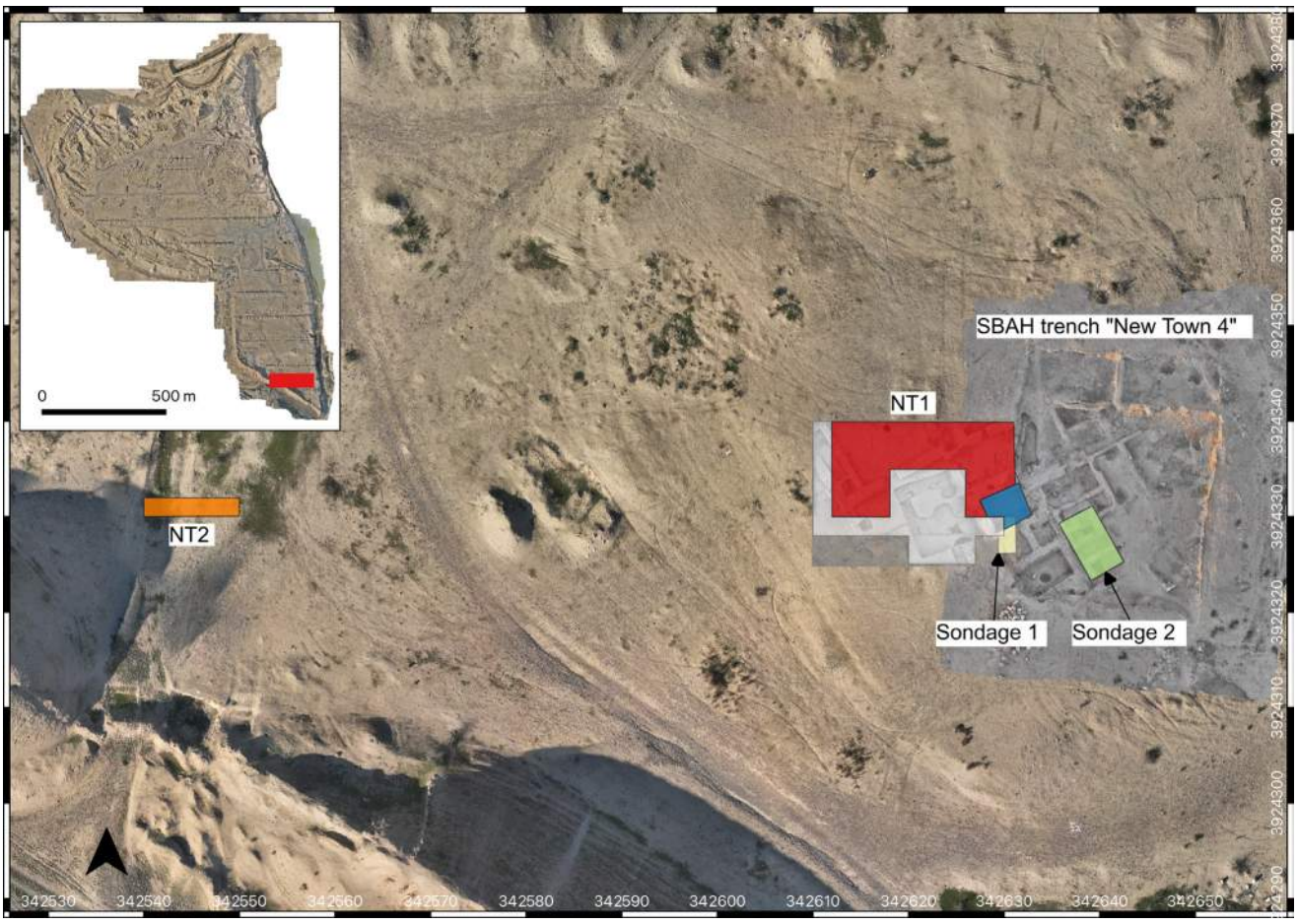

Fig. C1.1: The 2023 and 2024 excavation trenches next to the "New Town 4" trench of the 2002 SBAH excavations. Orange: trench NT2, white: trench NT1 in 2023, red: trench NT1 in 2024, yellow: Sondage 1 in 2023, blue: Sondage 1 in 2024 (= "Room 5"), green: Sondage 2. Created by Jens Rohde, annotated by Andrea Squitieri.

35 Based on the radiocarbon dates: 341-57 BC (95.4% probability), 176-52 BC (95.4% probability), 173-53 BC (95.4% probability), see Radner/Squitieri 2024b, Table D1.1.

36 Radner/Squitieri 2024b, 128.

- The excavation of a sondage, referred to as Sondage 1, within the baulk separating NT1 and the SBAH trench (yellow colour in **Fig. C1.1**).[37] Sondage 1 revealed two partial units, named "Room 5" and "Room 6". The radiocarbon dates from the floor deposit of "Room 6" established its Iron Age horizon.[38] Meanwhile, the radiocarbon dating from the floor deposit of "Room 5" yielded a mix of Late Bronze Age and Iron Age dates,[39] in addition to Hellenistic/Parthian pottery collected from the room's fills. This dating discrepancy necessitated additional investigation into "Room 5" in the 2024 campaign.
- A comprehensive geophysical survey across the entire New Town using magnetic prospection and Electrical Resistivity Tomography (ERT).[40] This survey was supplemented by eight sediment cores taken throughout the New Town using a percussion coring machine (Cobra TT).[41] In the southern part of the New Town, near the city wall, both coring and ERT indicated the possible presence of an ancient road potentially connected to a city gate. This hypothesis required validation through excavation, which was undertaken in 2024.

Based on the results obtained in 2023, we planned the 2024 campaign with the following goals:

- Extend trench NT1 to the north by 142 m² (red colour in **Fig. C1.1**) to further explore the structures of Building A and Building B (**§C2**).
- Continue excavating "Room 5" and collecting additional information about its stratigraphic relationship with the surrounding structures (blue colour in **Fig. C1.1**). A crucial result of the 2024 campaign is that "Room 5" belonged to Building A, and thus, it will be discussed alongside the latter in **§C2.8.7**.
- Open a new sondage, Sondage 2, within the 2002 SBAH trench "New Town 4" (green colour in **Fig. C1.1**) to obtain a complete stratigraphic sequence below the structures exposed by SBAH and collect samples suitable for radiocarbon dating.
- Open a new operation, referred to as NT2 (orange colour in **Fig. C1.1**), to test the presence of an ancient road in the spot where the ERT prospection and the coring had hinted at its presence.

C1.1 Updates to the registration method

F. Janoscha Kreppner & Andrea Squitieri

The registration method adopted during the 2024 campaign follows the one implemented in the 2023 campaign,[42] with minor additions. It is worth offering a summary here. All archaeological features are registered within a 10 × 10 m square grid using the locus/collection system (**Fig. C1.2**). Each grid square receives a six-digit number derived from the WGS84/UTM 38N coordinates of each square's southwest vertex. A locus (pl. loci), i.e. a stratigraphic unit, is labelled as Locus:[square number]:[progressive number], so, e.g., Locus:261433:001 is Locus 1 in Square 261433. Collections of fragmentary materials (e.g., pottery sherds, bones), samples (e.g., charcoal, flotation samples, phytoliths), and individual finds are indicated by the prefix AS, which stands for Assur. They receive an additional progressive number following the locus number, e.g., AS 261433:001:001 is collection/sample/find 1 in Locus 1 in Square 261433. The excavation data are stored in a server-based MySQL-based database, accessible remotely by all team members, both in the field and in the excavation house, via a web interface.[43] The database is directly connected to QGIS, making it possible to visualise the points and the lines measured on the field using a Leica dGPS (base model: GS10, rover models: GS10 and

Fig. C1.2: The 2024 excavation grid. Prepared by Andrea Squitieri.

37 Radner/Squitieri/Rohde 2024, 138.

38 Based on the radiocarbon dates: 756-481 calBC (95.4% probability) and 734-412 (95.4% probability), see Radner/Squitieri 2024b, Table D1.1.

39 1416-1278 calBC (95.4% probability) and 771-545 calBC (95.4% probability), see Radner/Squitieri 2024b, Table D1.1.

40 Fassbinder *et al.* 2024.

41 Altaweel 2024.

42 Radner/Squitieri 2024b, 93-98.

43 The Assur database was designed by Christoph Forster (www.datalino.de).

GS18). These measurements constitute the basis for the architectural plans generated after the excavation campaign. At the end of each excavation day, a DJI Mavic 3 Pro drone is used to take photos of the excavation areas. These photos are then elaborated in Agisoft Metashape to obtain orthophotos, 3D, and digital elevation models (DEMs). The 3D documentation helps keep track of the excavation progress daily, thus ensuring a minimal loss of information.

At the start of the 2024 campaign, we introduced a secondary labelling system for archaeological features. In our system, it is common for features to be registered with multiple loci. For example, a pit receives at least two loci: one for the cut and one for the fill. Similarly, a grave may have a locus for the cut, one for the fill, one for the skeleton and one for the grave architecture. Additionally, since our locus system is tied to a 10 × 10 m grid, an archaeological feature crossing several grid squares, such as a wall or a floor, is also described by multiple loci, each with a different number in each square. Consequently, the number of loci increases rapidly. Managing a high number of loci can be challenging and obscure the fact that different locus numbers may refer to the same feature (a pit, a floor or a grave, for instance). To address this, specific archaeological features, such as walls, floors, and installations, now receive a progressive number following their designation. For floors and installations, this number also includes a reference to the room and building in which they are located. Deposits are assigned numbers that reflect their stratigraphic position. The table below lists the new labels for the archaeological features, along with examples.

Feature	Nomenclature	Example
Pit	Pit [progressive number]	Pit 4
Grave	Grave [progressive number]	Grave 9
Wall	Wall [progressive number]	W01
Floor	[Building-Room] - F [progressive number]	A01-F1 (= Floor 1 in Building A Room 1)
Deposit/Fill	[Building-Room] - D [progressive number based on deposit's stratigraphy]	B11-D02-01 (= Deposit 02-01 in Building B Room 11)
Installation	[Building-Room] - I [progressive number]	B11-I1 (= Installation 1 in Building B Room 11)

The stratigraphic **Table C2.1** also provides the correspondence between archaeological features and locus numbers.

C1.2 The radiocarbon dates from the 2024 campaign

Karen Radner & Andrea Squitieri

In 2023, the first steps toward establishing the absolute chronology of the excavated contexts were initiated through the submission of 17 samples, comprising human teeth, charcoal, and seeds, for radiocarbon dating.[44] Building on these results, 18 samples were collected in 2024 and submitted for analysis to the Curt-Engelhorn-Zentrum Archäometrie (CEZA) of the Reiss-Engelhorn-Museen in Mannheim. These new samples were collected from graves excavated during the 2024 field season and from newly uncovered contexts in trench NT1, Sondage 2, and trench NT2. The results of these radiocarbon analyses are summarised in **Table C1.1**, with detailed dates organised by context as listed below.

- Two human bones from Graves 3 and 8 and a human tooth from Grave 9 were selected for radiocarbon dating. The two human bones, however, did not contain enough collagen to produce a date. Additional teeth from Graves 6, 8 and 9 were sent in May 2024 for DNA extraction to the Max-Planck-Institut für evolutionäre Anthropologie in Leipzig.
- Two charcoal and three organic samples from trench NT2 were selected for radiocarbon dating. Four additional samples from the same contexts were sent to Katleen Deckers (University of Tübingen) for wood analysis (**§I1**).
- Five charcoal samples and four seeds from the structures uncovered in Sondage 2 were selected for radiocarbon dating. A charcoal sample from the same sondage was also sent for wood analysis (**§I1**).
- One seed from the flotation of the floor deposit in Room 11 in Building B was sent for radiocarbon dating.

Table C1.1 lists the radiocarbon results according to material and laboratory number. The signature AsRC (for Assur RadioCarbon) is used to identify each sample, with progressive numbers that continue the 2023 list.[45]

- From trench NT1, the sample AsRC 31 (**Fig. C1.3**) is a seed collected through the flotation of the floor deposit of Room 11 in Building B (**§C2.9**). This sample has provided us with the first radiocarbon date relative to this building, which had already been partially exposed in 2023. The radiocarbon date obtained, 778-551 calBC (95.4 % probability), aligns with the Iron Age pottery re-

44 Radner/Squitieri 2024b, Table D1.1.
45 Radner/Squitieri 2024b, Table D1.1.

AsRC no.	LAB ID	Sample AS no.	Material	Context	Relative stratigraphy	14C Age (yr BP)	68.30%	95.40%	C%	Coll. %	Eastings (UTM)	Northings (UTM)	Elevation (m asl)
AsRC 18	MAMS 69978	AS 254433:038:005	Charcoal	Trench NT2: fill	NT2 Phase 1	2488 ± 19	cal BC 756-547	cal BC 770-541	51.4		342547.11	3924330.68	152.6
AsRC 19	MAMS 69979	AS 254433:041:006	Charred vitrified organic material**	Trench NT2: fill	NT2 Phase 1	>49000	/	/	66.0				
AsRC 20	MAMS 69980	AS 263432:018:003	Charcoal	Sondage 2: fill on the virgin soil	Sondage 2 Phase 1	2926 ± 20	cal BC 1196-1055	cal BC 1214-1048	45.0		342638.85	3924328.62	158.9
AsRC 21	MAMS 69981	AS 263432:021:004	Charcoal	Sondage 2: fill of Pit 16	Sondage 2 Phase 1	3060 ± 20	cal BC 1386-1282	cal BC 1406-1261	28.4		342638.58	3924328.4	158.54
AsRC 22	MAMS 69982	AS 254433:039:006	Organic material, not necessarily charred**	Trench NT2: fill	NT2 Phase 1	8992 ± 53	cal BC 8287-8016	cal BC 8295-7963	0.2		342547.55	3924330.79	151.43
AsRC 23	MAMS 69983	AS 254433:041:001	Humified organic material**	Trench NT2: fill	NT2 Phase 1	38920 ± 680	cal BP 42949-42317	cal BP 43875-42104	31.0		342547.35*	3924330.65*	150.5*
AsRC 24	MAMS 69984	AS 254433:025:003	Charcoal	Trench NT2: fill	NT2 Phase 2	2516 ± 20	cal BC 773-572	cal BC 777-548	58.5		342547.68	3924330.71	153.15
AsRC 25	MAMS 69985	AS 262433:093:004	Human bone	Grave 8	NT1 Phase 8a	/	/	/		none			
AsRC 26	MAMS 69986	AS 262433:090:007	Human tooth	Grave 9	NT1 Phase 8a	1853 ± 18	cal AD 133-234	cal AD 130-236	39.5	4.2	342624.1*	3924338.4*	161.5*
AsRC 27	MAMS 69987	AS 262433:060:019	Human bone	Grave 3	NT1 Phase 6	/	/	/		none			
AsRC 28	MAMS 70418	AS 263432:012:003	Seed	Sondage 2: drainage fill	Sondage 2 Phase 3	3389 ± 16	cal BC 1732-1631	cal BC 1740-1622	46.5		342638.62	3924328.52	159.54
AsRC 29	MAMS 70419	AS 263432:016:005	Seed	Sondage 2: floor deposit	Sondage 2 Phase 2	2587 ± 16	cal BC 796-780	cal BC 801-775	58.0		342639.06	3924328.69	159.49
AsRC 30	MAMS 70420	AS 263432:021:005	Seed	Sondage 2: fill of Pit 16	Sondage 2 Phase 1	3034 ± 16	cal BC 1375-1260	cal BC 1385-1222			342638.67	3924328.52	158.61
AsRC 31	MAMS 70421	AS 262433:158:001	Seed	Trench NT1: Building B Room 11 floor deposit	NT1 2023 Phase 4	2521 ± 16	cal BC 774-590	cal BC 778-551	59.3		342622.13	3924337.67	160.68
AsRC 32	MAMS 73966	AS 263432:044:003	Charcoal	Sondage 2: fill below floor (SBAH Unit 14)	Sondage 2 Phase 2	2650 ± 16	cal BC 815-801	cal BC 827-794	58.6		342638.62	3924327.04	159.44
AsRC 33	MAMS 73967	AS 263432:035:002	Seed	Sondage 2: floor deposit with burnt traces (SBAH Unit 14)	Sondage 2 Phase 2	2589 ± 16	cal BC 796-781	cal BC 802-776	55.0		342638.64	3924327.01	159.63
AsRC 34	MAMS 73968	AS 263432:031:006	Charcoal	Sondage 2: floor deposit (SBAH Unit 14)	Sondage 2 Phase 2	2539 ± 16	cal BC 781-596	cal BC 791-569	63.5		342638.5	3924326.48	159.53
AsRC 35	MAMS 73969	AS 263432:031:005	Charcoal	Sondage 2: floor deposit (SBAH Unit 14)	Sondage 2 Phase 2	2634 ± 16	cal BC 809-798	cal BC 816-791	62.5		342638.05	3924326.87	159.53

* approximate coordinates

** identifications by Katleen Deckers; not linked to any occupation phase at the site

Table C1.1: Summary table of the radiocarbon dates obtained from the areas excavated during the 2024 season. Compiled by Andrea Squitieri.

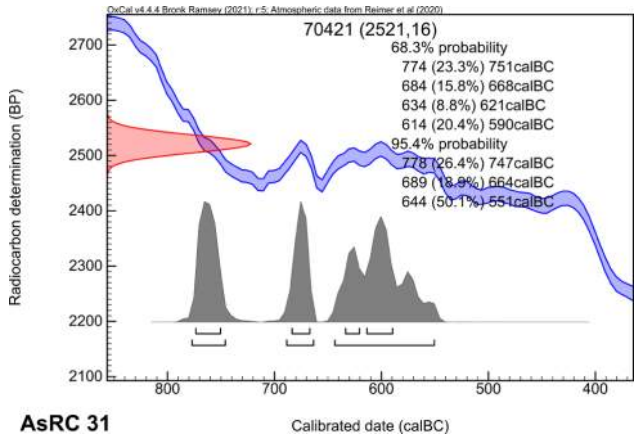

Fig. C1.3: Calibrated radiocarbon determination of the sample AsRC 31 (MAMS 70421). Prepared by Andrea Squitieri.

trieved from this building,[46] and the building's relative stratigraphic position (**§C2.1**).

The tooth from Grave 9 (AsRC 26 = **Fig. C1.4**) was radiocarbon dated to the Parthian period (130-236 calAD). This date fits the relative stratigraphy of this grave, which was assigned to the NT1 2024 Phase 8a (**§C2.1**). The chamber tomb excavated in 2023, dated to 83-215 calAD, also belongs to this phase.[47] Unfortunately, the samples AsRC 25 and AsRC 27, coming from Graves 8 and 3, respectively, did not contain enough collagen, rendering them undatable.

- From the trench NT2 (**§C4**), the sample AsRC 19, made of charred vitrified organic material, was collected from the lowest excavated level, approximately 6 m below the site surface. It failed to produce a date. The sample AsRC 23, made of humified organic material (**Fig. C1.5**), also coming from NT2's deepest level, yielded a date corresponding to the Upper Palaeolithic Age (43,875-42,104 calBP), while the sample AsRC 22, made of organic material not necessarily charred (**Fig. C1.6**), was dated to the Neolithic period (8295-7963 calBC). Given the nature of the features excavated in trench NT2 (discussed in **§C4**), the dates obtained from both AsRC 23 and AsRC 22 cannot be directly connected to any occupation period at Assur; hence, we assume that they were deposited at the bottom of NT2 through natural processes. Lastly, two charcoal samples (AsRC 24 = **Fig. C1.7** and AsRC 18 = **Fig. C1.8**), located stratigraphically higher than the earlier ones, were dated to 777-548 calBC and 770-541 calBC, respectively. Both date ranges align with the Iron Age pottery collected from the same contexts (**§C4**).
- From Sondage 2 (**§C3**), nine radiocarbon dates are available. The charcoal samples AsRC 20 (**Fig. C1.9**) and AsRC 21 (**Fig. C1.10**) were collected from the lowest level of the sondage, that is from a fill lying right above the virgin soil and the fill of a pit (named Pit 16), which cut the virgin soil; they were dated to 1214-1048 calBC and 1406-1261 calBC, respectively. The date of AsRC 21 is nearly as old as the earliest date obtained in 2023 close to the virgin soil reached below the structures unearthed in NT1.[48] The date range obtained from AsRC 21 fits well with the earliest mention of building activities in the New Town during the reign of Puzur-Aššur III (conventionally dated to 1521-1498 BC).[49]

  The seeds AsRC 28, AsRC 29, and AsRC 30 (**Figs. C1.11-13**) were dated to 1740-1622 calBC, 801-775 calBC, and 1385-1222 calBC, respectively. The mixture of dates from various periods can be explained by considering the stratigraphy of Sondage 2 (see also **§C3**). The sample AsRC 30, dating to 1375-1260 calBC, was found at the lowest level reached by the sondage, close to the virgin soil, as did the sample AsRC 21. The sample AsRC 29 (**Fig. C1.12**), dated to 801-775 calBC, was found on a pebble floor above the earlier deposits. Above this floor, the drainage installation was discovered, from which sample AsRC 28, dated to 1740-1622 calBC, was collected. This is the oldest radiocarbon date obtained so far, predating the reign of Puzur-Aššur III. However, since the seed came from the fill of a drainage installation, it is highly possible that older material originating from elsewhere on the site could have ended up in this fill (see **§C3** and **§I2.6.5**, where the plant remains are discussed).

  The samples AsRC 32, AsRC 33, AsRC 34 and AsRC 35 (three charcoal pieces and one seed) were radio-

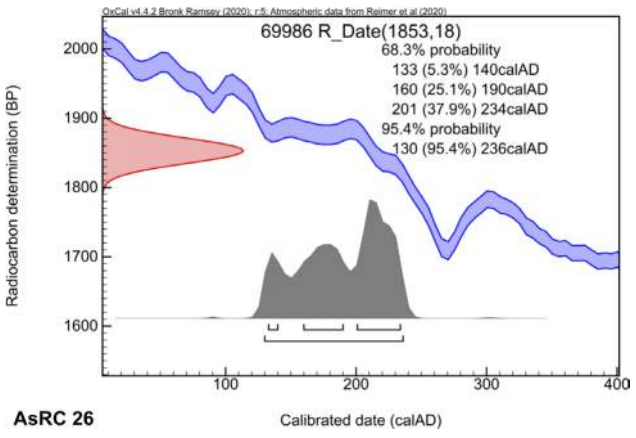

Fig. C1.4: Calibrated radiocarbon determination of the sample AsRC 26 (MAMS 69986). Prepared by Andrea Squitieri.

46 Kreppner/Rohde/Squitieri 2024, 127-130.
47 Radner/Squitieri 2024b, Table D1.1.
48 Kreppner/Rohde/Squitieri 2024, 135.
49 Radner/Kreppner 2024, 224.

carbon dated to 815-801 calBC, 796-781 calBC, 781-596 calBC, and 809-798 calBC (**Figs. C1.14-17**). They came from the southern part of Sondage 2, where the continuation of the pebble floor was found, the same floor on which the drainage was discovered. Their dates fall within the Iron Age horizon, thus confirming that the structures uncovered in this sondage belong to the Iron Age (see discussion in **§C3**).

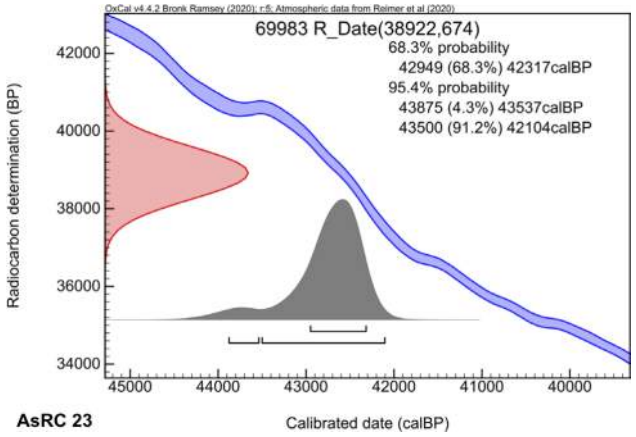

Fig. C1.5: Calibrated radiocarbon determination of the sample AsRC 23 (MAMS 69983). Prepared by Andrea Squitieri.

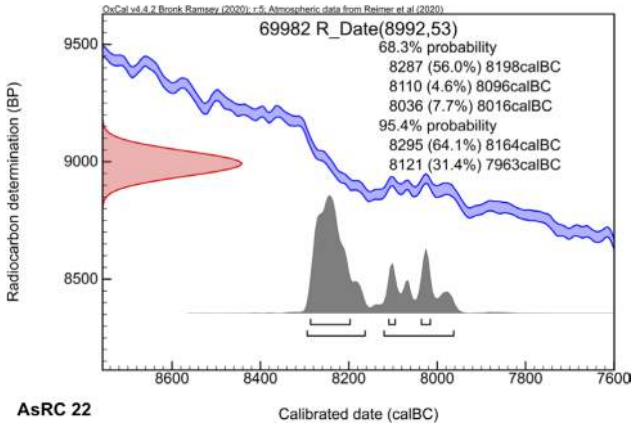

Fig. C1.6: Calibrated radiocarbon determination of the sample AsRC 22 (MAMS 69982). Prepared by Andrea Squitieri.

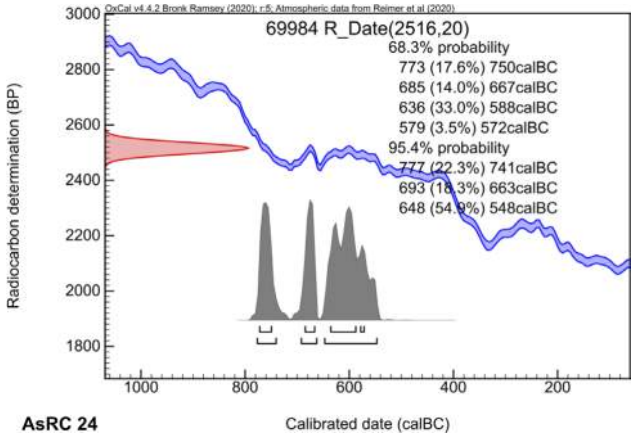

Fig. C1.7: Calibrated radiocarbon determination of the sample AsRC 24 (MAMS 69984). Prepared by Andrea Squitieri.

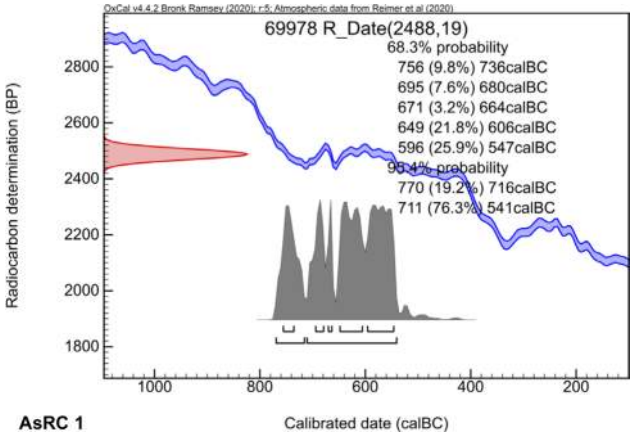

Fig. C1.8: Calibrated radiocarbon determination of the sample AsRC 1 (MAMS 69978). Prepared by Andrea Squitieri.

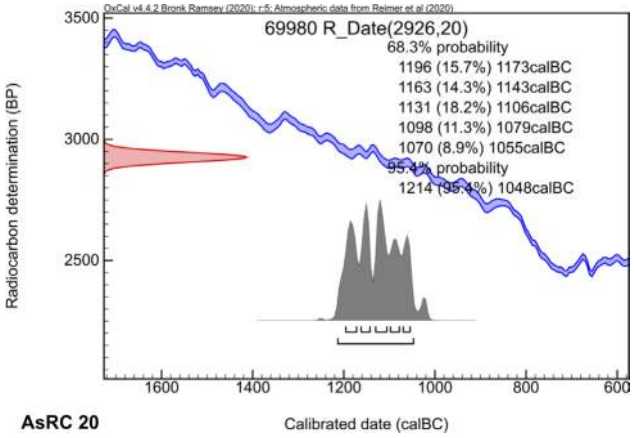

Fig. C1.9: Calibrated radiocarbon determination of the sample AsRC 20 (MAMS 69980). Prepared by Andrea Squitieri.

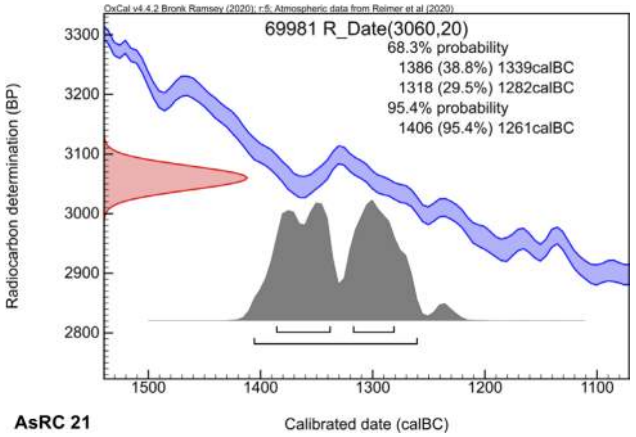

Fig. C1.10: Calibrated radiocarbon determination of the sample AsRC 21 (MAMS 69981). Prepared by Andrea Squitieri.

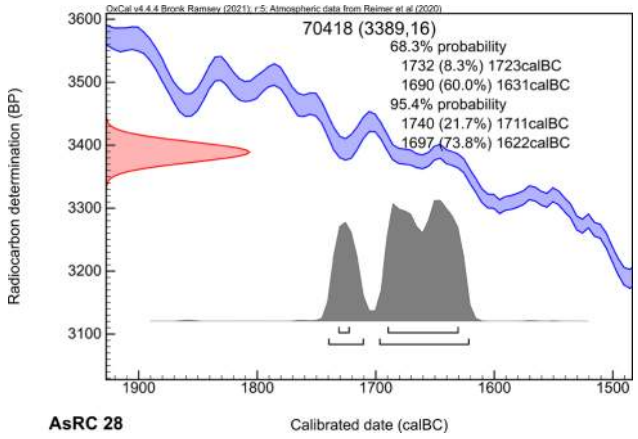

Fig. C1.11: Calibrated radiocarbon determination of the sample AsRC 28 (MAMS 70418). Prepared by Andrea Squitieri.

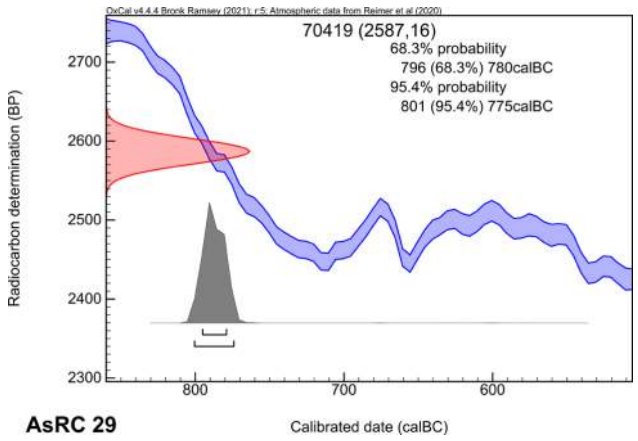

Fig. C1.12: Calibrated radiocarbon determination of the sample AsRC 29 (MAMS 70419). Prepared by Andrea Squitieri.

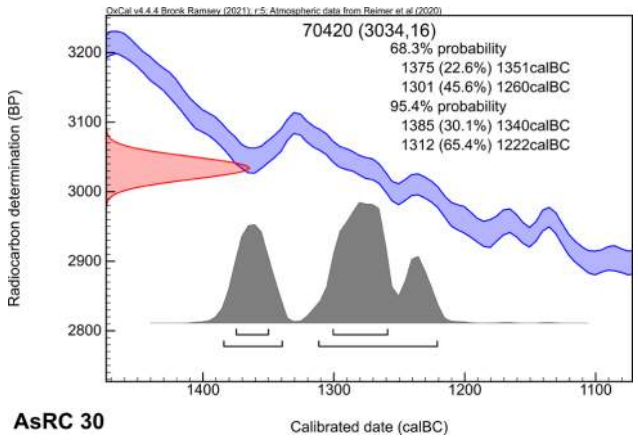

Fig. C1.13: Calibrated radiocarbon determination of the sample AsRC 30 (MAMS 70420). Prepared by Andrea Squitieri.

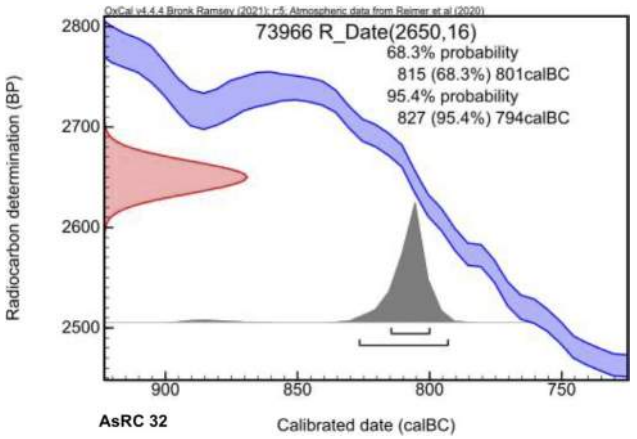

Fig. C1.14: Calibrated radiocarbon determination of the sample AsRC 32 (MAMS 73966). Prepared by Andrea Squitieri.

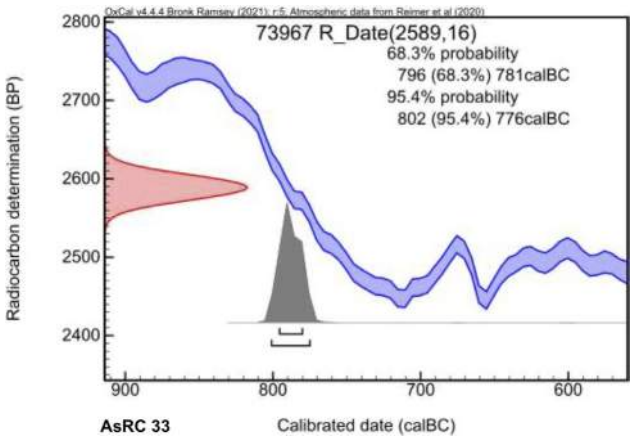

Fig. C1.15: Calibrated radiocarbon determination of the sample AsRC 33 (MAMS 73967). Prepared by Andrea Squitieri.

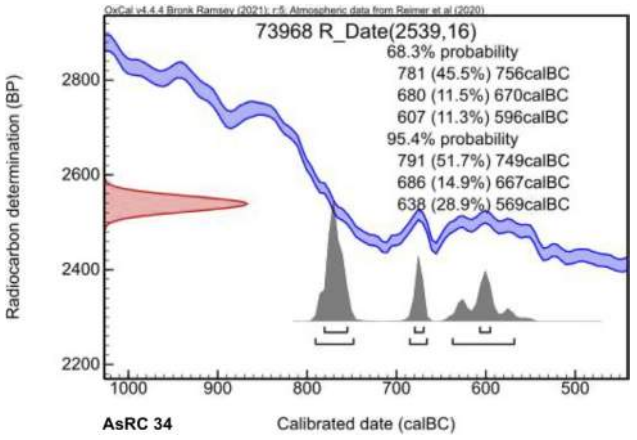

Fig. C1.16: Calibrated radiocarbon determination of the sample AsRC 34 (MAMS 73968). Prepared by Andrea Squitieri.

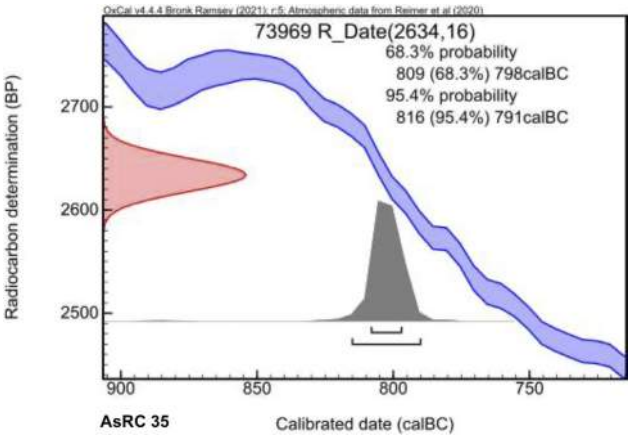

Fig. C1.17: Calibrated radiocarbon determination of the sample AsRC 35 (MAMS 73969). Prepared by Andrea Squitieri.

C2. Excavating trench NT1 2024 in the New Town of Assur

F. Janoscha Kreppner, Jens Rohde, Andrea Squitieri, Veronica Hinterhuber, Alessio Palmisano, Poppy Tushingham & Marco Wolf

C2.1 The relative stratigraphy

The trench NT1 (**Fig. C2.1.1**) comprises nine stratigraphic phases between the topsoil and the virgin soil. These were designated with progressive numbers following the label NT1 2023 for phases identified in the 2023 campaign or NT1 2024 for those identified during the 2024 campaign. Overall, the identified stratigraphic phases range from phase NT1 2023 Phase 9, dated to the modern period, down to NT1 2023 Phase 1, dated to the Late Bronze Age.[50]

During the 2024 campaign, we continued the exploration of NT1 2023 Phases 9, 8, 7, 5 and 4. Phase 8 was subdivided into two new phases, referred to as NT1 2024 Phase 8b and NT1 2024 Phase 8a. The latter contained graves dated to the Parthian period, while the former contained pits that had damaged these graves and the structures of Building A (NT1 2023 Phase 5). The table below summarises the relative stratigraphy of the 2023 and 2024 campaigns combined, with the phases discussed in the present book in italics.

Stratigraphic phases / periods / absolute dates[51]	**Main features**
Topsoil	Soft brown soil
NT1 2023 Phase 9 Modern	2023: Looting pit and looted Grave 2 2024: Pit 8 and Pit 17
NT1 2024 Phase 8b Between the Parthian and Early Islamic periods	2024: Pits 1 to 6, Pits 9 to 15 and Pit 18.
NT1 2024 Phase 8a Chamber tomb: 83-215 calAD Grave 9: 130-236 calAD	2023: Chamber tomb (Grave 1) 2024: Graves 6, 7, 8, 9, 11
NT1 2023 Phase 7 Parthian period (?)	2023: Architecture (wall) 2024: Pit 7 and stone installations
NT1 2023 Phase 6 159/158 BC (Grave 3)[52]	2023: Grave 3 and Grave 4
NT1 2023 Phase 5 173-53 calBC 176-52 calBC 341-57 calBC[53]	2023: Building A (Rooms 1, 2 and 3) 2024: Building A (Rooms 1, 2, 7, 8, 9, Courtyard 10 and "Room 5")
NT1 2023 Phase 4 778-551 calBC	2023: Building B (Outdoor Area 4) 2024: Building B (Room 11)
NT1 2023 Phase 3 770-542 calBC 775-545 calBC	2023: Grave 5
NT1 2023 Phase 2 Late Bronze Age/Early Iron Age	2023: Architecture (walls)
NT1 2023 Phase 1 1506-1440 calBC	2023: Deep sounding (no architecture)
Virgin soil	Hard reddish soil

50 Kreppner/Rohde/Squitieri 2024, 93.

51 95.4% probability for calibrated radiocarbon dates.

52 Date from alphabetic inscription on Grave 3, see Gzella 2024.

53 Three additional and older radiocarbon dates obtained from seeds collected from the floors of Building A have been omitted in this table. The presence of older seeds in the floor deposits of Building A may be due to the reuse of cultural debris as construction material for the floors, or the collapse of mudbricks containing older seeds in their matrix, see also Radner/Squitieri 2024b, 100.

Fig. C2.1.1: Trench NT1, delimited by a white dash line, and the SBAH trench "New Town 4" of 2002, overlaid by the excavation grid. Orthophoto by Jens Rohde, prepared by Andrea Squitieri.

C2.2 The stratigraphic table

The complete relative stratigraphy of the trench NT1, combining the 2023 and the 2024 excavation results, is shown in **Table C2.1**. This table is organised as follows:

- The rows are ordered chronologically from the most recent to the oldest phases;
- The columns refer to spaces such as rooms;
- Roughly contemporary deposits and archaeological features are organised horizontally;
- The cells contain a short description of each locus;
- The most relevant background colours are yellow, which indicates occupation and use of floors and installations; brown, which indicates post-occupation periods; and grey, which indicates graves.

Each occupation phase (yellow rows) is divided into the following sub-phases:

- First Construction: construction of walls and their foundations;
- Construction: construction of floors and installations;
- Occupation: use of floors and installations;
- End of occupation: destruction and/or abandonment of floors and installations.

The sections below describe the archaeological features in stratigraphic order, from the youngest to the oldest.

C2.3 NT1 2023 Phase 9

Pits 8 and 17 were assigned to NT1 2023 Phase 9, ascribed to the modern period (**Fig. C2.3.1**). The former was a shallow oval pit, about 55 × 33 cm in diameter, located in the southwestern part of the excavation area. The fill, excavated to a depth of c. 15 cm, consisted of greyish brown soil containing bones, a modern green glass bottle fragment, and a tin can. Towards the northeast, Pit 17 was

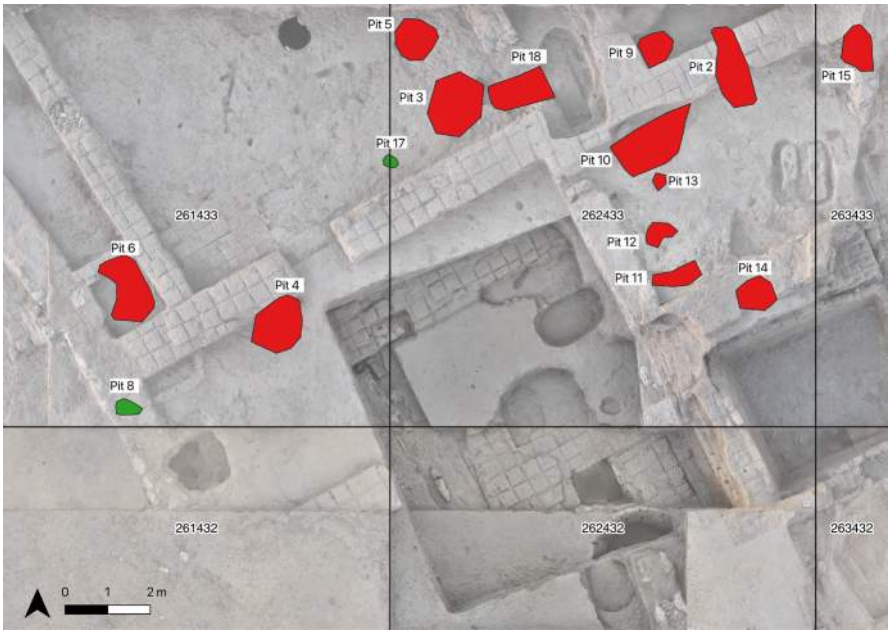

Fig. C2.3.1: Pits of NT1 2023 Phase 9 (green) and NT1 2024 Phase 8b (red). Orthophoto by Jens Rohde, prepared by Andrea Squitieri.

Fig. C2.4.1: Honeycomb decorated jar AS 261433:036:005 from Pit 4, dated to the Early Islamic period. Photo by Marco Wolf.

identified as an animal burrow. Both pits damaged the structures of Building A **(§C2.8)**.

C2.4 NT1 2024 Phase 8b

The NT1 2024 Phase 8b is composed of several pits (**Fig. C2.3.1**) that damaged Grave 9 (NT1 2024 Phase 8a) as well as the architecture of Building A (NT1 2023 Phase 5). The pits did not contain any chronological diagnostic finds, with the notable exception of Pit 4, which included a complete water jar with a honeycomb decoration typical of the Early Islamic period (AS 261433:036:005, see **§D1.3**). Based on the pits' stratigraphic position and the vessel's date in Pit 4, we may suggest that NT1 2024 Phase 8a pits were dug between the Parthian and the Early Islamic period.

Pit 4, located in the southwestern part of the excavation area, partially damaged wall W04 belonging to Building A (NT1 2023 Phase 5). It was c. 60 cm deep and had a diameter between 1 and 1.3 m. Its fill consisted of a crumbly, brown clayey soil mixed with reddish-brown clay, yielding fragments of gypsum plaster, pottery sherds, bones, and brick fragments. The pit accommodated the jar AS 261433:036:005, which was found in a complete state of preservation lying on its side, with its opening facing slightly downwards (**Fig. C2.4.1**). The jar was oriented in a southwest-northeast direction, and some brick fragments and stones were in front of the vessel's mouth. This could indicate that the vessel had been deliberately laid into the pit and sealed. The jar was almost empty, except for some very loose dark-brown clayey soil (registered as Locus:261433:045) mixed with small pottery sherds, fragments of bones, and pebbles. A concentration of bitumen could be observed at the bottom of the vessel. As shown in **§D1.3**, this jar can be dated to the Early Islamic period based on parallels found in Iraq. A very similar jar (AS 262433:021:007, see **§D1.3**) was found in 2023 in a complete state of preservation within the structures of the Parthian-period chamber tomb (Grave 1).[54] Though not directly related to a looting pit, this jar can now be assigned to NT1 2024 Phase 8b. It most likely belonged to the looting events that targeted the chamber tomb in antiquity.

C2.5 NT1 2024 Phase 8a

NT1 2024 Phase 8a consists of the Parthian-period chamber tomb (Grave 1) unearthed in 2023 and removed in that year,[55] as well as five looted graves (Graves 6, 7, 8, 9, and 11)

54 Kreppner/Richter/Squitieri 2024, 141-142.

55 Kreppner/Rohde/Squitieri 2024, 105-118. Note that in Kreppner/Rohde/Squitieri 2024, the chamber tomb (Grave 1) had been assigned to the NT1 2023 Phase 8. After the results of the 2024 excavations, this phase was subdivided into Phases 8a and 8b. The chamber tomb has now been assigned to Phase 8a, along with the other Parthian graves excavated in 2024.

Assur New Town trench NT1: 2023 and 2024		261433	261432	262432	262433, 263433			
Present surface		Locus:261433:001, Locus:261433:013, Locus:261433:028	Locus:261432:003, Locus:261432:005	Locus:262432:002, Locus:262432:011, Locus:262432:014	Locus:262433:001		Locus:262433:083, Locus:263433:006	Locus:263433:005
Topsoil		Locus:261433:002, Locus:261433:014, Locus:261433:029	Locus:261432:004, Locus:261432:006	Locus:262432:003, Locus:262432:005, Locus:262432:012, Locus:262432:015	Locus:262433:002		Locus:262433:084, Locus:263433:007	Locus:263433:003
Modern	NT1 2023 Phase 9	Locus:261433:027 refill of 2023 excavation	looting of Grave 2: Locus:261432:012, Locus:261433:049 pit cut, Locus:261432:013, Locus:261432:015, Locus:261433:050 fills, Locus:261432:016 stone collapse, Pit 8: Locus:261433:071 cut, Locus:261433:072 fill				Locus:262433:082 refill of 2023 excavation, Pit 17 (Locus:261433:081 cut, Locus:261433:082 fill)	
Parthian to Islamic	NT1 2023 Phase 8b	Pit 4: Locus:261433:035 cut, Locus:261433:036 fill, Locus:261433:045 fill of vessel	Pit 6: Locus:261433:042 cut, Locus:261433:043 fill	Pit 1: Locus:262432:008 cut, Locus:262432:009 fill	Pit 9: Locus:262433:112 cut, Locus:262433:114 fill	Pit 10: Locus:262433:114 cut, Locus:262433:115 fill	Pit 2: Locus:262433:085 cut, Locus:262433:086 fill, Pit 3: Locus:262433:087 cut, Locus:262433:088 fill, Pit 5: Locus:262433:099 cut, Locus:262433:100 fill, Pit 11: Locus:262433:118 cut, Locus:262433:119 fill, Pit 12: Locus 262433:120 cut, Locus:262433:121 fill, Pit 13: Locus:262433:122 cut, Locus:262433:123 fill, Pit 14: Locus:262433:133 cut, Locus:262433:134 fill, Pit 15: Locus:263433:015 cut, Locus:263433:013 fill, Pit 18 : Locus:262433:108 cut, Locus:262433:109 fill	
Parthian	NT1 2023 Phase 8a	Chamber Tomb (= Grave 1) (see Radner/Squitieri 2024, Table 02.1)				Grave 8: Locus:262433:091 cut, Locus:262433:092 pit fill, Locus:262433:093 fill of coffin, Grave 9: Locus:262433:089 cut, Locus:262433:090 pit fill (C14 sample), Locus:262433:094 fill of coffin, Locus:262433:111 mud bricks, Grave 11: Locus:263433:008 cut, Locus:263433:009 pit fill, Locus:263433:010 sarcophagus fill	Grave 7: Locus:262433:095 cut, Locus:262433:096 fill, Locus:262433:097 skeleton
	NT1 2023 Phase 7	Locus:261433:024 two rows of stones, Locus:261433:055 collapse, Locus:261433:033 stone installation, Locus:261433:054 stone installation, Locus:261433:057 stone installation Pit 7: Locus:261433:059 stone capping, Locus:261433:060 cut, Locus:261433:061 fill		Locus:262432:016 fill Locus:262432:017 wall	Locus:262433:103 mudbrick installation			
159/158 BC	NT1 2023 Phase 6			Grave 4: Locus:262432:052 pit cut with fill Locus:262432:053 and Locus:262432:054, Locus:262432:055 skeleton	Grave 3: Locus:262433:057 and Locus:262433:066 pit cut with fills Locus:262433:056, Locus:262433:067 and Locus:262433:058 with skeleton Locus:262433:060. Inscription date: 159/158 BC			

Table C2.1 (Part 1.A): The relative stratigraphy of the trench NT1. Prepared by F. Janoscha Kreppner.

	Assur New Town trench NT1: 2023 and 2024 (cont.)	Building A							
		Room 1	Courtyard 10	Room 2	Room 3	Room 7	Room 8	Room 9	"Room 5"
Hellenistic	NT1 2023 Phase 5: POST-OCCUPATION	A01-D01-01 (Locus:261433:003 mudbrick collapse), A01-D01-02 (Locus:261433:004 mudbrick debris), A01-D01-03 (Locus:261433:034 brownish silty soil with mudbrick debris), A01-D01-04 (Locus:261433:037 mudbrick debris), A01-D01-05 Locus:261433:038 mudbrick debris southern part	A09/10-D01-01 brownish mudbrick debris (Locus:262433:104) A10-01-01 mudbrick collapse (Locus:261433:012, Locus:261433:048, Locus:261433:051, Locus:261433:056), A10-01-02 loose silty and well sorted soil with a yellowish-brown colour (Locus:261433:053, Locus:261433:058)	A02-D01-01 silty soil (Locus:262433:008, Locus:262433:009) A02-D01-02 mudbrick debris (Locus:261432:007, Locus:261433:017, Locus:261433:021 and Locus:261433:039, Locus:262433:065 and Locus:262433:098)	A03-D01-01 greyish mudbrick debris (Locus:262432:051	A07-01-01 brownish mudbrick debris (Locus:262433:101)	A08-D01-01 brownish mudbrick debris (Locus: 262433:102, Locus:263433:011, Locus:262433:143) brownish mudbrick debris with stones, baked brick fragments pebbles	A09/10-D01-01 brownish mudbrick debris (Locus:262433:104) A09-D1-02 light brown, loose dry soft silty soil with mudbrick fragments and pebbles (Locus:262433:144)	Sondage 01-05-D01-01 soft, greyish-brown silty soil with sherds, pebbles, mudbrick debris (Locus:262432:056, Locus:263432:004), Sondage 01-05-D01-02 light brown loose soil (262433:135, 263433:004), Sondage 01-05-01-03 reddish loose soil with mudbrick fragments, ashes and bones (Locus:262433:137), Sondage 01-05-D01-04 ashes with mudbrick fragments (Locus:262433:139), Sondage 01-05-D01-05 reddish brown silty soil with chunks of mudbricks (Locus:262433:140), Sondage 01-05-D01-06 loose ashes with mudbrick fragments, whitish inclusions (Locus:262433:141), Sondage 01-05-D01-07 reddish silty soil with mudbrick fragments, ashes with white traces (Locus:262433:142), Sondage 01-05-D01-08 soft loose ashes with white traces and some mudbrick fragments (Locus:262433:148, Locus:263433:016), Sondage 01-05-D01-09 reddish soil with mudbricks (Locus:262433:155)
	NT1 2023 Phase 5: END OF OCCUPATION	A01-D02-01 (Locus261433:005 and Locus:261433:040 brownish silty soil with ceramics and some ash), A01-D02-02 (Locus:261433:007 local ashes)	A10-D02-01 greyish brown and moderately sorted silty soil, with some sherds and some bones, few ashes and pebbles (Locus:261433:067, Locus:262433:136)	A02-D02-01 greyish-brown, dry soft, poorly sorted, silty soil with abundant sherds, some pebbles and some mudbrick debris, few bones, few charcoal (Locus:261432:011 (C14 sample), Locus:261433:020 (C14 sample), Locus:261433:046, Locus:262433:105), A02-D02-02 yellowish-brown sandy soil, mixed with mudbrick fragments and remains of plaster (Locus:262433:068, C14 sample)	A03-D02-01 soft brownish-reddish mud material with very few sherds and bones (Locus:262432:058, C14 sample)	A07-02-01 soft, greyish-brown soil with a few pottery sherds, pebbles, mudbrick debris, and some bones (Locus:262433:110)	A08-D02-01 soft, greyish-brown soil with a few pottery sherds, pebbles, mudbrick debris, and some bones (Locus:262433:107, Locus:263433:012)		Sondage 01-05-D02-01 dry soft, well sorted, brown silty soil with few sherds, few bones and some charcoal and few ashes (Locus:262432:066, two C14 samples) , Sondage 01-05-D02-02 patches of soft ashy and harder reddish silty moderately sorted soil (Locus:262433:156, Locus:263433:017)
	NT1 2023 Phase 5: OCCUPATION	W-03 (Locus:261433:009, Locus:261433:063), A01-I1 small baked brick wall (Locus:261433:066), A01-F1 beaten earth floor (Locus:261433:006, Locus:261433:041, Locus:261433:044)	W-03 (Locus:261433:009, Locus:261433:063), A10-I1 mudbrick installation (Locus:261433:062), A10-F1a beaten earth floor (Locus:261433:073)				A08-I3 door blocking installation (Locus:262433:159)		
	NT1 2023 Phase 5: CONSTRUCTION		A10-I3 Locus:261433:076 baked brick pavement, A10-I4 row of mudbricks (Locus:261433:075), A10-F1b beaten earth floor (Locus:261433:068, Locus:262433:138), A10-I2 mudbrick with a circular mark (Locus:261433:069), A10-D03-01 brownish clay soil (Locus:261433:074), A10-I5 surface for construction (Locus:261433:077)	A02-I1 mudbrick installation (Locus:261433:052), A02-I2 door jamb hole (Locus:261433:070) A02-F1 beaten earth floor (Locus:261432:014, Locus:261433:023, Locus:261433:047, Locus:262433:069, Locus:262433:106), Locus:261433:026 passage	A03-F1 beaten earth floor Locus:262432:060	A07-F1 beaten earth floor Locus:262433:116	A08-F1 beaten earth floor (Locus:262433:124), A08-I1 threshold (Locus:262433:146), A08-I2 door socket (Locus:262433:147)	A09-I1 threshold (Locus:262433:145), A09-F1 beaten earth floor (Locus:262433:149)	Sondage 01-05-F1 beaten earth floor with white plaster (Locus:262432:072, Locus:262433:157, Locus:263433:018)
	NT1 2023 Phase 5: FIRST CONSTRUCTION	W-01 (Locus:261433:010, Locus:261433:064), W-02 (Locus:261433:008), W-04 (Locus:261433:022, Locus:261433:065, Locus:262433:126, Locus:262433:127, Locus:262433:128) walls	W-04 (Locus:261433:022, Locus:261433:065, Locus:262433:126, Locus:262433:127, Locus:262433:128), W-06 (Locus:262433:078, Locus:262433:129, Locus:262433:131) walls	W-01 (Locus:261432:008, Locus:261433:064), W-04 (Locus:261433:022, Locus:261433:065, Locus:262433:126, Locus:262433:127, Locus:262433:128), W-05 (Locus:261432:009), W-06 (Locus:262433:078, Locus:262433:129, Locus:262433:132) walls	W-05 (Locus:261432:009) wall	W-04 (Locus:261433:022, Locus:261433:065, Locus:262433:126, Locus:262433:127, Locus:262433:128), W-07 (Locus:262433:130)	W-06 (Locus:262433:078, Locus:262433:129, Locus:262433:131), W-08 (Locus:262433:131), W-09 (Locus:263433:014) walls	W-06 (Locus:262433:078, Locus:262433:129, Locus:262433:131), W-07 (Locus:262433:130) walls	Sondage 01-05-I1 lining of half mudbricks (Locus:262433:160)

Table C2.1 (Part 1.B): The relative stratigraphy of the trench NT1. Prepared by F. Janoscha Kreppner.

Assur New Town trench NT1: 2023 and 2024 (cont.)		262432	262433
		Building B	
		Unroofed Area 4	Room 11
Iron Age	NT1 2023 Phase 4: POST-OCCUPATION	Locus:262432:031 soft greyish soil, Locus:262432:032 soft greyish soil, Locus:262432:033 fill, Locus:262432:034 fill, Locus:262433:029 fill, Locus:262433:032 fill Locus:262432:047 mudbrick collapse, Locus:262433:051 fill, Locus:262433:061 fill, Locus:262432:067 fill, Locus:262433:152 and Locus:262432:069 mudbrick debris, Locus: 262432:065 mudbrick debris	B11-001-01 fill with mudbrick collapse (Locus:261433:150), Locus:262433:151 and Locus:261433:078, Locus:262433:153 and Locus:261433:079 and Locus:261433:085)
	NT1 2023 Phase 4: END OF OCCUPATION		B11-002-01 fill with ash (Locus:261433:080, Locus:262433:161), B11-002-02 fill with white inclusions and ashes (Locus:262433:158) (C14 sample), B11-02-03 fill of installation B11-I2 (Locus:262433:166)
	NT1 2023 Phase 4: OCCUPATION	Locus:262433:059 pit cut with fill Locus:262433:055, Locus:262432:062 pit cut with fill Locus:262432:063, Locus:262433:052 pit cut with fill Locus:262433:053, Locus:262433:081 pit cut; Locus:262433:062 fill; Locus:262433:063, Locus:262432:050 and Locus:262432:064 fills; Locus:262433:064 mudbrick installation; Locus:262433:071 white plaster installation with fill Locus:262433:070; Locus:262432:048 pit cut with brick lining Locus:262432:090 and fill Locus:262432:049	B11-I3 brick and stone installation (Locus:261433:087), B11-F2 top of floor package (Locus:261433:086, Locus:262433:163), B11-I2 mudbrick installation (Locus:262433:164) with floor (Locus:262433:167), second phase of the entrance (Locus:261433:084)
	NT1 2023 Phase 4: CONSTRUCTION	Locus:262432:088 and Locus:262433:080 beaten earth floor, Locus:262432:061 and Locus:262432:073 substruction of floor	B11-F1 beaten earth floor, B11-I1 entrance
	NT1 2023 Phase 4: FIRST CONSTRUCTION	W-11 (Locus:262433:054) wall, Locus:262433:077 construction pit cut with fill Locus:262433:073, W-12 (Locus:262432:075) wall	W-10 (Locus:261433:083, Locus:262433:162), W-11 (Locus:262433:054), W-12 (Locus:262433:165)
	NT1 2023 Phase 3	Grave 5: Locus:262432:069 pit cut with looted fill Locus:262432:070 (two C14 samples) and Locus:262432:071	
	NT1 2023 Phase 2: POST-OCCUPATION	Locus:262433:072 fill with stones and burnt brick fragments, Locus:262432:067 fill, Locus:262432:074 fill, Locus:262432:088 fill	
	NT1 2023 Phase 2: END OF OCCUPATION		
	NT1 2023 Phase 2: OCCUPATION	Locus:262433:075 fill, Locus:262433:076 reddish-brown fill	
	NT1 2023 Phase 2: CONSTRUCTION	Locus:262433:074 row of stones: drain (?)	
	NT1 2023 Phase 2: FIRST CONSTRUCTION	Locus:262432:080, Locus:262432:081, Locus:262432:082, Locus:262432:083 southern walls; Locus:262432:084 and Locus:262432:085 northern walls	
Late Bronze Age	NT1 2023 Phase 1	Locus:262432:076 soft greyish and well sorted mud material with larger and smaller stones, lots of sherds; Locus:262432:086 and Locus:262432:087 beaten earth floors (?); Locus:262432:078 pit cut with fill Locus:262432:079	
	VIRGIN	Locus:262432:077	

Table C2.1 (Part 2): The relative stratigraphy of the trench NT1. Prepared by F. Janoscha Kreppner.

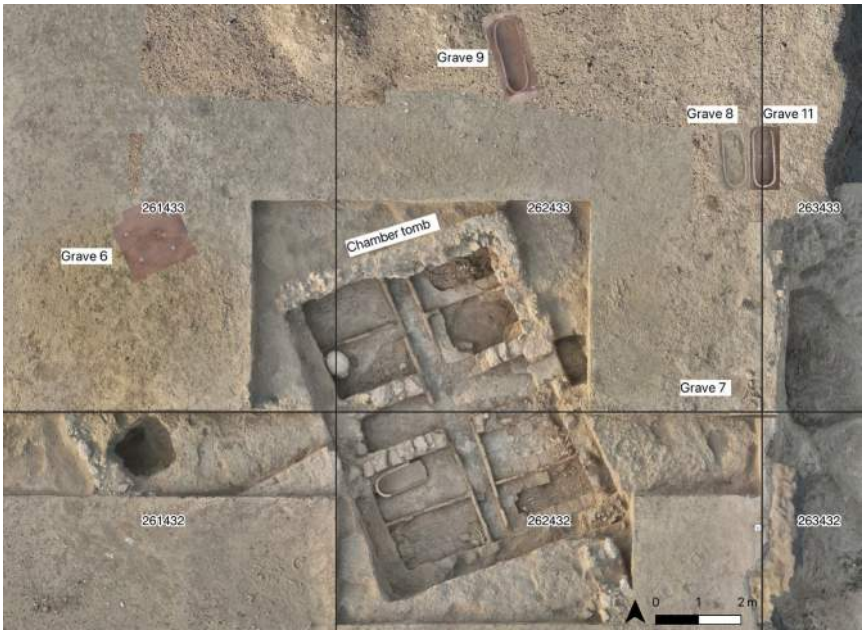

Fig. C2.5.1: The chamber tomb (Grave 1), as excavated in 2023, and the graves of NT1 2023 Phase 8a. Orthophotos by Jens Rohde, prepared by Andrea Squitieri.

discovered in 2024 (**Fig. C2.5.1**). These graves were also dated to the Parthian period based on their relative stratigraphy, the sarcophagi from Graves 8, 9, and 11, and the radiocarbon dates from Grave 9. Graves 6 and 7 were pit graves cutting the upper fills of Building A (**§C2.8**). Graves 8, 9, and 11, also cutting the structures of Buiding A, contained tub sarcophagi similar to those previously excavated at Assur by Andrae, which had been in use during the Parthian period.[56] Finally, a tooth sample from Grave 9 was radiocarbon dated to 130-236 calAD, a date range falling within the Parthian period (**§C1.2**). It is not sure if Graves 6, 7, 8, 9, and 11 were installed at the same time as the chamber tomb (Grave 1), from which a tooth sample was radiocarbon dated to 83-215 calAD.[57] In this respect, it is worth noting that the graves did not cut the chamber tomb but were located around it, which seems to indicate that they were roughly contemporaneous with it. The radiocarbon dates from the chamber tomb and Grave 9 would allow this possibility.

Below is a description of Graves 6, 7, 8, 9, and 11. A discussion of the human remains retrieved from them is provided in **§H**, while the sarcophagi from Graves 8, 9, and 11 are discussed in **§E1.1**.

Fig. C2.5.2: The skeleton of Grave 6, with the jug AS 261433:031:002 (1) and the miniature aryballos AS 261433:031:003 (2) next to the head. Photo by Marco Wolf.

C2.5.1 Pit graves

Grave 6 was located in the southwestern part of the excavation area and was identified as the burial of an infant of about 2 years old (**Fig. C2.5.2**, see also **§H2.4**). The grave pit had an oval shape measuring c. 82 × 32 cm. The fill had a depth of c. 20 cm and consisted of greyish loose and very soft silty soil, yielding some loose animal and human bones but no pottery sherds. It seems that the skeleton had been laid directly on the soil. Directly next to the skull, an almost complete jug (AS 261433:031:002), with the handle broken, and a white glazed aryballos (AS 261433:031:003) were found (**Figs. C2.5.3-4**). The jug has a possible parallel from Seleucia, reconstructed with a loop handle, dated to the 2nd century AD.[58] The miniature aryballos seems to

56 In German: *Wannensarkophage*, see Andrae/Lenzen 1933, 93.
57 Radner/Squitieri 2024b, Table D1.1.
58 Valtz 2024, pl. 4.59.

Fig. C2.5.3: Jug AS 261433:031:002 from Grave 6. Photo and drawing by Andrea Squitieri (drawing generated in GigaMesh from the 3D model).

Fig. C2.5.4: Aryballos AS 261433:031:003 from Grave 6. Photo and drawing by Andrea Squitieri (drawing generated in GigaMesh from the 3D model).

Fig. C2.5.5: The skeleton of Grave 7, with the globular jar AS 262433:096:003 (1) near the head. Photo by Marco Wolf.

take inspiration from small Hellenistic oil jugs (also called gutti), such as those from the agora of Athens.[59]

Grave 7, situated in the southeastern corner of the excavation area, was partially excavated in 2023 (**Fig. C2.5.5**). At that time, the lower limbs of the skeleton were excavated. In the 2024 campaign, we could define the grave's limits and expose the rest of the skeleton (discussed in **§H2.5**). The skeleton was north-south oriented and lying in the supine position. Next to the skull, an almost complete jar with a globular body was found (AS 262433:096:003, **Fig. C2.5.6**).

Grave 6 finds		
AS number	**Short object description**	**Fig.**
AS 261433:031:002	Jug with globular body, cylindrical neck and broken handle	**C2.5.3**
AS 261433:031:003	Miniature aryballos with white glaze	**C2.5.4**
Grave 7 finds		
AS number	**Short object description**	
AS 262433:096:003	Jar with globular body	**C2.5.6**

C2.5.2 Graves with sarcophagi

Grave 8, looted in antiquity, was in the eastern part of the excavation area. It cut the floor of Building A Room 8 (**Fig. C2.5.7**). Its fill yielded fragmented potsherds and disarticulated human bones belonging to at least four individuals (described in **§H2.6**). The grave contained a relatively well-preserved tub sarcophagus measuring 1.38 × 0.52 × 0.38 m (**§E1**, **no. 299**.), whose contents had also been looted.

Grave 9 was located to the northwest of Grave 8. It, too, had been targeted by a looting pit (Pit 18), which had also damaged wall W06 of Building A (**Fig. C2.5.8**). The grave cut the floor of Building A's Room 9 and part of the wall W04, which also belonged to Building A. As mentioned, a tooth collected from the grave fill was radiocarbon dated to 130-236 calAD (**§C1.2**). The grave consisted of a partially preserved mudbrick structure with a rectangular shape

59 Rotroff 1997, pl. 83.1138-41. Thanks to Alessandra Cellerino and Enrico Foietta for pointing out the parallels of the jug and the aryballos from Grave 6.

measuring c. 2.5 × 1.5 m, covered with plaster (**Fig. C2.5.9**). Inside the mudbricks, a bone shaft was found (**§E1**, **no. 438**). This structure housed a tub sarcophagus (**§E1**, **no. 300**) measuring 1.85 × 0.60 × 0.39 m, which contained disarticulated bones belonging to at least two individuals (discussed in **§H2.7**). A hollowed bronze tube and two glass beads (**§E1**, **nos. 396**, **315**, **316**) were found in the sarcophagus. Some fragments of the sarcophagus lid (**§E1**, **no. 301**) were found lying on top of the sarcophagus (**Fig. C2.5.9**), while others were scattered in the surrounding fill. In the grave fill, a fragment of an terracotta animal figurine was found (**§E1**, **no. 368**).

Grave 11, also targeted by looting, was situated next to Grave 8 and was parallel to it (**Fig. C2.5.10**). The two graves seemed to have been installed at different times because Grave 11 was partially cut by Grave 8. Grave 11

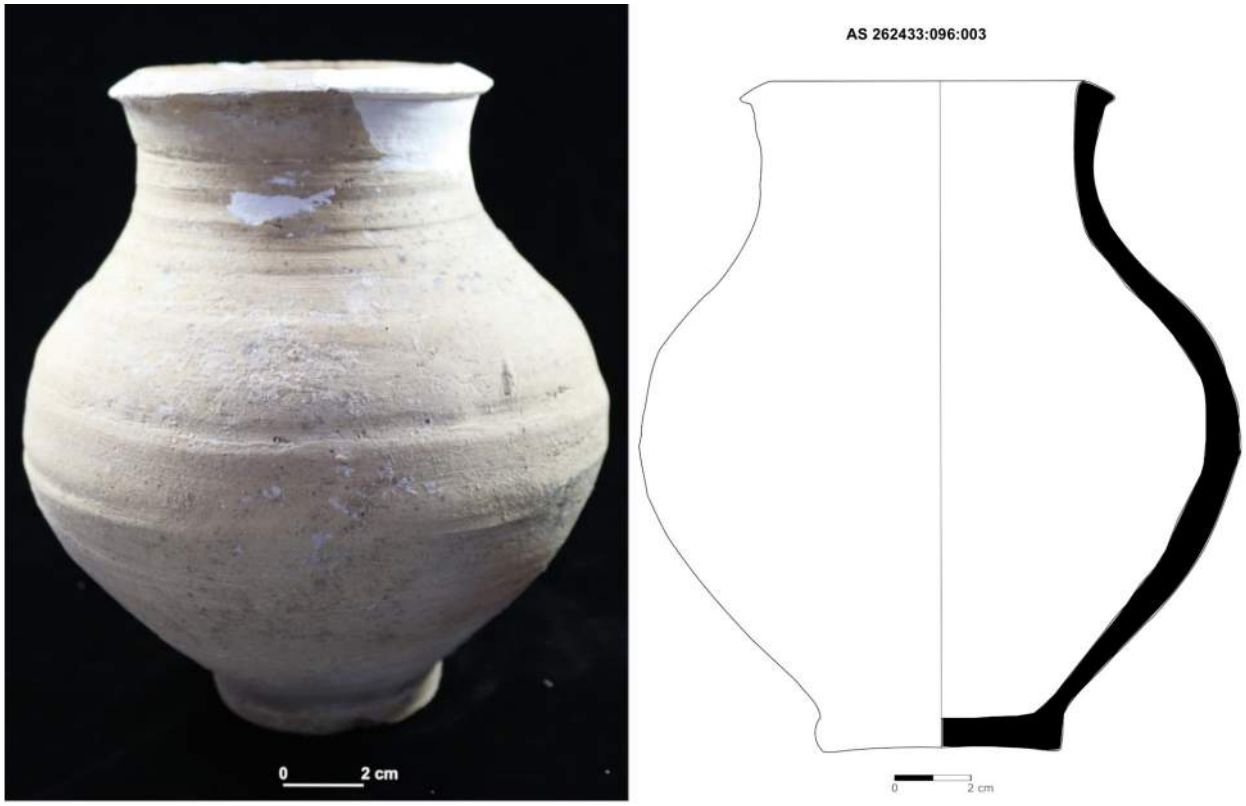

Fig. C2.5.6: Jar AS 262433:096:003 from Grave 7. Photo and drawing by Andrea Squitieri (drawing generated in Gigamesh from the 3D model).

Fig. C2.5.7: The tub sarcophagus of Grave 8, with traces of plaster along the cracks on the long side, indicating an ancient repair. Photo by Alessio Palmisano.

Fig. C2.5.8: The tub sarcophagus of Grave 9. The grave's mudbrick architecture is visible towards the southeast. Photo by Jens Rohde.

contained an almost wholly preserved tub sarcophagus measuring 1.35 × 0.50 × 0.39 m (**§E1, no. 302**), set parallel to that of Grave 8. The fill inside the sarcophagus contained some loose animal bones and pottery sherds.

Fig. C2.5.9: In situ remains of the lid of Grave 9's tub sarcophagus. Photo by Jens Rohde.

Fig. C2.5.10: The tub sarcophagus of Grave 11, next to that of Grave 8. The traces of plaster on the cracks along the base of the sarcophagus indicate ancient repairs. Photo by Jens Rohde.

Grave 8 finds			
AS number	**Short object description**	**Context**	**§E1, no.**
AS 262433:092:003	Tub sarcophagus	Grave fill	299
Grave 9 finds			
AS number	**Short object description**	**Context**	**§E1, no.**
AS 262433:094:003	Hollowed bronze tube	Sarcophagus fill	396
AS 262433:094:004	Bead, probably glass	Sarcophagus fill	315
AS 262433:094:005	Glass bead	Sarcophagus fill	316
AS 262433:090:003	Tub sarcophagus	Grave fill	300
AS 262433:090:004	Sarcophagus lid fragments	Grave fill	301
AS 262433:090:006	Terracotta animal figurine	Grave fill	368
AS 262433:111:003	Bone shaft	Mudbrick structure	438
Grave 11 finds			
AS number	**Short object description**	**Context**	**§E1, no.**
AS 263433:009:003	Tub sarcophagus	Grave fill	302

C2.6 The entrance shaft of the chamber tomb (Grave 1)

NT1 2024 Phase 8s also includes the Parthian-period chamber tomb (Grave 1) that was excavated in 2023 and removed during that campaign to investigate the struc-

Fig. C2.6.1: The steps leading to the entrance of the chamber tomb (Grave 1), carved into the older wall Locus:262433:075. Photo by Jens Rohde.

tures below.[60] During the 2024 campaign, we completed the excavation of the fill of the entrance shaft leading to the chamber tomb, which had been only partially excavated in 2023 as Locus:262433:017. The remaining fill was removed in 2024 as Locus:262433:117.

Glazed and decorated ceramic fragments (**§E1**, **no. 298**) were recovered from this fill. They were identified as belonging to sarcophagi, which were destroyed during ancient looting.

After removing the fill, the stepped entrance to the chamber tomb was uncovered (**Fig. C2.6.1**). The entrance, approximately 1.4 m wide, comprised five steps (recorded as Locus: 262433:154). These steps were cut into the earlier wall Locus: 262432:075 (excavated in 2023 and belonging to Building B, **§C2.9**). Traces of white plaster were still visible on the surface of the steps, with the bottom step consisting of a row of stones also coated in plaster.

C2.7 NT1 2023 Phase 7

NT1 2023 Phase 7 is positioned stratigraphically below NT1 2024 Phase 8a and above the structures of Building A (NT1 2023 Phase 5). This phase was already identified in 2023 as consisting of two features: the scanty remains of a wall (Locus:262432:017), cut by the chamber tomb to the southeast, and a partially excavated stone installation (Locus:261433:024), located in the northwestern part of the excavated area, which had damaged the wall Wo2 of Building A.[61] In 2024, we uncovered additional features belonging to this phase, namely three stone installations (Locus:261433:033, Locus:261433:054, and Locus:261433:057), the Pit 7, and a mudbrick installation (Locus:262433:103) (**Fig. C2.7.1**).

The three stone installations (Locus:261433:033, Locus:261433:054, and Locus:261433:057) were unearthed in the northern part of the excavation area. They had been badly eroded since they were found only 10-15 cm beneath the modern site surface. Nevertheless, it was possible to observe that they aligned in a northeast-southwest direction, spaced approximately 2.3 m apart, and showed a similar construction technique.

The best-preserved installation, Locus:261433:033, was located between the other two (**Fig. C2.7.2**). It had a square plan of 1.2 × 1.2 m and a maximum height of 35 cm. It was made of gypsum and river stones, placed somewhat irregularly to form two courses. The gap between the stones was filled with smaller gypsum stones and baked brick fragments.

The installation Locus:261433:054, located to the southwest of Locus:261433:033, despite being much more eroded, was similar to Locus:261433:033 in shape and orientation. Only one gypsum stone (measuring 47 × 54 × 25 cm) was preserved, but the remains of the installation's foundation, made of mudbrick fragments, were still visible on the ground (**Fig. C2.7.3**).

The third installation, Locus:261433:057, situated northeast of Locus:261433:033, was found in a very poor state of preservation, with only two gypsum stones remaining (**Fig. C2.7.4**). Part of it continued under the northern limit of the excavation area. Its orientation and location suggest it originally had a structure similar to the previous two installations.

The fill between the installations Locus:261433:033 and Locus:261433:054, designated as Locus:261433:055, contained many stones, fragments of baked bricks and plaster, which were most likely the result of the installations' erosion.

The function of these three installations is unclear. Given their alignment and construction technique, it is tempting to suggest that they are the remains of an architectural structure that has since been eroded.

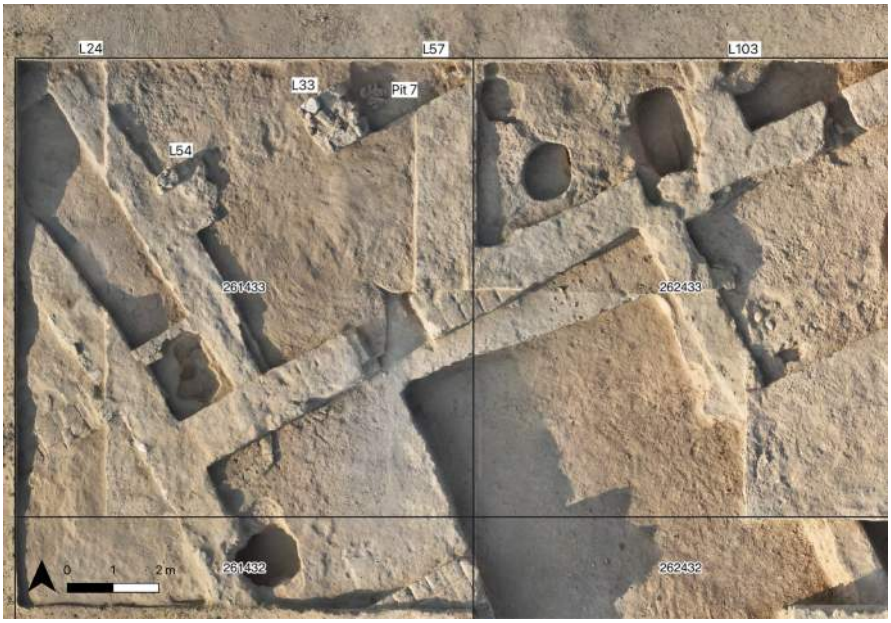

Fig. C2.7.1: The remains of NT1 2023 Phase 7 below the Parthian-period burials of Phase 8a and above the structures of Building A of NT1 2023 Phase 5. The labelled features belong to Phase 7. Orthophoto by Jens Rohde, annotations by Andrea Squitieri.

60 Kreppner/Rohde/Squitieri 2024, 105-118.

61 Kreppner/Rohde/Squitieri 2024, 118.

Fig. C2.7.2: The stone installation Locus:261433:033. Photo by Marco Wolf.

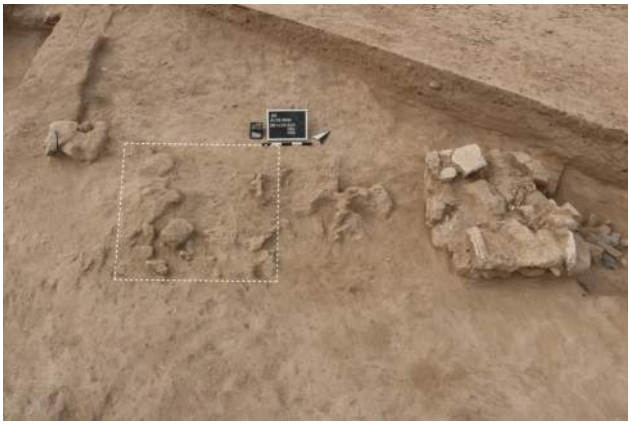

Fig. C2.7.3: The stone installation Locus:261433:054. Photo by Marco Wolf.

Fig. C2.7.4: The stone installation Locus:261433:057. Photo by Marco Wolf.

Fig. C2.7.5: The stone capping of Pit 7. Photo by Veronica Hinterhuber.

To the northeast of installation Locus:261433:033, we uncovered Pit 7. This pit cut the floor of Building A Courtyard 10. It was marked by a circular stone capping with a diameter of c. 65 cm, made of stones mixed with a few pottery sherds and gypsum fragments (**Fig. C2.7.5**). The pit cut had a diameter of c. 65 cm, increasing to 85 cm at a depth of 70 cm. The fill consisted of brown and soft soil with some ashes. It yielded many pottery sherds, bones, larger stones, and fragments of baked bricks, which had probably been exposed to fire. Small finds of various materials were also recovered from this fill (see table below). At a depth of 20 cm, a large quantity of mudbrick debris was found mixed with a considerable number of pottery sherds, including the neck of a green glazed amphora (registered as 00-00-J06, **Fig. C2.7.6**), datable to the Parthian period, and the fragments of a globular pot with two handles (registered as 00-00-J07, **Fig. C2.7.6**). The pit was excavated to a depth of c. 2.7 m, without reaching the bottom.

Finds from Pit 7 fill		
AS number	**Short object description**	**§E1, no.**
AS 261433:061:002	Simple handstone	413
AS 261433:061:005	Perforated stone	414
AS 261433:061:006	Ceramic stilt	445
AS 261433:061:007	Ceramic object (part of foot or handle)	463
AS 261433:061:008	Two fragments of a bronze shaft	385
AS 261433:061:010	Bead, probably glass	318
AS 261433:061:011	Carnelian bead	304
AS 261433:061:016	Bead, probably glass	319

Fig. C2.7.6: The green-glazed amphora (AS 00-00-J06) and the globular vessel (AS 00-00-J07) from Pit 7. Photos and LAP drawings by Poppy Tushingham.

Finally, a mudbrick installation, registered as Locus: 262433:103, was also assigned to NT1 2023 Phase 7. It was identified in the northeastern portion of the excavated area, where it cut wall W07 of Building A (see **Fig. C2.7.1**). The original shape and function of this installation are not clear.

D2.8 NT1 2023 Phase 5: Building A and "Room 5"

The excavation of Building A started in 2023 when we partially exposed three rooms, named Rooms 1, 2, and 3 (**Figs. C2.8.1-2**).[62] The building was assigned to the stratigraphic phase NT1 2023 Phase 5. Soon after the 2023 campaign, we obtained radiocarbon dates from the floor deposits of these rooms that ranged between 341 calBC and 52 calBC (95.4% probability).[63] During the 2024 campaign, we resumed excavations in Rooms 1 and 2 and uncovered additional rooms belonging to Building A, namely Rooms 7, 8, and 9, along with the remains of an open area named

62 Kreppner/Rohde/Squitieri 2024, 122-126.
63 Radner/Squitieri 2024, Table D1.1.

Fig. C2.8.1: Building A and its features, with the white-coloured squares covering older features. Created by Jens Rohde, annotated by Andrea Squitieri.

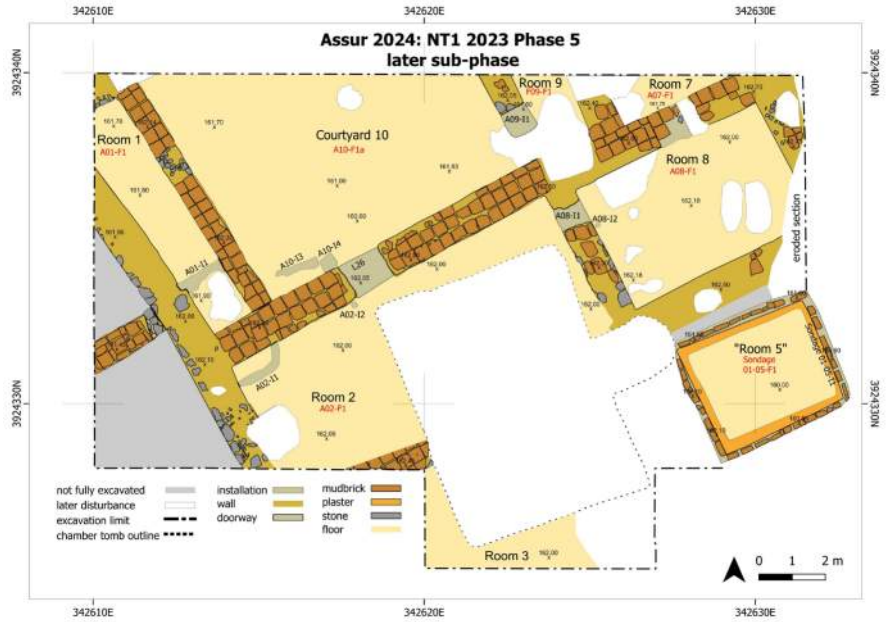

Fig. C2.8.2: Plan of the later sub-phase of Building A (NT1 2023 Phase 5). Plan and annotations generated in QGIS by Adrian Westermann.

Courtyard 10. A significant outcome of the 2024 campaign was the discovery that the unit called "Room 5," which was partially excavated in 2023 within the baulk between our trench and the 2002 SBAH trench ("Sondage 1", see **§C1.1**),[64] belonged, in fact, to Building A and was originally designed as an underground structure, identified as a silo. The following sections discuss the remains uncovered in the rooms and courtyard of Building A, with "Room 5" presented in **§C2.8.7**.

C2.8.1 Room 1

Room 1 is in the northwestern part of the excavated area of Building A, to the west of Courtyard 10 (**Figs. C2.8.1-2**). In 2023, c. 5 m² of this room was uncovered; in 2024, an additional 6 m² was exposed. The room is bounded to the northwest by wall W02, northeast by wall W03, southwest by wall W01, and southeast by wall W04. The latter is a long wall of about 17 m that crosses Building A in an east-west direction, shared by Room 1, Courtyard 10, Room 9, Room 7 to the north, and Room 2 and Room 8 to the south. The 2024 investigations established that Room 1 belonged to a later architectural sub-phase of Building A. Room 1 did not exist in the earlier sub-phase when Courtyard 10 occupied a much larger space. In the later sub-phase, Wall W03 was erected, thus creating Room 1.

Walls W01 and W02, bordering Room 1 to the southwest and northwest, respectively, were already uncovered in 2023 and badly preserved. Their stone foundations were still visible, but almost no mudbrick was distinguishable. W02, moreover, had been damaged by a younger installation, assigned to NT1 2023 Phase 7 (**§C2.7**).[65]

W03, bordering Room 1 to the northeast, extended for about 7.7 m, and it was thinner than all the other walls of Building A. It had a width of 65 cm, corresponding to one and a half mudbricks, measuring 38 × 39 cm and 38 × 20 cm, respectively (**Fig. C2.8.3**). This wall did not bind with walls W02 and W04, indicating a later construction. The faces of W03 were covered with plaster, particularly well preserved on

64 Radner/Squitieri/Rohde 2024, 138-139.

65 Kreppner/Rohde/Squitieri 2024, 118-119.

Fig. C2.8.3: Walls W2 and W3 bordering Room 1 of Building A. Photo by Veronica Hinterhuber.

Fig. C2.8.4: The installation A01-I1, separating Room 1 into two spaces. Photo by Veronica Hinterhuber.

the western side of the wall, approximately 3 cm thick, and made of brownish-red clay with inclusions. As the plaster on the east side was damaged, we could observe that the wall was built on a series of stones 20 to 25 cm in diameter. These stones were located approximately 25 cm above the older floor of Courtyard 10 (**§C2.8.6**), confirming the wall's construction in a later building phase. No entrance leading to Room 1 could be identified. Upon examination, a disturbance in the northern segment of wall W03 proved not to be a doorway. A square ceramic object was found within this damaged portion of W03 (**§E1**, **no. 462**).

At some point after its creation, Room 1 was divided into two smaller spaces by a narrow installation named A01-I1, which was approximately 1.5 m long and c. 30 cm wide (**Fig. C2.8.4**). The resulting two spaces measured c. 9 m² to the north and 2 m² to the south. This installation was constructed using baked bricks mixed with stones to form four courses and reached a maximum height of 30 cm above the floor level. The baked bricks varied in size, with the largest on the uppermost course measuring 33 × 28 × 7 cm. Sparse remains of plaster were also noted. The installation was partially disturbed by the younger Pit 6, belonging to phase NT1 2024 Phase 8b (**§C2.4**).

The floor of Room 1 was better preserved to the north of the installation A01-I1, where it consisted of a greyish beaten earth surface with some white inclusions, ashy spots, and embedded pottery sherds and small pebbles. The floor deposit, A01-D02-01, consisted of light brown silty soil with charcoal pieces, many pottery sherds, bones, and pebbles. Seven beads and a circular bronze item were collected from this deposit (**§E1**, **nos. 320-325**, **337**, **393**). To the south of installation A01-I1, the room floor and the floor deposit above it had been badly damaged by Pit 6 (**§C2.4**).

The upper fills of Room 1 (registered as A01-D01-01 to A01-D01-05) contained mudbrick debris and baked brick fragments embedded in greyish-brown soil, which yielded pottery sherds and bones. Loom weights, stone, metal, and ceramic items were collected from this fill (see table below).

Room 1 finds			
AS number	**Short object description**	**Context**	**§E1, no.**
AS 261433:037:003	Ceramic stilt	Upper room fill	443
AS 261433:037:004	Iron ring	Upper room fill	344
AS 261433:037:005	Bronze open ring	Upper room fill	345
AS 261433:037:007	Loom weight	Upper room fill	425
AS 261433:037:008	Bronze ring	Upper room fill	346
AS 261433:037:009	Loom weight	Upper room fill	426
AS 261433:037:011	Stone weight or polisher	Upper room fill	411
AS 261433:040:008	Circular bronze item	Floor deposit	393
AS 261433:040:009 -014	Six glass beads	Floor deposit	320-325

Room 1 finds			
AS number	**Short object description**	**Context**	**§E1, no.**
AS 261433:040:015	Coral bead	Floor deposit	337
AS 261433:063:001	Rectangular ceramic object	From inside wall W03	462

C2.8.2 Room 2

Room 2 is southeast of Room 1 and south of Courtyard 10 (**Figs. C2.8.1-2**). It was partially excavated in 2023 when it was established that a large portion of it had been obliterated by the construction of the chamber tomb (Grave 1) in the Parthian period (NT1 2023 Phase 8a). In 2024, we exposed the remaining portions of Room 2. If one considers the portion cut by the chamber tomb, Room 2 originally had an area of about 47 m². The room was bordered to the north by wall W04, to the east by wall W06, to the south by wall W05, and to the west by wall W01.

Wall W01 was not well preserved as it was damaged by Pit 8 and by the looted Grave 2 (Locus:261432:012: NT1 2023 Phase 9), already identified in 2023 (**§C2.1**).[66]

Wall W04 was constructed on a foundation of stones measuring 16 to 35 cm in diameter. The mudbricks were laid on top in a pattern consisting of two full-sized bricks and one half-sized brick (measuring c. 38 × 38 × 8 cm and 38 × 20 × 8 cm, respectively). A gap of about 1.2 m in wall W04 constituted the passage (registered as Locus: 261433:026) connecting Room 2 to Courtyard 10. To the west of the passage, and up to the corner with wall W01, wall W04 was preserved to a height of 38-58 cm above the floor; it had a width of c. 1 m and a length of c. 4.5 m. To the east of the passage and up to the corner with wall W06, wall W04 had a preserved height of 45-55 cm above the floor, a width of about 1 m, and a length of c. 5 m. The wall plaster, preserved on the southern face, was made of brownish-red clay with white inclusions. It had a thickness of 3-4 cm.

The floor of Room 2, designated as A02-F1, consisted of a greyish-brown beaten clay surface with white inclusions and some ashy spots. Some pottery sherds, pebbles, and animal bones were embedded in it.

In the northwestern corner of Room 2, we found the installation A02-I1, set on top of the floor (**Fig. C2.8.5**). It consisted of a row of mudbricks enclosing a small area measuring c. 1.5 × 0.5 m. Another installation, A02-I2, was found next to the passage Locus:261433:026 (**Fig. C2.8.5**). It consisted of a hole that may have accommodated a door socket, which was not found in the excavation.

The deposit right above the floor of Room 2, named A02-D02-01, consisted of crumbly, greyish-brown silty soil mixed with pottery sherds, animal bones, pebbles, mudbrick debris, and charcoal fragments. A carnelian bead (**§E1**, **no. 305**) and an obsidian blade (**§E1**, **no. 377**) were collected from this deposit.

The upper fill of Room 2, A02-D01-02, was made of light-brown soil with a soft consistency. The material was a mix of pottery sherds, pebbles, animal bones, and mudbrick debris. A small bronze disc (**§E1**, **no. 397**) was found in this deposit, which may be a very corroded and now unrecognisable coin. It is worth mentioning that a bronze fibula was found while cleaning the upper deposit of Room 2 in the area excavated in 2023 (**§E1**, **no. 343**).

Room 2 finds			
AS number	**Short object description**	**Context**	**§E1, no.**
AS 261433:046:012	Carnelian bead	Floor deposit	305
AS 261433:046:015	Obsidian blade	Floor deposit	377
AS 262433:098:003	Bronze disc	Upper room fill	397
AS 261432:007:008	Bronze fibula	Upper room fill	343

C2.8.3 Room 7

Room 7 is located east of Room 9 and north of Room 8 (**Figs. C2.8.1-2**). Only 2.5 m² of this room was exposed, as the rest extended below the northern excavation limits. Wall W07 delimits the room to the west, and wall W04 to the south.

Wall W04, damaged by Pit 2 (**§C2.4**), was preserved to 50-60 cm above the room's floor. Wall W07 had a preserved width of about 1 m and was exposed over a length of c. 1 m. In its northernmost part, it had been cut by the later installation Locus:262433:103, belonging to NT1 2023 Phase 7 (**§C2.7**). In the southern part of the wall, it was possible to see that it was preserved to a height of c. 70 cm above the floor level and had a base composed of stones of diameters ranging from 15 to 20 cm. The wall was covered by plaster, approximately 1-2 cm thick, which was only preserved on the eastern side and consisted of brownish-red clay with pebbles and white inclusions.

The floor of Room 7, registered as A07-F1, consisted of a greyish-coloured beaten earth surface with some pottery sherds, pebbles, and stones embedded in it. It was

66 Kreppner/Rohde/Squitieri 2024, 105.

Fig. C2.8.5: Room 2, bordered to the north by wall W04, with installations A02-I1 and A02-I2. Photo by Veronica Hinterhuber.

covered by the deposit A07-02-01, which consisted of soft, greyish-brown soil with a few pottery sherds, pebbles, mudbrick debris, and some bones.

The upper fill of Room 7, A07-01-01, consisted of brown soil with a soft consistency, containing a few potsherds. Notably, a bronze coin (registered as AS 262433:101:002, discussed in **§E2**), dating to the reign of either Antiochus VIII (r. 125-96 BC) or Antiochus XII (r. 87-82 BC), was discovered within this deposit. As it came from the upper fill of the room, the coin cannot be directly related to the building's use period.

Room 7 finds		
AS number	**Short object description**	**Context**
AS 262433:101:002	Seleucid bronze coin (**§E2**) (Antiochus VIII or Antiochus XII)	Upper room fill

D2.8.4 Room 8

Room 8 is located south of Rooms 7 and 9 and east of Room 2 (**Figs. C2.8.1**, **C2.8.2**). Approximately 22 m² of this room was exposed. The eastern portion of the room had been damaged by Pit 15 (**§C2.4**) and by the erosion of the western section of the 2002 SBAH trench (**Fig. C2.8.2**). The room is bordered by wall W04 to the north, W06 to the west, W08 to the south, and W09 to the east.

Wall W04, excavated over a length of about 4 m, had been damaged by Pit 2 of the NT1 2023 Phase 8b (**§C2.4**). This pit also damaged the passage between Room 8 and Room 7; nevertheless, it was possible to observe that this passage underwent two phases. While it was open in the earlier phase, it was blocked later by extending wall W04 towards the east by adding two and a half mudbricks, which were set differently from the rest of the wall's bricks. These added bricks that blocked the passage have been registered as installation A08-I3.

Wall W06 was excavated over a length of c. 4.5 m and was about 90 cm wide. The northern section of the wall reached a height of 60 cm above the floor level, while the southern portion was preserved to a height of 20 cm. At the base of the wall, one course of stones could be observed, varying in diameter from 15 to 25 cm. The plaster, approximately 2-3 cm thick, was partially preserved on both sides of the wall. In wall W06, the passage between Room 8 and Room 2 was located. This was marked by a door socket (A08-I2) and a threshold (A08-I1), about 60 cm wide, consisting of a slightly elevated and more reddish beaten earth surface, with pottery sherds lying flat on it.

Wall W08 had a preserved width of about 1 m and was exposed over a length of about 5 m. It was severely damaged by the construction of the Parthian-period chamber tomb to the west and by the cut of Pit 14 **(§C2.4)**. As a result, only the stone base of the wall had survived. This

was composed of stones of different sizes, with dimensions ranging from 6 to 15 cm, and larger stones 30 cm long and 15 cm wide.

Wall W09 was poorly preserved because it had been damaged by Pit 15 (**§C2.4**) and by the erosion affecting the western section of the 2002 SBAH trench. As a result, the wall's preserved part had a length of about 65 cm and a height of less than 40 cm. Only four incomplete mudbricks of this wall were discernible. This wall appears bound to the northern wall W04, indicating a contemporaneous construction.

The floor of Room 8 (A08-F1) consisted of a greyish-coloured beaten earth surface with pottery sherds, pebbles, and stones embedded in it. Unfortunately, it was not well preserved due to severe damage caused by later disturbances, namely the installation of Graves 8 and 11 and Pits 10, 11, 12, and 13 (**§C2.4-5**).

The floor deposit of Room 8, named A08-D02-01, was made of soft, greyish-brown soil containing a few pottery sherds, pebbles, bones, and charcoal. A terracotta bird head fragment (**§E1**, **no. 369**), a stone pounder/polisher (**§E1**, **no. 416**), and a carnelian bead (**§E1**, **no. 309**) were collected from this deposit. This deposit was, in turn, covered by the upper fill A08-D01-01, containing mudbrick debris and additional small finds, including a terracotta human head (**§E1**, **no. 354**) (see table below).

Room 8 finds			
AS number	**Short object description**	**Context**	**§E1, no.**
AS 262433:107:005	Stone pounder/ polisher	Floor deposit	416
AS 262433:107:008	Carnelian bead	Floor deposit	309
AS 262433:107:012	Terracotta bird head	Floor deposit	369
AS 262433:102:003	Terracotta human head	Upper room fill	354
AS 262433:102:004	Stone tool, possibly a pestle	Upper room fill	418
AS 262433:102:005	Bead, possibly carnelian	Upper room fill	307
AS 262433:102:006	Bronze shaft	Upper room fill	388

D2.8.5 Room 9

Room 9 is between Courtyard 10 and Room 7 (**Figs. C2.8.1-2**). Only 2.5 m² of this room has been exposed as it continued under the northern limit of the excavation area. This room had a narrow, elongated shape, with the excavated area measuring 1.6 m in width and 2.3 m in length. To the west, it was delimited by wall W06, to the east by wall W07, and to the south by wall W04. The southern part of wall W06 was poorly preserved due to the damage caused by the construction of Grave 9 and Pit 18 (**§C2.4-5**).

Nevertheless, it was possible to identify a passage within this wall connecting Room 9 to Courtyard 10. This passage was marked by the threshold A09-I1, made of a beaten earth surface, slightly more elevated than the room's floor, with pottery sherds lying flat. Room 9's floor (A09-F1) was poorly preserved due to the disturbance caused by Grave 9 and Pit 18, which also damaged the grave. These disturbances also made distinguishing a distinct deposit above the floor impossible. The upper room's mudbrick debris fills were named A09-D01-02 and A09/10-D01-01 (the latter also covered the doorway leading to Courtyard 10).

C2.8.6 Courtyard 10

Courtyard 10 is located east of Room 1 and north of Room 2 (**Figs. C2.8.1-2**), with about 48 m² of this space uncovered. It was delimited to the southwest by the wall W04, which accommodated the passage Locus:261433:026 connecting the courtyard to Room 2. As mentioned above when describing Room 1, the courtyard underwent two construction phases. In the earlier phase, it was bordered to the west by wall W01, as Room 1 did not yet exist. In the later phase, wall W03 was constructed parallel to wall W01. This reconfiguration created Room 1 and led to a significant reduction in the courtyard's size.

The structural changes that Courtyard 10 underwent can also be observed in the sequence of superimposed floors identified in the courtyard. In the southwestern courtyard area, where we excavated to investigate the structures below Building A, we identified the construction surface, A10-I5, of Courtyard 10's older floor (**Fig. C2.8.6**). It consisted of beaten earth with a greyish colour, with some stones and pebbles embedded in it. Directly above it, there was a 10 cm thick deposit, named A10-D03-01, consisting of a brownish and very crumbly clayey soil mixed with mudbrick debris, pottery sherds, bones, and a ceramic disc (**§E1**, **no. 456**).

On the construction surface A10-I5 and embedded in the deposit A10-D03-01, the installations A10-I3 and A10-I4 had been built (**Fig. C2.8.7**). The installation A10-I3 consisted of baked bricks extending over 3 × 1.2 m. It was made of three rows of 10 baked bricks measuring c. 25 × 23 × 5 cm, with a trapezoid shape, which was bordered to the north by larger baked bricks measuring c. 33-35 × 36 × 6 cm. This installation extended to the west under wall W03, confirming its stratigraphic relation to the ear-

lier construction phase of Courtyard 10. The installation A10-I4, located immediately north of A10-I3, consisted of one row of 10 mudbricks measuring c. 40 × 40 cm, set in a northeast-southwest orientation, with the westernmost bricks continuing under wall W03.

The courtyard's earlier floor, A10-F1b, extended around these two installations and was exposed over the entire excavated area of Courtyard 10. This floor abutted wall W04 to the south and the installations A10-I3 and A10-I4 and wall W06 to the east. Towards the west, it went below the later wall W03, while to the north, it was limited by the trench borders. This floor was made of a beaten earth surface of a greyish colour with some white spots and ashy spots, containing only a few embedded pottery sherds and bones. It had been severely damaged by wall collapse and numerous animal burrows.

Adjacent to the passage Locus:261433 :026 was the installation A10-I2 (**Fig. C2.8.8**), located directly on top of floor A10-F1b and abutting wall W04. This installation consisted of a single mudbrick,

Fig. C2.8.6: Excavation below the older floor of Courtyard 10, in which the construction surface A10-I5 was uncovered. Photo by Veronica Hinterhuber.

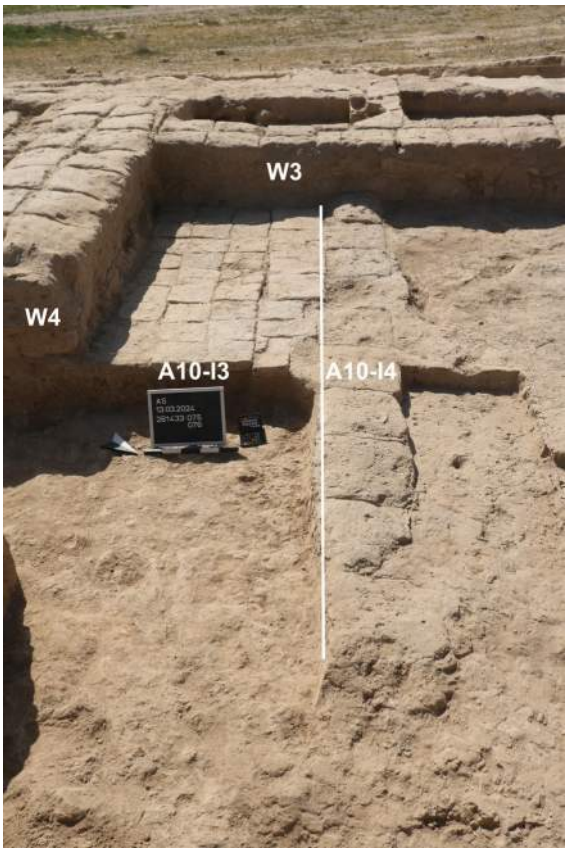

Fig. C2.8.7: The installations A10-I2 and A10-I4 in the southwestern corner of Courtyard 10, which belong to the courtyard's older construction phase. Photo by Veronica Hinterhuber.

Fig. C2.8.8: Installation A10-I1 in the southwestern corner of Courtyard 10, which belongs to the courtyard's younger construction phase, and installation A10-I2, which belongs to both the older and the younger construction phases. Photo by Veronica Hinterhuber.

Fig. C2.8.9: The younger floor of Courtyard 10 with the installation A10-I1 in the background. Photo by Veronica Hinterhuber.

measuring c. 42 × 42 cm, with a circular mark on the top. The mudbrick was covered with two layers of plaster, each about 1 cm thick. Interestingly, the upper layer of plaster extended to the later floor of Courtyard 10, indicating that the installation's use was related to both the earlier and the later floor of Courtyard 10.

Above floor A10-F1b, we encountered the younger floor of Courtyard 10, registered as A10-F1a (**Fig. C2.8.9**). It consisted of a beaten earth surface of a greyish colour with only a few embedded pottery sherds, bones, and pebbles. This floor abutted walls W02, W03, and W04 and covered the previously mentioned installations A10:I3 and A10:I4. This floor was visible towards the western and southern edges of the courtyard; however, towards the middle of the courtyard, it was challenging to distinguish it from the older floor A10-F1b.

On top of floor A10-F1a, the installation A10-I1 was found in the corner between walls W04 and W03 (**Figs. C2.8.8-9**). It was made of a row of half-sized mudbricks measuring c. 30 × 16 cm, with a total length of 1.8 m and a width of 70 cm, covered with plaster. The deposit within the installation consisted of very soft, greyish soil with a noticeable concentration of ashes. The installation's fill yielded a bone ring (**§E1**, **no. 348**) and a loom weight (**§E1**, **no. 427**).

The courtyard's younger floor, A10-F1a, was covered by a deposit designated as A10-D02-01. This deposit was made of greyish-brown soil with a few ashy spots. Only a few pottery sherds, bones, and tiny bronze fragments were collected from this deposit. Above A10-D02-01, we identified three superimposed deposits: A10-D01-01, A10-D01-02, and A09/10-D01-01, with the latter also covering the adjacent Room 9. Various items were collected from these upper deposits, listed in the table below. The most notable among them is a bronze fibula dated to the 7th/6th century BC (**§E1**, **no. 342**), which, given its context and chronology, cannot be related to the use period of Building A.

Courtyard 10 finds			
AS number	**Short object description**	**Context**	**§E1. no.**
AS 262433:104:004	Carnelian bead	Upper fill	309
AS 262433:104:003	Polisher	Upper fill	415
AS 261433:048:002	Bronze shaft with braid decoration	Upper fill	384
AS 261433:048:003	Carnelian bead	Upper fill	306
AS 261433:056:004	Glass bead	Upper fill	327

Courtyard 10 finds			
AS number	**Short object description**	**Context**	**§E1. no.**
AS 261433:058:006	Bronze needle	Upper fill	381
AS 261433:058:007	Possibly a ceramic spindle whorl	Upper fill	436
AS 261433:058:003	Flat bronze object	Upper fill	395
AS 261433:058:012	Bronze fibula	Upper fill	342
AS 261433:058:014	Conic ceramic object	Upper fill	461
AS 261433:058:016	Stone tool	Upper fill	417
AS 261433:058:017	Egyptian blue bead	Upper fill	334
AS 261433:058:018	Lapis lazuli pendant	Upper fill	314
AS 261433:058:021	Bronze applique	Upper fill	394
AS 261433:058:022	Polisher	Upper fill	412
AS 261433:058:023	Glass bead	Upper fill	328
AS 261433:058:024	Glass bead	Upper fill	329
AS 261433:058:025	Snail shell, possibly a bead	Upper fill	340
AS 261433:058:026	Ceramic stilt	Upper fill	444
AS 261433:062:002	Bone ring	Installation A10-I1	348
AS 261433:062:004	Loom weight	Fill A10-I1	427
AS 261433:074:003	Ceramic disc	Fill A10-D03-01	456

C2.8.7 "Room 5"

The unit "Room 5" was partially excavated in 2023 within a separate sounding area, Sondage 1, between the 2023 trench NT1 and the 2002 SBAH trench (see **§C1**). At the very start of the 2023 excavations, it was possible to see the fills of "Room 5" along the western section of the SBAH trench (**Fig. C2.8.10**). These fills resembled those of a pit, as they formed a deep concave depression containing thick layers of ashes. During the 2023 excavations, we reached the southern and western portions of the floor of "Room 5" and exposed an area of about 1.5 m².[67]

At that time, a charcoal sample and a seed were collected from the deposit right above the floor and sent for radiocarbon dating. The first was dated to 1416-1278 calBC, with 95.4% probability, while the second was dated to 771-545 calBC, with 95.4% probability.[68] These two contrasting dates

Fig. C2.8.10: Photo of the western section of the 2002 SBAH trench, taken at the start of the 2023 excavation campaign, showing the fills of "Room 5" before excavation. Photo by Jens Rohde.

were also at odds with the evidence from the pottery coming from the fills, which suggested a Hellenistic/Parthian date.[69]

This discrepancy in dating prompted us to resume investigations in "Room 5". During the 2024 campaign, we identified the borders of "Room 5". We established not only that this unit belonged to Building A but also that it constituted an underground unit without a doorway, akin to a silo (**Figs. C2.8.1-2**).

C2.8.7.1 The architecture and fills of "Room 5"

The main characteristic of "Room 5" is that it was not bound by walls but rather by a lining (registered as Sondage 01-05-I1) made of a row of half mudbricks, measuring 36 × 16 × 12 cm (**Fig. C2.8.11**). These mudbricks were set in 13 preserved courses and were covered by plaster, still partially preserved. The lining narrowed down towards the bottom so that at the top, "Room 5" measured about 15 m², while it measured about 10 m² at the bottom. The height of the lining was c. 2.3 m, thus defining a preserved volume of c. 20 m³.

Another characteristic of "Room 5" is that its floor, registered as Sondage 01-05-F1, was about 2.3 m lower than the floors of the other rooms of Building A. It was a greyish-whitish hard surface covered with plaster, directly connected to the plaster covering the room's lining. Some stones were embedded in the floor, which may indicate the existence of a stone substructure beneath it.

Right above the floor, we identified a deposit of hard, reddish, silty-clayey soil mixed with patches of soft and

67 Radner/Rohde/Squitieri 2024, 138-139.

68 Radner/Squitieri 2024b, Table D1.1.

69 Kreppner/Richter/Squitieri 2024, 149.

Fig. C2.8.11: "Room 5" at the end of the 2024 excavation. The white lines show the gap between the unit's mudbrick lining and the surrounding structures. Photo by Jens Rohde.

ashy soil (registered as Sondage 01-05-D02-01). From this deposit, the rim fragment of a frit vessel was collected (**§E1**, **no. 376**). Above the floor deposit, we encountered a thick sequence of fills containing mudbrick debris mixed with abundant ashes. These fills, along with the room's mudbrick lining, were, in turn, covered by the deposit registered as Sondage 01-05-D01-02.

C2.8.7.2 Stratigraphic relations of "Room 5" and its function

Because of the peculiar architecture of "Room 5" among the other structures of Building A, it is worth offering additional detail about its stratigraphic relations and an interpretation of its function. As we have seen above, "Room 5" was surrounded not by walls but rather by a mudbrick lining. To the east, this lining cut the Iron Age walls excavated by the SBAH team in 2002 (**Figs. C2.8.12**). Towards the south, the lining was against the wall Locus:262432:089, excavated in 2023, which separated "Room 5" from another unit, also excavated in 2023, and called Room 6 (the latter yielded charcoal samples on its floor dated to the Iron Age)[70] (**Figs. C2.8.12**). The stone base of wall Locus:262432:089 sat on top of a row of mudbricks likely belonging to an older wall, which was also cut by the construction of "Room 5". Towards the west, the lining of "Room 5" was set against the wall Locus:262432:075, excavated in 2023, which constituted the eastern border of Building B Unroofed Area 4, dated to the Iron Age (**§C2.9**) (**Figs. C2.8.12**). Finally, to the north, the lining of "Room 5" was set against a partially excavated wall located just beneath the wall W08, belonging to Building A (**Fig. C2.8.13**).

These observations indicate that the construction of "Room 5" damaged parts of the surrounding Iron Age architecture; therefore, we can rule out a construction date before the Iron Age. This makes the Middle Assyrian radiocarbon date, obtained from the charcoal piece collected in 2023, irrelevant to the construction date of "Room 5". This charcoal piece was presumably part of the mudbrick remains that had collapsed on the floor.

Another relevant observation is that the mudbrick lining of "Room 5" was covered by the deposit named Sondage 01-05-D01-02 (**Fig. C2.8.14**), which had been cut by Grave 7 (NT1 2024 Phase 8a). As this grave was dated to the Parthian period (**§C2.5**), this period represents the *terminus ante quem* for the construction of "Room 5", further suggesting that this unit belonged to Building A.

Fig. C2.8.12: The walls cut by "Room 5": W8 of Building A (north), L75 of Building B (west) and L89 (south). Photo by Jens Rohde.

Fig. C2.8.13: The mudbrick lining of "Room 5" leaning against wall W08 of Building A. Photo by Jens Rohde.

70 Radner/Squitieri/Rohde 2024, 137.

Fig. C2.8.14: The deposit 01-05-D01-02, covering the mudbrick lining of "Room 5" and cut by Grave 7. Photo by Jens Rohde.

Concerning its use, we interpret "Room 5" as an underground silo used for storing food resources.[71] This interpretation is based on its significantly lower floor level than the other floors of Building A and the plaster covering its lining and floor (see also a discussion in **§I2.4.1**). After the abandonment of Building A, "Room 5" appears to have gradually filled with waste material and ashes. This is also suggested by the wide range of artefacts recovered from the fills, including textile tools, stone tools, figurines, weapons, beads, and metal production waste.

"Room 5" finds		
AS number	**Short object description**	**§E1, no.**
AS 262433:148:003	Fragment of a mortar bowl	421
AS 263433:016:004	Carnelian bead	311
AS 263433:016:006	Two fragments of pottery slag	473
AS 263433:016:007	Fragment of an 'Assyrian clay hand'	372
AS 262433:141:003	Bone shuttle fragment	432
AS 262433:141:004	Blue glass fragment	330
AS 262433:141:005	Bone shuttle fragment	433
AS 262433:141:006	Loom weight	428
AS 262433:141:007	Loom weight	429
AS 262433:140:003	Carnelian bead	310
AS 262433:139:003	Bronze ring fragment	349
AS 262433:139:004	Bent lead item	398
AS 262433:137:003	Bronze nail shaft	379
AS 262433:137:004	Iron rod fragment	389
AS 262433:137:006	Spearhead	391
AS 262433:137:007	Spindle whorl	437
AS 262433:135:003	Perforated pottery sherd	450
AS 262433:135:004	Bronze arrowhead	390
AS 263433:017:004	Fragment of a vessel rim made of frit	376

71 Such underground silos are commonly used in the region until today, as Sakhar Mohammad Ajaj (SBAH Sherqat) explained to us in detail, emphasising the cooling and the protection against pests this architecture provides. For the palaeobotanical view on the matter, which supports the identification, see **§I2.4.1.4**.

C2.9 NT1 2023 Phase 4: Building B

Building B, assigned to the NT1 2023 Phase 4, was partially exposed in 2023. At that time, we uncovered two walls, namely W11 to the north and Locus:262432:075 to the southeast, which defined an open space dubbed Unroofed Area 4, measuring about 44 m². In 2024, we uncovered a space north of wall W11, named Room 11 **(Figs. C2.9.1–2)**. A seed collected through flotation from the floor deposit of Room 11 was radiocarbon dated to 778-551 calBC (**§C1.2**).

C2.9.1 Room 11

Room 11 is bordered to the south by wall W11, which also separates this unit from the Unroofed Area 4 (**Figs. C2.9.1–2**). The room is further defined by wall W10 to the north and, possibly, by wall W12 to the east. The room's

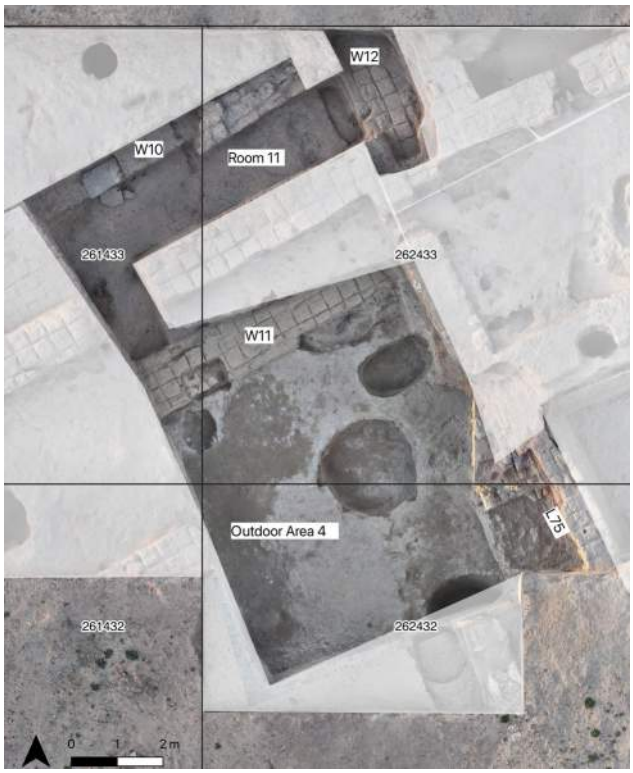

Fig. C2.9.1: Building B and its features. White-coloured areas serve to cover up older structures. Created by Jens Rohde, annotated by Andrea Squitieri.

Fig. C2.9.2: Plan of Building B. Plan and annotations generated in QGIS by Adrian Westermann.

Fig. C2.9.3: Room 11 with the installations B11-I1 (threshold) and B11-I3. The white dashed line indicates the mudricks used to block, or narrow, the entrance. Photo by Veronica Hinterhuber, annotated by Andrea Squitieri.

western portion could not be investigated as it continued under the structures of Building A. Building A's wall W04, occupying the middle of the room, was not removed; hence, only 13 m² of Room 11 could be exposed. Despite being only partially excavated, Room 11 is notable for its size as it has an excavated length of c. 7 m and a width of about 4 m.

The wall W10 (**Fig. C2.9.3**) was exposed over a length of c. 7.5 m, it had a maximum width of c. 60 cm and a preserved height ranging from 65 to 95 cm from the floor level. It was found in very poor condition, thus making it difficult to delineate the single mudbricks. The mortar between the bricks was made of greyish-brown clay with a dry and crumbly consistency. The wall plaster, up to 4 cm thick and preserved only in some spots, was made of reddish-brown clayey soil with white inclusions.

Within wall W10, we identified a doorway marked by the stone threshold B11-I1 (**Fig. C2.9.3**). Based on the threshold structure, we determined that the doorway underwent three phases. In the latest phase, the doorway had been completely sealed off with mudbricks, found lying directly on the threshold (**Fig. C2.9.3**). In the intermediate phase, the passage was clear, and the threshold, made of multiple stone slabs, was c. 85 cm wide and c. 45 cm high (**Fig. C2.9.4**). A stone step, approximately 50 cm long, was added directly in front of the threshold to accommodate this height. Finally, in the oldest phase, the threshold was 1.3 m wide and only about 35 cm high, thus eliminating the need for a step. The threshold's oldest phase could be reconstructed because the stone slabs belonging to this phase protruded into the wall masonry (**Fig. C2.9.4**).

Wall W12, only partially exposed, had been severely damaged by the later construction of Building A in the Hellenistic period and the installation of Grave 9 in the Parthian period. It likely served as the eastern boundary of Room 11, though this is difficult to confirm for two main reasons. Firstly, the connection between W12 and walls W10 and W11 could not be identified. Secondly, the bricks of W12, measuring 33 × 33 cm, are smaller than those of W10 and W11, which measure 36-38 × 36-38 cm. Hence, further investigation is needed to clarify the eastern limit of Room 11.

The floor of Room 11 (registered as B11-F1) consisted of a package of closely superimposed earth surfaces that had been laid out throughout the period of use. The uppermost floor of the package represents the last floor used (B11-F2). Room 11's floor (registered as B11-F1) was a brown,

Fig. C2.9.4: The older phase of threshold B11-I1, indicated by the white arrow. Photo by Veronica Hinterhuber, annotated by Andrea Squitieri.

Fig. C2.9.5: The installation B11-I2 in the western portion of Room 11. Photo by Veronica Hinterhuber, annotated by Andrea Squitieri.

beaten-earth surface with pottery sherds, charcoal fragments, and pebbles embedded in it. Some parts showed burnt traces, which were reddish, black, and white. The floor abutted W10 to the north and W11 to the south.

On the floor and west of the entrance B11-I1, we found the installation B11-I3 **(Fig. C2.9.3)**. It was made of one baked brick, measuring 35 × 35 cm, placed on top of stones and two reused fragments of grinding stones (**§E1**, **nos. 406**, **407**), for a total size of 55 × 45 cm. The function of this installation is not clear.

In the easternmost part of Room 11, a mudbrick installation named B11-I2 (**Fig. C2.9.5**) was identified. It comprises a severely preserved row of five half mudbricks, aligned north-south. The room's floor abutted the western side of this installation.

Room 11's floor deposit was excavated in two portions: B11-D02-01 to the west and B11-D02-02 to the east. In the western part, the floor deposit consisted of brown clayey soil, including mudbrick debris from the wall collapse, mixed with ashes, charcoal fragments, pottery sherds, animal bones, and bronze fragments. In the eastern part, the floor deposit was made of hard brown clayey soil with 2-10 mm white inclusions, loose ashes, and chunks of charcoal up to 3 cm in size.

The floor deposit yielded various items, including a spherical lead weight, beads, and grinding stone fragments (see table below). The upper room's fill (B11-D01-01) was a reddish brown, hard clayey soil. It contained mudbrick debris and various small finds, including the torso of a human terracotta figurine (**§E1**, **no. 353**).

Room 11 finds			
AS number	**Short object description**	**Context**	**§E1, no.**
AS 261433:080:003	Lead weight	Floor deposit	392
AS 261433:080:005	Glass bead	Floor deposit	332
AS 261433:080:006	Grinding stone fragment	Floor deposit	405
AS 261433:080:007	Carnelian bead	Floor deposit	312
AS 261433:080:008	Spherical bead	Floor deposit	335
AS 261433:080:011	Perforated pottery sherd	Floor deposit	449
AS 262433:161:004	Grinding stone fragments	Floor deposit	408
AS 262433:161:005	Loom weight	Floor deposit	431
AS 261433:087:001-2	Grinding stone fragments	Installation B11-I3	406, 407
AS 261433:079:004	Ceramic disc	Upper room fill	457
AS 261433:079:008	Bronze shaft	Upper room fill	386
AS 261433:079:011	Bronze needle with a hook	Upper room fill	387
AS 261433:079:015	Human clay figurine (torso)	Upper room fill	353
AS 261433:085:003	Weaving shuttle	Upper room fill	434
AS 261433:085:004	Loom weight	Upper room fill	430
AS 261433:085:005	Drilled shell, probably a bead	Upper room fill	341
AS 261433:085:007	Ceramic disc	Upper room fill	458
AS 262433:150:003	Lead wire	Upper room fill	399
AS 262433:150:004	Bead, probably glass	Upper room fill	331

Room 11 finds			
AS number	**Short object description**	**Context**	**§E1, no.**
AS 262433:150:008	Metal fragment, probably lead	Upper room fill	400
AS 262433:153:004	Bronze nail	Upper room fill	380
AS 262433:153:005	Fragments of a small lead tube	Upper room fill	401

C3. Sondage 2: Excavations within the SBAH trench "New Town 4"

Jens Rohde, Jana Richter & Andrea Squitieri

During the 2024 campaign, we began a limited excavation dubbed "Sondage 2" within the large trench that is located right next to our NT1 trench and that was excavated in 2002 by the Iraqi team of the State Board of Antiquities and Heritage (SBAH), which at that time was called the "New Town 4" trench (**Fig. C3.1**). Excavating this sondage aimed to achieve two primary objectives. Firstly, we sought to confirm the elevation of the virgin soil, tentatively identified in core C10 at a height of around 158 m above sea level (**Fig. C3.2**; **§B2**). Secondly, we wanted to determine whether any older structures existed beneath structures unearthed by the Iraqi team in 2002, ideally collecting samples suitable for radiocarbon dating.

Fig. C3.1: Orthophoto of the SBAH trench "New Town 4" next to trench NT1, overlaid by the excavation grid. The green rectangle indicates the location of Sondage 2. Orthophotos by Jens Rohde, prepared by Andrea Squitieri.

Sondage 2 measures approximately 23 m² and targeted an area where the SBAH excavations had uncovered three units. Based on the original room numbers assigned by the Iraqi team, we labelled them SBAH Unit 18, SBAH Unit 14, and SBAH Unit 15 (**Fig. C3.2**). These units are bounded by a wall to the west running roughly north-south, while two walls perpendicular to it separate SBAH Unit 18 from SBAH Unit 14 and the latter from SBAH Unit 15, respectively. SBAH Unit 18 was accessible through doorways from the north and the east, whereas no doorway was identified within the walls of SBAH Units 14 and 15. Therefore, the two southern units are the remains of wall foundations belonging to a younger architectural phase from which no floor is preserved.

In SBAH Unit 18, the Iraqi team had uncovered a backed brick floor, marking the lowest level reached at that time (**Fig. C3.2**). After removing the brick floor, our excavations revealed three stratigraphic phases between it and the virgin soil, summarised in **Table C3.1**. We also unearthed a structure below the brick floor, below SBAH Unit 18, interpreted as a drainage, resting on a pebble floor. Below the drainage, our excavations reached the virgin soil. The sections below describe the deposits and structures encountered below each SBAH unit.

C3.1 The first structures below SBAH Unit 18

The baked brick floor was made of bricks measuring c. 34 × 34 cm. After removing the bricks, we found remains of plaster embedded in a 10 cm thick layer of reddish brown, loose soil (registered as Locus:263432:010) containing pebbles and pottery sherds. We assume this deposit was made to prepare the brick floor, thus sealing all the deposits and installations below. After removing the layer Locus:263432:010, the fill Locus:263432:013 was excavated. This was made of a greyish-brown hard soil containing mudbrick debris, ashes, pottery sherds, bones and some tiny bronze fragments. This fill covered the installation Locus:263432:014, made of large stones set to form an enclosure (**Fig. C3.3**). This stone installation continued towards the southwest corner of the unit (here registered as Locus:263432:036), covering the entire southwestern third of the unit. The stone layer abutted the western wall,

Fig. C3.2: Orthophoto of Sondage 2. The brick floor is the level reached by the SBAH team in 2002. Created by Jens Rohde, annotated by Andrea Squitieri.

which is set against another neighbouring building, and the southern wall, which separates SBAH Unit 18 from SBAH Unit 14.

In the southwest corner of SBAH Unit 18, after removing the stone installation Locus:263432:036, we uncovered a door socket (Locus:263432:039) that did not seem to be related to any of the surrounding walls because no doorway was visible in the brickwork in this area. To the south of the door socket, we found a partially preserved beaten earth surface with white inclusions (Locus:263432:042) that abutted the western wall. The remnant of this surface was in the direct vicinity of a mudbrick installation made of three mudbricks in a row (Locus:263432:041). Still, the relationship between both features could not be established because the mudbricks had been cut by the door socket Locus:263432:039. The surface Locus:263432:042 continued to the south below the southern wall, separating SBAH Unit 18 from Unit 14. It, therefore, predates the visible mudbrick architecture.

C3.2 The drainage installation below SBAH Unit 18

Moving towards the east, still within the area delimited by SBAH Unit 18, after removing the stone installation Locus:263432:014, we encountered the deposit Locus:263432:011, made of reddish brown silty soil containing mudbrick fragments and a few pebbles. Below Locus:263432:011, we found a circular installation defined by a lining, about 2-3 cm thick, made of blackish clay. The installation, named Locus:263432:015, had a maximum diameter of 53 cm (**Fig. C3.3**). It contained the fill Locus:263432:012, made of yellow-greenish clayey-silty soil with traces of ashes. Inside this fill, we found deteriorated fragments of what may have originally been an unfired clay tablet (AS 263432:012:002), but with no traces of cuneiform script preserved. We interpret this installation as a part of a drainage system.

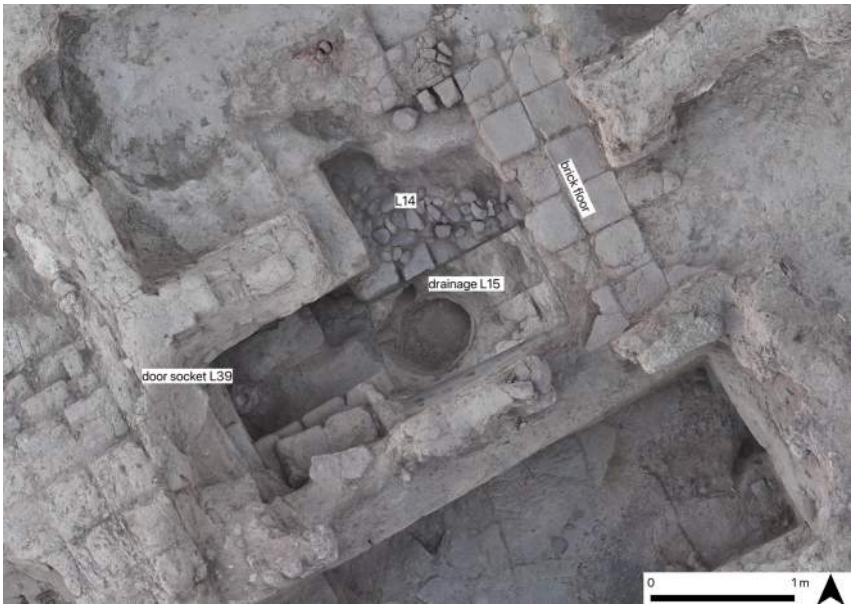

Fig. C3.3: SBAH Unit 18. Orthophoto by Jens Rohde, annotated by Andrea Squitieri.

Interestingly, the drainage fill (Locus:263432:012) yielded a very high amount of seeds separated through flotation, which are discussed in **§I2.6**. One of these seeds was radiocarbon-dated to 1732-1631 calBC (95.4% probability; **§C1.2**). This is the oldest date range obtained in our excavations, predating the reign of Puzur-Aššur III (conventially dated to 1521–1428 BC), who was the first Assyrian ruler to mention the New Town of Assur in his inscriptions.[72] However, such an early date may be explained by the context in which the seed was collected, as the drainage sys-

72 Radner/Kreppner 2024, 224f.

Table C3.1: Stratigraphy of Sondage 2. Prepared by Jens Rohde and Jana Richter.

Sondage 2 stratigraphy										
Stratigraphic phase	Main features and radiocarbon dates (95.4% probability)									
	SBAH Unit 18					SBAH Unit 14			SBAH Unit 15	
	Baked brick floor reached by SBAH in 2002					Level reached by SBAH in 2002			Level reached by SBAH in 2002	
Phase 3	Locus:263432:010 plaster fill mixed with clay Locus:263432:013 grey-brown hard soil Locus:263432:014 stone enclosure installation Locus:263432:011 fill covering the drainage Locus:263432:015 drainage lining Locus:263432:012 drainage fill **(1740-1622 calBC)**	=	Locus:263432:027 plaster fill mixed with clay Locus:263432:032 mudbrick cover Locus:263432:036 layer of river stones abutting S wall Locus:263432:037 clay with reed traces below stone layer			Locus:263432:024 fill Locus:263432:026 disturbance in the east Locus:263432:025 fill			Locus:263432:029 fill Locus:263432:033 pit cut; Locus:263432:034 pit fill	
Phase 2	not excavated		Locus:263432:040 pit cut for door socket Locus:263432:039 door socket Locus:263432:042 clay surface abutting W wall Locus:263432:041 mudbrick installation Locus:263432:017 pebble floor	= ? =	Locus:263432:035 burnt material on the surface **(802-776 calBC)** Locus:263432:030 clay surface Locus:263432:031 floor deposit **(816-791 calBC; 791-569 calBC)** Locus:263432:038 pebble floor Locus:263432:044 floor package made of pebbles mixed with bitumen **(827-794 calBC)** Locus:263432:046 paved floor with stone slabs	= ? = ? = ?	Locus:263432:048 hard clay surface rubble fill Locus:263432:049 reddish floor abutting W wall Locus:263432:050 grey surface abutting W wall	
Phase 1	Locus:263432:018 brown clayey soil above virgin soil **(1214-1048 calBC)** Locus:263432:020 cut of Pit 16 Locus:263432:021 fill of Pit 16 **(1385-1222 calBC; 1406-1261 calBC)**	not excavated				Locus:263432:047 compact grey surface below W wall			not excavated	
	Locus:263432:019 virgin soil: hard reddish soil with white inclusions									

tem could have been filled with older material transported by water from distant locations across the site. The plant remains recovered from the drainage fill also align with the presence of waterborne waste material (**§I2.6.5**).

The drainage rested on a pebble floor registered as Locus:263432:017. This floor, which had already become vis-

Fig. C3.4: The drainage with its clay lining (Locus:263432:015) and the pebble floor (Locus:263432:017) reached below the drainage fill in SBAH Unit 18. Photo by Jens Rohde, annotated by Andrea Squitieri.

Fig. C3.5: The pebble floor Locus:263432:017. Photo by Jens Rohde.

ible below the fill of the drainage (**Figs. C3.4**, **C3.5**), was made of two layers of pebbles intermixed with whitish particles for a total thickness of 15 cm. In our reconstruction, the pebble floor Locus:263432:017 lies stratigraphically below the beaten earth surface Locus:263432:042, identified in the southwestern corner of SBAH Unit 18. Lying on the pebble floor, we identified a thin deposit named Locus:263432:016, made of light brown clayey soil, yielding pottery sherds and bones. The flotation of this deposit isolated a seed radiocarbon dated to 801-775 calBC (95.4 % probability; **§C1.2**).

The deposits encountered below SBAH Unit 18 yielded the small finds listed below.

AS number	Short object description	§E1, no.
AS 263432:016:004	Whetstone fragment	419
AS 263432:013:004	Flat bronze fragment	403
AS 263432:012:002	Illegible clay tablet fragments	—
AS 263432:011:003	Fragment of a lower grinding stone	409
AS 263432:010:003	Basalt mortar bowl	422

C3.3 The virgin soil below SBAH Unit 18

After removing a portion of the pebble floor Locus:263432:017, we reached the fill Locus:263432:018, made of brown clayey soil with mudbrick remains and pottery sherds (SE section in **Fig. C3.6**). The fill Locus:263432:018 covered the virgin soil (Locus:263432:019) and Pit 16, cutting the latter (**Fig. C3.7**). This fill yielded a charcoal sample radiocarbon dated to 1214-1048 calBC (95.4 % probability; **§C1.2**).

Pit 16 was filled with brown clayey soil, yielding a few pottery sherds. In this fill, a charcoal sample was radiocarbon dated to 1406-1261 calBC, and a seed isolated through flotation was radiocarbon dated to 1385-1222 calBC (both 95.4 % probability; **§C1.2**). These three dates, coming from the lowest levels of Sondage 2, postdate Puzur-Aššur III's reign and thus may well indicate human activities in this part of the New Town after its foundation. They are slightly younger than the date to 1506-1440 calBC, which was obtained in 2023 from the sounding that reached the virgin soil under the NT1 trench.[73]

The virgin soil, Locus:263432:019, was reached at the bottom of Sondage 2, and was characterised by hard reddish soil with white inclusions (**Fig. C3.7**). It was at an elevation of 158.90 m above sea level, about 90 cm below the level where virgin soil was observed in core C10, taken about 2 m to the north (**§B2**).

C3.4 The structures below SBAH Unit 14

To provide more context to the drainage and the pebble floor Locus:263432:017, on which it rested, we excavated below the level reached by the SBAH team in 2002 in both SBAH Unit 14 and Unit 15 (**Fig. C3.2**). In SBAH Unit 14, we first encountered a series of fills located stratigraphically below the wall foundations reached by the SBAH team. We reached an accumulation of concentrated burnt material (Locus:263432:035) resting on a clay surface (Locus:263432:030) (**Fig. C3.8**). In our reconstruction, the surface Locus:263432:030 might be equivalent to the surface Locus:263432:042 encountered in SBAH Unit 18. From the burnt deposit Locus:263432:035, a seed was isolated through flotation, which yielded the radiocarbon date 802-776 calBC (95.4% probability; **§C1.2**). After removing the clay surface Locus:263432:030, we encountered the thick floor deposit Locus:263432:031 resting on a pebble floor, registered as Locus:263432:038 (**Fig. C3.9**). This pebble floor has been equated to the pebble floor Locus:263432:017, identified in SBAH Unit 18, on which the drainage rested (see **§C3.2**). Interestingly, from the floor deposit Locus:263432:031, we collected two charcoal samples radiocarbon dated to 816-791 calBC and 791-569 calBC (both 95.4% probability; **§C1.2**), respectively.

When we removed the pebble floor Locus:263432:038, we uncovered another floor made of pebbles set between two layers of bitumen, registered as Locus:263432:044. The latter may represent the construction layer for the pebble floor Locus:263432:038, or an earlier phase in a sequence of floors renovated several times. From Locus:263432:044, a charcoal sample was collected, radiocarbon dated to 827-794 calBC (95.4% probability; **§C1.2**). Locus:263432:044 covered a stone slab floor (Locus:263432:046) abutting the western wall (**Fig. C3.10**). Below the stone slabs, we encountered a compact clay surface (Locus:263432:047) going under the western wall.

C3.5 The structures below SBAH Unit 15

Moving south to the SBAH Unit 15, right below the level reached by the SBAH in 2002, we found a pit (cut: Locus:263432:033; fill: Locus:263432:034 fill) disturbing the southwestern portion of the unit (**Fig. C3.2**). It was impossible to tell from which level the pit had been originally dug. Because of time constraints, we did not extend the exca-

73 Radner/Squitieri 2024c, 99: Table D1.1.

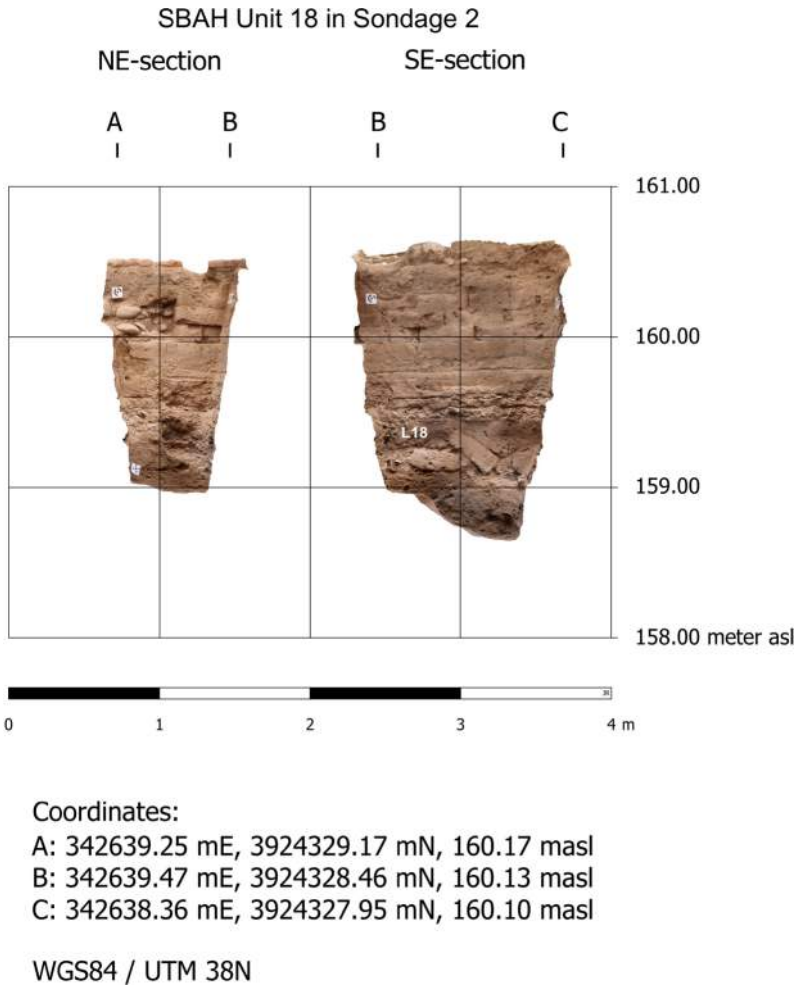

Fig. C3.6: The northeastern and the southeastern sections of SBAH Unit 18. Created by Jens Rohde.

Fig. C3.7: The virgin soil (Locus:263432:019) and the pit cutting it (Locus: 263432:021) reached below SBAH Unit 18. Photo by Jens Rohde.

vation across the rest of the unit but focused on the southwestern corner area around the pit. Around the latter, we identified the surface Locus:263432:048, a hard clay surface, most likely corresponding stratigraphically to the surface Locus:263432:030 in SBAH Unit 14 and Locus:263432:042 in SBAH Unit 18. The clay surface lay immediately below the wall foundation separating SBAH Unit 15 from SBAH Unit 14. We interpret it as the level on which the mudbrick walls were founded rather than a beaten mud floor built to be walked on. The surface Locus:263432:048 rests on a package of soil intermingled with mudbrick debris. Below this fill, we found a reddish clay surface, Locus:263432:049, probably corresponding stratigraphically to the pebble floors Locus:263432:038 (in SBAH Unit 14) and Locus:263432:017 (in SBAH Unit 18), though not made of pebbles. Below Locus:263432:049 was a greyish surface, Locus:263432:050, possibly connected stratigraphically to Locus:263432:046 in Unit 14, as they both abutted the western wall. No sample suitable for radiocarbon dating could be collected.

C3.6 Preliminary observations

The excavations we undertook within the SBAH trench "New Town 4" revealed a complex sequence of deposits, structures and floors below the level reached by the SBAH team in 2002. Due to the limited nature of our sondage, it is not clear yet how to interpret our findings. However, some preliminary conclusions can be drawn.

Our investigations have shown that the SBAH trench "New Town 4" contains more than one building, indicating a complex architectural history. Evidence of Late Bronze Age occupation in the area (Phase 1 in **Table C3.1**) has been identified, although no architectural structures associated with this phase have been found. On the other hand, the Iron Age occupation comprised multiple building phases. Notably, the building layout as visible in the SBAH trench does not represent the earliest phase of construction. Radiocarbon-dated Iron Age floors (Phase 2 in **Table C3.1**) predate all the currently visible walls

Fig. C3.8: Accumulation of burnt material Locus:263432:035, resting on the clay surface Locus:263432:030 in SBAH Unit 14. Photo by Jens Rohde.

included in our sondage. This suggests that either the related architecture had been completely removed before subsequent deposits accumulated and the foundations of SBAH Units 14 and 15 were built, or that the area we investigated was originally an open space without internal subdivisions when the Phase 2 floors were constructed. As a working hypothesis, we interpret the area east of the "western wall" in **Fig. C3.2** as an outdoor area where the inhabitants levelled the ground and reinforced it using construction materials such as stone slabs and bitumen/pebble floors beneath SBAH Unit 14, along with the pebble floor below SBAH Unit 18. Following this preliminary interpretation, the thick floor deposit Locus:263432:031 beneath SBAH Unit 14 is thought to have formed through the accumulation of trodden mud floors over successive rainy seasons, likely spanning no more than half a century, as indicated by comparisons with the radiocarbon dates obtained from Locus:263432:044 (below Locus:263432:031) and Locus:263432:035 (above Locus:263432:031). Finally, the drainage system below SBAH Unit 18 was constructed using a floor surface (Locus:263432:017) that yielded the radiocarbon date range of 801-775 calBC (95.4% probability; **§C1.2**). The drainage itself may have been built within or soon after this date range, though still within the time of the Assyrian occupation at the site.

C4. Excavating trench NT2 2024 in the New Town of Assur

John MacGinnis & F. Janoscha Kreppner

In 2023, the magnetic prospection revealed a large area devoid of constructions near the gap within the southern wall of the New Town (**Fig. C4.1**). In that year, the ERT measurements indicated an anomaly (**Fig. C4.2**, letter a) that might have been interpreted as a road.[74] Moreover, the core C7, also taken in 2023, had revealed a thick pebble layer at a depth of about 1 m, which could have been an ancient road level.[75] To explore the hypothesis of the existence of an ancient road, in 2024, we opened trench NT2, measuring 2 m north-south and 10 m west-east, and located about 65 m to the west of trench NT1 (**Fig. C4.3**).

The excavations in NT2 did not confirm the existence of an ancient road. Instead, they uncovered a sequence of deposits, which we explored to a depth of 6 m and arranged into four distinct stratigraphic phases: from Phase 4, the youngest, to Phase 1, the oldest (**Fig. C4.4**). The only discernible

Fig. C3.9: Pebble floor Locus:263432:038 in SBAH Unit 14. Photo by Jens Rohde.

Fig. C3.10: Stone slab floor Locus:263432:046 abutting the western wall in SBAH Unit 14. Photo by Jens Rohde.

74 Fassbinder *et al.* 2024.
75 Altaweel 2024.

Fig. C4.1: Trench NT2, located close to a wide gap in the southern wall of the New Town. Orthophoto by Jens Rohde, annotations by Andrea Squitieri.

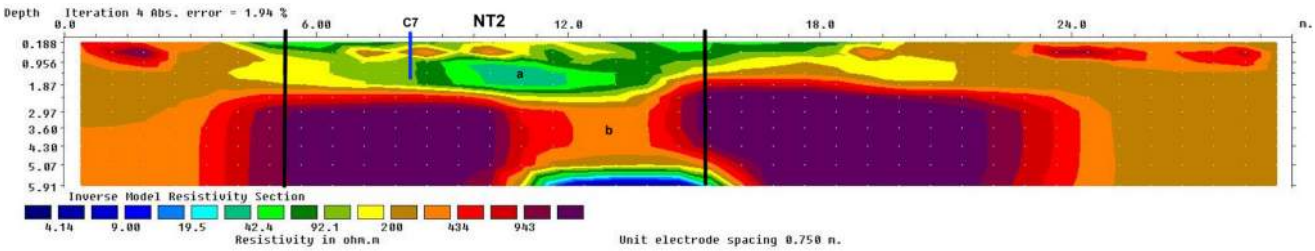

Fig. C4.2: ERT Profile 3 (dipole-dipole, 30 m long, probe separation 0.75 m) measured in 2023 by Jörg Fassbinder and Marco Wolf. The anomaly (a) was initially interpreted as a possible ancient road level. The vertical black lines indicate the size of trench NT2 as dug in 2024, while the blue line indicates the reach of core C7 taken in 2023 (see Altaweel 2024 and Fassbinder/Wolf 2024). Created by Jörg Fassbinder, annotated by Andrea Squitieri.

Fig. C4.3: Orthophoto of trench NT2. Created by Jens Rohde, annotated by Andrea Squitieri.

structure was a circular shaft about 3 m in diameter that we encountered at a depth of about 3 m, cutting into the natural ground (**Fig. C4.2**, letter b). We interpret this shaft as a deliberate feature constructed to improve the infiltration of rainwater and wastewater, which accumulated throughout Assur's occupation history.

A mixture of pottery material, ranging from the 14th century BC to the Parthian period, was found in the NT2 deposits, with a tendency for Middle Assyrian and Neo-Assyrian pottery to be found in the lowest level (Phase 1) (**§D1.2**). The chronological sequence of the fills uncovered in this trench was also established using radiocarbon samples, yielding late Iron Age date ranges in Phase 2 and 1 (see **Table C1.1**). Various finds in different materials and chronologies were collected from the fills alongside several metal slags and crucible fragments. The latter items indicate that waste from workshops across the site accumulated in the shaft throughout Assur's history. Notably, a small potsherd with cuneiform writing was collected from Phase 1 (**§F1**, Text 11). Finally, a child burial, designated Grave 10, was discovered (**§H2.8**). The stratigraphy of trench NT2 is shown in **Table C4.1**.

C4.1 NT2 2024 Phase 4

Beneath the site surface and the topsoil, a reddish-brown clayey soil deposit with pebbles, termed NT2-D01-01, overlaid the surface NT2-F1 (**Fig. C4.4**), which consisted of a thick gravel pack. The surface lay at an altitude of 255.5 m above sea level. The proportion of pebbles became smaller and smaller from the western end of the trench towards the east, so that the surface was difficult to define from the centre of the trench.

C4.2 NT2 2024 Phase 3

Phases 3 and 2 were differentiated based on their distinct soil compositions, which are expressed in particular in the low (Phase 3) and high (Phase 2) levels of ash content. The uppermost deposit of Phase 3 (NT2-D02-01) was made of a soft brown silty soil. It overlaid loose brown soil (NT2-D02-02) with some sand, patches of clay, numerous pebbles and small pottery sherds. In the eastern half of the trench, a hard, light red clay layer (NT2-D02-03) was present towards the northern profile. There was also an area of compact pebblestones (NT2-D02-04) and one flat stone laid horizontally down on smaller stones (registered as installation NT2-I1) at the western end of the trench.

The compact pebblestone layer (NT2-D02-04) was cut towards the west by the pit of Grave 10. An approximately two-year-old child was buried in this grave in a crouching position (**§H2.8**), wearing a bronze anklet (**§E1**, **no. 351**) (**Fig. C4.5**). Towards the east, the soil deposits of Phase 3 accumulated into a depression, the lowest point of which lay at c. 154 m above sea level.

Two broken ceramic stilts (**§E1**, **nos. 439**, **441**) and two fragments of terracotta figurines (**§E1**, **nos. 358**, **361**) were found in Phase 3's fills.

AS number	Short object description	§E1, no.
AS 254433:014:003	Broken ceramic stilt	439
AS 254433:016:004	Broken ceramic stilt	441
AS 254433:016:005	Fragment of a terracotta horse figurine	358
AS 254433:016:006	Fragment of a terracotta horseman figurine	361
AS 254433:029:002	Bronze anklet in Grave 10	351

D4.3 NT2 2024 Phase 2

The NT2 2024 Phase 3 soil overlaid the thick package of grey-reddish soil NT2-D03-01 of the NT2 2024 Phase 2, with some sand and clay mixed with a lot of ashes. This thick package formed a wide depression towards the eastern part of the trench (**Fig. C4.4**).

In the northeastern part of the trench, the ash-rich deposit NT2-D03-01 was at the same level as the Phase 3 deposits (see L15 in **Fig. C4.4**). Towards the west, the heavily ash-rich deposit NT2-D03-01 extended over the entire trench.

Below NT2-D03-01 was the deposit NT2-D03-02, which lay directly on a mud surface, registered as NT2-F2. This deposit yielded the radiocarbon date range 777-548 calBC (95.4 % probability, **§C1.2**). Interestingly, this date fits with the large amount of Iron Age/Neo-Assyrian pottery in this deposit, although younger pottery was also found (**§D1.2**). This deposit, in turn, overlaid a layer of very thickly deposited pebbles in a matrix of grey dirt (NT2-D04-01), which may have been a substructure of the surface. The surface and the overlying ash-rich soil accumulated into a depression, the lowest point of which was located in the centre of the eastern part of the trench on the southern profile (**Fig. C4.4**).

Several fragments of slags, iron, bronze, crucibles, and an almost complete stilt were found in the heavily ash-laden soil (see table below). These finds indicate that rubbish from workshops accumulated in the depression. Other finds collected include terracotta figurines, a core-moulded glass vessel, ceramic discs, and a loom weight (see table below). A complete miniature vessel,

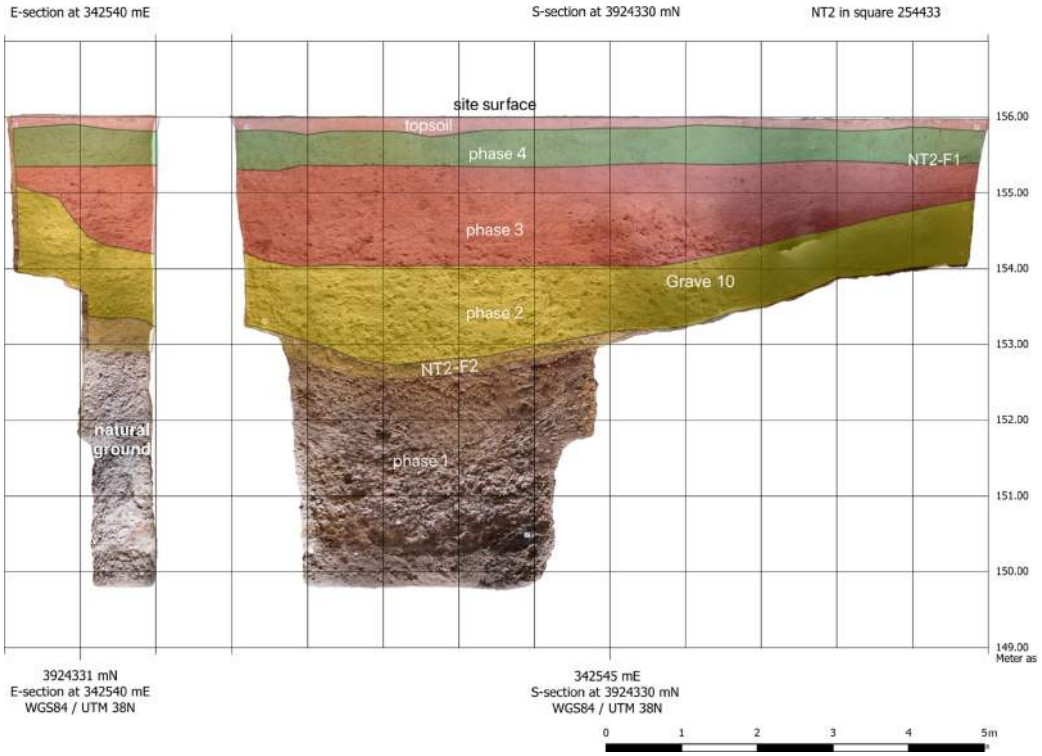

Fig. C4.4: Southern section of trench NT2 with indications of phases and main features. Created by Jens Rohde, annotated by Andrea Squitieri.

NT2 stratigraphy	
Stratigraphic phases and pottery periods	**Main features and radiocarbon dates (95.4% probability)**
NT2 Phase 4 Parthian, Hellenistic and Iron Age pottery	NT2-D01-01 reddish-brown clayey soil with pebbles (Locus:254433:004, Locus:254433:005, Locus:254433:012) NT2-F1 surface with pebbles (Locus:254433:006, Locus:254433:009)
NT2 Phase 3 Parthian, Hellenistic and Iron Age pottery	NT2-D02-01 soft brown silty soil (Locus:254433:007, Locus:254433:008, Locus:254433:013) NT2-D02-02 loose brown soil with patches of clay and pebbles (Locus:254433:014, Locus:254433:022, Locus:254433:016, Locus:254433:023) Grave 10 (cut: Locus:254433:031, fill: Locus:254433:032, skeleton: Locus:254433:029) NT2-D02-03 tough, light red clayey layer (Locus:254433:017) NT2-D02-04 compact pebble layer (Locus:254433:018 and Locus:254433:026) NT2-I1 flat stone laid down on smaller stones (Locus:254433:024)
NT2 Phase 2 Parthian, Hellenistic and Iron Age pottery	NT2-D03-01 grey-reddish silty-clayey soil, mixed with a lot of ashes (Locus:254433:015, Locus:254433:019, Locus:254433:027, Locus:254433:020, Locus:254433:033, Locus:254433:021, Locus:254433:034) NT2-D03-02 silty-clayey soil mixed with a lot of ashes (Locus:254433:025, Locus:254433:036) **(777-548 calBC)** NT2-F2 muddy surface below ashes (Locus:254433:028, Locus:254433:037) NT2-D04-01 pebble layer (Locus:254433:030)
NT2 Phase 1 Neo-Assyrian and Middle Assyrian pottery	NT2-D05-01 pebbles in grey soil with pottery and bones (Locus:254433:035, Locus:254433:038, Locus:254433:039, Locus:254433:041) **(770-541 calBC)**
Locus:254433:040 natural ground	

Table C4.1: Stratigraphy of trench NT2. Prepared by F. Janoscha Kreppner.

datable to the Hellenistic or Parthian period, was also found (**Fig. D1.2.4**).

AS number	Short object description	§E1, no.
AS 254433:019:004	Loom weight	423
AS 254433:019:005	Bronze bracelet	350
AS 254433:019:007	Stilt fragment	442
AS 254433:019:009	Head of a terracotta figurine	355
AS 254433:021:004	Fragment of a stone basin	420
AS 254433:021:008	Fragment of the torso of a human terracotta figurine	352
AS 254433:021:013	Fragment of a terracotta horseman figurine	362
AS 254433:021:014	Miniature vessel (see **Fig. D1.2.4**)	-
AS 254433:025:008	Fragment of a terracotta horseman figurine	363
AS 254433:025:009	Fragment of an 'Assyrian clay hand'	373
AS 254433:025:010	Fragment of a core-formed glass vessel	374
AS 254433:028:004	Fragment of a terracotta wheel	370
AS 254433:027:003	Fragment of a terracotta horseman figurine	364
AS 254433:028:005	Broken terracotta horse figurine	356
AS 254433:033:003	Parallelepiped-shaped ceramic object	459
AS 254433:033:004	Fragment of a terracotta horseman figurine	365
AS 254433:028:006	Perforated ceramic disc	447
AS 254433:028:007	Ceramic disc	448
AS 254433:015:004	Ceramic stilt fragment	440
AS 254433:015:005	Fragment of a perforated sherd	446

C4.4 NT2 2024 Phase 1 and the drainage shaft

The mud surface NT2-F2 extended over a circular vertical shaft, about 3.3 m wide, which cut through the natural ground (**Fig. C4.6**). The fill of the shaft consisted of pebbles embedded in grey soil with pottery and bones, and was registered as NT2-D05-01. It was excavated for about 3 m, to a depth of 148.80 m above sea level, without reaching the bottom.

In the ERT image (**Fig. C4.2**: letter b), the shaft appears as an orange, red and purple area and has a high electrical resistance. The shaft reached the deeper soil layers with lower electrical resistance (blue). This could mean

Fig. C4.5: The skeleton of a two-year-old child in Grave 10, with a bronze anklet (**§E1, no. 351**). Photo by John MacGinnis.

that the shaft was dug down through the impermeable upper layer of the natural soil to reach the deeper layers and allow better infiltration of rainwater and wastewater. The shaft was constructed at the lowest point of the New Town, where water still collects during rainfall (**Fig. C4.7**). The fill of the shaft, consisting of a lot of gravel and pottery sherds, ensured water permeability and prevented the earth from becoming too heavy. Our find could, therefore, be interpreted as a drainage shaft that allowed rainwater and wastewater from the settlement to seep away.

The fill of the shaft produced the radiocarbon date range 770-541 calBC (95.4 % probability; **§C1.2**). This date range contrasts with the Middle Assyrian pottery retrieved from this fill, further indicating that both older and younger material was mixed in the shaft's fill.

Particularly noteworthy finds from the fill of the shaft were a sherd inscribed with cuneiform (AS 254433:039:004; **§F**, Text 11) and a large terracotta wheel (**§E1, no. 371**). Other finds included ceramic discs, two fragments of Egyptian blue, and a spindle or loom weight (see table below). Slag and fragments of crucibles (**§E1, nos. 466, 472**)

were also found in the shaft's upper part, suggesting that production waste also got into the fill before the surface NT2-F2 finally sealed it.

Fig. C4.6: The shaft dug through the natural ground, corresponding to the anomaly (b) in **Fig. C4.2**. Photo by John MacGinnis.

AS number	Short object description	§E1, no.
AS 254433:035:002	Fragments of very coarse clay with traces of bronze	472
AS 254433:038:006	Spindle whorl or loom weight	435
AS 254433:038:008	Fragment of grinding stone	404
AS 254433:039:004	Potsherd with cuneiform writing (see **§F1**, Text 11)	-
AS 254433:039:007	Ceramic disc	452
AS 254433:039:008	Ceramic disc	453
AS 254433:039:009	Ceramic disc	454
AS 254433:039:010	Ceramic disc	455
AS 254433:039:003	Iron slag fragments	466
AS 254433:041:003	Two fragments of Egyptian Blue	375
AS 254433:041:005	Rectangular baked brick with a circular cavity	-
AS 254433:041:008	Terracotta wheel	371

Fig. C4.7: Rainwater accumulated close to trench NT2 (covered by a blue tarp) at the end of March 2024. Photo by F. Janoscha Kreppner.

D. Pottery from Assur, 2023 and 2024

This chapter has two parts. The first (**§D1**) presents three focused studies on selected pottery unearthed during the 2023 and 2024 excavation campaigns. The second (**§D2**) outlines the findings from petrographic and pXRF analyses conducted on pottery samples collected in the 2023 and 2024 campaigns.

During the field campaign in February and March 2024, the pottery team was headed by Jana Richter and Andrea Squitieri and comprised Poppy Tushingham, Amr Mohammad Jasim (SBAH Sherqat), and Omar Laith Allawi (SBAH Sherqat). The same team also worked during the study season from 24 October to 11 November 2024. The pottery workflow implemented during both the 2024 excavation campaign and the study season followed and improved upon the one established in 2023,[76] with the notable addition of a second Laser Aided Profiler (LAP),[77] which helped us increase the number of sherds that could be drawn. Poppy Tushingham and Amr Mohammad Jasim operated the two LAP devices. As in 2023, the complete vessels were first rendered in 3D models by Andrea Squitieri using the Agisoft Metashape software, and subsequently, two-dimensional drawings were generated from these 3D models and exported in SVG using the free software GigaMesh.[78]

To register the pottery sherds, joins, and vessels, we followed the same system applied in 2023, which we summarise briefly here for clarity. Every sherd receives the following label: AS [square number]:[locus number]:[collection number]:[sherd number] (e.g. AS 261433:005:001:023). Joined sherds and complete vessels receive a different label incorporating the abbreviations "J" for join or "V" for vessel, respectively. The join and the vessel labels contain the name of the building where the join/vessel was recovered and the room number. In the case of joins/vessels found outside buildings, the number 0 is used (e.g., A-01-V01 is Vessel 1 found in Room 1 of Building A).

76 Kreppner/Richter/Squitieri 2024.

77 https://www.laseraidedprofiler.com.

78 https://gigamesh.eu.

D1. Studies on the pottery excavated in 2023 and 2024 at Assur

D1.1 Preliminary study of selected post-Assyrian pottery from Building A in the New Town of Assur (2023-2024)

Alessandra Cellerino & Enrico Foietta

D1.1.1 Introduction

This chapter presents descriptions and comparisons of 22 pottery sherds from Building A, collected during the 2023 and 2024 campaigns (**§C2.8**). These sherds belong to a group of 26 pottery samples selected during the 2024 campaign, which were initially exported to the University of Torino for direct study conducted by the authors of this chapter and later brought to Germany for petrographic and pXRF analysis, the results of which are discussed in **§D2**. Four of the 26 samples are body sherds with no reconstructable shape and have been excluded from this study.

The sherds in this study originate from various units of Building A, specifically Room 1, Room 2, Room 3, Room 7, Room 8, and Courtyard 10. All were recovered from floor deposits except for one sherd (**5**), which was found in the fill of Courtyard 10. Based on a range of evidence, Building A is dated to the Hellenistic period (**§C2.8**).

The following section provides shape descriptions for each sherd (or group of sherds) and their comparative analysis. Comparisons are drawn from previous excavations at Assur and sites in its vicinity. Most parallels were identified among Hellenistic, post-Assyrian and late Neo-Assyrian ceramics from excavations at Nimrud and sites explored during the Eski Mosul Dam rescue project. More recent comparative material comes from investigations in the Iraqi Kurdistan region. For specific shapes widely distributed across the ancient Near East during the Hellenistic period and likely influenced by western pottery prototypes, comparisons with the Athenian Agora repertoire are also included.

For further details about the fabric groups mentioned in the text, we refer to **§D2**. Colours are provided according to the Munsell colour system. The abbreviations used are H. for height, D. for diameter, and Th. for thickness.

D1.1.2 Sherd descriptions and comparisons

(1) AS 261433:067:014:001 (Fig. D1.1.1)
Findspot: Courtyard 10, floor deposit;
Ware: Fabric group 2A;[79] light green glazed outer and inner surfaces; core colour: 10YR 8/3; oxidising firing atmosphere;
Manufacturing technique: wheel-made;
Dimensions: H. 3.9 cm; D. 26.6 cm; Th. 0.7 cm;
Description: Rolled rim and part of the body of a glazed plate. The glaze is opaque with some opalescence and craquelures.

Place	Period	References
Nimrud, Hellenistic settlement, Level 3	post 150 BC	Oates 1968, fig. 15: 5
Khirbet Khatuniyeh, Levels 3-2	probably 3rd century BC	McKenzie 1997, fig. 59: 402
Tell Deir Situn	3rd–first half of 2nd century BC	Curtis *et al.* 1987-1988, fig. 3: 4-5
Tell Mohammed 'Arab, Hellenistic pits	mid-3rd–mid-2nd century BC	Roaf 1984, fig. 3c
Khirbet Hatara, Level 9b	second half of 3rd–2nd century BC	Venco Ricciardi 1997, fig. 3: 33
Qasr Shemamok, Pit e6	second half of 2nd–early 1st century BC	Calini 2022, fig. 3u-v
Iraqi Kurdistan, LoNAP survey area	late 4th–late 2nd century BC	Palermo 2016, fig. 20: 11
Athens, Athenian Agora	200–175 BC	Rotroff 1997, fig. 48: 678-681

The sherd (**1**) belongs to a plate with a slightly upturned, thickened rim. This form was very popular in the ancient Near East from the 3rd century BC to the 1st century AD. It was probably borrowed from the Attic rolled-rim plate,[80] which was one of the most common types in the Hellenistic pottery repertoire. This plate type originated in Attica in the early 4th century BC and was exported elsewhere,[81] mainly in the early Hellenistic period. Attic rolled-rim plates are always black glazed, and all examples made before c. 200 BC have stamped decoration on the inner floor of the base.[82]

There is a wide range of sizes and rim variations among these plates, which may have served many purposes, from individual food serving to large sharing platters. Larger plates became popular at the end of the 4th century and throughout the 3rd and 2nd centuries BC, with an average diameter of 23-27 cm. Although much less popular than the fishplate in the Near East, this plate shape was imitated and locally produced in Glazed, Common or Red Painted Ware at many Mesopotamian sites.[83]

All the comparisons listed above refer to plates manufactured in Red Painted Ware. In northern Mesopotamia, from the 3rd century to the beginning of the 1st century BC,[84] pottery types inspired by or reproducing Greek models were manufactured in Red Painted Ware,[85] but this type of ware was also used, even if more rarely, for shapes belonging to the late Assyrian tradition. The matte red paint (whose colours can vary from orange to very dark brown or black)[86] usually appears on the rim (both inside and outside), and only occasionally, the paint covers the whole body. The spatial distribution of this type, present not only at Nimrud but also in the pottery collected in more recent surveys and excavations,[87] indicates that Red Painted Ware should be considered a northern Mesopotamian decorative technique rather than an imitation of western models.

The sherd (**1**) analysed here is a glazed example of this type of plates. The manufacture of glazed pottery significantly increased from the 4th century BC, becoming very common from the end of the 3rd and the beginning of the 2nd century BC, in the macro-area defined by Hannestad as "the glazed ware area",[88] which also includes central-southern Mesopotamia, the Persian Gulf region[89] and southwest Iran.[90] This surface treatment was much less common in northern Mesopotamia, even if the production of polychrome-glazed vessels was attested during the late Neo-Assyrian period.[91]

The technological characteristics of Mesopotamian glaze (calcareous clay fabric, glaze consisting of silica as

79 For all fabric groups mentioned in this section, see **§D2**.
80 Rotroff 1997, 142-145.
81 Hannestad 1983, 53; Rotroff 1997, 143, note 6.
82 Rotroff 1997, 143.
83 Hannestad 1983, 32-34.
84 Oates 1968, 122.
85 Oates 1968, 123; Venco Ricciardi 1997, 134.
86 E.g., Oates 1968, 123; Venco Ricciardi 1997, 132; Calini 2022, 472-473.
87 See references in Gavagnin/Iamoni/Palermo 2016 and Calini 2022.
88 Hannestad 1983, 107-112.
89 For a survey of the Hellenistic pottery in the Near East and at the site of Failaka, see Hannestad 1983.
90 On the Hellenistic and Parthian pottery in ancient Elymais, see Haerinck 1983 and Cellerino 2023.
91 See e.g., Curtis 1989, 50-51; Hausleiter 2010, 261-264, pls. 123-126. On the Neo-Assyrian glaze technique, see Nunn 1988, 142-156; Moorey 1994, 159-162.

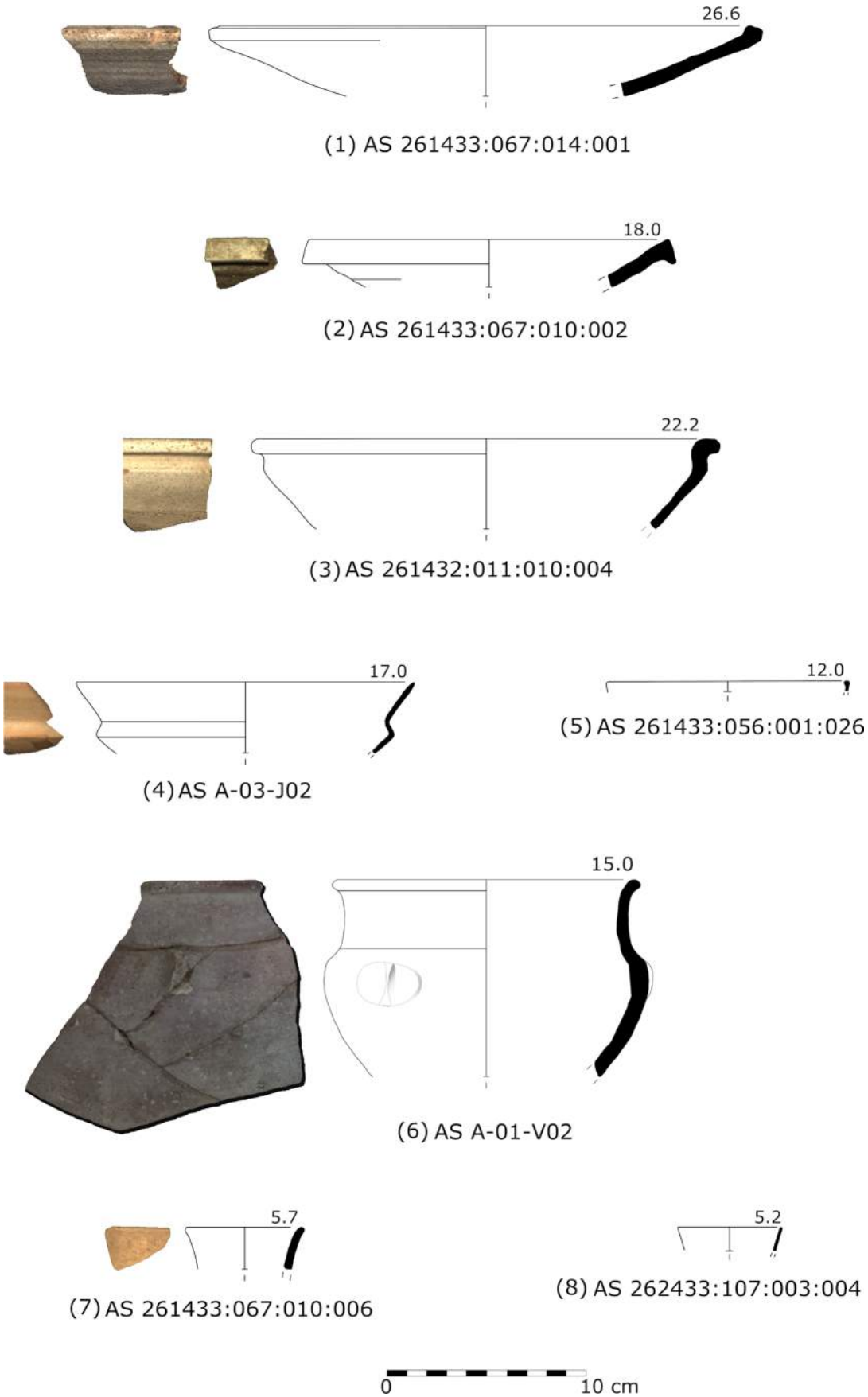

Fig. D1.1.1: Pottery from Building A. Scale 1:3. LAP drawings by Poppy Tushingham and Amr Mohammad Jasim, drawing (6) by Claudio Fossati.

the vitrifying agent, soda-rich plant ashes with high magnesium and potash contents as the flux, and copper, iron and manganese oxides as the main colouring agents) appear to have been much the same over a wide area,[92] and remain substantially unchanged from the second half of the second millennium BC to the Sasanian era.

Glazed pottery represents a tiny proportion of the Hellenistic pottery found at Nimrud.[93] Bowls, fishplates, and amphoriskoi are the most common types made in Glazed Ware, although most of the shapes inspired by the Greek types are produced in Red Painted Ware. The glaze is commonly blue-green in colour, but a yellow tinge is also attested. The glazed forms are attested in Nimrud from Level 4 onwards and tend to become more common in Levels 1 and 2 after the mid-2nd century BC.[94]

At Assur, during the 1988-1989 excavation by the Freie Universität Berlin of the Parthian-period levels dated between the 1st century AD and the middle of the 3rd century AD,[95] glazed pottery represented only c. 4% to 1.23% (in the most recent phase) of the sherds collected.

In contrast to the scarcity of glazed pottery in northern Mesopotamia, the Achaemenid and early Hellenistic glazed pottery collected for example during the excavation campaigns at Babylon conducted by the *Centro Ricerche Archeologiche e Scavi di Torino per il Medio Oriente e l'Asia* represents 25% of the diagnostic sherds.[96] Additionally, the glazed pottery from the excavated late Hellenistic-Parthian levels of Seleucia on the Tigris amounts to 36% of the total of the diagnostic sherds collected.[97]

(2) AS 261433:067:010:002 (Fig. D1.1.1)
Findspot: Courtyard 10, floor deposit;
Ware: Fabric group 4A; outer surface colour: 2.5Y 8/2; core colour: 2.5Y 8/2; inner surface colour: 2.5Y 8/2; oxidising firing atmosphere;
Manufacturing technique: wheel-made, self-slipped surfaces;
Dimensions: H. 3.3 cm; D. 18 cm; Th. 0.6 cm;
Description: Rim and part of the body of a fishplate. The rim is almost triangular in section.

Place	Period	References
Assur, Arsacid Buildings, Phase I	1st century AD	Hauser 1996, fig. 4a
Nimrud, Hellenistic settlement, Levels 5-3	215–post 150 BC	Oates 1968, fig. 15: 3-4
Nimrud, Hellenistic settlement, Levels 1-2	145–post 140 BC	Oates 1968, fig. 15: 33
Nimrud, Hellenistic settlement, Levels 5-1	215–post 140 BC	Oates 1968, fig 16: 51
Nimrud, Hellenistic settlement, Levels 3-1	post 150–post 140 BC	Oates 1968, fig. 16: 68-69
Tell Mohammed 'Arab, Hellenistic pits	mid-3rd–mid-2nd century BC	Roaf 1983, fig. 6: 41-42
Khirbet Hatara, Level 9a	second half of 3rd–2nd century BC	Venco Ricciardi 1997, fig. 9: 112
Iraqi Kurdistan, LoNAP survey area	late 4th–late 2nd century BC	Palermo 2016, fig. 20: 7, 9
Girdi Qala, Trench B, sub-surface	2nd century BC–2nd century AD	Mas 2015, fig. 2: 39
Athens, Athenian Agora	200–175 BC	Rotroff 1997, fig. 51: 729-730[98]

The sherd (**2**) belongs to a type of plate commonly known as fishplate.[99] The fishplate is one of the most widespread forms in the Hellenistic world[100] and exemplifies the adoption by local potters of a genuine Greek type. The original Greek version appeared between the late 5th century to the early 4th century BC[101] within the Attic Red Figure corpus.[102] The date when the fishplate and other Western shapes began to be produced in the ancient Near East is a subject of debate, but a period between the end of the 4th century and the beginning of the 3rd century BC is generally accepted.

In the Near East, the fishplate was produced in Glazed Ware,[103] particularly in southern Mesopotamia,[104] or in the northern Mesopotamian Red Painted Ware, and more rarely in Common Ware, as this example from Assur. The

92 Oates 1968, 125. On the technological characteristics of the Mesopotamian glazed pottery, see Hedges/Moorey 1975; Hedges 1982; Tite/McCarthy/Paynter 2008.
93 Oates 1968, 125-126.
94 Oates 1968, 66.
95 Hauser 1996, 61-62, 73-74.
96 Cellerino 2004, 97-99.
97 Valtz 2024, 11.
98 In the Athenian Agora assemblage, it is interesting to note a tendency towards a deeper fishplate, an evolution that probably began in the first quarter of the 2nd century BC (Rotroff 1997, 147).
99 For a general analysis of the type, see Hannestad 1983, 29-32.
100 See e.g., Rotroff 1997, 146, note 13.
101 Hannestad 1983, 29.
102 Rotroff 1997, 146-150.
103 "Ces formes se rencontrent principalement dans la céramique à glaçure, comme c'est le cas en général en Orient", (Boucharlat 1987, 197). Rutten 1996, 10 underlines, regarding the pottery from Tell ed-Der, dated to the second half of the 3rd century BC, the relative frequency in Mesopotamia of fishplates produced in Common Ware during the Seleucid period.
104 Cellerino 2004, 103-105.

fishplate is considered a 'fossile directeur' of the Hellenistic period,[105] even though this type continued to be made during the Parthian period.[106] Interestingly, fishplates appear in all three wares at Nimrud and are ring-based, like the black glazed examples further west.[107] A disk or flat base is a common feature in the Near Eastern versions that often replaces the ring base of the western prototypes. The central depression[108] in the middle of the base floor, characteristic of the Greek type, is sometimes substituted in the Near East by an incised circle or concentric circles.

(3) AS 261432:011:010:004 (part of A-02-J02) (Fig. D1.1.1)

Findspot: Room 2, floor deposit;

Ware: Fabric group 4A; outer surface colour: 7.5YR 8/2; core colour: 7.5YR 5/8; inner surface colour: 7.5YR 8/3; oxidising firing atmosphere, flame marks on the inner surface;

Manufacturing technique: wheel-made, slipped surfaces;

Dimensions: H. 5 cm; D. 22 cm; Th. 0.6 cm;

Description: Rim and part of the body of a large carinated bowl with a projecting rim, almost rectangular in section.

Place	Period	References
Assur	8th–7th century BC	Hausleiter 2010, pl. 23: Ass. 11748: g1; pl. 29: Ass. 12054: k; pl. 35: Ass. 6304: a2
Assur	7th century BC	Hausleiter 2010, pls. 38-39: Ass. 7787, Ass. 7788, Ass. 7793f, Ass. 8715
Nimrud, Fort Shalmaneser	last decade of 7th century–first half of 6th century BC	Oates 1959, pl. XXXV: 23-24
Nimrud, Fort Shalmaneser	post-Assyrian levels	Chiocchetti 2008, fig. 1: 9-10
Nimrud, Hellenistic settlement, Level 6	end of c. 225 BC but probably Achaemenid	Oates 1968, fig. 20: 139
Nimrud, Hellenistic settlement, Levels 5-2	post 215–145 BC	Oates 1968, fig. 15: 13, 36-37, 143
Nineveh, MG 22 Area	7th century BC	Lumsden 1999, fig. 5: 22
Khirbet Khatuniyeh, Level 4	late 7th century BC	Curtis/Green 1997, fig. 36: 142
Khirbet Khatuniyeh, Level 3	post-Assyrian	Curtis/Green 1997, fig. 56: 360
Khirbet Khatuniyeh, Level 2	3rd–2nd century BC	McKenzie 1997, fig. 60: 424, 426
Khirbet Hatara, Level 9	second half of 3rd–2nd century BC	Venco Ricciardi 1997, fig. 3: 84
Khirbet Qasrij	Late Neo-Assyrian–Achaemenid period	Curtis 1989, fig. 24

Carinated bowls with a projecting rim, in various sizes and proportions, are typical of the late Neo-Assyrian pottery repertoire.[109] As the above comparisons illustrate, these bowls were also popular in the post-Assyrian period and continued to be produced, with little or no alteration, during the Hellenistic period. In Hellenistic Nimrud, they represent the most common open forms made in Red Painted Ware and Common Ware.[110] Oates highlights that, although the Assyrian forms are generally more sharply carinated, it is nearly impossible to distinguish the Hellenistic versions from authentic Assyrian bowls based solely on shape.[111]

(4) AS 262432:058:015:001 (part of join AS A-03-J02) (Fig. D1.1.1)

Findspot: Room 3, floor deposit;

Ware: Fabric group 1A; outer surface colour: 5YR 7/8; core colour: 5YR 6/8; inner surface colour: 5YR 7/6; oxidising firing atmosphere;

Manufacturing technique: wheel-made, the outer and inner surfaces are evenly smoothed;

Dimensions: H. 3.6 cm; D. 17 cm; Th. 0.3 cm;

Description: Rim and part of the body of a carinated bowl with a flaring rim.

105 de Miroschedji 1987, 43

106 See e.g., the fishplates in Common Ware found in Phase I of the buildings excavated in 1988-1989 by the Freie Universität Berlin at Assur and dated to the 1st century AD (Hauser 1996, 59-60, 73, fig. 4a).

107 Oates 1968, 123.

108 Lecomte, studying the pottery from Larsa dated to the 2nd century BC, suggests that the depression is an "older morphological feature", which persists into the end of the 2nd-beginning of the 1st century BC (Lecomte 1993, 21).

109 Oates 1959, 132; Curtis/Green 1997, 89.

110 Oates 1968, 124.

111 Oates 1968, 132.

Place	Period	References
Nimrud, T.W. 53, Rooms 16-19, Level 3	second half of 7th century BC	Lines 1954, pl. XXXVII: 7
Nimrud, Hellenistic grave	probably dated to 175–140 BC[112]	Oates 1968, fig. 16: 45
Nineveh, MG 22 Area	7th century BC	Lumsden 1999, fig. 8: 58
Khirbet Qasrij, Trench A4/1	Late Neo-Assyrian–Achaemenid period	Curtis 1989, fig. 31: 140

Carinated bowls with flaring rims were typical of the late Neo-Assyrian period, spreading across the empire's vast regions. They were made of metal,[113] pottery, and glass.[114] This class of bowls, produced mostly in Palace Ware,[115] is characterised by a ring foot or a rounded base, in the case of metal vessels, sometimes with a solid knob in the centre or proto-omphalos, a shallow semi-elliptical body, and a sharp carination between the body and the everted rim.[116] It is debated if the pottery versions were created first[117] or if they were imitations of metal counterparts.[118] Establishing cause-effect relationships in skeuomorphism processes is often complicated. Usually, skeuomorphs of metal and stone vessels are regarded as imitations manufactured in a less precious and less expensive material, but this is not always the case.[119]

A sub-type of this bowl type, with a larger diameter and more shallow, survived into the Achaemenid and post-Achaemenid periods.[120] However, the sharp carination was progressively modified and became less pronounced.[121] This bowl type continued to enjoy popularity until the early Parthian era, when it was produced in Glazed Ware or different local wares such as the Festoon or Triangle Wares in the regions of western Iran.[122]

112 See also Oates/Oates 1958, 130-131.
113 For the Assyrian metal bowls, see Curtis 2013, 69-72, pls. XXXVI-XXXIX.
114 See e.g., Saldern 1970, 226, no. 46, fig 41.
115 Hunt 2015, 48-49, fig. 3.10 ("Form A").
116 On the social meaning and function of these bowls, see Hunt 2015, 183-191.
117 As argued by Curtis 2013, 69.
118 As argued by Oates 1959, 132 and by Hunt 2015, 188-189.
119 On the skeuomorphism between glass, metal and stone vessels in the Neo-Assyrian tableware, see Cellerino 2021.
120 Also known as "cream bowl" (Stronach 1978, 184, fig. 106).
121 Curtis 1989, 48; 2013, 71.
122 Cellerino 2015, 133-134; Valtz 2024, 47-48.

(5) AS 261433:056:001:026 (Fig. D1.1.1)
Findspot: Courtyard 10, fill;
Ware: Fabric group 1A; chemical outlier (see **§D2**); black glazed outer and inner surfaces; core colour: 10YR 7/3; oxidising and reducing firing atmosphere;
Manufacturing technique: wheel-made;
Dimensions: H. 1.2 cm; D. 16 cm; Th. 0.3 cm;
Description: In-turned, rounded rim of an imported black glazed echinus bowl.[123]

Place	Period	References
Athens, Athenian Agora	200–175 BC	Rotroff 1997, fig. 48: 678-681
Athens, Athenian Agora	325–275 BC	Rotroff 2006, fig. 52: 307

This sherd, whose chemical analysis has shown it to be most likely an import (see **§D2**), belongs to a type of bowl with an incurved rim, also known as an echinus bowl,[124] which is one of the most common shapes of the Hellenistic period. It was probably used for serving food rather than as a drinking bowl.[125] The form was very popular in the 4th century BC in the Athenian Agora repertoire but survived into the late Hellenistic period when echinus bowls were manufactured in three variants: a shallow bowl with stamped decoration on the inner floor, a similar bowl without decoration, and a deep variant which became more popular in the 3rd century BC, replacing the shallow echinus bowl type.[126]

Hellenistic echinus bowls typically feature shiny black glazes, which in some cases may show red shades due to an inhomogeneous reducing firing. Semi-glazed or Common Ware echinus bowls are quite rare, indicating a sporadic production.[127]

Attic imports into the eastern Mediterranean and the Near East are common, particularly among the 3rd-century BC Hellenistic sites, and are produced in various wares. The echinus bowls and other Greek-inspired forms were never produced in the Near East in Black Glaze Ware, like their western prototypes. They were made in white, yellow, and turquoise Glazed Ware in central-southern Mesopotamia and Red Painted Ware in the northern Mesopotamian regions. Oates highlights that the examples

123 The body sherd AS 261433:058:001:019 (not included in this section) is another fragment of an imported black glazed open form.
124 Rotroff 1997, 161-163.
125 Rotroff 1997, 161, note 55.
126 According to Rotroff, the mid-3rd century BC could be considered the terminal date of production (Rotroff 1997, 162).
127 Rotroff 2006, 115.

from Nimrud, made in Red Painted Ware, typically have a ring base, a typical feature of the Greek echinus bowls. In contrast, a disk base characterises the bowls produced in Common Ware at Nimrud and in southern Mesopotamia.[128]

The production of similar bowls in the Neo-Babylonian and Achaemenid periods was probably a crucial factor in the significant increase in popularity of the shape, which certainly met local taste. On the one hand, the echinus bowl was linked to the emerging Hellenistic culture, but on the other hand, it followed a local, well-established pottery tradition.[129]

(6) AS 261433:005:001:023 (part of A-01-V02) **(Fig. D1.1.1)**
Findspot: Room 1, floor deposit;
Ware: Fabric group 4A; Red Painted Ware; outer surface colour: 2.5YR 7/6; core colour: 2.5Y 8/3; inner surface colour: 2.5Y 8/3; oxidising firing atmosphere;
Manufacturing technique: wheel-made, slipped surfaces;
Dimensions: H. 8,1 cm; D. 15 cm; Th. 0.6 cm;
Description: Rim, neck, and part of the body of a beaker. Simple, rounded rim and a slightly flaring neck.

Place	Period	References
Nimrud, Burnt Palace	7th century BC	Hausleiter 2010, pl. 81: BT 1.10

The sherd (**6**) belongs to a goblet manufactured in Red Painted Ware. The light red paint is poorly preserved up to the rim. The shape is undoubtedly inspired by the late Neo-Assyrian common beakers characterised by a wide flaring neck, spherical or ovoid body, and round, pointed or button base. Some rare variants have a small flat or disk base. A good parallel is a beaker from Nimrud (rim diameter: 16.4 cm). Our sherd (rim diameter: 15 cm) and the Nimrud goblet are very similar in shape and stand out from normal Assyrian goblets by their large size, hence, they may represent an unusual variant of the type. Some beakers from Tell Halaf, produced in Red Slip Ware,[130] show some similarities to our sherd, but they are considerably smaller.[131] Katzy suggests a Mesopotamian origin for this type of beaker, which is attested at Tell Halaf from the beginning of the Seleucid period until the 1st century BC.[132]

The decoration on our goblet's shoulder confirms a Seleucid date. The extruded hump formed by a fingertip on the shoulders of the goblet is considered as a distinctive feature of the Hellenistic period. The finger indentations were usually completed by impressed stamp motifs, generally rosettes, stars, or palmettes. The use of stamps is attested in the Achaemenid period, and this practice persisted into the Seleucid period, when it became even more popular.[133] In northern Mesopotamia, the stamped decoration became a common feature of the Hellenistic period. Here, the finger indentations are usually much less deep and less popular than in the southern Mesopotamia.[134]

On our goblet, the knob pushed out by the pressure of the finger from the inside of the vessel was simply pinched. This specific type of decoration has no parallels in the northern Mesopotamian pottery repertoire. According to Oates and Hannestad, the use of the two different stamp techniques (simple impressed stamps or stamps on a hump) could have a chronological significance. In fact, based on the stratigraphy of the Failaka and Nimrud excavations, simple impressions are more prevalent in upper levels, which may indicate a later date.[135]

(7) AS 261433:067:010:006 (Fig. D1.1.1)
Findspot: Courtyard 10, floor deposit;
Ware: Fabric group 1B; chemical outlier (see **§D2**); outer surface colour: 7.5YR 7/6; core colour: 7.5YR 7/6; inner surface colour: 7.5YR 7/6; oxidising firing atmosphere;
Manufacturing technique: wheel-made, the outer and inner surfaces are evenly smoothed;
Dimensions: H. 2.2 cm; D. 5.7 cm; Th. 0.3 cm;
Description: Rim and neck of a small jar or goblet. Simple, rounded rim and flaring neck.

(8) AS 262433:107:003:004 (Fig. D1.1.1)
Findspot: Room 8, floor deposit;
Ware: Fabric group 1A; chemical outlier (see **§D2**); outer surface colour: 10YR 8/2; core colour: : 10YR 8/2; inner surface colour: : 10YR 8/2; oxidising firing atmosphere;
Manufacturing technique: wheel-made, the outer and inner surfaces are evenly smoothed;
Dimensions: H. 1.9 cm; D. 5.2; Th. 0.2 cm;

128 Oates 1968, 123.
129 Cellerino 2004, 105-106.
130 This more recent definition corresponds to Oates' Red Painted Ware. See e.g., Martín Galán 2007, 228-229; Katzy 2015, 60-62.
131 Katzy 2015, 99-101, pl. 33, 03-2A, pl. 60, no. 7, rim diameter: 10 cm.
132 Katzy 2015, 101-105.
133 On the impressed stamp decoration, see Hannestad 1983, 57-58; Cellerino 2004, 118.
134 Oates 1968, 124-125.
135 Hannestad 1983, 60. At Nimrud the indentations are less marked in Level 2 (mid-2nd century BC) than in the earlier levels (Oates 1968, 125).

Description: Rim and neck of a goblet. Simple, rounded rim and a slightly flaring neck.

Place	Period	References
Assur	Late Neo-Assyrian–post Assyrian, 7th–6th/5th century BC	Hausleiter 2010, pl. 77: BZ 1.10
Assur	8th–7th century BC	Hausleiter 2010, pl. 78: BR 1.3; pl. 80: BE 2.2
Assur	7th century BC	Hausleiter 2010, pl. 80: BE 2.2
Nimrud, Fort Shalmaneser	last decade of 7th century–first half of 6th century BC	Oates 1959, pl. XXXVI: 38-39, 41-47, 49
Nimrud, Fort Shalmaneser	Late Neo-Assyrian, 8th–7th century BC	Hausleiter 2010, pl. 80: BE 2.1, 2.3
Hellenistic settlement, Levels 4-2	post-175–145 BC	Oates 1968, fig. 17: 70-72
Khirbet Khatuniyeh, Level 4	late 7th century BC	Curtis/Green 1997, fig. 50: 234
Khirbet Khatuniyeh, Level 3	post-Assyrian	Curtis/Green 1997, fig. 58: 381
Khirbet Qasrij, Trenches A3-A4/1-B4/1	Late Neo-Assyrian–Achaemenid period	Curtis 1989, fig. 31: 116-120

The sherds (**7**) and (**8**) are rim fragments of probably thin-walled beakers. The small preserved part of the vessels has allowed only generic comparisons based on the rim diameter and the curve of the wall. The attribution to a specific variant is problematic. Still, the small diameter (5.7 and 5.2 cm) and the plain, rounded rim may point to the class of narrow cylindrical beakers. This shape, called by Oates "istikan",[136] is well represented in the late Neo-Assyrian pottery repertoire, especially at Assur and Nimrud,[137] and was manufactured in several varieties of size and base. They are, on average, 8-9 cm high but exist in larger or smaller variants. Comparisons are also possible with another class of small beaker, far less common than the cylindrical type, with a round-walled body, a pointed or button base, and a high, usually flaring, neck, found almost exclusively in late Neo-Assyrian contexts during the excavation of the Citadel of Nimrud and in Fort Shalmaneser. The cylindrical beakers with a low disk base found in the Hellenistic levels 4-2 of the Nimrud Citadel illustrate the persistence and development of this shape during the 2nd century BC.

136 Oates 1959, 132-133.

137 Hausleiter 2010, 295, fig. 53.

(9) AS 262433:136:001:009 (Fig. D1.1.2)
Findspot: Courtyard 10, floor deposit;
Ware: Fabric group 4A; outer surface colour: 10YR 8/2; core colour: 10YR 8/3; inner surface colour: 10YR 8/3; oxidising firing atmosphere;
Manufacturing technique: wheel-made, slipped surfaces;
Dimensions: H. 2.5 cm; D. 6.3 cm; Th. 0.4 cm;
Description: Rim and neck of a small jar. Folded rim with an indentation on the outer side, cylindrical neck. Black paint at the rim.

(10) AS 262433:107:003:001 (Fig. D1.1.2)
Findspot: Room 8, floor deposit;
Ware: Fabric group 4A; outer surface colour: 2.5Y 8/1; core colour: 10YR 8/4; inner surface colour: 2.5Y 8/2; oxidising firing atmosphere;
Manufacturing technique: wheel-made, slipped surfaces;
Dimensions: H. 5.3 cm; D. 10 cm; Th. 0.75 cm;
Description: Rim and neck of a jar. Folded rim with an indentation on the outer side, cylindrical neck.

(11) AS 262433:107:007:003 (Fig. D1.1.2)
Findspot: Room 8, floor deposit;
Ware: Fabric group 1A; chemical outlier (see **§D2**); outer surface colour: 10YR 10/3; core colour: 10YR 10/3; inner surface colour: 10YR 10/3; oxidising firing atmosphere;
Manufacturing technique: wheel-made;
Dimensions: H. 2.5 cm; D. 7 cm; Th. 0.5 cm;
Description: Rim and neck of a small jar. Projecting thickened rim, flaring neck.

(12) AS 262433:136:001:004 (Fig. D1.1.2)
Findspot: Courtyard 10, floor deposit;
Ware: Fabric group 3A; outer surface colour: 2.5Y 7/2; core colour: 10YR 7/4; inner surface colour: 2.5Y 7/2; oxidising firing atmosphere;
Manufacturing technique: wheel-made;
Dimensions: H. 4.2 cm; D. 8 cm; Th. 0.5 cm;
Description: Rim and neck of a jar. Projecting thickened rim, flaring neck.

(13) AS 262433:107:006:001 (Fig. D1.1.2)
Findspot: Room 8, floor deposit;
Ware: Fabric group 4A; outer surface colour: 5Y 7/2; core colour: 5Y 7/1; inner surface colour: 5Y 7/1; oxidising firing atmosphere, overfired;
Manufacturing technique: wheel-made;
Dimensions: H. 5 cm; D. 12 cm; Th. 0.7 cm;

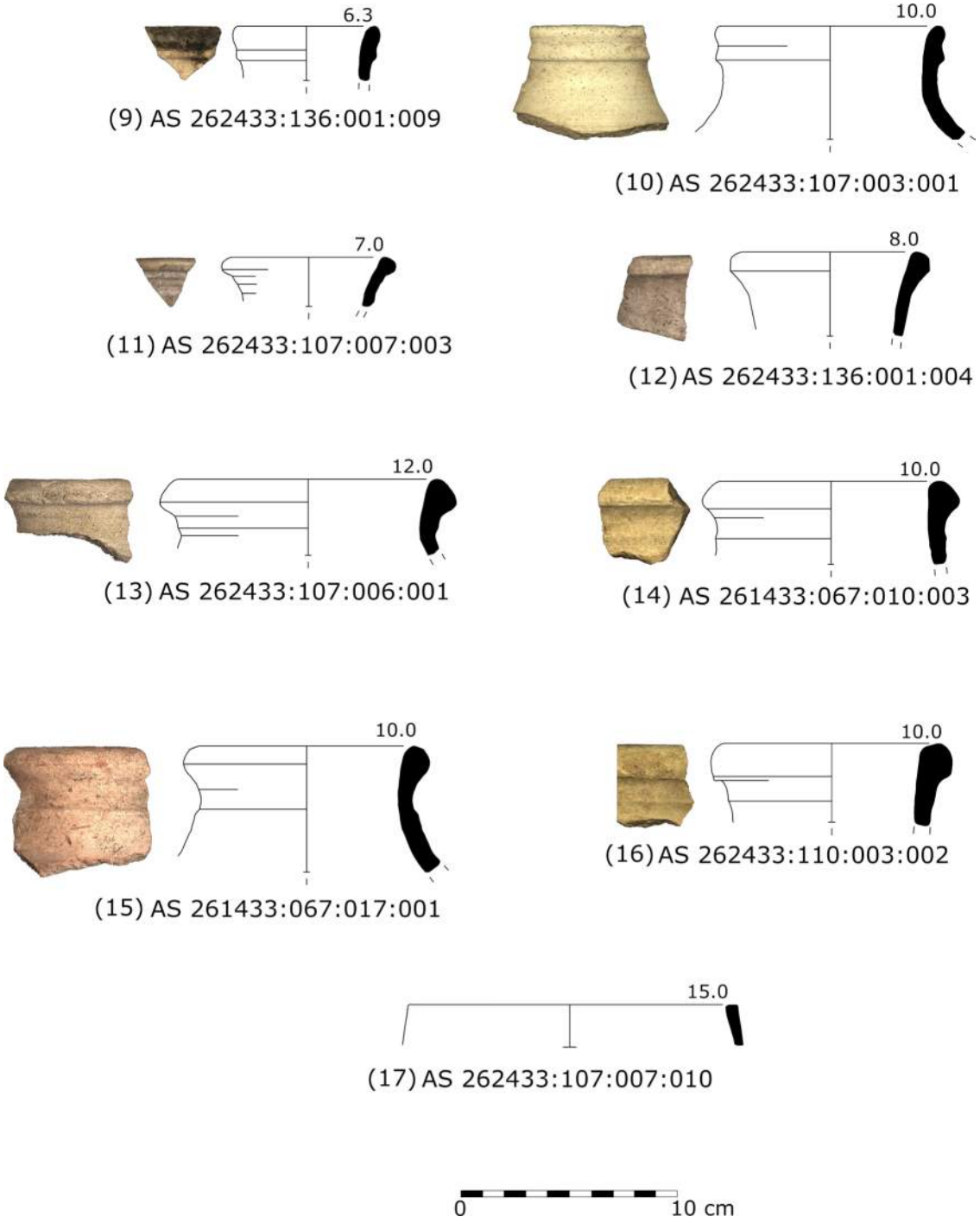

Fig. D1.1.2: Pottery from Building A. Scale 1:3. LAP drawings by Poppy Tushingham and Amr Mohammad Jasim.

Description: Rim and neck of a jar. Projecting thickened rim, almost triangular in section, cylindrical short neck decorated by a low ridge.

(14) AS 261433:067:010:003 (Fig. D1.1.2)
Findspot: Courtyard 10, floor deposit;
Ware: Fabric group 4A; outer surface colour: 2.5Y 8/2; core colour: 7.5YR 6/3; inner surface colour: 2.5Y 8/2; oxidising firing atmosphere;
Manufacturing technique: wheel-made;
Dimensions: H. 3.9 cm; D. 10 cm; Th. 0.6 cm;
Description: Rim and neck of a jar. Projecting thickened rim, almost triangular in section, cylindrical neck decorated by a low ridge.

(15) AS 261433:067:017:001 (Fig. D1.1.2)
Findspot: Courtyard 10, floor deposit;
Ware: Fabric group 2B; outer surface colour: 7.5YR 8/3; core colour: 7.5YR 6/8; inner surface colour: 7.5YR 6/7; oxidising firing atmosphere;
Manufacturing technique: wheel-made, slipped outer surface;
Dimensions: H. 7.1 cm; D. 10 cm; Th. 0.9 cm;
Description: Rim and neck of a jar. Projecting thickened rim, cylindrical short neck, a ridge between neck and shoulder.

(16) AS 262433:110:003:002 (Fig. D1.1.2)
Findspot: Room 7, floor deposit;
Ware: Fabric group 3A; outer surface colour: 2.5Y 8/3; core colour: 2.5Y 8/3; inner surface colour: 2.5Y 8/3; oxidising firing atmosphere;
Manufacturing technique: wheel-made;
Dimensions: H. 3.9 cm; D. 8 cm; Th. 0.85 cm;
Description: Rim and neck of a jar. Projecting thickened rim almost square in section, cylindrical neck decorated by a low ridge.

The sherds (**9**) to (**16**) show several varieties of rims that may be associated with closed forms. The same rim type could have been used for various jars or pots of different sizes and functions. The sherds described above probably belong to small or medium-necked jars, a heterogeneous group of vessels, measuring between 6.3 and 12 cm in diameter. Four types of rims can be identified:

- Sherds (**9**) and (**10**) are folded rims of small-medium jars, 6.3-10.8 cm in diameter. The neck is straight. Folded rims are considered characteristic of the Hellenistic period;[138] however, they appeared already in the Neo-Babylonian and Achaemenid levels of many Mesopotamian sites,[139] as the comparisons demonstrate, and were adopted for necked jars, collar jars, and a variety of pots. This rim type seems to be an expression of the northern pottery tradition,[140] possibly a development of a late Neo-Assyrian type,[141] because it is less popular in the Hellenistic sites of southern Mesopotamia.[142] Moreover, this rim type is frequently decorated with red paint, as in (**9**), which is a typical feature of the northern Hellenistic pottery tradition.[143]

Place	Period	References
Nimrud, Hellenistic House / Hellenistic settlement, Level 4	3rd century BC, 175–150 BC	Oates 1968, fig. 19: 107, 117
Khirbet Khatuniyeh, Level 4	late 7th century BC	Curtis/Green 1997, fig. 50: 245
Khirbet Khatuniyeh, Level 3	post-Assyrian	Curtis/Green 1997, fig. 57: 377
Khirbet Khatuniyeh, Level 2	3rd–2nd century BC	McKenzie 1997, fig. 63: 449-453
Tell Mohammed 'Arab, Hellenistic pits	mid-3rd–mid-2nd century BC	Roaf 1983, fig. 6: 26
Khirbet Qasrij, Trenches B4/1, B5/2, A2, A3, B2, B3, B4/2, A4/1	Late Neo-Assyrian–Achaemenid period	Curtis 1989, fig. 37: 230-234
Khirbet Hatara, Levels 9a-9b	second half of 3rd–2nd century BC	Venco Ricciardi 1997, fig. 5: 63-64; fig. 6: 79-81
Qasr Shemamok, Pit e6	second half of 2nd–early 1st century BC	Calini 2022, figs. 5, 6a-f
Girdi Qala, Trench B, sub-surface	2nd century BC–2nd century AD	Mas 2015, fig. 4
Iraqi Kurdistan, LoNAP survey area	late 4th–late 2nd centuries BC	Palermo 2016, fig. 22: 1-2

- Sherds (**11**) and (**12**) are rims of relatively small jars with a flaring neck, not chronologically diagnostic as they belong to a long-lasting type. For these two examples from Assur, it is possible to indicate only approximate parallels.

138 See e.g., Oates 1968, 142; Calini 2022, 491-492.

139 Curtis 1989, 48-49.

140 Calini 2022, 492.

141 See e.g., Hausleiter 2010, pl. 107: FG 5 R1; pl. 108: FV 1.1; pl. 111: FV 4.2-FV 4.3.

142 Cellerino 2004, 114, 156, fig. 20: 157-159.

143 See e.g., Khirbet Hatara (Venco Ricciardi 1997, 135-136).

Place	Period	References
Khirbet Qasrij, Trenches A3/2, A4/2	Late Neo-Assyrian–Achaemenid period	Curtis 1989, fig. 32: 152, 155
Khirbet Khatuniyeh, Level 3	post-Assyrian	Curtis/Green 1997, fig. 56: 366
Khirbet Khatuniyeh, Level 2	3rd–2nd century BC	McKenzie 1997, fig. 60: 424, 426
Khirbet Hatara, Level 9b	second half of 3rd–2nd century BC	Venco Ricciardi 1997, fig. 6: 78; fig. 8: 105
Gird-i Matrab, Area A, Building A	4th–early 2nd century BC	Palermo 2024, fig. 9: 12

- Sherds (**13**), (**14**), and (**15**) are rims of medium-sized jars with a relatively short neck, characterised by a low ridge at the junction of the typically ovoid body. This type has a long history in northern Mesopotamia, appearing in various closed shapes from the late Neo-Assyrian period to the end of the 2nd century BC.

Place	Period	References
Assur	Late Neo-Assyrian, 8th–7th century BC	Hausleiter 2010, pl. 97: FM 2.2, FM 2.5; pl. 103: FG 3.4, FG 3.5
Nimrud, North West Palace	8th–7th century BC	Hausleiter 2010, pl. 89: FW 1.3
Nimrud, Fort Shalmaneser	last decade of 7th century–first half of 6th century BC	Oates 1959, pl. XXXVIII: 97-99
Nimrud, Hellenistic House	3rd century BC	Oates 1968, fig. 19: 113, 115
Nineveh, MG 22 Area	7th century BC	Lumsden 1999, fig. 6: 32
Khirbet Khatuniyeh, Level 4	late 7th century BC	Curtis/Green 1997, fig. 39: 170-171; fig. 41: 178, 183
Khirbet Khatuniyeh, Level 2	3rd–2nd century BC	McKenzie 1997, fig. 62: 444
Gird-i Matrab, Area A, Building A	4th–early 2nd century BC	Palermo 2024, fig. 9: 14

- Sherd (**16**) belongs to the same type of jars as the previously described sherds. Thick squared rims appeared in the late Neo-Assyrian period and are still used in the Achaemenid and early Hellenistic periods, associated with different-sized jars. The type is also quite common in southern Mesopotamia.[144]

Place	Period	References
Assur	Late Neo-Assyrian, 8th–7th century BC	Hausleiter 2010, pl. 26: Ass. 11951d; pl. 27: Ass. 11960a; pl. 30: Ass. 12054, g 3.4, FG 3.5
Nimrud, Hellenistic House	3rd century BC	Oates 1968, fig. 19: 112
Khirbet Khatuniyeh, Level 4	late 7th century BC	Curtis/Green 1997, fig. 41: 179-180
Khirbet Khatuniyeh, Level 2	3rd–2nd century BC	McKenzie 1997, fig. 62: 444

(17) AS 262433:107:007:010 (Fig. D1.1.2)
Findspot: Room 8, floor deposit;
Ware: Fabric group 5; outer surface colour: 7.5YR 5/6; inner surface colour: 5YR 5/6; oxidising firing atmosphere, dark core;
Manufacturing technique: probably hand-made, self-slipped surface;
Dimensions: H. 2.2 cm; D. 17.3 cm; Th. 0.7 cm;
Description: Rim and neck of a cooking pot. Simple, rounded rim, flat on top.

Place	Period	References
Khirbet Qasrij, Trenches B1-B2	first half of 6th century BC	Curtis 1989, fig. 41: 282
Qasr Shemamok, Pit e6	second half of 2nd–early 1st century BC	Calini 2022, fig. 8e-f

This sherd belongs to the class of cooking pots, whose function is identifiable based on technical and morphological criteria. Functional criteria dictate the form; therefore, the latter is scarcely influenced by changing ceramic styles, making it difficult to date cooking pots precisely. Only during the Seleucid period new types of cooking vessels, adapted from Greek prototypes, became part of the Near Eastern pottery repertoire.

Cooking pots have a coarse mineral-organic fabric that enhances heat resistance, a rounded or slightly flattened base, and walls of consistent thickness. Small gravel, quartzite, calcite, and straw may be added to the clay mixture. The cooking pot fragment (**17**) exhibits careless manufacturing and was probably handmade. The dark core, resulting from the incomplete removal of carbonaceous matter, indicates

144 Cellerino 2004, 113-114, 154, fig. 19: 142-143.

inadequate firing or relatively low temperature. Cooking pots from the 2nd millennium BC onwards typically have a globular or biconical shape; the mouth is always wide, the neck is short, and the rim is plain, slightly everted, or inwardly oriented. The cooking pots of this type are medium-sized, with a rim diameter between 11 and 20 cm.

(18) AS 261433:067:021:004 (Fig. D1.1.3)
Findspot: Courtyard 10, floor deposit;
Ware: Fabric group 4B; outer surface colour: 10YR 8/2; core colour: 5YR 6/6; inner surface colour: 10YR 8/2; oxidising firing atmosphere;
Manufacturing technique: wheel-made;
Dimensions: H. 2.2 cm; D. 17.3 cm; Th. 0.7 cm;
Description: Rim and small part of the body of a large-mouth pot. Projecting rim, almost rectangular in section.

Place	Period	References
Assur	Late Neo-Assyrian, 8th–7th century BC	Hausleiter 2010, pl. 117: TG1R3
Nimrud, Hellenistic House	3rd century BC	Oates 1968, fig. 19: 111
Nimrud, Fort Shalmaneser	post-Assyrian levels	Chiocchetti 2008, fig 2: 20
Nineveh, MG 22 Area	7th century BC	Lumsden 1999, fig. 7: 39
Khirbet Khatuniyeh, Level 6	Late Neo-Assyrian	Curtis/Green 1997, fig. 32: 71
Khirbet Khatuniyeh, Level 4	late 7th century BC	Curtis/Green 1997, fig. 51: 260
Khirbet Khatuniyeh, Level 2	3rd–2nd century BC	McKenzie 1997, fig. 63: 456
Qasr Shemamok, Pit e6	second half of 2nd–early 1st century BC	Calini 2022, fig. 6m

(19) AS 262433:136:001:001 (Fig. D1.1.3)
Findspot: Courtyard 10, floor deposit;
Ware: Fabric group 4A; outer surface colour: 2.5Y 8/2; core colour: 10YR 8/3; inner surface colour: 2.5Y 8/2; oxidising firing atmosphere;
Manufacturing technique: wheel-made, slipped surfaces;
Dimensions: H. 4.1 cm; D. 32 cm; Th. 0.7 cm;
Description: Rim and part of the body of a large-mouth pot. Broad out-turned rim, slightly offset on the interior. The external face is concave.

Place	Period	References
Kar-Tukulti-Ninurta, surface	post-Assyrian period	Schmidt 1999, fig. 7a: 9
Khirbet Khatuniyeh, Level 2	3rd–2nd century BC	McKenzie 1997, fig. 63: 455
Gird-i Matrab, Area A, Building A	4th–early 2nd century BC	Palermo 2024, fig. 9: 6
Iraqi Kurdistan, LoNAP survey area	late 4th–late 2nd centuries BC	Palermo 2016, fig. 22: 11

Although quite different in size, the sherds (**18**) and (**19**) belong to the same type of storage vessel. Bell-shaped or ovoid vessels with a slightly constricted, wide mouth, without a neck, with a rim diameter slightly smaller than or the same as the maximum diameter of the vessel, and usually a disk or ring base, were very common storage containers in ancient Mesopotamia, produced in countless variants from at least the second millennium BC onwards.

These movable storage jars were used for the short-term storage of daily amounts of various foodstuffs, both liquid and dry, and may have been placed in the house storeroom or kitchen area.[145] The sherd (**18**), in particular, has a shape elaborated during the late Neo-Assyrian period but still used in the Hellenistic period, as the comparisons above demonstrate.

The sherd (**19**) features a distinctive out-turned rim that resembles the rims of certain Attic kraters,[146] which date from the 3rd to the early 2nd century BC. These kraters were common household vessels,[147] used not only for mixing wine and water at the symposium but also for various other functions.[148] The comparisons date this type from the late 4th to the 2nd century BC.

(20) AS 261433:046:020:001 (part of A-01-J04) **(Fig. D1.1.3)**
Findspot: Room 2, floor deposit;
Ware: Fabric group 4A; core colour: 10YR 7/4; bitumen on the inner and outer surface; oxidising firing atmosphere;
Manufacturing technique: wheel-made;
Dimensions: H. 4.8 cm; D. 15 cm; Th. 1.2 cm;
Description: Rim and neck of a large jar. Folded rim with an indentation on the outer side, short cylindrical neck.

Place	Period	References
Nimrud, Hellenistic settlement	probably Achaemenid, but also from Levels 3-2, post-150-145 BC	Oates 1968, fig. 20: 143
Khirbet Khatuniyeh. Level 2	3rd–2nd century BC	McKenzie 1997, fig. 63: 453

145 Rotroff 2006, 93.
146 Rotroff 2006, fig. 36: 214; fig. 37: 216.
147 Sparkes/Talcott 1970, 54.
148 Rotroff 2006, 105-107.

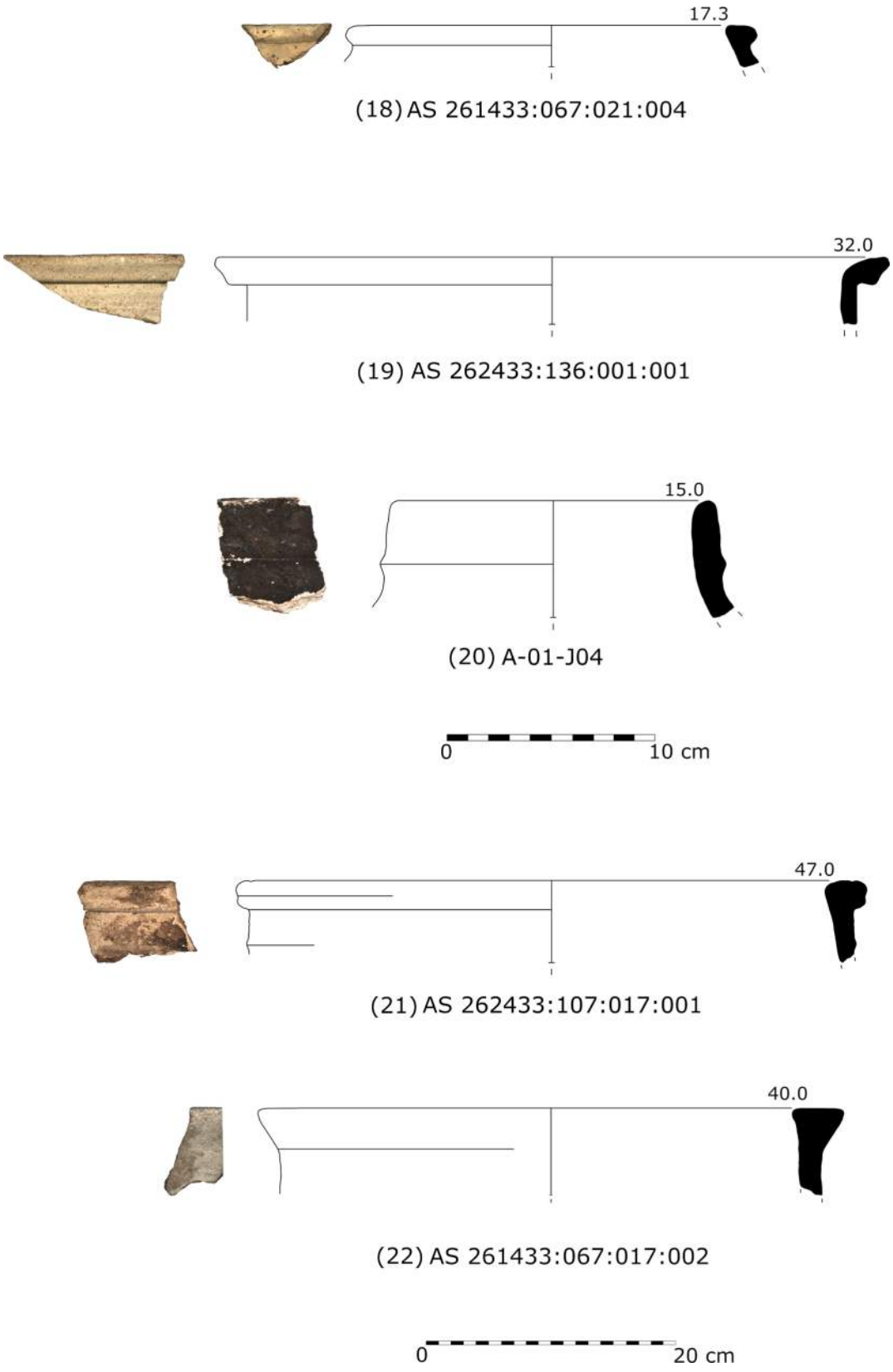

Fig. D1.1.3: Pottery from Building A. AS 261433:067:021:004, AS 262433:136:001:001 and A-01-J04 in scale 1:3; AS 262433:107:017:001 and AS 261433:067:017:002 in scale 1:5. LAP drawings by Poppy Tushingham and Amr Mohammad Jasim.

Place	Period	References
Tell Mohammed 'Arab, Hellenistic pits	mid-3rd–mid-2nd century BC	Roaf 1983, fig. 6: 26
Khirbet Qasrij, Trench B4/2	Late Neo-Assyrian–Achaemenid period	Curtis 1989, fig. 37: 234
Khirbet Hatara, Level 9b	second half of 3rd–2nd century BC	Venco Ricciardi 1997, fig. 7: 84
Qasr Shemamok, Pit e6	second half of 2nd–early1st century BC	Calini 2022, fig. 6e-f
Girdi Qala, Trench B, sub-surface	2nd century BC–2nd century AD	Mas 2015, fig. 4: 40
Iraqi Kurdistan, LoNAP survey area	late 4th–late 2nd century BC	Palermo 2016, fig. 20: 11

The sherd (**20**) belongs to a typical storage jar, probably ovoid in shape, with a short neck, a relatively small diameter, and a rounded or pointed base. The morphology, the thickness of the walls (1.2 cm), and the coating of the jar with bitumen for waterproofing and reducing porosity to retard seepage, indicate that it could have been used for storing liquids. The very elongated folded rim might suggest a date to the end of the 2nd century BC.[149]

(21) AS 262433:107:017:001 (Fig. D1.1.3)
Findspot: Room 8, floor deposit;
Ware: Fabric group 3A; outer surface colour: 10YR 8/3; core colour: 2.5Y 6/6; inner surface colour: 2.5Y 8/2; oxidising firing atmosphere;
Manufacturing technique: wheel-made, self-slipped surfaces;
Dimensions: H. 6.5 cm; D. 47 cm; Th. 1.6 cm;
Description: Rim and part of the body of a large storage jar. Projecting rim, almost rectangular in section.

Place	Period	References
Khirbet Khatuniyeh, Level 4	late 7th century BC	Curtis/Green 1997, fig. 51: 263
Khirbet Khatuniyeh, Level 3	post-Assyrian	Curtis/Green 1997, fig. 57: 380
Khirbet Khatuniyeh, Level 2	3rd–2nd century BC	McKenzie 1997, fig. 63: 456
Khirbet Hatara, Level 9b	second half of 3rd–2nd century BC	Venco Ricciardi 1997, fig. 7: 84
Khirbet Qasrij, Trench A1	Late Assyrian–Achaemenid period	Curtis 1989, fig. 38: 251

The sherd (**21**) belongs to a large storage container, a class of vessels common in all periods and regions in antiquity. These containers feature wide mouths, deep bodies, thick walls, and large capacities. Large vessels of this type were utilised for the long-term storage of foodstuffs, particularly grains and legumes. They may have also contained water in household pantries. The design of these storage pithoi reflects their function, as the wide mouths facilitate easy access to their contents. In the Mesopotamian pottery tradition, they are often adorned with applied ribbings that cover the junctions of the different parts used in their construction,[150] simplifying transport.

(22) AS 261433:067:017:002 (Fig. D1.1.3)
Findspot: Courtyard 10, floor deposit;
Ware: Fabric group 3A; outer surface colour: 2.5Y 8/2; core colour: 5YR 6/6; inner surface colour: 2.5Y 8/2; oxidising firing atmosphere;
Manufacturing technique: hand-made;
Dimensions: H. 8.2 cm; D. 40 cm; Th. 1.5 cm;
Description: Rim and part of the body of a large tray. Projecting thickened rim with flat lip.

The sherd (**22**) is a rim of a large vessel variously called by scholars tray, basin, mortar, mortar plate, or 'plat à râper'.[151] These vessels belong to a well-known class of handmade shallow containers characterised by their coarse ware, thick walls, irregular, often oval shape, and sometimes fitted with a pinched spout. The average diameter varies from 30 to 40 cm. Although this type of vessel was widespread in Mesopotamia from at least the second millennium BC,[152] it is considered a hallmark of the Achaemenid and Seleucid periods.[153] Scholars have suggested that they could have served for grinding grains[154] but, as Rotroff pointed out, such pottery trays could instead be used to crush spices, vegetables, and garlic in the preparation of sauces or other recipes, or, in the Greek world, for pressing a small amount of grapes.[155] It seems likely that this type of vessel ceased to be made around the mid- or end of the 2nd century BC, as indicated by the archaeological contexts of Failaka, Susa, and Seleucia on the Tigris. The reasons for their disappearance are unclear but plausibly linked to economic changes and agricultural

149 McKenzie 1997, 93; Calini 2022, 492.

150 As is well known, large storage jars were made by separate parts (being) joined together, a process dubbed "slab building" (see Lecomte 1987, 230; Rice 1987, 125).

151 Adams 1965, 130; Hannestad 1983, 67; Bernard/Gachet/Salles 1990, 270; Petrie 2002, 99; Rotroff 2006, 116-117.

152 See e.g., Gabutti 2002-2003, pls. 41-42.

153 Gibson 1972, 165.

154 See e.g., Hannestad 1983, 67; Valtz 2024, 218.

155 Rotroff 2006, 100, 117. Ceramic vessels are too fragile for grinding grains or pressing olives.

developments that occurred after the Parthian conquest of Mesopotamia.[156] The closest parallels to (**22**) are restricted to central-southern Mesopotamia, where such trays are common.[157]

Place	Period	References
Babylon, ShuAnna	Seleucid levels	Cellerino 2004, fig. 14: 97
Larsa, Ebabbar, Room 23	2nd–1st century BC	Lecomte 1987, pl. 52: 9
Larsa, Ebabbar, Room 24	2nd century BC	Lecomte 1987, pl. 28: 3
Seleucia, North Agora, Stoa area, Archive area, Level IIIa	mid-2nd century BC	Valtz 2024, pl. 47: 152-157
Failaka, Hellenistic fortress	mid-3rd–beginning 1st century BC	Hannestad 1983, pl. 63: 656

D1.1.3 Preliminary conclusions

This study examined a selection of pottery sherds recovered from Hellenistic Building A, categorised by vessel shape. While the findings highlight patterns in storage (large jars), domestic activities (a cooking pot fragment and tray fragment), and possible communal usage (tableware such as fishplates), these observations remain tentative as they rely on a small selection of sherds. The presence of a fragment of an imported Attic echinus bowl represents an intriguing discovery that illuminates the interregional connections that the inhabitants of Building A had with other areas of the world. In this regard, the wood charcoal remains from Building A indicate a similar pattern of interregional connections regarding the import of wood from distant regions (**§I1**). Future studies that incorporate a larger dataset and additional analysis should further refine our understanding of pottery distribution and spatial organisation within Building A.

D1.2 The pottery from trench NT2 in the New Town of Assur (2024)

John MacGinnis, Jana Richter & F. Janoscha Kreppner

The trench NT2 with the drainage shaft (**§C4**), excavated close to the southern portion of the fortification walls of the New Town, yielded a mixture of pottery material ranging from the 14th century BC to the Parthian period. While there is a noticeable tendency for older pottery to be more prevalent in the lower layers (Phases 2 and 1) and younger pottery in the upper layers (Phases 4 and 3), the stratigraphic phases and the pottery levels do not align consistently. Consequently, older and younger materials are often intermixed within the same stratigraphic phase.

In addition to numerous older pieces, Phases 4 and 3 contained pieces that can be assigned to the Parthian (**Fig. D1.2.1**) and Hellenistic periods (**Fig. D1.2.2**), which is why the formation of the accumulations of these two phases can be assigned to these periods. The heavily ash-rich deposits of Phase 2 contained Neo-Assyrian pottery, more concentrated above the surface NT2-F2 (**Fig. D1.2.3**). The presence of pottery from different periods suggests that the fills accumulated in the depression without a hiatus in the stratigraphic sequence being recognisable (see also **§C4.3**).

The fill of the shaft identified in Phase 1 contained mainly Middle Assyrian pottery from the 13th century BC (**Fig. D1.2.4**). Some pieces can be dated to the 14th century BC (**Fig. D1.2.5**). However, a few pieces from the upper part of the shaft can be dated to the Neo-Assyrian period (**Fig. D1.2.6**). The pottery finds suggest that this shaft was already in use in the second millennium BC, soon after the foundation of the New Town. At the same time, Neo-Assyrian pottery in the shaft fill indicates that material was filled in at least in the upper area, which was already in the Iron Age before the surface NT2-F2 was created. The charcoal sample from the shaft fill, radiocarbon-dated to 770-541 calBC (95.4% probability; **§C1.2** and **§C4.4**), further supports this scenario.

D1.3 Honeycomb jars of the Early Islamic period from Assur (2023 and 2024)

Mustafa Ahmad

D1.3.1 Introduction

"Honeycomb ware" is a distinctive decorative pattern applied primarily to a specific class of vessels, most notably large-sized storage jars. Although the ware had previously been described under various terms and classifications, the designation "honeycomb" was first explicitly introduced by Robert McC. Adams in 1965. Earlier publications had documented similar pottery types but employed differing terminologies and descriptive frameworks.[158]

156 Bernard *et al.* 1990, 270; Valtz 2024, 218.

157 Petrie 2002, 99.

158 For details about the different terminologies used for honeycomb ware, see Ahmad 2025, 456-457.

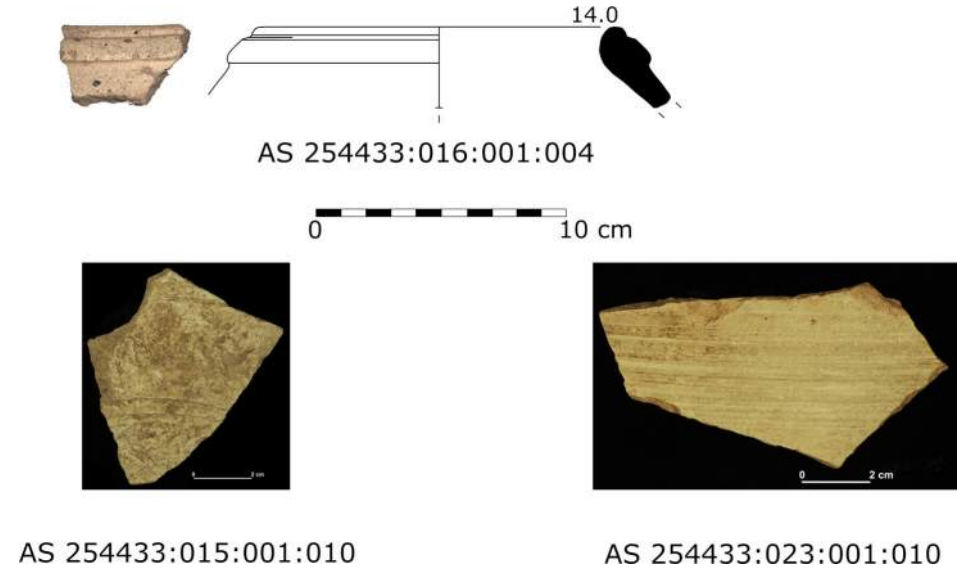

Fig. D1.2.1: Parthian-period pottery from trench NT2, Phases 4 and 3. Drawing in scale 1:3. Created by Andrea Squitieri from LAP drawings by Poppy Tushingham and Amr Mohammad Jasim.

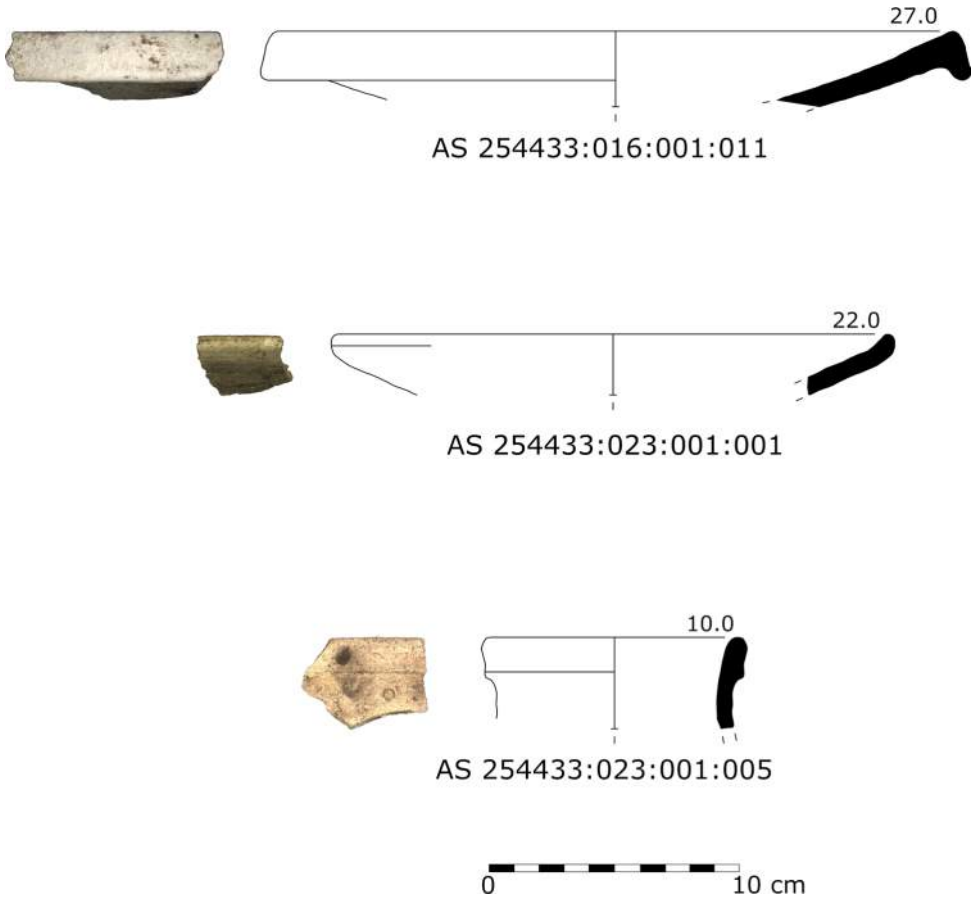

Fig. D1.2.2: Hellenistic pottery from trench NT2, Phases 4 and 3. Scale 1:3. Created by Andrea Squitieri from LAP drawings by Poppy Tushingham and Amr Mohammad Jasim.

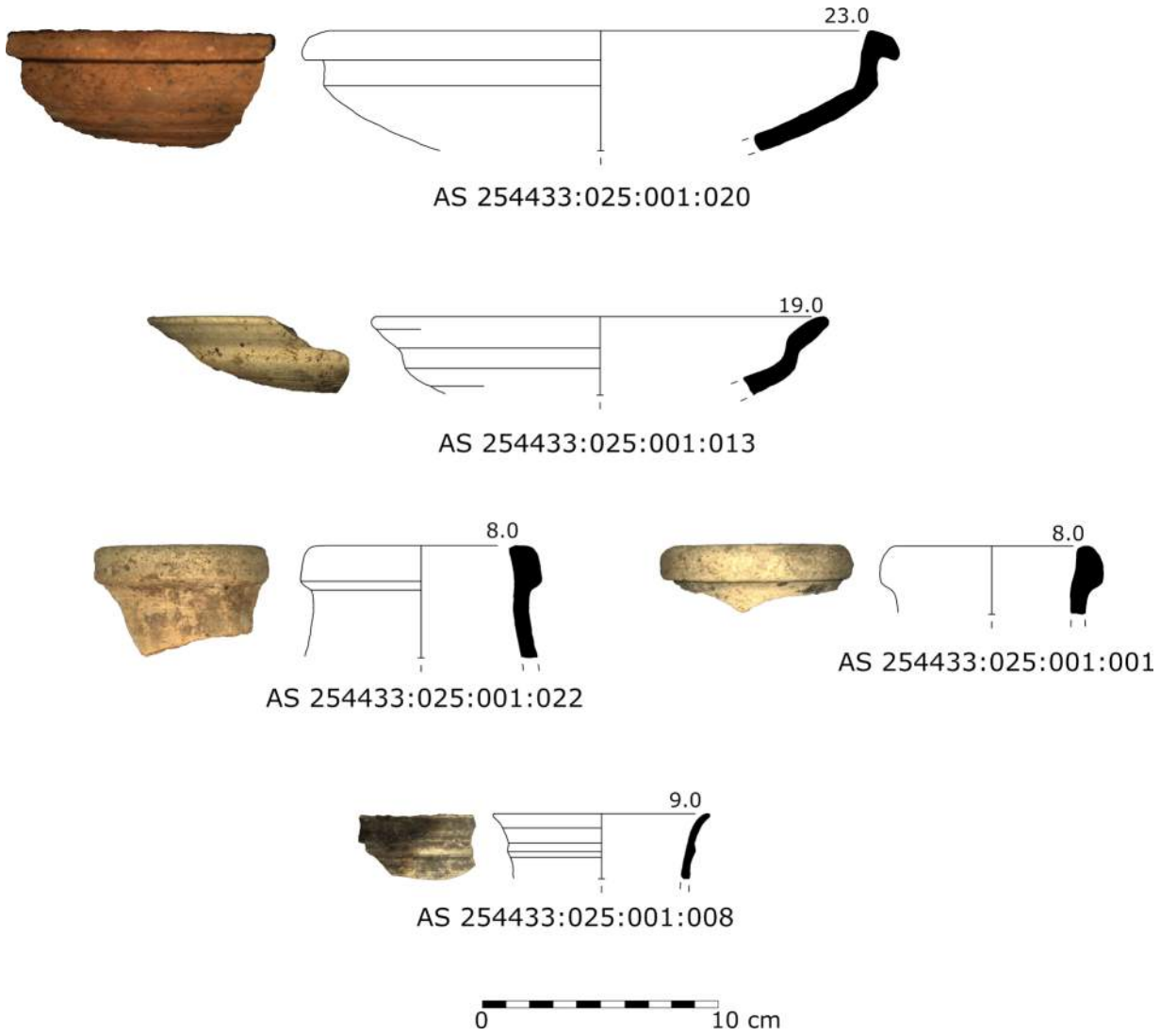

Fig. D1.2.3: Neo-Assyrian pottery from trench NT2, above surface NT2-F2. Scale 1:3 Created by Andrea Squitieri from LAP drawings by Poppy Tushingham and Amr Mohammad Jasim.

The honeycomb ware technique involves modifying the texture of the vessel's exterior by pressing fingertips into the wet clay before firing, resulting in intricate decorative patterns. The fabrics used for this ware typically incorporate mineral-tempered, sandy, or gritty inclusions and, occasionally, vegetal temper. The predominant fabric colour is greenish buff, though variations in buff, reddish buff, and reddish-brown are also observed. Honeycomb ware encompasses a range of decorative patterns, including cellular impressions, vertical or wavy lines, and broad thumb impressions. Despite the diversity in patterns, these designs are collectively categorised under the term "honeycomb ware".

This section deals with two complete honeycomb-decorated jars found in Assur during the 2023 and 2024 excavation seasons[159]. Honeycomb-decorated pottery is frequently encountered in Iraq in both excavated sites and archaeological surveys, and it has long been misattributed to the Sasanian period. A significant reassessment of its chronology was undertaken by St. John Simpson in 1992, who redefined honeycomb ware as belonging exclusively to the Early Islamic period. This revision was grounded in the absence of honeycomb pottery in securely dated, stratified Sasanian contexts, in contrast with its widespread presence at monophase Early Islamic sites in the Mosul Dam Lake region.[160]

159 Kreppner/Richter/Squitieri 2024, 141, and see **§C2.4**.
160 Simpson 1992, 296.

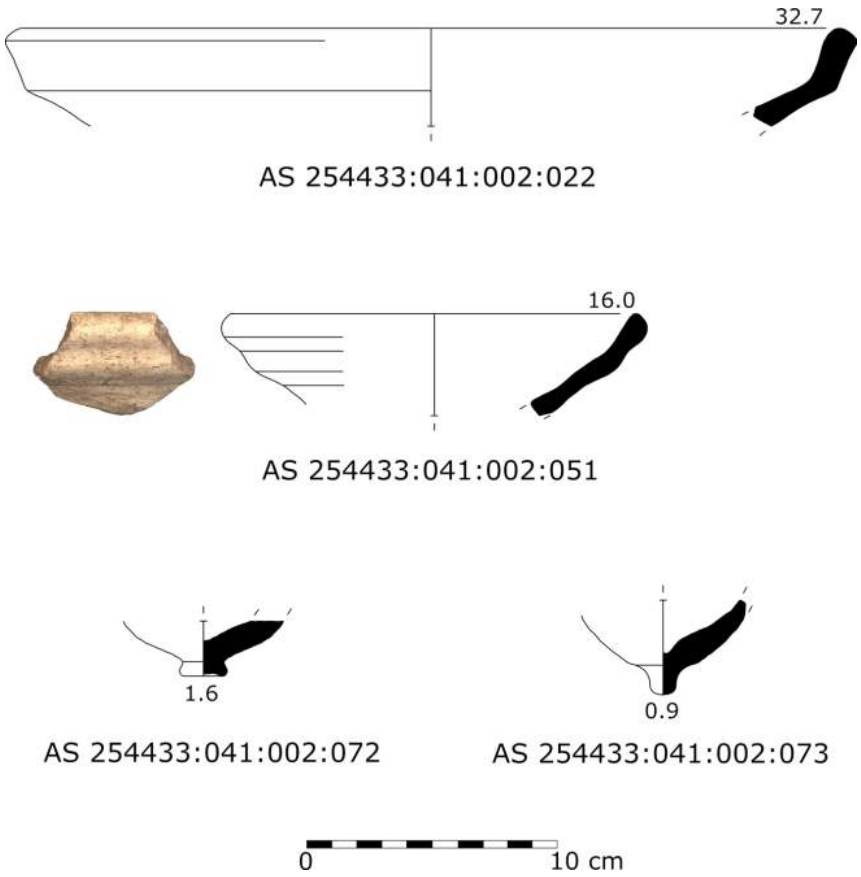

Fig. D1.2.4: Middle Assyrian pottery from trench NT2, Phase 1. Scale 1:3. Created by Andrea Squitieri from LAP drawings by Poppy Tushingham and Amr Mohammad Jasim.

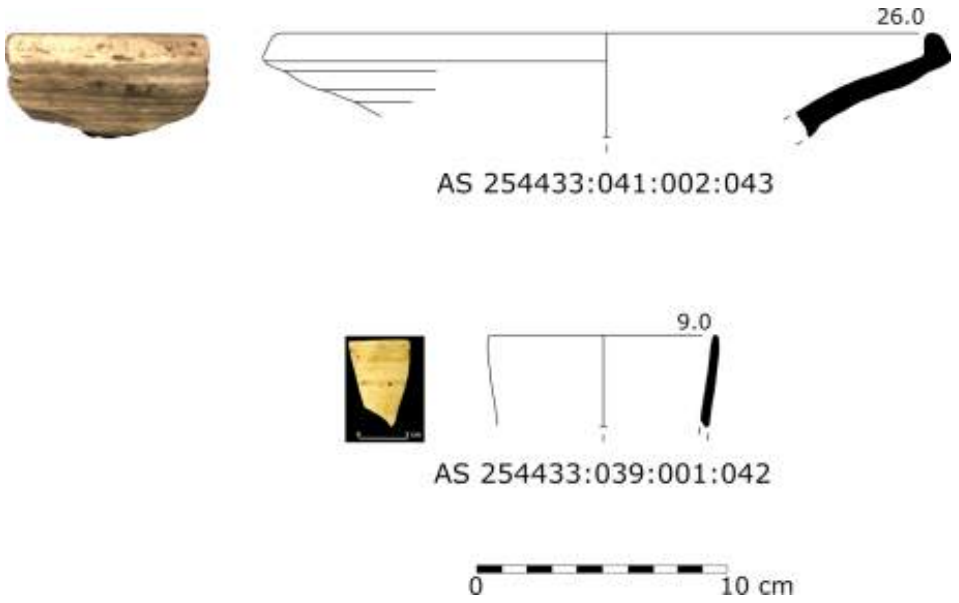

Fig. D1.2.5: 14th century BC pottery from trench NT2, Phase 1. Drawings in scale 1:3. Created by Andrea Squitieri from LAP drawings by Poppy Tushingham and Amr Mohammad Jasim.

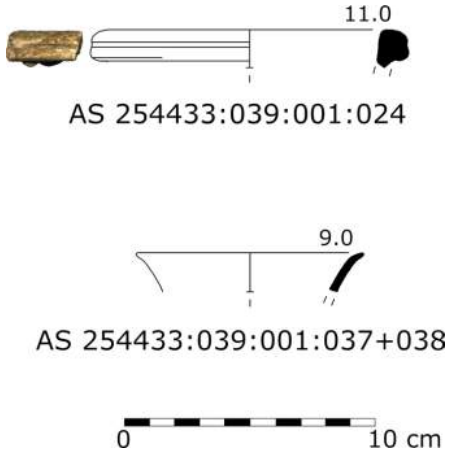

Fig. D1.2.6: Neo-Assyrian pottery from trench NT2, Phase 1. Scale 1:3. Created by Andrea Squitieri from LAP drawings by Poppy Tushingham and Amr Mohammad Jasim.

1.3.2 The honeycomb jars from Assur

Walter Andrae found honeycomb ware fragments during his excavations at the caravanserai in Assur.[161] However, the honeycomb pattern visible on the photograph of a published sherd differs from the pattern in evidence on the two jars studied in this chapter.

During the 2023 and 2024 excavation seasons, two complete honeycomb jars were found at the New Town of Assur. The jar AS 262433:021:007 (**Fig. D1.3.1**) is referred to in the following text as Jar 1 (with four handles), and jar AS 261433:036:005 (**Fig. D1.3.2**) is Jar 2 (with three handles).

From a morphological point of view, Jar 1 has a rounded ovoid shape, while Jar 2 has a more spherical shape. While equipped with different numbers of handles, both jars share the same handle type: oval-sectioned, ear-shaped handles (onto which Jar 2 has round thumb-stops applied), and they have the same rounded base. Also, they share the same decorative patterns, namely the honeycomb decoration applied to the body.

The honeycomb decoration comprises successive vertical bands of two decorative elements: impressed finger imprints and thumb-smeared imprints. These are confined within finger-trailled vertical lines, which are executed in the zones below the handles. Jar 2 has three vertical bands underneath its three handles (**Fig. D1.3.2**), while Jar 1 (**Fig. D1.3.1**) has four vertical bands underneath its four handles. This might be a standardised technique for applying this pattern in Assur, whereas such correspondence between handles and bands is not common in honeycomb jars from other sites.

Although the jars share the main morphological features and the honeycomb decoration pattern, they differ in the rim shapes and the decorative elements applied to the jars' rims, necks, and upper bodies. Jar 1 has a triangular folded rim with grooves on top, while Jar 2 has a banded rim with hatched decoration on the outer surface.

Jar 1's set of decorations is composed of an incised wavy-grooved line, a rib with interval impressions, another incised wavy line, and hatched decoration confined between two horizontal grooved lines, respectively, from the rim to the end of the jar's shoulders.

Jar 2 has a plain short neck without any decoration, followed by an impressed rib at the base of the neck and a series of oblique impressed comb tips (head of seven tips), a wavy combed decoration, a horizontal combed decoration, and another wavy combed decoration on the shoulder of the jar. The shoulders are also adorned with an applied decoration made of a moon shape with a solid round appliqué. Three of these sets of appliques are executed on the areas between the handles.

161 Andrae/Lenzen 1933, pl. 56n (photograph).

D1.3.3 Comparisons

Only a few complete honeycomb jars are known from excavations, including those found at Khirbat Salih (**Fig. D1.3.3:1**),[162] Eski Makhmur (**Fig. D1.3.3:2**),[163] Sin al-Dhibban (**Fig. D1.3.3:3**),[164] Yorgan Tepe (**Fig. D1.3.3:4**),[165] Tulul al-Hamediyat (**Fig. D1.3.4:1**),[166] and Tell Tuneinir **(Fig. D1.3.4:2-4)**.[167] Attested are jars that are rounded hemispherical;[168] ovoid; elongated ovoid;[169] and rounded with a bulbous base.[170] In archaeological excavations and surveys, most honeycomb ware vessels are usually found in fragmented conditions as broken body sherds. Therefore, it is sometimes difficult to attribute a body sherd of this ware to a specific type of honeycomb jar.

The relative lack of complete honeycomb jars makes comparing the two Assur examples difficult. A complete jar displayed at the Duhok Museum in the Kurdish Autonomous Region of Iraq resembles Jar 1. Unfortunately, it originated from a non-stratified context found at a salvage excavation site named Kalatè, located in Duhok province.[171] Remarkably, the decoration of a moon-like shape applied on the shoulders of the second jar is similar to a decorated jar found in Tikrit (**Fig. D1.3.4:5**).[172] The latter has additional elements,[173] but they both share the overall shape and the hatched incised impressions on the moon-shaped line. The lower part of the Tikrit jar is decorated with a honeycomb decoration.

The hatched decorated rim in Jar 2 from Assur is common in rims of jars usually found in northern Mesopo-

162 Cinti Luciani 1993, pl. CXI: 1.

163 Nováček *et al.* 2016, fig. 133. Nováček/Melčák 2016, fig. 7 (almost complete).

164 Reitlinger 1951, fig. 7-8.

165 Ehrich 1939, pl. 137A (broken).

166 Kawamata 1990, fig. 8: 34, 11 (broken).

167 See the Tell Tuneinir website at http://users.stlcc.edu/mfuller/Area1opotteryPhotos.html.

168 A complete honeycomb jar of this type is displayed at Duhok Museum in Iraq (author's observation).

169 Examples of the ovoid and elongated ovoid jars are displayed at Aleppo Museum (thanks to Marie-Odile Rousset for providing this information).

170 See the Tell Tuneinir website at http://users.stlcc.edu/mfuller/Area1opotteryPhotos.html.

171 Information obtained by the author from the Directorate of Antiquities and Heritage of Duhok.

172 Reitlinger 1951, 15, fig. 4.

173 Similar decoration patterns were found on body sherds from the old excavations at Assur, see Andrae 1977, 271-272, fig. 247.

Fig. D1.3.1: The honeycomb Jar 1 from Assur, AS 262433:021:007. Photos by Andrea Squitieri, collage by Mustafa Ahmad.

Fig. D1.3.2: The honeycomb Jar 2 from Assur, AS 261433:036:005. Photos by Andrea Squitieri, collage by Mustafa Ahmad.

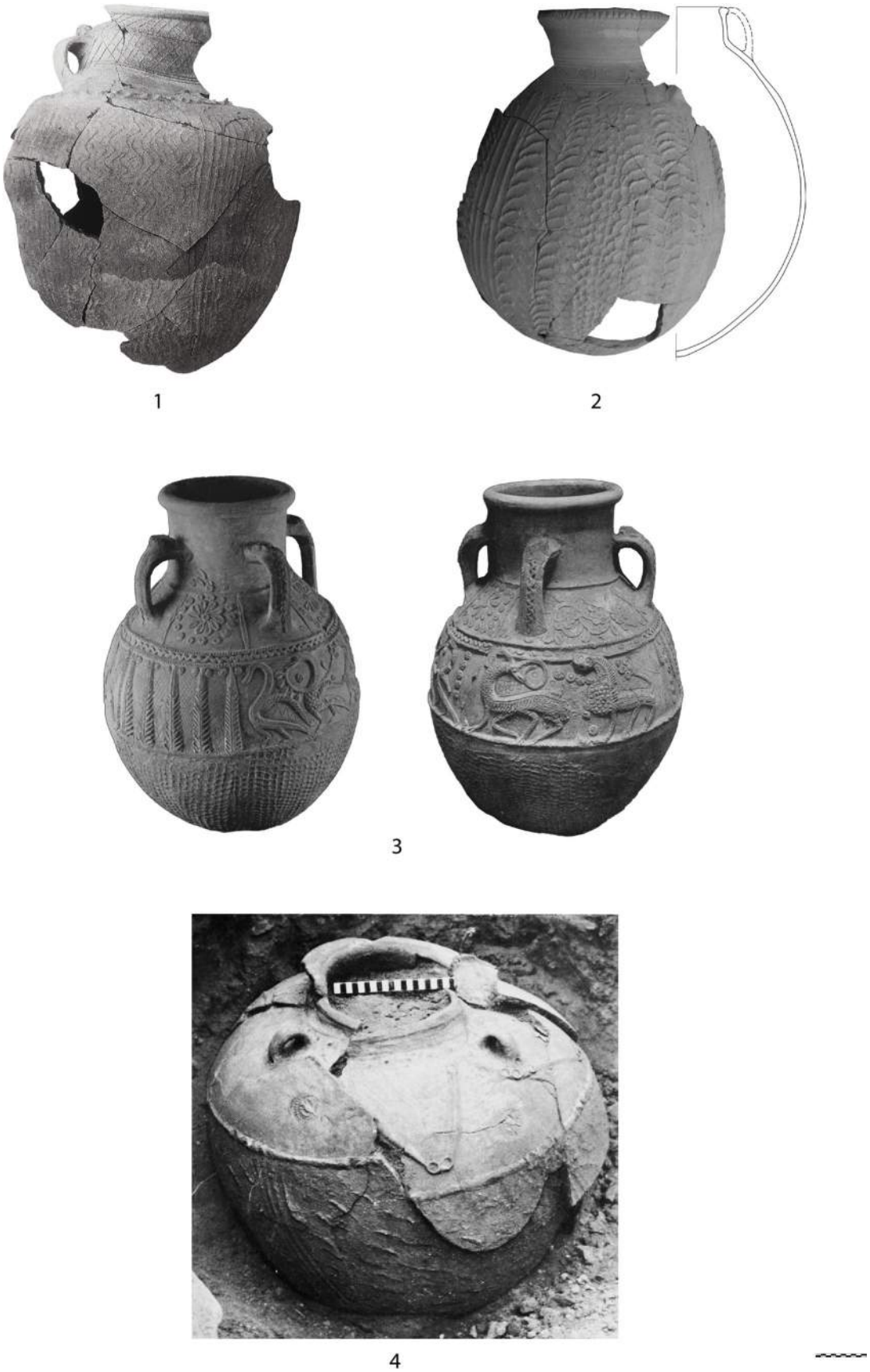

Fig. D1.3.3: Honeycomb jars from Khirbat Salih (1), Eski Makhmur (2), Sin al-Dhibban (3), and Yorgan Tepe (4). Created by Mustafa Ahmad.

Fig. D1.3.4: Honeycomb jars from Tulul al-Hamediyat (1), Tell Tuneinir (2-4), and Tikrit (5). Created by Mustafa Ahmad.

tamia. Similar rims were used as chrono-markers in the North Jazira Survey and dated to the Late Sasanian / Early Islamic period, side by side with honeycomb ware.[174] Hatched decorated rims were also found with honeycomb jars at Resafa and dated to the 8th century AD.[175] It is also attested on a rim found at Eski Makhmur near Erbil, but it is uncertain if the sherd in question is part of a honeycomb ware jar.[176] However, among the associated pottery at the site, an almost complete honeycomb ware jar bears honeycomb patterns similar to the Assur jars.[177]

D1.3.4 Chronology

Neither of the honeycomb jars discovered in Assur came from primary contexts. Jar 1 was recovered from the floor of Subdivision 5 of the chamber tomb (Grave 1), excavated in the 2023 season and dated to the Parthian period.[178] However, it was placed there at a later time, possibly during a looting event, long after the tomb had ceased to serve its original funerary function.[179] Jar 2 was found in a pit, likely a later intrusive feature, possibly a looting pit (**Fig. C2.4.1**), which cut through the Parthian-period deposits (see **§C2.4**).

Based on comparative features, such as jar typology, the honeycomb decoration pattern, and the associated applied motifs, the two honeycomb jars from Assur can tentatively be assigned to the Early Islamic period, specifically the 7th–8th centuries AD. However, the presence of an impressed hatched motif applied to the crescent-shaped applied band is not attested before the first half of the 8th century AD. This suggests that the jars under discussion may more precisely be dated to the early 8th century AD. Continued excavations of the later occupational phases at Assur may yield further data to refine the chronology of the Early Islamic occupation at the site.

D1.3.5 Conclusions

Honeycomb ware is among the more readily identifiable ceramic types within archaeological assemblages, primarily due to its distinctive decorative style. Nevertheless, the scarcity of well-stratified excavation contexts has hindered the development of a comprehensive understanding of this ware. As a result, our current knowledge of honeycomb ware remains fragmented, based mainly on a limited number of complete vessels and dispersed body sherds recovered from excavations and surveys.

The honeycomb jars from Assur discussed in this section significantly contribute to this limited corpus. Their importance lies not only in their intact and complete preservation but also in the notable consistency of the honeycomb decoration applied to both jars, despite variations in overall form and the decorative treatment of the rims, necks, and upper body sections. Conversely, the discovery of these jars in earlier, unrelated contexts raises questions concerning the circumstances of their deposition, particularly the rationale behind their deliberate placement in an intact state within such contexts.

D2. Chemical and petrographic analysis of Hellenistic and Parthian-period pottery from Assur, 2023 and 2024

Michaela Schauer & Silvia Amicone

This section presents the results of portable X-ray fluorescence (p-XRF) and petrographic analyses conducted on a total of 75 pottery samples from the Hellenistic and Parthian periods. Of these, 25 samples were exported to Germany after the 2023 spring campaign and analysed, with their results already discussed in the publication detailing that campaign's findings.[180] Following the 2024 spring campaign, an additional 50 samples were exported and subsequently analysed.

In this chapter, we have consolidated the results from the initial 25 samples and the subsequent 50 samples to provide a more comprehensive discussion of the findings from the Hellenistic and Parthian periods.

This chapter provides chemical and mineralogical groupings and connects the results to vessel contexts and types whenever applicable. While working with a substantial sample set, our interpretations are constrained by the specific samples, contexts, and vessel types chosen for this study. As a result, conclusions may evolve as additional data becomes available in the future. Nevertheless, the current analysis offers significant insights into pottery production and exchange networks during Assur's Hellenistic and Parthian occupation periods, allowing us to draw valuable conclusions about these phases of the site's history.

174 Wilkinson/Tucker 1995, hatched rims: fig. 77:22, and honeycomb ware: fig. 22:18-19.

175 Müller/Wiener 2016, 414–15, fig. 1.

176 Nováček *et al.* 2016, fig. 135:12.

177 Nováček *et al.* 2016, fig. 133. Nováček/Melčák 2016, 103, fig. 7.

178 Kreppner/Richter/Squitieri 2024, 142. See also **§C2.5**.

179 Kreppner/Richter/Squitieri 2024, 142.

180 Amicone/Schauer 2024.

D2.1 Materials

D2.1.1 Samples dating to the Hellenistic period

A total of 36 samples from Building A, dated to the Hellenistic period, were analysed. These include 11 samples from the 2023 campaign and 25 samples from the 2024 campaign. The majority of fragments were recovered from Courtyard 10 (n=10), Room 1 (n=8), and Rooms 2 and 8 (both n=7). Less well represented are Room 3 (n=3) and Room 7 (n=1).

Most samples are classified as body sherds (n=14), followed by jars (n=10), bowls (n=3), beakers (n=3), pots (n=3), and bottle/jar hybrids (n=3). Beakers, bowls, and rim sherds are each represented by two samples, while all other types, including bottles, bottle/jar, beaker/jar, and plates, are represented by a single example each.

D2.1.2 Samples dating to the Parthian period

A total of 39 samples from the chamber tomb (Grave 1), dated to the Parthian period, were analysed.[181] These include 14 samples from the 2023 campaign and 25 samples collected during the 2024 campaign. Most fragments were recovered from the floor of Subdivision 3 (n=11), Subdivision 4 (n=8), the fill of the southern corridor (n=7) and Subdivision 7 (n=5). Two samples each came from the floors of Subdivisions 5 and 8. One sample each was obtained from the floor of Subdivision 2 and the fills of Subdivision 1, the main corridor, and the upper fill.

Most samples are classified as body sherds (n=16), followed by bowls (n=6), jars (n=3), bottles (n=4), kraters (n=3), and jar/pot types (n=2). All other types – bottle/jar, bowl/jug, jar/juglet, large vessel and rim sherd – are represented by a single sample each.

D2.2 Methods

D2.2.1 Portable X-ray fluorescence analysis (p-XRF)

The portable X-ray fluorescence analysis (p-XRF) conducted to determine the elemental bulk chemistry[182] of the samples followed the same procedure as in our previous study.[183]

As in 2023, data acquisition for the 2024 pottery samples was carried out using the Niton XL3t (serial no. 97390), previously owned by LMU Munich's Department of Cultural Studies and Archaeology and, since late 2023, hosted by LMU Munich's Department of Geology. Three measurements were taken per sample on different areas of a fresh break, using the TestAllGeo mode with an 8 mm collimator and a measurement time of 300 seconds (60 seconds each for the main, low, and high filters, and 120 seconds for the light filter).

Sampling and data collection were conducted by Marco Wolf from November 15 to 25, 2024, under laboratory conditions (temperature: 20° C; relative humidity: 35–42%) in LMU Munich's Department of Geology. Data processing and interpretation were carried out by Michaela Schauer.[184]

The data provided by the device after its internal processing – i.e., the analytical data – forms the basis of this study. Following the data quality control procedures outlined in our previous study, the process includes two main steps. First, all samples are routinely checked for excessively high measurement uncertainties (value ≤ ± error 2σ) and variation coefficients (CV ≥ 20%). Samples were remeasured if more than 20% of the reliable elements exhibited too high CVs. Chemical elements for which fewer than 20% of the samples violate the CV benchmark, and which can be corrected using the appropriate coefficient correction, are considered reliable.[185] These include: SiO_2, TiO_2, Al_2O_3, Fe_2O_3, MnO, CaO, K_2O, V, Cr, Ni, Rb, Sr, Y, Zr, and Nb. Second, quantitative values were calculated using coefficient correction IV (coefcor IV), which was developed following the Munich Procedure.[186] Data interpretation is based on the analysis of element-based scatter plots of the processed data (**Table D2.1**).

D2.2.2 Ceramic petrography

The petrography of archaeological ceramics involves the description, classification, and interpretation of ceramic pastes or fabrics, using techniques adapted from geology and soil micromorphology for the analysis of rocks and soils. This method provides valuable insights into various technological aspects (e.g., forming techniques and tem-

181 See Kreppner/Rohde/Squitieri 2024, 105-118.

182 For the p-XRF analysis see e.g., Potts 2008; Liritzis/Zacharias 2011; Shackley 2012; Johnson 2014; Neff/Voorhies/Umaña 2014; Shugar/Mass 2014.

183 Amicone/Schauer 2024.

184 All steps of data processing and interpretation as well as the raw p-XRF data of the pottery discussed here is accessible in the LMU online data repository: Schauer 2025b.

185 Schauer/Amicone 2024; Schauer/Truntschnig/Almstädter 2025; Schauer 2025a.

186 Schauer 2024; Schauer *et al.* 2024.

Sample ID	Registration No.	SiO2	TiO2	Al2O3	Fe2O3	MnO	CaO	K2O	V	Cr	Ni	Cu	Zn	Rb	Sr	Y	Zr	Nb	Period	Context	Vessel type	Group	Petrofabric
AS001	AS 262432:022:001:014	50.39	0.55	16.73	6.09	0.13	14.59	1.29	113	274	325	35	433	34	727	30	138	14	Parthian	Chamber Tomb Subdivision 4 floor	body sherd	PO1	1A
AS002	AS 262432:022:009:050	51.55	0.49	18.18	6.27	0.10	12.27	2.11	94	196	213	45	102	77	454	26	123	14	Parthian	Chamber Tomb Subdivision 4 floor	body sherd	PG2	1B
AS004	AS 262433:021:001:026	52.94	0.54	17.97	5.69	0.09	12.14	2.31	108	203	217	291	331	82	617	26	135	14	Parthian	Chamber Tomb Subdivision 3 floor	body sherd	PG2	2A
AS005	AS 262433:023:001:034	53.70	0.63	14.73	6.60	0.12	14.00	2.06	106	279	193	40	81	47	447	27	151	13	Parthian	Chamber Tomb Southern Corridor fill	body sherd	PG1	2A
AS006	AS 262432:022:009:052	52.95	0.64	16.17	7.33	0.15	13.21	2.10	111	297	235	43	96	44	398	29	143	15	Parthian	Chamber Tomb Subdivision 4 floor	body sherd	PG1	3A
AS007	AS 262432:022:009:053	55.51	0.69	16.50	6.88	0.20	11.89	2.92	116	189	161	40	128	67	768	31	172	17	Parthian	Chamber Tomb Subdivision 4 floor	body sherd	PO2	2B
AS008	AS 262433:023:001:035	52.31	0.60	15.90	6.29	0.12	14.36	1.57	97	217	205	35	96	43	408	28	132	15	Parthian	Chamber Tomb Southern Corridor fill	body sherd	PG1	4A
AS009	AS 262433:023:001:036	52.85	0.79	15.10	7.52	0.21	14.94	2.73	121	189	199	44	112	82	315	33	201	19	Parthian	Chamber Tomb Southern Corridor fill	body sherd	PO3	3B
AS010	AS 262433:023:001:037	52.10	0.59	15.32	6.08	0.12	15.37	1.57	89	217	199	43	89	55	333	28	139	15	Parthian	Chamber Tomb Southern Corridor fill	body sherd	PG1	4A
AS011	AS 262433:023:001:038	52.94	0.61	15.90	6.30	0.12	13.66	2.00	104	195	189	49	97	61	460	29	146	15	Parthian	Chamber Tomb Southern Corridor fill	body sherd	PG1	4B
AS012	AS 262432:021:001:036	53.86	0.66	12.78	7.02	0.13	14.34	2.56	101	264	188	82	99	47	503	27	144	14	Parthian	Chamber Tomb Subdivision 3 floor	body sherd	PG1	3A
AS013	AS 262432:022:009:054	60.20	0.61	13.45	6.46	0.10	10.19	2.62	93	188	179	24	66	61	321	23	115	12	Parthian	Chamber Tomb Subdivision 4 floor	body sherd	PG3	4B
AS014	AS 262432:022:001:015	54.29	0.60	13.73	5.76	0.12	15.69	2.26	103	180	166	40	71	47	472	24	125	12	Parthian	Chamber Tomb Subdivision 4 floor	body sherd	PG1	4B
AS015	AS 262433:023:001:039	53.28	0.66	13.66	7.43	0.13	13.39	2.64	104	238	252	37	79	61	363	24	107	11	Parthian	Chamber Tomb Southern Corridor fill	body sherd	PG1	4B
AS033	AS 261433:005:001:045	49.84	0.62	18.05	7.15	0.13	11.68	2.26	119	286	260	45	83	64	285	27	129	16	Hellenistic	Room 1 floor	body sherd	HG5	1A
AS034	AS 261433:005:001:046	53.23	0.60	15.75	5.56	0.10	12.47	2.88	106	224	202	51	139	58	519	24	122	13	Hellenistic	Room 1 floor	body sherd	HG1	2A
AS035	AS 261433:005:001:047	53.29	0.62	15.10	6.96	0.13	12.41	2.92	98	186	210	42	80	87	434	26	142	14	Hellenistic	Room 1 floor	body sherd	HG1	2A
AS036	AS 261432:011:013:005	48.29	0.58	16.16	6.47	0.11	17.30	1.07	108	227	230	39	90	29	549	28	138	17	Hellenistic	Room 2 floor	body sherd	HO1	1B
AS037	AS 261433:005:001:048	52.36	0.53	14.83	5.86	0.10	15.71	2.40	89	189	216	32	71	50	567	24	131	12	Hellenistic	Room 1 floor	body sherd	HG1	2A
AS038	AS 261433:005:001:049	58.14	0.61	13.56	5.43	0.09	12.39	3.23	100	169	155	54	72	54	375	22	104	10	Hellenistic	Room 1 floor	body sherd	HG3	4A
AS039	AS 261432:011:013:006	54.76	0.56	15.47	5.89	0.11	14.11	1.33	106	212	201	40	79	31	419	26	123	13	Hellenistic	Room 2 floor	body sherd	HG2	4A
AS040	AS 261432:011:013:007	54.20	0.60	13.95	6.45	0.12	13.60	2.91	101	190	164	37	75	56	395	25	118	12	Hellenistic	Room 2 floor	body sherd	HG1	4A
AS041	AS 261433:005:001:050	54.15	0.66	10.58	6.95	0.14	16.58	3.15	88	179	156	54	81	54	365	22	108	11	Hellenistic	Room 1 floor	body sherd	HG3	4A
AS042	AS 261433:005:001:051	52.19	0.64	12.66	8.08	0.14	17.04	1.98	104	181	145	43	76	34	595	28	138	15	Hellenistic	Room 1 floor	body sherd	HG2	3A
AS043	AS 262432:058:015:004	53.72	0.69	15.26	7.29	0.16	14.16	2.07	104	273	203	31	79	28	328	28	135	16	Hellenistic	Room 3 floor	body sherd	HG2	1B
AS064	AS 261433:067:010:006	52.00	0.41	15.49	7.18	0.13	14.13	1.83	72	134	241	29	86	66	483	27	127	12	Hellenistic	Courtyard 10 floor	thin walled beaker	HO2	1B
AS065	AS 261433:046:001:007	53.61	0.66	17.55	7.01	0.11	9.63	2.90	122	232	226	75	287	89	459	27	138	15	Hellenistic	Room 2 floor	beaker/jar	HG5	1A
AS066	AS 261433:067:017:002	57.40	0.67	15.09	6.87	0.10	12.05	1.96	105	135	101	27	88	45	246	28	139	15	Hellenistic	Courtyard 10 floor	large storage jar	HO3	2E
AS067	AS 262433:136:001:009	53.68	0.56	15.99	6.30	0.11	12.59	2.06	103	202	238	40	99	64	399	26	135	13	Hellenistic	Courtyard 10 floor	folded rim jar	HG1	4A
AS068	AS 262433:136:001:004	51.32	0.58	14.50	6.81	0.12	14.50	1.63	104	201	230	147	200	32	474	26	123	13	Hellenistic	Courtyard 10 floor	small jar	HG2	3A
AS069	AS 261433:046:020:001	54.51	0.63	13.89	6.68	0.11	14.58	2.20	96	149	163	26	81	54	320	25	126	13	Hellenistic	Room 2 floor	bottle	HG1	4A
AS070	AS 261433:067:021:004	56.90	0.60	11.25	6.27	0.13	15.23	2.80	85	123	164	47	68	62	453	22	118	10	Hellenistic	Courtyard 10 floor	large-mouth pot	HG3	4C
AS071	AS 261433:067:010:003	50.73	0.59	13.76	6.50	0.11	17.80	2.05	95	197	198	43	134	38	665	25	133	13	Hellenistic	Courtyard 10 floor	medium jar	HG2	4A
AS072	AS 261433:046:004:004	59.02	0.55	12.04	6.17	0.11	13.90	1.95	82	128	154	36	225	58	331	22	103	11	Hellenistic	Room 2 floor	body sherd	HG3	4B
AS073	AS 262433:136:001:001	52.92	0.66	14.44	6.98	0.13	15.29	1.88	103	158	183	33	87	42	415	27	136	12	Hellenistic	Courtyard 10 floor	large-mouth pot	HG2	4A
AS074	AS 262433:107:003:004	51.28	0.48	18.17	7.68	0.14	11.01	2.52	89	192	264	14	156	60	357	29	127	13	Hellenistic	Room 8 floor	thin walled beaker	HO4	1A
AS075	AS 262433:107:007:003	50.13	0.73	15.35	7.02	0.16	19.63	1.77	107	186	164	72	366	39	509	32	201	17	Hellenistic	Room 8 floor	small jar	HO5	1A
AS076	AS 262433:107:017:001	50.77	0.66	12.32	7.41	0.14	18.27	2.95	96	216	200	66	85	59	514	25	134	14	Hellenistic	Room 8 floor	large storage jar	HG4	3A
AS077	AS 262433:110:003:002	52.67	0.57	13.59	6.13	0.12	16.15	1.70	88	204	222	53	80	42	539	27	127	13	Hellenistic	Room 7 floor	jar	HG2	3A
AS078	AS 262433:107:003:001	54.14	0.58	14.35	6.39	0.12	15.36	1.44	95	168	213	59	234	35	459	26	124	12	Hellenistic	Room 8 floor	folded rim jar	HG2	4A
AS079	AS 262433:107:006:001	56.66	0.61	12.53	6.60	0.13	15.27	1.64	93	262	203	36	95	37	405	25	141	13	Hellenistic	Room 8 floor	medium jar	HG2	4A
AS080	AS 261433:067:014:001	53.34	0.58	12.96	5.63	0.11	17.26	1.39	83	165	172	630	78	43	482	24	121	12	Hellenistic	Courtyard 10 floor	rolled rim plate	HG2	4A
AS081	AS 262433:107:007:010	52.68	0.83	15.26	7.00	0.12	16.08	2.67	118	236	200	73	95	55	123	27	148	13	Hellenistic	Room 8 floor	cooking pot	HO6	5
AS082	AS 261433:067:017:001	52.47	0.64	11.99	6.24	0.12	17.56	3.30	99	196	171	43	97	57	532	23	126	12	Hellenistic	Courtyard 10 floor	medium jar	HG4	2B
AS083	AS 262433:107:004:004	57.11	0.75	16.79	5.78	0.12	9.65	2.62	139	171	107	43	70	44	305	25	148	11	Hellenistic	Room 8 floor	body sherd	HO7	6
AS084	AS 261433:056:001:026	53.91	0.60	21.18	7.39	0.10	6.57	2.80	110	410	342	48	265	140	202	29	143	11	Hellenistic	Courtyard 10 fill	echinus bowl	HO8	1A
AS085	AS 262432:058:015:001	50.45	0.50	19.98	6.84	0.11	8.87	2.75	110	228	281	24	122	100	399	27	142	15	Hellenistic	Room 3 floor	carinated bowl	HO9	1A
AS086	AS 261432:011:010:004	56.16	0.59	13.31	6.60	0.13	11.41	2.78	91	193	236	39	98	63	495	24	123	10	Hellenistic	Room 2 floor	carinated bowl	HG1	4A
AS087	AS 261433:005:001:023	53.36	0.60	15.07	6.80	0.13	13.64	2.39	104	188	235	31	93	66	430	25	128	14	Hellenistic	Room 1 floor	beaker	HG1	4A
AS088	AS 261433:058:001:019	52.25	0.55	15.14	6.45	0.11	15.43	1.28	93	196	226	29	249	35	396	25	122	12	Hellenistic	Room 3 floor	body sherd	HG2	1A
AS090	AS 262432:022:009:011	49.20	0.53	13.85	9.04	0.14	17.62	2.29	75	126	218	38	159	78	650	27	129	13	Parthian	Chamber Tomb Subdivision 4 floor	large flat bowl	PO4	1A
AS091	AS 262433:023:001:001	51.11	0.63	14.12	7.84	0.16	16.46	1.71	94	222	251	83	99	63	518	29	164	15	Parthian	Chamber Tomb Subdivision 7 floor	open bowl	PG1	2A
AS092	AS 262433:023:001:002	52.01	0.51	16.84	6.59	0.12	13.81	1.20	92	188	274	1626	111	29	447	28	122	12	Parthian	Chamber Tomb Subdivision 7 floor	bottle	PO5	1B
AS093	AS 262433:014:001:005	54.09	0.61	13.52	6.37	0.14	15.87	1.52	95	229	184	1129	122	31	379	27	143	13	Parthian	Chamber Tomb Subdivision 5 fill	jar	PG1	2A
AS094	AS 262433:024:001:002	55.06	0.60	14.67	7.42	0.15	12.32	2.79	93	214	188	53	106	74	394	26	146	14	Parthian	Chamber Tomb Subdivision 8 floor	small jar or juglet	PG1	2C
AS095	AS 262433:011:001:001	51.51	0.61	16.32	5.98	0.12	15.16	1.84	107	222	217	48	190	66	570	28	147	14	Parthian	Chamber Tomb Subdivision 5 fill	jar	PG1	2B
AS096	AS 262432:021:001:028	53.72	0.61	14.60	5.68	0.12	15.27	2.01	100	216	186	35	84	63	386	25	151	14	Parthian	Chamber Tomb Subdivision 3 floor	bottle	PG1	2B
AS097	AS 262432:007:001:054	53.00	0.61	15.10	5.94	0.13	14.89	1.81	103	277	245	272	82	50	368	26	128	13	Parthian	Chamber Tomb Southern Corridor fill	bottle or jar	PG1	2B
AS098	AS 262432:013:001:019	53.95	0.61	15.79	6.61	0.11	14.15	1.62	112	226	202	30	76	37	554	28	148	14	Parthian	Chamber Tomb Subdivision 1 fill	large vessel	PG1	2A
AS099	AS 262432:021:001:020	53.79	0.64	15.29	6.74	0.14	12.60	1.92	105	227	247	38	99	66	348	28	136	14	Parthian	Chamber Tomb Subdivision 3 floor	krater	PG1	4A
AS100	AS 261432:010:001:004	56.51	0.58	15.18	6.11	0.10	9.15	2.83	107	202	208	64	226	71	454	23	134	12	Parthian	Chamber Tomb Main Corridor fill	bowl	PG3	4C
AS101	AS 262433:006:001:041	53.43	0.60	15.14	6.70	0.14	14.25	1.76	97	206	233	32	91	54	354	27	126	14	Parthian	Chamber Tomb upper fill	deep bowl	PG1	4A
AS102	AS 262432:021:001:039	53.44	0.59	14.63	5.84	0.11	14.50	1.96	95	193	173	27	76	46	388	26	157	13	Parthian	Chamber Tomb Subdivision 3 floor	jar	PG1	2B
AS103	AS 262433:023:001:022	50.50	0.59	15.80	6.77	0.14	15.17	1.73	94	227	240	36	105	65	395	28	141	14	Parthian	Chamber Tomb Subdivision 7 floor	krater	PG1	4A
AS104	AS 262433:022:001:013	54.21	0.66	16.53	6.50	0.12	10.09	2.79	129	275	198	38	95	70	395	27	135	14	Parthian	Chamber Tomb Subdivision 4 floor	krater	PG1	2C
AS105	AS 262433:021:001:005	53.49	0.53	13.78	6.34	0.14	15.58	1.58	81	181	231	4935	81	36	554	28	134	12	Parthian	Chamber Tomb Subdivision 3 floor	bowl or jug	PG1	2A
AS106	AS 262432:020:001:012	50.77	0.59	17.59	6.94	0.14	12.45	1.82	115	261	291	34	105	65	417	28	138	14	Parthian	Chamber Tomb Subdivision 2 floor	bottle	PG1	2A
AS107	AS 262432:021:001:027	53.15	0.58	13.88	5.64	0.12	16.29	1.89	92	212	200	29	77	44	395	25	130	12	Parthian	Chamber Tomb Subdivision 3 floor	bottle	PG1	2B
AS108	AS 262432:021:001:023	54.60	0.71	14.20	7.54	0.16	12.62	2.34	112	245	229	43	126	66	367	27	133	14	Parthian	Chamber Tomb Subdivision 3 floor	jar or pot	PG1	4C
AS109	AS 262433:023:001:017	54.14	0.57	13.59	7.28	0.14	15.29	1.57	93	176	221	38	94	54	436	27	131	13	Parthian	Chamber Tomb Subdivision 7 floor	closed bowl	PG1	2A
AS110	AS 262433:024:001:011	52.51	0.64	14.35	7.00	0.13	13.74	2.95	105	221	227	46	90	74	514	26	135	13	Parthian	Chamber Tomb Subdivision 8 floor	bowl	PG1	2C
AS111	AS 262433:023:001:018	57.96	0.70	15.22	7.18	0.14	8.15	2.64	115	254	242	34	96	69	277	25	126	13	Parthian	Chamber Tomb Subdivision 7 floor	rim sherd	PO6	4C
AS112	AS 262433:021:001:009	51.40	0.65	14.90	7.23	0.15	15.08	1.33	98	234	261	35	94	42	407	27	136	14	Parthian	Chamber Tomb Subdivision 3 floor	hole-mouth jar or pot	PG1	4B
AS113	AS 262433:021:001:008	53.78	0.61	14.24	6.64	0.12	15.02	1.43	97	204	217	23	80	44	497	26	132	14	Parthian	Chamber Tomb Subdivision 3 floor	body sherd	PG1	4A
AS114	AS 262433:021:001:035	53.28	0.62	14.93	6.69	0.13	14.40	1.36	98	223	237	42	92	44	337	25	112	12	Parthian	Chamber Tomb Subdivision 3 floor	body sherd	PG1	4B

Table D2.1: Results of the chemical analysis, with the chemical groups indicated in the column "Group" and petrographic group in the column "Petrofabric". Prepared by Michaela Schauer and Silvia Amicone.

pering) and aids in identifying the raw material sources used in pottery production.

The petrographic analysis on the Assur samples was carried out by Silvia Amicone at the Competence Center Archaeometry–Baden-Württemberg (University of Tübingen). Once the exported pottery sherds arrived in Tübingen, thin sections were prepared. First, a slice was cut from the vertical cross-section of each sherd. After consolidation with epoxy resin, the slices were lapped with silica powder (600 grain size) and mounted on glass slides. The samples were then ground to approximately 40 µm using a Buehler PetroThin thin-sectioning system. Finally, they were further thinned to around 20–30 µm using silica powder (600 to 900 grain size) and coated with a removable transparent varnish.

The thin sections were examined under a polarising microscope (Leica DM2500 P) to identify the compositional and technological characteristics of the materials under investigation.[187]

D2.3 Results of p-XRF analysis

As it was already observed in the previous study,[188] the Hellenistic and Parthian-period samples cannot be easily distinguished only based on their chemistry. In the scatter plots, their clusters broadly overlap, providing a solid foundation for defining the local chemistry.[189] Working from this basis, the following interpretation of chemical groups and outliers is carried out for each period separately.

D2.3.1 Samples dating to the Hellenistic period

The 36 Hellenistic samples can be separated, based on their chemistry, into five clusters (HG1 to HG5) and nine outliers (HO1 to HO9; **Fig. D2.1**[190]). Hellenistic Chemical Group 1 (HG1; n=8) is defined by its high K_2O and Rb, but low CaO values, while Chemical Group 2 (HG2; n=9) shows low K_2O and Rb, and comparatively high CaO concentrations. In general, lower Al_2O_3 and SiO_2 values can also be observed for HG2 compared with HG1. The clear differences, most apparent in the CaO/Sr and K_2O/Rb ratios, are due to the use of two different clay sources.

Chemical Group 3 (HG3; n=4) is distinguished particularly by its low Al_2O_3, Zr, and Y, but high SiO_2 concentrations, as well as the specific Nb/Ni ratio,[191] clearly indicating the use of a second local clay source. It is worth noting that this group, when compared with values from the other groups of the Hellenistic period,[192] shows little to no overlap in the defining elements and therefore appears to represent a specific method of clay selection or paste preparation.

Low SiO_2 and Al_2O_3, combined with high K_2O and CaO values, as well as very tightly clustered Rb, Sr, and V concentrations, define Chemical Group 4 (HG4; n=2). These samples are repeatedly found overlapping with either HG1 or HG2, suggesting the possibility of clay mixing and/or specific tempering approaches.

High Al_2O_3 and V, but also low CaO and Sr values, along with a specific Nb/Si and Zr/Y ratio, characterise Chemical Group 5 (HG5; n=2).[193] These samples show a closer resemblance to HG1, indicating a special tempering method using the raw clay typical of that group.

In addition to these five chemical groups, nine outliers have been defined: Hellenistic Outlier 1 (HO1; sample AS036) is characterised by low SiO_2, K_2O, and Rb, and high Nb concentrations.[194] As this sample is consistently found in the vicinity of HG2, it seems likely that the differences are due to a specific method of tempering or processing of this raw clay.

Hellenistic Outlier 2 (HO2; sample AS064) is distinguished by its low TiO_2, V, and Cr concentrations, as well as a specific K_2O/Rb ratio.[195] This might result from a particular selection of tempering material, though a non-local origin cannot be ruled out.

Hellenistic Outlier 3 (HO3; sample AS066) is chiefly defined by its low Ni and high Nb concentrations. Additionally, high SiO_2 and comparatively low Sr and CaO values are attested. Due to its varying position – at times

187 Quinn 2022 (with literature therein).

188 Amicone/Schauer 2024.

189 For details, see Schauer 2025b: R-Script section 8.2 and 9.2.

190 To view an interactive plot including the parthian material, see Schauer 2025b: R-Script section 8.2.

191 The variation coefficients of samples AS041 and AS70 are too high for Zr, and of sample AS72 for Ni. Yet, as they form a coherent group also in the not-affected elements, this chemical cluster is solidly defined.

192 For details, see Schauer 2025b: R-Script section 8.2.

193 For sample AS033, the variation coefficients are too high for Al_2O_3 and V but in a range of 1% and 3%, respectively. If this is taken into consideration the possible range of concentration for Al_2O_3 is still outside of the main clusters and therefore reliable to define this tandem. On the other hand, V has to be viewed with great caution.

194 The variation coefficient of sample AS036 for Nb is 1% above the benchmark, yet taking this into consideration, the value is still outside the main cluster.

195 The variation coefficient of sample AS064 is too high for Cr but by less then 1%, which would still count as a comparably low value range.

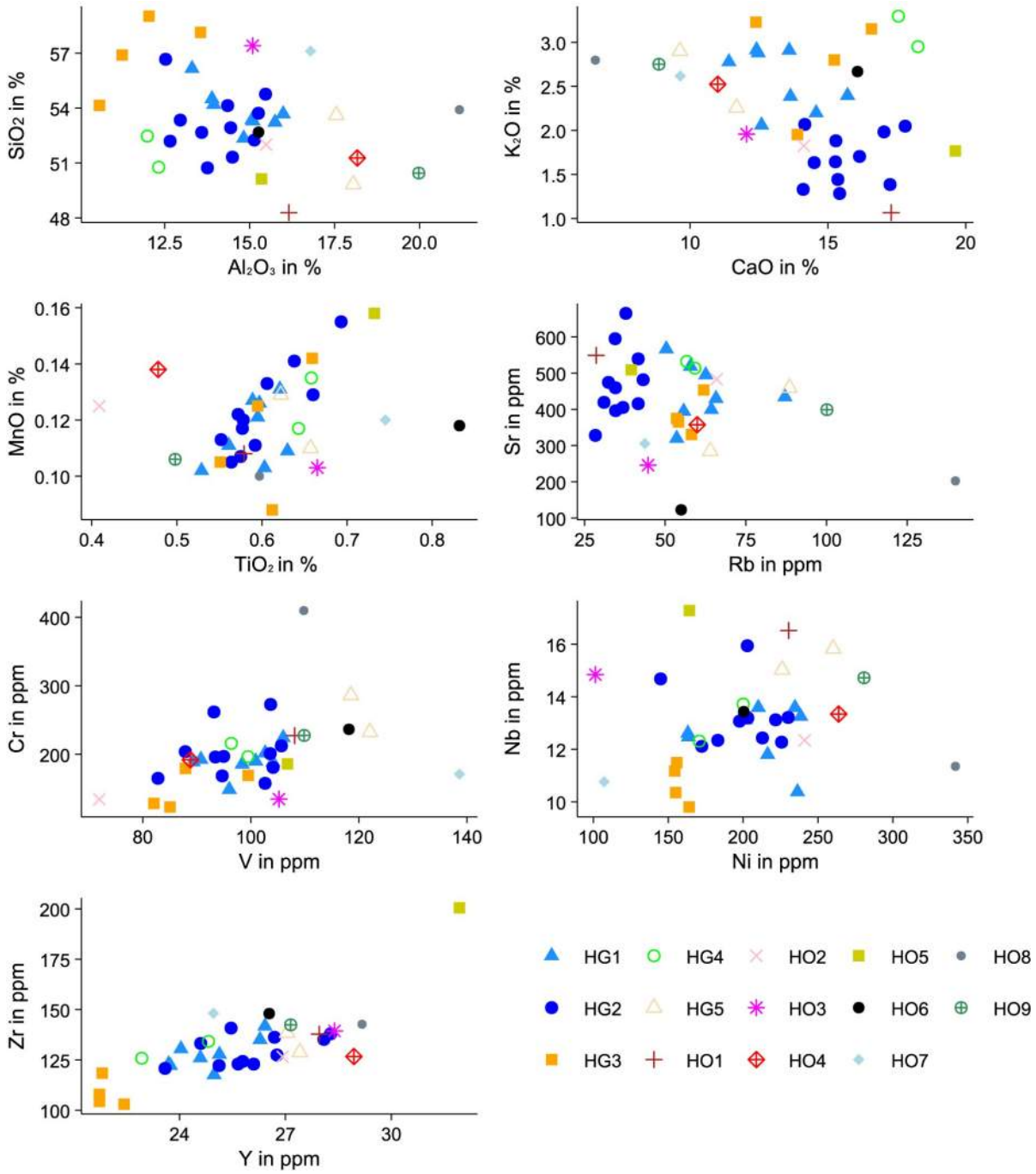

Fig. D2.1: Scatterplots of selected elements for the Hellenistic Chemical Groups (n=36). Prepared by Michaela Schauer.

closer to HG1 or HG2 – it is likely that a mixing of clays produced this individual chemical fingerprint.

Hellenistic Outlier 4 (HO4; sample AS074) differs from the other objects due to its low TiO_2 and CaO, but high Fe_2O_3, Al_2O_3, Ni, and Y concentrations[196]. It appears on the fringes of the clusters, with no clear relation to any of the major groups. As this sample is an outlier not only among the Hellenistic samples but also among the Parthian-period samples, a non-local origin of this outlier is likely.

Hellenistic Outlier 5 (HO5; sample AS075) is characterised by high MnO, CaO, TiO_2, Rb, Nb, Zr, and Y concentrations, clearly distinguishing this pottery from contemporary material. When comparing it with the Parthian-period samples, it falls within the range of two outliers of that period.

196 The variation coefficient for Al_2O_3 is too high for sample AS074.

Hellenistic Outlier 6 (HO6; sample AS081), with its high TiO2 and V but low Sr values, otherwise shows concentrations largely comparable to HG1. This suggests a different clay paste preparation method involving a specific type of temper, but starting with similar raw clay material.

Hellenistic Outlier 7 (HO7; sample AS083), with low Fe_2O_3, CaO, Ni, Nb, and Cr, but high TiO_2, SiO_2, and V concentrations, falls outside the local signature, particularly with regard to V, Cr, Nb, and Ni values. This supports a non-local origin.

Hellenistic Outlier 8 (HO8; sample AS084) exhibits high Al_2O_3, Rb, Cr, and Ni, but low MnO, CaO, and Sr concentrations.[197] As with Outlier 7, its values for key trace elements, such as Rb and Ni, but also CaO, fall outside the local signature, making a non-local origin highly likely.

Hellenistic Outlier 9 (HO9; sample AS085) is characterised by low TiO_2, SiO_2, and CaO, but high Al_2O_3, Rb, and Ni values. Considering the local signature of all samples, it seems likely that this vessel's chemical fingerprint is affected by the temper rather than by the use of a different clay source.

In summary, various clay sources and tempering approaches can be identified from the p-XRF of the Hellenistic period samples. Most samples are of local origin, while five samples, namely AS064 (HO2), AS074 (HO4), AS075 (HO5), AS083 (HO7), and AS084 (HO8), are potentially of non-local origin.

D2.3.2 Samples dating to the Parthian period

The 39 Parthian-period samples cluster, based on their chemistry, into three groups (PG1 to PG3) and six outliers (PO1 to PO6; **Fig. D2.2**[198]). Unlike the Hellenistic samples, no separation based on K_2O/Rb or CaO/Sr ratios is visible. Therefore, one main Chemical Group (PG1), including 29 of the 39 samples, can be defined.

Chemical Group 2 (PG2; samples AS002, AS004) shows low TiO_2 and MnO, but high Al_2O_3 and Rb concentrations.[199] These values are most likely the result of a selective tempering method or paste preparation by sorting out specific mineral inclusions.

Chemical Group 3 (PG3; samples AS013, AS100) is characterised by low MnO, CaO, Sr, and Y, yet high SiO2 values. These characteristics clearly distinguish PG3 from the other groups. Interestingly, these samples frequently appear in close proximity to Hellenistic Chemical Group 3 (HG3), suggesting the possibility of similar clay use and/or preparation techniques.

Besides these three groups, six outliers have been defined: Parthian Outlier 1 (PO1; AS001) is defined by its low TiO_2 and SiO_2, yet high Sr, Ni, and Y concentrations.[200] The differences in trace elements compared not only to the Parthian samples but also to the Hellenistic samples provide strong evidence for a non-local origin of this sample.

Parthian Outlier 2 (PO2; sample AS007)[201] is characterised by high values of MnO, K_2O, Sr, Nb, Zr, and Y, but low Ni. Taken together, these values suggest the use of a different clay source.

Parthian Outlier 3 (PO3; AS009),[202] which shows high concentrations of TiO_2, MnO, Rb, Zr, Y, and Nb. Both PO2 and PO3 are clearly distinguishable from the Hellenistic local ware in terms of the relevant elements.[203]

Parthian Outlier 4 (PO4; sample AS090) exhibits high CaO, and Rb, but low SiO_2, TiO_2, Cr, and V concentrations. This sample stands out from all other Parthian and Hellenistic pottery, making a non-local origin highly likely. It is worth noting, however, that PO4 shows notable similarities with HO2, especially in terms of Cr, V, Y, and Zr concentrations.

Parthian Outlier 5 (PO5; sample AS092) is characterised by low TiO_2, SiO_2, K_2O, and Rb, yet high Ni concentrations[204]. While these values support the possibility of non-local production when compared to other Parthian samples, the inclusion of the Hellenistic data suggests that this outlier is more likely the result of a specific paste preparation method that excluded certain mineral tempers.

Parthian Outlier 6 (PO6; sample AS111) shows high TiO_2, SiO_2, and K_2O, but low CaO and Sr concentrations. Interpretation is challenging, as its differences from the main cluster are not dramatic, though they are consistent. The fact that this sample often aligns with Hellenistic outliers (HO8, HO9) in key elements may support a non-local origin.

In summary, among the Parthian-period samples, three local production groups and six outliers can be defined.

197 The variation coefficient for sample AS084 in regard to Al_2O_3 is 1% above the benchmark, yet taking this into account, it does not affect its position in relation to the other samples.

198 To view an interactive plot including the Hellenistic material, see Schauer 2025b: R-Script section 9.2.

199 The variation coefficient for TiO_2 is too high for sample AS002.

200 The variation coefficient for Sr is too high for sample AS001.

201 The variation coefficient for MnO is too high for sample AS007.

202 The variation coefficient for MnO is too high for sample AS009.

203 In the report on the 2023 analysis, these samples were defined as "Parthian pottery outlier 7" (= PO2 = AS007) and "Parthian pottery outlier 6" (= PO3 = AS009), respectively.

204 The variation coefficient for K_2O is too high for sample AS092.

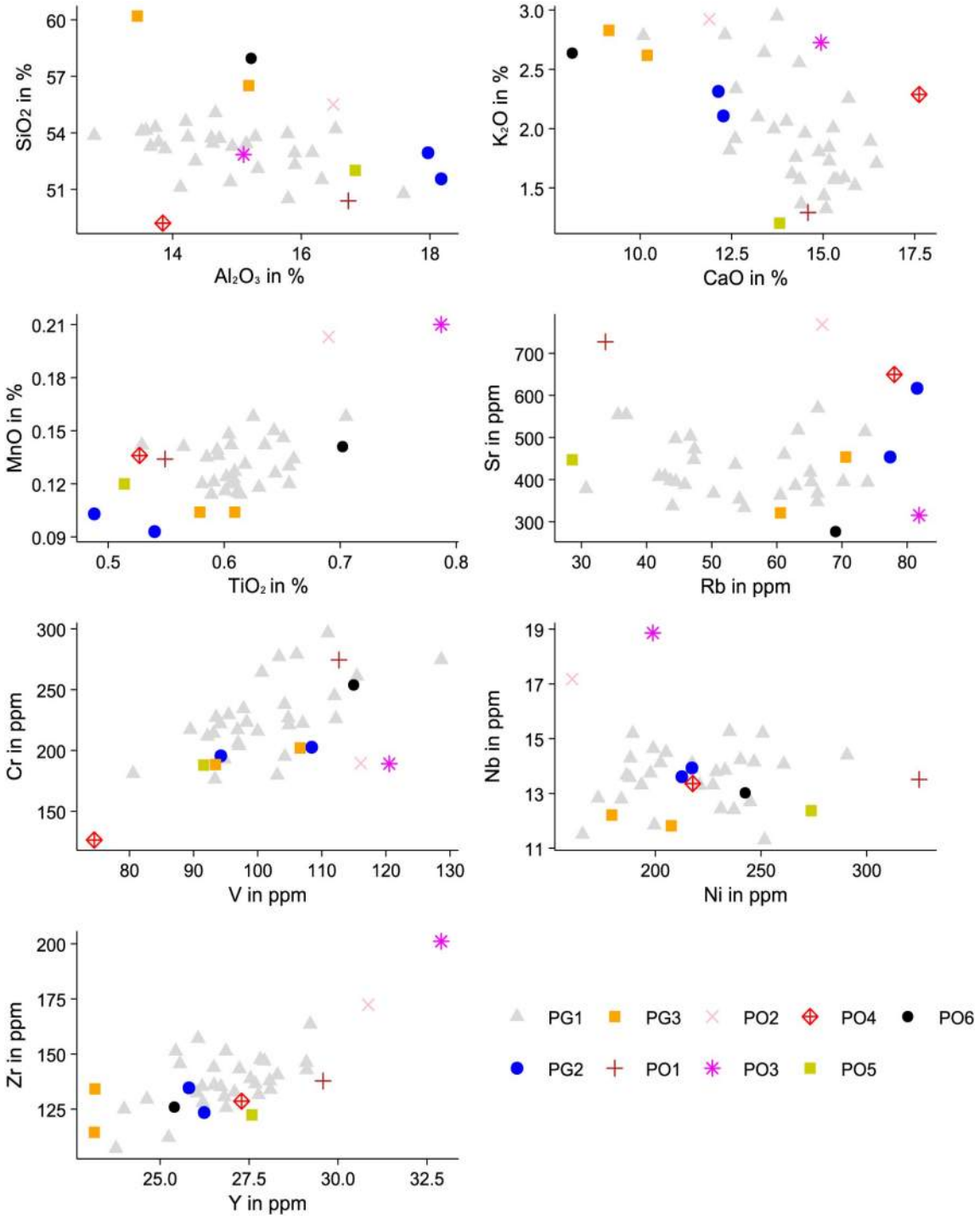

Fig. D2.2: Scatterplots of selected elements for the Parthian-period Chemical Groups (n=39). Prepared by Michaela Schauer.

Fabric	Name	Subfabric	Technology	Coarseness
1	Fine fabric	A	Levigated clay?	Very fine (0.05 mm average size)
1		B	Levigated clay?	Fine (0.1 mm average size)
2	Medium coarse fabric	A	Unprocessed?	Medium coarse (0.25 mm average size)
2		B	Unprocessed?	Medium coarse with common serpentinite (0.25 mm average size)
2		C	Unprocessed?	Medium coarse with abundant inclusions (0.25 mm average size)
2		D	Unprocessed?	Medium coarse scarce inclusions (0.25 mm average size)
2		E	Clay mixing	Medium coarse (0.25 mm average size)
3	Chaff tempered fabric	A	Chaff tempered	Fine (0.1 mm average size)
3		B	Chaff tempered	Coarse micritic calcite (1 mm calcite average size)
4	Mineral tempered fabric	A	Mineral tempered	Coarse calcareous (0.5 mm average size)
4		B	Mineral tempered	Very coarse calcareous chaff tempering (1-2 mm average size)
4		C	Mineral tempered	Coarse calcareous (0.5 mm average size), more abundant fine fraction
5	Calcite tempered fabric		Calcite tempering	Coarse (0.5 mm average size)
6	Micritic calcite		Unprocessed?	Coarse (0.5 mm average size)

Table D2.2: Fabric groups identified in the pottery samples selected from Assur in 2023 and 2024. Prepared by Silvia Amicone.

Of these outliers, five, PO1 to PO4 and PO6, are likely of non-local origin. Compared with the Hellenistic period, this reflects a reduction in the complexity of local paste preparation techniques, as the Parthian-period outliers tend to represent true imports or non-local productions rather than variations in local clay paste processing.

D2.4 Results of the petrographic analysis

Five different fabric groups were recognised according to compositional and textural characteristics, reflecting both provenance and technology (**Tables D2.1–2**).

Fabric 1: Fine fabric (**Fig. D2.3 a-f**; **Fig. D2.4 a**, **b**)
This fabric is marked by inclusions between 0.05 and 0.1 mm average size. The main inclusions are quartz and feldspars (plagioclases), but muscovite, amphibole, serpentinite and opaques are also common; more rarely, tiny fragments of metamorphic rocks, calcite and chert can be observed. The presence of elongated voids in some samples might suggest organic tempering, but they could also be derived from the combustion of naturally occurring organic materials present in the original clay used to produce this fabric. The fineness of this fabric suggests that the original raw material has been cleaned (probably through levigation).

This group includes the following chemical outliers, which also present some petrographic peculiarities:

- AS74 (HO4): Fits within the fabric description but contains more muscovite (**Fig. D2.3b**);
- AS75 (HO5): Matches the general fabric but displays more calcareous clay and abundant postpositional calcite (**Fig. D2.3c**);
- AS84 (HO8): Exhibits a black glossy coating and lacks amphibole and serpentinite (**Fig. D2.3d**);
- AS85 (HO9): Contains fewer inclusions but aligns with the general fabric description (**Fig. D2.3e**);
- AS92 (PO5): Fits the general fabric description but likely also contains fragments of sedimentary rocks (**Fig. D2.4b**).

Fabric 2: Medium-coarse fabric (**Fig. D2.3g**; **Fig. D2.4c-e**)
This fabric is characterised by inclusions of 0.25 mm average size. The main inclusions are quartz and feldspars (plagioclases), but muscovite, amphibole and serpentinite are also common; more rarely, tiny fragments of metamorphic rocks, calcite and chert can be observed. The presence of elongated voids in the same samples might suggest organic tempering. Still, it could also be derived from the combustion of naturally occurring organic materials present in the original clay used to produce this fabric.

Within this fabric, minor compositional and textural characteristics enable the identification of subgroups:

- 2A: standard Fabric 2;
- 2B: serpentinite is more common;
- 2C: inclusions are more abundant;
- 2E: clay mixing (see HO3 = sample AS66).

Fabric 3: Chaff-tempered fabric (**Fig. D2.3h**)
This fabric is characterised by inclusions of 0.1 mm average size. The main inclusions are quartz and feldspars (plagioclases); more rarely, tiny fragments of metamorphic rocks and chert and tiny little fragments of serpentinite and amphiboles were observed. Big elongated voids filled with charred materials are surely evidence of tempering with organic materials (probably chaff). The finesse of this fabric suggests that the original raw materials have been cleaned (probably through levigation). However, one sample (PO3 = sample AS09) also contains relatively big fragments of micritic calcite (1 mm average size), and it

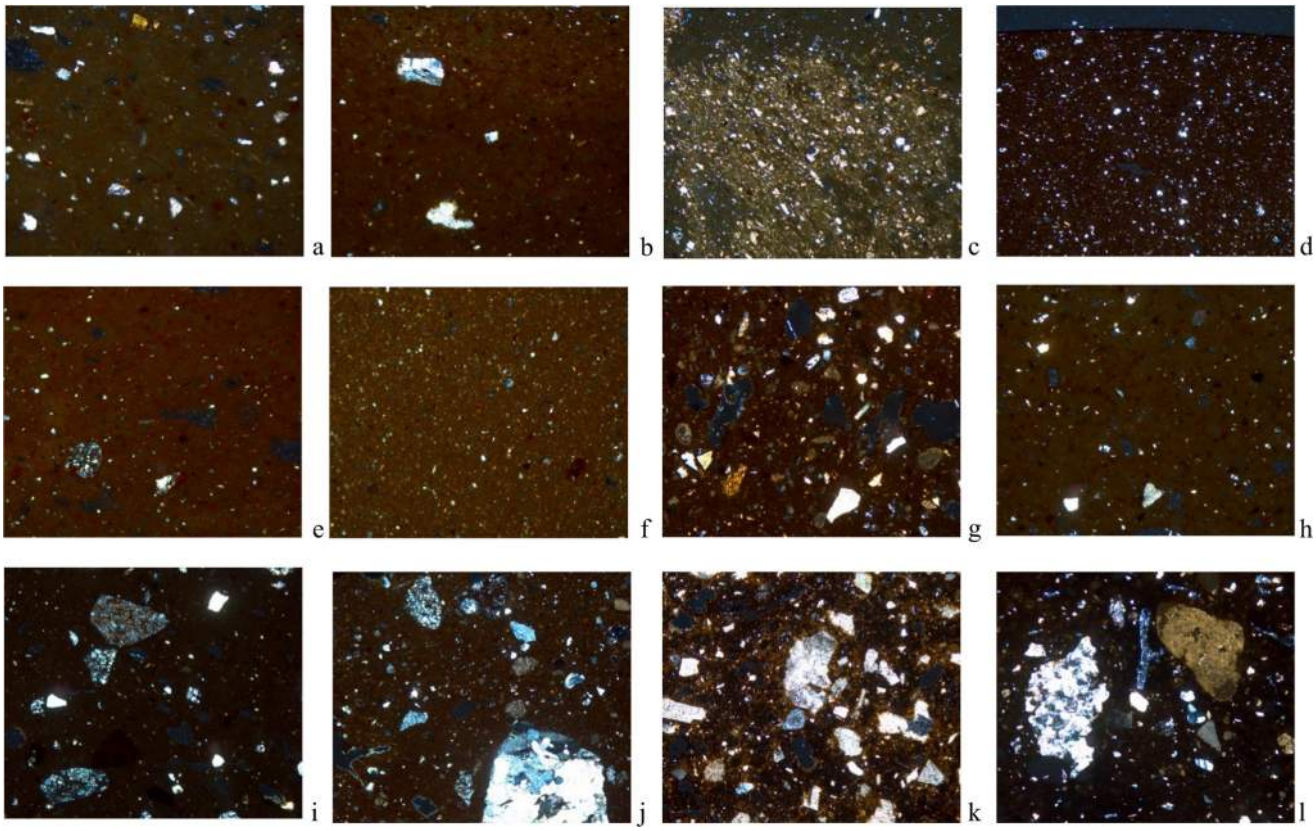

Fig. D2.3: Thin section micrographs of selected Hellenistic samples from Assur: a) AS64 Fabric: 1B; b) AS74 Fabric: 1A; c) AS75 Fabric: 1A; d) AS84 Fabric: 1A; e) AS85 Fabric: 1A; f) AS65 Fabric: 1A; g) AS82 Fabric: 2B; h) AS68 Fabric: 3A; i) AS67 Fabric: 4A; j) AS70 Fabric: 4B; k) AS81 Fabric: 5; l) AS83 Fabric: 6. All images were taken in XP. Field of view 1.5 mm (a–c, e, f). Field of view 3 mm (d, g–l). Prepared by Silvia Amicone.

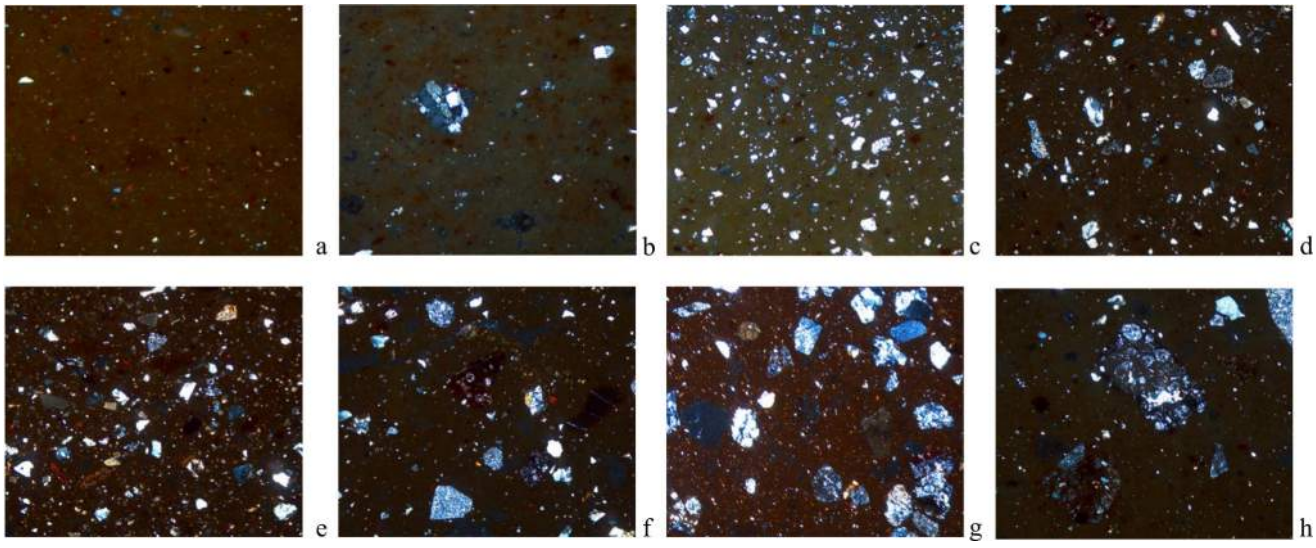

Fig. D2.4: Thin section micrographs of selected Parthian-period samples from Assur: a) AS90 Fabric: 1A; b) AS92 Fabric: 1B; c) AS91 Fabric: 2A; d) AS95 Fabric: 2B; e) AS94 Fabric: 2B; f) AS99 4A; g) AS111 Fabric: 4C; h) AS112 Fabric: 4B. All images were taken in XP. Field of view 1.5 mm (a,b). Field of view 3 mm (b-h). Prepared by Silvia Amicone.

might represent the use of a slightly different clay source and uncleaned clay (subgroup Fabric 3B).

Fabric 4: Coarse fabric, mineral-tempered (**Fig. D2.3i, j**; **Fig. D2.4f-h**)
This fabric is marked by inclusions between 0.5 and 2 mm average size. The main inclusions are quartz and feldspars (plagioclases), but muscovite, amphibole and serpentinite are also common; more rarely, tiny fragments of metamorphic rocks, calcite and chert can be observed. The presence of elongated voids in the same samples might suggest organic tempering. Still, it could also be derived from the combustion of naturally occurring organic materials present in the original clay used to produce this fabric. The strong bimodal distribution of the inclusions suggests mineral tempering. The samples AS070, AS100, AS108, and AS111 (= PO6) show more inclusions in the fine fraction (**Fig. D2.3j**).

Fabric 5: calcite-tempered fabric (**Fig. D2.3k**)
This fabric (observed only in HO6 = sample AS81) is dominated by the presence of sparitic calcite of 0.5 mm average size. There is also very fine quartz. The finesse of this fabric suggests that the original raw materials have been cleaned (probably through levigation) and tempered with sparitic calcite.

Fabric 6: micritic calcite fabric (**Fig. D2.3l**)
This fabric (observed only in HO7 = sample AS83) is an addition to the fabrics identified based on the first set of samples exported after the 2023 campaign.[205] It is dominated by micritic calcite with an average grain size of 0.5 mm. Very coarse quartz is also present. The main inclusions, aside from calcite, are quartz and feldspars (plagioclase), along with common occurrences of chert, muscovite, amphibole, and serpentinite. Less frequently, tiny fragments of metamorphic, sedimentary, and volcanic rocks are also observed.

D2.5 Discussion

The sections below explore the relationships between the chemical and petrographic groups, their spatial distribution within the excavated features of the Hellenistic Building A and the Parthian-period chamber tomb, and, finally, their connections to vessel typology.

D2.5.1 Combining the results from p-XRF and petrographic analyses

Overall, most petrographic groups are attested in both the Hellenistic and the Parthian periods (**Table D2.3**), although it is possible to observe that Fabrics 1A and 4A are more common in the Hellenistic period, whereas Fabrics 2A, 2B, 4B and 4C occur more frequently during the Parthian period.

The analyses have shown that rare petrographic fabrics often correspond to chemical outliers.[206] Fabric 2E is attested only in one, non-local Hellenistic outlier, HO3 (= sample AS066); Fabric 5 is linked to HO6 (= sample AS081), and Fabric 6 to HO7 (= sample AS083). A non-local origin is likely for HO7, while the chemical peculiarities of HO6 are due to a specific tempering method involving a high amount of calcite. PO3 (= sample AS009) is the only representative of Fabric 3B, which, based on its chemical composition, indicates a foreign production, thus rendering this fabric non-local as well.

It is worth noting that Hellenistic Group 1 (HG1) includes only samples with Fabrics 2A and 4A, while Group 3 (HG3) comprises only Fabrics 4A, 4B and 4C, and Group 5 (HG5) contains just objects of Fabric 1A. For the Parthian period, Group 1 (PG1) does not include any samples with Fabric 1 or 3B, while Group 3 (PG3) relates exclusively to Fabrics 4B and 4C.

Finer fabrics, especially 1A and 1B, can be more precisely distinguished through the p-XRF analysis. Hellenistic outliers HO4 (= sample AS074), HO5 (= sample AS075), and HO9 (= sample AS085) belong to Fabric 1A. Of these, HO4 and HO9 are chemically identified as non-local, while HO5 is highly contaminated by post-depositional calcite. Fabric 1A is also defined for the non-local outlier HO8 (= sample AS084), which is petrographically marked by a lack of amphibole and serpentinite. HO1 (= sample AS036) and HO2 (= sample AS064) belong to Fabric 1B, which is too fine to be clearly differentiated through petrography. However, chemical data strongly suggest that HO1 reflects a different temper while HO2 is of non-local origin.

Among the Parthian outliers with fine fabrics, PO1 (= sample AS001) and PO4 (= sample AS090) belong to Fabric 1A. While petrographically unremarkable, they are chemically distinct and indicate two different non-local origins. PO5 (= sample AS092), of Fabric 1B, is more likely distinguished by a specific tempering approach. However, due to the fineness of the fabric, this cannot be confirmed petrographically. PO2 belongs to the medium-coarse Fab-

205 Amicone/Schauer 2024.

206 This outcome was already observed in the analysis of the first set of Hellenistic samples: Amicone/Schauer 2024.

Group	Origin	Period	1A	1B	2A	2B	3A	4A	4B	4C	2E	5	6	2C	3B
HG1	Local	Hellenistic			3			5							
HG2	Local	Hellenistic	1	1			3	6							
HG3	Local	Hellenistic						2	1	1					
HG4	Local	Hellenistic				1	1								
HG5	Local	Hellenistic	2												
HO1	Local (temper)	Hellenistic		1											
HO2	Non-local	Hellenistic		1											
HO3	Non-local	Hellenistic									1				
HO4	Non-local	Hellenistic	1												
HO5	Local (temper)	Hellenistic	1												
HO6	Local (temper)	Hellenistic										1			
HO7	Non-local	Hellenistic											1		
HO8	Non-local	Hellenistic	1												
HO9	Non-local	Hellenistic	1												
PG1	Local	Parthian			7	5	2	6	5	1				3	
PG2	Local	Parthian		1	1										
PG3	Local	Parthian							1	1					
PO1	Non-local	Parthian	1												
PO2	Non-local	Parthian				1									
PO3	Non-local	Parthian													1
PO4	Non-local	Parthian	1												
PO5	Local (temper)	Parthian		1											
PO6	Local (temper)	Parthian								1					

Table D2.3: Matrix of chemical and petrographic groups. Prepared by Michaela Schauer and Silvia Amicone.

ric 2B, which is not a petrographic outlier, yet its chemistry suggests non-local production. PO6 (= sample AS111) is made of Fabric 4C with a high amount of inclusions. Its chemical peculiarities may result from the p-XRF measuring a higher proportion of temper, thus skewing the signature to reflect temper rather than the clay matrix. A non-local origin in this case may be doubtful.

When examining the chemical fingerprint in conjunction with fabric types in the element-based scatterplots, particularly for the Hellenistic but also for the Parthian period, it appears that fine fabrics (1A/B) are quite distinct. This is primarily due to their lower SiO_2 but higher Al_2O_3, V, Y, Ni, and Nb contents.[207] In the case of Hellenistic pottery of Fabric 1A, CaO values are also lower. These results are broadly consistent with those from the previous year. Beyond this, no clear chemical differentiation can be made for the remaining petrographic fabrics.

D2.5.2 Hellenistic period: combining contexts, chemistry and fabrics

The Hellenistic period samples were collected from the floors of Building A (**Fig. C2.8.2**), except for AS84 (HO8), which was found in the fill. Because of their context, all samples except AS84 can be connected to the building's main period of use. Interesting patterns emerge when the Hellenistic chemical/petrographic groups and outliers are analysed spatially.

Vessels of HG1 (n=8) are only found in Room 1 (n=4) or Room 2 (n=3), with one exception collected from the floor of Courtyard 10. The same applies to HG3 (n=4), with the highest number attested in Room 1 (n=2), followed by Room 2 (n=1) and Courtyard 10 (n=1). The two sherds of HG5 also originate exclusively from Rooms 1 and 2. HG2 (n=11), on the other hand, appears to be more spread out, with the highest number found in Courtyard 10 (n=4). Rooms 3 and 8 each yielded two samples, while Rooms 1, 2 and 7 yielded one each. The two sherds of HG4 were found in Courtyard 10 and Room 8.

Most chemical outliers (n=9) come from Room 8 (HO4, HO5, HO6, HO7), with all except HO6 likely to be non-local. The other two non-local samples come from the Courtyard 10 floor (HO2) and fill (HO8). The three outliers differing from the main clusters due to temper were found in Courtyard 10 (HO3), Room 2 (HO1), and Room 3 (HO9). It can, therefore, be concluded that different chemical groups are linked to different areas of the building. HG1, HG3 and HG5 are restricted to Rooms 1 and 2 and Courtyard 10, while HG4 is found only in Courtyard 10 and Room 8. Non-local samples predominantly come from the latter two units, with no chemical outlier found in Room 1. HG2 is mainly attested in Courtyard 10 and Rooms 3 and 8 but rarely in Rooms 1 and 2. This indicates a spatial divide, with HG1, HG3 and HG5 concentrated in the western part of the building, HG2 and HG4 in the eastern part, and an area of overlap in the courtyard. Non-local vessels appear more closely associated with Room 8 and the eastern section of the building.

Looking at fabric types and their distribution within the building, Fabric 1A is most commonly found in Room 3 (n=2) and Room 8 (n=2), but is also present in the Courtyard 10 fill, Room 1 and Room 2 (one sample each), the latter two also yielding one sample each of Fabric 1B. One further sample of Fabric 1B was found on the floor of Courtyard 10, which also yielded the only example of Fabrics 2B and 2E of this period. Fabric 2A is confined to Room 1 (n=3), while Fabric 3A was found on the courtyard floor, in Room 1, Room 7 and Room 8 (one each). The dominant fabric of the period, Fabric 4A, appears on the courtyard floor (n=4), in Room 1 (n=3), Room 2 (n=4) and

207 To view interactive scatterplots of the petrographic groups in regard to their chemistry in both periods, see Schauer 2025b: R-Script sections Z and X.

Room 8 (n=2); the single vessels of Fabric 4B in Room 2 and Fabric 4C on the courtyard floor. The samples of Fabrics 5 and 6 are both found in Room 8.

Thus, Fabrics 4A and 4B tend to occur more frequently in the western part of the building, while Fabric 1A is slightly more common in the southern rooms. The restriction of Fabric 2A to a specific context and the appearance of unusual fabrics in Room 2 and Room 8 are noteworthy. The latter observation corresponds well with the presence of chemical outliers in Room 8.

D2.5.3 Hellenistic period: combining vessel typology, chemistry and fabrics

Several vessel types stand out as chemical outliers: the two thin-walled beakers (HO2, HO4), two body sherds (HO1, HO7), a large storage jar (HO3), a small jar (HO5), the only cooking pot (HO6), an echinus bowl (HO8), and a carinated bowl (HO9; **Fig. D2.5**). Notably, the two beakers, the large storage jar, the carinated bowl, the echinus bowl, and the body sherd HO7 are considered non-local. Although thin-walled beakers are well represented at Assur, they also show close parallels with material from other sites, such as Nimrud (see **§D1.1**), suggesting a broader exchange network for these objects beyond Assur. Additionally, the mobility of even large vessels is demonstrated by the case of the non-local, otherwise unremarkable, storage jar (see **§D1.1**), which appears to have been brought in from elsewhere.

Whether the contents or the vessel itself were of primary interest cannot be determined.

The carinated bowl (HO9) is particularly intriguing. Since this form is almost indistinguishable between Assyrian and Hellenistic contexts (see **§D1.1**), it is possible that HO9 not only has a non-local origin but may also belong to a different chronological horizon than the other Hellenistic examples. Hence, an Assyrian-period origin for this sample is very likely.

The outlier H08 has also yielded remarkable results as the chemical, petrographic, and typological analyses contribute to its distinctiveness: all analyses clearly show that this bowl differs from the other Hellenistic finds in the study, and the typological analysis suggests an Attic origin (see **§D1.1**, sherd no. 5).

In the case of the cooking pot HO6 (Fabric 5 = sample AS81), its distinct tempering method is likely linked to its function. Calcite temper is exceptionally well suited to vessels exposed to rapid temperature changes, as expected in cooking.

The chemistry of most vessel types shows no strong correlation with a specific clay source or preparation method, indicating that no single raw material source or production technique was used consistently for a given form **(Fig. D2.5)**. However, the two thin-walled beakers stand out for their low TiO_2 and high Fe_2O_3 and Ni values, which may reflect functional aspects of this specific vessel type. Additionally, local bottles (AS069, AS071, AS087) and folded rim jars (AS067, AS077, AS078) form tightly clustered groups within the local chemical spectrum, particularly with respect to Fe_2O_3, MnO, TiO_2 and Y concentrations. This strongly suggests deliberate and consistent paste preparation. This also applies to the glazed rolled-rim plate (AS080), which shows relatively low Fe_2O_3, K_2O, V and Y, but high CaO values.[208]

As for fabrics and vessel types, smaller forms such as beakers, bowls, and jars are generally produced in finer fabrics (1A/1B; **Fig. D2.5**), while larger forms such as storage jars, cooking pots, and plates tend to be made from medium to coarser fabrics (3A, 4). No further detailed observations can be made at this stage.

D2.5.4 Parthian period: combining contexts, chemistry and fabrics

The chemical grouping of the Parthian-period material from the chamber tomb is less detailed, making the relationship between context and chemistry less informative than that of the Hellenistic Building A. Furthermore, the interpretation is complicated because the tomb was heavily looted, which means that the fragments collected cannot be relied upon to be in their original depositional positions.

Nevertheless, the samples belonging to PG1 (n=29) were found across almost all floors of the chamber tomb:[209] on the floors of Subdivisions 2 (n=1), 3 (n=10), 4 (n=3), 7 (n=3), and 8 (n=2), and in the fills of Subdivisions 1 (n=1) and 5 (n=2), the southern corridor (n=6), and the upper fill (n=1). The PG2 samples (n=2) come from the floors of Subdivisions 3 and 4. One of the two samples assigned to PG3 was also found in Subdivision 4, while the other was recovered from the tomb's main corridor fill. Most outliers, which are most likely non-local, were found on the floor of Subdivision 4 (PO1, PO2, and PO4), while PO3 was found in the fill of the southern corridor. The only vessel defined by a special type of temper, PO5, came from the floor of Subdivision 7. For PO6, also from Subdivision 7, it is unclear whether the object is of local or non-local origin.

208 To view interactive scatterplots of the Hellenistic vessel types in regard to their chemistry, see Schauer 2025b: R-Script section W.

209 For the layout of the chamber tomb (Grave 1), see Kreppner/Rohde/Squitieri 2024, fig. D2.2.

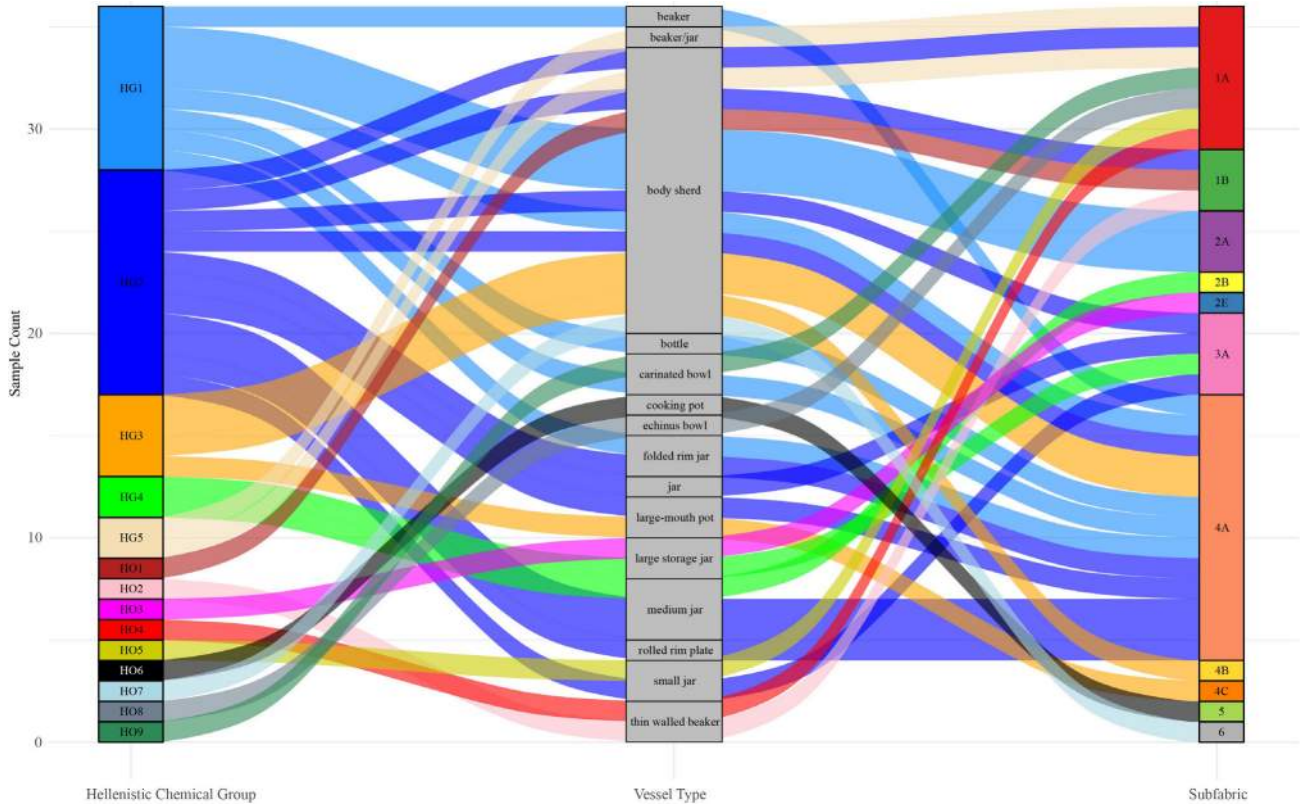

Fig. D2.5: Visualisation of the relationship between Hellenistic Chemical Groups, vessel types, and fabrics. Prepared by Michaela Schauer.

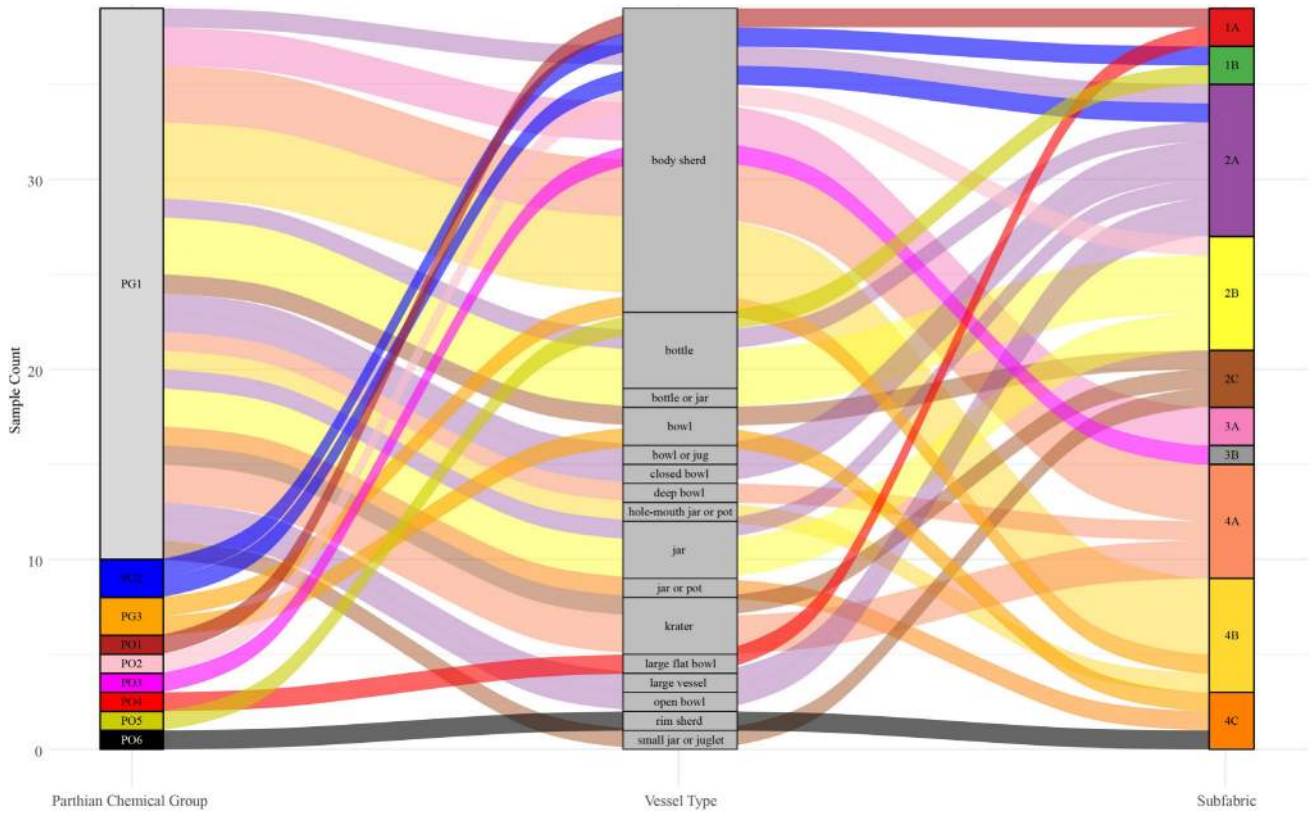

Fig. D2.6: Visualisation of the relationship between Parthian-period Chemical Groups, vessel types, and fabrics. Prepared by Michaela Schauer.

The main conclusion is that non-local material, where attribution is possible, is mostly concentrated in the eastern compartments of the tomb, especially Subdivision 4. Specially tempered vessels appear to be confined to Subdivision 7.

Fine fabric types are limited to the floors of Subdivisions 4 (1A; n=2 / 1B; n=1) and 7 (1B; n=1). Medium fabrics appear in nearly all subdivisions. Fabric 2B (n=3) and 2A (n=2) are somewhat concentrated in Subdivision 3; Fabric 2A also appears in Subdivision 7 (n=2), as well as Subdivision 1, 2 and 5 and the Southern Corridor Fill (one sample each), while Fabric 2B is found in Subdivision 4, 5 and the Southern Corridor Fill (one sample each). Fabric 2C has a focus on Subdivision 8 (n=2) and 4 (n=1). Medium Fabric 3A was found in Subdivisions 3 and 4 (one sample each), while 3B was recovered from the southern corridor fill. Coarser fabrics are mainly associated with Subdivision 3 (4A: n=2 / 4B: n=3 /4C: n=1) and the southern corridor fill (4A: n=2 / 4B: n=2). Fabric 4A and C also occur in Subdivision 7 (one sample each), the former additionally in the tomb fill (n=1), the latter in the main corridor fill (n=1); 4B in Subdivision 4 (n=2).

Overall, it can be concluded that fine and coarse fabric types are found mixed across a variety of areas in the tomb, with no strong spatial focus. It is, however, interesting to note that fine wares occur more frequently in the northeastern and southeastern subdivisions. This may suggest some variation in the selection of grave goods or reflect differences in the social status of the individuals buried in these specific compartments. However, the dataset is too limited to draw firm conclusions.

D2.5.5 Parthian period: combining vessel typology, chemistry and fabrics

No clear chemical distinctions between different vessel types can be made chemically or petrographically. However, it should be noted that the typological analysis for this material is still preliminary and considerably less detailed than for the Hellenistic period, as further study is ongoing. In general terms, kraters and large vessels show slightly higher Al_2O_3 concentrations, whereas bowls and jars tend to have lower Al_2O_3 values.[210] However, no consistent pattern emerges across other elements, and it appears that no vessel type can be reliably linked to a specific clay source or paste preparation technique.

210 To view interactive scatterplots of the Hellenistic vessel types in regard to their chemistry, see Schauer 2025b, R-Script section W.

Looking at the relationship between fabric and vessel type, bottles, bowls, and interestingly, also plates or large bowls, were produced in finer fabrics (see **Fig. D2.6)**. As with the Hellenistic material, larger vessels are more likely to have been made from coarser fabrics.

D2.6 Conclusions

This section showcased the results of chemical and petrographic analyses conducted on Hellenistic and Parthian-period samples from Building A and the chamber tomb, respectively. The analyses revealed that most of the pottery from both periods was locally produced; however, there were distinct differences in the production strategies employed during the two time periods.

The Hellenistic assemblage reveals a wider range of chemical compositions and tempering methods, with five distinct chemical groups and several outliers. These reflect the use of different clay sources and paste preparation techniques, including clay mixing and specialised tempering. Some vessels, particularly fine wares like beakers and bowls, are identified as non-local, suggesting active exchange networks during this period. Spatially, local groups cluster in the western rooms of Building A, while chemically distinct and non-local samples tend to appear in the eastern areas of the building, particularly Room 8 and Courtyard 10.

One especially notable non-local vessel is an echinus bowl, chemically and petrographically distinct from the rest of the assemblage. Its composition suggests it originated outside of Assur, and both its form and material characteristics point toward production traditions more commonly associated with Attic wares. The echinus bowl, along with other outliers such as thin-walled beakers and a large storage jar, likely arrived at the site through trade or movement of goods and people. Their presence indicates that even fine or delicate wares, and in some cases, larger utilitarian forms, were circulating regionally or inter-regionally during the Hellenistic period (see also **§D1.1**).

In contrast to the Hellenistic samples, the Parthian-period samples are more chemically homogenous. One dominant group accounts for most of the assemblage, with only a few outliers standing apart. These outliers are likely imports, though fewer in number and variety compared to the Hellenistic period. Petrographically, the Parthian-period material shows a narrower range of fabrics, with less variation in tempering and paste preparation.

The combination of chemical and petrographic results highlights the relationship between vessel function, form, and manufacturing choices. Fine fabrics are typically as-

sociated with small forms like beakers and bowls, while coarser fabrics are used for larger or functional vessels, such as storage jars and cooking pots. Calcite tempering appears in some cooking vessels, likely due to its thermal properties, pointing to functional considerations in material selection.

In conclusion, the chapter illustrates a shift from the Hellenistic period's more varied and interconnected pottery practices to a more uniform and localised production system in the Parthian phase. These findings offer valuable insight into technological traditions, resource use, and exchange patterns at Assur during these two key historical periods.

E. Small finds from Assur, 2023 and 2024

This section is composed of two parts. The first part (**§E1**) presents a typological analysis of the small finds recovered from Assur during the 2023 and 2024 excavation campaigns. The finds are arranged according to the following categories: sarcophagi (**§E1.1**), personal items, including jewellery (**§E1.2**), figurative terracotta objects (**§E1.3**), glass objects (**§E1.4**), and, finally, tools, including metal tools, weapons, textile tools in various materials, stone tools and metal production waste (**§E1.5**). The second part (**§E2**) deals with a bronze coin discovered in Building A, identified as belonging to the late Seleucid period.

E1. Typological study of the small finds from the New Town of Assur, 2023 and 2024

Andrea Squitieri & Helen Gries[211]

The 2024 campaign provided new insights into the archaeological features partially discovered in 2023, expanding the corpus of items available for study. Consequently, we are better positioned to discuss the small finds from the 2023 and 2024 campaigns in a typological classification. Moreover, the use in the field of a DinoLite microscope (model: AM4113T 200×) during the 2024 campaign significantly enhanced our ability to identify particular materials and improve the descriptions of many finds.[212] The DinoLite microscope proved crucial in distinguishing frit from glass, documenting beads and the worn-out late Seleucid bronze coin (discussed in **§E2**).

Throughout the chapter, the following abbreviations are used in the object descriptions: L. for length, W. for width, H. for height, Th. for thickness, D. for diameter, and Wt. for weight. The catalogue numbers (= no.) assigned to the finds follow directly after those assigned to the finds from 2023, continuing the same sequence. References to the catalogue numbers of the items already published in the Exploring Assur Volume 1[213] are preceded by the abbreviation "ExA1" (e.g., ExA1: 45). The AS numbers refer to the find registration number, composed as follows: AS [square number]:[locus number]:[find number].

E1.1 Sarcophagi and sarcophagus lids

Two types of sarcophagi were discovered during the 2023 and 2024 campaigns at Assur. The first type is the inverted sarcophagus (German: *Stülpsarkophag*) with an ovoid-elliptic shape. Two such sarcophagi were unearthed in Graves 3 and 4, both of which cut the floors of Building A.[214] Grave 3's sarcophagus bore an alphabetic inscription reporting the date 159/158 BC.[215]

The second type is the tub sarcophagus, made from a single ceramic piece in a rectangular shape with curved short sides (German: *einteiliger Wannensarkophag*). Four such sarcophagi were unearthed during the 2023 and 2024 campaigns, in addition to many fragments of this type from the chamber tomb (Grave 1) excavated in 2023. The sections below detail the tub sarcophagi and their respective lids.

E1.1.1 The sarcophagi from the chamber tomb

The Parthian-period chamber tomb (Grave 1) excavated during the 2023 campaign had a rectangular layout measuring about 6 × 8 m and was composed of eight smaller chambers, named subdivisions, separated by two perpendicular corridors.[216] The tomb had been looted in antiquity, leaving its artefacts and bones scattered everywhere. On the floor of Subdivision 2, a partially preserved tub sarcophagus (ExA1: **56**) was found (**Figs. E1.1.1a**, **E1.1.1b**). Since this sarcophagus was restored in 2024, we can offer more details about it. It is an unglazed sarcophagus, measuring 186 × 59 × 44 cm, with a flat base, straight long sides, and curved short sides. Notably, the long sides are

211 Andrea Squitieri wrote **§E1.1**, **§E1.2.1.3**, **§E1.4.3**, **§E1.5.1**, **§E1.5.2**, **§E1.5.4**, **§E1.5.5**; Helen Gries wrote: **§E1.2.1.1**, **§E1.2.1.2**, **§E1.3**, **§E1.4.1-2**, **§E1.4.2**, and **§E1.5.3**.

212 During the 2024 campaign, the small finds were processed and photographed in the field by Helen Gries and Andrea Squitieri. They were cleaned and restored by Akam Omar Ahmed Al-Qaradaghi.

213 Squitieri 2024.

214 Kreppner/Rohde/Squitieri 2024, 119-122.

215 Gzella 2024.

216 Kreppner/Rohde/Squitieri 2024, 105-118. For a plan of the tomb, see Kreppner/Rohde/Squitieri 2024, fig. D.2.2.

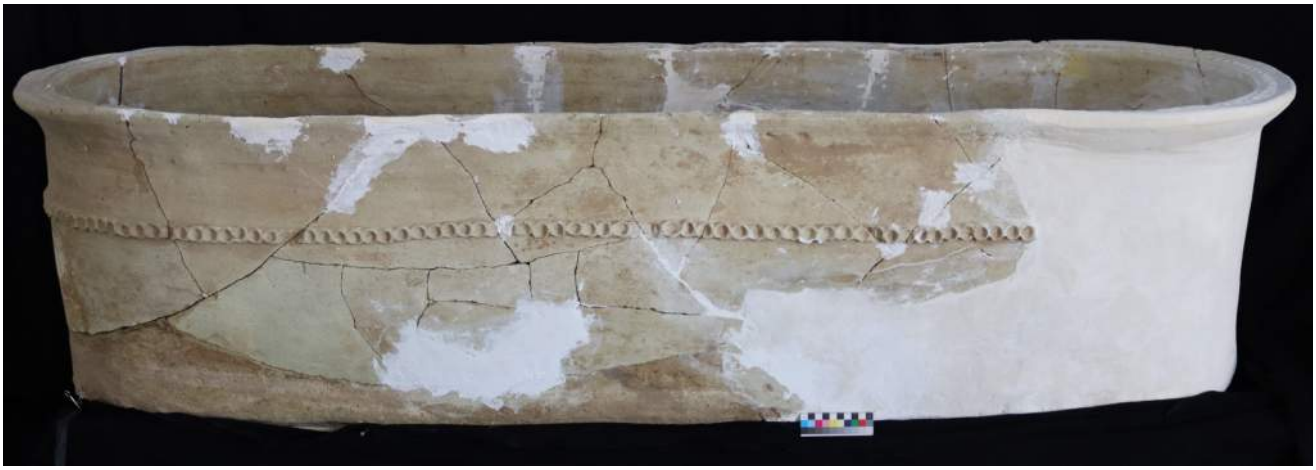

Fig. E1.1.1a: The tub sarcophagus **56** (see Squitieri 2024, 165) from the chamber tomb (Grave 1) of the Parthian period. Restored by Akam Omar Ahmed Al-Qaradaghi. Photo by Andrea Squitieri.

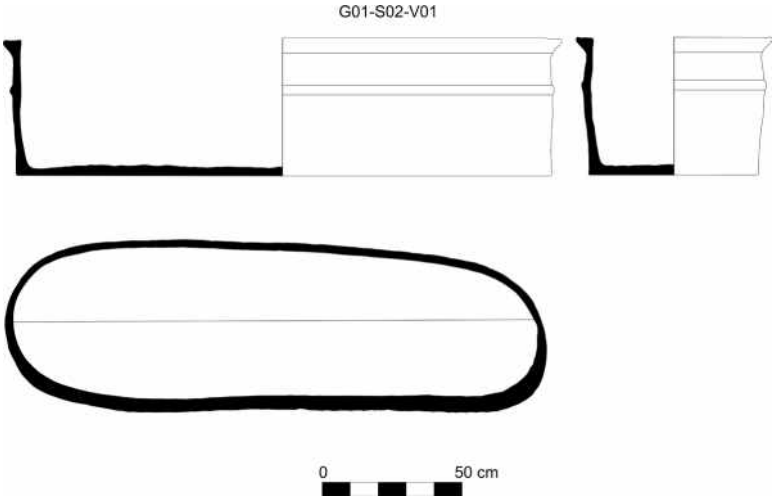

Fig. E1.1.1b: Drawing of the tub sarcophagus **56** generated using GigaMesh by Marco Wolf from a 3D model generated by Andrea Squitieri using the LiDAR sensor of iPhone 12 Pro.

Fig. E1.1.2: A decorated fragment belonging to the sarcophagus **294**, found in the chamber tomb (Grave 1) of the Parthian period. Photo by Ellen Coster.

Fig. E1.1.3: Glazed fragments **296** of walls and rims belonging to various tub sarcophagi. Photo by Omar Laith Allawi.

not perfectly straight as they widen slightly on one end (see discussion below, **§E1.2.3**). The rim, approximately 5 cm wide, is decorated with two parallel grooves and a central ridge with rounded impressions. About 14 cm below the rim, a rope-like decorative band runs around the outer surface.

The sarcophagus ExA1: **56** was not the only one housed within the chamber tomb. Fragments from at least three additional tub sarcophagi were identified. A sarcophagus base was found in Subdivision 7 (**293**), and wall fragments with a rope-like decoration (**294**) were collected in Subdivisions 2, 6, 7, and the southern corridor (**Fig. E1.1.2**). Two joining fragments with top rim decoration, similar to that on ExA1: **56**, were found in Subdivision 5 (**295**). All these fragments were unglazed. Glazed fragments of tub sarcophagus rims, displaying a rope-like decoration (**296**), were found in the fill of the tomb's entrance shaft (**Fig. E1.1.3**). They likely belong to glazed sarcophagi that were destroyed during ancient looting.

Two unglazed and incomplete ceramic lids for sarcophagi were also collected in the chamber tomb. Six fragments of one lid (**297**) were found on the floor of Subdivision 9 (**Fig. E1.1.4**). Its original width was 58 cm, with a preserved length of 48 cm and a thickness ranging between 2.5 cm and 3 cm. The top surface is decorated with a groove along the outer edge and two parallel lines along the central long axis. Two curved lines flank the central double-line band, all drawn with fingers. A dog's paw print, measuring 4.7 × 5.3 cm, is visible on the top surface.

Another lid (**298**) was found in nine fragments in Subdivision 2 (**Fig. E1.1.5**); however, not all fragments could be joined together. The two curved extremities of the lid were reconstructed, though much of the central body was missing. It had a maximum preserved width of 54 cm and a thickness of 3 cm. The top surface has a greenish-beige slip or coating up to 2.5 mm thick, while the bottom surface is very coarse, with impressions of chaff up to 8 cm in length.

Fragments of sarcophagi from the chamber tomb (Grave 1)		
No.	**Reg. number**	**Description**
ExA1: 56	G01-S02-V01	Restored tub sarcophagus, measuring 186 × 59 × 44 cm (**Figs. E1.1.1a**, **E1.1.1b**)
293	G01-S07-J08	Fragments of a tub sarcophagus
294	G01-S07-J03	Fragments of a tub sarcophagus (**Fig. E1.1.2**)
295	G01-S05-J02	Fragments of a tub sarcophagus
296	AS 262433:117:004	Glazed fragments of different sarcophagi (**Fig. E1.1.3**)
297	G01-S09-J02	Sarcophagus lid fragments (**Fig. E1.1.4**)
298	G01-S02-J01	Sarcophagus lid fragments (**Fig. E1.1.5**)

E1.1.2 The sarcophagi from Graves 8, 9 and 11

Graves 8, 9 and 11 were identified and excavated around the chamber tomb. Grave 8 (**§C2.5.2**) contained an unglazed ceramic tub sarcophagus (**299**), measuring 138 × 52 × 38 cm, with straight long sides and curved short sides (**Figs. E1.1.6a**, **E1.1.6b**). About 10 cm below the rim, a 2 cm wide band with a rope-like motif made of rounded impressions runs along the outer surface. Unlike ExA1: **56** (discussed above), this sarcophagus has no sinusoid profile on the long sides and no decorations on the rim

Fig. E1.1.4: Fragments of the sarcophagus lid **297** found in the chamber tomb (Grave 1) of the Parthian period. Photo by Ellen Coster.

Fig. E1.1.5: Fragments of the sarcophagus lid **298** found in the chamber tomb (Grave 1) of the Parthian period. Photo by Ellen Coster.

Fig. E1.1.6a: The tub sarcophagus **299** found in Grave 8. Restored by Akam Omar Ahmed Al-Qaradaghi. Photo by Andrea Squitieri.

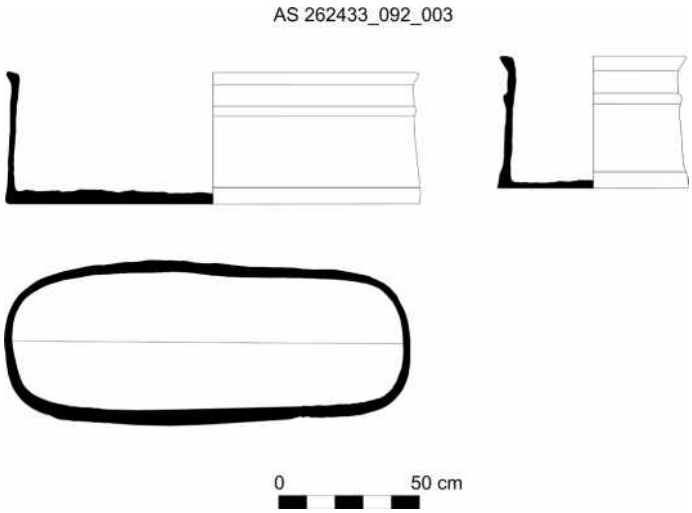

Fig. E1.1.6b: Drawing of the tub sarcophagus **299** generated using GigaMesh by Marco Wolf from a 3D model generated by Andrea Squitieri using the LiDAR sensor of iPhone 12 Pro.

surface. Before restoration, traces of plaster were noted along some cracks on the long sides, indicating ancient repairs (see **Fig. C2.6**).

Grave 9 (**§C2.5.2**) contained an unglazed ceramic tub sarcophagus (**300**) measuring 184/177 × 61/56 × 39 cm, with one straight long side and one with a slight sinusoid shape, causing the width to vary from 56 to 61 cm (**Figs. E1.1.7a**, **E1.1.7b**). The shorter sides are curved and slightly taper upwards, resulting in a length of 184 cm at the base and 177 cm at the top. The rim is flat and slightly everted, decorated with a series of rounded impressions on the top. The outer surface features two horizontal bands marked by rounded impressions, with the top band 5 cm below the rim and the bottom one 30 cm below the rim. Fragments of the lid (**301**) were found on top of the sarcophagus, while others were found scattered in the grave fill (**Figs. C2.9**, **Fig. E1.1.8**). The lid, made of ceramic, could only be partially reconstructed due to some fragments not joining. Its original measurements were about 80 × 70 cm. It is flat with an upright thick rim and a thick ridge running longitudinally in the centre. The surface is crossed by linear depressions, possibly finger-made, in a sinusoid pattern.

Grave 11 (**§C2.5.2**) contained an almost wholly preserved and unglazed tub sarcophagus (**302**) (**Figs. E1.1.9a**, **E1.1.9b**). The sarcophagus measures 130 × 43 × 38 cm, with straight long sides and curved short sides. Its overall shape is regular, lacking the slight sinusoid profile seen in ExA1: **56** and **300**. The rim is flat and slightly everted. About 7 cm below the rim, a 2 cm wide band with a rope-like motif runs along the outer surface. An interesting feature is the ancient repairs made with plaster along cracks on the long sides and base (see **Fig. C2.10**), as observed on Grave 8's sarcophagus.

Sarcophagi from Graves 8, 9 and 11		
No.	**AS number/ Grave**	**Description**
299	AS 262433:092:003 Grave 8	Tub sarcophagus, 138 × 52 × 38 cm (**Figs. E1.1.6a**, **E1.1.6b**)
300	AS 262433:090:003 Grave 9	Tub sarcophagus, 184/177 × 61/56 × 39 cm (**Figs. E1.1.7a**, **E1.1.7b**)

Fig. E1.1.7a: The tub sarcophagus **300** found in Grave 9. Restored by Akam Omar Ahmed Al-Qaradaghi. Photo by Andrea Squitieri.

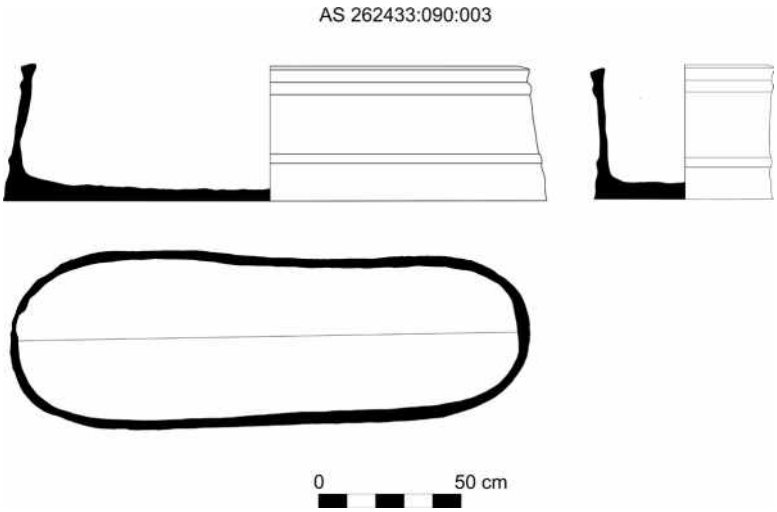

Fig. E1.1.7b: Drawing of the tub sarcophagus **300** generated using GigaMesh by Marco Wolf from a 3D model generated by Andrea Squitieri using the LiDAR sensor of iPhone 12 Pro.

Fig. E1.1.8: Fragments of the lid **301** belonging to the sarcophagus **300** from Grave 9. Photo by Andrea Squitieri.

Sarcophagi from Graves 8, 9 and 11		
No.	**AS number/ Grave**	**Description**
301	AS 262433:090:004 Grave 9	Sarcophagus lid fragments, reconstructed size: c. 80 × 70 cm (**Figs. C2.9**, **E1.1.8**)
302	AS 263433:009:003 Grave 11	Tub sarcophagus, 130 × 43 × 38 cm (**Figs. E1.1.9a**, **E1.1.9b**)

E1.1.3 Observations on the tub sarcophagi

The tub sarcophagi discovered during the 2023 and 2024 campaigns, both in the chamber tomb (Grave 1) and in Graves 8, 9 and 11, belong to the "one-piece tub sarcophagus" type (German: *einteiliger Wannensarkophag*). These sarcophagi were made in a single piece, and the deceased was placed inside them in a stretched position. Several such sarcophagi had already been uncovered at Assur by Andrae.[217] This design first appeared in Assur during the Neo-Assyrian period, marking an innovation from the

217 Andrae/Lenzen 1933, 93.

Fig. E1.1.9a: The tub sarcophagus **302** found in Grave 11. Restored by Akam Omar Ahmed Al-Qaradaghi. Photo by Andrea Squitieri.

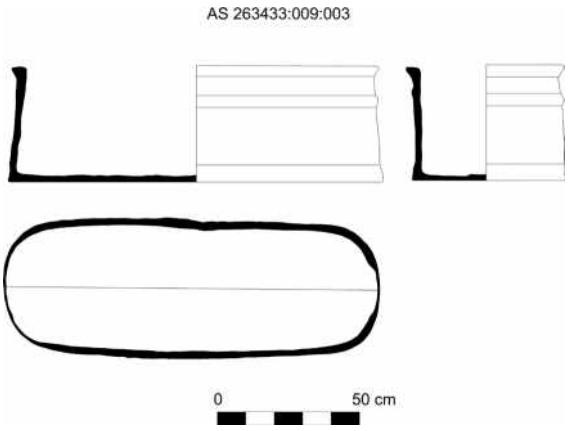

Fig. E1.1.9b: Drawing of the tub sarcophagus **302** generated using GigaMesh by Marco Wolf from a 3D model generated by Andrea Squitieri using the LiDAR sensor of iPhone 12 Pro.

earlier Middle Assyrian period, when tub sarcophagi were typically made of two joined pieces (German: *zweiteiliger Wannensarkophag*).[218] Among the Parthian graves unearthed by Andrae, some yielded sarcophagi that closely parallel ours in both shape and decoration, registered as Ass 13368, Ass 13413, and Ass 13500. Andrae had suggested that some Neo-Assyrian tub sarcophagi were reused in Parthian times, particularly around the Nabu Temple ruins.[219] These possibly reused sarcophagi often showed signs of repair, such as plaster applied to breakage points. Interestingly, signs of repair can also be observed on our sarcophagi from Graves 8 and 11.

As highlighted by Haller,[220] despite the continuity in design from the Neo-Assyrian to the Parthian period, two design features seem to have appeared only in the Parthian period, these are:

- Vertical flat raised bands connecting the rim to the base on the outer surface (not attested on our sarcophagi)
- Enlargement of the sarcophagus walls at one end, presumably for the deceased's head.

It appears that Neo-Assyrian tub sarcophagi always have straight, long sides, while the head-enlargement feature appeared in Assur only after the Neo-Assyrian period.[221] Even though not very pronounced, the head enlargement feature can be seen in our sarcophagus ExA1: **56** and in the sarcophagus **301** from Grave 9. Hence, while it is possible that the sarcophagi from Graves 8 and 11 broke after manufacture and were repaired before use, it is also plausible that they may have been Neo-Assyrian sarcophagi reused during the Parthian period. On the other hand, the sarcophagus ExA1: **56** and the sarcophagus **300** should be considered genuinely Parthian, as they display the characteristic head-enlargement feature and no signs of ancient repair.

218 Haller 1954, 74.

219 Andrae/Lenzen 1933, 93.

220 Haller 1954, 81.

221 The head-enlargement feature can be found in the Neo-Assyrian period only on sarcophagi with a curved shape and one straight side (German: *Hockersarkophag*), in which the deceased was placed in a crouched position, see Haller 1954, fig. 108.

E1.2 Personal items

E1.2.1 Personal ornaments

E1.2.1.1 Beads and pendants

One of the primary objectives during the processing of finds from the 2024 campaign was to refine the material identification of the numerous beads unearthed. To achieve this, the beads were re-examined macroscopically and documented using a DinoLite microscope. This detailed analysis led to revisions in some material identifications. The beads from the 2023 campaign are listed here according to their updated material classifications, which, in some cases, differ from those published in *Exploring Assur Volume 1*.[222]

E1.2.1.1.1 Stone beads and pendants

During the 2024 campaign, 11 stone beads (**303-313**) and the fragment of a lapis lazuli pendant (**314**) were found. Ten of the 11 beads are likely made of carnelian and exhibit different shapes. Another tiny spherical bead is made of lapis lazuli (**313**). They are all relatively small (up to 1 cm in diameter), with perforation diameters ranging from 0.1 to 0.3 cm.

2024 campaign		
No.	**AS number/ context**	**Description**
	Carnelian	
303	AS 262433:084:003 Topsoil	Bead with biconical shape, most probably made of carnelian. The surface is whitish, and the core is light red. L. 0.6 cm; D. 0.8 cm; perforation D. ca. 0.1 cm.
304	AS 261433:061:011 NT1 2023 Phase 7 / Pit 7 / fill	Barrel-shaped bead (not very regular), red-brownish colour, likely carnelian. L. 0.5 cm; D. 0.4 cm; perforation D. 0.1 cm.
305	AS 261433:046:012 NT1 2023 Phase 5 / Building A Room 2 / Floor deposit	Short cylindrical carnelian bead, dark red colour. L. 0.3 cm; D. 0.6 cm; perforation D. 0.3 cm.
306	AS 261433:048:003 NT1 2023 Phase 5 / Building A Courtyard 10 / Upper fill	Carnelian bead with a hexagonal, long truncated bicone shape. L. 1.5 cm; D. 1.0 cm; perforation D. 0.1 cm. (**Fig. E1.2.1**)
307	AS 262433:102:005 NT1 2023 Phase 5 / Building A Room 8 / Upper fill	Barrel-shaped bead, red-brown colour, probably carnelian. L.0,6 cm; D. 0.5 cm; perforation D. ca. 0.1 cm.
309	AS 262433:107:008 NT1 2023 Phase 5 / Building A Room 8 / Floor deposit	Cylindrical carnelian bead, light red to transparent colour, partially broken. L. 0.5 cm; D. 0.3 cm; perforation D. 0.1 cm. (**Fig. E1.2.2**)
309	AS 262433:104:004 NT1 2023 Phase 5 / Building A Courtyard 10 / Upper fill	Short iconic carnelian bead, light red to transparent colour. L. 0.4 cm; D. 0.7 cm; perforation D. ca. 0.1 cm.
310	AS 262433:140:003 NT1 2023 Phase 5 / Building A "Room 5" / Fill	Oblate carnelian bead, dark red colour. L. 0.3 cm; D. 0.5 cm; perforation D. 0.1 cm.
311	AS 263433:016:004 NT1 2023 Phase 5 / Building A "Room 5" / Fill	Spherical carnelian bead, light red to transparent colour. L. 0.7 cm; D. 0.9 cm; perforation D. 0.2 cm.
312	AS 261433:080:007 NT1 2023 Phase 4 / Building B Room 11 / Floor deposit	Small spherical carnelian bead. D. 0.4 cm; perforation D. 0.1 cm. (**Fig. E1.2.3**)
	Lapis lazuli	
313	AS 262433:117:003 NT1 2024 Phase 8a / Grave 1 / Entrance shaft	Spherical lapis lazuli bead. D. 0.4 cm; perforation D 0.1 cm.
314	AS 261433:058:018 NT1 2023 Phase 5 / Building A Courtyard 10 / Upper fill	Fragment of a small cylindrical lapis lazuli pendant with a brilliant blue colour, slightly wider on one side. The surface has longitudinal shallow grooves. The upper part is broken off in the perforation. L. 0.9 cm; D. 0.5 cm; perforation D. ca. 0.1-0.2 cm. (**Fig. E1.2.4**)
2023 campaign		
ExA1: 16,[223] 44, 57, 58, 66, 68 (?),[224] 69, 70, 71, 72, 73, 74, 75, 139 (?), 150 (?), 206, 254.		

222 Squitieri 2024.

223 Of the 15 beads grouped under ExA1: **16**, nine are made of different stones and six of glass, see **§E1.2.1.1.2**.

224 ExA1: **68**, **139**, **150** could also be spindle whorls, see **§E1.5.3.3**.

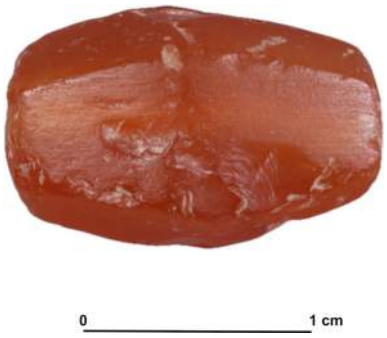

Fig. E1.2.1: Carnelian bead **306**. Photo by Helen Gries.

Fig. E1.2.3: Carnelian bead **312**. Photo by Helen Gries.

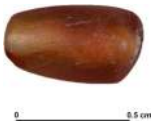

Fig. E1.2.2: Carnelian bead **309**. Photo by Helen Gries.

Fig. E1.2.4: Fragment of a lapis lazuli pendant **314**. Photo by Helen Gries.

1.2.1.1.2 Glass beads

Determining composite materials such as glass or frit on heavily corroded surfaces can be challenging. However, reliable identification was often achieved through the DinoLite microscopic examination of fractures or damaged areas. This revealed that some beads, initially identified as frit due to their whitish corroded surface, were, in fact, made of glass.

Six nearly identical spherical beads with a dark, spotty, corroded surface (**320-325**) were recovered from the floor deposit of Room 1 in Building A (NT1 2023 Phase 5; **§C2.8.1**). Two of these beads were broken or damaged, allowing the material on the fractured surfaces to be identified as glass (**Fig. E1.2.9**). A spherical glass bead (**332**) was also collected from the floor deposit of Room 11 in Building B (NT1 2023 Phase 4; **§C2.9.1**).

Spherical shapes predominate among the 2024 glass bead finds, particularly those recovered from NT1 2023 Phases 4 and 5. The perforation diameters in these beads are generally larger than those in stone beads (**§E1.2.1.1.1**), ranging from 0.1 to 0.7 cm. Their colour spectrum includes yellow, green, and blue turquoise. In contrast, the glass beads from the younger chamber tomb (Grave 1) and looted Grave 2, both excavated in 2023, display a much wider variety of shapes, including ring, oblate, cylindrical, triangular, and spherical beads (ExA1: **10**, **11**, **12**, **13**, **16**, **61**, **62**, **63**, **64**, **65**).

2024 campaign		
No.	**AS number/ context**	**Description**
315	AS 262433:094:004 NT1 2024 Phase 8a / Grave 9 / Sarcophagus fill	Short cylindrical bead, probably made of glass. The surface is whitish, corroded. L. 1.0 cm; D. 1.4 cm; perforation D. 0.7 cm.
316	AS 262433:094:005 NT1 2024 Phase 8a / Grave 9 / Sarcophagus fill	Spherical glass bead, broken in two. The surface is whitish, corroded, and the core dark blue-grey. L. 0.8 cm; D. 1.1 cm; perforation D. 0.3 cm. (**Fig. E1.2.5a**, **E1.2.5b**)
317	AS 261433:043:003 NT1 2024 Phase 8b / Pit 6 / Fill	Spherical glass bead; translucent, shiny turquoise colour. D. 0.5 cm; perforation D. 0.2 cm. (**Fig. E1.2.6**)
318	AS 261433:061:010 NT1 2023 Phase 7 / Pit 7 / Fill	Spherical bead; probably made of glass; surface whitish with black fine lines, corroded. D. 1.0 cm; perforation D. 0.4 cm.
319	AS 261433:061:016 NT1 2023 Phase 7 / Pit 7 / Fill	This fragment of a tubular bead is probably made of glass. The surface is whitish, with dark spots, corroded. L. 1.5 cm; D. 0.3 cm; perforation D. 0.1 cm. (**Fig. E1.2.7**)
320	AS 261433:040:009 NT1 2023 Phase 5 / Building A Room 1 / Floor deposit	Spherical bead, probably made of glass. The surface is dark, spotty, and corroded. D. 0.5 cm; perforation D. 0.2 cm. (**Fig. E1.2.8**)
321	AS 261433:040:010 NT1 2023 Phase 5 / Building A Room 1 / Floor deposit	Spherical bead, probably made of glass. The surface is dark, spotty, and corroded. D. 0.7 cm; perforation D. 0.2 cm.
322	AS 261433:040:011 NT1 2023 Phase 5 / Building A Room 1 / Floor deposit	Spherical bead, probably made of glass. The surface is dark, spotty, and corroded. D. 0.5 cm; perforation D. 0.2 cm.
323	AS 261433:040:012 NT1 2023 Phase 5 / Building A Room 1 / Floor deposit	Spherical glass bead, broken in two. The surface is dark, spotty, and corroded. The core is yellowish. D. 0.5 cm; perforation D. 0.2 cm. (**Fig. E1.2.9**)
324	AS 261433:040:013 NT1 2023 Phase 5 / Building A Room 1 / Floor deposit	Spherical bead, probably made of glass. The surface is dark, spotty, and corroded. D. 0.5 cm; perforation D. 0.2 cm.
325	AS 261433:040:014 NT1 2023 Phase 5 / Building A Room 1 / Floor deposit	Spherical glass bead with a damaged surface, dark, spotty and corroded. The core is yellowish. D. 0.5 cm; perforation D. 0.2 cm.

2024 campaign		
No.	**AS number/ context**	**Description**
326	AS 261433:052:001 NT1 2023 Phase 5 / Building A Room 2 / Installation A02-I1	Fragment of an originally spherical glass bead. The surface is dark, spotty, and corroded. The core is turquoise. D. 1.0 cm (preserved); perforation D. 0.4 cm. (**Fig. E1.2.10a**, **E1.2.10b**)
327	AS 261433:056:004 NT1 2023 Phase 5 / Building A Courtyard 10 / Upper fill	Spherical glass bead broken into two halves. The surface is corroded, white-black-brown. The core is almost completely corroded with smaller dark blue-green spots. D. 1.0 cm; perforation D. 0.4 cm. (**Fig. E1.2.11a**, **E1.2.11b**)
328	AS 261433:058:023 NT1 2023 Phase 5 / Building A Courtyard 10 / Upper fill	Fragments of a spherical glass bead. The surface is white-black-brown, corroded, and the core almost completely corroded with small yellow spots. D. 1.0 cm (preserved); perforation D. ca. 0.3-0.4 cm.
329	AS 261433:058:024 NT1 2023 Phase 5 / Building A Courtyard 10 / Upper fill	Fragment of a conical glass bead. The surface is white-grey, corroded. The core is light green and dark red. L. 0.9 cm; D. 0.6 cm; perforation D. ca. 0.2 cm. (**Fig. E1.2.12a**, **E1.2.12b**)
330	AS 262433:141:004 NT1 2023 Phase 5 / Building A "Room 5" / Fill	Shapeless glass fragment, maybe belonging to a bead. Blue colour. L. 0.5 cm.

Fig. E1.2.5a: Glass bead **316**. Photo by Helen Gries.

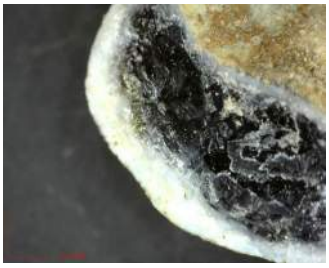

Fig. E1.2.5b: Detail photo showing the core of glass bead **316**, taken with a DinoLite microscope. Photo by Helen Gries.

Fig. E1.2.6: Glass bead **317**. Photo by Helen Gries.

Fig. E1.2.7: Tubular bead **319**, probably made of glass. Photo by Helen Gries.

2024 campaign		
No.	**AS number/ context**	**Description**
331	AS 262433:150:004 NT1 2023 Phase 4 / Building B Room 11 / Upper fill	Barrel-shaped bead, probably made of glass. Light green-bluish colour. L. 0.5 cm; D. 0.3 cm; perforation D. 0.1 cm. (**Fig. E1.2.13**)
332	AS 261433:080:005 NT1 2023 Phase 4 / Building B Room 11 / Floor deposit	Fragmented spherical glass bead. The surface is whitish, corroded. The core is yellow-greenish. D. 0.8-1.0 cm; Perforation D. ca. 0.3 cm. (**Fig. E1.2.14a**, **E1.2.14b**)
2023 campaign		
ExA1: 10, 11, 12, 13,[225] 16,[226] 61, 62, 63, 64, 65, 67,[227] 134 (?), 135, 136, 274.[228]		

Fig. E1.2.8: Spherical glass bead **320**. Photo by Helen Gries.

Fig. E1.2.9: Fragments of glass bead **323**. Photo by Helen Gries.

Fig. E1.2.10a: Glass bead **326**. Photo by Helen Gries.

Fig. E1.2.10b: Detail photo showing the core of glass bead **326**, taken with a DinoLite microscope. Photo by Helen Gries.

225 The five greenish spherical beads (ExA1: **12**, **13**), originally assumed to be metal, are now identified as glass, similar to the whitish ring beads found alongside them (ExA1: **10**).

226 Of the 15 beads grouped under ExA1: **16**, six are made of glass. These correspond to the whitish ring beads (ExA1: **10**) and the greenish spherical beads (ExA1: **12**) from the same context.

227 The bead (ExA1: **67**) was first identified as stone due to its dull gray surface, but restoration in February 2025 revealed its original deep blue glass with a white iridescent corroded surface.

228 The large cylindrical bead (L. 5.3 cm), initially identified as stone, has been reclassified as a heavily corroded glass bead, likely dating to the Late Bronze Age. Similar beads are known from Middle Assyrian tombs at Assur (see e.g. Pedde 2015, graves 25.6, 43.1, 111.3, 158.9, 159.15, 201.1 pls. 29, 36, 85, 116, 117, 132 where they are sometimes described as frit beads).

Fig. E1.2.11a: Glass bead **327**. Photo by Helen Gries.

Fig. E1.2.11b: Detail photo showing the core of glass bead **327**, taken with a DinoLite microscope. Photo by Helen Gries.

Fig. E1.2.12a: Glass bead **329**. Photo by Helen Gries.

Fig. E1.2.12b: Detail photo showing the core of glass bead **329**, taken with a DinoLite microscope. Photo by Helen Gries.

Fig. E1.2.13: Barrel-shaped bead **331**, probably made of glass. Photo by Helen Gries, taken with a DinoLite microscope.

Fig. E1.2.14a: Glass bead **332**. Photo by Helen Gries.

Fig. E1.2.14b: Detail photo showing the core of glass bead **332**, taken with a DinoLite microscope. Photo by Helen Gries.

E1.2.1.1.3 Frit and Egyptian Blue beads

Frit and Egyptian Blue beads represent only a tiny fraction of the finds from the 2023 and 2024 campaigns. Alongside the two beads discovered in 2023 (ExA1: **141**, **243**), the 2024 campaign yielded a fragment of an Egyptian Blue bead (**334**) and a bead possibly made of frit (**333**). However, the latter is so heavily corroded that we could not easily identify its material. The material of **335** also remains undetermined without chemical analysis, as it could be frit, glass, or ceramic.

2024 campaign		
No.	**AS number/context**	**Description**
333	AS 261433:005:010[229] NT1 2023 Phase 5 / Building A Room 1 / Floor deposit	Cylinder bead, probably made of frit. The surface is whitish and corroded. L. 0.8 cm, D. 0.5 cm; perforation D. 0.2 cm. (**Fig. E1.2.15**)
334	AS 261433:058:017 NT1 2023 Phase 5 / Building A Courtyard 10 / Upper fill	Fragment of a conical Egyptian Blue bead. L. 1.0 cm; D. 0.4-0.6 cm; perforation D. 0.1 cm. (**Fig. E1.2.16**)
335	AS 261433:080:008 NT1 2023 Phase 4 / Building B Room 11 / Floor deposit	Small spherical bead, perhaps made of frit, glass or ceramic. The surface is dark grey-black with white corrosion. D. 0.6 cm; perforation D. max. 0.1 cm.
2023 campaign		
ExA1: 141, 243.		

Fig. E1.2.15: Cylinder bead **333**, probably made of frit. Photo by Helen Gries.

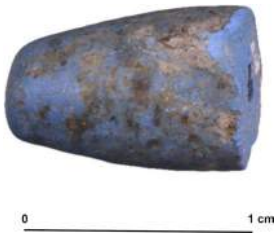

Fig. E1.2.16: Fragment of Egyptian blue bead **334**. Photo by Helen Gries.

229 This bead was found in the heavy fraction separated through flotation and coming from the deposit Locus:261433:005, excavated during the 2023 campaign. On this deposit, see Kreppner/Rohde/Squitieri 2024, 122-123.

E1.2.1.1.4 Coral beads

During the 2023 and 2024 excavations, four beads likely made of coral were recovered from topsoil and from the floor deposit of Room 1 of Building A (NT1 2023 Phase 5). Coral beads and pendants were occasionally found during earlier excavations in Assur,[230] but coral appears to have been rarely used in Mesopotamia before the Hellenistic period.[231]

2024 campaign		
No.	**AS number/context**	**Description**
336	AS 261433:029:009 Topsoil	Cylindrical bead, possibly coral. L. 0.6 cm; D. 0.4 cm. (**Fig. E1.2.17**)
337	AS 261433:040:015 NT1 2023 Phase 5 / Building A Room 1/ Floor deposit	Cylindrical bead, possibly coral, light red/orange colour. L. 0.4 cm; D. 0.3 cm. (**Fig. E1.2.18**)
2023 campaign		
ExA1: 15 (two beads).		

Fig. E1.2.17: Cylindrical bead **336**, probably made of coral. Photo by Helen Gries.

Fig. E1.2.18: Cylindrical bead **337**, probably made of coral. Photo by Helen Gries.

E1.2.1.1.5 Worked shells

Four worked shells discovered during the 2024 campaign feature perforations, suggesting they may have been used as beads or pendants.

2024 campaign		
No.	**AS number/context**	**Description**
338	AS 000001:001:030 Site surface	Shell with perforation, possibly a bead. L. 3.4 cm; D. 0.8 cm; perforation D. 0.1 cm.
339	AS 261433:036:004 NT1 2024 Phase 8b / Pit 4 / Fill	Bead from a Conus advertex shell, white with brownish dots. H. 0.9 cm; D. max. 0.6 cm; perforation D. 0.2 cm.
2024 campaign		
No.	**AS number/context**	**Description**
340	AS 261433:058:025 NT1 2023 Phase 5 / Building A Courtyard 10 / Upper fill	Snail shell with a perforation on the top. It is unclear whether it is a bead. L. 2.5 cm.
341	AS 261433:085:005 NT1 2023 Phase 4 / Building B Room 11 / Upper fill	Shell with drilled perforation, probably a bead. L. 1.5 cm; D. 0.6 cm; perforation D. ca. 0.1 cm. (**Fig. E1.2.19**)
2023 campaign		
ExA1: 14, 156, 158, 199, 253.		

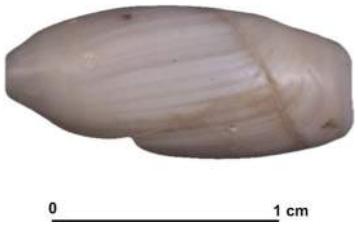

Fig. E1.2.19: Shell **340** with a drilled perforation, possibly used as a bead. Photo by Helen Gries.

E1.2.1.2 Fibulae

Two fibulae were recovered during the 2023 campaign: one from inside the Parthian chamber tomb's (Grave 1) walls (ExA1: **29**) and the other from the fill of Grave 5, dated to the Iron Age[232] (ExA1: **236**). Two additional bronze fibulae, **342** and **343**, were unearthed during the 2024 excavation. Both were found in the post-occupation fills of Building A (NT1 2023 Phase 5). The fibula **342** belongs to type D1.1 in Pedde's classification and likely dates to the 7th/6th century BC (**Fig. E1.2.20**). Comparable examples have been documented in earlier excavations at Assur and from other Assyrian centres (Sheikh Hamad, Khorsabad, and Nimrud), as well as sites like Godin Tepe, Susa, and Amlash.[233] Based on its dating and location in the upper fill of Courtyard 10, the fibula is likely unrelated to the use of Building A (**§C2.8.6**).

The exceptionally large fibula **343** (**Fig. E1.2.21a**, **E1.2.21b**), measuring 10.0 cm in length, was recovered from the upper fill of Room 2 in Building A (**§C2.8.2**). It corresponds to Pedde's type C.3.3, typically dated to the 6th-4th centuries BC, and thus the Achaemenid period.

230 See e.g., Gries 2017, 231, nos. 1522, 1523.

231 Tosi 1980-83, 212.

232 Radner/Squitieri 2024b, Table D1.1.

233 Pedde 2000, 251-253, nos. 770-778, pl. 57.

Fibulae of this type are often sizable and primarily known from the southern Levant and Deve Hüyük but have not previously been documented in Assur.[234] Given its dating, a connection to the building's use cannot be ruled out, even though the fibula was found in the post-occupation phase of Building A.

2024 campaign		
No.	**AS number/context**	**Description**
342	AS 261433:058:012 NT1 2023 Phase 5 / Building A Courtyard 10 / Upper fill	Only the bow is preserved in this triangular fibula, while the pin is missing. The pin was attached to a terminal segment, which is not preserved. On the other side, the pin was accommodated into a folded end. The bow top is bent but not pointed. Decorative elements adorn both sides of the bow, with a central bead flanked by discs on either side. The fibula bow was originally cast straight and bent over a thin, round top to assume the final bow shape. L. 5.0 cm. (**Fig. E1.2.20**)
343	AS 261432:007:008[235] NT1 2023 Phase 5 / Building A Room 2 / Upper fill	Large triangular fibula with triple beading and two discs between the beads. The arm with the pin holder consists of two discs, one bead, two discs, one bead, two discs, one bead and another bead (from the centre to the top). The arm with the pin attachment consists of two discs, one bead, two discs, one bead, two discs and one bead. The pin is not preserved, but the attachment suggests it was made of iron. L. 10.0 cm; H. 7.1 cm; D. max. 1.3 cm; Wt. 58.0 g. (**Fig. E1.2.21a**, **E1.2.21b**)
2023 campaign		
ExA1: 29, 236.		

Fig. E1.2.20: Fibula **342**.
Photo by Helen Gries.

234 Pedde 2000, 214-216, nos. 542-550, pl. 40; there is also a certain similarity to Pedde's D3.1 type, which, however, usually only has double discs in the middle and the beads are significantly thicker than the discs.

235 This fibula was found at the end of the 2024 campaign while cleaning the southern portion of the upper fill of Room 2. On this upper fill, see Kreppner/Rohde/Squitieri 2024, 126.

Fig. E1.2.21a: Fibula **343** (side 1).
Photo by Helen Gries.

Fig. E1.2.21b: Fibula **343** (side 2).
Photo by Helen Gries.

E1.2.1.3 Earrings, rings, bracelets

Earrings, rings, and bracelets were predominantly made of bronze, with iron being a less common material, and one example was found made of bone. In the fills of Building A, five metal rings were discovered: four made of bronze and one of iron. The iron ring (**344**) (**Fig. E1.2.22**) features a circular, flat, thickened part with a diameter of 2 cm that may have served as a sealing plate, though its heavy corrosion makes this uncertain. The bone ring (**348**) was found in the fill of the installation A10-I1 in Courtyard 10 of Building A.

In the NT2 trench, a simple iron anklet with touching ends (**351**) still encircled the ankle of a child's skeleton in Grave 10 (see **Figs. C4.5** and **E1.2.23**).

2024 campaign		
No.	**AS number/context**	**Description**
344	AS 261433:037:004 NT1 2023 Phase 5 / Building A Room 1 / Fill	Fragment of an iron ring with a circular flat and thicker part, probably a sealing plate with a D. of 2 cm. L. 2.4 cm; W. 2.1 cm; Th. 2 cm. (**Fig. E1.2.22**)
345	AS 261433:037:005 NT1 2023 Phase 5 / Building A Room 1 / Fill	Bronze open ring. D. 1 cm.
346	AS 261433:037:008 NT1 2023 Phase 5 / Building A Room 1 / Fill	Bronze ring with overlapping ends. D 1.5 cm.

2024 campaign		
No.	**AS number/context**	**Description**
347	AS 262433:107:020 NT1 2023 Phase 5 / Building A Room 8 / Floor deposit	Bronze crescent-shaped (ear-) ring, about 0.5 cm thick and 1.3 cm long. Made of bronze.
348	AS 261433:062:002 NT1 2023 Phase 5 / Building A Courtyard 10 / Installation A10-I1	Broken ring with a squarish section made of bone. It has a shallow groove on the surface. D. 2.0 cm.
349	AS 262433:139:003 NT1 2023 Phase 5 / Building A Room 5 / Fill	Bronze (ear-)ring. D. 1.0 cm.
350	AS 254433:019:005 NT2 2024 Phase 2 / Fill	Thin (0.3 cm) bronze bracelet covered by patina. D. 4.5 cm but bent. No sign of decoration.
351	AS 254433:029:002 NT2 2024 Phase 3 / Grave 10 skeleton	Iron anklet with touching ends. Oval section. D 0.5 cm. (**Fig. E1.2.23**)
2023 campaign		
ExA1: 18, 33, 89, 90, 96, 126, 225.		

Fig. E1.2.22: Iron ring **344** with a possible sealing plate. Photo by Andrea Squitieri.

Fig. E1.2.23: Bronze anklet **351** from Grave 10. Photo by Andrea Squitieri.

E1.3 Figurative terracotta objects

E1.3.1 Terracotta figurines

The terracotta figurines unearthed during the 2023 and 2024 campaigns date from the Neo-Assyrian to the Parthian period. They find parallels in the broader repertoire from the same time frame documented in earlier excavations at Assur.[236] The finds include fragments of human figures (**§E1.3.1.1**), horseman figures (**§E1.3.1.2**), animal figures with and without wheels (**§E1.3.1.3**/**§E1.3.1.4**), a bird-shaped vessel or flute (**§E1.3.1.5**), and terracotta wheels (**§E1.3.1.6**). All the figurines are handmade, with notable variations in clay composition between the different types.

E1.3.1.1 Human figures

Two fragments of male figurines (**352**, **353**) can be identified as belonging to the 'man in a bell skirt' type (German: *Mann im Glockenrock*), characterised by a cylindrically shaped hollow body. Similar figurines were frequently uncovered during earlier excavations in Assur.[237] However, relatively few examples have been found in stratified contexts until now, so the type can only be broadly dated to the Neo-Assyrian period (10th-7th century BC). This dating is further supported by the contexts of the two pieces discussed here. **352** was recovered from a fill in trench NT2 (NT2 2024 Phase 2) containing mixed Parthian, Hellenistic, and Iron Age pottery (**§D1.2**). In contrast, **353** came from Building B Room 11 (NT1 2023 Phase 4), where a seed was radiocarbon dated to 778-551 calBC (**§C2.9**).

Additionally, two male heads (**354**, **355**) may belong to this figurine type or to handmade horseman figures dating to the 10th-7th century BC (**§E1.3.1.2**). Applied headbands and hair rolls are common features of both types.[238] A similar head was previously discovered during the 2023 campaign (ExA1: **186**).

236 Klengel-Brandt 1978; Miglus 2016, 61-62, pls. 81-84; Klengel-Brandt/Onasch 2020; for additions and critical comments on this publication, see Katzy 2024; Roßberger 2024.

237 Klengel-Brandt 1978, 55-59; Miglus 2016, 61, pl. 82b-d; Klengel-Brandt/Onasch 2020, nos. 495-591. Examples of a similar hand position as in **352** can be found there under nos. 538-542, 544.

238 For this type of head, see Klengel-Brandt/Onasch 2020, nos. 676-825.

2024 campaign		
No.	**AS number/ context**	**Description**
352	AS 254433:021:008 NT2 2024 Phase 2 / Fill	Fragment of a handmade hollow human male figurine, preserving only the upper body. The head, left hand, and lower body below the waist are broken off. The left arm is bent upward, while the right arm extends downward in front of the body. Elongated, slightly diagonal incisions on the back may represent clothing. The surface is smooth, and the figurine is made of reddish-brown clay with an organic temper. L. 4.1 cm; W. 5.9 cm; H. 5.5 cm. (**Fig. E1.3.1a–b**)

Fig. E1.3.1a–b: Torso of the male terracotta figurine **352**, front side and reverse. Photos by Helen Gries.

Fig. E1.3.2a–b: Torso of the male terracotta figurine **353**, front side and reverse. Photos by Helen Gries.

Fig. E1.3.3: Head fragment **354** of a male terracotta figurine. Photo by Helen Gries.

Fig. E1.3.4: Head fragment **355** of a male terracotta figurine. Photo by Helen Gries.

2024 campaign		
No.	**AS number/ context**	**Description**
353	AS 261433:079:015 NT1 2023 Phase 4 / Building B Room 11 / Fill	Fragment of a handmade hollow human male figurine, preserving only the right half of the upper body. The right arm is extended downward, resting against the body. Elongated incisions on the back run slightly diagonally outward, possibly representing clothing. The surface is smoothed, and the yellowish clay is organically tempered with chaff. W. 2.9 cm; L. 3.1 cm; H 5.3 cm. (**Fig. E1.3.2a–b**)
354	AS 262433:102:003 NT1 2023 Phase 5 / Building A Room 8 / Fill	Head fragment of a handmade human male figurine, preserving only the head and parts of the neck. The face is modelled, with the eye sockets pressed in using fingers and the nose and chin pulled slightly out of the clay. The mouth is not indicated. The eyes, headband, earflaps, and hair roll have been added separately. The headband and hair roll feature vertical incisions. The earflaps suggest the figure may have worn a helmet. The surface is smoothed, and the reddish clay contains very little organic temper. W. 3.0 cm; L. 2.9 cm; H. 3.60 cm. (**Fig. E1.3.3**)
355	AS 254433:019:009 NT2 2024 Phase 2 / Fill	Head fragment of a handmade human male figurine, preserving only the head and neck. The face is modelled, with the eye sockets pressed in using fingers and the nose and chin pulled slightly out of the clay. The mouth is not indicated, and the chin area is damaged. The eyes, headband, and hair roll have been applied separately. The surface is smoothed, and the yellowish clay contains an organic temper. L. 3.0 cm; W. <3.0 cm; H. 4.2 cm. (**Fig. E1.3.4**)
2023 campaign		
ExA1: 186 (head fragment of a terracotta male figurine).		

E1.3.1.2 Horseman figures

Alongside human figures from the Neo-Assyrian to the Parthian periods, handmade horseman figurines represent the largest group of terracotta figurines in Assur.[239] The rider and horse were typically crafted separately and only assembled before firing. Handmade horseman figurines were widely produced in northern Mesopotamia between the first half of the 10th to the 7th century BC, and have been discovered at numerous sites.[240] Several distinct handmade riders can be identified within the terracotta corpus from Assur dating to the 1st millennium BC (for wheeled horses and riders, see §**E1.3.1.3**). These types often overlap chronologically.

Six rider and horse fragments likely belong to Neo-Assyrian horseman figurines. The fragment of a horse's body, **356**, belongs to the group of glazed figurines, a relatively small subset within the corpus of Neo-Assyrian horseman figurines from Assur.[241] These glazed figures are minimally detailed and feature a monochrome white-yellowish glaze, which is often heavily corroded today. The fragment was discovered in the drainage shaft in trench NT2 (NT2 2024 Phase 2) alongside Parthian, Hellenistic, and Iron Age pottery (**§D1.2**).

In addition to the previously published torso of a horseman (ExA1: **194**), two more fragments of this type were discovered in 2024. Due to their poor state of preservation, the precise identification of these fragments is not possible. However, the compact posture of **357**, with arms bent close to the body, is a common feature of horseman figurines from Assur, allowing for a general attribution to this group. Similarly, the arm position and hairstyle of **359** suggest that it could also represent a Neo-Assyrian horseman figure.[242] Both were found in the topsoil, providing no additional clues for their dating. With its applied bridle, the fragment of a horse's snout (**358**) likely belongs to a horseman figurine from this group, similar to ExA1: **280**.

An almost wholly preserved figurine (**360**) of an elaborately crafted horseman was recovered from the floor deposits of the Parthian-period chamber tomb (Grave 1).[243] Notably, no remains of the horse that presumably accompanied the rider were found in the tomb. Comparable horseman figurines, often found separated from their accompanying horses, are already known from earlier excavations in Assur.[244] These horsemen are typically dated to the Parthian period based on features such as dress, hairstyles, and stratified contexts of some figurines. This new find now supports this dating. Additionally, at least one other horseman terracotta figurine (rider not preserved) has been documented from a Parthian chamber tomb complex in Assur.[245]

2024 campaign		
No.	**AS number/ context**	**Description**
356	AS 254433:028:005 NT2 2024 Phase 2 / Pebble surface	Fragment of a handmade horseman figure, preserving only the horse's body and the rider's base, which merges directly into the horse's neck. The horse's head and legs are broken off, while the tail is indicated on the body as a clay coil. The terracotta core is made of reddish clay, overlaid with a 0.3-0.4 cm thick layer of fine whitish clay with no visible temper. The surface is coated with a white-yellow glaze that contains small bubbles. This glaze is heavily corroded and only partially preserved. W. 2.9 cm; L. 5.8 cm; H. 4.2 cm. (**Fig. E1.3.5**)
357	AS 261433:029:008 Topsoil	Fragment of a rider from a handmade horseman figurine. The horse, as well as the rider's head and lower body, is missing. The rider was separately modelled, and the impression on the underside of the figure indicates that the upper body was originally attached directly to the horse. The rider holds his arms close to his body, with his hands resting on his legs. A diagonal incised line on the back may represent clothing. The surface is heavily abraded. The figurine is made of greyish-yellowish clay, partially reddish, with an abundant organic temper (chaff). W. 3.7 cm; L. 2.6 cm; H. 5.0 cm. (**Fig. E1.3.6**)

239 Klengel-Brandt 1978, nos. 313-332 (Neo-Assyrian), 466-486 (Parthian), 522-579 (various horses); Miglus 2016, 61, pl. 82a; Klengel-Brandt/Onasch 2020, nos. 592-675 (Neo-Assyrian), 910-944 (Parthian), 996-1256 (various horses); only the Hellenistic rider no. 1096 is made in a double mold.

240 For the Syrian horses and riders, see Pruß 2010, 233-245; Bolognani 2017, 177-225.

241 Klengel-Brandt/Onasch 2020, nos. 636-642, 1038-1071.

242 For possible comparisons, see Klengel-Brandt/Onasch 2020, nos. 592-635.

243 Kreppner/Rohde/Squitieri 2024, 116-118.

244 Klengel-Brandt/Onasch 2020, nos. 910-944, 1072-1096.

245 Klengel-Brandt 1978, 91, no. 596, pl. 18; Klengel-Brandt/Onasch 2020, no. 1086. For the find context in the chamber tomb, see Andrae/Lenzen 1933, 98, pl. 49n; Miglus 1996, 312-313, Plan 72, 146.

2024 campaign		
No.	**AS number/ context**	**Description**
358	AS 254433:016:005 NT2 2024 Phase 3 / Fill	Fragment of the head of a handmade horse figurine, preserving only the snout. A straight incision indicates the mouth, and round punctures represent the two nostrils. Remnants of elongated clay applications on both sides likely depict the horse's bridle, suggesting that it is probably a horseman figure. The surface is only slightly smoothed. The figurine is made of beige-yellowish clay with an organic temper. W. 2.3 cm; L. 3.4 cm; H. 1.9 cm. (**Fig. E1.3.7**)
359	AS 261433:029:005 Topsoil	Fragment of the upper body of a handmade human male figure, probably a horseman. The head, left arm, front, and lower body are broken off, leaving only the back and the right arm up to the elbow. The right arm is bent against the body. On the back, the end of a hair roll is preserved. The surface is smoothed, and the figurine is made of reddish clay with no visible temper. L. 4.2 cm; W. 2.1 cm; H. 4.2 cm. (**Fig. E1.3.8a–b**)
360	AS 262432:022:077 Chamber tomb (Grave 1) / Subdivision 4 / Floor deposit	Rider of a handmade horseman figure. The rider is fully preserved except for minor damage to the head and the left side. The face is modelled, with an impressed semicircular mouth and applied clay lenses featuring circular impressions to represent the eyes. The rider wears a round headdress with a broad, turned-up rim decorated with impressed semicircles. Similar impressions are found on the arms, upper body, and a clay coil applied to the neck, which likely represents a necklace or collar. The lower body, including the base of the legs, was modelled separately, with the impression on the underside indicating that the upper body was originally attached directly to the horse. The rider holds his arms, adorned with bracelets, close to his body, with his hands positioned in front of his abdomen. The surface is carefully smoothed, with numerous visible fingerprints. The figurine is made of fine reddish clay without visible inclusions. W. 4.9 cm; L. 2.8 cm; H. 8.7 cm. (**Fig. E1.3.9a–c**)
2023 campaign		
ExA1: 194 (torso of a rider), 280 (head of a horse).		

Fig. E1.3.5: Fragment **356** of a glazed terracotta horseman figurine. Photo by Helen Gries.

Fig. E1.3.6: Rider fragment **357** of a terracotta horseman figurine. Photo by Helen Gries.

Fig. E1.3.7: Horse head fragment **358** of terracotta horseman figurine. Photo by Helen Gries.

Fig. E1.3.8a–b: Fig. E1.3.8a–b: Upper body fragment **359** of a male terracotta rider figurine, front side and reverse. Photos by Helen Gries.

Fig. E1.3.9a–c: Rider **360** of a terracotta horseman figurine, front side, reverse and lateral side. Photos by Helen Gries.

E1.3.1.3 Wheeled animal figures

Six figurine fragments from the 2024 campaign have been identified as parts of wheeled animal figurines. Similar figurines were discovered in large numbers during earlier excavations in Assur. While horse figurines, both with and without riders, are common, cattle figurines, particularly those representing humped cattle, are attested but much rarer. These figurines are dated to the first half of the 1st millennium BC.[246] Five of the six fragments from the 2024 campaign were found alongside pottery dating from the Iron Age to the Parthian period in trench NT2 (NT2 2024 Phase 2 and 3, see **§D1.2**). The figures are made from coarse clay mixed with a significant amount of chaff, and their bodies are minimally detailed. The front and hind legs are formed as single strands, drilled horizontally to attach the wheels. The bodies have a rounded cross-section with minimal modelling. The tail is typically represented by a simple, often irregular clay coil attached to the hind legs. Features such as the shaping of the animal's head, the horse's bridle, or remnants of a rider on the horse's back and neck help distinguish between the various types: horse, rider, or cattle. However, when only the animal's body or legs are preserved, identifying the specific type becomes uncertain.

Of the six figurines discussed here, two (**362**, **364**) can be identified as horsemen. The remaining fragments are too incomplete to determine the type of animal with certainty.

2024 campaign		
No.	**AS number/context**	**Description**
361	AS 254433:016:006 NT2 2024 Phase 3 / Fill	Fragment of the hind legs of a handmade animal figurine with wheels. The two hind legs are joined and undifferentiated, featuring a drilled perforation (D. 0.9 cm) for attaching the wheels. The lower section of the left leg is damaged. A clay coil represents the tail. The surface is only slightly smoothed. The figurine is made of yellow-greenish clay with a reddish core, containing abundant organic temper (chaff). W. 4.2 cm; L. 5.0 cm; H. 6.1 cm. (**Fig. E1.3.10**)
2024 campaign		
No.	**AS number/context**	**Description**
362	AS 254433:021:013 NT2 2024 Phase 2 / Fill	Fragment of a handmade horseman figurine with wheels, preserving parts of the horse's head, neck, and chest. From the horse's head, the right eye and portions of a browband with parallel incisions are intact, while the muzzle and ears are broken off. The harness is indicated by flat, irregular clay coils on the horse's neck. The damage on the neck was likely caused by the hand of the originally attached rider. The surface is only slightly smoothed. The figurine is made of yellow-greenish clay with a significant amount of organic temper (chaff). W. 3.7 cm; L. 4.9 cm; H. 10.5 cm. (**Fig. E1.3.11a–b**)
363	AS 254433:025:008 NT2 2024 Phase 2 / Fill	Fragment of the hindquarters of a handmade animal figurine with wheels. The rounded body is broken at an angle, leaving the front legs, neck, head, and any traces of a rider unpreserved. The two hind legs are joined and undifferentiated, featuring a drilled perforation (D. 0.6-0.9 cm) for attaching the wheels. A flat, irregular clay coil represents the tail. The surface is only slightly smoothed. The figurine is made of yellow-greenish clay with a reddish core and contains a significant amount of organic temper (chaff). W. 5.4 cm; L. 8.4 cm; H. 7.7 cm. (**Fig. E1.3.12**)

Fig. E1.3.10: Hind leg fragment **361** of a wheeled terracotta animal figurine. Photo by Helen Gries.

246 Klengel-Brandt 1978, nos. 523-528 (horses), 590-594 (cattle); Miglus 1996, 61-63, pls. 42a, 83; Klengel-Brandt/H.-U. Onasch 2020, nos. 996-1037 (horseman), 1109-1151 (animals), 1263-1271 (cattle).

2024 campaign		
No.	**AS number/context**	**Description**
364	AS 254433:027:003 NT2 2024 Phase 2 / Fill	Parts of the horse's neck, chest, and body from a handmade horseman figurine with wheels. The head, legs, and the lower and rear portions of the horse's body are missing. Remnants of the harness, made of flat, irregular clay coils, are preserved on the horse's neck, with one end hanging down on the right side. The imprint of the rider's left leg is faintly visible. The surface is only slightly smoothed. The figurine is made of yellow-greenish clay with a reddish core and contains a significant amount of organic temper (chaff). W. 4.0 cm; L. 7.1 cm; H. 9.2 cm. (**Fig. E1.3.13**)
365	AS 254433:033:004 NT2 2024 Phase 2 / Fill	Fragment of the hindquarters of a handmade animal figurine with wheels. The rounded body is broken at an angle, leaving the front legs, neck, and head, as well as any traces of a rider, unpreserved. The left side of the back is also damaged. The two hind legs are joined and undifferentiated, with the lower parts broken off at the drilled perforation for attaching the wheels. The tail is represented by a clay coil. The surface is only slightly smoothed. The yellow-reddish clay contains a significant amount of organic temper (chaff). W. 5.1 cm; L. 9.7 cm; H. 5.7 cm. (**Fig. E1.3.14**)

Fig. E1.3.11a–b: Fragment **362** of a wheeled terracotta horse figurine, front and lateral sides. Photos by Helen Gries.

2024 campaign		
No.	**AS number/context**	**Description**
366	AS 262433:152:002 Collapse of wall Locus: 262432:075 (Building B)	Fragment of the hindquarters of a handmade animal figurine with wheels. The rounded body is broken at an angle, leaving the front legs, neck, head, and any traces of a rider unpreserved. The two hind legs are joined and undifferentiated, with the lower parts broken off at the drilled perforation for attaching the wheels. The tail was originally indicated by a clay coil, of which only the impression remains. The surface is only slightly smoothed. The yellow-greenish clay contains a significant amount of organic temper (chaff). W. 4.8 cm; L. 8.8 cm; H. 5.2 cm. (**Fig. E1.3.15**)

Fig. E1.3.12: Hindquarter fragment **363** of a wheeled terracotta animal figurine. Photo by Helen Gries.

Fig. E1.3.13: Fragment **364** of a wheeled terracotta horseman figurine. Photo by Helen Gries.

Fig. E1.3.14: Hindquarter fragment **365** of a wheeled terracotta animal figurine. Photo by Helen Gries.

Fig. E1.3.15: Hindquarter fragment **366** of a wheeled terracotta animal figurine. Photo by Helen Gries.

2024 campaign		
No.	**AS number/context**	**Description**
368	AS 262433:090:006 Grave 9 / Fill	Fragment of the hind legs of a handmade animal figurine. The left leg is intact, while the right leg is broken off beneath the body. The figurine is irregularly modelled, with a minimally smoothed surface. It is made of fine reddish clay with a small amount of organic temper (chaff). L.3.5 cm; W. 3.0 cm; H. 5.2 cm. (**Fig. E1.3.17**)

Fig. E1.3.16: Fragment **367** of an terracotta animal figurine. Photo by Helen Gries.

Fig. E1.3.17: Hind leg fragment **368** of a terracotta animal figurine. Photo by Helen Gries.

E1.3.1.4 Animal figures

Two handmade terracotta fragments belong to animal figurines. Due to their poor state of preservation, it is no longer possible to identify the animals they represent. The fragment **368** was found in the grave fill of the looted Grave 9 (**§C2.5.2**). Since the terracotta figurine originates from the surrounding fill rather than the grave itself, the possibility of an earlier date cannot be excluded.

2024 campaign		
No.	**AS number/context**	**Description**
367	AS 000001:001:026 Site surface	Fragment of the body of a handmade animal figurine, with the legs and neck broken off. The short, bent tail, shaped by pulling the clay, suggests it may represent a dog. The figurine is irregularly modelled, with a minimally smoothed surface. It is made of yellowish clay containing mineral temper. W. 3.3 cm; L. 4.4 cm; H. 2.3 cm. (**Fig. E1.3.16**)

E1.3.1.5 Bird vessel / flute

Fragment **369** depicts a bird's head with a round beak and a circular perforation. The body's base indicates that it was part of a hollow figure. Similar bird-shaped vessels, with openings on the back and through the beak, are known from various periods in Mesopotamia and were also discovered during earlier excavations at Assur.[247]

Such vessels, due to their dual openings, are interpreted as either libation vessels or musical instruments, such as flutes or pipes.[248] The bird fragment discussed here was found in Room 8 of Building A, dated to approximately the 4th to 2nd century BC (**§C2.8**), though the fragment itself is likely older than its findspot.[249] It features a perforation through the beak that does not connect to the interior, indicating it may have been a misproduction.

247 Klengel-Brandt 1978, 107, nos. 715-719, pl. 22; Miglus 2015, 62, pls. 46a, 84a; Klengel-Brandt/Onasch 2020, 204-2028, nos. 1512-1527, pls. 264-268; for comparisons from other sites see Wrede 2003, 62-64.

248 Klengel-Brandt 1978, 107 suggests that they are libation vessels; for an interpretation as a flute see Rittig 2010, 85-87, pls. 86-87; on vessel flutes in Mesopotamia in general, see Rashid 1984, 46.

249 However, the dating proposed by Klengel-Brandt 1978, 107 for this type in the Ur III/Isin-Larsa period seems too early.

2024 campaign		
No.	**AS number/context**	**Description**
369	AS 262433:107:012 NT1 2023 Phase 5 / Building A Room 8 / Floor deposit	Fragment of a bird's head belonging to a bird vessel or a bird-shaped vessel flute. The round eyes are applied in the form of clay lenses, of which only one is preserved (the imprint of the other can still be recognised). The round beak has a round hole. There is also an impression of a drill hole on the inside, but it does not appear to have been drilled through as a spout. Elongated parallel incisions have been preserved on the neck, which probably represent the plumage. The clay is tempered, and the surface is smoothed with partial damage. L. 3.9 cm; W. 3.1 cm; H. 4.5 cm. (**Fig. E1.3.18**)

Fig. E1.3.18: Bird's head fragment **369** of a bird vessel or a bird-shaped vessel flute. Photo by Helen Gries.

E1.3.1.6 Terracotta wheels

During the 2023 and 2024 campaigns, three flat, round ceramic objects with central perforations were discovered, likely terracotta wheels. Unlike spindle whorls, these wheels are thinner at the edges than at the centre, with some featuring a pronounced thickening in the middle, possibly representing a wheel hub. However, due to their poor state of preservation and the limited number of such finds, distinguishing terracotta wheels from spindle whorls remains challenging at this stage (**§E1.5.3**).

The two wheels found in 2024 originate from the drainage shaft in trench NT2 (**§C4**). Item **370** was recovered from stratigraphic phase NT2 2024 Phase 2, which contains pottery ranging from the Iron Age to the Parthian period. In contrast, **371** was found in the oldest phase of the structure (NT2 2024 Phase 1), characterised by Middle Assyrian and Neo-Assyrian pottery. The wheel ExA1: **288** lacks stratification, as it was uncovered during cleaning of the 2002 SBAH trench.

The three terracotta wheels show significant differences in material composition, clay colour, and size, with diameters ranging from 5.0 to 11.6 cm. Wheel **371**, in particular, stands out. Measuring 11.6 cm in diameter,[250] it exhibits clear signs of use on its surface, along with traces of black material, likely bitumen, that extend over some of the damage. This material suggests it may not have served as the wheel of a terracotta chariot or figure but rather functioned as a tool, such as a spool or a similar implement.

2024 campaign		
No.	**AS number/context**	**Description**
370	AS 254433:028:004 NT2 2024 Phase 2 / Pebble surface	Fragment of a terracotta wheel that is thicker at the centre. The surface is barely smoothed. The relatively coarse clay is yellowish on the surface and reddish on the inside and contains an organic temper (chaff). D. 5.5 cm; Th. max. 2.8 cm; D. of the perforation 0.8-1.0 cm. (**Fig. E1.3.19**)
371	AS 254433:041:008 NT2 2024 Phase 1 / Fill	Terracotta wheel with battered edges. The centre around the perforation is thicker. The area is damaged on both sides. There are traces of black colour (bitumen?) on the surface extending beyond the damage. The surface is barely smoothed. The relatively coarse clay is yellowish on the surface and light red on the inside and contains an organic temper (chaff). D. 11.6 cm; Th. 1.4 (edges) to 4.5 cm (centre); D. of the perforation 1.0 cm. (**Fig. E1.3.20**)
2023 campaign		
ExA1: 288 (Terracotta wheel with damage to the edges. Thicker in the centre around the perforation. D. 5.0 cm; max. Th. 2.0 cm.)		

Fig. E1.3.19: Fragment **370** of a terracotta wheel. Photo by Helen Gries.

250 The majority of terracotta wheels uncovered during the Andrae excavations have diameters ranging from 5-7 cm, with only six wheels exceeding 10 cm in diameter, see Klengel-Brandt/Onasch 2020, 243, nos. 1820-1825.

Fig. E1.3.20: Terracotta wheel **371**. Photo by Helen Gries.

E1.3.2 Architectural elements / "Assyrian clay hands"

Two heavily corroded clay objects from the 2024 campaign have been identified as "Assyrian clay hands," also referred to as "hands of Ishtar".[251] Unlike figurines, these architectural elements likely served as corbels. Similar clay hands are well-documented from Assyrian centres such as Assur, Nimrud, Nineveh, and Khorsabad, as well as from sites in present-day Syria and Turkey, and are generally dated to the 9th and 8th centuries BC.[252] Some examples feature a blue-green glaze or bitumen coating, and approximately one-third bear inscriptions of Shalmaneser III or Ashurnasirpal II, linking them to palaces or temples.[253] The two fragments from the 2024 campaign lack preserved surfaces and show no evidence of inscriptions or glazes. They are made of relatively coarse clay with a high content of chaff.

"Assyrian clay hands" are typically associated with official buildings such as temples and palaces. In Assur, examples have been found on the city wall and gates, the Nabu temple, the Ziggurat, and in the palaces.[254] Notably, clay hands discovered in a collapsed wall of the Old Palace were still in situ, demonstrating that they were originally attached to the brickwork.[255]

The two clay hand fragments from the 2024 campaign were not found in their primary contexts. Item **372** was recovered from the fill of "Room 5" in Building A and is likely much older than its findspot (**§C2.8.7**). The second fragment (**373**) was discovered in the drainage shaft (NT2 2024 Phases 2), alongside pottery from the Parthian, Hellenistic, and Iron Age periods, as well as various other small finds (**§C4.3**). The damaged or misproduced object appears to have been discarded in the drainage shaft.

2024 campaign		
No.	**AS number/context**	**Description**
372	AS 263433:016:007 NT1 2023 Phase 5 / Building A "Room 5" / Fill	Heavily eroded fragment of an "Assyrian clay hand". The middle three fingers are still preserved. The back, underside, and both sides are broken off. The relatively coarse green-yellowish clay contains an organic temper (abundant chaff). L. 7.4 cm; W. 6.7 cm; H. 8.3 cm. (**Fig. E1.3.21**)
373	AS 254433:025:009 NT2 2024 Phase 2 / Fill	Heavily eroded fragment of an "Assyrian clay hand". The middle three fingers are still recognisable, and the two lateral ones are battered, as is the top. The back is broken off. The relatively coarse, yellowish and reddish clay contains an organic temper (abundant chaff). L. 8.3 cm; W. 11.0 cm; H. 5.9 cm. (**Fig. E1.3.22**)

Fig. E1.3.21: Fragment **372** of an "Assyrian clay hand". Photo by Helen Gries.

251 The popular name 'Hand of Ishtar' should be avoided, as there is no evidence of a connection to the goddess Ishtar; see Moorey 1985, 180; Frame 1991, 357-359; Moorey 1994, 315.

252 Frame 1991; Guralnick 2008; Soldi 2017, 11, fig. 4.

253 Frame 1991, 343-355.

254 Andrae 1913, 7, 36, 43 fig. 5, pl. LXXIX, CII; Preusser 1955: 21, pl. 17; Pedde/Lundström 2008, 45, figs. 54, 55; Miglus 2016, 60-61, pls. 40, 41, 44, 80; only in one case were clay hands also found in a grave, see Haller 1954, 153-156.

255 Preusser 1955, 21, pl. 14; Pedde/Lundström 2008, 45, figs. 54, 55.

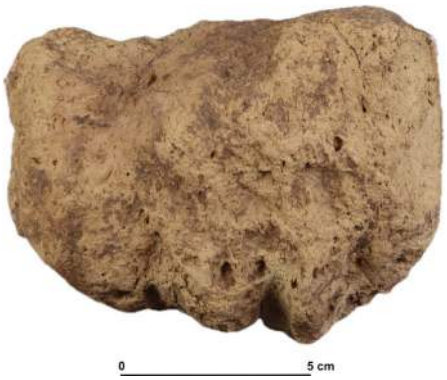

Fig. E1.3.22: Fragment **373** of an "Assyrian clay hand". Photo by Helen Gries.

E1.4 Glass and glassy objects

E1.4.1 Glass vessels

Only one glass vessel fragment (**374**) was recovered during the 2024 campaign. This body sherd, originating from a core-formed glass vessel dating to the Late Bronze Age, is too incomplete to determine the original shape of the vessel (**Fig. E1.4.1a**). Due to extensive corrosion, the original colours cannot be identified with certainty. However, it appears to feature yellow, white, and possibly green glass threads forming a feather pattern (**Fig. E1.4.1b**). This decorative motif is commonly found on Assur's core-formed glass bottles and bowls.[256] Similar glass vessels were previously discovered at the site, particularly in the Ištar temple of Tukulti-Ninurta I and less frequently in the graves of Middle Assyrian elites.[257]

During the 2023 campaign, 21 glass fragments, likely from glass vessels, were found. Most fragments are tiny and heavily corroded, limiting detailed evaluation. None appear to belong to Middle Assyrian core-formed vessels. Instead, most seem to be blown glass, a technique introduced in the late first century BC.[258] This aligns with the contexts in which they were found: the topsoil (ExA1: **8**), the Parthian chamber tomb (Grave 1) (ExA1: **31**, **32**, **35**, **36**, **39**, **40**, **46**, **51**, **54**, **76**, **77**, **78**, **79**), and the upper deposits of this tomb (ExA1: **110**, **129**). Two fragments from Grave 3 (ExA1: **137**, **144**), dated to the mid-2nd century BC, are too small to identify. Similarly, three fragments from Building B (NT1 2023 Phase 4) cannot be attributed to blown glass due to their thicker walls (ExA1: **179**, **220**, **229**).

2024 campaign		
No.	**AS number/context**	**Description**
374	AS 254433:025:010 NT2 2024 Phase 2 / Fill	Body sherd of a core-formed glass vessel. Made of different coloured glass threads and decorated with a feather pattern in yellow, white, and maybe green. The remains of the core are still visible on the inside. W. 4.1 cm; H. 3.1 cm; Th. 0.7 cm. (**Fig. E1.4.1a**, **E1.4.1b**)
2023 campaign		
ExA1: 8, 31, 32, 35, 36, 39, 40, 46, 51, 54, 76, 77, 78, 79, 110, 129, 137 (?), 144 (?), 179, 220, 229.		

Fig. E1.4.1a: Body sherd **374** of a core-formed glass vessel. Photo by Helen Gries.

Fig. E1.4.1b: Detail photo showing the different coloured glass threads of body sherd **374**, taken with a DinoLite microscope. Photo by Helen Gries.

E1.4.2 Frit and Egyptian Blue objects

Only a small number of frit or Egyptian Blue objects were recovered during the 2023 and 2024 campaigns. Apart from the few beads (see above, **§E1.2.1.1.3**), these include two fragments of Egyptian Blue and a rim fragment of a frit vessel. Due to their poor state of preservation, neither their function nor their dating could be determined further. The scarcity of objects in this material group may be attributed to the layers investigated during the first two campaigns, which primarily date to the Iron Age through the Parthian period. In contrast, frit and Egyptian Blue were predominantly used during the Late Bronze Age.[259] As stratigraphic phases of the Middle Assyrian period have been explored only to a limited extent so far, a more significant number of frit or Egyptian Blue finds might emerge on a larger scale in future excavations of this phase.

256 Gries/Schmidt 2020, 247-251, Tab. 1-3.

257 For vessel shapes, decorations and find spots of core-formed glass vessels from Assur, see Gries/Schmidt 2020 with further references.

258 Saldern 2004, 218-224; Freestone 2021, 246-247.

259 For the distribution of frit (faience) in the Middle Assyrian period, see Puljiz 2021 with further references.

2024 campaign		
No.	**AS number/context**	**Description**
375	AS 254433:041:003 NT2 2024 Phase 1 / Fill	Two fragments of Egyptian Blue. One is a thin disc, and the other looks more like an imprint on a tiny bit of soil; max. D. 1.5 cm. (**Fig. E1.4.2**)
376	AS 263433:017:004 NT1 2023 Phase 5 / Building A Room 5 / Floor deposit	Small rim fragment of a vessel made of whitish frit. Two circular indented lines on the outside. W. 1.7 cm; H. 3.0 cm; D. perhaps between 15-20 cm (cannot be determined with certainty). (**Fig. E1.4.3**)

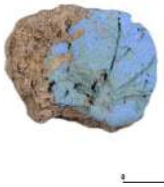

Fig. E1.4.2: Two fragments of Egyptian blue **375**. Photo by Helen Gries.

Fig. E1.4.3: Rim fragment **376** of a frit vessel. Photo by Helen Gries.

E1.4.3 Obsidian blade

A fragment of an obsidian blade (**377**) was discovered on the floor of Building A, Room 2. While obsidian items became increasingly rare after the Chalcolithic period, they did not vanish entirely.[260] Given that this is the only obsidian artefact recovered, and that no evidence of Neolithic or Chalcolithic occupation has been identified at Assur thus far, the presence of this item in Building A remains challenging to interpret.

2024 campaign		
No.	**AS number/context**	**Description**
377	AS 261433:046:015 NT1 2023 Phase 5 / Building A Room 2 / Floor deposit	Fragment of an obsidian blade, partially preserved. W. 0.8 cm; L. 2.0 cm. (**Fig. E1.4.4**)

Fig.E1.4.4: Fragment **377** of an obsidian blade. Photo by Helen Gries.

E1.5 Tools

E1.5.1 Metal tools

E1.5.1.1 Pins, needles and nails

Several thin and elongated metal fragments could potentially be identified as pins, needles, or nails. Unfortunately, due to varying levels of preservation, it is often challenging to precisely determine their original shape, leading us to group these fragments. Needles are typically thinner than nails and feature a hole at one end. We identified two fragments with holes, one from Building A (**381**) (**Fig. E1.5.1**) and another from Building B (**382**), which can be classified as needles. Additional thin shaft fragments from both buildings, with diameters of less than 1 cm, might also be parts of needles or pins. In contrast, nails tend to be thicker. Thick shaft fragments, approximately 3 cm in diameter, found in the NT2 trench are likely to be iron nails (**378**).

2024 campaign		
No.	**AS number/context**	**Description**
378	AS 254433:013:004 NT2 2024 Phase 3 / Fill	Fragments of iron nails with a thickness of c. 3 cm. The longest is 8 cm long. Highly corroded.
379	AS 262433:137:003 NT1 2023 Phase 5 / Building A Room 5 / Fill	Bronze nail. One end is rounded and slightly thicker than the opposite end, which is also rounded. L. 10 cm; D. 0.5 cm.
380	AS 262433:153:004 NT1 2023 Phase 4 / Building B Room 11 / Fill	Two fragments of a bronze nail with a flattish head with a diameter of 1.2 cm.

260 See e.g., Matney *et al.* 2011, 95.

2024 campaign		
No.	**AS number/context**	**Description**
381	AS 261433:058:006 NT1 2023 Phase 5 / Courtyard 10 Building A / fill	Fragment of a bronze needle with a pinhole. The point is broken off. L. 6.5 cm; D. 0.3 cm. (**Fig. E1.5.1**)
382	AS 261433:083:001 NT1 2023 Phase 4 / Building B Room 11 / from inside wall W10	Fragments of a bronze needle with a pinhole. Total L. 8 cm; D. 0.2 cm.
383	AS 261433:036:003 NT1 2024 Phase 8a / Pit 4 fill	Fragment of a bronze shaft. L. 2 cm.
384	AS 261433:048:002 NT1 2023 Phase 5 / Courtyard 10 Building A / fill	Small fragment of a bronze shaft with a braid decoration. L. 1.5 cm.
385	AS 261433:061:008 NT1 2023 Phase 7 / Pit 7 / Fill	Two fragments of a bronze shaft. Each fragment is about 2 cm long.
386	AS 261433:079:008 NT1 2023 Phase 4 / Building B Room 11 / Fill	Fragment of a bronze shaft. L. 3.1 cm; D. 0.3 cm.
387	AS 261433:079:011 NT1 2023 Phase 4 / Building B Room 11 / Fill	Fragment of a bronze shaft with a bent end or a hook (perhaps a nail). L. 2.6 cm; D. 0.6 cm.
388	AS 262433:102:006 NT1 2023 Phase 5 / Building A Room 8 / Fill	Fragment of a bronze shaft. L. 2.2 cm.
389	AS 262433:137:004 NT1 2023 Phase 5 / Building A Room 5 / Fill	A highly corroded fragment of an iron shaft. L. c. 4.5 cm.
2023 campaign		
ExA1: 4, 17, 49, 81, 83, 120, 175, 191, 195, 211, 232, 262, 273.		

Fig. E1.5.1: Fragment **381** of the bronze needle with pinhole. Photo by Andrea Squitieri.

E1.5.1.2 Weapons

One arrowhead and one spearhead were found in the upper fills of "Room 5" of Building A (**§C2.8.7**). The arrowhead (390), made of bronze, has a trilobate shape with a socket (**Figs. E1.5.2a**, **E1.5.2b**). It belongs to the so-called "Scythian" type,[261] which spread from around the 9th-8th centuries BC onwards across a wide area encompassing the Pontic-Caspian steppes, the Caucasus, Anatolia, northwest Iran and Mesopotamia.[262] Andrae reported some examples of this type of arrowhead from Assur in the area of the southern city wall ("*Südwall*"). Andrae associated them with the final conquest of Assur in 614 BC.[263]

In Neo-Assyrian times, the standard arrowhead was made of iron and had a leaf shape with a tang, but by the end of the 7th century BC, bronze socketed trilobate arrowheads reached Assyria and the wider Near East as a consequence, as it is often assumed, of the Scythian and Cimmerian invasions.[264] Such arrowheads continued to be attested long after the Neo-Assyrian period, only to be substituted by a new type of iron tripartite arrowhead, and with a tang, in the Roman-Parthian period.[265] Our example comes from the upper fill of "Room 5", a post-occupation fill which formed during the Hellenistic period after the primary use of Building A (**§C2.8.7**). Our arrowhead **390** may come from the Hellenistic occupation of Assur, though it cannot be ruled out that it is an heirloom from an earlier date.

The spearhead **391**, made of iron, is too corroded to reconstruct its shape in detail (**Fig. E1.5.3**). From what is preserved, it seems likely that it originally had a long, slender, leaf-shaped blade with a socket. Iron spearheads developed from their older bronze counterparts, and they spread in north Mesopotamia from the 8th century BC onwards.[266]

2024 campaign		
No.	**AS number/context**	**Description**
390	AS 262433:135:004 NT1 2023 Phase 5 / Building A "Room 5" / Fill	Socketed trilobate arrowhead made of bronze. L. 4.1 cm; W. max. 0.9 cm; D. base 0.7 cm; D. point 0.3 cm; Wt. 6 g. (**Figs. E1.5.2a**, **E1.5.2b**)

261 This type of arrowhead is thought to have originated in Central Asia in the Scythian area, hence the name, see Cleuziou 1977.

262 Hellmuth Kramberger 2016, 27-34, fig. 33 ("Typ Ib-reiternomadisch Variante a"); Muscarella 1988, 212-213; Cleuziou 1977.

263 Andrae 1977, fig. 185.

264 Curtis 2013, 39; Cleuziou 1977.

265 Hellmuth Kramberger 2016, 32-34; Curtis 2013, 42.

266 Curtis 2013, 38.

2024 campaign		
No.	**AS number/context**	**Description**
391	AS 262433:137:006 NT1 2023 Phase 5 / Building A "Room 5" / Fill	Highly corroded spearhead made of iron. L. 10 cm; max. Th. 3.5 cm. (**Fig. E1.5.3**)

Figs. E1.5.2a-b: Bronze trilobate arrowhead **390**. Photo by Andrea Squitieri.

Fig. E1.5.3: Iron spearhead **391**. Photo by Andrea Squitieri.

E1.5.1.3 Weights

Only two items have been recognised as possible weights. ExA1: **38** (**Fig. E1.5.4**) was found during the 2023 excavations in the Parthian period chamber tomb (Grave 1). It had a biconical shape, with no perforation, and was made of a dark mottled stone with a weight of 1.27 g. The second (**392**) was found in 2024 during the excavation of the floor deposit of Room 11 in Building B, dated to the Iron Age (**§C2.9.1**). It was made of lead and had a sub-spherical shape, weighing 20.43 g (**Fig. E1.5.5**).

2024 campaign		
No.	**AS number/context**	**Description**
392	AS 261433:080:003 NT1 2023 Phase 4 / Building B Room 11 / Floor deposit	Lead weight with a sub-spherical shape. D. 1.6 cm; Wt. 20.43 g. (**Fig. E1.5.5**)
2023 campaign		
ExA1: 38 (**Fig. E1.5.4**).		

Fig. E1.5.4: Bi-conical stone weight **38** (see Squitieri 2024, 163). Photo by Andrea Squitieri.

Fig. E1.5.5: Sub-spherical lead weight **392**. Photo by Andrea Squitieri.

F1.5.1.4 Miscellaneous metal fragments

Several metal fragments were collected, whose original shape and function were difficult to determine due to their poor state of preservation. They comprise small metal sheets, discs, tubes and wires from Buildings A and B, mostly made of bronze, while four were made of lead. A highly corroded bronze disc (**397**) from the fill of Room 2 in Building A might have been a coin (**Fig. E1.5.6**), but it was not possible to determine this for sure (for the Seleucid coin from Room 7 of the same building, see **§E2**).

2024 campaign		
No.	**AS number/context**	**Description**
393	AS 261433:040:008 NT1 2023 Phase 5 / Building A Room 1 / Floor deposit	Small circular bronze item with a dome shape and three tiny protrusions, possibly an applique. L. 0.8 cm; Th. 0.7 cm.
394	AS 261433:058:021 NT1 2023 Phase 5 / Building A Courtyard 10 / Fill	A small, rounded bronze item with a dome shape, possibly an applique. D. 1 cm; Th. 0.5 cm.
395	AS 261433:058:003 NT1 2023 Phase 5 / Building A Courtyard 10 / Fill	Flat bronze item (0.3 cm thin), rectangular shape with a narrower side and a blunt tip. Perhaps part of a decorative element.
396	AS 262433:094:003 NT1 2024 Phase 8a / Grave 9 / Fill of sarcophagus	A thin sheet of bronze, wrapped to make a hollow tube. Broken at both ends. L. 1 cm; D. 2 cm.

2024 campaign		
No.	**AS number/context**	**Description**
397	AS 262433:098:003 NT1 2023 Phase 5 / Building A Room 2 / Fill	Bronze disc, possibly a very corroded and unrecognisable coin. (**Fig. E1.5.6**)
398	AS 262433:139:004 NT1 2023 Phase 5 / Building A "Room 5" / Fill	Bent metal item, covered by a grey-whitish corrosion. It has a circular section, but one end is flat. Possibly made of lead.
399	AS 262433:150:003 NT1 2023 Phase 4 / Building B Room 11 / Fill	Thin wire, slightly curved. Covered by a whitish and powdery patina, a grey colour is visible below it. It could be made of lead. L. 4 cm; Th. 0.3 cm.
400	AS 262433:150:008 NT1 2023 Phase 4 / Building B Room 11 / Fill	Flattish fragment, covered by a greyish-yellow patina. It could be made of lead.
401	AS 262433:153:005 NT1 2023 Phase 4 / Building B Room 11 / Fill	Three fragments of a small lead tube. D. 1 cm; Th. 0.7 cm.
402	AS 262433:162:001 NT1 2023 Phase 4 / Building B Room 11 / from inside wall W10.	Flattened bronze object with a rounded end that forms a loop. The hole has an oval shape (D. 0.2-0.5 cm). L. 1.3 cm; W. 0.9 cm; Th. 0.2 cm.
403	AS 263432:013:004 Sondage 2 Phase 3 / Fill	Two fragments of a disc-shaped object made of bronze. The 0.4 cm preserved L. 2 cm. Highly corroded.
2023 campaign		
ExA1: 27, 172, 219 (lead fragments).		

Fig. E1.5.6: Corroded bronze disc **397**, possibly an unidentifiable coin. Photo by Andrea Squitieri.

F1.5.2 Stone tools

During the 2024 excavation campaign, 19 stone tools were recovered. As in the 2023 campaign, most of these tools were found in secondary contexts and in fragmentary conditions, making reconstructing their original forms and functions challenging. Despite these difficulties, four main morphological categories were identified: grinding stones, rounded or disc-shaped stones, elongated tools/pestles, and mortars. Basalt remained the most commonly used raw material, while various types of local limestone appeared less frequently, consistent with findings from 2023.

In Building A (**§C2.8**), four hand-sized disc-shaped limestone stones with polished, shiny surfaces were recovered from various rooms (**411**, **412**, **416**, **417**). Given the presence of polished surfaces, these may have been used primarily as polishers (**Fig. E1.5.7**). They seem unsuitable for food processing, likely serving instead in the manufacture or maintenance of objects or as floor polishers. Because of their diverse shapes and the local origin of the limestone, these stones appear to be expedient tools, likely made from nearby pebbles and used in various activities. The only potential food-processing tools found in Building A were a possible basalt pestle (**418**), found in the fill of Room 8 (**Fig. E1.5.8**), and a fragment of a lower grinding stone, also in basalt, discovered on the floor of Room 2 (ExA1: **165**). The presence of only these two items suggests a very limited level of food processing activities occurring within the building (see also **§I2.4.4**, but see the cooking pot fragment from Room 8, **§D1.1**).

In Room 11 of Building B, dated to the Iron Age, fragments of two semi-porous basalt grinding stones were found on the floor (**405**, **408**). Two additional fragments

Fig. E1.5.7: Pebble **412**, possibly used as a polisher. Photo by Andrea Squitieri.

Fig. E1.5.8: Elongated basalt tool **418**, possibly used as a pestle. Photo by Andrea Squitieri.

(**406**, **407**) were reused in installation B11-I3 near the room's entrance (**§C2.9.1**). In the Unroofed Area 4 of Building B, located south of Room 11, and excavated in 2023,[267] fragments of whetstones and stone vessels were found in the occupation level (ExA1: **204**, **205**, **210**), but no grinding stones were recovered. The excavated area of Building B is too small to conclude whether food processing activities took place in or near the building.

2024 campaign		
No.	**AS number/context**	**Description**
404	AS 254433:038:008 NT2 2024 Phase 1 / Fill	Fragment of a possible lower grinding stone made of semi-porous basalt L. 9 cm; W. 5 cm; Th. 3 cm.
405	AS 261433:080:006 NT1 2023 Phase 4 / Building B Room 11 / Floor deposit	Fragment of a lower grinding stone. The dorsal side is very rough and slightly convex, and the working surface is flat and smoothed through use. The edges are broken off. Made of semi-porous basalt. L. 13 cm; W. 12 cm; Th. 7 cm.
406	AS 261433:087:001 NT1 2023 Phase 4 / Building B Room 11 / Part of installation B11-I3.	Half-broken saddle quern with a rectangular shape. The edges are roughly cut, and the working surface is flat and smooth but still retains roughness, indicating it was not used for a long time. The dorsal side is slightly convex and rough. Made of semi-porous basalt. L. 27 cm; W. 18-27 cm; Th. 2-5 cm.
407	AS 261433:087:002 NT1 2023 Phase 4 / Building B Room 11 / Part of installation B11-I3.	Fragment of a lower grinding stone, possibly originally with a loaf shape. Only one end is preserved. It has a flat and smooth working surface and a convex dorsal side. Made of semi-porous basalt. L. 10 cm; W. 14 cm; Th. 5 cm.

2024 campaign		
No.	**AS number/context**	**Description**
408	AS 262433:161:004 NT1 2023 Phase 4 / Building B Room 11 / Floor deposit	Two small fragments of a grinding stone, too small to say if they belong to a lower or an upper stone. One fragment shows a flat and smooth surface. Both are made of semi-porous basalt. Larger piece: L. 7 cm; W. 7 cm; Th. 2 cm. Smaller piece: L. 4.5 cm; W. 3 cm; Th. 2.5 cm.
409	AS 263432:011:003 Sondage 2 Phase 3 / Fill	Fragment of a lower grinding stone with a smooth working surface. The dorsal side is very rough. Made of semi-porous basalt. L. 12 cm; W. 10 cm.
410	AS 263433:011:003 Sondage 2 Phase 3 / Fill	Fragment of a lower grinding stone. One curved edge is partially preserved, the working surface is smooth, and the dorsal side is rough. Made of semi-porous basalt. L. 15 cm; max Th. 5 cm.
411	AS 261433:037:011 NT1 2023 Phase 5 / Building A Room 1 / Fill	Roundish pebble with two polished surfaces. It could be a stone weight or a polisher. Possibly limestone. D. 3.8 cm; Wt. 88 g.
412	AS 261433:058:022 NT1 2023 Phase 5 / Building A Courtyard 10 / Fill	Pebble with an ovoid section and two opposite flattish and polished areas. The remaining surface is rough with horizontal striations due to the degradation of the stone. Made of limestone. Possibly a polisher. L. 5.5 cm. (**Fig. E1.5.7**)
413	AS 261433:061:002 NT1 2023 Phase 7 / Pit 7 / Fill	A roughly disc-shaped item with two opposite flat and smooth sides and some tiny striations visible on them. The edges are rounded. Made of a reddish medium-grained stone. Possibly a simple handstone made of limestone. L. 12 cm; W. 9 cm; Th. 4.5 cm.
414	AS 261433:061:005 NT1 2023 Phase 7 / Pit 7 / Fill	Ovoid limestone pebble with a wide perforation, slightly off-centre, and with a concave section. The surface is smooth. Max. L. 4 cm; min. L. 3.5 cm; perforation D. 1.5 cm.
415	AS 262433:104:003 NT1 2023 Phase 5 / Building A / Upper fill	Dome-shaped object with a flat and shiny side made of limestone. Possibly a polisher. L. 4.2 cm; H. 2.8 cm.

267 Kreppner/Rohde/Squitieri 2024, 127.

2024 campaign		
No.	**AS number/context**	**Description**
416	AS 262433:107:005 NT1 2023 Phase 5 / Building A Room 8 / Floor deposit	Roundish pebble with a smooth and shiny surface, with the exception of one side, which is rough and shows tiny pecking marks. Possibly used as a pounder and as a polisher. Made of limestone. D. 7 cm.
417	AS 261433:058:016 NT1 2023 Phase 5 / Building A Courtyard 10 / Fill	Flat, wide object with one side polished. One end is rounded, and the other is broken off. L. 7 cm; Th. 1.2 cm. Made of limestone.
418	AS 262433:102:004 NT1 2023 Phase 5 / Building A Room 8 / Fill	An elongated tool made of compact basalt. Rectangular shape with rounded edges and smooth faces. The ends are roundish, and one of them has some pecking marks. Possibly used as a pestle. L. 11.5 cm; W. 5 cm. (**Fig. E1.5.8**)
419	AS 263432:016:004 Sondage 2 Phase 2	Fragment of a perforated stone object with one side flat and the other rounded. Broken in the perforation. Dark grey stone. Polished surface. Most likely used as a whetstone. L. 3.4 cm; W. 1.6 cm; Th. 1.2 cm.
420	AS 254433:021:004 NT2 2024 Phase 2	The corner piece of a basalt basin with a pierced-through base. The corner is regular and has flat surfaces. L. 8.5 cm; W. 7 cm.
421	AS 262433:148:003 NT1 2024 Phase 5 / Building A "Room 5" / Fill	Fragment of a mortar bowl, made of compact basalt. L. 6.5 cm; H. 5 cm.
422	AS 263432:010:003 Sondage 2 Phase 3	Rim to base fragment of a mortar bowl with a slightly pointed rim, upright wall and flattish base. The cavity is gently sloping down, and it is smooth. The outside surface is very rough. Made of semi-porous basalt. L. 11 cm; Th. 6.5 cm.
2023 campaign		
ExA1: 5, 6, 7, 22, 23, 24, 45, 60, 107, 111, 114, 118, 119, 122, 123, 124, 125, 131, 154, 155, 165, 176, 177, 182, 188, 204, 205, 210, 221, 222, 231, 239, 240, 285.		

E1.5.3 Textile production tools in various materials

Various finds from the 2023 and 2024 campaigns, including loom weights, weaving shuttles, spindle whorls, and bone pins, suggest textile production in the New Town of Assur. These tools, which are likely associated with textile production, are discussed in this chapter, though it is acknowledged that some may have served other purposes. However, their frequent co-occurrence in the same contexts in Assur supports their interpretation as textile tools. Concentrations of these tools are particularly notable in the fill of "Room 5" of Building A (NT1 2023 Phase 5), as well as in Room 11 and Unroofed Area 4 of Building B (NT1 2023 Phase 4).

E1.5.3.1 Loom weights

In addition to the nine loom weights discovered in 2023, eight more were found during the 2024 campaign. All loom weights are handmade from unfired clay and spherical or flattened spherical.[268] The loom weights from Buildings A and B are relatively small, measuring 3.0-5.5 cm in diameter and 3.1-4.5 cm in height.[269] Only the loom weight **424**, found in the topsoil, is significantly larger, with a diameter of up to 7.0 cm.

Building A (NT1 2023 Phase 5) yielded six loom weights across several locations: Room 1 (**425**, **426**), Room 3 (ExA1: **171**), "Room 5" (**428**, **429**), and Courtyard 10 (**427**). Furthermore, six loom weights were recovered from Building B (NT1 2023 Phase 4). These were found in the occupation

Fig. E1.5.9: Loom weight **423** with one flattened and one pointed side. Photo by Helen Gries.

268 The terminology for loom weight shapes follows Mårtensson/Nosch/Strand 2009, fig. 9.

269 For comparison, loom weights uncovered during the 1989–1990 and 2000–2001 excavations of Neo-Assyrian dwelling houses in Assur measured 5.1-7.7 cm in diameter, see Miglus 2016, 62.

level of the Unroofed Area 4 (ExA1: **192**, **193**, **215**, **216**) and Room 11 (**430**, **431**).

2024 campaign		
No.	**AS number/context**	**Description**
423	AS 254433:019:004 NT2 2024 Phase 2 / Fill	Spherically shaped loom weight with one side flattened, and one pointed. D. 4.3-4.5 cm; D. of the perforation 1.0 cm; Wt. 71.0 g. (**Fig. E1.5.9**)
424	AS 261433:029:003 Topsoil	Loom weight broken into two halves. The surface is damaged. Originally, it had a spherical shape. D. max. 7.0 cm; D. of the perforation 1.3 cm; Wt. 96.0 g.
425	AS 261433:037:007 NT1 2023 Phase 5 / Building A Room 1 / Fill	Flattened spherically shaped loom weight. One part is broken off. D. max. 5.0 cm; H 3.4 cm; D. of the perforation 0.8 cm; Wt. 56.0 g. (**Fig. E1.5.10**)
426	AS 261433:037:009 NT1 2023 Phase 5 / Building A Room 1 / Fill	Slightly irregularly spherically shaped loom weight, slightly damaged. D. max. 5.0 cm; H. 4.5 cm; D. of the perforation 0.8 cm; Wt. 95.0 g.
427	AS 261433:062:004 NT1 2023 Phase 5 / Building A Courtyard 10 / From installation A10-I1	Flattened spherically shaped loom weight. D. 5.5 cm; H. 3.5 cm; D. of the perforation 1.0 cm; Wt. 44.0 g.
428	AS 262433:141:006 NT1 2024 Phase 5 / Building A "Room 5" / Fill	Spherically shaped loom weight with one side pointed out and one side broken off. D. 3.5 cm; H. 2.7 cm; D. of the perforation 1.0 cm; Wt. 25.0 g.
429	AS 262433:141:007 NT1 2024 Phase 5 / Building A "Room 5" / Fill	Half-broken loom weight with a spherical shape. It shows traces of burning. D. c. 3 cm; D. of the perforation 0.8 cm; Wt. 16.0 g.
430	AS 261433:085:004 NT1 2023 Phase 4 / Building B Room 11 / Fill	Fragment of a loom weight with a spherical shape, about ⅔ preserved. D. 4.5 cm; H. 3.1 cm; Wt. 60.0 g. (**Fig. E1.5.11**)
431	AS 262433:161:005 NT1 2023 Phase 4 / Building B Room 11 / Floor deposit	Half of a spherical loom weight (modern break). D. 4.7; H. 1.6 cm.
2023 campaign		
ExA1: 171, 192, 193, 212, 215, 216, 283, 284.		

Fig. E1.5.10: Loom weight **425** with flattened spherical shape. Photo by Helen Gries.

Fig. E1.5.11: Loom weight **430** with a spherical shape. Photo by Helen Gries.

F1.5.3.2 Weaving shuttle

Five flat, polished bone spatulas were unearthed in Assur during the 2023 and 2024 campaigns. Where preserved, each features a rounded and pointed end with a meticulously smoothed surface (**Fig. E1.5.12**). Comparable bone tools, often found alongside other textile production implements such as loom weights and spindle whorls, have been documented at various sites from the Iron Age onwards.[270] These tools are, therefore, interpreted here as weaving shuttles, used on handlooms to thread the weft alternately through the warp threads.[271]

During the 2023 and 2024 excavations in Assur, these spatulas were found alongside other textile production tools, reinforcing their interpretation as weaving shuttles.[272] Thus, in the fill of "Room 5" in Building A (**§C2.8.7**), two weaving shuttles (**432**, **433**), two loom weights (**§E1.5.3.1**), and a spindle whorl (**§E1.5.3.3**) were recovered. In Building B, the weaving shuttles were also found

270 E.g., Assur (Wicke 2010, 188-190, pls. 39-41; Miglus 2016, 65-66); Khirbet Khatuniyeh (Curtis/Green 1997, 20, no. 77, fig. 23); Tille Höyük (Blaylock *et al.* 2016, 229-231); Tell Afis (Cecchini 2000, 223-229); Tell Mastuma (Iwasaki *et al.* 2009, fig. 8.27.19-22); Tell Halaf (Mönninghoff/Skaletz 2022, 331-332); Nush-i Jan (Curtis 1984, 44-45, nos. 393-415, fig. 13).

271 For a discussion of alternative uses of the object type, see Wicke 2010, 188-190; for an interpretation as weaving shuttles, see in particular Cecchini 2000, 225-228.

272 Miglus observed similar associations of bone spatulas and loom weights during the 2001 excavations in Assur, see Miglus 2016, 66. Wicke 2010, 189, on the other hand, sees no evidence of textile production in connection with bone spatulas in Assur.

in contexts that yielded other tools related to textile production. In Room 11, a weaving shuttle (**434**) and a loom weight (**§E1.5.3.1**) were uncovered. Additionally, four loom weights (ExA1: **192**, **193**, **215**, **216**) and a weaving shuttle (ExA1: **227**) were found in Unroofed Area 4 of the building, which had been excavated in 2023.[273]

2024 campaign		
No.	**AS number/context**	**Description**
432	AS 262433:141:003 NT1 2024 Phase 5 / Building A "Room 5" / Fill	A flat, thin bone tool with one rounded and one pointed end. L. 8.0 cm; W. 1.4 cm; Th. 0.1 cm. (**Fig. E1.5.12**)
433	AS 262433:141:005 NT1 2024 Phase 5 / Building A "Room 5" / Fill	Fragments of a flat and thin bone tool with a pointed end. L. 7 cm; W. 2 cm; Th. 0.2 cm.
434	AS 261433:085:003 NT1 2023 Phase 4 / Building B Room 11 / Fill	Fragments of a flat, elongated bone object with a point; the fragments are glued together. L. 6.4 cm; W. 1.9 cm; Th. 0.15 cm.
2023 campaign		
ExA1: 167, 227.		

Fig. E1.5.12: Thin bone tool **432**, possibly a weaving shuttle. Photo by Helen Gries.

F1.5.3.3 Spindle whorls

Three ceramic objects from the 2024 campaign may be interpreted as spindle whorls (**435-7**). Unlike terracotta wheels (**§E1.3.1.6**), these are not thicker around the perforation, and in contrast to loom weights, they are not made of clay but of ceramic or stone.[274] However, due to the very poor state of preservation, it must remain uncertain whether all three objects are indeed spinning whorls, or a different type of terracotta wheels, loom weights (perhaps secondarily fired), or even simple perforated sherds (see below **§E1.5.4.2**).

Additionally, three stone beads, shaped like a spherical cap or conical frustum, which may have also served as spindle whorls, were found during the 2023 campaign (ExA1: **68**, **139**, **150**). All three are made of dark polished stone, possibly steatite, and originated from the chamber tomb (Grave 1), and Graves 3 and 4.

2024 campaign		
No.	**AS number/context**	**Description**
435	AS 254433:038:006 NT2 2024 Phase 1 / Fill	Fragment of a round perforated ceramic object with irregular edges. Some damage along the edges. It has quite a regular perforation (D. 1.3 cm), slightly thicker towards the perforation. D. max. 5.8 cm; Th. max. 1.9 cm at the centre; Th. 1.0 cm along the edges. (**Fig. E1.5.13**)
436	AS 261433:058:007 NT1 2023 Phase 5 / Building A Courtyard 10 / Upper fill	Fragment of a round ceramic object, maybe a spindle whorl, about half preserved. It tapers towards the edge and has vertical incisions. D. c. 3.0 cm.
437	AS 262433:137:007 NT1 2024 Phase 5 / Building A "Room 5" / Fill	Fragment of round perforated ceramic object, about half preserved. Slightly thicker towards the perforation. D. of the perforation 0.9 cm; Th. max. 1.7 cm.
2023 campaign		
ExA1: 68, 139, 150.		

Fig. E1.5.13: Perforated ceramic object **435**, possibly a spindle whorl. Photo by Helen Gries.

F1.5.3.4 Bone shaft

From the Late Bronze Age onwards, shafts made of bone or ivory, often found alongside other textile production tools, have been documented in the Eastern Mediterrane-

273 Kreppner/Rohde/Squitieri 2024, 127-129.

274 Völling 2008, 113; Bianchi/Wissing 2009, 218-220; Helms 2010.

an. These objects were likely used as spindles for whorls (**§E1.5.3.3**). During the 2024 excavations, a fragment of a bone shaft (**438**) with a pointed end was uncovered within the mud bricks forming the structure of Grave 9 (**§C2.5**). While it may have been a spindle shaft, it could also have served as an awl or needle.

2024 campaign		
No.	**AS number/context**	**Description**
438	AS 262433:111:003 NT1 2024 Phase 8a / Grave 9 / Mudbrick structure	Fragment of a bone object with an elongated shape and a pointed end. L. 8 cm; D. 0.5 cm. (**Fig. E1.5.14**)

Fig. E1.5.14: Bone shaft **438**, possibly a spindle shaft, an awl or a needle. Photo by Helen Gries.

E1.5.4 Ceramic tools and recycled ceramic objects

E1.5.4.1 Ceramic stilts

Stilts are three-armed ceramic supports used in pottery kilns to ensure adequate spacing between glazed vessels during firing. They help prevent the glaze from melting and causing the vessels to fuse during the firing process.[275] A total of 10 tripod stilts were collected during the 2023 and 2024 campaigns in Assur. Most of them are fragmented, with only one or two arms preserved. The intact arms end with either a knob or a T-shape. The best-preserved example, **442**, has all three preserved arms, each approximately 4 cm long and 2.5 cm thick, ending with small knobs (**Fig. E1.5.15**). In contrast, the fragment **439** has a T-shaped terminal. Some stilt fragments show the remains of a greenish or yellowish glaze on their surface (**440**, **441**, **443**), while others show traces of a red painting (**444**, **445**). Three-armed stilts are commonly found across various periods and cultural contexts, particularly in areas with significant pottery production.[276] In our excavations,[277] four out of 10 examples were discovered in operation NT2 (**§C4**), where they were collected alongside waste material from metal production (**§E1.5.5**). Since NT2 is interpreted as a collection area for wastewater and waste material, these stilts likely originated from pottery workshops scattered throughout the site.

Fig. E1.5.15: Three-arm ceramic stilt **442** with knobs at the terminal ends. Photo by Andrea Squitieri.

The remaining six stilts were recovered from operation NT1. One (**445**) came from the fill of Pit 7 of the NT1 2023 Phase 7, dated to the Parthian period. Three were found within the deposits of Building A (**443**, **444**, ExA1: **163**) dated to the Hellenistic period. Their presence in this building may suggest a nearby pottery production area. The final two examples (ExA1: **202**, **226**) were retrieved from the fills of the Unroofed Area 4 of Building B (NT1 2023 Phase 4), dated to the Iron Age.[278]

2024 campaign		
No.	**AS number/context**	**Description**
439	AS 254433:014:003 NT2 2024 Phase 3 / Fill	Ceramic stilt. Terminal end fragment with T-shape. L. 5 cm; Th. 3.5 cm.
440	AS 254433:015:004 NT2 2024 Phase 2 / Fill	Ceramic stilt. Terminal end fragment with T-shape. Traces of green glaze. L. 4.5 cm; Th. 1.9 cm.
441	AS 254433:016:004 NT2 2024 Phase 3 / Fill	Ceramic stilt. Two arms are preserved with knobs at the terminal ends. Traces of greenish glaze. L. 6.5 cm.
442	AS 254433:019:007 NT2 2024 Phase 2 / Fill	Almost complete ceramic tripod stilt with knobs at the terminal ends. L. 8 cm; Th. 4.5 cm. (**Fig. E1.5.15**)
443	AS 261433:037:003 NT1 2023 Phase 5 / Room 1 Building A / Fill	Ceramic stilt. T-shaped end fragment with yellow glaze traces. L. 2.2 cm; Th. 3.6 cm.
444	AS 261433:058:026 NT1 2023 Phase 5 / Courtyard 10 Building A / Fill	Ceramic stilt. Body fragment. Traces of red painting. L. 4 cm.

275 Waksman 2017.

276 Waksman 2017.

277 No such items have been reported by W. Andrae during his work at Assur.

278 Kreppner/Rohde/Squitieri 2024, 130.

2024 campaign		
No.	**AS number/context**	**Description**
445	AS 261433:061:006 NT1 2023 Phase 7 / Pit 7 / Fill	Ceramic stilt. Two arms are preserved, each with a knob at the terminal end. Traces of red painting. L. 6 cm; Th. 1.6 cm.
2023 campaign		
ExA1: 163, 202, 226.		

E1.5.4.2 Pottery sherds with perforations or depressions

Reused ceramic sherds with perforations or depressions carved on both sides were discovered in the fills of trenches NT1 and NT2. Specifically, they were found within the structures of Building B, Building A, and the chamber tomb (Grave 1). These artefacts vary in shape, from rectangular to disc-like, measuring approximately 5-7 cm in length and less than 2 cm in thickness, and feature irregular edges (**Fig. E1.5.16**).

Six (**446**, **447**, **450**, **451**, ExA1: **55**, **224**) of the eight sherds have a central perforation with a bi-conical section ranging from 0.3 to 0.7 cm in diameter. The remaining two sherds (**448**, **449**) display depressions on both sides, suggesting an intended but unfinished perforation. The function of these items remains uncertain. Perforated sherds similar to ours are common in the archaeological records of various chronological and cultural contexts.[279] When interpreted as textile tools, such as spindle whorls (see **§E1.5.3.3**), they tend to have a very regular disc shape.[280] Our examples, however, have irregular edges and rough manufacture, making their use as textile tools less likely. Consequently, our examples might have served as weights for fishing nets or as tokens or gaming pieces in the case of the non-perforated ones.

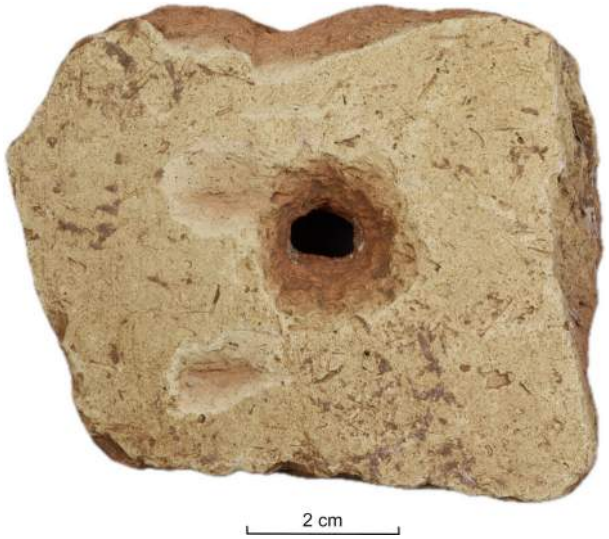

Fig. E1.5.16: Perforated pottery sherd **450**. Photo by Andrea Squitieri.

2024 campaign		
No.	**AS number/context**	**Description**
446	AS 254433:015:005 NT2 2024 Phase 2 / Fill	Perforated pottery sherd with irregular shape. Yellowish fabric with a reddish core and much chaff. L. 5.2 cm; W. 4.2 cm; Th. 1.7 cm; perforation D. 0.6 cm.
447	AS 254433:028:006 NT2 2024 Phase 2 / Pebble surface	Perforated pottery sherd with disc shape and irregular edges. D. 5.2 cm; Th. 1.6 cm; perforation D. 0.3 cm.
448	AS 254433:028:007 NT2 2024 Phase 2 / Pebble surface	A reworked pottery sherd with a disc shape and very irregular edges. Worked on both sides to create a depression but not perforated. D. max. 5.1 cm; Th. 1.6 cm.
449	AS 261433:080:011 NT1 2024 Phase 4 / Building B Room 11 / Floor deposit	A reworked pottery sherd with a rectangular shape, one corner broken off. Worked on both sides to create a depression but no perforation. L. 5.7 cm; W. 5.1 cm; Th. 1.4 cm.
450	AS 262433:135:003 NT1 2023 Phase 5 / Building A "Room 5" / Fill	Perforated pottery sherd with a rectangular shape and slightly curved in section. Irregular edges and perforation. L. 7 cm; W. 5.5 cm; Th. 1.5 cm; perforation D. 0.4-0.7 cm. (**Fig. E1.5.16**)
451	AS 263432:009:005 Surface find collected in the 2002 SBAH trench	Perforated pottery sherd with irregular shape. L. 7 cm; Th. 1.2 cm; perforation D. c. 0.5 cm. Yellowish and reddish clay with a lot of chaff.
2023 campaign		
ExA1: 55, 224 (both with perforation).		

E1.5.4.3 Ceramic discs

Eight ceramic discs were found, made from reworked sherds without perforations, with more or less regular

279 See e.g., Squitieri 2020, fig. E1.24 (Dinka Settlement Complex, Iraqi Kurdistan).

280 See e.g., Welton *et al.* 2019, fig. 24.12 (Tell Tayinat, south-east Turkey); Good 2012, fig. 2.2 (Iranian plateau).

edges and diameters varying from 2 to 5 cm (**Fig. E1.5.17**). They come from the fills of the NT2 trench and the structures of Building B (Iron Age), Building A (Hellenistic) and the Parthian chamber tomb (Grave 1).

Discs made from potsherds are common in the archaeological record across various cultural landscapes and chronological horizons. Their exact purpose remains unclear. Proposed uses include pot lids, gaming pieces, tokens, or, intriguingly, "pessoi", which were small tools for personal hygiene.[281] Recent experimental research has shown that such ceramic discs may also be suitable as a potter's rib to curve or straighten the walls of pottery vessels during the manufacturing process.[282] Unfortunately, the contexts in which the pieces from Assur were found do not provide further clues about their function.

2024 campaign		
No.	**AS number/context**	**Description**
452	AS 254433:039:007 NT2 2024 Phase 1 / Fill	Ceramic disc with irregular edges. D. 4.9 cm; Th. 0.9 cm.
453	AS 254433:039:008 NT2 2024 Phase 1 / Fill	Ceramic disc with irregular edges. D. 4 cm; Th. 0.9 cm.
454	AS 254433:039:009 NT2 2024 Phase 1 / Fill	Ceramic disc with irregular edges. D. 3.5 cm; Th. 0.9 cm.
455	AS 254433:039:010 NT2 2024 Phase 1 / Fill	Ceramic disc with irregular edges. D. 2.9 cm; Th. 0.8 cm.
456	AS 261433:074:003 NT1 2023 Phase 5 / Courtyard 10 Building A / Fill	Ceramic disc with regular edges. D. 4 cm; Th. 1.1 cm. (**E1.5.17**)
457	AS 261433:079:004 NT1 2023 Phase 4 / Building B Room 11 / Fill	Ceramic disc with regular edges. D. 2.6 cm; Th. 0.8 cm
458	AS 261433:085:007 NT1 2023 Phase 4 / Building B Room 11 / Fill	Ceramic disc with regular edges. D. 2.8 cm; Th. 0.8 cm
2023 campaign		
ExA1: 37.		

Fig. E1.5.17: Ceramic disc **456**. Photo by Andrea Squitieri.

E1.5.4.4 Miscellaneous ceramic objects

Several ceramic objects of unclear function were found in both the NT1 and NT2 trenches. Two small, roughly conical objects (**461**, **463**) may be broken feet of pottery vessels with legs, though no such shapes have been identified so far in the existing pottery collections. Two small ceramic balls, each approximately 2.5 cm in diameter and collected in 2023 from the Parthian chamber tomb (Grave 1) (ExA1: **100**, **101**), are low-fired and do not show any signs of burning or incisions. It is possible they were used as gaming pieces, such as marbles, or even as blowgun projectiles for hunting small animals. To this list, we can add two small ceramic items, also found in the fills of the Parthian chamber tomb, with a rectangular shape measuring 4.7 × 3 × 1 cm and 4.8 × 2.8 × 1 cm respectively, made of reddish high-fired ceramic with small mineral inclusions (ExA1: **47**, **118**).[283] They both show irregular striations on their surfaces alternated with polished zones, indicating they may have been used as polishers or burnishers used in pottery manufacture (ExA1: **47**, **Fig. E1.5.18**).

Finally, a rectangular object, **462**, about 1 cm thick, shows rows of small rectangular depressions on one of the flat sides and two parallel protruding ridges on the opposite side. Its function is unclear; it could have been the base of a figurine or a tool.

2024 campaign		
No.	**AS number/context**	**Description**
459	AS 254433:033:003 NT2 2024 Phase 2 / Fill	Parallelepiped-shaped object with rounded edges on one side. Broken on one narrow side. L. 15 cm; W. 6 cm; Th. 4.5 cm.

281 Charlier *et al.* 2012.

282 Gawron-Szymczyk 2022.

283 ExA1: **118** was wrongly published as made of stone.

2024 campaign		
No.	**AS number/context**	**Description**
460	AS 261433:058:007 NT1 2023 Phase 5 / Courtyard 10 Building A / Fill	Disc-shaped fragment with vertical grooves along the edge. D. c. 3 cm; Th. 1 cm.
461	AS 261433:058:014 NT1 2023 Phase 5 / Courtyard 10 Building A / Fill	Conic fragment, maybe the foot of an object. H 3.5 cm; bottom D 2.3 cm; top D 1.4 cm.
462	AS 261433:063:001 NT1 2023 Phase 5 / Building A / From inside wall W03.	Rectangular ceramic object, about 1 cm thick. One of the flat sides shows rows of small rectangular, carved depressions, while the opposite side shows two protruding ridges. L. 7 cm; W. 5 cm; Th. 1 cm.
463	AS 261433:061:007 NT1 2023 Phase 7 / Pit 7 / Fill	Cylindrical shaft (broken) ending with a broader base, slightly concave. It may be a broken foot or a handle. Shaft D. 2.3 cm; base D 3.1 cm.
2023 campaign		
ExA1: 47 (**Fig. E1.5.18**), 118, 100, 101.		

Fig. E1.5.18: Rectangular ceramic tool (ExA1: **47**, see Squitieri 2024, 164), possibly used as a polisher. Photo by Andrea Squitieri.

E1.5.5 Metal production waste

During the excavation of the NT2 trench (**§C4**), a significant amount of waste material from metal production was uncovered. Several metal slag fragments (**464-466**) were discovered in the lowest layers (**Figs. E1.5.19**, **E1.5.20**) and in the fill of the rounded shaft cut into the natural ground. Additionally, various fragments of roughly worked clay (**468-472**) were found throughout all layers of NT2. These clay fragments exhibited traces of bronze sheets on their surfaces; hence, they are believed to be remnants of crucibles used in bronze object production. Slags and crucible fragments indicate that metal workshops were dispersed throughout the city. Their waste, along with wastewater and other debris, was most likely carried into the shaft excavated in NT2 by rainwater. Though more rarely, metal production waste has also been found in the NT1 trench (**§C2**). A few slags were recovered from the fills of Building B (**467**), while some pottery slag fragments and possible crucible fragments were collected from the fills of Building A (**473**, **474**).

2024 campaign		
No.	**AS number/context**	**Description**
464	AS 254433:020:003 and AS 254433:021:005 NT2 2024 Phase 2 / Fill	Five iron slag fragments. L. < c. 5 cm.
465	AS 254433:025:005 NT2 2024 Phase 2 / Fill	Three metal slags with reddish and green stains. L. < c. 5 cm.
466	AS 254433:039:003 NT2 2024 Phase 1 / Fill	Three iron slag fragments. L. < c. 7 cm.
467	AS 261433:079:006 NT1 2023 Phase 4 / Building B Room 11 / Fill	Two metal slag fragments. L. < c. 7 cm.
468	AS 254433:021:009 NT2 2024 Phase 2 / Fill	Four fragments made of coarse unbaked clay with a worked rim. Possibly part of a stand for a crucible. (**Fig. E1.5.19**)
469	AS 254433:025:004 NT2 2024 Phase 2 / Fill	26 fragments of rough clay, some burnt. Some pieces have worked parts like a rim or base or are in the shape of a foot. Some have traces of bronze on the inside. (**Fig. E1.5.20**)
470	AS 254433:025:006 NT2 2024 Phase 2 / Fill	12 fragments of burnt, very rough clay, showing red, black and brownish stains. Some pieces show traces of bronze on the inside. They are most likely part of one or more crucibles.
471	AS 254433:030:003 NT2 2024 Phase 2 / Surface	Rim fragment made of very coarse clay, maybe part of a crucible.
472	AS 254433:035:002 NT2 2024 Phase 1 / Fill	Fragments of very coarse clay with traces of bronze. Most likely part of one or more crucibles.

Fig. E1.5.19: Coarse and unbaked clay fragments **468**, interpreted as crucible fragments. Photo by Andrea Squitieri.

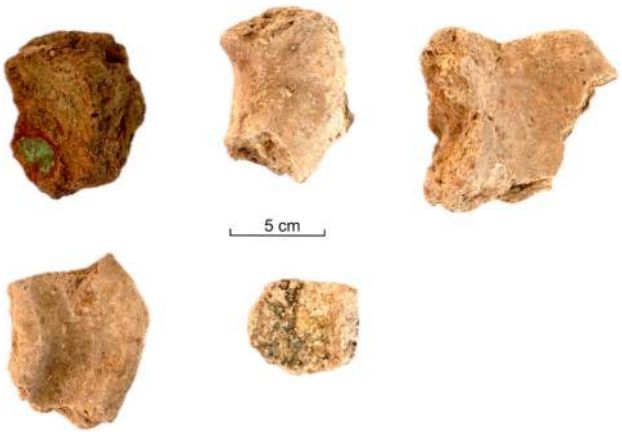

Fig. E1.5.20: Coarse clay fragments **469** with traces of burnt and bronze, interpreted as crucible fragments. Photo by Andrea Squitieri.

2024 campaign		
No.	**AS number/context**	**Description**
473	AS 263433:016:006 NT1 2023 Phase 5 / Building A Room 5 / Fill	Two small fragments of pottery slags.
474	AS 261433:058:027 NT1 2023 Phase 5 / Courtyard 10 Building A / Fill	Stone rim with traces of bronze attached to it. Possibly from a stone crucible.
2023 campaign		
ExA1: 173, 187.		

E2. A late Seleucid bronze coin from Room 7 in Building A in the New Town of Assur

Kay Ehling

During the excavations of Building A, a bronze coin (AS 262433:101:002, **Figs. E2.1a-e**) dating to the Seleucid period was discovered in the fill of Room 7 (**§C2.8.3**). To date, approximately 50 Seleucid coins have been found at Assur, with a noticeable increase in coins from the reign of Antiochus III.[284] This finding aligns with discoveries from the nearby site of Nimrud, where coins from Seleucus III, Antiochus III, Seleucus IV, Alexander I, and Demetrius II have been documented.[285]

Unfortunately, the condition of the newly discovered coin from Assur, weighing 4.48 g with a diameter of 17 mm, and classified as a "Denomination C", is relatively poor. The reverse image is no longer discernible, making precise identification impossible.[286] However, the outline of the head, the base of the forehead, the eyes, nose and mouth area are clearly visible on the front.

Ultimately, the only feature remaining to aid in identifying the depicted figure is the profile line. If we can rule out the presence of a beard, including a narrow, slightly curled beard along the chin, which could have been worn away through circulation or damage while lying in the rubble, two rulers, Seleucus VI and Demetrius III, can be excluded. Antiochus XI must also be ruled out; although the portrait style would be appropriate, no smaller, lighter denomination C bronze coins were issued for this king, only denomination B types (S C 2443). The sharply curved nose also eliminates Antiochus X as a candidate, as he is typically depicted with a snub nose.

The pronounced curve of the nose, however, points to either Antiochus VIII (**Fig. E2.2**) during his final reign (109–96 BC) or Antiochus XII, who ruled from 87/86 to 83/82 BC (**Fig. E2.3**).[287] An explanation for the great physiognomic similarity of the two Seleucids is easily found. The son of Antiochus VIII, Antiochus XII, had his portrait aligned with his father's.

284 Heidemann/Miglus 1996, 354 lists 30 coins; Butcher 2017, 26-28, nr. 3–53 lists 50 specimens from Seleucus I to Antiochus VIII.

285 Jenkins 1958, 158-168.

286 According to the catalogue Houghton/Lorber/Hoover 2008 (hereafter abbreviated as S C)

287 The end of his reign is based on a dated tetradrachm that became known in 2008: Classical Numismatic Group, Lancaster, PA, Mail Bid Sale 79, September 17, 2008, No. 429 = S C 2472 A: ΛΕ (Year 230 of the Seleucid Era = 83/82 BC).

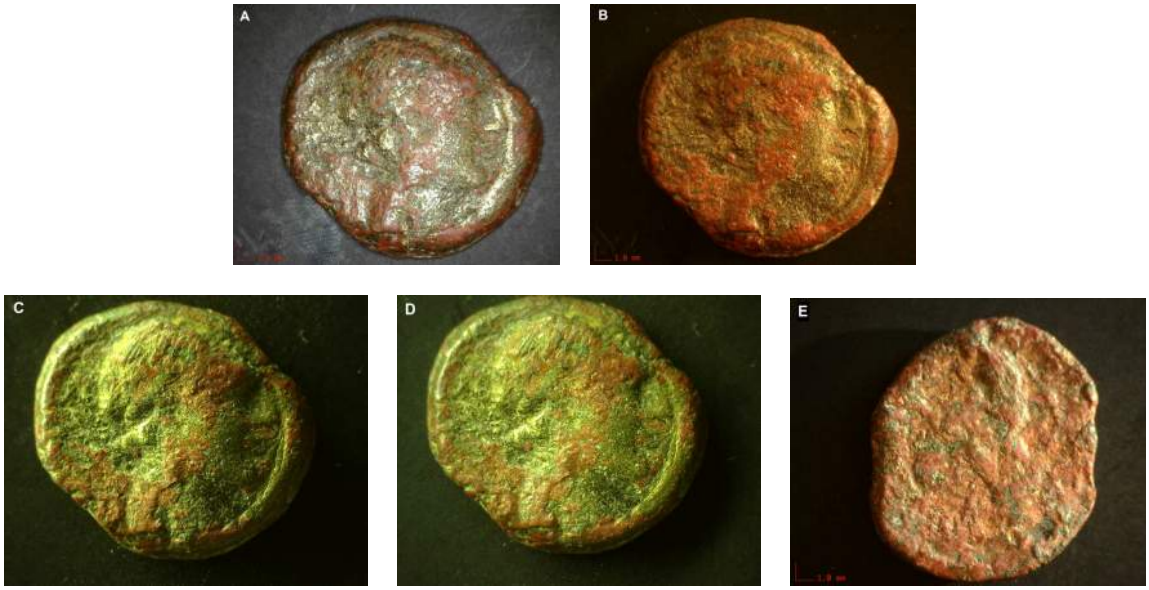

Fig. E2.1: Late Seleucid bronze coin (AS 262433:101:002) found in Room 7 of Building A. A-D: front, E: reverse. 17 mm, 4.48 g. Photos taken by Andrea Squitieri using a DinoLite microscope.

What speaks in favour of Antiochus VIII is that among the coins found in Assur, at least one piece is documented for this king.[288] However, an attribution to Antiochus XII is also quite possible, although he ruled almost exclusively over the Damascus area. As recent research has shown,[289] after the death of Antiochus XII, the remaining Seleucid troops gathered near Damascus and, led by the *strategos autokrator* Hippocrates, escaped from the advancing soldiers of the Nabataean king Aretas III, probably via Palmyra and Dura-Europos towards the Euphrates and Babylon. Under the date September/October 83 BC, the Babylonian Astronomical Diaries report unrest in this region, which can probably be seen in this context.[290] If it originated under Antiochus XII, the new coin from Assur may have travelled with the troops led by Hippocrates to eventually reach the site.

In conclusion, the coin AS 262433:101:002 is probably either a bronze of Antiochus VIII (S C 2314: standing Tyche) or a bronze of Antiochus XII (S C 2474: standing Apollo next to column; or S C 2477: standing Apollo next to tripod). On balance, the most likely option is the bronze S C 2474 of Antiochus XII, as the faint traces on the reverse suggest (Fig. E2.4).

Fig. E2.2: Antiochus VIII: Denomination B for S C 2317. Photo: American Numismatic Society, http://numismatics.org/collection/1944.100.77958 (public domain mark).

Fig. E2.3: Antiochus XII: Denomination B for S C 2478. Photo: American Numismatic Society, http://numismatics.org/collection/1944.100.78017 (public domain mark).

Fig. E2.4: Left: Reverse of a bronze coin of Antiochus XII, showing Apollo standing left, resting his arm on a column (S C 2474). Photo: Bibliothèque nationale de France, Département Monnaies, Médailles et Antiques, Luynes.3431 (43-51-66), https://gallica.bnf.fr/ark:/12148/btv1b11318536m (public domain mark). Right: Reverse of AS 262433:101:002, oriented to match the comparison and annotated by Paul van Koppen, after a sketch by Kay Ehling.

288 Butcher 2017, no. 40 = AMz 63.

289 See Ehling/Pangerl/Wünsch 2019/20, 35–48 and 42–45.

290 Sachs/Hunger 1996, no. -82 A, rev. 19-24. For December/January 83/82 BC and February/March 82 BC, further fragmentary references to fighting in Babylonia can be found in the Astronomical Diaries (Sachs/Hunger 1996, no. -82 B, obv. 18-21; rev. 3-7).

F. Cuneiform finds from Assur, 2024

Karen Radner

The text numbers continue the sequence of the epigraphic report of the 2023 spring season.[291] The badly preserved clay fragments excavated in an Assyrian drainage installation unearthed in Sondage 2 **(§D3.2)** may well constitute a clay tablet that was once inscribed with cuneiform text, but nothing remains of its surface and the object is therefore not included here.

F1. Texts from excavation

Text 11: **AS 254433:039:004**. Pottery sherd with incised cuneiform writing. Measurements: max. 4.6 × max. 3 × 0.6 cm (**Fig. F1**). It comes from the fill of the trench NT2 (**§C4**).

This fragmentary cuneiform text is inscribed onto a sherd from the body of a vessel with a diameter of about 20 cm and a wall thickness of 6 mm. The three preserved lines of text are placed at a right angle, rather than parallel, to the striations of the vessel. This means that the inscription was placed perpendicular to the axis of the vessel and ran from the rim to the bottom. When Assyrian vessels are inscribed, the text typically runs around their rims or shoulders.[292] Liane Jakob-Rost knows of only one example of a perpendicularly inscribed vessel from Assur.[293]

While the second and third line run parallel to each other the first line does not and is set at an angle of about 30 degrees. It is unclear whether the space between the first and second line was left empty or whether there originally was a shorter line in between them that did not reach as far as the preserved part of the sherd.

Most of the known Assyrian vessel inscriptions fall into one of two categories. They either name the vessel's owner or donor,[294] or else they identify the vessel's capacity.[295] Neither seems to apply to the present text, which appears to mention a person by name (Ahhe-eriba or DN-ahhe-eriba, with a divine name as the first element), followed by the mention of an associated group of people.

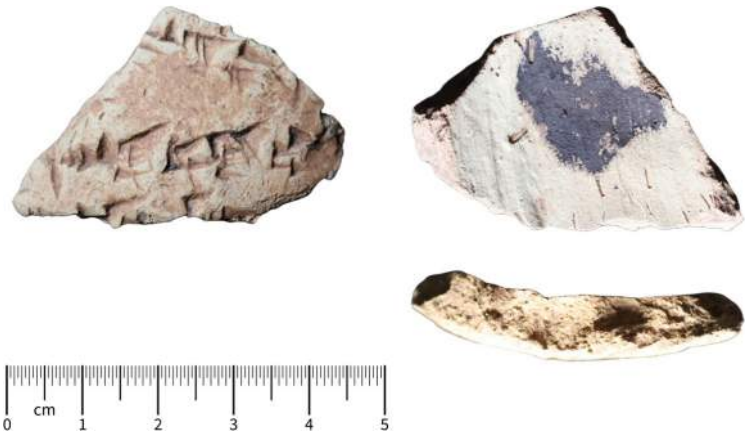

Fig. F1: AS 254433:039:004 = Text 11. Pottery sherd with incised cuneiform writing. Photos by Andrea Squitieri, figure prepared by Karen Radner.

1' [...] TA* UŠ [...]
space
2' [... ^{m}(DN–)PAP].MEŠ–SU *ù* LÚ*.[...]
3' [...] ⌜x.MEŠ ^{m}x⌝ [...]

291 Radner 2024.

292 The best Middle Assyrian examples from Assur are the inscriptions on the large clay vessels used for the banquet (*tākultu*) ritual at the Aššur temple under Adad-nerari I (1305-1274 BC; RIMA 1 A.0.76.27-28) and Shalmaneser I (1273-1244 BC; RIMA 1 A.0.77.25-27); see Frankena 1954, 51-52 and, most recently on the ritual, Heeßel 2020, 64-67. The inscriptions on the smaller Middle and Neo-Assyrian vessels from Assur were published by Jakob-Rost 1991 (sadly, without photos). A further Neo-Assyrian example is the inscribed carinated bowl fragment found at Gird-i Rostam in the Kurdish Autonomous Region of Iraq, see Radner 2021.

293 VA Ass 4455 = Jakob-Rost 1991, 61 no. 30. VA Ass 4482 = Jakob-Rost 1991, 62 no. 42 may be a further example but may have been stamped rather than inscribed. Stamping vessels with an inscription that runs along the axis is rather common; see Jakob-Rost 1991, 55.

294 For Neo-Assyrian vessels with ownership inscriptions, presumably gifted by the Assyrian king to banquet participants, see Radner 2021, 119-120; for vessels gifted to the Aššur temple by various Middle Assyrian kings who are then identified by name in the inscription, see Frankena 1954, 51-52.

295 Chambon/Kreppner 2010.

F2. Surface finds

Except for the bricks from the quay wall of Adad-nerari I (Texts 12 and 13) and a brick of Tukulti-Ninurta I (Text 17), the inside of all the bricks and brick fragments edited in the following has the pinkish-reddish colour indicative of a firing temperature of around 700° C.[296]

Text 12: **AS 000001:001:013**. Fragmentary brick with a stamped inscription of Adad-nerari I of Assyria (1305-1274 BC). Measurements: max. 14.5 × max. 18.5 × 6 cm (**Fig. F2**).

This brick fragment was found on 8 March 204 by F. Janoscha Kreppner on the surface south of the excavation house, just outside of the fence enclosing its perimeter.

It is the fifth attested example of a series of bricks from the northern quay wall of Adad-nerari I to be stamped with two inscriptions. The obverse features a five-line inscription (RIMA 1 A.0.76.39), while the one-line inscription is stamped on one of its narrow sides (RIMA 1 A.0.76.46). That text would be upside-down if the brick was laid in a way that made the inscription on the surface visible. As is routinely the case with examples of this brick series, the inside is greenish, indicating a high firing temperature of more than 1000° C.[297] Moreover, there are traces of bitumen on its bottom side, which is also typical for the bricks from the quay wall. There are also circular markings on the surface that were created when the mud was smoothed into the brick mould.

Front:

1 [É.GAL ^{m}10–ERIM.TÁH MAN KIŠ]
2 [A GÍD–DI–DINGIR MAN KUR.*Aš-šur*]
3 [*šá ki-si-ir*]-*t*[*i*]
4 [*šá* KA-*i na-ar*]-*ti*
5 [*šá* É.GAL-*la*]-*ti*

(1) "[Palace of Adad-nerari (I), king of the universe, (2) son of Arik-den-ili, king of Assyria. (3) (Brick) belonging to the fa]ci[ng (of the quay wall) (4) at the mouth of the can]al (5) [of the palace comp]lex."

Side:

1 [É.GAL ^{m}10]–ˈERIMˀ.TÁH MAN KIŠ

"[Palace of Adad]-nerari (I), king of the universe."

Fig. F2: AS 000001:001:013 = Text 12. Brick fragment with stamped inscriptions of Adad-nerari I of Assyria (1305-1274 BC) on the front and one of the narrow sides. Photos by Andrea Squitieri, figure prepared by Karen Radner.

Text 13: **AS 000001:001:011**. Fragmentary brick with a stamped inscription of Adad-nerari I of Assyria (1305-1274 BC). Measurements: max. 13 × max. 13 × 6.5 cm (**Fig. F3**).

This brick fragment was found by Christoph Forster on 5 March 2024 on the surface west of the 2023-24 excavation area. It is a new example of Adad-nerari's stamp inscription from the southern stretches of the quay wall (RIMA 1 A.0.76.40). As is very common for this brick series, there are traces of bitumen, visible both on the top and bottom sides of the brick. Its inside has the yellow-greenish colour that is typical of the quay wall bricks, indicating a firing temperature of more than 1000° C.[298]

1 [É.GAL ^{m}10–ERIM.TÁH UGULA]
2 ˈA GÍD–Dˀ[I–DINGIR UGULA-*ma*]
3 *šá ki*-[*si-ir-ti*]
4 *šá* I[GI ÍD]

(1) "[Palace of Adad-nerari, overseer], (2) son of Arik-d[en-ili, also overseer]. (3) (Brick) belonging to the fa[cing (of the quay wall)] (4) which fro[nts onto the river (Tigris)]."

296 Kreppner 2006, 99; Schneider 2006, 404.
297 Kreppner 2006, 99; Schneider 2006, 404.
298 Kreppner 2006, 99; Schneider 2006, 404.

Fig. F3: AS 000001:001:011 = Text 13. Brick fragment with a stamped inscription of Adad-nerari I of Assyria (1305-1274 BC). Photo by Andrea Squitieri.

Text 14: **AS 000001:001:031**. Brick with a stamped inscription of Shalmaneser I of Assyria (1273-1244 BC). Measurements: 33.5 × 33.5 × 5 cm (**Fig. F4**).

Eileen Eckmeier and Helen Gries found this brick on the surface on 2 April 2024 in the area of the Aššur temple, broken in two pieces but otherwise complete.

A four-line text was stamped on the brick's obverse. The fourth line is so shallowly impressed that its traces are barely visible. This is a new example of a brick series of Shalmaneser I associated with his renovation of the Aššur temple (RIMA 1 A.0.77.31). The brick stamp used is different from the one used for AS 000001:001:007 and AS 000001:001:009 (see below, Text 15), as the royal name in the second line begins with the vertical wedge used to introduce a personal name (*Personenkeil*). There is no secondary inscription on either of the narrow sides of the brick.

1 É.GAL
2 ^{md}D[I-*ma*]-˹*nu*˺–MAŠ
3 MAN KIŠ [A 10]– ˹ERIM.TÁH˺
4 ˹MAN˺ [KIŠ]-˹*ma*˺

(1) "Palace of (2) Sha[lma]neser (I), (3) king of the universe, [son of Adad]-nerari (I), (4) also king of [the universe]."

Fig. F4: AS 000001:001:031 = Text 14. Brick, in two pieces, with a stamped inscription of Shalmaneser I of Assyria (1273-1244 BC). Photo by Andrea Squitieri.

Text 15: **AS 000001:001:009**. Fragmentary brick with a stamped inscription of Shalmaneser I of Assyria (1273-1244 BC). Measurements: 33.5 × max. 30 × 5 cm (**Fig. F5**).

Jörg Fassbinder found this brick on the surface on 26 February 2024 during the magnetometer prospection in the main part of Assur, in the area south of the Sin-Šamaš temple.

Stamped on the brick's obverse, the four-line text is a new example of the brick inscription of Shalmaneser I associated with his renovation of the Aššur temple (RIMA 1 A.0.77.31). This brick was stamped with the same stamp as the obverse of a brick found in 2023 (**Fig. F6**).[299] In the new example, the stamp impression is very faint, and some signs are barely visible: they are marked with an underline in the following edition. Unlike AS 000001:001:031 (above, Text 14), the royal name is written without *Personenkeil*. There is no secondary inscription on the three surviving narrow sides of the brick.[300]

299 AS 000001:001:007, published as Radner 2024, 190-191: Text 7.

300 Unlike AS 000001:001:007, which has the secondary one-line inscription ^{m}DI-*ma-nu*–MAŠ MAN KIŠ "Shalmaneser (I), king of the universe" on one of its narrow sides.

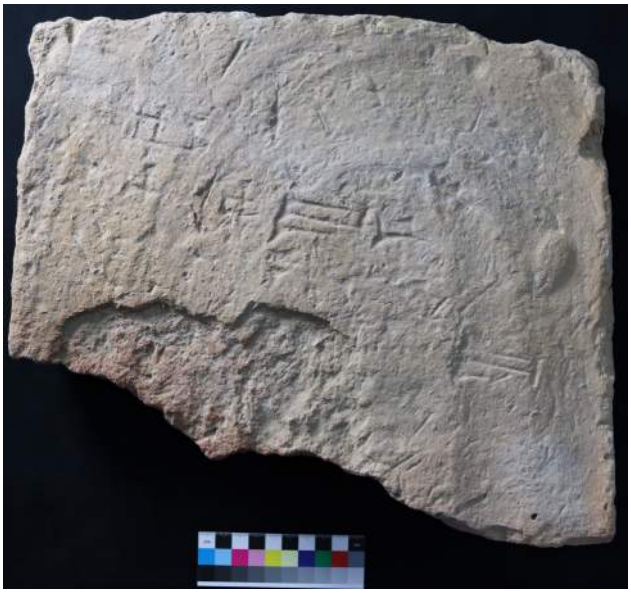

Fig. F5: AS 000001:001:009 = Text 15. Brick fragment with a stamped inscription of Shalmaneser I of Assyria (1273-1244 BC). Photo by Andrea Squitieri.

Fig. F6: The same stamp was impressed on the bricks AS 000001:001:007 (top, found in 2023) and AS 000001:001:009 (bottom), albeit by exercising different levels of strength. Photo by Karen Radner.

1 É.GAL
2 ^{d}DI-*ma-nu*–MAŠ
3 MAN KIŠ A 10–ERIM.TÁH
4 [MAN KI]Š-*ma*

(1) "Palace of (2) Shalmaneser (I), (3) king of the universe, son of Adad-nerari (I), (4) also [king of the unive]rse."

Text 16: **AS 000001:001:033**. Fragmentary brick with a stamped inscription of Shalmaneser I of Assyria (1273-1244 BC). Measurements: max. 16 × max. 17 × 5.5 cm (**Fig. F7**).

This brick fragment was found on 2 April 2024 by Akam Omar Ahmed Al-Qaradaghi on the surface in the area of the Aššur temple.

This is a new example of the brick series of Shalmaneser I associated with his renovation of the Aššur temple (RIMA 1 A.0.77.31). Only the ends of the first two lines of the stamped four-line inscription are preserved. Unlike in the case of the brick stamps used for AS 000001:001:031 (see above, Text 14) as well as AS 000001:001:007 and AS 000001:001:009 (see above, Text 15), the text in this stamp is structured by dividing lines. There are no traces of a secondary inscription on the remaining two narrow sides of the brick.

Fig. F7: AS 000001:001:033 = Text 16. Brick fragment with a stamped inscription of Shalmaneser I of Assyria (1273-1244 BC). Photo by Andrea Squitieri.

1 [É.GA]L
2 [^{md}DI-*ma-n*]*u*–MAŠ
3 [MAN KIŠ A 10–ERIM.TÁH]
4 [MAN KIŠ-*ma*]

(1) "[Palac]e of (2) [Shalma]neser (I), (3) [king of the universe, son of Adad-nerari (I), (4) also king of the universe]."

Text 17: **AS 000001:001:014**. Fragmentary brick with a stamped inscription of Tukulti-Ninurta I of Assyria (1243-1207 BC). Measurements: max. 17 × max. 18.5 × 6.5 cm (**Fig. F8**).

This brick fragment was found on the surface on 8 March 2024 by Andrea Squitieri in the area of the cella of the Aššur temple. Its inside has a yellow-greenish colour, indicating a firing temperature of more than 1000° C.[301]

This three-line stamped inscription is a new example of a well-known text of Tukulti-Ninurta I that is attested in Assur as well as several other sites (RIMA 1 A.0.78.38). The same stamp was used for some much better-preserved bricks excavated by Walter Andrae, now kept in the Vorderasiatisches Museum in Berlin (VA Ass 3245h and VA Ass 3245k; **Fig. F9**).

Fig. F8: AS 000001:001:014 = Text 17. Brick fragment with a stamped inscription of Tukulti-Ninurta I of Assyria (1243-1207 BC). Photo by Andrea Squitieri.

301 Kreppner 2006, 99; Schneider 2006, 404.

Fig. F9: The same stamp was used for the inscription of Tukulti-Ninurta I on the brick fragment AS 000001:001:014 and the bricks VA Ass 3245h and VA Ass 3245k from the excavations of Walter Andrae, now in the Vorderasiatisches Museum Berlin. Photos by Andrea Squitieri and Karen Radner, figure prepared by Karen Radner.

1 [É.GAL ^{m}GIŠ. *tukul-ti*–]
2 [^{d}*Nin-urta*] MAN KIŠ
3 [A ^{d}DI-*ma-nu*–MA]Š MAN KIŠ-*ma*

(1-2) "[Palace of Tukulti-Ninurta (I)], king of the universe, (3) [son of Shalmanes]er (I), also king of the universe."

Text 18: **AS 000001:001:012**. Fragmentary brick with a stamped inscription of Tukulti-Ninurta I of Assyria (1243-1207 BC). Measurements: max. 14.5 × max. 11.5 × 6 cm (**Fig. F10**).

This brick fragment was found on 7 March 204 by Marco Wolf on the surface during the magnetometer prospection near the Parthian Palace.

This inscription was shallowly stamped into the obverse of a brick of Tukulti-Ninurta I. The stamp was pressed into the clay twice, as the double imprint of the

signs in the second line illustrates. It is either a new example of the inscription RIMA 1 A.0.78.32 if there are only two lines or of RIMA 1 A.0.78.38 if there was originally a third line, of which nothing survives today. The present edition assumes the first option to be correct.

1 É.GAL ^{m}[GIŠ. *tukul-ti*–]
2 [^{d}]^{r}*Nin-urta* MAN$^{?}$ [KIŠ]

(1-2) "Palace of [Tukulti]-Ninurta (I), king of the [universe]."

Fig. F10: AS 000001:001:012 = Text 18. Brick fragment with a stamped inscription of Tukulti-Ninurta I of Assyria (1243-1207 BC). Photo by Andrea Squitieri.

Text 19: **AS 000001:001:015**. Fragmentary brick with a stamped inscription, most likely of Tukulti-Ninurta I of Assyria (1243-1207 BC). Measurements: max. 18 × max. 15 × max. 6 cm (measurements taken along the lines of text; **Fig. F11**).

This brick fragment was found on the surface on 21 March 2024 by Helen Gries in the area of the Aššur temple near the ziggurat.

While the surface of this fragment from the middle of a brick is badly worn and in part broken off, it still preserves traces of a stamped inscription that consists of three lines with a height of 1.8 cm, with dividing lines. What at first glance appear to be traces of a fourth line are more likely to be damages to the surface whose erosion exposed shallow cavities originating from the straw added to the clay mixture of the mudbrick. These sometimes look like cuneiform wedges; note also the two cavities resembling a Winkelhaken at the start of the first line, which obscure the beginning of the sign GAL. In addition to the surface's poor state of preservation, the stamp was also unevenly impressed so that its imprint is very shallow on the right-hand side; note e.g. how the dividing line underneath the third line of the inscription disappears in the middle of the text.

The clearly visible signs DI-*ma-nu* in the third line refer to a Shalmaneser, and the best option is to assign this brick to Tukulti-Ninurta I son of Shalmaneser I. Like Text 15 = AS 000001:001:014, this is another new example of an inscription of Tukulti-Ninurta I (RIMA 1 A.0.78.38) that is well attested in Assur and other sites.

1 [É.G]^{r}AL$^{?}$ [^{m}GIŠ. *tukul-ti*–]
2 [^{d}]^{r}*Nin-urta*$^{?}$ [MAN KIŠ]
3 [A ^{d}]DI-*ma-nu*–[MAŠ MAN KIŠ-*ma*]

(1-2) "[Pal]ace of [Tukulti]-Ninurta (I), [king of the universe, (3) son of] Shalman[eser (I), also king of the universe]."

Fig. F11: AS 000001:001:015 = Text 19. Brick fragment with a stamped inscription, likely of Tukulti-Ninurta I of Assyria (1243-1207 BC). Photo by Andrea Squitieri.

Text 20: **AS 000001:001:027**. Fragmentary brick with a stamped inscription of Ashurnasirpal II of Assyria (883-859 BC). Measurements: max. 29 × max. 21 × 6.5 cm (**Fig. F12**).

This brick was found on the surface on 28 March 2024 by Eileen Eckmeier at the eastern side of the ziggurat of the Aššur temple. There are traces of bitumen on the surface.

This is a new example of a brick series of Ashurnasirpal II with a stamped three-line inscription (RIMA 2

A.0.101.1006). In our piece, the ends of two lines are preserved. The height of the lines of text is 2.5 cm, and there are dividing lines.

1 [É.GAL ^{m}AŠ–PAP–A MAN ŠÚ]
2 [MAN KUR] AŠ A GIŠKIM–^{r}MAŠ^{1}
3 [MAN] KUR AŠ-*ma*

(1) "[Palace of Ashurnasirpal (II), king of the universe, king of] Assyria, son of Tukulti-Ninurta (II), also [king] of Assyria."

Fig. F12: AS 000001:001:027 = Text 20. Brick fragment with a stamped inscription of Ashurnasirpal II of Assyria (883-859 BC). Photo by Andrea Squitieri.

Text 21: **AS 000001:001:032**. Fragmentary brick with a hand-written inscription of Shalmaneser III of Assyria (858-824 BC). Measurements: max. 27 × 16 × 13.5 cm (**Fig. F13**).

This fragmentary brick was found by Eileen Eckmeier and Helen Gries on 2 April 2024 just outside of the northern fence enclosing the excavation house.

This is a new example of a brick series of Shalmaneser III from the city wall of Assur (RIMA 3 A.0.102.100).

1 ^{md}DI-*ma-nu*–MAŠ MAN ŠÚ
2 A AŠ–PAP–A MAN ŠÚ
3 A TUKUL–MAŠ MAN ŠÚ-*ma*
4 *šá* BÀD URU.ŠÀ–URU

(1) "Shalmaneser (III), king of the universe, (2) son of Ashurnasirpal (II), king of the universe, (3) son of Tukulti-Ninurta (II), also king of the universe: (4) belonging to the wall of Libbi-Ali (i.e., Assur)."

Fig. F13: AS 000001:001:032 = Text 21. Fragmentary brick with a hand-written inscription of Shalmaneser III of Assyria (858-824 BC). Photo by Andrea Squitieri.

Text 22: **AS 000001:001:029**. Fragmentary brick with a stamped inscription of Shalmaneser III of Assyria (858-824 BC). Measurements: 37 × max. 30 × 9.5 cm (**Fig. F14**).

F. Janoscha Kreppner and Eileen Eckmeier found this fragmentary brick, broken into two pieces, on 31 March 2024 on the surface near the inner side of the western city wall of the New Town, close to the SBAH excavations of 1979-80.[302]

Parts of the brick's surface are heavily eroded, exposing shallow cavities that originate from the straw in the mudbrick's clay mixture and that make the cuneiform characters of the stamped inscription hard to recognise. Nevertheless, enough of the signs survive to read the entire text with confidence. The stamp was impressed deeply into the centre of the brick, parallel to its edges. The stamp field measures 24 × 8.5 cm, and the three lines of text of the inscription are 2.7 cm high and separated by dividing lines. There are no traces of a secondary inscription on either of the brick's two preserved narrow sides.

This is a new example of an inscription that is well-attested at Assur, where it was used for Shalmaneser's refurbishment of the city walls (RIMA 3 A.0.102.106). Several bricks excavated by Walter Andrae and now kept in the Vorderasiatisches Museum are stamped with the same stamp used for our brick: VA Ass 03265a, VA Ass 03265b, VA Ass 03265c, VA Ass 03265d, and VA Ass 03265e.

1 ^{r}É.GAL ^{md}DI-*ma-nu*–MAŠ^{1}
2 MAN ŠÚ MAN KUR.AŠ ^{r}A AŠ^{1}–PAP–A ^{r}MAN ŠÚ MAN KUR.AŠ^{1}
3 A TUKUL–^{d}MAŠ ^{r}MAN ŠÚ MAN^{1} KUR.AŠ-*ma*

302 See Ahmad 1996.

(1) "Palace of Shalmaneser (III), (2) king of the universe, king of Assyria, son of Ashurnasirpal (II), king of the universe, king of Assyria, (3) son of Tukulti-Ninurta (II), also king of the universe, king of Assyria."

Fig. F14: AS 000001:001:029 = Text 22. Fragmentary brick with a stamped inscription of Shalmaneser III of Assyria (858-824 BC). Photo by Andrea Squitieri.

Text 23: **AS 000001:001:010**. Fragmentary brick with a hand-written inscription of Sennacherib of Assyria (704-681 BC). Measurements: max. 29 × 35 × 11 cm (**Fig. F15**).

This brick fragment was found by Marco Wolf on 27 February 2024 during the magnetometer prospection in the area south of the Ištar temple, west of trench W-1 of the excavations of Barthel Hrouda and Peter Miglus.[303] The piece was found as a part of a recently constructed fireplace, likely for a picnic – a popular weekend pastime of Sherqat's inhabitants. This has resulted in the partial blackening of the surface; the decolouring is not linked to an exposure of the brick to bitumen in antiquity.

With a thickness of 11 cm, the brick is remarkable for its size and weight. This is characteristic of a brick series created for Sennacherib's work on the "Palace of Rest" (*ekal tapšuhti*), of which this is a new example (RINAP 3/2 no. 203). There are no traces of a secondary inscription on the three preserved narrow sides of the brick.

Sennacherib's "Palace of Rest, an eternal dwelling, the firmly founded family house," is the king's burial place.[304] Steven Lundström suggested that the bricks of this series, and their inscription, do not belong to the grave itself but to an above-ground structure dedicated to ancestor worship that he locates in the Old Palace whereas he assigns a second brick series, with a different inscription mentioning Sennacherib's "Palace of Sleep, the tomb of rest, the eternal dwelling" (RINAP 3/2 no. 204: ll. 1-3: É.GAL *ṣa-la-li ki-mah tap-šu-uh-ti šu-bat da-ra-a-ti*), to the underground structure that would have housed the body.[305] Be that as it may, the burial place of Sennacherib remains unlocalised, and all bricks bearing the two inscriptions have been found in secondary positions. Many of them (but not ours) have been found near the Old Palace. This strongly suggests that the structure was located in or near that building and that it was looted and destroyed, presumably already in antiquity and most likely during the fall of Assur at the hands of the Medes in 614 BC. [306]

The brick's five-line inscription is written by hand and arranged into a frame with line divisions, which takes up most of the obverse. The height of the resulting boxes varies considerably, with the first line measuring 7.5 cm, the

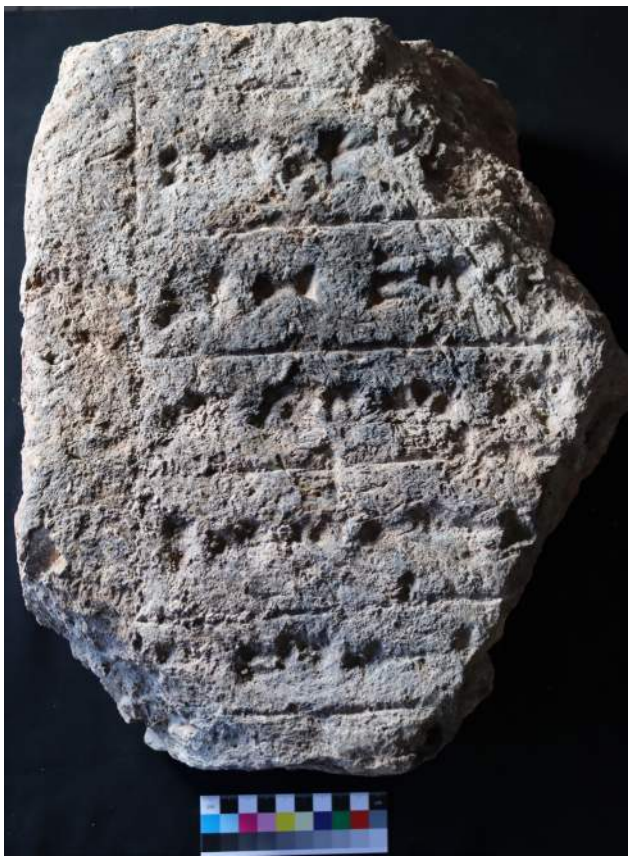

Fig. F15: AS 000001:001:010 = Text 23. Brick fragment with a hand-written inscription of Sennacherib of Assyria (704-681 BC). Photo by Andrea Squitieri.

303 For the location, see Miglus/Radner/Stępniowski 2016, pl. 3.
304 Frahm 1997, 181-182; Lundström 2009, 206-213.
305 Lundström 2009, 207, 209-210.
306 For a survey of the suggested locations of Sennacherib's tomb, see Grayson/Novotny 2014, 24 with n. 70.

second and fourth lines 6 cm, the third line 5.5 cm and the fifth line 5 cm.

1 É.GAL *tap-*[*šu-uh-ti*]
2 *šu-bat da-r*[*at*]
3 É *kim-ti šur-*[*šu-du*]
4 *šá* ^{md}30–PAP.MEŠ–S[U MAN GAL]
5 MAN *dan-nu* MA[N ŠÚ MAN KUR.*Aš-šur*]

(1) "Palace of R[est], (2) an eter[nal] dwelling, (3) the firmly-[founded] family house (4) of Sennacher[ib, great king], (5) strong king, ki[ng of the universe, king of Assyria]."

G. Geochemical analysis and building techniques of bricks from Assur

Marta Lorenzon & Melis Uzdurum

G1. Introduction

In Assur, monumental and residential structures predominantly used mudbricks and fired bricks as primary building materials. Analysing these bricks provides valuable insights into the city's resource management, architectural practices, labour organisation, and climate adaptation strategies, thus shedding light on the socio-political dynamics and technological advancements of the time.

This chapter presents results from geochemical analyses addressing the following key questions:

- Which raw materials were used, and where were they sourced?
- Can patterns of resource distribution be identified through brick composition?
- How did Assur's inhabitants adapt their building materials to environmental and societal changes?

Through these analyses, we seek to enhance our understanding of the economic, environmental, and technological practices that underpin Assur's history.

G2. Samples and sampling strategy

This study focuses on 36 samples identified by an "M" followed by a progressive number (**Table G1**), which are categorised as Earthen Building Materials (EBM). They were exported to Germany in May 2024 and subsequently sent to the University of Helsinki Centre of Excellence in Ancient Near Eastern Empires for geochemical analysis.

The samples comprise mudbricks (N=16), mud mortar (N=2), fired bricks (N=14), and soil samples (N=4).

Mudbrick samples were collected from different locations to capture a diachronic perspective from the Old Assyrian to the Hellenistic periods (**Fig. G1**). These locations are:

- the Iron Age and the Hellenistic walls unearthed in trench NT1 (**§C2**);
- a gap within the New Town's southern fortification walls;
- the ziggurat core, along a tunnel excavated in modern times,[307] which provides access to the internal structure (see **Figs. B1.5-6**).

The mud mortar samples were extracted from the gap in the New Town's southern fortification walls.

The fired brick samples were taken from inscribed baked bricks collected from different spots across the site surface during both the 2023 and 2024 campaigns (**§F**).[308] Their inscriptions, dating from Adad-nerari I (r. 1305-1274 BC) to Sennacherib (r. 704-681 BC), served as chronological markers, thus enhancing our understanding of raw material sources and compositional changes in building materials over time.

Finally, four soil samples used as comparative material were taken from cores extracted by the river north of Assur (cores C13, C19 and C20, see **§B2** and **Fig. B2.1**).

As shown in **Table G1**, the chronological arrangement of the samples is as follows:

- Hellenistic period: M1, M2 and M3, taken from the walls of Building A (**§C2.8**);
- Iron Age/Neo-Assyrian period: M4, M5, M6, M10, M19, M24, M32, M33, taken from the walls of Building B (**§C2.9**), and from the walls of Room 6;[309]
- Late Bronze Age/Middle Assyrian period: M7, M8, M9, M11, M12, M13, M14, M15, M16, M17, M18, M20, M21, M22, M23, M25, M26, M27, and M28, taken from the walls of NT1 2023 Phase 2[310], and from the gap in the southern fortification wall of the New Town;[311]

307 On this tunnel, probably excavated by Rassam, see Andrae 1977, 130; Miglus 1985.

308 For the 2023 bricks, see Radner 2024.

309 On Room 6, excavated in 2023, see Radner/Squitieri/Rohde, 136-138.

310 About the walls exposed in trench NT1 and assigned to the NT1 2023 Phase 2, see Kreppner/Rohde/Squitieri 2024, 132-135.

311 Andrae noted two construction phases in the southern fortification walls of the New Town, in the section where our samples were taken, with the older phase most likely to be dated to the Middle Assyrian period and the younger to the Neo-Assyrian period (Andrae 1977, 201-210; see also Miglus 2010, 235-240). As the samples

Fig. G1: Location of the mudbrick samples analysed in this study (without the samples from the ziggurat and the fired bricks, for which see **§F** and Radner 2024). For the soil samples' provenance, see **Fig. B2.1**. Prepared by Andrea Squitieri.

- Middle Bronze Age/Old Assyrian period: M29 and M30, taken from the ziggurat core.[312] In particular, M29 was taken at c. 1.5 m from the tunnel floor level, while M30 was sampled at c. 20 cm above the floor level.

discussed in this study were collected from the lower phase, they were assigned to the Middle Assyrian period.

312 The construction of the ziggurat took place during the reign of Sam-su-Addu of Ekallatum = "Šamši-Adad I" of Assyria (conventionally dated to 1833-1775 BC, see Radner/Moeller/Potts 2022, p. xii).

G3. Methods

G3.1 Colourimeter analysis

The colour measurement was conducted using a CM-23d portable sphere-type spectrophotometer designed for accurate colour assessment across various surface types. With its horizontal alignment, the CM-23d is particularly suited for measuring the colour of flat or large surfaces, making it ideal for archaeological samples like mudbricks. The sphere-type geometry allows for precise colour measurements by minimising the impact of surface texture and gloss. The device provides SCI (Specular Component Included) and SCE (Specular Component Excluded) data in a single measurement sequence. This dual capability allows for a comprehensive evaluation of the influence of surface conditions, such as gloss or roughness, on the colour measurement results, ensuring a more nuanced analysis of the samples. Digital colourimetric results, unlike the Munsell colour description system, are numerical, enabling their use in statistical analyses.[313] Colour distribution analyses were conducted using R open-source software.

G3.2 p-XRF analysis

The p-XRF analysis was chosen due to its non-destructive nature and ability to provide quantitative data suitable for statistical evaluations, including principal component analysis (PCA), hierarchical cluster analysis (HCA), and ternary diagrams. These methods facilitated the detection of patterns related to the procurement of raw materials. Elemental analysis was conducted at the University of Helsinki using a Bruker S1 TITAN handheld XRF. The device features a 4 W, 50 kV tantalum anode X-ray tube, a graphene high-performance silicon drift detector with a resolution of 145 eV (Mo-Kα), and a 20 mm detector window. Each sample was meas-

313 Love 2017.

Sample ID	AS no.	Sample type	Context	Type of context	Period	Date from inscription
M01	AS 261433:065:001	Mudbrick	Building A	Urban	Hellenistic	
M02	AS 262433:126:001	Mudbrick	Building A	Urban	Hellenistic	
M03	AS 261433:063:002	Mudbrick	Building A	Urban	Hellenistic	
M04	AS 262433:054:002	Mudbrick	Building B	Urban	Neo-Assyrian	
M05	AS 262433:054:003	Mudbrick	Building B	Urban	Neo-Assyrian	
M06	AS 262433:054:004	Mudbrick	Building B	Urban	Neo-Assyrian	
M07	AS 262432:085:001	Mudbrick	NT1 2023 Phase 2	Urban	Middle Assyrian	
M08	AS 262432:085:002	Mudbrick	NT1 2023 Phase 2	Urban	Middle Assyrian	
M09	AS 262432:084:001	Mudbrick	NT1 2023 Phase 2	Urban	Middle Assyrian	
M10	AS 262432:089:001	Mudbrick	Room 6	Urban	Neo-Assyrian	
M11	AS 244436:001:001	Mud mortar	New Town southern wall opening (W)	Fortification	Middle Assyrian	
M12	AS 244436:001:002	Mudbrick	New Town southern wall opening (W)	Fortification	Middle Assyrian	
M13	AS 244436:001:004	Mudbrick	New Town southern wall opening (E)	Fortification	Middle Assyrian	
M14	AS 244436:001:005	Mud mortar	New Town southern wall opening (E)	Fortification	Middle Assyrian	
M15	AS 244436:001:003	Mudbrick	New Town southern wall opening (W)	Fortification	Middle Assyrian	
M16	AS 244436:001:006	Mudbrick	New Town southern wall opening (W)	Fortification	Middle Assyrian	
M17	AS 000001:001:022	Fired brick	Site surface	Public	Middle Assyrian	Adad-nerari I (1305-1274 BC)
M18	AS 000001:001:020	Fired brick	Site surface	Public	Middle Assyrian	Adad-nerari I (1305-1274 BC)
M19	AS 000001:001:017	Fired brick	Site surface	Public	Neo-Assyrian	Tiglath-pileser III (744-727 BC)
M20	AS 000001:001:019	Fired brick	Site surface	Public	Middle Assyrian	Tukulti-Ninurta I (1243-1207 BC)
M21	AS 000001:001:018	Fired brick	Site surface	Public	Middle Assyrian	Adad-nerari I (1305-1274 BC)
M22	AS 000001:001:023	Fired brick	Site surface	Public	Middle Assyrian	Tukulti-Ninurta I (1243-1207 BC)
M23	AS 000001:001:024	Fired brick	Site surface	Public	Middle Assyrian	Adad-nerari I (1305-1274 BC)
M24	AS 000001:001:021	Fired brick	Site surface	Public	Neo-Assyrian	Sennacherib (704-681 BC)
M25	AS 000001:001:016	Fired brick	Site surface	Public	Middle Assyrian	Shalmaneser I (1273-1244 BC)
M26	AS 262433:049:005	Fired brick	Reused in walls of chamber tomb (Grave 1)	Public	Middle Assyrian	Adad-nerari I (1305-1274 BC)
M27	AS 262433:003:004	Fired brick	Reused in walls of chamber tomb (Grave 1)	Public	Middle Assyrian	Adad-nerari I (1305-1274 BC)
M28	AS 000001:001:025	Fired brick	Site surface	Public	Middle Assyrian	Tukulti-Ninurta I (1243-1207 BC)
M29	AS 220540:001:001	Mudbrick	Internal tunnel (1.50 m from the floor)	Ziggurat	Old Assyrian	
M30	AS 220540:001:002	Mudbrick	Internal tunnel (0.50 m from the floor)	Ziggurat	Old Assyrian	
M32	AS 000001:001:027	Fired brick	Site surface	Public	Neo-Assyrian	Ashurnasirpal II (883-859 BC)
M33	AS 000001:001:029	Fired brick	Site surface	Public	Neo-Assyrian	Shalmaneser III (858-824 BC)
Soil 05	AS 229570:001:001:001	Soil	Core C20 (outside settlement)			
Soil 06	AS 229570:001:001:002	Soil	Core C20 (outside settlement)			
Soil 07	AS 300608:001:001:001	Soil	Core C13 (outside settlement)			
Soil 08	AS 252592:001:001:001	Soil	Core C19 (outside settlement)			

Table G1: List of samples collected during the 2024 excavation season. Prepared by Marta Lorenzon and Melis Uzdurum.

ured three times, with an acquisition time of 180 seconds (about 6 minutes) per measurement.[314]

Concentrations of 45 elements and compounds were measured in wt% (including MgO, Al_2O_3, SiO_2, P_2O_5, S, Cl, K_2O, CaO, Ti, V, Cr, Mn, Fe, Co, Ni, Cu, Zn, As, Se, Rb, Sr, Y, Zr, Nb, Mo, Rh, Pd, Ag, Cd, Sn, Sb, Ba, La, Ce, Hf, Ta, W, Pt, Au, Hg, Tl, Pb, Bi, Th, and U). Elements that exhibited higher error margins (V, Co, Ni, As, Se, Y, Nb, Mo, Rh, Pd, Ag, Cd, Sn, Sb, Ba, La, Ce, Hf, Ta, W, Pt, Au, Hg, Tl, Pb, Bi, Th, U) were excluded from the analysis. The 13 elements and compounds chosen for statistical analysis (Al_2O_3, SiO_2, P_2O_5, S, Cl, CaO, Ti, Mn, Fe, Sr, Rb, Zn, Zr) were selected due to their high level of reliability in p-XRF measurements and minimal error margins.[315]

The quantitative analysis results were reported in wt%, then averaged and normalised before applying Hierarchical Cluster Analysis, Principal Component Analysis (PCA), and creating a Ternary Diagram with JMP Pro 17 software.

G3.3 Loss-on-ignition analysis

Loss-on-ignition (LOI) analysis was performed on EBM and soil samples to quantify the mudbrick samples' organic material and carbonate content. The LOI method involves heating the samples at specific temperature ranges to measure weight loss due to the combustion of organic matter and the decomposition of carbonates. First, the samples were dried at 105° C to remove residual moisture. The samples were then heated to 550° C to burn off organic materials. Finally, the temperature was increased to 950° C to measure the loss related to the decomposition of carbonates, primarily $CaCO_3$. The total weight loss at each stage corresponds to the amount of moisture, organic content, and carbonate content in the samples, respectively.[316] One-way analyses and t-tests for the LOI analysis were conducted using JMP 17 Pro software.

G4. Results

G4.1 Macroscopic observations

The mudbricks examined in situ in trench NT1 measure 40 × 40 cm in the Hellenistic period (Building A) and 35 × 35 cm in the Iron Age/Neo-Assyrian period (Building B). They feature a thick mud mortar layer, approximately 2 cm, as a horizontal joint between bricks, while vertical joints are thinner, averaging 1 cm in width. Macroscopically, the mudbricks from the Neo-Assyrian context exhibit a clay-rich composition with a high percentage of vegetal temper. The external wall surface of both Hellenistic and Iron Age walls was finished with a 4-5 cm layer of mud plaster, as observed also on the New Town's southern fortification wall.

G4.2 Colourimeter results

Colourimeter analysis provides macroscopic data on the composition and properties of the unfired mudbricks and soil samples collected in Assur. By measuring subtle colour variations, colourimeter analysis helps identify different soil sources and organic additives used in the bricks, offering insights into the materials employed during manufacturing (**Table G2**).

Sample ID	L* lightness	a* red/green	b* yellow/blue
M01	59.84	4.8	13.26
M02	58.49	4.91	12.95
M03	57.83	4.65	12.28
M04	58.87	4.77	12.88
M05	56.14	4.38	11.82
M06	56.03	5.68	12.82
M07	52.53	5.35	13.4
M08	48.71	5.28	12.69
M09	46.7	5.26	11.51
M10	54.24	3.88	9.89
M11	55.43	5.54	13.66
M12	43.33	3.34	7.02
M13	47.99	6.46	12.01
M14	55.12	5.84	14.13
M15	46.16	6.16	12.56
M16	36.92	3.14	4.12
M29	46.09	4.87	9.28
M30	51	5.11	10.51
Soil 05	46.23	5.31	13.67
Soil 06	42.5	3.29	11.3
Soil 07	42.93	4.68	10.62
Soil 08	52.83	3.31	6.21

Table G2: Results of the colourimeter analysis. Prepared by Marta Lorenzon and Melis Uzdurum.

The colourimetric results, covering periods from the Old Assyrian to the Hellenistic period, reveal notable variations in colour properties as measured by L*, a*, and b* values (**Fig. G2**). The lightness (L*) values ranged from a maximum of 59.84 for sample M01 to a minimum of 36.92 for sample M16, suggesting a trend towards darker materials during the Neo-Assyrian period. The a* values, representing red-green variations, were positive across most samples, indicating a consistent presence of red hues, particularly strong in samples M11 and M14. The b* values, which reflect yellow-blue variations, ranged from 6.21 for soil sample Soil 08 to 14.13 for M14, suggesting prominent yellow hues in some samples, potentially indicating distinct material sources.

314 Lorenzon *et al.* 2024.

315 Emery/Morgenstein 2007; Hunt/Speakman 2015.

316 Davies 1974; Stein 1984; Love 2012; Lorenzon *et al.* 2023.

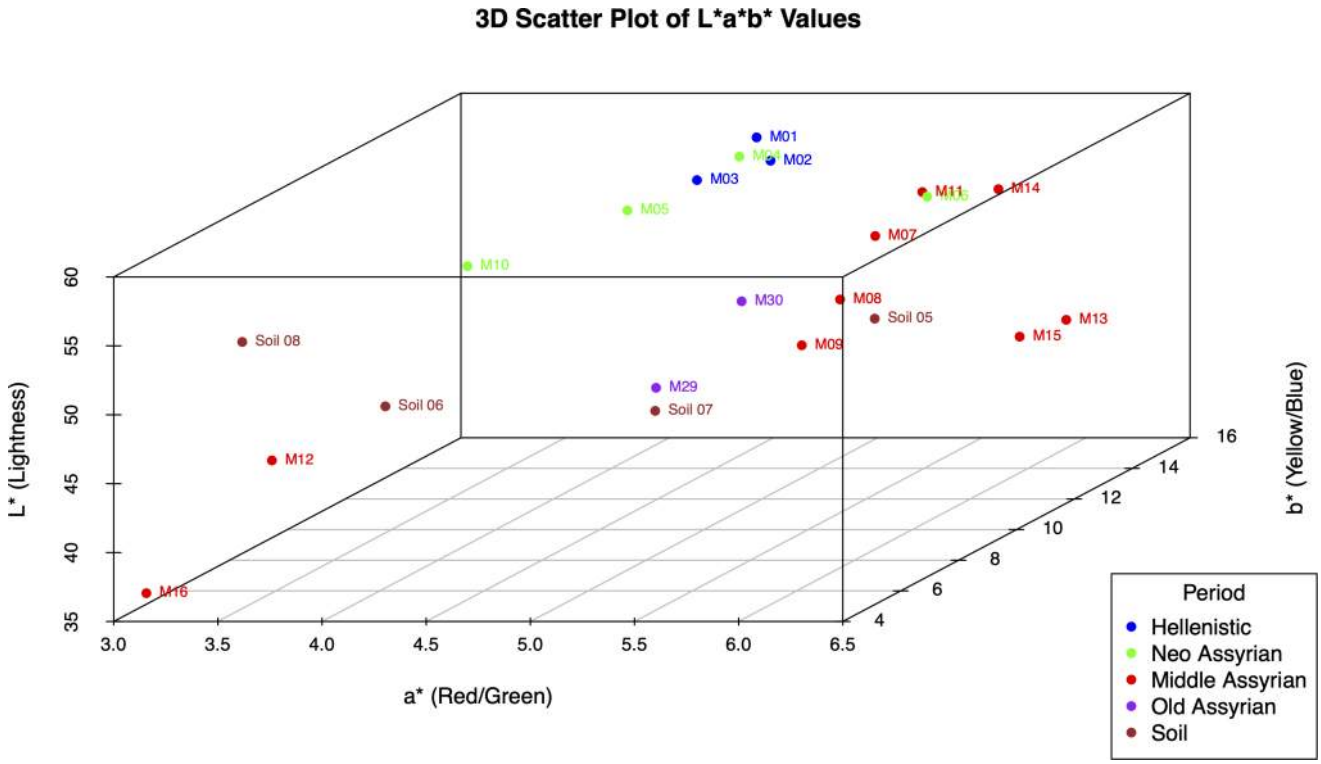

Fig. G2. 3D plot of the L*a*b values. Prepared by Marta Lorenzon and Melis Uzdurum.

In general, Middle Assyrian material exhibits a broader range of lower L* values, pointing to a shift toward darker hues and more muted colour palettes. This trend is accompanied by varied a* and b* values, with specific Middle Assyrian samples leaning towards redder and less yellow hues. While the soil samples are generally darker, they reinforce the observation that materials from different periods show distinct colourimetric characteristics, aligning more closely with Neo-Assyrian samples. These variations may reflect cultural preferences or shifts in soil availability.

G4.3 p-XRF results

The principal component analysis (PCA) highlights the differences and similarities between material types and historical periods, providing insights into the consistency or variability in raw materials used across time (**Table G3**). The clear separation or overlap of clusters informs us about Assur's technological advancements, resource use, and construction practices. PC1 accounts for 36% of the variation, while PC2 explains 28.5% of the total variance (**Fig. G3**). Together, PC1 and PC2 account for around 64.5% of the variance in the dataset. This means the two components capture a large portion of the significant variations in the samples' geochemical compositions. The biplot visualises the relationships between the variables and the principal components. Samples with high values of CaO and P_2O_5 are likely situated on the positive end of Component 1, possibly indicating materials related to plaster or lime-rich sources, often associated with construction practices. Conversely, SiO_2 and Al_2O_3 align with Component 2, which might represent materials with a higher silicate or alumina composition, potentially indicative of clay or mud-based building materials.

The PCA plot shows that fired brick samples are widely dispersed, indicating high variability in their chemical composition, suggesting significant differences in the materials or production processes used (**Fig. G3**). Likewise, mud mortar samples are widely spread along the axis linked to SiO_2 and Al_2O_3, indicating high compositional variability. Mudbrick samples are grouped along the axis where CaO and P_2O_5 show high loadings, suggesting higher concentrations of these components.

The Hellenistic samples present a high percentage of P_2O_5, S, Sr and Zr compared to other samples, possibly indicating the use of dung in the recipe. Assyrian samples have a more balanced elemental composition with moderate levels of elements except Rb. The reference soil samples are distinct from the construction materials, with higher levels of iron and related elements. This suggests that the natural soils of Assur are more iron-rich than the processed construction materials. The lack of P_2O_5 and Sr

Sample ID	Al_2O_3	SiO_2	P_2O_5	MgO	CaO	S	Cl	Ti	Mn	Fe	Sr	Rb	Zn	Zr
M01	5.6550	23.0720	0.7304	10.9191	15.3591	5.6773	0.0683	0.2570	0.0428	2.6347	0.0784	0.0038	0.0050	0.0186
M02	4.3870	19.5295	0.4815	6.8329	13.3635	5.6265	0.0565	0.2301	0.0336	2.0560	0.0721	0.0035	0.0047	0.0163
M03	4.5750	21.3139	0.5785	6.8507	14.2381	5.3869	0.0995	0.2615	0.0382	2.2702	0.0696	0.0032	0.0046	0.0167
M04	5.9730	27.0681	0.6079	6.9584	13.4619	2.4783	0.1154	0.2998	0.0459	2.4974	0.0437	0.0038	0.0046	0.0134
M05	5.4371	24.5395	0.5459	6.6858	13.0621	3.2645	0.1129	0.2571	0.0391	2.1414	0.0515	0.0036	0.0043	0.0143
M06	4.1385	18.4255	0.1919	5.7356	11.2224	3.6262	0.0512	0.2169	0.0307	1.9640	0.0315	0.0039	0.0034	0.0125
M07	3.2966	15.7574	0.3816	5.3918	11.0579	3.9040	0.0658	0.2036	0.0273	1.5663	0.0440	0.0031	0.0041	0.0128
M08	4.0108	19.5633	0.4146	6.0783	12.1273	4.2853	0.2300	0.2454	0.0357	2.0422	0.0431	0.0033	0.0039	0.0129
M09	3.2740	16.1711	0.3302	4.4212	10.2614	2.7671	0.1324	0.2148	0.0298	1.7541	0.0455	0.0035	0.0039	0.0144
M10	4.5446	19.8235	0.5930	6.9551	11.9628	6.7158	0.3343	0.2123	0.0263	1.8635	0.0473	0.0033	0.0041	0.0133
M11	3.1685	15.3462	0.2439	3.7172	8.9897	2.0738	0.6321	0.1820	0.0252	1.4219	0.0512	0.0037	0.0036	0.0135
M12	3.6178	17.2595	0.1110	3.4991	7.2140	0.6585	0.5752	0.2197	0.0327	1.8568	0.0339	0.0048	0.0051	0.0122
M13	3.2695	16.0118	0.1367	3.4283	7.4205	0.1634	0.6210	0.2171	0.0258	1.4670	0.0324	0.0037	0.0033	0.0128
M14	5.5911	24.5369	0.4442	5.9667	14.2052	3.1856	0.9424	0.3014	0.0412	2.5191	0.0528	0.0036	0.0038	0.0143
M15	5.5271	28.2285	0.0848	4.3091	8.8820	0.2514	0.1883	0.3376	0.0563	3.1486	0.0186	0.0037	0.0037	0.0100
M16	5.8835	25.9512	0.1500	6.1310	9.8293	1.1712	0.5454	0.2644	0.0355	2.1664	0.0483	0.0047	0.0033	0.0148
M17	3.9847	17.1453	0.3106	5.0844	10.3063	3.8464	0.0475	0.2556	0.0439	2.5624	0.0338	0.0040	0.0051	0.0162
M18	2.1314	14.8111	0.0711	2.0712	6.0310	0.6487	0.0567	0.2049	0.0236	1.3586	0.0343	0.0049	0.0058	0.0156
M19	5.3973	25.6113	0.1619	4.3448	10.3256	0.2634	0.0311	0.2823	0.0493	2.6651	0.0347	0.0041	0.0050	0.0146
M20	3.4616	18.0655	0.4351	6.2380	10.1119	3.7710	0.0153	0.2239	0.0421	2.2556	0.0364	0.0042	0.0078	0.0159
M21	5.1495	25.7617	0.5228	3.6596	9.1369	0.3616	0.0285	0.3026	0.0434	2.6454	0.0303	0.0048	0.0058	0.0155
M22	5.5152	19.8457	0.3597	7.5316	13.8777	5.8525	0.0396	0.2352	0.0381	2.3264	0.0335	0.0041	0.0044	0.0135
M23	3.2770	16.6712	0.2423	4.3998	8.6481	1.7435	0.1607	0.2167	0.0347	1.7704	0.0364	0.0044	0.0050	0.0152
M24	4.7701	18.2814	0.5489	7.1401	9.5598	5.9738	0.1413	0.2174	0.0438	2.4143	0.0391	0.0047	0.0056	0.0144
M25	6.3685	25.7697	0.3680	7.8165	12.4695	5.4799	0.0712	0.3262	0.0576	3.1326	0.0357	0.0039	0.0092	0.0149
M26	4.8256	18.1095	0.4088	8.4439	12.8057	8.2568	0.0413	0.2055	0.0318	2.0695	0.0375	0.0035	0.0037	0.0149
M27	5.9658	30.3727	0.1556	6.5428	10.6287	0.3824	0.0352	0.3300	0.0559	3.1276	0.0274	0.0043	0.0056	0.0135
M28	1.9127	10.7445	0.0833	2.6024	6.4456	0.9155	0.0231	0.1520	0.0217	1.1931	0.0399	0.0035	0.0043	0.0146
M29	4.8490	22.4936	0.3277	6.4174	11.2814	2.0601	0.7152	0.2766	0.0388	2.1949	0.0483	0.0037	0.0040	0.0142
M30	4.1568	19.6958	0.0908	3.7966	8.2115	1.2314	0.4634	0.2172	0.0226	1.3936	0.0465	0.0044	0.0030	0.0134
M32	5.4698	25.1355	0.1467	4.5525	9.9794	1.0116	0.0198	0.2505	0.0374	2.2216	0.0302	0.0055	0.0039	0.0132
M33	3.5805	17.0893	0.2015	4.0063	8.0632	2.8751	0.0239	0.2305	0.0347	1.8199	0.0376	0.0042	0.0051	0.0134
Soil 05	3.1768	17.4013	0.0464	3.6213	6.7048	0.0421	0.1472	0.2591	0.0506	2.8821	0.0219	0.0042	0.0040	0.0135
Soil 06	3.8935	29.4756	0.0661	3.0982	8.1064	0.0258	0.0142	0.2426	0.0442	2.3390	0.0178	0.0031	0.0027	0.0088
Soil 07	6.3451	28.0040	0.0922	4.8627	8.5232	0.3259	0.2223	0.3867	0.0574	3.2388	0.0191	0.0038	0.0041	0.0107
Soil 08	6.3427	27.2059	0.0774	4.9662	10.0163	0.4024	0.3284	0.3834	0.0673	3.8682	0.0189	0.0041	0.0043	0.0104

Table G3: Results of p-XRF analysis. Prepared by Marta Lorenzon and Melis Uzdurum.

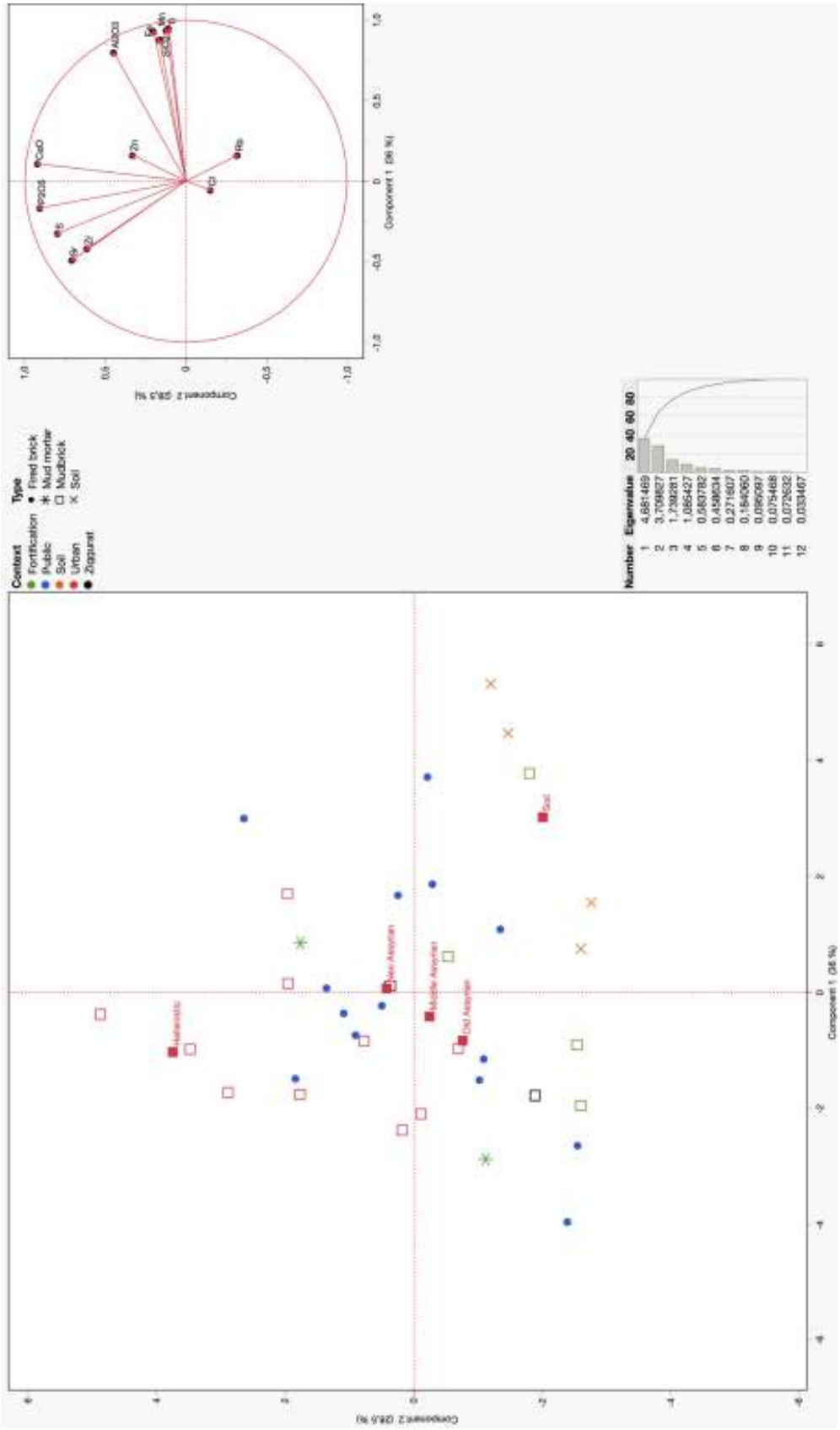

Fig. G3: Results of PCA showing correlation by period, sample type and context with 13 variables: Al_2O_3, SiO_2, P_2O_5, S, Cl, CaO, Ti, Mn, Fe, Sr, Rb, Zn, Zr for the 32 mudbrick, fired brick, mortar samples, and four reference soil samples collected from Assur. Prepared by Marta Lorenzon and Melis Uzdurum.

implies these elements were added or concentrated during brick-making or other construction processes, further separating the soil samples from the built environment. There is no distinction in the elemental composition between the Middle Assyrian and Neo-Assyrian samples. Mudbrick samples are scattered across the PCA plot, with many closer to the centre. These samples may have a more balanced geochemical profile, reflecting various sources or lesser degrees of chemical alteration during production.

Mudbricks and fired bricks are spread across the PC1 and PC2 axes (**Fig. G3**), indicating variability in their geochemical composition. Some are positioned along the positive PC1 axis, while others appear in the negative PC1 or PC2 quadrants, meaning they do not share a uniform geochemical signature. Some have higher concentrations of Fe, Mn, Ti, and SiO_2, while others have higher levels of P_2O_5, CaO, S, Sr, and Zr.

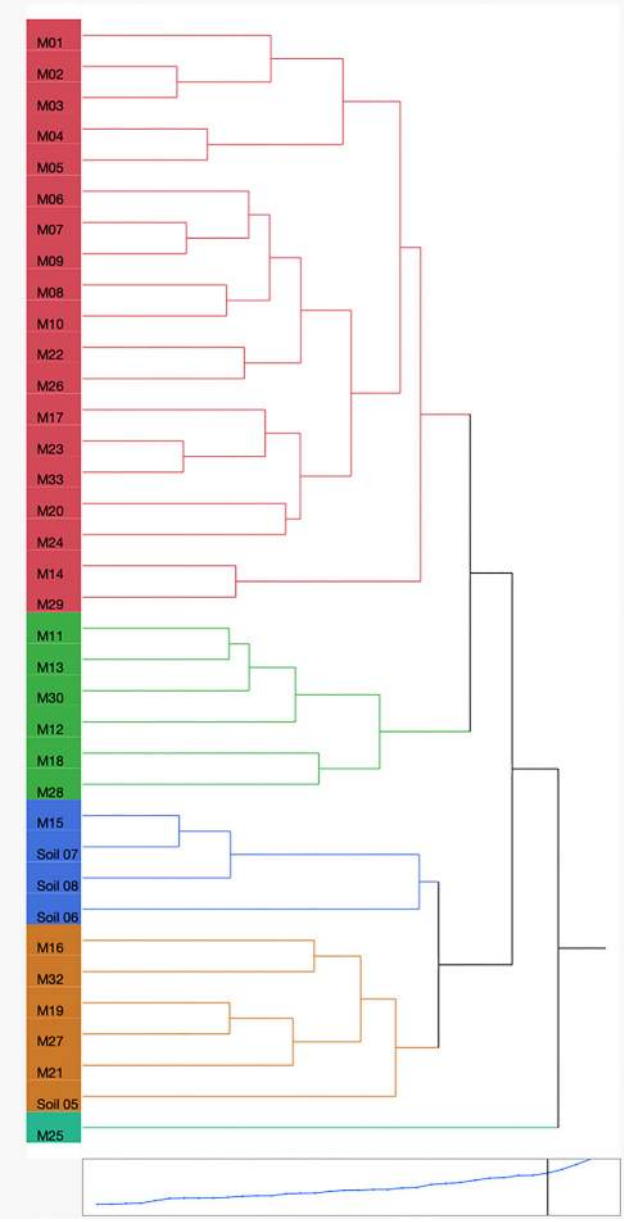

Fig. G4: Results of hierarchical cluster considering 13 variables (Al_2O_3, SiO_2, P_2O_5, S, CI, CaO, Ti, Mn, Fe, Sr, Rb, Zn, Zr) for the 32 mudbrick, fired brick, mortar samples, and four reference samples collected from the Assur settlement. Prepared by Marta Lorenzon and Melis Uzdurum.

Public and fortification samples are scattered, some showing higher values along PC1 and others more centred. Some of these samples exhibit high Fe, Mn, and Ti, indicating potential differences in their treatment or exposure to iron-bearing materials. One of the ziggurat samples is in the lower left quadrant (negative PC1, positive PC2). In contrast, the other ziggurat sample is located near the centre of the plot, indicating a balanced composition in terms of both PC1 and PC2 elements and closer to the Neo-Assyrian samples.

A hierarchical cluster analysis (HCA) based on average clustering was conducted on 13 variables, revealing the separation of the samples into five distinct groups based on their geochemical composition. In the dendrogram (**Fig. G4**), each branch represents a group of samples with similar properties, with the proximity of samples or clusters indicating greater similarity. The distance between clusters reflects the degree of difference in elemental composition, meaning clusters farther apart in the dendrogram are more dissimilar. The HCA offers insights into various samples that share compositional relationships, such as mudbrick, fired brick, and mortar. The Assur samples are divided into five distinct clusters, suggesting similarities in their elemental composition. These clusters may indicate that the materials share a common source or manufacturing technique. Most reference soil samples fall within the same elemental cluster, including the mudbrick sample M15.

Notably, mudbrick and fired brick samples from public contexts, like fortification and ziggurat structures, are grouped in the same clusters (Cluster 2: M11, M13, M30, M12, M18, M28; Cluster 4: M16, M32, M19, M27, M31, Soil 05). Cluster 1, the largest cluster, contains all urban context samples and some from public contexts, pointing towards consistency of raw source procurement between buildings of different typologies and across different periods.

A ternary plot visualises the proportions of three variables in a dataset. The plot represents the geochemical composition of mudbrick, fired brick, mortar, and reference samples using three key elements, including SiO_2, Al_2O_3, CaO+MgO (**Fig. G5**). We selected these elements as SiO_2 functions as the proxy for quartz, CaO+MgO for the calcite content and Al_2O_3 for clay and feldspar.[317] The

317 Nodarou/Frederick/Hein 2008.

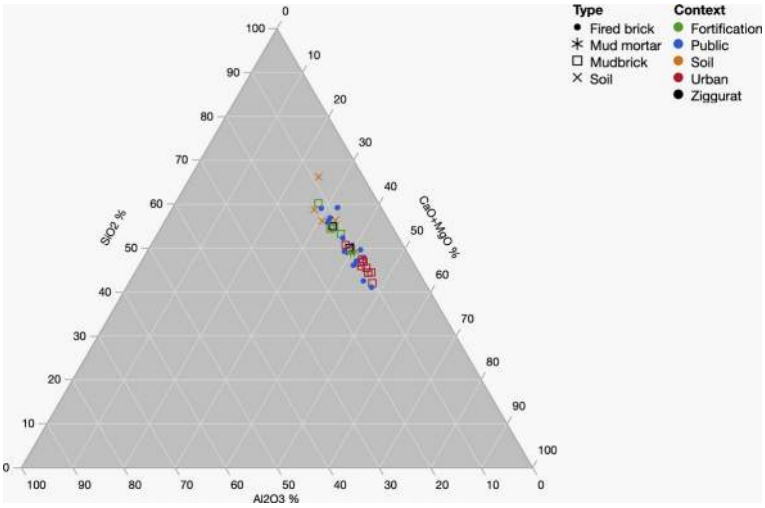

Fig. G5: Triangular scattergram SiO_2 – Al_2O_3 – CaO+MgO. Prepared by Marta Lorenzon and Melis Uzdurum.

SiO_2 component has higher values across all samples, suggesting that these materials have a siliceous composition, which is common in clay-rich materials. The Al_2O_3 values are lower than SiO_2, indicating that the clay may not be as high in aluminium-rich minerals (such as kaolinite). The CaO+MgO content is moderate, suggesting the use of partially calcitic clays or calcite in the materials, but this latter could act as a stabiliser in the construction.

G4.4 Loss-on-ignition results

The results from one-way ANOVA and Student's t-tests on organic matter content (%) show significant differences across periods, particularly between the soil and the archaeological samples (**Fig. G6**). The markedly higher organic content in the reference soil compared to the Hellenistic ($p = 0.0011$) and Neo-Assyrian ($p = 0.0027$) mudbricks suggests that the natural soil was not directly used in construction materials but was likely processed to reduce organic matter. Additionally, there are notable differences between the Middle Assyrian and Hellenistic periods ($p = 0.0535$), suggesting that although both exhibit relatively low organic matter percentages, slight variations in processing or the choice of source material and temper may have influenced mudbrick production. Soil samples display the highest organic matter levels, ranging from 4.17% to 7.79%. In contrast, the Hellenistic, Neo-Assyrian and Old Assyrian (ziggurat) samples have lower median organic content, around 3.7% and 4.2%, respectively. Urban samples dated to the Middle Assyrian period show slightly higher organic matter percentages than the other urban samples, with a median of 4.8%, implying possible changes in source materials, processing methods, or tempering strategies during this period. Urban contexts generally display lower organic content, particularly in the Hellenistic period, where values range from 0.83% to 4.39% (**Table G4**). In contrast, fortification contexts show higher organic content in the period of Middle Assyrian, with values around 4.54%. Ziggurat samples associated with monumental religious architecture exhibit intermediate organic matter levels, ranging from 3.14% to 4.07%. The high organic content in soil samples suggests that raw materials were processed before use, particularly in urban and ziggurat contexts, except for Middle Assyrian samples, where refining materials was likely essential to ensure structural integrity. In fortification contexts and some urban contexts dated to the Middle Assyrian period, however, the broader range of organic content suggests that large-scale constructions may have used less processed materials.

The one-way ANOVA and Student's t-test results on $CaCO_3$ content (%) indicate significant differences across periods (**Fig. G7**). Neo-Assyrian samples exhibit notably higher $CaCO_3$ percentages than other Assyrian samples ($p < 0.0001$), suggesting a purposeful shift in material selection during the Neo-Assyrian period. Neo-Assyrian samples show the highest median $CaCO_3$ content at 11.69%. Similarly, Middle Assyrian urban mudricks and soil samples have relatively high $CaCO_3$ levels, with medians of 10.79% and 10.64%, respectively. Hellenistic urban samples show slightly lower $CaCO_3$ levels, with a median of 10.36%, while fortification and Old Assyrian (ziggurat) samples exhibit the lowest $CaCO_3$ percentages, with a median of 9.58%. The differences between Old Assyrian and Hellenistic samples ($p = 0.0035$) point to potential variations in sourcing or processing materials between these periods. Although the $CaCO_3$ content in the reference soil is comparable to some Assyrian samples, no significant differences are observed. The ziggurat samples exhibit $CaCO_3$ levels between 11.5% and 12.1%. Urban contexts in the Hellenistic period show $CaCO_3$ values from 10.18% to 10.59%, while Middle Assyrian fortification contexts have levels around 10.79%.

The $CaCO_3$ analysis of mudbrick samples from the Assur settlement demonstrates clear variations across periods and contexts (**Table G4**). The high $CaCO_3$ content in Neo-Assyrian and Middle Assyrian samples, particularly in urban contexts, suggests a focus on enhancing durability and strength in construction. In contrast, the ziggurat samples in the Old Assyrian period exhibit lower $CaCO_3$ levels, indicating that material selection may have prioritised factors other than longevity.

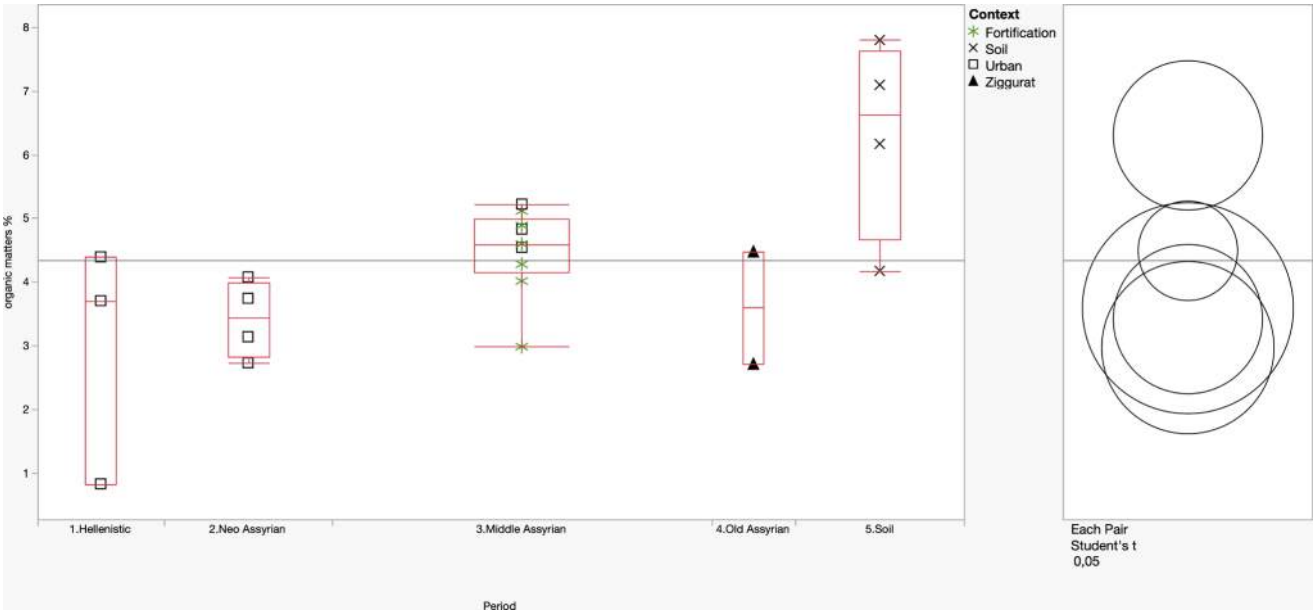

Fig. G6: One-way analysis and Student's t-test of organic matter (%) in different mudbricks and reference samples by period (N=22). Prepared by by Marta Lorenzon and Melis Uzdurum.

Sample ID	Crucible	Wet weight	105° C	550° C	Organic material %	950° C	CO_2	$CaCO_3$
M01	8.2351	13.2344	12.7341	12.6278	0.8348	12.1699	0.4579	10.1778
M02	9.5028	14.5101	14.0870	13.9881	3.7055	13.5026	0.4855	10.5907
M03	9.2081	14.2121	13.7129	13.6097	4.3929	13.1454	0.4643	10.3068
M04	8.2464	13.2408	12.8202	12.7179	4.0787	12.1912	0.5267	11.5156
M05	8.6358	13.6618	13.3653	13.2421	3.1402	12.6663	0.5758	12.1746
M06	9.5966	14.5988	14.3303	14.207	2.7341	13.6674	0.5396	11.3991
M07	9.5193	14.5387	14.0069	13.9025	4.5420	13.407	0.4955	11.0415
M08	9.5619	14.5743	13.9691	13.8452	5.2194	13.3836	0.4616	10.4738
M09	9.5284	14.5211	13.9611	13.8469	4.8291	13.3686	0.4783	10.7903
M10	8.7419	13.7761	13.4750	13.2716	3.7440	12.8319	0.4397	9.2899
M11	9.4647	14.4999	14.1538	13.7763	5.1124	13.3686	0.4077	8.6946
M12	9.5233	14.5226	14.2102	13.8697	4.5946	13.4252	0.4445	9.4839
M13	9.8930	14.8926	14.5949	14.2684	4.2768	13.7855	0.4829	10.2703
M14	8.8014	13.8334	13.4702	13.1752	4.8863	12.7326	0.4426	9.4800
M15	9.5489	14.5768	14.3493	14.0009	4.0134	13.5013	0.4996	10.4075
M16	9.1448	14.1790	13.9533	13.7625	2.9850	13.3109	0.4516	9.3917
M29	8.7209	13.7369	13.4272	13.1358	4.4767	12.6825	0.4533	9.6318
M30	9.0151	14.0254	13.8005	13.6506	2.7158	13.1907	0.4599	9.6105
Soil 05	8.5247	13.5341	13.1243	12.9865	4.1724	12.5322	0.4543	9.8769
Soil 06	8.3001	13.3049	12.5014	12.4187	7.0888	11.9364	0.4823	11.4798
Soil 07	8.6684	13.6766	12.8531	12.675	7.7927	12.2296	0.4454	10.6435
Soil 08	8.8421	13.8573	13.2202	13.0424	6.1641	12.5794	0.463	10.5754

Table G4: Results of the loss-on-ignition analysis on the unfired bricks (mudbricks). Prepared by Marta Lorenzon and Melis Uzdurum.

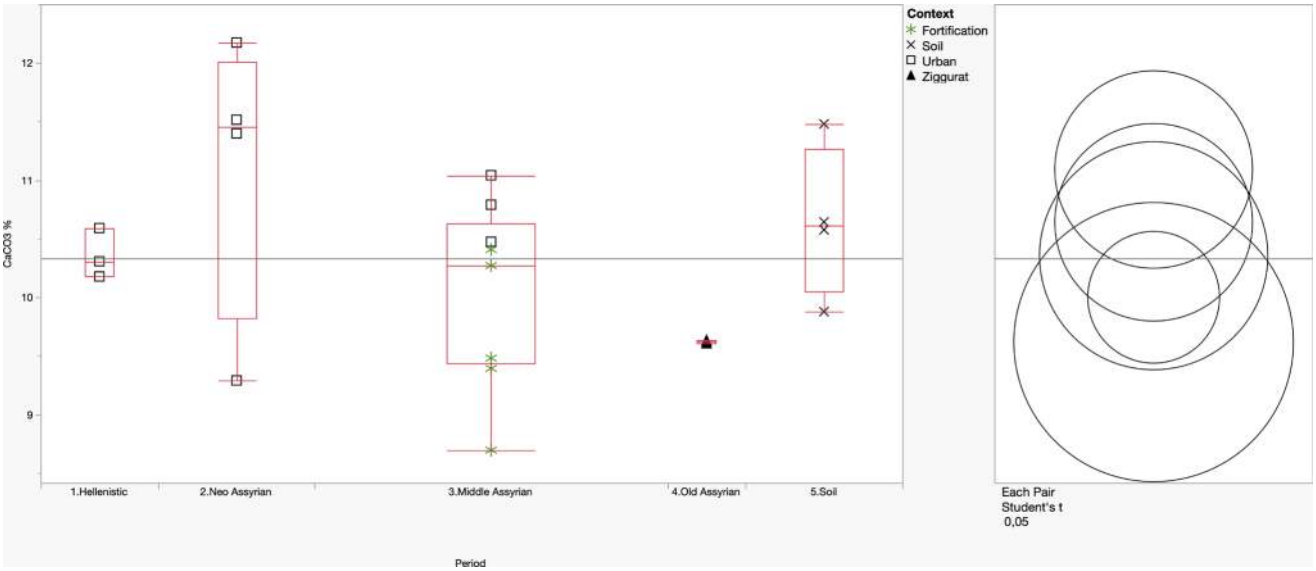

Fig. G7: One-way analysis and Student's t-test of $CaCO_3$ (%) in different mudbricks and reference samples by period (N=22). Prepared by Marta Lorenzon and Melis Uzdurum.

A comparative analysis of organic matter and $CaCO_3$ content in the mudbrick samples reveals a pattern divergence between the two components. While organic matter percentages are higher in soil samples than in mudbrick samples, this trend reverses with $CaCO_3$ content. In specific mudbrick samples, particularly Neo-Assyrian urban structures, the $CaCO_3$ percentage exceeds that of natural soil. This contrast suggests that while organic matter content was minimised, $CaCO_3$ was deliberately increased, potentially by adding lime, during the construction process in Neo-Assyrian urban structures.

G5. Discussion

G5.1 Material variability and elemental contribution

The geochemical analyses reveal significant variability in the elemental composition of construction materials, primarily driven by P_2O_5, CaO, S, Sr, Zr, Zn, Cl, and Rb (PC1), as well as SiO_2, Al_2O_3, Fe, Mn, and Ti (PC2). These elements differentiate between materials used in various periods and structural contexts. Analytical results suggest significant material variability across the different sample types. Urban samples are tightly clustered, indicating a uniform chemical composition. This suggests a standardised selection or processing method reflecting controlled material sources.

In contrast, mud mortar samples exhibit widespread along the SiO_2 and Al_2O_3 axis, indicating higher variability and possibly a more diverse range of clay or silicate sources. Mudbrick samples from urban structures, positioned along the component axis with high CaO and P_2O_5 loadings, show a concentration of these elements, suggesting using lime or calcium-based additives for structural reinforcement. The unique chemical profile of the soil samples, used as a reference, indicates that local raw materials were not used directly in construction; instead, they were processed or modified to create suitable building materials.

SiO_2 is the predominant component across all construction materials, especially in fired bricks and mudbricks, reflecting the use of silica-rich clays. Al_2O_3 improves clay plasticity during moulding and strengthens both fired and unfired bricks. Its presence in all sample types indicates a consistent use of alumina-rich clays, which is critical for shaping and ensuring durability. CaO+MgO content is generally low, except in one ziggurat sample, suggesting selective use of calcitic clays for specific structural elements. This selective use may have strengthened parts of the ziggurat, setting these samples apart from those used in urban or public structures. Additionally, two clusters have formed due to the higher CaO+MgO percentage in urban mudbricks and the higher SiO_2 percentage in fortification mudbricks. This clustering suggests that distinct compositional choices for urban versus fortification structures were made, likely reflecting differing functional requirements or construction practices.

G5.2 Chronological variability

Regarding the chronological variability, the PCA results show a distinct separation between the Hellenistic and Assyrian samples. Hellenistic samples are notable for their higher levels of Sr, P_2O_5, S, and Zr, which suggest different material sources or construction methods compared to other periods, including dung as a tempering agent. Hellenistic materials have been sourced and processed to reduce exposure to iron-rich elements, resulting in relatively low organic content and moderate $CaCO_3$ levels. This careful material selection may have enhanced durability without extensive calcite addition.

In contrast, Assyrian materials are more homogenous, suggesting consistent construction practices and standardised material sourcing. The Assyrian samples' relatively low organic matter and moderate $CaCO_3$ content imply that materials were carefully chosen to balance durability and processing. The low organic matter percentage suggests an intentional reduction of organic components to improve durability, while moderate $CaCO_3$ levels indicate that lime, if naturally present in the soil, was not heavily supplemented. This suggests using materials with minimal modification yet sufficient for constructing durable structures.

Assyrian samples reveal some variability in geochemical composition attributed to diverse soil sources. Public and fortification structures highlight significant variation, with some samples showing high iron content while others are more balanced, likely reflecting different construction requirements for fortifications versus public buildings. The two samples from the ziggurat display distinct geochemical profiles. One sample has a balanced composition, while the other shows lower P_2O_5, S, Sr, CaO and iron levels, which differ from the Hellenistic samples. This suggests that the ziggurat's construction may have involved distinct phases or specialised material treatments to enhance durability.

The combined PCA and ternary plot analyses offer a complementary view of the geochemical composition of Assur's construction materials. The Hellenistic period is characterised by distinctive material compositions with higher levels of P_2O_5, S, Sr, Zr, and CaO, whereas Assyrian samples reflect more uniform construction practices. The ziggurat samples (Old Assyrian) also display variability, suggesting that specialised materials were used in certain parts. Across all material types, reliance on locally sourced silica-rich clays is evident, with minimal lime or other additives except in specific cases, such as in the ziggurat. High iron content in reference soils suggests natural enrichment, while construction materials show modifications due to firing or adding specific stabilisers. These findings contribute to a nuanced understanding of technological advancements and material selection in ancient Assur. The ternary plot enhances this understanding by emphasising the importance of silica-rich clays, the selective use of lime, and the consistency in raw material sourcing across different periods and structures. It reinforces the narrative of material sourcing and technological practices suggested by the PCA results.

G5.3 Technological perspectives

Variations in organic matter and $CaCO_3$ content in Assur's mudbrick samples shed light on construction technologies and material processing techniques across periods and contexts. In the Neo-Assyrian urban structures, the low organic matter paired with higher $CaCO_3$ content suggests organised material selection to minimise decomposition risk and maintain structural integrity over time. The elevated $CaCO_3$ content points to using calcitic clay and/or calcitic inclusions in the building materials, enhancing the mudbricks' durability. This indicates that builders had a sophisticated understanding of material properties, adapting techniques to suit different construction needs, whether prioritising durability in urban buildings, volume and strength in fortifications, or standardised processes in monumental structures.

H. Human remains from Assur, 2023 and 2024

Rafał A. Fetner

H1. Registration, sampling and method of analysis

This chapter presents the results of the osteological analysis conducted in the field by the present author in March 2024 on the human remains unearthed at Assur during the 2023 and 2024 excavation campaigns (**Table H1**). The human remains from the chamber tomb (Grave 1), also excavated in 2023, are not included in this study as they are still undergoing analysis. During the fieldwork study, the human remains were documented following the established procedures outlined by Buikstra and Ubelaker,[318] as well as Brickley and McKinley.[319]

In addition to documenting the human remains, several samples were collected during the fieldwork for various scientific analyses, namely radiocarbon dating, DNA analysis, strontium isotope analysis, and parasitological examination. Radiocarbon dating samples were taken from Graves 3, 8, and 9; however, only the sample from Grave 9 contained sufficient collagen for accurate dating (see **Table H1** and **§C1.2)**. For DNA analysis, samples from Graves 6, 8, 9, and the chamber tomb were selected and sent in May 2024 to the Max-Planck-Institut für Evolutionäre Anthropologie in Leipzig for extraction and analysis. For strontium isotope analysis, bone samples were collected from Graves 3, 9, and the chamber tomb. Modern plant samples from the Assur area were also collected to provide comparative data. Finally, parasitological samples were gathered from Graves 3, 4, 7, and 10. The samples for strontium isotope and parasitological analyses were exported to Germany in May 2024 and forwarded to the author at the Department of Archaeology, University of Warsaw, for further examination. The findings from these analyses will be published in separate studies.

The following sections present the results of the osteological analysis from Graves 3, 4, 5, 6, 7, 8, 9 and 10, covering skeletal descriptions, age-at-death estimates, stature and sex determinations, and any observed pathological changes. To maintain clarity, the completeness of the human skeletons is summarised in a concise, descriptive format.

The age-at-death was initially determined based on the degree of physiological development of the bones (subadults and adults), with further age refinement applied in subsequent analytical stages. For subadults, age estimation was based on the degree of bone development, including measured bone length,[320] the development of deciduous and permanent teeth,[321] and the degree of tooth eruption.[322] Adult age was determined based on the morphology of the pubic symphyseal surface[323] and the auricular surface of the ilium,[324] the sternal ends of the ribs,[325] and the degree of dental wear on permanent

Grave no.	Bone collection	MNI	Sex determination	Age-at-death	Pathologies	Period/Date
Grave 3	AS 262433:060:013	1	female	young adult	osteoarthrosis, Schmorl's nodes	159/158 BC (alphabetic inscription)
Grave 4	AS 262432:055:001	1	female	young adult	osteoarthrosis	Hellenistic
Grave 5	AS 262432:070:002	1	female	young adult	periostosis, osteoarthrosis , porotic hyperostosis, linear enamel hypoplasia	770-542 calBC and 775-545 calBC (95.4%)
Grave 6	AS 261433:031:001	1		infant		Parthian
Grave 7	AS 262433:097:001	1	female (?)	young-middle adult		Parthian
Grave 8	AS 262433:093:002	4	male, male, female, female (?)	young adult, middle adult, middle adult, middle adult (?)	osteoarthrosis	Parthian
Grave 9	AS 262433:094:002	2	female, unknown	senile adult, adolescent	osteoarthrosis	130-236 calAD (95.4%)

Table H1: Summary of the osteological analysis of the human remains unearthed in Assur, 2023 and 2024. Prepared by Rafał Fetner.

318 Buikstra/Ubelaker 1994.
319 Brickley/McKinley 2004.
320 Schaefer/Black/Scheuer 2009.
321 Smith 1991.
322 Ubelaker 1989.
323 Brooks/Suchey 1990.
324 Lovejoy *et al.* 1985.
325 İşcan/Loth/Wright 1984; 1985.

teeth.[326] Age-at-death was expressed in the following categories: infant (birth–3 years of age), child (3–12 years of age), adolescent (12–20 years of age), young adult (20–35 years of age), middle adult (35–50 years of age), and old adult (more than 50 years of age).

The sex of adults was determined based on sexual dimorphism traits in the skull, as recommended by Buikstra and Ubelaker,[327] as well as sexual dimorphism in the pubic bone,[328] the ilium,[329] and measurements of the proximal and distal ends of the humerus[330] and femur.[331]

Stature was estimated based on measurements of the maximum length of long bones using regression equations.[332]

Pathological changes were documented following the standards established by Brickley and McKinley,[333] taking into account the type of bone, body side, affected area, detailed descriptions of the alterations, and relevant measurements. Diagnoses were made based on the operational definitions proposed by Waldron and the diagnostic guidelines outlined by Buikstra.[334]

H2. Results of the osteological analysis

The results of the osteological analysis are presented below according to the grave identification number.

H2.1 Grave 3 (159/158 BC)

Grave 3, excavated in 2023, yielded an inverted sarcophagus bearing an alphabetic inscription that reports the date 159/158 BC.[335] Below the sarcophagus, the skeleton of the adult individual was preserved in parts of the skull, the cervical, thoracic, lumbar, and sacral vertebrae, the shoulder girdles, the right, and left humeri, forearms, hand bones, the pelvic girdle, femora, and lower leg bones of both sides and the foot phalanges. Additionally, some molar and incisor teeth were preserved.

The sex of the individual was determined to be female, based on the sexual dimorphism of the pubic bone, where the presence of a subpubic concavity was noted, and the pubic angle was wide. A preauricular sulcus was observed on the ilium (grade 3 on both the right and left sides). It was also possible to measure the diameter of the humeral head (38 mm). The age-at-death of the individual was determined solely based on the morphology of the pubic symphyseal surface (phase 2), corresponding to the young adult age category. The individual's stature was estimated based on the length of the radius (235 mm) to be 161.8 cm.

Among the pathological changes, osteoarthrosis was identified on the articular surface of the coracoid process of the left scapula, and Schmorl's nodes were observed on four thoracic vertebrae, one of which also exhibited osteoarthrosis on the articular surface. These changes are not typical for a young adult and indicate spinal overloading, either systematic or due to exertion beyond the spine's accustomed load. Similarly, osteoarthrosis in the acromioclavicular joint, one of the more common pathological changes in humans, was also present.

H2.2 Grave 4 (mid-2nd century BC)

Grave 4, unearthed in 2023, yielded an inverted sarcophagus similar to that of Grave 3 but without an inscription. It is assumed to date to the same period as Grave 3.[336] Under the sarcophagus, the skeleton of the adult individual was preserved in parts of the skull, cervical, thoracic, lumbar, and sacral vertebrae, thorax, shoulder girdle, both humeri, forearm bones, and hand bones, as well as the pelvic girdle, femora, lower leg bones, and foot bones.

The sex of the individual was determined to be female based on sexual dimorphism traits of the pubic bone, including the presence of a subpubic concavity, absence of a ventral arc, a narrow ischiopubic ramus ridge, and a wide subpubic angle, as well as traits of the ilium, with the preauricular sulcus graded as 2.

The age-at-death of the individual was estimated based on the morphology of the pubic symphyseal surface (phase 3) and the sternal end of the rib (phase 2). Both indicators correspond to the young adult age category.

The only pathological change observed in this individual was osteoarthrosis on the articular surface of a thoracic vertebra. Similar to the individual from Grave 3, osteoarthrosis at a young adult age is less common, and this change in the spine suggests occasional activities that placed strain on this structure beyond its normal capacity.

326 Lovejoy 1985.
327 Buikstra/Ubelaker 1994.
328 Phenice 1969.
329 Walker 2005; Steckel *et al.* 2018.
330 Mall *et al.* 2001.
331 Šlaus *et al.* 2003.
332 Ruff *et al.* 2012.
333 Brickley/McKinley 2004.
334 Waldron 2008; Buikstra 2019.
335 Gzella 2024.
336 Kreppner/Rohde/Squitieri 2024, 121.

H2.3 Grave 5 (Neo-Assyrian)

Grave 5 was a pit grave identified in 2023. Two molars retrieved from this grave were radiocarbon dated to 770-542 calBC and 775-545 calBC (both 95.4% probability).[337] The characteristic burial goods establish the Neo-Assyrian date of this burial.[338] The skeleton of an adult individual was preserved in parts of the skull, cervical, thoracic, lumbar, and sacral vertebrae, thorax, shoulder girdle bones, humeri, both forearms and hands, pelvic girdle, both femora, lower leg bones, and foot bones. Among the remains was a single bone (the shaft of a femur) belonging to another individual.

The sex of the individual was determined to be female based on the morphology of the mastoid process of the temporal bone (grade 3) and the diameter of the femoral head (39 mm). The age-at-death of the individual was estimated as young adult, based on the sternal end of the clavicle in the process of fusion.

The individual bore extensive bone changes, particularly on the distal ends of the legs and foot (**Fig. H1**). New bone formation, namely porous bone tissue deposited on the surface of the compact bone without any signs of penetration into the cortical bone, was noted in several locations on all the metatarsals of the left foot and two metatarsals of the right foot, on the distal ends of both the tibiae and fibulae, as well as on the left ulna. These changes are indicative of chronic periostosis in areas free from muscle attachments, where there is only a thin layer of skin.

Additionally, osteoarthrosis was noted on the navicular bone, and an advanced stage of porotic hyperostosis (**Fig. H2**) in the process of healing was observed on the parietal bones, typically associated with anaemia. Linear enamel hypoplasia was recorded on the incisor and canine teeth, indicating that this individual had survived a non-specific stress episode during childhood, leaving marks on their teeth in the form of underdeveloped enamel (hypoplasia). This condition can be caused by various disruptions, and it is generally not recommended to diagnose a specific cause beyond acknowledging the occurrence of a physiological stress episode. During the individual's life, signs of porotic hyperostosis also developed, a condition often associated with megaloblastic anaemia, typically caused by a deficiency in vitamin B12, which is primarily found in meat and animal-derived products. At the time of death, this condition was in the process of healing, suggesting that before death, the individual received the necessary

Fig. H1: Case of multi-loci new bone formation on left metatarsals. Photo by Rafał Fetner.

Fig. H2: Close-up of the parietal bone surface with visible healing signs of porosity, an indicator of porotic hyperostosis. Photo by Rafał Fetner.

nutrients to reduce the volume of red marrow and attempt to restore the integrity of the compact bone on the skull.

Another significant factor is the changes observed on the distal surfaces of the lower legs and feet. This type of non-specific inflammation is commonly a result of trauma or bacterial infection, such as a skin infection or wound. No injuries were noted on the surfaces of the foot bones, which does not exclude the possibility of soft tissue wounds that could have served as an entry point for

337 Kreppner/Rohde/Squitieri 2024, 130-132.

338 Kreppner/Richter/Squitieri 2024, 147; Squitieri 2024, 178-179

bacteria. The porotic hyperostosis and periostosis coexisted for several years before the individual's death. These conditions may have been unrelated or manifestations of a non-specific metabolic disease.

H2.4 Grave 6 (Parthian period)

Grave 6 was a pit grave identified during the 2024 campaign (**§C2.5.1**). The skeleton of a subadult individual was preserved in parts of the skull and mandible, including both permanent and deciduous teeth, the cervical, thoracic, and lumbar vertebrae, thorax, both clavicle and humeri, the right forearm and metacarpal bones, iliac bones, both femora and fibulae, as well as the metatarsal bones.

The individual's age-at-death can be estimated based on the development of the first permanent molars (Cr3/4) as two years, corresponding to the infant age category.

H2.5 Grave 7 (Parthian period)

Grave 7 was a pit grave identified in 2023, whose excavation was completed in 2024 (**§C2.5.1**). The adult individual was preserved in parts of the skull, cervical, thoracic, and lumbar vertebrae, thorax, both clavicles, humeri, ulnae, the right radius, both wrists, the right metacarpals, hand phalanges, and both pelvic bones.

The individual's sex can be tentatively determined based on the presence of a weakly pronounced preauricular sulcus (grade 2). This feature is more commonly observed in females but is not uncommon in males.

The age-at-death can be estimated based on the sternal end of a true rib (phase 5), corresponding to the young and middle adult age category.

H2.6 Grave 8 (Parthian period)

Grave 8, excavated in 2024 (**§C2.5.2**), contained a tub sarcophagus in which the remains of at least four individuals were found. This number was estimated based on the presence of a right talus, a left ischium, and a proximal tibia. Where possible, bones belonging to different individuals were distinguished. Remains from all skeletal elements and permanent teeth were well-represented.

The sex of the individuals was determined based on the sexual dimorphism traits of the right pubic bone (1. absence of a subpubic concavity, 2. presence of a subpubic concavity, 3. absence of a subpubic concavity), and the left pubic bone (presence of a subpubic concavity). Based on these, it can be inferred that at least two males and one female were present. Further support comes from measurements of the humeral and femoral heads. The femoral head measurements are as follows: a pair of heads (right and left) measuring 44 mm each, a right femoral head measuring 40 mm, and an unclassified femoral head measuring 45 mm. These likely represent at least three individuals of different sizes, all of whom can be classified as female. Two measurements from the humeral head diameter (40 mm) and bicondylar width (54 mm) also indicate a female. The only sexually dimorphic cranial feature present (slightly pronounced glabella—grade 2) is more commonly observed in females. In summary, the grave contained the remains of at least four adult individuals, including two short-statured males and at least one, possibly two, females.

The age-at-death of the individuals can be determined based on the morphological development of the pubic symphyseal surface: the lowest grade (2), found on the right pubic bone along with the absence of a subpubic concavity (one of the males), indicates a young adult; two other right pubic symphyseal surfaces with a grade of 4 suggest two middle adult individuals. Two preserved left pubic bones (phases 4 and 5 of development) indicate two middle adults. Age can also be estimated based on the degree of dental wear on the permanent teeth. One individual's molar wear (grades 2 and 3) corresponds to stage G, indicating a middle adult. In conclusion, the collection predominantly consisted of individuals in the middle adult age category, with one male in the young adult category.

Among the pathological changes, secondary osteoarthrosis was noted on one metacarpal bone, associated with a prior fracture. Secondary osteoarthrosis is a common consequence of fractures near joints.

H2.7 Grave 9 (Parthian period)

Grave 9, also excavated in 2024 (**§C2.5.2**), yielded a tub sarcophagus which contained the remains of at least two individuals. A molar collected from this grave was radiocarbon dated to 130–236 calAD (95.4%). The number of individuals was estimated based on bones that still showed signs of development, including the humerus, left ilium, metatarsal bone, sacrum, and right tibia.

The skeleton of the physiologically mature individual was preserved in parts of the mandible with teeth, cervical, thoracic, and lumbar vertebrae, thorax, scapulae and clavicles, humeri, ulnae, wrists, metacarpals and hand phalanges, pelvic bones, femora, lower leg bones, tarsals, and metatarsals.

The sex of the physiologically mature individual can be determined based on sexual dimorphism traits of the

pelvis: the preauricular sulcus is well and very well-developed (grades 3 and 4, respectively, for the left and right ilium), a trait more commonly found in females and rarely in males.

The age-at-death of this individual was estimated based on the morphology of the auricular surface (grade 8 and 7 for the left and right ilium, respectively) and the morphological variability of the sternal rib ends (two bones with grade 5), indicating an old adult age (over 50 years).

The age-at-death of the younger individual can be determined based on the degree of physiological development of the bones: the fusion of the first rib head (17–25 years), the absence of fusion in the iliac crest (under 18 years), and the degree of molar wear corresponding to phase B2 (16–20 years), placing this individual in the adolescent age category.

The observed pathological changes are typical of advanced age and should be associated with the older individual. These include osteoarthrosis on the cervical vertebra body and the articular surfaces of the thoracic and lumbar vertebrae, which, similar to previous individuals, are likely related to spinal strain.

H2.8 Grave 10 (period unclear)

Grave 10 is a pit burial identified in trench NT2 (**§C4.1**). The skeleton of a subadult individual was preserved in parts of the skull with teeth, the spine and chest, both humeri and forearms, as well as the lower limb bones.

The individual's age-at-death can be estimated at 2 years of age based on the development of the first permanent molars (Cr3/4).

H3. Preliminary conclusions

During the 2023 and 2024 campaigns at Assur, the remains of 12 individuals were found (in addition to the not yet analysed remains from the Parthian-period chamber tomb), spanning from the Iron Age to the Parthian period, with the majority being female skeletons in the young adult age category. The youngest individuals buried were around 2 years old. The most common pathological conditions were joint diseases, which are frequent among humans. However, their prevalence in younger adults was somewhat surprising. These primarily consisted of spinal conditions related to physical activity. In the case of one young adult female (Grave 5), there is a possibility of a non-specific metabolic disease that affected various skeletal elements.

I. Plant remains from Assur, 2024

I1. Wood identifications from charcoal remains of the 2024 season at Assur

Katleen Deckers

The results from the 2023 excavation season offered an initial glimpse into vegetation patterns and wood use at Assur.[339] Building on this foundation, five additional charcoal samples from the 2024 campaign underwent analysis, the results of which are presented in this chapter. These samples comprise 118 newly identified fragments. Three samples are attributed to the Hellenistic period and are associated with Building A, while the remaining two originate from Iron Age and Late Bronze Age contexts (**Table I1.1**).

The charcoals were identified using standard methodology, i.e., microscopic investigations of transversal, tangential, and radial sections with varying magnifications between 60× and 500×, depending on the intended diagnostic features to be investigated. The Tübingen charcoal reference collection and identification literature were used for this.[340]

A minimum of six taxa were identified amongst the 2024 samples (**Table I1.1**): *Alnus*, *Populus*, *Salix*, *Quercus*, *Tamarix* and indeterminate Dicoyledoneae. While *Populus*, *Salix*, and *Tamarix* were identified in the previous season's samples, *Quercus* and *Alnus* represent newly discovered taxa from Assur. For a few of the fragments that were too small, it could not be discerned whether it was *Quercus* or *Castanea*, though it was most likely *Quercus*, as it could be identified more precisely from other fragments in these samples.

Considering the region's climatic conditions, only receiving approximately 250 mm of rainfall annually, making it unsuitable for *Quercus* growth, the wood from this tree was likely imported to the site.[341] *Alnus* represents a possibly local taxon from the riverine environment,[342] though it is not reported as part of the local riparian vegetation today.[343] However, even along the Euphrates, it seems to have occurred more extensively in the past as well.[344]

Adding the 2024 season identification results to those of the previous season for Building A[345] (**Fig. I1.1**), we observe a dominant presence of likely local taxa within the complex, such as *Tamarix*, *Populus*, *Salix*, and *Alnus*, that were all possibly belonging to the Tigris riverine woodland. *Lycium* was also likely locally available, though it was retrieved further away from the river. In contrast, *Abies* and *Quercus* represent imported taxa from a further distance, while *Juglans* is a cultivated taxon (**Fig. I1.1**). The latter is not grown today in the surroundings of Assur since the climate and soil conditions are not ideal for it, as it is too hot and dry, and the soils are too shallow, saline, and alkaline. It occurs today at higher elevations, such as Pirmam, Shaqlawa, Soran, and Choman, c. 130 km to the northeast in what is today the Kurdish Autonomous Region of Iraq.[346] This is also the zone/direction from which *Quercus* may have derived.[347]

There is some variation in the distribution of taxa within the different rooms of Building A (**Fig. I1.2**). All rooms have *Populus*/*Salix*, and most also *Tamarix*. Imported taxa were found in Rooms 2, 3, and 5, represented by *Quercus*

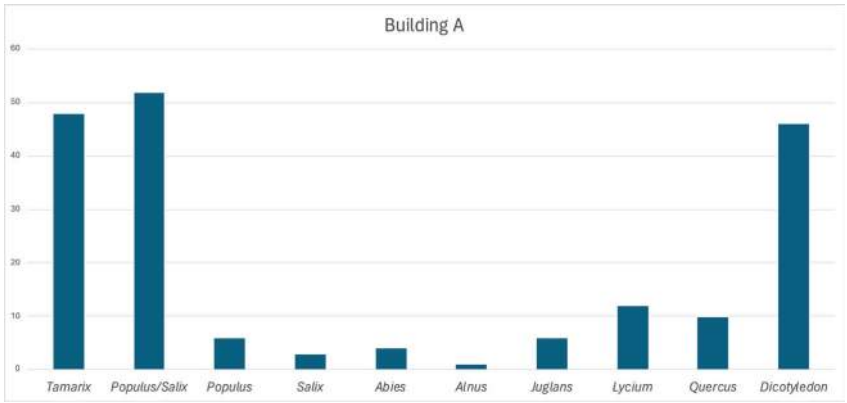

Fig. I1.1: Results of wood analysis from Hellenistic Building A (2023 and 2024 excavations). Prepared by Katleen Deckers.

339 Deckers 2024.
340 e.g., Fahn/Werker/Baas 1986; Gale/Cutler 2000; Schweingruber 1990; Crivellaro/Schweingruber 2013.
341 Khwarahm 2020.
342 Pessin 2004.
343 Handel-Mazzetti 1914.
344 Deckers/Pessin 2010.
345 Deckers 2024, fig. H2.1.
346 Ragheb Kamal Mohammad, personal communication, 2023.
347 Khwarahm 2020.

Sample AS no.	Context	Context information	Date/Period	Retrieval method	*Alnus* sp.	Dicotyledon	*Populus* sp./*Salix* sp.	*Populus* sp.	*Quercus* sp., deciduous	*Quercus* sp.	*Quercus* sp./ *Castanea* sp.	*Tamarix* sp.	*Salix* sp.
AS 263432:021:004	Sondage 2	Fill of a pit cutting the virgin soil below a building, charcoal from bottom of pit	1406-1261 calBC (see **Table C1.1**)	handpicked			24	3					
AS 254433:038:005	Trench NT2	Fill	770-541 calBC (see **Table C1.1**)	handpicked					5	3			
AS 262433:156:002	Building A	"Room 5", originally a silo that was likely used as refuse pit when the building was abandoned.	Hellenistic	flotation	1	30	18			7	3	4	
AS 261433:046:017	Building A	Floor deposit of Room 2	Hellenistic	handpicked			2						
AS 261433:040:003	Building A	Floor deposit of Room 1	Hellenistic	handpicked			12	4					2

Table I1.1: Charcoal identification results of the 2024 campaign samples. Prepared by Katleen Deckers.

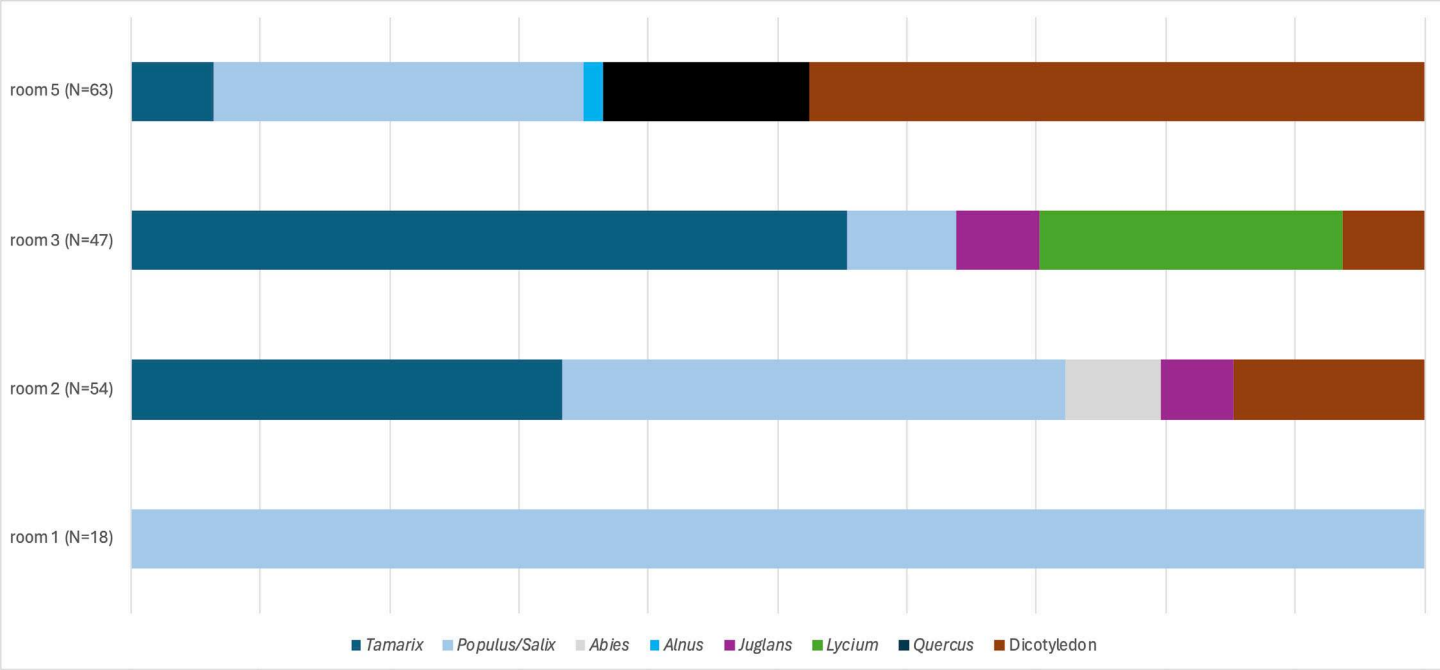

Fig. I1.2: Results of wood analysis from Hellenistic Building A (2023 and 2024 excavations), sorted per room. *Quercus/Castanea* is indicated as *Quercus*. Prepared by Katleen Deckers.

in "Room 5," *Juglans* in Room 3, and *Juglans* and *Abies* in Room 2. *Lycium* was only represented in Room 3, and *Alnus* was only found in "Room 5."

In addition to the Hellenistic period samples from Building A, one Iron Age sample (AS 254433:038:005) was identified from the NT2 trench and a Late Bronze Age sample from Sondage 2 (AS 263432:021:004). While the latter contained only *Populus*/*Salix* fragments, the former contained *Quercus*. The presence of this taxon indicates that this wood was already being imported into Assur in the Iron Age.

In conclusion, the charcoal identifications shed new light on wood use and vegetation at Assur. The results show a variety of wood species used, some of which were likely locally available, while others were imported. The importation of wood from a further distance may relate to a scarcity of local wood resources and/or the high status of the users of this wood, and overall, it indicates long-distance connections.

I2. Plant identification from light fraction samples of the 2024 season at Assur

Claudia Sarkady

I2.1 Methodology: field sampling, sample processing in the lab and palaeobotanical identification

During the 2024 excavation season at Assur, 10 soil samples and one hand-picked sample for palaeobotanical analysis were collected from the following contexts (see also **Table I2.1**):

- the fill of Pit 7 (Parthian period);
- the floor deposits in Rooms 5, 7, and 8 of Building A (Hellenistic period);
- the floor deposit in Room 11 of Building B (Late Iron Age);
- the fills in Sondage 2 (Late Bronze Age to Iron Age);
- the fills in trench NT2 (Late Bronze Age to Parthian period).

The hand-picked sample was comprised of date stone remains recovered during the excavation of Pit 7.[348] Meanwhile, the 10 soil samples were collected from the floor deposits of Rooms 5, 7, 8, and 11, following a slightly modified protocol compared to the 2023 campaign.[349] Instead of using a floor grid to collect multiple soil samples, only one sample was taken per floor deposit. This adjustment was necessitated by significant disturbances in these rooms, caused by later pits, graves, and wall collapses, which complicated the identification of intact floor deposits. Consequently, soil samples were collected exclusively from areas where the floor deposits could be confidently associated with the rooms' original phase of use.

After collection, the soil samples were processed on-site by Jana Richter, Andrea Squitieri and Poppy Tushingham using the flotation machine that was also used during the 2023 campaign[350] in order to separate the light fraction (floating material containing plant remains) from the heavy fraction (non-floating material). Due to the varying archaeological contexts from which the samples were collected, the soil sample volumes ranged from 1.5 to 23.5 litres (**Table I2.1**). In total, 85 litres were processed using a mesh size of less than 1 mm. The heavy fraction, upon inspection, was found to contain no residual plant material and was therefore left in Assur. The light fraction samples were sun-dried in bags on a clothesline before being packed in plastic bags.

The samples were subsequently exported to Munich in May 2024 by Jana Richter and Poppy Tushingham, and they were then handed over to the present author for palaeobotanical analysis. The analysis was conducted at the Archaeobotanical Laboratory in Eggstätt, Germany, operated by the author. All charred and uncharred specimens were identified from each sample under a low-power stereo-microscope manufactured by Helmut Hundt GmbH in Wetzlar (Germany) with 6.7 to 45× magnification. The light fraction samples contained 107.9 grams of charred and uncharred plant seeds, for a total of 6252 seeds. Of these, 5317 were identified as belonging to cultivated species, while 935 were from wild plants. Notably, the number of seeds recovered during the 2024 campaign is not far from that of the 2023 campaign (N=8665) despite a total of 32 samples being collected during the latter.[351]

Plant material	**2023 campaign**	**2024 campaign**
Total seeds	8665	6252
Total cultivar count	5207	5317
Total wild plants	3458	935
Total cereal chaff	54	44
Cultivated/wild plants	3/2	28/5

After the analysis, each specimen was conserved in gelatin capsules to avoid further damage and then placed in small rectangular plastic boxes.

348 On hand-picked samples in palaeobotanical analysis, see van der Veen 2011, 17.

349 Radner/Squitieri 2024b, 96-97.

350 Radner/Squitieri 2024b, 96-97.

351 Sarkady 2024, 202.

Sample ID	Context	Context period	Short context description	Volume (lt)
AS 261433:061:012	Pit 7	Parthian	Fill	Hand-picked sample
AS 262433:156:002	Building A "Room 5"	Hellenistic	Floor deposit	2
AS 262433:107:014	Buidling A Room 8	Hellenistic	Floor deposit	23.5
AS 262433:110:002	Building A Room 7	Hellenistic	Floor deposit	13
AS 262433:158:001	Building B Room 11	Iron Age	Floor deposit	5
AS 263432:012:003	Sondage 2	Middle Bronze Age	Fill of drainage (see **Table C1.1**)	20
AS 263432:016:005	Sondage 2	Iron Age	Deposit on pebble floor, below the drainage Locus:263432:012. (see **Table C1.1**)	2.5
AS 263432:021:003	Sondage 2	Late Bronze Age	Fill of a pit cutting the virgin soil (see **Table C1.1**)	2.5
AS 263432:021:005	Sondage 2	Late Bronze Age	Fill of a pit cutting the virgin soil (see **Table C1.1**)	11
AS 254433:036:002	NT2	Iron Age to Parthian	Fill in trench NT2, stratigraphic Phase 2	1.5
AS 254433:037:002	NT2	Iron Age to Parthian	Mud surface in trench NT2, stratigraphic Phase 2	4

Table I2.1: List of the 2024 campaign flotation samples arranged by context. Prepared by Andrea Squitieri.

The author carried out the plant identification with the use of specific seed atlases[352] and a reference collection of modern seeds collected by the author herself in Syria. The reference collection was adequate for cultivated plants such as cereals, but the representation of the wild flora was insufficient for detailed determinations. The descriptions and drawings published in archaeobotanical papers of other sites in the Near East were very helpful, especially those of van Zeist and Bakker-Heeres.[353] Thanks to this reference material, most plant remains could be identified among the Assur samples.

I2.2 Overview of the plant identifications

The results of the seed identifications are summarised in **Table I2.2**.[354] For each sample, the archaeological context, the pre-flotation volume, the total weight with packaging (g), and the net weight (g) are provided. The table is divided into two sections: the first lists cultivated plants, and the second lists wild plants (broadly referred to as weeds). Both sections are organised alphabetically by the full scientific plant names in Latin, with the standard English names included where applicable.[355]

The nomenclature and classification of the taxa follow the traditional names of morphological species.[356] Taxa were identified to the species level in cases of good preservation, otherwise, they were identified to genus or family. In cases where specimens were poorly or partially preserved, making the identification uncertain, the prefix cf. (for Latin *confer* "compare") is used before the botanical name. This indicates a close but not definitive identification, either at the genus or species level.[357] The abbreviation sp. (for Latin *species* "species") in some cases indicates that determination of the exact species was not possible.[358] All samples contained a certain number of charred plant remains that could not be determined, not even to the classification level of the family. They are classified in the group of indeterminate seeds (abbreviated as indet. for Latin *indeterminata* "indeterminates"). These were small fragments of badly preserved charred seeds, seeds without recognisable surface structure, small twigs/stems, and lumps of seeds of undefined shape that were stuck together (called amorphous objects in the table). These fragments may represent remnants of bread or porridge with their characteristic porous and irregular surfaces. Many seeds, especially cereal grains, were preserved only in small, porous, highly distorted fragments, which are unidentifiable (Cerealia indet. in the table). The scarcity of carbonised plant remains is often due to preservation issues, particularly in saline soils, where preservation tends to be poor. Additionally, dust storms can lead to rapid sedimentation at a site, resulting in a low concentration of botanical remains and contributing to the fragmentation of grains.[359]

In addition to plant remains (seeds, fruits, stems), **Table H2.2** also includes other material classes that were identified, such as charcoal, animal bones, insect remains, molluscs, and small artefacts. These are listed in the third section of the table under "Varia." Medium-sized

352 Cappers/Bekker/Jans 2012; Beijerinck 1976.

353 van Zeist/Bakker-Heeres 1982; 1984a; 1984b; 1985.

354 For detailed information about the plant families listed in the table and in the present text, see Sarkady 2024.

355 For the English names of plants, see Erhardt *et al.* 2008.

356 Oberdorfer 1990; Zohary/Hopf/Weiss 2012.

357 van der Veen 2011, 17.

358 This procedure is consistent with the publications of van Zeist and Bakker-Heeres.

359 Neef 1991, 321.

Archaeobotanical Laboratory CS Claudia Sarkady														
Assur 2024, Archaeobotanical Investigations: Pit 7, Building A (Rooms 5,7,8), Building B (Room 11), Sondage 2, trench NT2														
	Context	Pit 7	Building A "Room 5"	Building A Room 7	Building A Room 8	Building B Room 11	Sondage 2	Sondage 2	Sondage 2	Sondage 2	Trench NT2	Trench NT2		
	Sample ID (AS number)	261433:061:012	262433:156:002	262433:110:002	262433:107:014	262433:158:001	263432:012:003	263432:016:005	263432:021:003	263432:021:005	254433:036:002	254433:037:002		
	Volume of samples (l)	0.0	2.0	13.0	23.5	5.0	20.0	2.5	2.5	11.0	1.5	4.0	85.0	
	Weight incl. package (g)	6.0	17.6	9.1	15.3	9.1	42.7	8.7	6.9	35.9	9.2	12.3	172.8	
	Netweight (g)	0.1	11.7	3.2	9.4	3.2	36.8	2.8	1.0	30.0	3.3	6.4	107.9	
TAXA	TAXA													Nm*
CEREALS	**CEREALS**												**Sum**	Ubiquity %
Hordeum vulgare	barley, grains			2	3	2	4		2	12		4	29	7 63.6
cf. *Hordeum vulgare*	prob. barley, grains				2								2	1 9.1
Hordeum vulgare	barley, internodes			1			3						4	2 18.2
Hordeum vulgare	barley, rachis nodes						7	4					11	2 18.2
Hordeum vulgare	barley, glume base						1						1	1 9.1
Triticum dicoccum	emmer wheat, grains		1		1								2	2 18.2
Triticum dicoccum	emmer wheat, spikelet fork		1					1					2	2 18.2
Triticum dicoccum	emmer wheat, glume base								1				1	1 9.1
Triticum monococcum	einkorn wheat, spikelet fork					2	1	2		2		1	8	5 45.5
Triticum monococcum	einkorn wheat, glume base								2				2	1 9.1
Triticum sp.	wheat grains indet.				1				3	4		239	247	4 36.4
Triticum sp.	wheat grains indet., rachis						2						2	1 9.1
Triticum sp.	wheat grains indet., spikelet fork						1						1	1 9.1
Cerealia indet.	cereal grains indet.		20	217	301	136	2650	165	305	1176	56		5026	9 81.8
Cerealia indet.	cereal spikelet fork						2						2	1 9.1
Cerealia indet.	cereal glume base									5			5	1 9.1
Cerealia indet.	cereal rachis nodes				1	2	1			1			5	4 36.4
OTHER FOOD PLANTS	**OTHER FOOD PLANTS**													
Lens culinaris	lentil		3						1	1			5	3 27.3
Vitis sp.	grape species, kernel						1						1	1 9.1
WILD PLANTS	**WILD PLANTS**													
Aegilops sp.	goat grass				1	5	2					1	9	4 36.4
Aizoon hispanicum	spanish aizoon						4						4	1 9.1
Apiaceae	parsley family					1							1	1 9.1
Astragalus sp.	milk vetch		2			2			3	13			20	4 36.4
Bromus sp.	brome grass									6			6	1 9.1
cf. *Carex divisa*	prob. divided sedge								3				3	1 9.1
Coronilla sp.	scorpion weed				1		1	2		4		1	9	5 45.5
Echinochloa	coxspur									2			2	1 9.1
Eremopyrum sp.	annual wheatgrass									11			11	1 9.1
Fabaceae	legumes						5		1	1	2		9	4 36.4
Fumaria densiflora	flowered fumitory									1			1	1 9.1
Galium spurium	false cleaver		1										1	1 9.1
Galium sp.	bedstraw						49	1	2	14		3	70	6 54.5
cf. *Glaucium* sp.	prob. horned poppy					1	1			1			3	3 27.3
Lithospermum arvense	field gromwell		16	17	90	13		22	5	6			169	7 63.6
Lotus sp.	trefoil						46						46	1 9.1
Malva sp.	mallow			1	4	1	6	1		4		1	18	7 63.6
Medicago sp.	bur clover			1	2	2	9	1	4	10		6	35	8 72.7
Melilotus sp.	melilot			6	4	1	1			15		2	29	6 54.5
cf. *Melilotus* sp.	melilot				7								7	1 9.1
Onobrychis sp.	sainfoin						3						3	1 9.1
Phoenix dactilifera	date palm	7											7	1 9.1
Plantago ovata	blond psyllium									1			1	1 9.1
Plantago lagopus	hare's foot plantain									1			1	1 9.1
Poaceae	grass family		5	2	14	9	13	3	9	46	1	3	105	10 90.9
Rumex pulcher	fiddle dock									1			1	1 9.1
Salsola sp.	Russian thistle						4						4	1 9.1
Scirpus maritimus	saltmarsh bulrush									3			3	1 9.1
Suaeda sp.	sea blite							1	4	2			7	3 27.3
Teucrium sp.	germander				1							1	2	2 18.2
Trifolium sp.	clover						1						1	1 9.1
Trigonella sp.	fenugreek							1		3			4	2 18.2
Vaccaria pyramidata	cowherb			1					2				3	2 18.2
Indet. seeds	Indeterminate seeds		6	23	37	10	68	17	24	122	6	28	341	10 90.9
Indet. stem	Indeterminate stem		4	5	7	11	13	13		34		1	88	8 72.7
Indet. seed shell	Indeterminate seed shell		6	12	8	17		4	6	30	2		85	8 72.7
													6464	
	Total	7	65	288	485	215	2899	238	377	1532	67	291	6464	
	density (seeds/litres)		32.5	22.2	20.6	43.0	145.0	95.2	150.8	139.3	44.7	72.8	76.0	
Varia	**Varia**													
	Wood charcoal (pieces)		577			1120				63			1760	
	Amorphous objects		2	1	2	3	15			39	3	11	76	
	Bone fragments (pieces)		6	6	6	2		415		17	1	1	454	
	Insect remains						6	3					9	
	Molluscs		1	2	2	1				1			7	
	Other finds									1 bead			1	
	Number of samples	1	1	1	1	1	1	1	1	1	1	1	11	

Table I2.2: List of plant remains recovered through flotation during the 2024 campaign. Prepared by Josef Grabmayr and Claudia Sarkady.

carbonised wood fragments were found only in samples AS 262433:156:002 and AS 263432:021:005, while charcoal fragments in other samples were too small to be recovered. Charcoal, zoological remains, and artefacts are not discussed in the present study (but see **§I1** for the charcoal remains from sample AS 262433:156:002).

Table I2.2 also presents values for density and ubiquity, commonly used by archaeobotanists to compare samples of varying sizes. Seed density is expressed as the number of seeds per litre of processed soil, while ubiquity, or relative abundance (also called percentage presence), indicates the percentage of samples in which a particular plant species is found.[360] The seed density value was beneficial for comparing samples of different sizes that were collected in the 2023 and 2024 campaigns (see also below **§I2.4.4**).

I2.3 Plant remains from Pit 7 (Parthian period)

AS 261433:061:012 is a hand-picked sample collected from the fill of Pit 7, which cut the floor of Building A Courtyard 10 and was assigned to the Parthian period (**§C2.7**). Seven fragments of a date palm stone (*Phoenix dactylifera*) from the palm family (Arecaceae) were identified; however, it is unclear whether they belong to the same kernel. Date fruits are cylindrical and contain a single stone. The largest fragment in this sample, which is exceptionally well-preserved, exhibits the characteristic large ventral groove. For a discussion about the presence of date palms in Assur, see **§I2.9**.

I2.4 Plant remains from Building A (Hellenistic period)

Three samples were collected from the floor deposits of Building A, specifically from the underground unit "Room 5" (**§C2.8.7**), Room 7 (**§C2.8.3**) and Room 8 (**§C2.8.4**).

I2.4.1 "Room 5"

The sample AS 262433:156:002 was collected from the floor deposit of "Room 5" , the deep-lying silo of Building A. 65 plant remains were recovered from this sample, resulting in a seed density of 32.5 per litre of soil.

I2.4.1.1 Cultivated plants

The occurrence of the hulled emmer wheat (*Triticum dicoccum*) is confirmed by one kernel and one spikelet fork. Twenty broken grains which were strongly deformed by charring are classified as indeterminate cereals (Cerealia indet.). They cannot be further identified, and it is not possible to decide whether they belong to barley or wheat. Edible plants from the Fabaceae family are represented by three lentil seeds (*Lens culinaris*), which are preserved without their seed coats. Domesticated lentils exhibit a wide range of morphological variation, typically classified into two groups: small-seeded lentils (microsperma) with a diameter of 3–4 mm, and large-seeded lentils (macrosperma) measuring 6–9 mm. The seeds in this sample have diameters of approximately 3.0–3.2 mm, indicating they belong to the small-seeded (microsperma) variety.[361] It is presumed that the cultivation of lentils took place at Assur; however, it cannot be ruled out that lentils were also gathered in the wild.

I2.4.1.2 Wild plants

The wild plants from "Room 5" include two seeds of milk vetch (*Astragalus* sp.), a small-seeded legume from the Fabaceae family, and likely one seed of false cleaver (*Galium spurium*) from the Rubiaceae family. Additionally, 16 uncharred fruitlets from the Boraginaceae family were identified as field gromwell (*Lithospermum arvense*). The grass family (Poaceae) is represented by five seeds, though their poor preservation prevents further identification. The legume seeds, like the grass grains, likely grew as weeds in crop fields and may have been unintentionally harvested with the crop. Six seeds, four small stems, and six seed shells could not be identified due to moderate preservation.

I2.4.1.3 Varia

More than 577 charcoal pieces, two amorphous objects (bread or porridge), six animal bones and one mollusc were recovered. The charcoal pieces could have been part of a roof or a wooden covering that collapsed when a fire broke out. They are discussed in **§I1**.

360 Pearsall 2015, 149; Jacomet/Kreuz 1999, 145.

361 Körber-Grohne 1988, 352; Zohary/Hopf/Weiss 2012, 77.

I2.4.1.4 The function of "Room 5" based on the plant remains

As discussed in **§C2.8.7**, "Room 5" was an underground unit surrounded by a mudbrick lining, with no entrance and a floor approximately 2 m lower than the other rooms in Building A. Both the floor and the mudbrick lining were covered with plaster. Based on these observations, it was suggested that "Room 5" may have functioned originally as a silo before being filled with refuse material after the abandonment of Building A.

The origins of the plants found in this unit remain uncertain. If the structure was indeed a silo, it may have been emptied before abandonment, as no stored crops were identified. The few charred plant remains retrieved might represent waste, potentially from secondary use. Alternatively, the charred plant remains may have entered the structure during plastering activities or been present in the matrix of the mudbricks that subsequently collapsed within the unit.

Nevertheless, the interpretation that this unit may have served as a silo is still convincing. In antiquity, silos, or storage facilities for cereals, can be found both underground and above the ground. Underground hermetic storage in airtight containers was a standard method for large-scale cereal and pulse storage worldwide.[362] Ethnographic evidence of such underground hermetic storage has been documented in the Greek islands (e.g., Crete, Kos), and archaeological evidence has been discovered globally, including the remarkable silo complex in the Hittite capital of Hattuša in modern Turkey.[363]

While the architectural design of these hermetic structures is often well-defined, direct evidence of their use as storage facilities is frequently lacking, as they are typically found empty, much like our "Room 5" at Assur was. In these structures, the mudbrick walls were coated with plaster to serve as a protective barrier against moisture and insect infestation, thus preserving the stored materials more effectively. This design indicates a deliberate strategy for long-term storage despite the absence of physical remnants within the structures.[364] The plaster helped protect crops from humidity, which could cause seed germination and mould growth. Furthermore, biological activity within the storage space created a low-oxygen atmosphere with elevated carbon dioxide levels, which is detrimental to any insects present in the stored crops.[365]

Although hermetic storage does not completely halt the deterioration of crops, it significantly slows decay, allowing cereals to be stored in these pits or other underground features for several years.[366] Once the pit was filled, an airtight seal was necessary to protect the content. This could involve covering the silo with a layer of ash or a roof made of clay combined with wood to prevent exposure to insects, humidity, and air. After the seal was broken, it was crucial to remove all goods quickly, as exposure to oxygen and moisture can accelerate the decomposition of the grains.[367]

This method of storage accommodates both short-term and long-term agricultural needs. Short-term storage is typically intended for daily meal preparation, while long-term storage is aimed at preserving agricultural surplus for times of famine, poor harvests, and for grains intended for sowing in the following year.[368]

The heat generated by the stored grain itself could potentially lead to spontaneous combustion, reducing the stored products to ash.[369] Due to the hermetic nature of these features, fires typically burn at lower temperatures and with limited oxygen for extended periods. This may explain why the fill of "Room 5" was rich in ash (**§C2.8.7**). However, another possible explanation for the presence of ashes in the fills of "Room 5" takes into account that, after the abandonment of Building A, this unit appears to have been repurposed as a refuse pit, where various items, possibly including ashes, accumulated (**§C2.8.7.2**).

I2.4.2 Room 7

The sample AS 262433:110:002 was collected from the floor deposit of Room 7 in Building A. 288 charred seeds were identified, with a density of 22.2 seeds per litre of soil.

I2.4.2.1 Cultivated plants

Cereals are represented by six-rowed barley (*Hordeum vulgare*) with two grains and one internode. 217 cereal fragments (Cerealia indet.) were isolated. These grains are deformed and corroded and have no characteristic features for further determination.

362 Diffey/Neef/Boogard 2017, 2.
363 Seeher 2000, 261-301.
364 Diffey/Neef/Boogard 2017, 2.
365 Seeher 2000, 264.
366 Seeher 2000, 268.
367 Diffey/Neef/Boogard 2017, 2; Seeher 2000, 269.
368 Diffey/Neef/Boogard 2017, 3.
369 Seeher 2000, 262.

I2.4.2.2 Wild plants

Wild plants from this sample include 17 seeds of field gromwell (*Lithospermum arvense*), one seed of mallow (*Malva* sp.), one seed of bur clover (*Medicago* sp.), six seeds of melilot (*Melilotus* sp.), two seeds of grasses (Poaceae), classified only to family level, and one seed of cowherb (*Vaccaria pyramidata*). 23 seeds, seven stems and 12 seed shells could not be further identified due to moderate preservation (Indet.).

I2.4.2.3 Varia

One amorphous object, probably a piece of bread or porridge, six small pieces of animal bones and two molluscs were recovered.

I2.4.3 Room 8

The sample AS 262433:107:014 was taken from the floor deposit of Room 8 of Building A. This sample yielded 485 plant remains, with a density of 20.6 seeds per litre of soil processed.

I2.4.3.1 Cultivated plants

Cereal crops occurring in this sample are three grains of six-rowed barley (*Hordeum vulgare*), two seeds identified with some uncertainty as barley (cf. *Hordeum vulgare*) and one grain of hulled emmer wheat. One grain of wheat could be identified only to the genus level (*Triticum* sp.). The remaining 301 cereal grains are less preserved and were identified as indeterminate cereals, as well as one cereal rachis node (Cerealia indet.).

I2.4.3.2 Wild plants

One grain of goat grass (*Aegilops* sp.) was identified to the genus level, and 14 grains of grasses were identified to the family level (Poaceae). Small-seeded legumes include one seed of scorpion weed (*Coronilla* cf. *scorpioides*), two seeds of bur clover (*Medicago* sp.), and four seeds of melilot (*Melilotus* sp.). At the same time, seven are uncertain (cf. *Melilotus* sp.). Other taxa attested are one seed of germander (*Teucrium* sp.), 90 seeds of uncharred field gromwell (*Lithospermum arvense*) and four seeds of mallow (*Malva* sp.). 37 seeds, seven stems and eight seed shells could not be further determined because of poor preservation (Indet.).

I2.4.3.3 Varia

Two amorphous objects, six animal bone fragments and two molluscs were recovered.

I2.4.4 The plant remains from Building A, 2023 and 2024: interpretation

By integrating the results of seed identifications from the 2023 and 2024 campaigns, distinct patterns in the distribution of plant remains across Building A emerge (**Figs. I2.1-2**). Overall, threshing remains were found in low quantities throughout the building, indicating that the plant remains did not originate from waste but rather from well-cleaned grains. The wild plant remains recovered across the building appear to be contaminants, suggesting that the samples represent a store of cereal grains infested with weed diaspores. The charred nature of the plant remains hints at the potential presence of ovens in the building, although none were identified during excavations.

The rooms of Building A, including the silo designated as "Room 5," exhibited seed densities ranging from 11.28 to 38.54 seeds per litre of processed soil. The lowest density was recorded in Room 2, while the highest was found in Room 3. Notably, when differentiating between cultivated and wild plant seeds, nearly half of the seeds in Room 3 were from wild plants. Despite this, Room 3 still had the highest density of cultivated plant seeds per litre, followed closely by Room 7.

Focusing on cereal seeds, the largest group among cultivated plants, it is noteworthy that while Room 2 yielded a substantial number of charred cereal grains (N=2577), its cereal seed density per litre of soil was the lowest in Building A. In contrast, Rooms 3 and 7 exhibited the highest cereal seed densities. Hence, it is possible that Rooms 3 and 7 were more closely associated with cereal consumption than Room 2. However, any interpretations regarding the functions of rooms in Building A based on plant remains must consider several limitations, as neither Room 3 nor Room 7 has been fully excavated, and a large portion of Room 2 had been obliterated by the construction of the chamber tomb in the Parthian period.

I2.5 Building B (Iron Age)

The sample AS 262433:158:001 was collected from the floor deposit of Room 11 in Building B (**§C2.9.1**). It yielded 215 charred plant remains, with a seed density of 43 seeds per litre of processed soil.

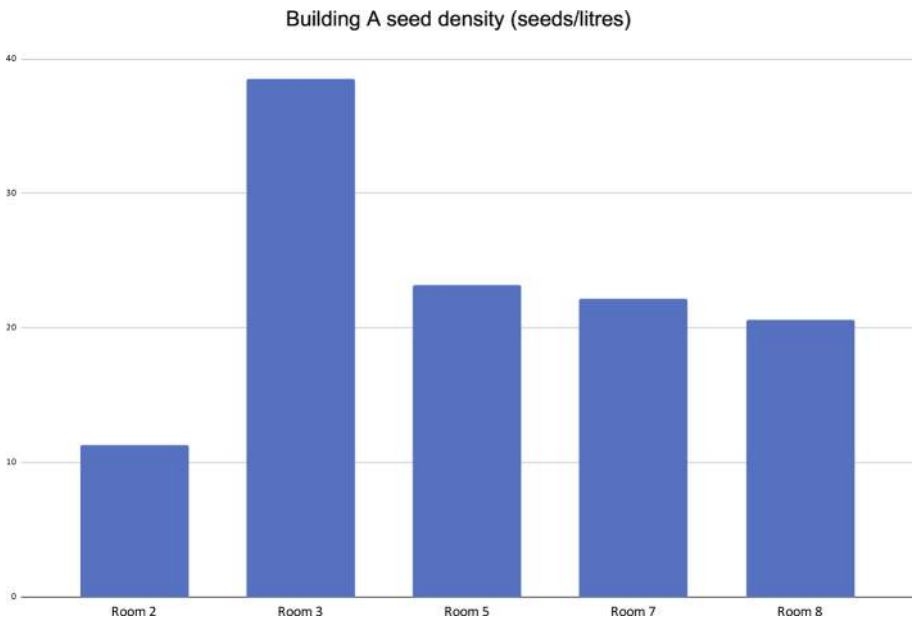

Fig. I2.1: Seed densities across the rooms of Building A. Prepared by Andrea Squitieri.

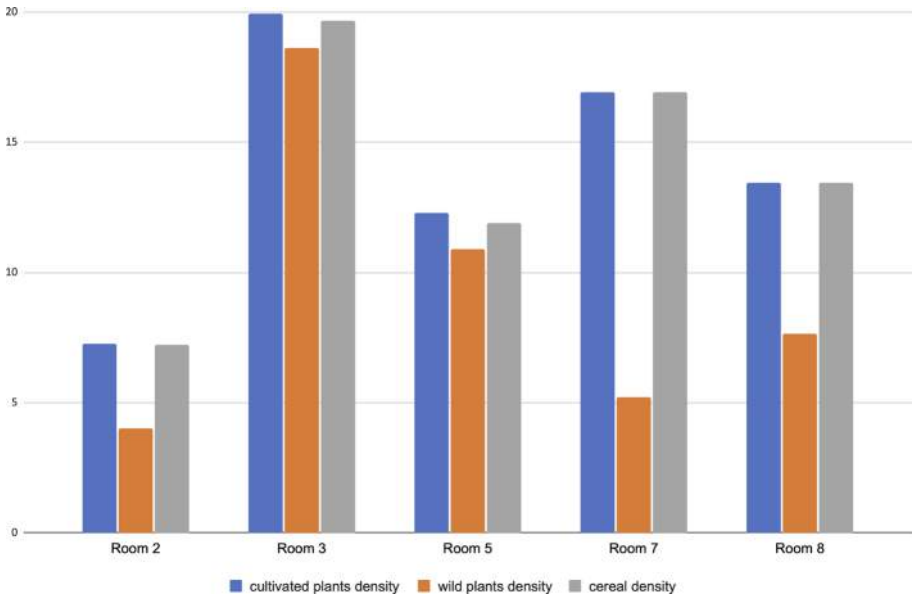

Fig. I2.2: Seed densities of the main plant types across the rooms of Building A. Prepared by Andrea Squitieri.

I2.5.1 Cultivated and wild plants

The cereal crops identified are two seeds of six-rowed barley (*Hordeum vulgare*) and two spikelet forks of hulled einkorn wheat (*Triticum monococcum*). 136 broken and deformed cereal grains and two cereal rachis nodes could not be further identified (Cerealia indet.).

Among the wild plants, five grains of goat grass (*Aegilops* sp.) and nine grains of other grass species were found, identified only to the family level (Poaceae). One seed of the parsley family (Apiaceae) was retrieved but could not be further identified. Two seeds of milk vetch represent wild small legumes (*Astragalus* sp.), two seeds of bur clover (*Medicago* sp.), and one seed of melilot (*Melilotus* sp.). Other species attested are one seed of horned poppy (cf. *Glaucium* sp.) but with uncertain identification, 13 uncharred fruitlets of field gromwell (*Lithospermum arvense*), and one seed of mallow (*Malva* sp.). Ten seeds, eleven stems and 17 seed shells, all badly preserved, could not be identified (Indet.).

I2.5.2 Varia

1120 wood charcoal fragments from very small to medium size, three amorphous objects (bread or porridge remnants), two animal bone fragments and one mollusc were retrieved.

I2.6 Plant remains from Sondage 2 (Middle Bronze Age to Iron Age)

The samples AS 263432:012:003, AS 263432:016:005, AS 263432:021:003 and AS 263432:021:005 were collected from Sondage 2 (**§C3**). They came from the layers identified below a paved brick floor that had been exposed by the SBAH team in 2002. Underneath this baked brick floor, a pebble floor was identified (on which the sample AS 263432:016:005 was taken), on which a structure interpreted as drainage was found (from which the sample AS 263432:012:003 was taken) (**§C3.2**). Below the pebble floor, the virgin soil was reached, which was cut by a pit (from whose fill the samples AS 263432:021:003 and AS 263432:021:005 were taken) (**§C3.3**). Overall, the flotation samples from Sondage 2 yielded a considerable amount of charred plant remains.

I2.6.1 The plant remains from sample AS 263432:012:003

The sample AS 263432:012:003 was taken from the fill of the drainage installation. It yielded 2899 seeds, with a seed density of 145 seeds per litre of soil processed. This is the highest number of charred plant remains among all the flotation samples collected during the 2024 campaign, constituting about 44% of the total.

I2.6.1.1 Cultivated plants

Two cereal species were identified: six-rowed barley and hulled einkorn wheat. The six-rowed barley *Hordeum vulgare* is represented by four kernels, three internodes, seven rachis nodes and one glume base. The grains have a typical spindle-like shape. The ear rachis fragments are represented by single internodes. At the top of the internode, a central scar can be seen, left by the detached fertile spikelet. The hulled wheat species einkorn (*Triticum monococcum*) is represented by one spikelet fork. Two rachis nodes and one spikelet fork of wheat, hulled or naked, could not be identified to the species level (*Triticum* sp.). The impressive number of 2650 cereal grains were retrieved, but they were so strongly deformed, broken and corroded by charring that they could not be further classified as either wheat or barley. Two cereal spikelet forks and one rachis node could not be identified even at the genus level (Cerealia indet.). Another food plant attested is grapevine; however, the preserved half-seed cannot be attributed to either wild wine or cultivated wine (*Vitis* sp.).

I2.6.1.2 Wild plants

Small-seeded legumes and seeds of bedstraw species are the most numerous remains among the weeds. The species of the family Fabaceae are difficult to identify because they are badly preserved. As a part of this group, there are one seed of scorpion weed (*Coronilla* cf. *scorpioides*), though with some degree of uncertainty, five seeds of legumes identified to family level (Fabaceae), 46 seeds of trefoil (*Lotus* sp.), nine seeds of bur clover (*Medicago* sp.), three seeds of sainfoin (*Onobrychis* sp.), and one seed of clover (*Trifolium* sp.).

Among the grasses, two seeds of the genus *Aegilops* sp., goat grass, were recovered. Other species are Spanish aizoon (*Aizoon hispanicum*) with four seeds, 49 seeds of bedstraw (*Galium* sp.), one seed of horned poppy (cf. *Glaucum* sp.), but identification is uncertain, six seeds of mallow (*Malva* sp.), 13 seeds of the grass family (Poaceae), and four seeds of Russian thistle (*Salsola* sp.). Most of the wild plants are identified to the genus level. The sample also contained 68 seeds and 13 stems that were not determined because of poor preservation (Indet.)

I2.6.1.3 Varia

15 amorphous objects (probably fragments of charred bread or porridge) and six remains of insects were found.

I2.6.2 The plant remains from sample AS 263432:016:005

This sample was collected from the deposit covering the pebble floor on which the drainage installation was found (**§C3.2**). It yielded 238 charred plant remains, with a seed density of 95.2 seeds per litre of soil processed.

I2.6.2.1 Cultivated plants

Cereals are represented by threshing remains: four rachis nodes of six-rowed barley (*Hordeum vulgare*), one spikelet fork of hulled wheat emmer (*Triticum dicoccum*), and two spikelet forks of einkorn (*Triticum monococcum*). Additionally, 165 corroded, porous and fragmented cereal fragments could be classified only as indeterminate cereal grains (Cerealia indet.), which can include wheat and barley.

I2.6.2.2 Wild plants

Small-seeded legumes are barely attested in this sample. There are only two seeds of scorpion weed (*Coronilla* cf. *scorpioides*), but identification is not quite certain; one seed of a bur clover (*Medicago* sp.) and one seed of fenugreek (*Trigonilla* sp.) were found. Other taxa found are one seed of bedstraw (*Galium* sp.), 22 uncharred fruitlets of field gromwell (*Lithospermum arvense*), one seed of mallow (*Malva* sp.), three grains of grasses, identified only to family (Poaceae) and one seed of sea blite (*Suaeda* sp.). 17 seeds, 13 stems and four seed shells could not be determined (Indet.).

I2.6.2.3 Varia

A large amount of small animal bones (415 pieces) and three remains of insects were found.

I2.6.3 The plant remains from sample AS 263432:021:003

The sample AS 263432:021:003 comes from the fill of a pit that cut the virgin soil, reached at the bottom of Sounding 2 (**§C3.3**). 377 seeds were identified, with a seed density of 150.8 seeds per litre of soil processed.

I2.6.3.1 Cultivated plants

Six-rowed barley (*Hordeum vulgare*) is represented by one grain, the hulled emmer wheat (*Triticum dicoccum*) by one glume base, and the einkorn (*Triticum monococcum*) by two glume bases. Three grains of wheat, naked or hulled, could be identified only to genus level (*Triticum* sp.). 305 cereal fragments could not be determined due to bad preservation (Cerealia indet.), which could include wheat as well as barley. The evidence of other cultivated plants is very poor, and only one lens seed is included (*Lens culinaris*). The diameter of the seed is 3.00 mm, indicating that it also belongs to the small-seeded variety (microsperma group).[370]

I2.6.3.2 Wild plants

A few seeds of three species of the small-seeded wild legumes were recovered: three seeds of milk vetch (*Astragalus* sp.), one seed of an undetermined legume (Fabaceae), and four seeds of bur clover (*Medicago* sp.). Other taxa represented are three seeds of divided sedge (cf. *Carex divisa*), but identification is uncertain, two seeds of bedstraw (*Galium* sp.), five fruitlets of uncharred field gromwell (*Lithospermum arvense*), nine grains of grasses (Poaceae), identified only to family level, four seeds of sea blite (*Suaeda* sp.) and two seeds of cowherb (*Vaccaria pyramidata*). Due to poor preservation, 24 seeds and six seed shell fragments could not be further identified (Indet.).

I2.6.3.3 Varia

Apart from plant seeds, no other remains were found in this sample.

370 Körber-Grohne 1988, 352; Zohary/Hopf/Weiss 2012, 77.

I2.6.4 The plant remains from sample AS 263432:021:005

The sample AS 263432:021:005 comes from the same context as the previous sample AS 263432:021:003. From this sample, 1532 seeds were recovered, with a seed density of 32.5 per litre of soil processed.

I2.6.4.1 Cultivated plants

Six-rowed barley (*Hordeum vulgare*) is represented by 12 grains, and the hulled einkorn wheat (*Triticum monococcum*) is represented by two spikelet forks. Four grains could be classified only as wheat, hulled or naked (*Triticum* sp.). 1176 poorly preserved, indeterminate cereals (Cerealia indet.) were identified, which could include wheat and barley. Five cereal glume bases and one rachis node were classified as indeterminate (Cerealia indet.). Another crop plant was found, namely one seed of domesticated lentil (*Lens culinaris*). The diameter is 3.1 mm; hence, this specimen also belongs to the small-seeded variety (microsperma group) mentioned above.[371]

I2.6.4.2 Wild plants

Small-seeded wild legumes and grasses are the most abundant groups of wild plants recovered in this sample. Six species of legumes are attested: milk vetch (*Astragalus* sp.) with 13 seeds, scorpion weed (*Coronilla* cf. *scorpioides*) with four seeds, but identification is uncertain, one seed of legumes not further identified (Fabaceae), ten seeds of bur clover (*Medicago* sp.), 15 seeds of melilot (*Melilotus* sp.) and three seeds of fenugreek (*Trigonella* sp.). Grasses are represented by six grains of brome grass (*Bromus* sp.), 11 grains of annual wheatgrass (*Eremopyrum* sp.), two seeds of coxspur (*Echinochloa* sp.), and 46 grains of grasses identified to family level (Poaceae). Other taxa are: one seed of dense flowered fumitory (*Fumaria densiflora*), 14 seeds of bedstraw (*Galium* sp.), one seed of horned poppy (cf. *Glaucium* sp.), but identification is not sure, six uncharred nutlets of gromwell (*Lithospermum arvense*), four seeds of mallow (*Malva* sp.), one seed of blond psyllium (*Plantago ovata*), one seed of hare's foot plantain (*Plantago lagopus*), one seed of fiddle dock (*Rumex pulcher*), three seeds of saltmarsh bulrush (*Scirpus maritimus*) and two seeds of sea blite (*Suaeda* sp.). 122 seeds, 30 seed shells and 34 small stems could not be further identified because of poor preservation.

371 Körber-Grohne 1988, 352; Zohary/Hopf/Weiss 2012, 77.

This sample is most promising from a palaeobotanical point of view because it yielded not only a significant quantity of plant remains but also many different plant species, especially wild plants.

I2.6.4.3 Varia

63 carbonised wood fragments and 39 amorphous objects, probably charred fragments of bread or porridge, were found, in addition to 17 animal bone fragments, one mollusc fragment, and one bead.

I2.6.5 Interpretation

The botanical content of the samples from Sondage 2 is of mixed origin and does not represent a specific stage of crop processing, such as dehusking or food preparation. Crop processing entails a series of operations required to convert the harvested cereals into clean grain (and potentially "useful" by-products).[372] The samples from Sondage 2 contained threshing refuse and crop-cleaning residues such as glume bases, internodes, and spikelet forks mixed with charred food plant remains and wild plants. In other words, the plant remains originated from various domestic activities. The mixing occurred after crop processing, probably near the unearthed floor and drainage system in Sondage 2.

The samples do not derive from particular features which could provide indications of the possible nature of the plant remains, such as a storage installation or a kitchen. It is evident that because of the mixed origin of the samples, an interpretation of the archaeobotanical data in terms of domestic activities is restricted. However, some conclusions on the crop-plant assortment and some notions on field weeds are possible.[373] Assuming that the charred plant material was primarily waste, it could be that the vegetable refuse derived from another place and reached some way through the drainage system by water. The fact that many zoological remains and a bead were found reinforces the assumption that the samples from Sondage 2 contained refuse material.

372 Charles/Bogaard 2001, 310.

373 van Zeist/Bakker-Heeres 1985, 165; For further information on crops and field weeds, see Sarkady 2024.

I2.7 Plant remains from the trench NT2 (Iron Age to Parthian period)

The samples AS 254433:036:002 and AS 254433:037:002 come from trench NT2 (**§C4**). They both derive from a mud surface, registered as NT2-F2, identified about 3 m below the site surface.

I2.7.1 Plant remains from sample AS 254433:036:002

This sample contained only 67 charred seeds, with a seed density of 44.7 seeds per litre of soil processed.

I2.7.1.1 Cultivated and wild plants

56 broken and poorly preserved seeds were classified as indeterminate cereal grains (Cerealia indet.). Only two seeds of wild legumes were recovered but could not be identified beyond the family level (Fabaceae). One grain of grass was found and classified only to the family level (Poaceae). Six seeds and two seed shells could not be identified due to poor preservation but may be attributed to wild plants (Indet.).

I2.7.1.2 Varia

In addition to the plant material, three amorphous objects (bread fragments or porridge fragments) and one animal bone fragment were found.

I2.7.2 Plant remains from the sample AS 254433:037:002

291 charred seeds were selected from this sample, with a density of 72.8 seeds per litre of soil processed.

I2.7.2.1 Cultivated plants

Cereals are represented by four grains of six-rowed barley (*Hordeum vulgare*) and one spikelet fork of hulled einkorn wheat (*Triticum monococcum*). 239 fragments of cereal grains could not be further identified because they were poorly preserved (Cerealia indet.); they could be either barley or wheat.

I2.7.2.2 Wild plants

One grain of goat grass (*Aegilops* sp.) and three other grains of grasses were found, but they could be identified only to the family level (Poaceae). The group of small-seeded wild legumes includes one seed of scorpion weed (*Coronilla* cf. *scorpioides*), identification is uncertain, six seeds of bur clover (*Medicago* sp.), and two seeds of melilot (*Melilotus* sp.). Other species are three seeds of bedstraw (*Galium* sp.), one seed of mallow (*Malva* sp.), and one seed of germander (*Teucrium* sp.). 28 less well-preserved seeds and one stem/twig could not be further identified (Indet.).

I2.7.2.3 Varia

11 amorphous objects (bread fragments or porridge fragments) and one animal bone fragment were found.

I2.8 Preliminary overall assessment

I2.8.1 Cultivated plants

The botanical record from Assur indicates that crop production was primarily centred around cereals. Three cereal species have been identified: hulled six-rowed barley (*Hordeum vulgare*) and two glume wheat species, emmer (*Triticum dicoccum*) and einkorn (*Triticum monococcum*). Free-threshing wheat species, such as bread wheat (*Triticum aestivum*), macaroni wheat (*Triticum durum*), and club wheat (*Triticum compactum*), appear to be absent from the 2024 samples. However, whether they might be among the unidentified cereal grains remains uncertain. Similarly, the 2023 samples yielded very few grains of free-threshing wheat species, suggesting that the cultivation of these wheat types was of minor importance, likely due to their higher water requirements and lower drought resistance.

Hordeum vulgare was the primary staple crop, dominating in each of the chronological periods to which the samples belonged and consistently present in most samples (63.6%), albeit in low quantities. The proportion of barley to wheat further indicates that barley was the most significant crop cultivated by the inhabitants of Assur. In addition to being a vital food source for humans, barley was used as fodder for animals. Its predominance can likely be attributed to its greater drought resistance compared to the more sensitive wheat varieties.[374] *Triticum dicoccum* (emmer) is attested by two grains, and *Triticum monococcum* (einkorn) only by chaff. Threshing remains from barley, emmer, and einkorn occur in very low numbers. It cannot be ascertained whether *Triticum monococcum* (einkorn) was an important crop. It seems to be less well adapted to the environmental conditions.[375] Another disadvantage of this crop is the relatively low productivity compared to emmer, and extra steps are needed during crop processing, such as dehusking to remove the glumes.[376] The overall low quantity of threshing remains and the presence of weeds in the samples suggest that most of the plant-food processing occurred outside the excavated areas. Since no deposits or storage of pure cereal grains were found, one could assume that the cereal grains identified from refuse layers may represent the waste fraction of food processing activities. In an advanced stage of crop processing, as described by Hillman, the cereals are passed through a sieve, which separates the bigger grains from the smaller grains, weed seeds, and threshing remains such as rachis remains or spikelet forks.[377]

Other cultivated plants are represented by very few seeds of lentils that belong to the domestic type (*Lens culinaris*). This finding confirms that this species was indeed cultivated at Assur but makes no suggestion concerning its relevance to human nutrition. It might not have been an important crop. The fact that pulses are sometimes rare in the archaeobotanical assemblages may result from the fact that lentils or peas are less likely to become charred than cereals due to the method used when they were prepared for meals.[378] However, if the site's economy was based on livestock, it is possible that pulses played a minor role in the human diet because of the availability of high-quality protein from meat. It should also be considered that the soil in Mesopotamia is formed by fluviatile sediments close to the main rivers Euphrates and Tigris, where sand is deposited. Flooding the plain not only maintained the fertility of the soil but also increased its salinity. Irrigation agriculture worsened this process. For this reason, several salt-intolerant crops were cultivated rarely or not at all, especially legume crops, such as peas and lentils.[379]

I2.8.2 Wild plants

Proving the use of the wild plant species identified in the samples poses significant challenges. Unfortunately, we

374 Wasylikowa/Kolinski 2013, 25.

375 Neef 1991, 325.
376 Hillman 1984, 114; 144.
377 van Zeist/Bekker-Heeres 1982, 242.
378 Sarkady 2024, 208.
379 Neef 1991, 321.

cannot determine whether these plants played a role in human consumption, were utilised for medicinal purposes or as spices, or whether they served solely as animal fodder.[380]

The majority of wild species found at Assur are leguminous plants and grasses. Grass seeds constitute 22.4% of the wild plant seeds, while wild legumes account for 49.8%. Additionally, the presence of certain wild plants can inform us about the locations of cultivated cereal fields, as some species, such as *Coronilla scorpioides* and *Vaccaria pyramidata*, likely grew in these areas; the latter is known to be a weed in winter crops.[381]

Other species, such as goat grass (*Aegilops* sp.), coxspur (*Echinochloa*), annual wheatgrass (*Eremopyrum*), and brome grass (*Bromus* sp.), are represented only in small quantities. Many other grass species, primarily small-grained, could only be classified at the family level (Poaceae). Plants such as *Plantago lagopus*, *Aizoon hispanicum* and *Suaeda* sp. could indicate fallow fields with moderate to severe salinity. *Malva* species occur in fields, in waste places and in disturbed ground.[382]

Small-seeded wild legumes include *Astragalus*, *Coronilla*, *Lotus*, *Medicago*, *Melilotus*, *Onobrychis*, *Trifolium*, and *Trigonella*. Their presence suggests that these species are pretty common near the site. Notably, the genera *Astragalus* and *Melilotus* comprise species that also grow in cultivated fields, making them likely to be harvested alongside crops since they produce seeds concurrently with cereals.[383] It is possible that seeds of field weeds were inadvertently brought to the site as admixtures in harvested crops, and the small-seeded legumes may represent residues from crop cleaning. However, it remains unclear whether these seeds were intentionally harvested.[384]

How did seeds from both crop plants and wild plants find their way into the settlement? There are various modes of transport to consider. As previously mentioned, crop plants were likely brought into the settlement after harvesting for further processing, often alongside weed species. The carbonisation of crop seeds could have been due to fire, but it is more plausible that they became charred during meal preparation. During cooking, cereal grains may have accidentally fallen near (not directly into) the fire or oven, leading to carbonisation. Additionally, accidents during cereal processing could result in carbonised grains and threshing remnants.

Wild plant species might have been introduced into the settlement accidentally by the wind or rain, by clinging to animal fur or clothing. They could also have been intentionally brought in via dried dung cakes made from cattle dung, which was used as fuel, particularly in areas where wood was scarce.[385] Miller has notably supported this dung theory as a source of carbonised seeds in archaeological deposits. Seeds can pass through an animal's digestive tract undamaged, and any straw or other plant material used to create these dung cakes would be burned for heating. This process could char the seeds present in the dung, leading to a significant number of charred seeds found at archaeological sites as a result of this practice.[386]

However, it is challenging to determine whether the seeds recovered from Assur originated solely from gathering wild plants or resulted from a combination of farming and foraging activities. Primarily, weed species may provide insights into past growing conditions. A significant issue arises because, in many cases, it is impossible to identify weed seeds at the species level. This limitation significantly reduces the utility of weed seeds as indicators of environmental conditions and the exploitation of wild flora during the settlement's occupation.[387] No palaeoecological conclusion can be drawn from weed seeds, which may include species from different habitats.[388] However, it is essential to highlight that some wild plants which grow in humid habitats and soils with intermediate salt content, like *Scirpus maritimus* and probably *Salsola* and *Suaeda* species, are attested in Assur.

I2.9 Appendix: Evidence for date palm in Assur

The hand-picked sample AS 261433:061:012, retrieved from the fill of Pit 7, dated to the Parthian period (**§C2.7**), contained seven fragments of date palm stone (*Phoenix dactylifera*). The date palm is one of the oldest cultivated fruit crops in the hot and arid regions of North Africa and the Middle East, with its domestication occurring in Southern Mesopotamia around 5000 BC.[389] Many of the earliest archaeobotanical remains of this plant are concentrated in the Gulf region and the valleys of the Tigris and Euphrates rivers.[390] Date palms thrive in what is known as the "date palm belt," an almost rainless area extending from

380 van Zeist/Bekker-Heeres 1982, 247.
381 van Zeist/Bakker-Heeres 1982, 240.
382 Neef 1989, 158.
383 Wasylikowa/Kolinski 2013, 23.
384 van Zeist/Bakker-Heeres 1982, 248.
385 van Zeist/Bakker-Heeres 1982, 233-234.
386 Miller 1984, 74-76.
387 Neef 1989, 158; Wasylikowa/Kolinski 2013, 23.
388 van Zeist/Bakker-Heeres 1982, 240.
389 Tengberg 2012.
390 Gros-Balthazard/Flowers 2021, 3.

southern Iran to the Atlantic coast of northwestern Africa ("Afro-Asian dry zone").[391] These palms grow in oases across hot deserts where sufficient underground water is available or are cultivated using artificial irrigation in arid zones. The optimal growing conditions are captured by the Arabic expression, "it prefers to grow with its head in the burning sun and its foot in the water," which describes the typical oasis environment.[392] Once planted, date palms begin to bear fruit after five years, achieving full production between eight and ten years. A single tree can yield between 100 and 200 kg of fruit annually. Palm dates are a high-energy food source, containing 72 to 88% sugar at maturity;[393] therefore, they have historically served as a crucial resource for food security during times of shortage and crisis.[394] The various uses of palm trees are extensive; every part of the tree—fruits, wood, bark, leaves, and fibres—can be utilised in multiple ways.[395] These parts have had numerous applications in medicine, for instance, to treat various diseases and injuries through ointments, bandages, and infusions. The fruit, rich in tannins, is medicinally used as a laxative, as well as for its detersive and astringent properties in treating intestinal issues.[396] In the arid regions of the Middle East, the date palm holds significant economic value as well as symbolic importance.[397]

Mesopotamia, often regarded as the "date palm country," boasts these trees throughout its landscape, except for the northern regions,[398] where Assur is located. Because date palm was not a local tree, it is likely that the inhabitants of Assur consumed not only locally grown agricultural products but also imported goods from greater distances, including both dried and fresh dates. Throughout history, people have sought foodstuffs from beyond their immediate environment, raising intriguing questions about how these foods were obtained and who had access to them. Exotic foods, spices, luxury items, and other goods were part of organised long-distance trade networks.[399] For transporting goods over longer distances, boats and ships were likely employed, aligning with the geomorphological features of the Southern Mesopotamian alluvial plain. Over shorter distances, goods were undoubtedly moved by porters and pack animals.[400]

I3. Preliminary observations on the phytolith assemblage at Assur from the 2023 and 2024 seasons

Doğa Karakaya

I3.1 Introduction

Phytoliths are microscopic silica structures formed by plants as they absorb monosilicic acid from groundwater and deposit it within intracellular or extracellular spaces during their lifespan. When plant material decays, these silica structures are preserved in natural and archaeological sediments, providing valuable evidence for archaeological research. The deposition of silica in plants is not uniform across species: some families exhibit a strong propensity for silica accumulation, while others do not. The genetic makeup of plants primarily determines this tendency, although environmental factors can also play a role. For instance, differences in agricultural practices, such as rain-fed versus irrigation farming, influence silica deposition, particularly in Southwest Asia.[401] Phytolith studies cover a wide range of critical archaeological questions in Southwest Asia, including, for instance, agricultural origins and dispersals,[402] combustion features,[403] ritual and burial practices,[404] and activity analysis.[405]

What is crucial to highlight is that plants incorporate not only opal into their metabolism but also a variety of other biogenic minerals, such as calcium oxalate and calcium carbonate, among others.[406] While the term *phytoliths* in archaeology typically refers to siliceous biogenic materials composed of opal, it also encompasses other biogenic minerals far less common in archaeological contexts. This distinction is particularly significant for calcium oxalate crystals, which are the most frequently produced minerals by plants. However, most probably due to their rapid recycling in the environment, calcium oxalate crystals are observed far less frequently than opaline phytoliths in the

391 Zohary/Hopf/Weiss 2012, Map 18.
392 Zohary/Hopf/Weiss 2012, 131.
393 Zabar/Borowy 2012, 42.
394 Zabar/Borowy 2012, 42.
395 Neef 1989, 160.
396 Zabar/Borowy 2012, 44; Hiller/Matthias/Melzig 2010, 443-444.
397 Tengberg 2012.
398 Zabar/Borowy 2012, 41.
399 van der Veen 2011, 1-2.
400 Selz 2014, 261 (for Mesopotamia in the third millennium BC); Radner 2016, 80-81 (for the use of donkeys Tigris-upstreams and rafts Tigris-downstreams in Assur in the late 7th century BC).
401 Rosen/Weiner 1994.
402 Ball *et al.* 2016.
403 Albert *et al.* 1999.
404 Cabanes/Albert 2011.
405 Shillito/Ryan 2013; Portillo *et al.* 2009.
406 Weiner 2010.

archaeological record.[407] Calcium oxalate is a significant source of calcitic ash, a by-product of burning wood and bark as fuel.[408]

This chapter offers initial observations on the opal phytolith assemblage, setting the stage for a deeper exploration. As detailed below, opal phytoliths are not the sole biogenic minerals found in the samples under study; they also include calcium oxalate crystals, varying levels of discoloured (blackened) phytoliths, and potentially calcitic ash.[409] While this section will not comprehensively examine the latter three additional categories of plant evidence, it will provide qualitative insights into their presence and relative abundance within the analysed samples.

I3.2 Methods

Nine sediment samples for phytolith analysis were collected from the Hellenistic Graves 3 and 4, the Neo-Assyrian Grave 5, the Parthian Graves 6 and 7, as well as from the floor deposits of Rooms 2, 3 and the Courtyard 10 of the Hellenistic Building A (**Table I3.1**),[410] following the sampling protocol established at the start of the 2023 campaign.[411] The samples ranged in weight from 26.5 mg to 46.1 mg and were processed following the method described by Katz and his colleagues, the so-called rapid extraction method.[412] Initially, the samples were sieved through a 224-micron mesh to remove larger soil particles. Carbonate minerals were then dissolved using 6N HCl, followed by density separation with a sodium polytungstate solution stabilised at 2.2639–2.3060 g/ml. A 50-microliter aliquot of each sample was placed on a microscope slide and covered with a 24 × 24 mm coverslip. Phytoliths were quantified by examining 20 visual fields at 200× magnification using a Zeiss Axio Imager 2 reflected light microscope in the Environmental Change Research Unit (ECRU) laboratory at the Faculty of Biological and Environmental Sciences, University of Helsinki. The same microscope was used to photograph the phytoliths.

In this section, the phytolith morphotypes are named using the nomenclature system established by the International Code for Phytolith Nomenclature (ICPN 2.0), as detailed by Neumann.[413] Morphological identification of phytoliths was conducted using references from multiple prior publications[414] and the Phytcore online phytolith database.[415] A minimum of 200 morphologically identifiable phytoliths is typically recommended to obtain a representative dataset.[416] This threshold, however, was not met in all samples. The factors contributing to the low phytolith counts in specific samples are also discussed below.

I3.3 Results

I3.3.1 Overall characteristics of the phytolith assemblage

Phytolith concentrations per gram of sediment range from 300,000 to 1,700,000. This study identified 1,097 opal phytoliths, with nearly one-fifth (19.53%) classified as weathered or melted. This category represents the largest group within the assemblage. Combined with the unknown and indeterminate categories, this group accounts for 25.16% of the total assemblage. A comparison of weathered and melted morphotypes reveals a ratio of approximately 1:2 in favour of melted morphotypes across the entire assemblage, though this proportion varies between contexts.

Another significant category is grass inflorescences and leaves (Poaceae) (**Fig. I3.1**). Elongate dentate/dendritics, representing long cell phytoliths formed in grass bracts (glumes, lemmas, and paleae), account for 17.89% of the assemblage. These phytoliths indicate that grass inflorescence parts were deposited in the analysed contexts to varying extents. This category includes only fragmented remains, while non-fragmented phytoliths of these two morphotypes (Elongate dentate and Elongate dendritics) make up an additional 5.38% of the assemblage. The ratio of fragmented to non-fragmented ones is 3.33, meaning there is one complete morphotype for every three fragmented ones. When specialised trichomes, such as Papillate, are included, this group constitutes 23.88% of the assemblage, providing clear evidence of grass inflorescence contributions to the studied deposits.

Rondel phytoliths, comprising 15.86% of the assemblage, represent one of the more enigmatic morphotypes. Morphologically, Rondel phytoliths exhibit distinct variations, including short, sutured types without ornamen-

407 Piperno 2006.

408 Weiner 2010.

409 See descriptions of dark-colored phytoliths in Parr 2006. Also see Canti 2003 for calcitic ash.

410 On Graves 3, 4, and 5, see Kreppner/Rohde/Squitieri 2024, 119-121, 130-132; on Graves 6 and 7, and Building A, see **§C2**.

411 Radner/Squitieri 2024b, 96-97.

412 Katz *et al.* 2010.

413 Neumann *et al.* 2019.

414 Rapp/Mulholland 1992; Piperno 2006; Pearsall 2015.

415 Albert/Ruíz/Sans 2016; https://www.phytcore.org [Access date: December 2024].

416 Albert/Weiner 2001.

	Sample ID.	AS 262432:070:006	AS 262432:058:019	AS 261432:011:021	AS 262433:105:004	AS 261433:067:011	AS 262432:055:005	AS 262433:060:018	AS 261433:032:003	AS 262433:096:002		
	Context	Grave 5	Room 3	Room 2	Room 2	Courtyard 10	Grave 4	Grave 3	Grave 6	Grave 7		
	Sample size (mg)	36	46.1	36.2	37.7	34.3	37	26.6	38	31.4		
	Phytoliths per gram of sediment	1,517,294	1,052,551	306,378	698,696	1,608,662	1,716,088	750,510	204,306	547,480		
	Period	770-542 calBC	314-57 calBC	314-57 calBC	314-57 calBC	314-57 calBC	159/158 BC	159/158 BC	83-215 calAD	83-215 calAD		
	Phase	3	5	5	5	5	6	6	8a	8a		
ICPN 2.0 codes	**Morphotypes**	**Ph40-2023**	**Ph30-2023**	**Ph04-2023**	**Ph03-2024**	**Ph01-2024**	**Ph19-2023**	**Ph25-2023**	**Ph06-2024**	**Ph04-2024**	**Absolute counts**	**Percentages**
ACU_BUL	**Acute bulbosus**	3	4		3	4	1			3	**18**	1.64
PAP	**Papillate**	3	3								**6**	0.55
BLO	**Blocky**		4	3	4	4	1	1		2	**19**	1.73
BUL_FLA	**Bulliform flabellate**			1	1	2				1	**5**	0.46
ELO_DET	**Elongate dendritic**	8	2				3	1			**14**	1.28
ELO_DEN	**Elongate dentate**	6	24		1	5	8			1	**45**	4.10
ELO_DEN/DET	**Elongate dentate/dentritic**	70	6	2	17	50	42	2		8	**197**	17.96
ELO_DEN/SIN	**Elongate dentate/sinuate**	3								1	**4**	0.36
ELO_ENT	**Elongate entire**	9	8		1	6	33	3	1	2	**63**	5.74
ELO_SIN	**Elongate sinuate**	1	9		3	9	14	1		3	**40**	3.65
ELO	**Elongate**	3	14	2	13	7		6	6	5	**56**	5.10
SPH_ECH	**Spheroid echinate**					2		2			**4**	0.36
SPH_ORN	**Spheroid ornate**		3	2							**5**	0.46
SPH_ORN/ECH	**Spheroid ornate/echinate**		1								**1**	0.09
SPH_RUG/ECH	**Spheroid rugose/echinate**					1					**1**	0.09
SPH_PSI	**Spheroid psilate**				1		2				**3**	0.27
BIL	**Bilobate**					2	1				**3**	0.27
CRO	**Cross**	3		2		1	5		1		**12**	1.09
RON	**Rondel**	24	41	5	19	38	33			14	**174**	15.86
SAD	**Saddle**		2		2	5	6			3	**18**	1.64
CRE	**Crenate**	3	3		5	6	4	1		3	**25**	2.28
TRZ	**Trapezoid**		8			5	7			1	**21**	1.91
CRE/TRZ	**Crenate/Trapezoid**	1									**1**	0.09
	Multicellular (articulated)	18	3	1		4	6	1		2	**35**	3.19
	Tabular	2	5	4	2	2	5	9	1		**30**	2.73
	Irregular thick		4		1						**5**	0.46
	Hat-shaped (sedges)	2				1		1	1	2	**7**	0.64
	Globular, indet.	1	2			2	2	1	1		**9**	0.82
	Indeterminate	6	10	4	4	3	1	3	12	4	**47**	4.28
	Unknown	2		2	4		6		3		**17**	1.55
	Wheathered	4	13	4	11	12	17	6		7	**74**	6.75
	Melted	25	6	8	3	28	32	34	2		**138**	12.58
	Total	**197**	**175**	**40**	**95**	**199**	**229**	**72**	**28**	**62**	**1097**	100.00
	Cyhrosphyta cysts	11	23			6	9			3	52	
	Diatoms					13					13	
	Sporomorphs		5	4							9	

Table I3.1: Results from the phytolith analysis of the 2024 samples from Assur. Prepared by Doğa Karakaya.

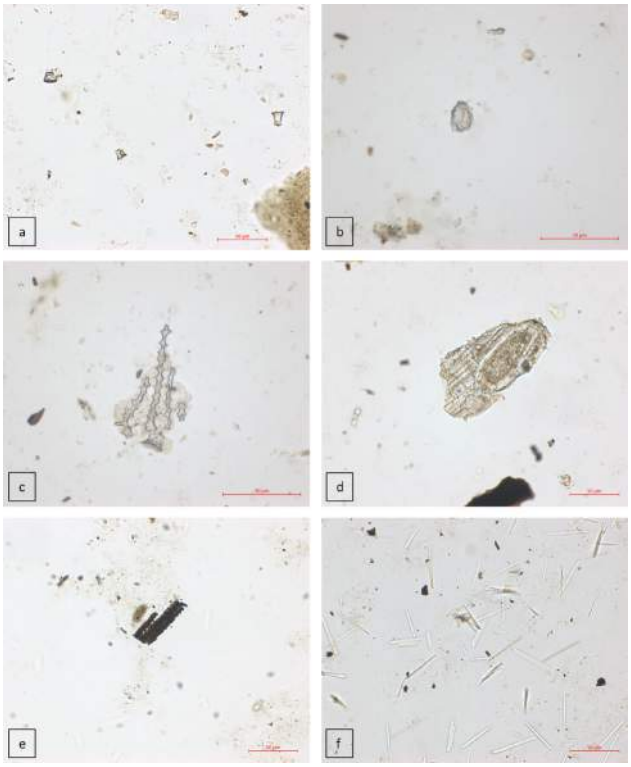

Fig. I3.1. Microphotographs of phytoliths and calcium oxalate crystals at Assur; a) GSSCP Rondel in sample AS 262432:070:006; b) Papillate in sample AS 262432:070:006; c) a slightly disoriented multicellular phytolith structure in sample AS 262432:070:006; d) a melted multicellular phytolith in sample AS 262432:055:005; e) a blackened multicellular phytolith structure in sample AS 261433:067:011; f) calcium oxalate crystals in sample AS 261433:067:011. Prepared by Doğa Karakaya.

tation or projection and short, non-sutured forms with a round, flat-topped inner periclinal surface view. Less common variants include crown-shaped or long-necked tall Rondels, present in significantly smaller quantities. In addition to Rondel, Grass Silica Short Cell Phytoliths (GSSCP) form the most abundant morphotype group in the assemblage. All GSSCP morphotypes described in ICPN 2.0 are represented, albeit in varying proportions. Crenate and Trapezoid morphotypes each account for approximately 4% of the assemblage, while Saddle, Cross, and Bilobate morphotypes contribute around 3%. Altogether, GSSCPs constitute 23.15% of the assemblage.

The remaining morphotypes have lower identification values, and assigning them to definitive categories is challenging. Elongate sinuate phytoliths, accounting for 3.65% of the assemblage, are consistently present across nearly all samples. This morphotype and acute bulbosus (1.64%), representing hair cells, indicate epidermal tissues from grass leaves. This association aligns with the abundant evidence of GSSCP. Similarly, the minor presence of bulliform flabellate phytoliths further supports this connection.

Elongate entire phytoliths, comprising 5.74% of the assemblage, are produced by various plants across numerous organs, limiting their diagnostic value. Other Elongate morphotypes (5.10%) were also left unidentified due to significant corrosion. A few Spheroid phytoliths were also observed, though they are scarce. Spheroid echinate phytoliths (0.35%) are indicative of palms (Arecaceae), a notable find at Assur, given its location outside the biogeographical range of the date palm (*Phoenix dactylifera*, see also **§I2.9**). Spheroid ornate and psilate phytoliths suggest the presence of woody dicots, but their contribution to the overall assemblage is minimal. Blocky phytoliths (1.73%) are relatively common; however, their origin remains ambiguous as none were found in their original anatomical position, leaving it unclear whether they derive from dicotyledonous or monocotyledonous plants.

I3.3.2 Sample descriptions

The sample AS 262432:070:006 was recovered from Grave 5, with typical late Neo-Assyrian burial goods and radiocarbon dated to 770-542 calBC (95.4% probability).[417] This sample was collected inside a small vessel within the grave,[418] ensuring minimal contamination from surrounding deposits.[419] 197 phytoliths were identified, with a notable 10% consisting of multicellular (articulated) phytoliths. Six of the 18 multicellular phytoliths observed were melted or weathered, precluding morphological identification. Though showing evidence of mechanical abrasion, corrosion, or burning, the remaining multicellular phytoliths retained identifiable features. Many were attributed to grass inflorescences, displaying evident characteristics of Elongated dentate, Elongated dendritic, and Papillate forms. The overall composition of the sample is consistent with the assemblage previously described: approximately 35% consists of fragmented Elongate dentate/dendritic phytoliths, with about 10% attributed to Rondels. Discoloured phytoliths are rare, while calcium oxalate crystals are abundant in this sample.

Four samples were recovered from Hellenistic Building A, specifically from Room 2, Room 3, and Courtyard 10. The two floor deposit samples from Room 2 (AS 261432:011:021 and AS 262433:105:004) yielded 135 identified phytoliths, a notably low number. Interestingly, based on the analysis

417 See Radner/Squitieri 2024b, Table D1.1
418 Kreppner/Richter/Squitieri 2024, fig. E1.9.
419 Kreppner/Rohde/Squitieri 2024, 130-132.

of flotation samples, Room 2 also yielded the lowest seed density across Building A (see **§I2** and **Fig. I2.1**).

Sample AS 261432:011:021 contained only 40 phytoliths, nearly half of which were unidentifiable due to weathering or melting. In contrast, AS 262433:105:004 had a slightly higher phytolith count, though one-fifth of its content was similarly unidentified or weathered. The remaining phytoliths in both samples were challenging to assign to specific morphotype categories, although Elongates, Rondels, and fragmented Elongate dentate/dendritic morphotypes were present. Notably, neither sample contained evidence of Chrysophyte cysts or diatoms. While discoloured phytoliths were rare, both samples were rich in calcium oxalate crystals.

The remaining two samples from Building A contain a richer phytolith assemblage. Sample AS 262432:058:019, from Room 3's floor deposit, yielded 175 identified phytoliths, with Rondels comprising nearly one-fourth of the assemblage. Notably, some Rondels are unusually large compared to those found elsewhere. Elongate Dentate phytoliths in this sample are less fragmented than in others, indicating better preservation. Additional phytolith types include GSSCP, Acute Bulbosus, Papillate, and Blocky forms. Furthermore, a multicellular phytolith and two Spheroid Ornate phytoliths were observed, suggesting the presence of dicot leaves.

In contrast, sample AS 261433:067:011, from Courtyard 10's floor deposit, shows more evidence of fragmentation, weathering, and melting than other samples from this phase. Despite this, the sample contained 199 phytoliths, with fragmented Elongate dentate/dendritic phytoliths and Rondels, each accounting for about one-fourth of the total. Discoloured phytoliths were relatively scarce in this sample, while calcium oxalate crystals were abundant.

Two samples were collected from Graves 3 and 4, both dated to the mid-2nd century BC, based on an alphabetic inscription incised on the sarcophagus of Grave 3, reporting the date 159/158 BC.[420] These burials are particularly significant due to their likelihood of being uncontaminated for phytolith deposition. The sample from Grave 3 (AS 262433:060:018) stands out for the unusually small calcium oxalate crystals. Despite showing evidence of burning, these crystals are abundant and better preserved than the phytoliths. This contrasts with other samples identified, where calcium oxalate crystals were consistently larger. Interestingly, no discoloured phytoliths were identified in this sample. Most of the 72 classified phytoliths were melted, while some showed weathering signs. Additionally, GSSCP phytoliths were notably absent, and grass inflorescence indicators were only minimally present in this particular depositional context.

The sample from Grave 4 (AS 262432:055:005) presents a contrasting pattern to the previous sample. Grave 4 sample, collected from above the skeleton, shows clear evidence of grass inflorescences, grass leaves/stems, and dicot phytoliths. Additionally, discoloured phytoliths are abundant. However, approximately one-fourth of the sample consists of weathered and melted phytoliths.

Finally, two samples came from graves dated to the Parthian period: Grave 6 (sample AS 261433:032:003) and Grave 7 (sample AS 262433:096:002) (**§C2.5**). These samples contained minimal phytolith evidence, with 28 and 62 identified phytoliths, respectively. Both samples included numerous blackened phytoliths and relatively fewer calcium oxalate crystals. Due to the limited phytolith content, drawing meaningful conclusions about their overall significance is challenging.

I3.4 Conclusions

This preliminary study has examined the phytolith assemblage at Assur, highlighting its significance for understanding ancient settlements when integrated with other micro-archaeological methods. The analysis of nine sediment samples revealed phytolith concentrations between 300,000 and 1,700,000 per gram, identifying 1,097 opal phytoliths, with nearly 20% categorised as weathered or melted. A notable ratio of melted to weathered phytoliths was observed, varying by context. The stability of phytoliths after burial is a well-researched area that provides valuable information on how fossil phytoliths survive in natural and archaeological sediments. Solubility and mechanical abrasion have been found to consistently impact the stability of fossil phytoliths. Therefore, the assemblage composition is subject to diagenetic changes after burial in archaeological sites.[421] Although phytoliths are durable inorganic bodies and can survive conditions when most organic remains can rapidly dissolve, they are strongly affected by the alkaline levels of the soil, and their solubility is thought to increase significantly under high pH and alkaline conditions.[422] The solubility of phytoliths increases significantly above pH 9, while water flow is needed for phytolith dissolution.[423] The temperature differences in wet and dry periods can also be factors for alternating pH values. Therefore, seasonal impact is equally crucial

420 Gzella 2024.

421 Cabanes/Weiner/Shahack-Gross 2011; Piperno 2006.

422 Cabanes/Weiner/Shahack-Gross 2011.

423 Pearsall 2015.

for phytolith dissolution.[424] High soil pH, water flow and seasonal temperature differences may have impacted the survival of phytoliths in Assur's archaeological strata.

Our analysis has also indicated significant amounts of calcium oxalate crystals, further enriching the findings related to plant evidence in the assemblages studied. Building on this evidence, analysing the phytolith assemblages at Assur in conjunction with other mineral components, such as calcium oxalate, calcitic ash, and discoloured phytoliths, is essential. This may provide valuable insights into the region's environmental and agricultural dynamics. Understanding the depositional histories of these mineral components will ultimately require detailed investigations using multidisciplinary archaeological techniques in future studies.

424 Karkanas 2010.

J. Preliminary conclusions for 2024

Karen Radner & Andrea Squitieri

Working in Assur continues to be a logistically, physically and emotionally challenging experience. Still, the results of our second year of fieldwork and the subsequent analyses of various finds made and samples taken during February and March 2024 have made the efforts worthwhile. In the excavation house, problems that caused delays and frustration in 2023 were successfully ironed out. In particular, our much better control of the electricity supply made the processing of flotation samples far more efficient and less time-consuming, and after Jana Richter and Andrea Squitieri had critically assessed the shortfalls of the pottery processing workflow during the short 2023 autumn study campaign, its speed was considerably increased by running a second Laser Aided Profiler and by training local colleagues Amr Mohammad Jasim and Omar Laith Allawi to complete the entire registration and recording process independently.

Moreover, the danger of running out of space because of the masses of pottery being stored in the excavation house was countered by renovating the second building to remain of Walter Andrae's original compound: the house known either as the House of Shaul Selman or more recently as *bayt ʿUmyān* ("Umyan's House"). Whereas the origin of the latter name remains unclear, Shaul Selman (also known as Saul Salomon) is familiar to us. Selman, the original accountant and treasurer of the Assur excavations, was a member of Hillah's significant and long-established Jewish community[425] and joined the Assur team through the mediation of Babylon's excavator Robert Koldewey. Our previous research in the archives of the German Oriental Society regarding Walter Andrae's construction activities at Assur had revealed that he had built a separate house for Selman just north of the excavation house in 1904.[426] Later, the Iraqi State Board of Antiquities and Heritage (SBAH) converted the building into a storage facility for the pottery found at Assur, and the ceramic finds of Peter Miglus' work in 2000 and 2001 were stored there, too. In 2016, when the Iraqi forces expelled a local ISIS terrorist cell from the excavation house that they had occupied since 2015, the Selman House was destroyed as well. Its restoration began in August 2024 and was completed in late October 2024 (**Figs. J1–J3**) under the supervision of Kamal Rasheed Raheem, with majority funding provided by the Patrimonies Fund of the Gerda Henkel Foundation (AZ 22/BE/24: "Renovation of the House of Shaul Salman in Assur"), and additional funding from Karen Radner's 2022 Gottfried Wilhelm Leibniz Award. During the 2025 spring campaign, the largest room of the house, situated in its northern part, was equipped with metal shelving to store human bones and pottery sherds

Fig. J1: The Selman House, view from southeast. Drone photo by Jens Rohde.

Fig. J2: The Selman House, view from northwest. Photo by Jana Richter.

425 On which see e.g. Cohen 1966, 3; Gat 1997.
426 Radner/Richter 2024, 28.

that have already been registered, processed and analysed (**Fig. J4**).

During the 2024 spring campaign, combining geomorphological and geophysical prospecting with a programme of sediment coring and excavations allowed us to considerably deepen our knowledge of the New Town's long occupational history and Assur's complex archaeological landscape. The latter is greatly affected by environmental and human-induced erosion (**§B1**). Contributing to the ongoing degradation of the site is the interplay of the region's climatic conditions, its soil composition, and its topography. The fragile mudbrick structures and the lack of humic topsoil make Assur especially vulnerable to water runoff and gully formation, particularly near the riverbank of the Tigris. These issues are massively exacerbated by past excavations that were left lying open, especially Walter Andrae's famous west-to-east trenches, as well as the activities of livestock and visitors.

Fig. J3: The inner courtyard of the Selman House. Photo by Jana Richter.

Fig. J4: The newly arranged storage space in the north room of the Selman House. Photo by Helen Gries.

The 2024 coring campaign had two goals. Firstly, we targeted the cellas of the sanctuaries of the gods Ishtar and Aššur to uncover the construction history of these most prominent temples in the Inner City of Assur (**§B2.3**). Whereas the many metres of fill left by past excavations and restorations made it impossible to reach layers elucidating the Aššur temple's early stratigraphy, coring beneath the cella of the Ishtar Temple was successful. We uncovered a thick layer of sand that had been placed directly underneath the original sanctuary. This sand was not sourced locally, which points to specific purification practices undertaken on the occasion of the temple's foundation.

Secondly, in the New Town (**§B2.2**), we aimed to find out more about the occupation layers situated underneath the Parthian-period architecture that had been brought to light by the 2023 magnetometer prospection.[427] The cores drilled in the New Town served as the crossing points of east-west- and north-south-oriented Electric Resistivity Tomography (ERT) profiles (**§B2.3**). Combined, the new coring and ERT results allow us to propose identification of architecture, open spaces, and pathways, all likely dating to the Assyrian period of the New Town's occupation. The results also highlight the uneven relief of the New Town, with the bedrock encountered at different levels in various areas. It emerges that the higher-lying parts of the New Town were the preferred sites for the construction of buildings, likely so that they were not affected by the water that accumulated in the lower-lying areas.

This specific hypothesis was put to the test by opening up trench NT2 (**§C4**) at the deepest-lying spot of the New Town, where a geophysical anomaly had been observed close to the southern city wall in the 2023 campaign.[428] This turned out to be a large drainage shaft dug straight through the bedrock, with its original opening situated about 3 m below the modern surface (**Fig. J5**). The shaft was presumably constructed at the same time as the New Town and its fortifications, or soon after, i.e. in the Late Bronze Age / Middle Assyrian period from which its old-

427 Fassbinder *et al.* 2024a, 72-77.
428 Fassbinder/Wolf 2024, 81 with figs. C2.14-15 (p. 80).

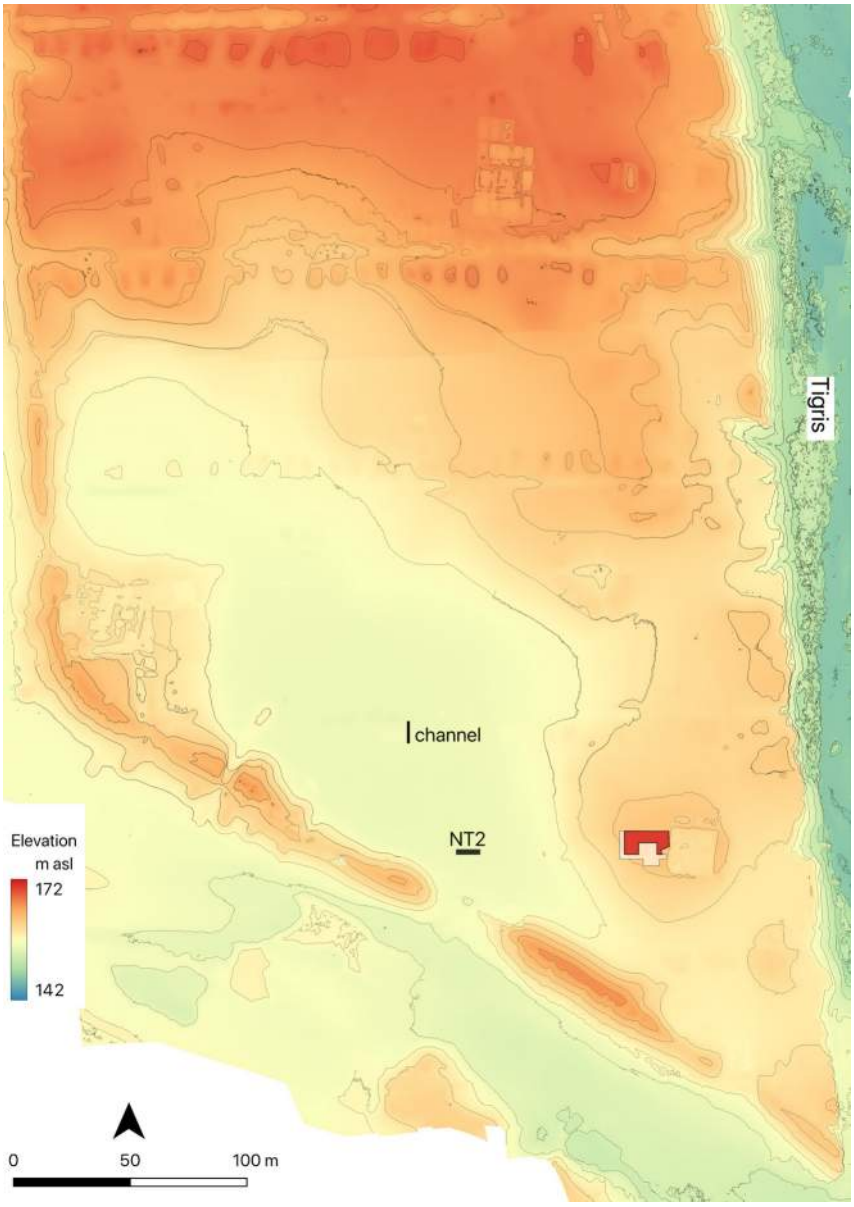

Fig. J5: Digital Elevation Model (DEM) of Assur's New Town, indicating the location of Trench NT2 and the possible underground channel identified in ERT Profile 8. Created by Andrea Squitieri using a DEM generated by Jens Rohde.

est ceramic finds date (**§D1.2**). Its purpose was to collect and drain rainwater as well as wastewater, as indicated not only by the wastewater drainage identified in the 2023 excavations of the Assyrian-period Building B,[429] but also by the possible channel visible in the results of the 2024 ERT prospection (**§B3**). The drainage shaft was used over centuries but no longer serviced after the end of the Neo-Assyrian period and the fall of the Assyrian Empire, as the accumulation of various later occupation layers indicates, which include a burial and much workshop refuse. A charcoal sample radiocarbon-dated to 770-541 calBC (**§C1.2** with **Fig. C1.8**) was identified as oak (*Quercus*), which must have been imported to Assur (**§I1**). The sinkhole's stratified pottery sequence goes from the Middle Assyrian to the Parthian period (**§D1.2**) and thus covers the entire occupational history of the New Town. One Neo-Assyrian sherd featured a fragmentary cuneiform inscription running in three lines from the vessel's rim to its bottom (**§F1**: Text 11).

This inscribed sherd was the only textual find made during the 2024 excavations. All other cuneiform texts published in this volume are surface finds of inscribed bricks of various kings of the Middle Assyrian (Adad-nerari I, Shalmaneser I, and Tukulti-Ninurta I) and Neo-Assyrian periods (Ashurnasirpal II, Shalmaneser III, Sennacherib: **§F2**). These and the inscribed bricks recovered in 2023 were sampled, among other brick specimens from well-dated building contexts, for the geochemical analysis of brick recipes used at Assur through the ages (**§G**). The results highlight differences and similarities in the design of Middle and Neo-Assyrian bricks. They all share a high calcium carbonate ($CaCO_3$) content, which indicates a deliberate strategy to enhance their durability. This is perhaps not surprising, as inscribed bricks were a key component in the Assyrian kings' attempts to preserve their "written names" (thus the Akkadian term for what we call "inscriptions" for eternity),[430] and their longevity was thus of utmost importance.

In 2024, we continued excavating the substantially enlarged trench NT1 (**§C2**). Here, five more Parthian-period graves of the pit and tub sarcophagus types were uncovered (**§C2.5**), just north of the chamber tomb excavated in 2023,[431] whose entrance shaft was explored in 2024 (**§C2.6**). During the detailed registration of the human bones unearthed in the tomb for the anthropological

429 Kreppner/Rohde/Squitieri 2024, 134.

430 Radner 2005, 114-155, 161-165.

431 Kreppner/Rohde/Squitieri 2024, 105-118.

analysis (**§H**), the rider of a horseman figure, handmade from clay (**§E**: **Fig. E1.3.9**), was identified, which confirms this figurine type's dating to the Parthian period; most other known examples from Assur lack a good find context. The new excavation results show the chamber tomb to be surrounded by burial plots, thus forming part of a larger Parthian-period cemetery in this area of the New Town. The individual graves often used tub sarcophagi (**§E1**, with **Figs. E1.1.1–9**), with some showing signs of ancient repair and reuse: this might suggest that Assyrian funerary objects were recycled and repurposed in the Parthian period. The people buried in the single graves were mostly young adult females (showing signs of joint disease, indicating that they conducted sustained manual labour), as well as two males and one infant. Disappointingly, only minimal evidence was found in the two assemblages of phytoliths sampled in 2023 from Graves 6 and 7 (**§I3**). On the other hand, a palaeobotanical sample handpicked from the fill of Pit 7, which held Parthian-period ceramics (**§C2.7**), contained pits of dates, which must be considered imports from southern Mesopotamia, where the date palm thrives (**§I2.9**).

Many of the Parthian-period cemetery's burials, including those in the chamber tomb, were disturbed and looted in antiquity. Two large water jars were likely left behind by the individuals who looted the cemetery in the Early Islamic period, as the vessels' characteristic honeycomb decoration allows their dating to the 8th century AD (**§D1.3**).

Situated underneath the cemetery, Building A is conclusively dated to the Hellenistic era by the radiocarbon datings derived from seeds and charcoals,[432] the date given in the alphabetic inscription incised on a sarcophagus,[433] and now also a newly discovered late Seleucid bronze coin (**§E2** with **Figs. E2.1a–e**). The pottery found in this substantial residential building further confirms its Hellenistic date and reflects its domestic, storage, and communal functions. We are extremely grateful to Alessandra Cellerino and Enrico Foietta (**Fig. J6**), members of the Italian Archaeological Expedition at Seleucia on the Tigris (IAES), led by the Centro Ricerche Archeologiche e Scavi di Torino (CRAST) and the University of Turin, for joining us in the spring of 2025 to work on the pottery assemblage from Building A, and especially for making their first results available already in this volume (**§D1.1**). A notable find is the fragment of an imported Attic echinus bowl, one of the most popular shapes of the Hellenistic vessel typology (**Fig. D1.1.1**), which illustrates the now important connection with the Mediterranean.

In 2024, Building A was further exposed, revealing new rooms and demonstrating that "Room 5" of the 2002 SBAH excavations was the Hellenistic building's deep grain silo (**§C2.8.7**); after its abandonment, this silo slowly filled up with waste material over time. The light fraction of the flotation samples from the new rooms yielded further material for the ongoing plant identification (**§I2**), adding to the 2023 results.[434] In addition, a first study of the phytolith samples taken in 2023 from Rooms 2, 3 and Courtyard 10 provided new insights into the plant life and plant preservation at Assur in the Hellenistic period (**§I3**).

Fig. J6: From left to right: Sakhar Mohammad Ajaj, Amr Mohammad Jasim, Omar Laith Allawi, Andrea Squitieri, Amer Abdullah Najm Aljumaily (University of Mosul), Kamal Rasheed Raheem, Poppy Tushingham, Alessandra Cellerino and Enrico Foietta (both University of Turin). 15 March 2025. Photo by Aziz Sharif.

432 Radner/Squitieri 2024c, 100.

433 Gzella 2024.

434 Sarkady 2024.

The chemical and petrographic analyses conducted on pottery from the Hellenistic Building A and from the Parthian-period chamber tomb (**§D2**) highlight considerable changes in manufacturing practices and also exchange patterns between these two periods of Assur's occupation. The Hellenistic pottery showed diverse chemical compositions and production strategies, indicating active trade. Notably, the already mentioned echinus bowl was conclusively identified as non-local, supporting the results of the typological study that classify it as an Attic import (**§D1.1**). Spatially, local ceramic groups cluster in the western rooms of Building A, while chemically distinct and non-local samples tend to appear in the eastern areas of the building. Notable patterns in the distribution of local and imported woods were also observed when analysing the charcoal remains from the same building (**§I1**). The Parthian-period pottery was found to be far more chemically uniform, with less variation and fewer imports. While this could indicate a shift towards localised production, it is important to stress that the Parthian-period material comes from a funerary context rather than a residential building.

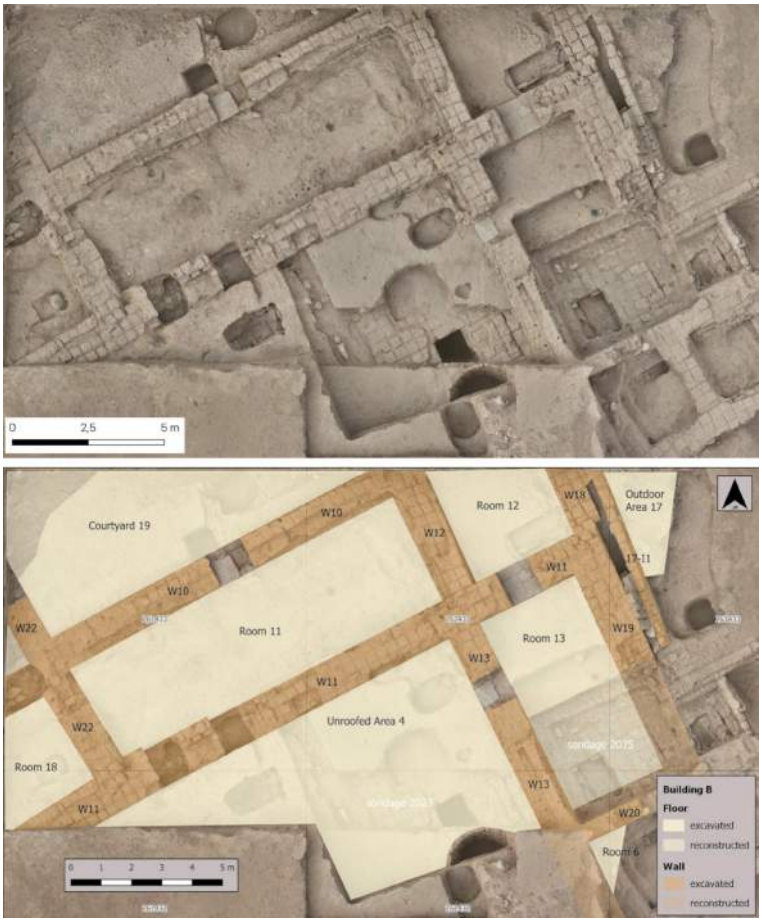

Fig. J7: Orthophoto (top) and plan (bottom) of Building B, dating to the Neo-Assyrian period, at the end of the 2025 excavation campaign. Created by Jens Rohde.

During the 2025 spring campaign, Building A was fully removed, and underneath, two earlier structures were uncovered: Buildings C1 and C2, as well as associated graves. These newly identified buildings, and the burials linked to them, likely date to the Achaemenid or early Seleucid period, and the radiocarbon samples taken and exported in May 2025 will hopefully clarify this.

Below these structures lie the remains of Building B, as first identified in the 2023 excavations (**Fig. J7**). Its pottery conclusively assign it to the later Neo-Assyrian period,[435] and this dating is now further strengthened by the radiocarbon date range gained from a carbonised seed from the newly excavated Room 11 (**§C2.9**; **Fig. C1.3**: 778-551 calBC; as is to be expected, this dating falls into the Hallstatt Plateau). The large and well-appointed Room 11, whose entrance features a stone threshold, yielded a good amount of light fraction from flotation that deepens our understanding of the domesticated and wild plants in evidence at Assur during the late Neo-Assyrian period (**§I2**), adding to the 2023 results.[436] Due to its position and its architectural characteristics, Room 11 most likely had a representative function within the very sizable Building B, whose wall and room dimensions dwarf those of Building A. The comparative geochemical analysis of the bricks from Buildings A and B highlighted pronounced differences between the brick recipes used to manufacture the Neo-Assyrian and the Hellenistic mudbricks (**§G**).

Connected to Building B is a Neo-Assyrian burial (Grave 5, providing two radiocarbon date ranges from 770-542 calBC and 775-545 calBC; again falling into the Hallstatt Plateau),[437] and the osteological analysis of the skeleton showed that it belonged to a woman suffering from a metabolic condition that affected several of her bones (**§H2.3**). A vessel from this grave yielded the first Iron Age assemblage of phytoliths to be analysed from Assur (**§I3**).

In the spring campaign of 2025, the excavation of Building B continued in an area of 250 m², bringing to light more of its typical Assyrian architectural layout (**Fig. J7**)

435 Kreppner/Richter/Squitieri 2024, 145-147.

436 Sarkady 2024.

437 Kreppner/Rohde/Squitieri 2024, 130-132.

and producing characteristic finds that include a bronze duck weight.

Overall, our excavations in Trench NT1 are notable for revealing the uninterrupted occupation of this part of the New Town from the Assyrian to the Parthian periods, with no signs of significant destruction. To learn more about the earlier Assyrian stratigraphy, we opened another sondage within the SBAH trench unearthed in 2002: Sondage 2 was excavated in spring and autumn 2024 (**§C3**). Multiple construction phases dating to the Iron Age were identified underneath the brick floor level reached by the Iraqi archaeologists, with features suggestive of open spaces such as courtyards. Below, there is evidence for Late Bronze Age occupation, but within the restricted space of the sondage, no corresponding architecture was preserved. A range of radiocarbon dates is available for the sondage, with the earliest, from a piece of charcoal, dating to 1406-1261 calBC (**Fig. C1.10**). This is relatively close to the radiocarbon dating range of 1506-1440 calBC from a lump of charcoal from above the virgin soil found in the 2023 excavations in Trench NT1.[438]

Therefore, our work continues to strengthen the hypothesis that the original occupation of the New Town dates back to the time of Puzur-Aššur III (conventionally dated to 1521-1498 BC), who, in his inscriptions, took credit for fortifying the New Town of Assur,[439] which he was the first to mention.

438 Kreppner/Rohde/Squitieri 2024, 136; Radner/Squitieri 2024c, 100 Fig. D1.5.

439 Miglus 2010, 236-237.

Bibliography

Bibliographic abbreviations
RIMA 1 = Grayson 1987
RIMA 2 = Grayson 1991
RIMA 3 = Grayson 1996
RINAP 3/2 = Grayson/Novotny 2014

Ahmad 1996
A.Y. Ahmad, "The archive of Aššur-mātu-taqqin found in the New Town of Aššur and dated mainly by post-canonical eponyms." *Al-Rafidan* 17 (1996), pp. 207–288.

Ahmad 2025
M. Ahmad, "Late Sasanian or Early Islamic? Honeycomb pottery revisited." In: S. Haddow, C. Mazzucato, and I. Thuesen (eds.), *Proceedings of the 13th International Congress on the Archaeology of the Ancient Near East*, Copenhagen 2025, pp. 455–463.

Albert/Ruíz/Sans 2016
R.M. Albert, J.A. Ruíz, and A. Sans, "PhytCore ODB: a new tool to improve efficiency in the management and exchange of information on phytoliths." *Journal of Archaeological Science* 68 (2016), pp. 98–105.

Albert/Weiner 2001
R.M. Albert and S. Weiner, "Study of phytoliths in prehistoric ash layers from Kebara and Tabun caves using a quantitative approach." In: J.D. Meunier and F. Coline (eds.), *Phytoliths: Applications in Earth Sciences and Human History*, Cape Town 2001, pp. 251–266.

Albert *et al.* **1999**
R.M. Albert, O. Lavi, L. Estroff, S. Weiner, A. Tsatskin, A. Ronen, and S. Lev-Yadun, "Mode of occupation of Tabun Cave, Mt Carmel, Israel during the Mousterian period: a study of the sediments and phytoliths." *Journal of Archaeological Science* 26 (1999), pp. 1249–1260.

Altaweel 2024
M. Altaweel, "Geoarchaeological coring in the New Town of Assur." In: Radner/Squitieri 2024a, pp. 81–87.

Andrae 1913
W. Andrae, *Die Festungswerke von Assur*, Leipzig 1913.

Andrae 1922
W. Andrae, *Der archaische Ischtar-Tempel in Assur*, Leipzig 1922.

Andrae 1935
W. Andrae, *Die jüngeren Ischtar-Tempel in Assur*, Leipzig 1935.

Andrae 1938
W. Andrae, *Das wiedererstandene Assur*, Leipzig 1938.

Andrae 1977
W. Andrae, *Das wiedererstandene Assur*, Munich 1977 (2nd edition, ed. by B. Hrouda).

Andrae/Lenzen 1933
W. Andrae and H. Lenzen, *Die Partherstadt Assur*, Leipzig 1933.

Atkinson 1946
R.J.C. Atkinson, *Field Archaeology*, London 1946.

Ball *et al.* **2016**
T. Ball, K. Chandler-Ezell, R. Dickau, N. Duncan, T.C. Hart, J. Iriarte, C. Lentfer, A. Logan, H. Lu, M. Madella, D.M. Pearsall, D.R. Piperno, A.M. Rosen, L. Vrydaghs, A. Weisskopf, and J. Zhang, "Phytoliths as a tool for investigating agricultural origins and dispersals around the world." *Journal of Archaeological Science* 68 (2016), pp. 32–45.

Bär 2003a
J. Bär, *Die älteren Ischtar-Tempel in Assur: Stratigraphie, Architektur und Funde eines altorientalischen Heiligtums von der zweiten Hälfte des 3. Jahrtausends bis zu Mitte des 2. Jahrtausends v.Chr.*, Berlin 2003.

Bär 2003b
J. Bär, "Sumerians, Gutians and Hurrians at Ashur? A re-examination of Ishtar Temples G and F." *Iraq* 65 (2003), pp. 143–160.

Becker 1991
H. Becker, "Zur magnetischen Prospektion in Assur: Testmessung 1989." *Mitteilungen der Deutschen Orient-Gesellschaft zu Berlin* 123 (1991), pp. 123–131.

Beijerinck 1976
W. Beijerinck, *Zadenatlas der nederlandsche flora ten behoeve van de botanie, palaeontologie, bodemcultuur en warekennis: omvattende, naast de inheemsche flora, onze belangrijkste cultuurgewassen en verschillende adventiefsoorten*, Amsterdam 1976.

Berna *et al.* 2007
F. Berna, A. Behar, R. Shahack-Gross, J. Berg, E. Boaretto, A. Gilboa, I. Sharon, S. Shalev, S. Shilstein, N. Yahalom-Mack, J.R. Zorn, and S. Weiner, "Sediments exposed to high temperatures: reconstructing pyrotechnological processes in Late Bronze and Iron Age Strata at Tel Dor (Israel)." *Journal of Archaeological Science* 34 (2007), pp. 358–373.

Bernard/Gachet/Salles 1990
V. Bernard, J. Gachet, and J.F. Salles, "Apostilles en marge de la céramique des États IV et V de la forteresse". In: Y. Calvet and J. Gachet, *Failaka, fouilles françaises 1986–1988*, Lyon 1990, pp. 241–284.

Bianchi/Wissing 2010
A. Bianchi and A. Wissing, *Ausgrabungen 1998-2001 in der Zentralen Oberstadt von Tall Mozan/Urkeš: die Kleinfunde*, Wiesbaden 2010.

Blaylock *et al.* 2016
S. Blaylock, D. Collon, M. Nesbitt, B.C. Coockson, and T. Çakar, *Tille Hoyuk, vol. 3.2: The Iron Age: Pottery, Objects, and Conclusions*, Ankara 2016.

Bolognani 2017
B. Bolognani, *The Iron Age Figurines from Karkemish (2011–2015 campaigns) and the Coroplastic Art of the Syro-Anatolian Region*. PhD thesis, University of Bologna, 2017. Available at: amsdottorato.unibo.it/8222/.

Boucharlat 1987
R. Boucharlat, "Les niveaux post-achéménides à Suse, secteur nord: Fouilles de l'Apadana-Est et de la Ville Royale ouest (1973-1978)." *Cahiers de la Délégation Archéologique Française en Iran* 15 (1987), pp. 145–311.

Brickley/McKinley 2004
M. Brickley and J.I. McKinley, *Guidelines to the Standards for Recording Human Remains*, Reading 2004.

Brooks/Suchey 1990
S. Brooks and J.M. Suchey, "Skeletal age determination based on the os pubis: a comparison of the Acsádi-Nemeskéri and Suchey-Brooks methods." *Human Evolution* 5 (1990), pp. 227–238.

Buikstra 2019
J.E. Buikstra (ed.), *Ortner's Identification of Pathological Conditions in Human Skeletal Remains*, London et al. 2019 (3rd edition).

Buikstra/Ubelaker 1994
J.E. Buikstra and D.H. Ubelaker (eds.), *Standards for Data Collection from Human Skeletal Remains*, Fayetteville 1994.

Butcher 2017
K. Butcher, "From the Achaemenids to the Arsacids." In: S. Heidemann and K. Butcher, *Regional History and The Coin Finds From Assur: From the Achaemenids to the Nineteenth Century*, Wiesbaden 2017, pp. 7–48.

Cabanes/Albert 2011
D. Cabanes and R.M. Albert, "Microarchaeology of a collective burial: Cova des Pas (Minorca)." *Journal of Archaeological Science* 38 (2011), pp. 1119–1126.

Cabanes/Weiner/Shahack-Gross 2011
D. Cabanes, S Weiner, and R. Shahack-Gross, "Stability of phytoliths in the archaeological record: a dissolution study of modern and fossil phytoliths." *Journal of Archaeological Science* 38 (2011), pp. 2480–2490.

Calini 2022
I. Calini, "Ceramic finds of the Hellenistic-Seleucid era from Qasr Shemamok: 2012 campaign, area A-Est." *Etudes Mésopotamiennes—Mesopotamian Studies* 2 (2022), pp. 470–512.

Canti 2003
M.G. Canti, "Aspects of the chemical and microscopic characteristics of plant ashes found in archaeological soils." *Catena* 54 (2003), pp. 339–361.

Cappers/Bekker/Jans 2012
R.T.J. Cappers, R.M. Bekker, and J.E.A. Jans, *Digitale Zadenatlas van Nederland*, Groningen 2012.

Cecchini 2000
S.M. Cecchini, "The textile industry in Northern Syria during the Iron Age according to the evidence of the Tell Afis excavations." In: G. Bunnens (ed.), *Essays on Syria in the Iron Age*, Leuven 2000, pp. 211–233.

Cellerino 2004
A. Cellerino, "La ceramica dal sondaggio di Shu-Anna a Babilonia." *Mesopotamia* 39 (2004), pp. 93–168.

Cellerino 2015
A. Cellerino, "The pottery." In: V. Messina (ed.), *Hung-e Azhdar: Research of the Iranian-Italian Joint Expedition in Khuzestan (2008-2011)*, Pisa 2015, pp. 123–176.

Cellerino 2021
A. Cellerino, "Transparent glass drinking bowls at the Assyrian court: visual appeal of wine consumption." *Mesopotamia* 61 (2021), pp. 125–138.

Cellerino 2023
A. Cellerino, "Ceramic innovations and conservatisms in Hellenizing Elymais: the glazed pottery from Shami." In: N. Marchetti, M. Campeggi, F. Cavaliere, C. D'Orazio, G. Giacosa, and E. Mariani (eds.), *Proceedings of the 12th International Congress on the Archaeology of the Ancient Near East, vol. 1*, Wiesbaden 2023, pp. 301–314.

Chambon/Kreppner 2010
G. Chambon and F.J. Kreppner, "Hohlmaßsysteme und deren Standardisierung in Assyrien und Volumina von Gefäßkeramik aus Dūr-Katlimmu." In: H. Kühne (ed.), *Dūr-Katlimmu 2008*, Wiesbaden 2010, pp. 11–32.

Charles/Bogaard 2001
M. Charles and A. Bogaard, "Third millennium BC charred plant remains from Tell Brak". In: D. Oates, J. Oates, and H. McDonald (eds.), *Excavations at Tell Brak, vol. 2: Nagar in the Third Millennium BC*, Oxford 2001, pp. 301–326.

Charlier *et al.* 2012
P. Charlier, L. Brun, C. Prêtre, and I. Huynh-Charlier, "Toilet hygiene in the classical era." *British Medical Journal* 345 (2012), e8287. DOI: 10.1136/bmj.e8287.

Chiocchetti 2008
L. Chiocchetti, "Post-Assyrian pottery from the Italian Excavations at Fort Shalmaneser, 1987–-1990." In: J. Córdoba, M. Molist, C. Pérez, I. Rubio, and S. Martínez (eds.), *Proceedings of the 5th International Congress on the Archaeology of the Ancient Near East*, Madrid 2008, pp. 417–440.

Cinti Luciani 1993
S. Cinti Luciani, "The late pottery of Tell Jikan and Tell Khirbet Salih." In: W. Gernot and C. Zaccagnini (eds.), *Tell Karrana 3 – Tell Jikan – Tell Khirbet Salih*, Mainz 1993, pp. 279–292.

Clark 1968
A.J. Clark, "A square array for resistivity surveying." *Prospezioni Archeologiche* 3 (1968), pp. 111–114.

Clark 1980
A.J. Clark, *Archaeological Detection by Resistivity*, PhD thesis, University of Southampton, 1980. Available at: eprints.soton.ac.uk/462734/.

Clark 1996
A.J. Clark, *Seeing Beneath the Soil: Prospecting Methods in Archaeology*, London 1996.

Cleuziou 1977
S. Cleuziou, "Les pointes de flèches 'scythiques' au proche et moyen Orient." In: J. Deshayes (ed.), *Le plateau iranien et l'Asie Centrale des origines à la conquête islamique*, Paris 1977, pp. 187–199.

Cohen 1966
H.J. Cohen, "The Anti-Jewish 'Farhūd' in Baghdad, 1941." *Middle Eastern Studies* 3 (1966), pp. 2–17.

Constable/Parker/Constable 1987
S.C. Constable, R.L. Parker, and C.G. Constable. "Occam's inversion: a practical algorithm for generating smooth models from electromagnetic sounding data." *Geophysics* 52 (1987), pp. 289–300.

Crivellaro/Schweingruber 2013
A.Crivellaro and F.-H. Schweingruber, *Atlas of Wood, Bark and Pith Anatomy of Eastern Mediterranean Trees and Shrubs, with a Special Focus on Cyprus*, London 2013.

Curtis 1984
J.E. Curtis, *Nush-i Jan, III: The Small Finds*, London 1984.

Curtis 1989
J.E. Curtis, *Excavations at Qasrij Cliff and Khirbet Qasrij*, London 1989.

Curtis 2013
J.E. Curtis, *An Examination of Late Assyrian Metalwork, with Special Reference to Nimrud*, Oxford 2013.

Curtis/Green 1997
J.E. Curtis and A. Green, *Excavations at Khirbet Khatuniyeh*, London 1997.

Curtis/Green/Knight 1987–1988
J.E. Curtis, A. Green, and W. Knight, "Preliminary report on the excavations at Tell Deir Situn and Grai Darki." *Sumer* 45 (1987–1988), pp. 49–53.

Curtis 2007
V.S. Curtis, "The Iranian revival in the Parthian period."

In: V.S. Curtis and S. Stewart (eds.), *The Age of the Parthians*, London/New York 2007, pp. 7–25.

Davies 1974
B.E. Davies, "Loss-on-ignition as an estimate of soil organic matter." *Soil Science Society of America Proceedings* 38 (1974), pp. 150–151.

de Miroschedji 1987
P. de Miroschedji, "Fouilles du chantier Ville Royale II à Suse (1975-77), II: Niveaux d'époques achéménide, séleucide, parthe et islamique." *Cahiers de la Délégation Archéologique Française en Iran* 15 (1987), pp. 11–143.

Deckers 2024
K. Deckers, "Wood identification from charcoal remains." In: Radner/Squitieri 2024a, pp. 201–202.

Deckers/Pessin 2010
K. Deckers and H. Pessin, "Vegetation development in the Middle Euphrates and Upper Jazirah (Syria/Turkey) during the Bronze Age." *Quaternary Research* 74.2 (2010), pp. 216–226.

Delrue 2007
P. Delrue, "Trilobate arrowheads at ed-Dur (U.A.E., Emirate of Umm al-Qaiwain)." *Arabian Archaeology and Epigraphy* 18 (2007), pp. 239–250.

Diffey/Neef/Boogard 2017
C. Diffey, R. Neef, and A. Bogaard, "The archaeobotany of large-scale hermetic cereal storage at the Hittite capital of Hattusha." In: A. Schachner (ed.), *Innovation versus Beharrung: Was macht den Unterschied des Hethitischen Reichs im Anatolien des 2. Jahrtausends v. Chr.?*, Istanbul 2017, pp. 185–200.

Ehling/Pangerl/Wünsch 2020
K. Ehling, A. Pangerl, and J. Wünsch, "Hippokrates – ein neuer Seleukidenkönig." *Jahrbuch für Numismatik und Geldgeschichte* 69/70 (2020), pp. 35–48.

Ehrich 1939
R.W. Ehrich, "Appendix E: The later cultures at Yorgan Tepa." In: R.F.S. Starr (ed.), *Nuzi: the Report of the Excavations at Yorgan Tepa near Kirkuk, Iraq, 1927-1931*, Cambridge MA 1939, pp. 545–552.

Emery/Morgenstein 2007
V.L. Emery and M. Morgenstein, "Portable EDXRF analysis of a mud brick necropolis enclosure: evidence of work organization, El Hibeh, Middle Egypt." *Journal of Archaeological Science* 34 (2007), pp. 111–122.

Erhardt *et al.* 2008
W. Erhardt, E. Götz, N. Bödecker, and S. Seybold, *Der große Zander: Enzyklopädie der Pflanzennamen*, Stuttgart 2008.

Everett 2013
M.E. Everet, *Near-Surface Applied Geoophysics*, Cambridge 2013.

Fahn/Werker/Baas 1986
A. Fahn, E. Werker, and P. Baas, *Wood Anatomy and Identification of Trees and Shrubs from Israel and Adjacent Regions*, Leiden 1986.

Fassbinder/Wolf 2024
J. Fassbinder and M. Wolf, "Electrical Resistivity Tomography (ERT) prospecting in the New Town of Assur, 2023." In: Radner/Squitieri 2024a, p. 81.

Fassbinder *et al.* 2024a
J.W.E. Fassbinder, J.-J. Herr, M. Wolf, and L. Ruider, "Geophysical prospecting in Assur, 2023." In: Radner/Squitieri 2024a, pp. 67–81.

Fassbinder *et al.* 2024b
J.W.E. Fassbinder, C. Lippolis, V. Messina, G. Patrucco, V. Santoro, and A. Spanò, "Preliminary report on the campaigns 2022-2023 of the Italian Archaeological Expedition at Seleucia on the Tigris (IAES)." *Mesopotamia* 59 (2024), pp. 55–82.

Frahm 1997
E. Frahm, *Einleitung in die Sanherib-Inschriften*, Vienna 1997.

Frame 1991
G. Frame, "Assyrian clay hands." *Baghdader Mitteilungen* 22 (1991), pp. 335–382.

Frankena 1954
R. Frankena, *Tākultu: de sacrale maaltijd in het assyrische ritueel, met een overzicht over de in Assur veererde goden*, Leiden 1954.

Freestone 2021
I.C. Freestone, "Glass production in the first millennium CE: a compositional perspective." In: F. Klimscha, H. Karlsen, S. Hansen, and J. Renn (eds.), *Vom künstlichen*

Stein zum durchsichtigen Massenprodukt, Berlin 2021, pp. 245–263.

Gabutti 2002–2003
A. Gabutti, "La ceramica dei livelli VIb-III", *Mesopotamia* 37/38 (2002–2003), pp. 87–263.

Gale/Cutler 2000
R. Gale and D. Cutler, *Plants in Archaeology: Identification Manual of Vegetative Plant Materials Used in Europe and the Southern Mediterranean to c. 1500*, Kew 2000.

Gat 1997
M. Gat, *The Jewish Exodus from Iraq, 1948-1951*, London 1997.

Gavagnin/Iamoni/Palermo 2016
K. Gavagnin, M. Iamoni, and R. Palermo, "The Land of Nineveh Archaeological Project: the ceramic repertoire from the Early Pottery Neolithic to the Sasanian period." *Bulletin of the American Schools of Oriental Research* 375 (2016), pp. 119-169.

Gawron-Szymczyk 2022
A. Gawron-Szymczyk, "Gaming pieces, pads or … anything else? Late Bronze Age ceramic discs in the light of experimental research." *Studia Archaeologica Brunensia* 27 (2022), pp. 5–18.

Gibson 1972
McG. Gibson, *The City and Area of Kish*, Miami 1972.

Good 2012
I. Good, "Changes in fiber use and spinning technologies on the Iranian Plateau: comparative and diachronic study of spindle whorls ca. 4500-2500 BCE." *Paléorient* 38 (2012), pp. 111–126.

Grayson 1987
A.K. Grayson, *Assyrian Rulers of the Third and Second Millennia BC (to 1115 BC)* (Royal Inscriptions of Mesopotamia: Assyrian Periods 1), Toronto 1987.

Grayson 1991
A.K. Grayson, *Assyrian Rulers of the Early First Millennium BC (1114-859 BC)* (Royal Inscriptions of Mesopotamia: Assyrian Periods 2), Toronto 1991.

Grayson 1996
A.K. Grayson, *Assyrian Rulers of the Early First Millennium BC (858-745 BC)* (Royal Inscriptions of Mesopotamia: Assyrian Periods 3), Toronto 1996.

Grayson/Novotny 2014
A.K. Grayson and J. Novotny, *The Royal Inscriptions of Sennacherib, King of Assyria (704-681 BC), part 2* (Royal Inscriptions of the Neo-Assyrian Period 3/2), Winona Lake IN 2014.

Gries 2017
H. Gries, *Der Assur-Tempel in Assur: das assyrische Hauptheiligtum im Wandel der Zeit*, Wiesbaden 2017.

Gries/Schmidt 2020
H. Gries and K. Schmidt, "The core-formed glass vessels from Middle Assyrian Aššur." *Zeitschrift für Assyriologie und vorderasiatische Archäologie* 110 (2020), pp. 242–275.

Griffiths/Barker 1993
D.H. Griffiths and R.D. Barker, "Two-dimensional resistivity imaging and modelling in areas of complex geology." *Journal of Applied Geophysics* 29 (1993), pp. 211–226.

Gros-Balthazard/Flowers 2021
M. Gros-Balthazard and J.M. Flowers, "A brief history of the origin of domesticated date palms." In: J.M. Al-Khayri, S. Mohan Jain, and D.V. Johnson (eds.), *The Date Palm Genome, vol. 1: Phylogeny, Biodiversity and Mapping*, Cham 2021, pp. 55–74.

Guralnick 2008
E. Guralnick, "Assyrian clay hands from Khorsabad." *Journal of Near Eastern Studies* 67 (2008), pp. 241–246.

Gzella 2024
H. Gzella, "The Aramaic inscription on the sarcophagus of Grave 3 from Assur." In: Radner/Squitieri 2024a, pp. 196–199.

Haerinck 1983
E. Haerinck, *La céramique en Iran pendant la période parthe (ca. 250 av. J.C. à ca. 225 après J.C.): Typologie, chronologie et distribution*, Ghent 1983.

Haller 1954
A. Haller, *Die Gräber und Grüfte von Assur*, Berlin 1954.

Haller/Andrae 1955
A. Haller and W. Andrae, *Die Heiligtümer des Gottes Assur und der Sîn-Šamaš-Tempel in Assur*, Berlin 1955.

Handel-Mazzetti 1914
H. von Handel-Mazzetti, "Die Vegetationsverhältnisse von Mesopotamien und Kurdistan." *Annalen des Naturhistorischen Museums in Wien* 28 (1914), pp. 48–111.

Hannestad 1983
L. Hannestad, *The Hellenistic Pottery from Failaka, with a Survey of Hellenistic Pottery from the Near East*, Aarhus 1983.

Hauser 1996
S.R. Hauser, "The production of pottery in the Arsacid Ashur." In: K. Bartl and S.R. Hauser (eds.), *Continuity and Change in Northern Mesopotamia from the Hellenistic to the Early Islamic Period*, Berlin 1996, pp. 55–85.

Hausleiter 2010
A. Hausleiter, *Neuassyrische Keramik im Kerngebiet Assyriens*, Wiesbaden 2010.

Hedges 1982
R.E.M. Hedges, "Early glazed pottery and faience in Mesopotamia". In: T.A. Theodore, A. Wertime, and S.F. Wertime (eds.), *Early Pyrotechnology: The Evolution of the First Fire-Using Industries*, Washington DC 1982, pp. 93–103.

Hedges/Moorey 1975
R.E.M. Hedges and P.R.S. Moorey, "Pre-Islamic ceramic glazes at Kish and Nineveh in Iraq." *Archaeometry* 17 (1975), pp. 25–43.

Heeßel 2020
N.P. Heeßel, "The king in ritual action: the Assyrian royal temple rituals." In: S. Görke and C.W. Steitler (eds.), *Cult, Temple, Sacred Spaces: Cult Practices and Cult Spaces in Hittite Anatolia and Neighbouring Cultures*, Wiesbaden 2020, pp. 57–70.

Heidemann/Miglus 1996
S. Heidemann and P.A. Miglus, "Fundmünzen aus Assur und Lokalgeschichte in islamischer Zeit." In: P.A. Miglus, *Das Wohngebiet von Assur. Stratigraphie und Architektur*, Berlin 1996, pp. 353–376.

Hellmuth Kramberger 2016
A. Hellmuth Kramberger, *Die Pfeilspitzen aus Tall Šēh Hamad/Dūr-Katlimmu von der mittelassyrischen bis zur parthisch-römischen Zeit in ihrem westasiatischen und eurasischen Kontext*, Wiesbaden 2016.

Helms 2010
T. Helms, "Wagenradmodelle oder Spinnwirtel? Überlegungen zum Gebrauchswert der Keramikscheiben mit zentraler, durchbohrter Verdickung aus Tell Chuera." In: J. Becker, R. Hempelmann, and E. Rehm (eds.), *Kulturlandschaft Syrien: Zentrum und Peripherie. Festschrift Für Jan-Waalke Meyer*, Münster 2010, pp. 207–226.

Herring/Pidlisecky/Cey 2021
T. Herring, A. Pidlisecky, and E. Cey, "Removing the effects of temperature on electrical resistivity tomography data collected in partially frozen ground: limitations and considerations for field applications." *Vadose Zone Journal* (2021), 20:e20146. DOI: 10.1002/vzj2.20146.

Hiller/Melzig 2010
K. Hiller and M.F. Melzig, *Lexikon der Arzneipflanzen und Drogen*, Heidelberg 2010.

Hillman 1984
G. Hillman, "Traditional husbandry and processing of archaic cereals in modern times, part 1: the glume wheats." *Bulletin on Sumerian Agriculture* 1 (1984), pp. 114–152.

Houghton/Lorber/Hoover 2008
A. Houghton, C. Lorber, and O. Hoover, *Seleucid Coins: A Comprehensive Catalogue, part II: Seleucus IV through Antiochus XIII*, New York/Lancaster/London 2008.

Hulin *et al.* 2018
G. Hulin, C. Maneuvrier, A. Tabbagh, and J.-B. Vincent, "What exists beneath the place where Conrad Schlumberger carried out the first (1912) electrical prospection experiment: the Val-Richer Abbey." *Near Surface Geophysics* 16 (2018), pp. 445–460. DOI: 10.3997/1873-0604.2017063.

Hunt 2015
A.M.W. Hunt, *Palace Ware Across the Neo-Assyrian Imperial Landscape: Social Value and Semiotic Meaning*, Leiden 2015.

Hunt/Speakman 2015
A.M.W. Hunt and R.J. Speakman, "Portable XRF analysis of archaeological sediments and ceramics." *Journal of Archaeological Sciences* 53 (2015), pp. 626–638. DOI: 10.1016/j.jas.2014.11.031.

İşcan/Loth/Wright 1984
M.Y. İşcan, S.R. Loth, and R.K. Wright, "Age estimation from the rib by phase analysis: white males." *Journal of Forensic Sciences* 29 (1984), pp. 1094–1104.

İşcan/Loth/Wright 1985
M.Y. İşcan, S.R. Loth, and R.K. Wright, "Age estimation from the rib by phase analysis: white females." *Journal of Forensic Sciences* 30 (1985), pp. 853–863.

Iwasaki *et al.* 2009
T. Iwasaki, S. Wakita, K. Ishida, and H. Wada (eds.), *Tell*

Mastuma: an Iron Age Settlement in Northwest Syria, Tokyo 2009.

Jacomet/Kreuz 1999
S. Jacomet and A. Kreuz, *Archäobotanik: Aufgaben, Methoden und Ergebnisse vegetations- und agrargeschichtlicher Forschung*, Stuttgart 1999.

Jakob-Rost 1991
L. Jakob-Rost, "Inschriften auf kleineren Tongefäßen aus Assur und Kar-Tukulti-Ninurta." *Forschungen und Berichte* 31 (1991), pp. 55–65.

Jenkins 1958
G.K. Jenkins, "Hellenistic coins from Nimrud." *Iraq* 20 (1958), pp. 158–168.

Johnson 2014
J. Johnson, "Accurate measurements of low Z elements in sediments and archaeological ceramics using portable X-Ray fluorescence (PXRF)." *Journal of Archaeological Method and Theory* 21 (2014), pp. 563–588.

Karkanas 2010
P. Karkanas, "Preservation of anthropogenic materials under different geochemical processes: a mineralogical approach." *Quaternary International* 214 (2010), pp. 63–69.

Katz *et al.* 2010
O. Katz, D. Cabanes, S. Weiner, A.M. Maeir, E. Boaretto, and R. Shahack-Gross, "Rapid phytolith extraction for analysis of phytolith concentrations and assemblages during an excavation: an application at Tell es-Safi/Gath, Israel." *Journal of Archaeological Science* 37 (2010), pp. 1557–1563.

Katzy 2015
E. Katzy, *Hellenisierung Nordmesopotamiens am Beispiel des Khabur-Gebietes*, Wiesbaden 2015.

Katzy 2024
E. Katzy, "Review of E. Klengel-Brandt und H.-U. Onasch, *Die Terrakotten aus Assur im Vorderasiatischen Museum Berlin: Von der frühdynastischen bis zur parthischen Zeit*." *Orientalistische Literaturzeitung* 118 (2024), pp. 386–389.

Kawatama 1990
M. Kawamata, "Telul Hamediyat near Tell Gubba and Songor, part II," *Al-Rafidan* 11 (1990), pp. 175–188.

Khwarahm 2020
N.R. Khwarahm, "Mapping current and potential future distributions of the oak tree (*Quercus aegilops*) in the Kurdistan Region, Iraq." *Ecological Processes* 9 (2020), 56. DOI: 10.1186/s13717-020-00259-0.

Klengel-Brandt 1978
E. Klengel-Brandt, *Die Terrakotten aus Assur im Vorderasiatischen Museum Berlin*, Berlin 1978.

Klengel-Brandt/Onasch 2020
E. Klengel-Brandt and H.-U. Onasch, *Die Terrakotten aus Assur im Vorderasiatischen Museum Berlin: Von der frühdynastischen bis zur parthischen Zeit*, Wiesbaden 2020.

Körber-Grohne 1987
U. Körber-Grohne, *Nutzpflanzen in Deutschland: Kulturgeschichte und Biologie*, Stuttgart 1987.

Kreppner 2006
F.J. Kreppner, *Die Keramik des 'Roten Hauses' von Tall Šēḫ Ḥamad / Dūr-Katlimmu. Eine Betrachtung der Keramik Nordmesopotamiens aus der zweiten Hälfte des 7. und aus dem 6. Jahrhundert v. Chr.*, Wiesbaden 2006.

Kreppner/Richter/Squitieri 2024
F.J. Kreppner, J. Richter, and A. Squitieri, "From Late Bronze Age to the early Islamic period: the pottery repertoire of the 2023 excavations of Assur." In: Radner/Squitieri 2024a, pp. 140–150.

Kreppner/Rohde/Squitieri 2024
F.J. Kreppner, J. Rohde, and A. Squitieri, "Excavating Trench NT1 2023 in the New Town of Assur." In: Radner/Squitieri 2024a, pp. 104–135.

Kunetz 1966
G. Kunetz, *Principles of Direct Current Resistivity Prospecting*, Berlin 1966.

Lanza/Mancini/Ratti 1972
R. Lanza, A. Mancini, and G. Ratti, "Geophysical surveys at Seleucia." *Mesopotamia* 7 (1972), pp. 27–41.

Leacroft/Leacroft 1974
H. Leacroft and R. Leacroft, *The Buildings of Ancient Mesopotamia*, Reading 1974.

Lecomte 1987
O. Lecomte, "Un probleme d'interpretation: l'Ebabbar de Larsa aux epoques hellenistique et seleucoparthe, approche archeologique, economique et culturelle". In : J.L. Huot (ed.), *Larsa 10e campagne (1983) et 'Oueili 4e campagne (1983): Rapport preliminaire*, Paris 1987, pp. 225–246.

Lecomte 1993
O. Lecomte, "Stratigraphical analysis and ceramic assemblages of the 4th-1st centuries BC: Ebabbar of Larsa (Southern Iraq)". In: U. Finkbeiner (ed.), *Materialen zur Archäologie der Seleukiden- und Partherzeit im siidlichen Babylonien und im Golfgebiet*, Tübingen 1993, pp. 17–39.

Lines 1954
J. Lines, "Late Assyrian pottery from Nimrud." *Iraq* 16 (1954), pp. 164–167.

Liritzis/Zacharias 2011
I. Liritzis and N. Zacharias, "Portable XRF of archaeological artefacts: current research, potential and limitations." In: M.S. Shackley (ed.), *X-Ray Fluorescence Spectrometry (XRF) in Geoarchaeology*, New York 2011, pp. 109–131.

Loke 2012
M.H. Loke, *Tutorial: 2-D and 3-D Electrical Imaging Surveys*, Malaysia 2012.

Loke/Acworth/Dahlin 2003
M.H. Loke, I. Acworth, and T. Dahlin, "A comparison of smooth and blocky inversion methods in 2D electrical imaging surveys." *Exploration Geophysics* 34 (2003), pp. 182–187. DOI: 10.1071/EG03182.

Loke *et al.* 2013
M.H. Lokem, J.E. Chambers, D.F. Rucker, O. Kuras, and P.B. Wilkinson, "Recent developments in the direct-current geoelectrical imaging method." *Journal of Applied Geophysics* 95 (2013), pp. 135–156. DOI: 10.1016/j.jappgeo.2013.02.017.

Lorenzon *et al.* 2023
M. Lorenzon, B. Cutillas-Victoria, E. Itkin, and A. Fantalkin, "Masters of mudbrick: geoarchaeological analysis of Iron Age earthen public buildings at Ashdod-Yam (Israel)." *Geoarchaeology* 39 (2023), pp. 35–62. DOI: 10.1002/gea.21977.

Lorenzon *et al.* 2024
M. Lorenzon, B. Cutillas-Victoria, A. Lichtenberger, and O. Tal, "Of mudbrick and stone: a geoarchaeological view on innovations in building practices at Hellenistic Tell Iẓṭabba." *Journal of Archaeological Science: Reports* 54 (2024), 104389. DOI: 10.1016/j.jasrep.2024.104389.

Love 2012
S. Love, "The geoarchaeology of mudbricks in architecture: a methodological study from Çatalhöyük, Turkey." *Geoarchaeology* 27 (2012), pp. 140–156. DOI: 10.1002/gea.21401.

Love 2017
S. Love, "Field methods for the analysis of mud brick architecture." *Journal of Field Archaeology* 42 (2017), pp. 351–363. DOI: 10.1080/00934690.2017.1345222.

Lovejoy 1985
C.O. Lovejoy, "Dental wear in the Libben population: its functional pattern and role in the determination of adult skeletal age at death." *American Journal of Physical Anthropology* 68 (1985), pp. 47–56.

Lovejoy *et al.* 1985
C.O. Lovejoy, R.S. Meindl, T.R. Pryzbeck, and R.P. Mensforth, "Chronological metamorphosis of the auricular surface of the ilium: a new method for the determination of adult skeletal age at death." *American Journal of Physical Anthropology* 68 (1985), pp. 15–28.

Lumsden 1999
S. Lumsden, "Neo-Assyrian pottery from Nineveh." In: A. Hausleiter and A. Reiche (eds.), *Iron Age Pottery in Northern Mesopotamia, Northern Syria and South-Eastern Anatolia*, Münster 1999, pp. 3–15.

Lundström 2009
S. Lundström, *Die Königsgrüfte aus dem Alten Palast von Assur: Aufarbeitung des archäologischen und inschriftlichen Befundes*, Wiesbaden 2009.

Mall *et al.* 2001
G. Mall, M. Hubig, A. Büttner, J. Kuznik, R. Penning, and M. Graw, "Sex determination and estimation of stature from the long bones of the arm." *Forensic Science International* 117 (2001), pp. 23–30.

Mårtensson/Nosch/Strand 2009
L. Mårtensson, M.L. Nosch, and E.A. Strand, "Shape of things: understanding a loom weight." *Oxford Journal of Archaeology* 28 (2009), pp. 373–398.

Martín Galán 2007
R. Martín Galán, "The Hellenistic pottery of Field A". In: M. Lebeau and A. Suleiman (eds.), *Tell Beydar: The 2000-2002 Seasons of Excavations, the 2003-2004 Seasons of Architectural Restoration: A Preliminary Report*, Turnhout 2007, pp. 227–241.

Mas 2015
J. Mas, "Pottery from Girdi Qala Trench B". In: R. Vallet (ed.), *Report of the First Season of Excavations at Girdi Qala and Logarand*, Paris 2015, pp. 37–46.

Matney *et al.* 2011
T. Matney, T. Greenfield, B. Hartenberger, C. Jalbrzikowski, K. Köro, J. MacGinnis, and A. Marsh, "Excavations at Ziyaret Tepe, Diyarbakir Province" *Anatolica* 37 (2011), pp. 67–114.

McKenzie 1997
L. McKenzie, "Discussion of pottery: Level 2". In: J.E. Curtis and A. Green, *Excavations at Khirbet Khatuniyeh*, London 1997, pp. 91–94.

Miglus 1985
P.A. Miglus, "Zur großen Ziqqurat in Assur." *Mitteilungen der Deutschen Orient-Gesellschaft zu Berlin* 117 (1985), pp. 21–45.

Miglus 1996
P.A. Miglus, *Das Wohngebiet von Assur: Stratigraphie und Architektur*, Berlin 1996.

Miglus 2010
P.A. Miglus, "Festungswerke von Assur im 2. Jahrtausend v. Chr." In: S.M. Maul and N.P. Heeßel (eds.), *Assur-Forschungen*, Wiesbaden 2010, pp. 229–244.

Miglus 2016
P.A. Miglus, "Architektur und Kleinfunde des Wohnquartiers." In: Miglus/Radner/Stępniowski 2016, pp. 57–70.

Miglus/Radner/Stępniowski 2016
P.A. Miglus, K. Radner, and F.M. Stępniowski, *Ausgrabungen in Assur: Wohnquartiere in der Weststadt, Teil I*, Wiesbaden 2016.

Miller 1984
N.F. Miller, "The use of dung as fuel: an ethnographic model and an archaeological example." *Paléorient* 10 (1984), pp. 71–79.

Mönninghoff/Skaletz 2022
H. Mönninghoff and M. Skaletz, "Beinobjekte." In: A. el-Massih Baghdo, L. Martin, M. Novák, and W. Orthmann (eds.), *Tell Halaf, VI: Der assyrische Statthalterpalast*, Wiesbaden 2022, pp. 331–332.

Moorey 1985
P.R.S. Moorey, *Materials and Manufacture in Ancient Mesopotamia – the Evidence of Archaeology and Art: Metals and Metalwork, Glazed Materials and Glass*, Oxford 1985.

Moorey 1994
P.R.S. Moorey, *Ancient Mesopotamian Materials and Industries: the Archaeological Evidence*, Oxford 1994.

Muscarella 1988
O.W. Muscarella, *Bronze and Iron: Ancient Near Eastern Artifacts in the Metropolitan Museum of Art*, New York 1988.

Müller-Wiener 2016
M. Müller-Wiener, "Material evidence for the transformation of Late-Umayyad economies: the case of pottery with applied and honeycomb decoration from Resafa (North Syria)." In: O. Kaelin, R. Stucky, and A. Jamieson (eds.), *Proceedings of the 9th International Congress on the Archaeology of the Ancient Near East*, Wiesbaden 2016, pp. 413–423.

Neef 1989
R. Neef, "Plant remains from archaeological sites in lowland Iraq: Hellenistic and Neo-Babylonian Larsa." In: J.L. Hout (ed.), *Larsa: Travaux de 1985*, Paris 1989, pp. 151–161.

Neef 1991
R. Neef, "Plant remains from archaeological sites in lowland Iraq: Tell el 'Oueili." In: J.L. Hout (ed.), *Oueili: Travaux de 1985*, Paris 1991, pp. 321–329.

Neff/Voorhies/Umaña 2014
H. Neff, B. Voorhies, and F.P. Umaña, "Handheld XRF elemental analysis of archaeological sediments: some examples from Mesoamerica." In: A.N. Shugar and J.L. Mass (eds.), *Handheld XRF for Art and Archaeology*, Ithaca 2014, pp. 379–399.

Neumann *et al.* 2019
K. Neumann, C.A.E. Strömberg, T. Ball, R.M. Albert, L. Vrydaghs, and L.S. Cummings, "International Code for Phytolith Nomenclature (ICPN) 2.0." *Annals of Botany* 124 (2019), pp. 189–199.

Nicholson/Shaw 2009
P.T. Nicholson and I. Shaw (eds.), *Ancient Egyptian Materials and Technology*, Cambridge 2009.

Nodarou/Frederick/Hein 2008
E. Nodarou, C. Frederick, and A. Hein, "Another (mud) brick in the wall: scientific analysis of Bronze Age earthen construction materials from East Crete." *Journal of Archaeological Science* 35 (2008), pp. 2997–3015.

Nováček/Melčák 2016
K. Nováček and M. Melčák, "The medieval urban landscape in Northeastern Mesopotamia (MULINEM): first two years of the project." In: O. Kaelin, R. Stucky, and A. Jamieson (eds.), *Proceedings of the 9th International Congress on the Archaeology of the Ancient Near East*, Wiesbaden 2016, pp. 95–105.

Nováček *et al.* 2016
K. Nováček, M. Melčák, and L. Starková (eds.), *Medieval Urban Landscape in Northeastern Mesopotamia*, Oxford 2016.

Nunn 1988
A. Nunn, *Die Wandmalerei und der glasierte Wandschmuck im Alten Orient*, Leiden 1988.

Oates 1968
D. Oates, *Studies in the Ancient History of Northern Iraq*, Oxford 1968.

Oates 1959
J. Oates, "Late Assyrian pottery from Fort Shalmaneser." *Iraq* 21 (1959), pp. 130–146.

Oates/Oates 1958
D. Oates and J. Oates, "Nimrud 1957: the Hellenistic settlement." *Iraq* 20 (1958), pp. 114–157.

Oberdorfer 1990
E. Oberdorfer, *Pflanzensoziologische Exkursionsflora*, Stuttgart 1990 (6th edition).

Palermo 2016
R. Palermo, "From Gaugamela to the Sasanians: the Hellenistic period (late fourth–late second centuries BC)." In: Gavagnin/Iamoni/Palermo 2016, pp. 119–169.

Palermo 2024
R. Palermo, "Exploring the Hellenistic period in North Mesopotamia: landscape studies and excavations at Gird-i Matrab (Iraqi Kurdistan)." *Parthica* 26 (2024), pp. 123–142.

Parr 2006
J.F. Parr, "Effect of fire on phytolith coloration." *Geoarchaeology* 21 (2006), pp. 171–185.

Parsi 2022
M. Parsi, *Analyzing and 3D modelling of Electrical Resistivity Tomography (ERT) data for archaeological prospection*, PhD thesis, LMU Munich, 2022. Available at: edoc.ub.uni-muenchen.de/30392/1/Parsi_Mandana.pdf.

Parsi/Fassbinder 2020
M. Parsi and J.W.E Fassbinder, "The 2019 Electrical Resistivity Tomography (ERT) survey." In: K Radner, F.J. Kreppner and A. Squitieri (eds.), *The Dinka Settlement Complex 2019: Further archaeological and geophysical work on Qalat-i Dinka and in the Lower Town*, Gladbeck 2020, pp. 24–36.

Parsi *et al.* 2019
M. Parsi, J.W.E. Fassbinder, N. Papadopoulos, M. Scheiblecker, and S. Ostner. "Revealing the hidden structure of the ancient city Ur (Iraq) with Electrical Resistivity Tomography." In: J. Bonsall (ed.), *13th International Conference on Archaeological Prospection*, Sligo 2019, pp. 206–208.

Parsi *et al.* 2023
M. Parsi, S. Hahn, J.E.W. Fassbinder, K. Kaniuth, M. Wolf, A. Asandulesei, and C. Brasoveanu, "Illuminating traces of an Achaemenid's monumental complex in the Southern Caucasus by Electrical Resistivity Tomography." *Journal of Applied Geophysics* 209 (2023), 104886. DOI: 10.1016/j.jappgeo.2022.104886.

Pearsall 2015
D.M. Pearsall, *Paleoethnobotany: a handbook of Procedures*, New York 2015 (3rd edition).

Pedde 2000
F. Pedde, *Vorderasiatische Fibeln von der Levante bis Iran*, Saarbrücken 2000.

Pedde 2015
F. Pedde, *Gräber und Grüfte in Assur: die mittelassyrische Zeit*, Wiesbaden 2015.

Pedde/Lundström 2008
F. Pedde and S. Lundström, *Der Alte Palast in Assur: Architektur und Baugeschichte*, Wiesbaden 2008.

Petrie 2002
C.A. Petrie, "Seleucid Uruk: an analysis of ceramic distribution", *Iraq* 64 (2002), pp. 85–123.

Phenice 1969
T.W. Phenice, "A newly developed visual method of sexing the os pubis." *American Journal of Physical Anthropology* 30 (1969), pp. 297–301.

Piperno 2006
D.R. Piperno, *Phytoliths: A Comprehensive Guide for Archaeologists and Paleoecologists*, Lanham 2006.

Portillo/Albert/Henry 2009
M. Portillo, R.M. Albert, and D.O. Henry, "Domestic activities and spatial distribution in Ain Abū Nukhayla (Wadi Rum, Southern Jordan): the use of phytoliths and spherulites studies." *Quaternary International* 193 (2009), pp. 174–183.

Potts 2008
P.J. Potts, "Introduction, analytical instrumentation and application overview" In: P.J. Potts and M. West (eds.), *Portable X-Ray Fluorescence Spectrometry: Capabilities for In Situ Analysis,* Cambridge 2008, pp. 1–12.

Preusser 1955
C. Preusser, *Die Paläste in Assur*, Berlin 1955.

Pruß 2010
A. Pruß, *Die Amuq-Terrakotten: Untersuchungen zu den Terrakotta-Figuren des 2. und 1. Jahrtausends v.Chr. aus den Grabungen des Oriental Institute Chicago in der Amuq-Ebene*, Turnhout 2010.

Puljiz 2021
I. Puljiz, "Faience for the empire: a study of standardized production in the Middle Assyrian State." *Zeitschrift für Assyriologie und Vorderasiatische Archäologie* 111 (2021), pp. 100–122.

Radner 2005
K. Radner, *Die Macht des Namens: Altorientalische Strategien zur Selbsterhaltung*, Wiesbaden 2005.

Radner 2016
K. Radner, "Die beiden neuassyrischen Privatarchive." In: Miglus/Radner/Stępniowski 2016, pp. 79-133.

Radner 2021
K. Radner, "A bit of Assyrian imperial culture: the fragment of an inscribed pottery bowl from Gird-e Rūstam (Iraqi Kurdistan)." *Altorientalische Forschungen* 48 (2021), pp. 118–124.

Radner 2024
K. Radner, "Cuneiform inscriptions from excavation and surface." In: Radner/Squitieri 2024a, pp. 184–196.

Radner/Kreppner 2024
K. Radner and F.J. Kreppner, "First conclusions." In: Radner/Squitieri 2024a, pp. 224–228.

Radner/Moeller/Potts 2002
K. Radner, N. Moeller, and D.T. Potts (eds.), *The Oxford History of the Ancient Near East, vol. 2: From the End of the Third Millennium BC to the Fall of Babylon*, New York/Oxford 2022.

Radner/Richter 2024
K. Radner and J. Richter, "The Andrae House, a monument in its own right: a brief history of the building and its use." In: Radner/Squitieri 2024a, pp. 18–64.

Radner/Squitieri 2024a
K. Radner and A. Squitieri (eds.), *Assur 2023: Excavations and Other Research in the New Town*, Gladbeck 2024.

Radner/Squitieri 2024b
K. Radner and A. Squitieri, "The 2023 work plan and its implementation." In: Radner/Squitieri 2024a, pp. 93–98.

Radner/Squitieri 2024c
K. Radner and A. Squitieri, "First radiocarbon dates from the 2023 excavations." In: Radner/Squitieri 2024a, pp. 98–104.

Radner/Squitieri/Rohde 2024
K. Radner, A. Squitieri, and J. Rohde, "Excavating a sondage linked to the 2002 SBAH trench." In: Radner/Squitieri 2024a, pp. 136–139.

Rapp/Mulholland 1992
G.R. Rapp and S.C. Mulholland (eds.), *Phytolith Systematics: Emerging Issues, vol. 1*, New York 1992.

Rashid 1984
S.A. Rashid, *Mesopotamien – Musikgeschichte in Bildern, Band 2: Musik des Altertums*, Leipzig 1984.

Ratti 1971
G. Ratti, "Applicazione di metodi geofisici per ricerche archeologiche in Iraq." *Bollettino Associazione Mineraria Subalpina* 8 (1971), pp. 3–4.

Reitlinger 1951
G. Reitlinger, "Unglazed relief pottery from Northern Mesopotamia." *Ars Islamica* 15–16 (1951), pp. 11–22.

Rice 1987
P.M. Rice, *Pottery Analysis: A Sourcebook*, Chicago/London 1987.

Rittig 2010
D. Rittig, "Musikinstrumente." In: E. Strommenger, P.A Miglus, and K. Kohlmeyer, *Altorientalische Kleinfunde*

(Ausgrabungen in Tall Biʿa/Tuttul, vol. 5), Wiesbaden 2010, pp. 85–87.

Roaf 1983
M.D. Roaf, "A report on the work of the British Archaeological Expedition in the Eski Mosul Dam Salvage Project from November 1982 to June 1983." *Sumer* 39 (1983), pp. 68–82.

Roaf 1984
M.D. Roaf, "Excavations at Tell Mohammed ʿArab in the Eski Mosul Dam Salvage Project." *Iraq* 46 (1984), pp. 141–156.

Rosen/Weiner 1994
A.M. Rosen and S. Weiner, "Identifying ancient irrigation: a new method using opaline phytoliths from emmer wheat." *Journal of Archaeological Science* 21 (1994), pp. 125–132.

Roßberger 2024
E. Roßberger, "Review of E. Klengel-Brandt and H.-U. Onasch, *Die Terrakotten aus Assur im Vorderasiatischen Museum Berlin: Von der frühdynastischen bis zur parthischen Zeit." Zeitschrift für Assyriologie und vorderasiatische Archäologie* 114 (2024), pp. 242–247.

Rotroff 1997
S.I. Rotroff, *Hellenistic Pottery: Athenian and Imported Wheelmade Table Ware and Related Material* (The Athenian Agora 29), Princeton 1997.

Rotroff 2006
S.I. Rotroff, *Hellenistic Pottery: the Plain Wares* (The Athenian Agora 33), Princeton 2006.

Ruff *et al.* 2012
C.B. Ruff, M.H. Brigitte, M. Niskanen, V. Sladék, M. Berner, E. Garofalo, and H.M. Garvin, "Stature and body mass estimation from skeletal remains in the European Holocene." *American Journal of Physical Anthropology* 148 (2012), pp. 601–617.

Rutten 1996
K. Rutten, "Late Achaemenid and Hellenistic pottery from the tombs of Mahmudiyah, Abu Qubur and Tell ed-Der", *Northern Akkad Project Reports* 10 (1996), pp. 7–39.

Sachs/Hunger 1996
A. Sachs and H. Hunger, *Astronomical Diaries and Related Texts from Babylonia, vol. 3: Diaries from 164 BC to 61 BC*, Vienna 1996.

Saldern 1970
A. von Saldern, "Other Mesopotamian glass vessels." In: A.L. Oppenheim, R.H. Brill, D. Barag, and A. von Saldern (eds.), *Glass and Glassmaking in Ancient Mesopotamia*, Corning 1970, pp. 201–228.

Saldern 2004
A. von Saldern, *Antikes Glas*, Munich 2004.

Sarkady 2024
C. Sarkady, "Plant identification from light fraction flotation samples." In: Radner/Squitieri 2024a, pp. 202–219.

Sauvage 2014
C. Sauvage, "Spindles and distaffs: Late Bronze and Early Iron Age Eastern Mediterranean use of solid and tapered ivory/bone shafts." In: M. Harlow, C. Michel, and M.L.B. Nosch (eds.), *Prehistoric, Ancient Near Eastern and Aegean Textiles and Dress: An Interdisciplinary Anthology*, Oxford 2014, pp. 184–226.

Schaefer/Black/Scheuer 2009
M. Schaefer, S. Black, and L. Scheuer, *Juvenile Osteology: A Laboratory and Field Manual*, London 2009.

Schauer 2024
M. Schauer, "Coefficient corrections for portable X-ray fluorescence data of the Niton XL3t No. 97390 (coefcor I-IV) developed according to the Munich procedure." *Data in Brief* 53 (2024), 109914. DOI: 10.1016/j.dib.2023.109914.

Schauer 2025a
M. Schauer, *Was ist 'La Hoguette' – Kultur, Phänomen, Subkultur? Archäologische Studien und portable, energiedispersive Röntgenfluoreszenzanalysen (p-ED-RFA) an Keramik zu einer altbekannten Frage*, Wiesbaden 2025.

Schauer 2025b
M. Schauer, "p-XRF data of Hellenistic and Parthian pottery from the 2023 and 2024 excavations at Assur." *Open Data LMU* (deposited 25 April 2025). DOI: https://doi.org/10.5282/ubm/data.608.

Schauer/Amicone 2024
M. Schauer and S. Amicone, "First steps towards a fabric classification for Assur: portable X-ray fluorescence (p-XRF) and petrographic analyses on the 2023 pottery." In: Radner/Squitieri 2024a, pp. 150–159.

Schauer/Truntschnig/Almstädter 2025
M. Schauer, T. Truntschnig, and G. Almstädter, "Portable Röntgenfluoreszenzanalyse (p-RFA): Qualitätskontrolle,

Datenaufbereitung & Datenvisualisierung zur Masterarbeit von T. Truntschnig ‚Keramikdeponierungen der Urnenfelderkultur in Österreich: Neue methodische Ansätze und interdisziplinäre Forschungen am Fallbeispiel Ebreichsdorf (NÖ, VB Baden).“ *NHMW Data Repository* (deposited 22 January 2025). DOI: 10.57756/3bmkjr.

Schauer *et al.* 2024
M. Schauer, F. Siegmund, M. Helfert, and B.L. Drake, “The Munich Procedure: Standardising linear regression documentation in p-XRF research.” *Software Impacts* 21 (2024), 100660. DOI: 10.1016/j.simpa.2024.100660.

Schlumberger 1912
C. Schlumberger, *Premières Expériences: Carte des Courbes Equipotentielles, Tracées au Courant Continu Val-Richer (Calvados). Août-Septembre 1912*, Calvados 1912.

Schmidt 2013
A. Schmidt, *Earth Resistance for Archaeologists*, Lanham 2013.

Schmidt 1999
C. Schmidt, “Die Keramik der Areale A-F in Kar Tukulti Ninurta”. In: A. Hausleiter and A. Reiche (eds.), *Iron Age Pottery in Northern Mesopotamia, Northern Syria and South-Eastern Anatolia*, Münster 1999, pp. 61–90.

Schmitt 2012
A. Schmitt, *Die jüngeren Ištar-Tempel und der Nabû-Tempel in Assur*, Wiesbaden 2012.

Schneider 2006
G. Schneider, “Mineralogisch-chemische Untersuchungen der mittel- und neuassyrischen Keramik von Tall Šēḫ Ḥamad.” In: Kreppner 2006, pp. 391–420.

Schweingruber 1990
F.H. Schweingruber, *Anatomie europäischer Hölzer: ein Atlas zur Bestimmung europäischer Baum-, Strauch- und Zwergstrauchhölzer*, Bern/Stuttgart 1990.

Seeher 2000
J. Seeher, “Getreidelagerung in unterirdischen Großsspeichern: Zur Methode und ihrer Anwendung im 2. Jahrtausend v. Chr. am Beispiel der Befunde in Ḫattuša.” *Studi Micenei ed Egeo-Anatolici* 42 (2000), pp. 261–301.

Selz 2014
G.J. Selz, “Feeding the travellers. On early dynastic travel, travel networks and travel provisions in the frame of third millennium Mesopotamia.” In: L. Milano (ed.), *Paleonutrition and Food Practices in the Ancient Near East: Towards a Multidisciplinary Approach*, Padova 2014, pp. 261–280.

Shackley 2012
M.S. Shackley, “Portable X-ray fluorescence spectrometry (pXRF): the good, the bad, and the ugly.” *Archaeology Southwest Magazine* 26 (2012), pp. 1–8.

Shillito/Ryan 2013
L.M. Shillito and P. Ryan, “Surfaces and streets: phytoliths, micromorphology and changing use of space at Neolithic Çatalhöyük (Turkey).” *Antiquity* 87 (2013), pp. 684–700.

Shugar/Mass 2014
A.N. Shugar and J.L. Mass, “Introduction.” In: A.N. Shugar and J.L. Mass (eds.), *Handheld XRF for Art and Archaeology*, Ithaca 2014, pp. 17–36.

Simpson 1992
St. J. Simpson, *Aspects of the Archaeology of the Sasanian period in Mesopotamia*. PhD thesis, University of Oxford, 1992. Available at: oai:union.ndltd.org:bl.uk/oai:ethos.bl.uk:577570.

Šlaus *et al.* 2003
M. Šlaus, D. Strinovic, J. Skavic, and V. Petrovecki, “Discriminant function sexing of fragmentary and complete femora: standards for contemporary Croatia.” *Journal of Forensic Science* 48 (2003), pp. 509–512.

Smith 1991
B.H. Smith, “Standards of human tooth formation and dental age assessment.” In: M.A. Kelly and C.S. Larsen (eds.), *Advances in Dental Anthropology*, New York 1991, pp. 143–168.

Soldi 2017
S. Soldi, “‘Assyrian clay hands’ in the architecture of the Ancient Near East.” *The Metropolitan Museum Journal* 52 (2017), pp. 8–23.

Sparkes/Talcott 1970
B.A. Sparkes and L. Talcott, *Black and Plain Pottery of the 6th, 5th and 4th Centuries BC* (The Athenian Agora 12), Princeton 1970.

Squitieri 2020
A. Squitieri, “Small finds from the Dinka Settlement Complex 2015-2019.” In: K. Radner, F. J. Kreppner, and A. Squitieri (eds.), *The Dinka Settlement Complex 2019: Further Archaeological and Geophysical Work in Qalat-i Dinka and in the Lower Town*, Gladbeck 2020, pp. 95–111.

Squitieri 2024
A. Squitieri, "Small finds from Assur, 2023." In: Radner/Squitieri 2024a, pp. 160–183.

Steckel *et al.* 2018
R.H. Steckel, C.S. Larsen, P.W. Sciulli, and P.L. Walker, "Data collection codebook." In: R.H. Steckel, C.S Larsen, C.A. Roberts, and J. Baten (eds.), *The Backbone of Europe*, Cambridge 2018, pp. 397–427.

Stein 1984
J.K. Stein, "Organic matter and carbonates in archaeological sites." *Journal of Field Archaeology* 11 (1984), pp. 239–245.

Strommenger/Miglus/Kohlmeyer 2010
E. Strommenger, P.A. Miglus, and K. Kohlmeyer, *Altorientalische Kleinfunde* (Ausgrabungen in Tall Bi'a/Tuttul, vol. 5), Wiesbaden 2010.

Stronach 1978
D. Stronach, *Pasargadae: A Report on the Excavations Conducted by the British Institute of Persian Studies from 1961 to 1963*, Oxford 1978.

Tengberg 2012
M. Tengberg, "Beginnings and early history of date palm garden cultivation in the Middle East." *Journal of Arid Environments* 86 (2012), pp. 139–147.

Tite/McCarthy/Paynter 2008
M.S. Tite, B. McCarthy, and S. Paynter, "Production of glazed pottery and brickwork in the Near East". In: M.S. Tite and A.J. Shortland (eds.), *Production Technology of Faience and Related Early Vitreous Materials*, Oxford 2008, pp. 187–198.

Tosi 1980–83
M. Tosi, "Koralle." *Reallexikon der Assyriologie und Vorderasiatische Archäologie* 6 (1980–83), p. 212.

Ubelaker 1989
D.H. Ubelaker, *Human Skeletal Remains: Excavation, Analysis, Interpretation*, Washington DC 1989.

Valtz 2024
E. Valtz, *Ceramica dagli scavi "storici" 1964-1976, 1985-1989*, Turin 2024 (2 volumes). Available at: www.centroscavitorino.it/wp-content/uploads/2024/06/01-TESTI_compressed.pdf; www.centroscavitorino.it/wp-content/uploads/2024/06/02-TAVOLE-_compressed-1.pdf.

van der Veen 2011
M. van der Veen, *Consumption, Trade and Innovation: Exploring the Botanical Remains from the Roman and Islamic Ports of Quseir al-Qadim, Egypt*, Frankfurt 2011.

van Zeist/Bakker-Heeres 1982
W. van Zeist and J.A.H. Bakker-Heeres, "Archaeobotanical studies in the Levant, 1: Neolithic sites in the Damas basin: Aswad, Ghoraife, Ramad." *Palaeohistoria* 24 (1982), pp. 156–256.

van Zeist/Bakker-Heeres 1984a
W. van Zeist and J.A.H. Bakker-Heeres, "Archaeobotanical studies in the Levant, 2: Neolithic and Halaf levels at Ras Shamra." *Palaeohistoria* 26 (1984), pp. 151–170.

van Zeist/Bakker-Heeres 1984b
W. van Zeist and J.A.H. Bakker-Heeres, "Archaeobotanical studies in the Levant, 3: Late Paleolithic Mureybit." *Palaeohistoria* 26 (1984), pp. 171–199.

van Zeist/Bakker-Heeres 1985
W. van Zeist and J.A.H. Bakker-Heeres, "Archaeobotanical studies in the Levant, 4: Bronze Age sites on the Syrian Euphrates." *Palaeohistoria* 27 (1985), pp. 247–316.

Venco Ricciardi 1997
R. Venco Ricciardi, "Hatara, Livello 9: la ceramica ellenistica", *Mesopotamia* 32 (1997), pp. 131-143.

Völling 2008
E. Völling, *Textiltechnik im alten Orient: Rohstoffe und Herstellung*, Würzburg 2008.

Waksman 2017
Y. Waksman, "Provenance studies: production and compositional groups." In: A.M.W. Hunt (ed.), *Archaeological Ceramic Analysis*, Oxford 2017, pp. 148–161.

Waldron 2008
T. Waldron, *Palaeopathology*, Cambridge 2008.

Walker 2005
P.L. Walker, "Greater sciatic notch morphology: sex, age, and population differences." *American Journal of Physical Anthropology* 127 (2005), pp. 385–391.

Wasylikowa/Kolinski 2013
K. Wasylikowa and R. Kolinski, "The role of plants in the economy of Tell Arbid, north-east Syria, in the post-Akkadian period and Middle Bronze Age." *Acta Palaeobotanica* 53 (2013), pp. 263–293.

Weiner 2010
S. Weiner, *Microarchaeology: Beyond the Visible Archaeological Record*, Cambridge 2010.

Welton *et al.* 2019
L. Welton, T. Harrison, S. Batiuk, E. Unlu, B. Janeway, D. Karkaya, D. Lipovitch, D. Lumb, and J. Roames, "Shifting networks and community identity at Tell Tayinat in the Iron I (ca. 12th to mid-10th century BCE)." *American Journal of Archaeology* 123 (2019), pp. 291–333.

Wicke 2010
D. Wicke, *Kleinfunde aus Elfenbein und Knochen aus Assur*, Wiesbaden 2010.

Wilkinson/Tucker 1995
T.J. Wilkinson and D.J. Tucker, *Settlement Development in the North Jazira, Iraq: A Study of the Archaeological Landscape*, Baghdad 1995.

Wrede 2004
N. Wrede, *Uruk, Terrakotten, I: Von der Ubaid- bis zur altbabylonischen Zeit*, Mainz 2004.

Zabar/Borowy 2012
A. Zabar and A. Borowy, "Cultivation of date palm in Iraq." *Annales Horticulturae* 22 (2012), pp. 39–53.

Zohary/Hopf/Weiss 2012
D. Zohary, M. Hopf, and E. Weiss, *Domestication of Plants in the Old World*, Oxford 2012 (4th edition).